The Development of DUAL BRD4 and CBP/p300 Degraders From ISOX-DUAL

Anthony Kai Edmonds

Supervisor: Professor John Spencer

Submitted to the University of Sussex in part fulfilment of the requirements for the degree of Doctor of Philosophy

July 2021

Declaration

I hereby declare that all work described in this thesis was carried out at the University of Sussex under the supervision of Professor John Spencer (Primary supervisor), Professor Simon Morley (co-supervisor) and Dr Timothy Chevassut (co-supervisor) or at Tocris Bio-Techne during an industrial placement under the supervision of Dr Graham Marsh and Dr Hannah Maple, from September 2017 to July 2021. Chapter 2 has formed the basis of a scientific paper and is currently under review. The enclosed work is my own unless otherwise stated and has not been submitted in whole or in part for any other degree.

Anthony Kai Edmonds

July 2021

Acknowledgements

Firstly, I would like to thank Professor John Spencer for his guidance, support and constant enthusiasm towards chemistry and life in general throughout my Ph.D. He was always there to assist when problems arose, or there for a good chat, a laugh and keeping me caffeinated. I hope to continue keeping in touch with or working with John in the future. Equally, I would like to thank Dr Hannah Maple for her guidance and support throughout the Ph.D. and for helping me with collaborative projects, learning how to communicate data scientifically, and for helping me understand data from biochemical assays.

I would like to thank Professor Simon Morley and Dr Ella Lineham for guidance and training during my initial journey into cell culture and immunoblotting, Dr Timothy Chevassut for guidance and support with biochemistry aspects and thank Dr Helen Stewart for the running of assays.

I would like to give a special thanks to Dr Graham Marsh for supervising me during my industrial placement, whose chemistry expertise and general laboratory tricks have been invaluable to my education and research. I would also like to thank Dr Catherine Oakes, Dr Mark Norley and Dr Simon Pridmore for their assistance with chemistry, laboratory work and friendliness during my time at Tocris. Additionally, I would like to thank the other employees of Tocris who assisted me during my industrial placement.

I would like to thank EPSRC and Tocris for funding my studies.

I would like to give a special thanks to Dr Jeff Cooper, Dr Cari Graber-Feesl, Dr Bradley Brasher and Dr Oleg Fedorov for collaborating and running assays on the compounds designed within this document, whose help was invaluable to the project. I would also like to thank Dr Alaa Abdul-Sala for carrying out mass spectrometry and the UK National Crystallography Service for X-ray crystallography and Dr Iain Day for help with NMR.

I would like to thank Dr Andrew McGown and Dr Storm Hassell-Hart for their guidance, helpful discussions, and input throughout my Ph.D., being there for both educational and comedic conversations. I would like to thank Dr Andrew McGown additionally for proof reading aspects of this document. I would also like to thank members of the Spencer group past and present for support help and distractions.

Finally, a special thanks to my family, especially my Mum, Dad and Sister for their support during my university career. They have always been there when I needed them, and I will be forever grateful for their love and encouragement.

Abbreviations

µM	Micromolar
µw	Microwave
AcCoA	Acetyl Co-enzyme A
ACR	Amide coupling reagent
ADCs	Antibody-Drug Conjugates
ADME	Absorption, Distribution, Metabolism and Excretion
Ala	Alanine
AML	Acute Myeloid Leukaemia
AR	Androgen Receptor
Arg	Arginine
ASGPR	Asialoglycoprotein receptor
Asn	Asparagine
Asp	Aspartic Acid
ATCC	American Type Culture Collection
ATP	Adenosine Triphosphate
ATTEC	Autophagosomes-Tethering Compounds
AUTACs	Autophagy-Targeting Chimeras
BAF	BRG1- or BRM-Associated Factors
BCA	Bicinchoninic Acid
BCR	Breakpoint Cluster Region
BD1	Bromodomain 1
BD2	Bromodomain 2
BET	Bromo- and Extra-Terminal
bHLHZip	Basic Helix Loop Helix Zipper
Boc	*tert*-butyloxycarbonyl
BRCA	Breast Cancer Gene
BRD	Bromodomain
BRM	Biological Response Modifier
cAMP	Cyclic Adenosine Monophosphate
CBP/CREBBP	CREB-binding Protein
CDI	Carbonyldiimidazole
CEI	Capillary Electrophoresis Immunoassay
CIP	Carbonyl Iron Powder

CLL	Chronic Lymphocytic Leukaemia
CRBN	Cereblon
CREB	cAMP Response Element Binding Protein
C-terminal	Carboxy Terminus
Cys	Cysteine
DC_{50}	Depletion with a Half-Maximal Degradation Concentration
DCM	Dichloromethane
DFT	Density-Functional Theory
DIPEA	*N*,*N*-Diisopropylethylamine
DMA	Dimethyl Acetamide
D_{max}	The Maximal Level of Degradation
DMEM	Dulbecco's modified Eagle's medium
DMF	Dimethyl Formamide
DMP	Dess Martin Periodinane
DMSO	Dimethyl Sulfoxide
DNA	Deoxyribonucleic acid
dTAG	Degradation Tag
EC_{50}	Concentration of the Drug at a Stable State Inducing Half of the Maximum Effect.
EMEM	Eagle's Minimal Essential Medium
ER	Estrogen Receptor
Et_2O	Diethyl ether
EtOAc	Ethyl Acetate
FDA	Food and Drug Administration
FP	Fluorescence Polarization
FRET	Fluorescence Resonance Energy Transfer
Gln	Glutamine
Glu	Glutamic Acid
Gly	Glycine
H3	Histone 3
H4	Histone 4
HAT	Histone Acetyl Transferase
HATU	Hexafluorophosphate Azabenzotriazole Tetramethyl Uronium
HBA	Hydrogen Bond Acceptor

HBD	Hydrogen Bond Donor
H-bond	Hydrogen bond
HBTU	Hexafluorophosphate Benzotriazole Tetramethyl Uronium
HCC	Hepatocellular Carcinoma
HDAC	Histone Deacetylase
HECT	Homologous to E6-AP Carboxy Terminus
HIF-1α	Hypoxia-Inducible Factor 1-alpha
His	Histidine
HLH	Helix Loop Helix
HPLC	High Performance Liquid Chromatography
HR-MS	High Resolution Mass Spectrometry
HTT	Huntington
IAP	Inhibitor of Apoptosis Proteins
IC_{50}	Half-maximal inhibitory concentration
IKZF	Ikaros family zinc finger
IMiDs	Immunomodulatory Drugs
imid	Imidazole
IRF	Interferon Regulatory Factor
K98	Lysine 98
KAc	Acetyl Lysine
K_d	Dissociation Constant
kDa	Kilodalton
K_i	Inhibition Constant
LAH	Lithium Aluminium Hydride
LC-MS	Liquid Chromatography-Mass Spectrometry
Leu	leucine
LTR	Lysosome Targeting Receptor
Lys	Lysine
LysCoA	Lysine Co-enzyme A
LYTACs	Lysosome-Targeting Chimeras
MAOS	Microwave Assisted Organic Synthesis
Max	Myc-associated factor X
MB	Myc Box
MCL	Mantle Cell Lymphoma

MDa	Mega Dalton
MDM2	Mouse Double Minute 2
MDS	Myelodysplastic syndrome
mHTT	Mutant Huntingtin Protein
MHz	Mega Hertz
MIDA	Methyliminodiacetic
MM	Multiple Myeloma
MOM	Methoxymethyl
Mono	Monowave
mRNA	Messenger RNA
NLS	Nuclear recognition sequence
nM	Nanomolar
NMP	*N*-Methyl-2-pyrrolidone
NMR	Nuclear Magnetic Resonance
N-terminal	Amino terminus
p300	E1 associated binding protein p300
p53	protein of 53 kDa
PAF	Platelet Activating Factor
PAIN	Pan Assay Interference Compound
PARP	Poly (ADP-ribose) polymerase
PBS	Phosphate-Buffered Saline
PCAF	p300 and CBP-Associated Factor
PD	Pharmacodynamics
$Pd(dppf)Cl_2 \cdot DCM$	[1,1'-bis(diphenylphosphino)ferrocene]dichloropalladium(II), complex with dichloromethane
PDB	Protein data bank
$PdCl_2(dtbpf)$	1,1'-bis(di-*tert*-butylphosphino)ferrocene] palladium(II) dichloride
PEG	Polyethylene glycol
PEL	Primary Effusion Lymphoma
Phe	Phenylalanine
PK	Pharmacokinetics
POI	Protein of Interest
PPI	Protein-Protein Interaction
ppm	parts per million

Pro	Proline
PROTAC	Proteolysis Targeting Chimera
qRT-PCR	Quantitative reverse transcription polymerase chain reaction
RING	Really Interesting New Gene
RIPK2	Receptor Interacting Serine/Threonine Kinase 2
RNA	Ribonucleic Acid
SAR	Structure Activity Relationship
SDS	Sodium Dodecyl Sulphate
Ser	Serine
SGC	Structural Genomics Consortium
SNIPERs	Specific and Non-genetic Inhibitors of Apoptosis Protein-Dependent Protein Erasers
T3P	Propanephosphonic acid anhydride
TAD	Transactivation Domain
TBS	*tert*-Butyldimethylsilyl
TFA	Trifluoroacetic acid
THF	Tetrahydrofuran
Thr	Threonine
TPD	Targeted Protein Degradation
TPSA	Total Polar surface Area
TR	Time-Resolved
Trp	Tryptophan
Tyr	Tyrosine
Ub	Ubiquitin
UbR	Ubiquitin Readers
UPS	Ubiquitin Proteasome System
VHL	Von Hippel-Lindau
WB	Western Blot
WDR5	WD repeat-containing protein 5
WT	Wild Type

Abstract

The development of Heterobifunctional molecules in the field of targeted degradation is a hot topic, with various modalities appearing over the past 20 years, with examples such as; PROTACs, SNIPERs, dTAGs, HaloTags, AUTACS, ATTECs and LYTACs. In 2019 alone there were 107 PROTAC publications, an increase of 55 from the previous year.[1]

ISOX-DUAL is an inhibitor of both BRD4 (IC_{50} = 1.5 μM) and CBP/p300 (IC_{50} = 0.65 μM) bromodomains and, as such, is a useful chemical probe for research into epigenetics.[2] The published and our in-house protocols toward this target molecule were poor yielding and not amenable to scale-up. Here, synthetic routes towards the title compound were re-investigated, and now achieves an overall yield of 42%, compared to the literature published 1%.

Using literature co-crystal structures in the bromodomains of BRD4 and CBP/p300 of the, structurally similar, inhibitor BDOIA383, two solvent exposed exit vectors were discovered for potential linkage to E3 recruiters. ISOX-DUAL was then re-designed with the optimised synthetic route to afford two degrader precursors (**3.07**) and (**3.27**) which were designed through replacement of the *N*,*N*-dimethylpropylamine to a propyl carboxylic acid (**3.07**) and the replacement of the morpholine moiety to a piperazine (**3.27**). Degrader mimics (**3.09**, **3.29**) were synthesised from these compounds and showed no loss in binding affinities to the bromodomains of BRD4 or CBP/p300.

A small library of 20 ISOX-DUAL based degraders were synthesised, guided by predicted physiochemical properties. Select degraders (**4.69**-**4.72**) were subjected to cell-free ubiquitination assays, to which, confirmed induction of ubiquitination of the target. The 20 synthesised degraders were initially treated in HeLa cells and **4.68** caused a reduction in BRD4 (75%) and CBP (73%), the most potent degrader in this assay. The investigation goes on to highlight the importance of cell lines when assessing these compounds and describes a series of future experiments, which, should be performed.

Contents

1 Chapter 1: Introduction

1.1 Cancer

Cancer is a general name given to more than 277 different types of disease, which result in the uncontrolled growth and division of cells.[3] It is currently one of the leading causes of death, contributing to an estimated 18.1 million new cases and 9.56 million deaths in 2018 worldwide and in 48 countries is ranked as the number one cause of premature death.[4] The global lifetime probability of being diagnosed with cancer is 37– 39%.[5]

More specifically in the UK, cancer deaths as a whole in 2016 were reported to be 30.3% in males and 25.6% in females, making cancer the leading cause of death for both sexes.[6] Statistics from Cancer Research UK show that in 2015 – 2017 there were around 367,000 new cases of cancer, breaking down to approximately 1000 new cases a day.[7] However, cancer survival has doubled within the last 40 years and is reported that half the people diagnosed with cancer in England and Wales survive their disease for more than 10 years.[7]

The burden of cancer will continue to grow each year due to longevity and growth of the world's population. Cancer growth is aided by behaviours adopted in the public with regards to an increase in available luxuries. Notable examples of these are: smoking, excessive alcohol consumption and eating, leading to obesity. Behavioural changes within society have resulted in a profound effect on the quantity of cancer cases and will continue to do so.[8] These statistics highlight how important it is to investigate new treatments and modalities to further increase the survival rate of this disease.

Tumorigenesis is the gain of malignant properties in normal cells, such properties include resisting cell death, genome instability and mutation, evading growth suppressors, avoiding immune destruction and have been described as the hallmarks of cancer.[9] Mutations in oncogenes and tumour suppressor genes might cause these genes to change the level of expression that could eventually lead to the gain of these hallmark properties.[10]

Epigenetics, originally defined by C.H.Waddington in 1942 as "The casual interactions between genes and their products, which bring the phenotype into being" involves understanding the structure of chromatin and its impact on gene function.[11] The definition of epigenetics has evolved over time to become "The study of heritable changes in gene expression that occur independent of changes in the primary DNA sequence".[12] This heritability of gene expression is mediated by epigenetic modifications of histone proteins.

Chromatin in the nucleus of a cell exists in one of two states, either open, which is favourable for transcription, or closed, which is favourable for transcriptional repression. Histones have a protruding *N*-terminus that is rich in lysine residues and therefore positively charged at physiological pH. This positive charge allows for an intimate interaction with the negative charge of the DNA phosphate backbone.[13] Acetylation of the histone proteins neutralise the charge, weakening interactions with DNA which results in an "open" chromatin formation.[13]

The post translational modification (PTM) *via* addition and removal of either methyl, acetyl or phosphate groups to histone proteins, and covalent modifications of DNA is known as the *epigenetic code* and allows for the control of gene expression.[14]

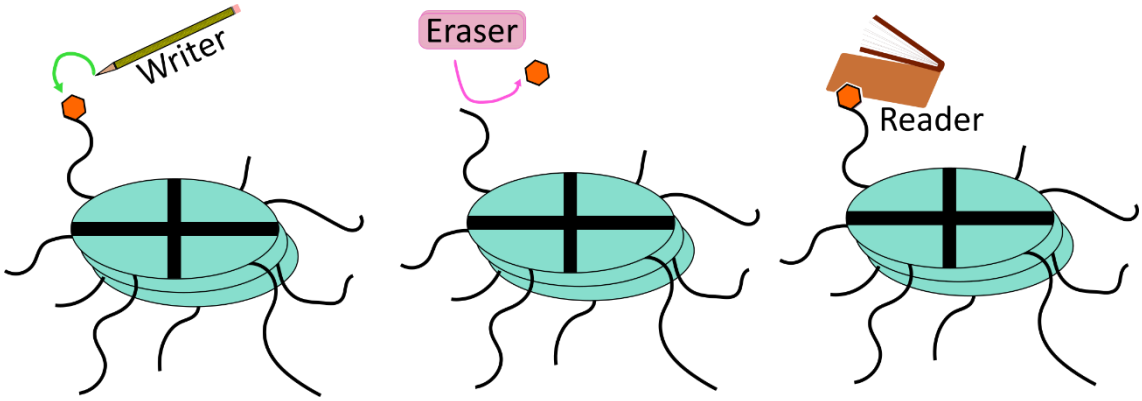

Figure 1.1: The series of proteins that govern the epigenetic code, Writers, Readers and Erasers.

The *epigenetic code* is governed by proteins that can be categorised as readers, writers and erasers (Figure 1.1). Readers are proteins that possess specialised domains capable of recognising specific epigenetic marks, for example, bromodomains (BRDs). Writers are enzymes that can add to nucleotide bases and specific amino acid residues on histones, with one example being Histone Acetyltransferases (HATs). Finally, erasers are the enzymes that are capable of removing the modifications, for example Histone deacetylases (HDACs).[15]

1.2 The Proto-Oncogene MYC

Proto-oncogenes are responsible for normal cell division and growth, but become oncogenes during genetic mutation.[3] Oncogenes are genes that have the potential to become cancer, and in these tumour cells, are often mutated or expressed at higher levels. One of the most notable proto-oncogenes is MYC and is one of the most highly amplified oncogenes in human cancers, observed in approximately 70% of human malignancies.[16–18]

The MYC family of oncogenes include c-Myc, N-Myc and L-Myc. The role of L-Myc is not fully understood but research is ongoing and reports have described L-Mycs role in gastric cancer through silencing of MYCL1 and its role in cancer stem-like cells.[19,20] N-Myc is tissue restricted and encoded by MYCN in neuroblastoma cells.[21] The members of the myc family of oncogenes are activated in many if not most human tumours. These structurally and functionally similar phosphoproteins are responsible for promoting cell growth and transformation by regulating the transcription of target genes required for proliferation.[22,23] The Myc family have motifs that are characteristic of transcription factors, the basic helix-loop-helix-leucine zipper (bHLHZip) dimerization and DNA binding domains. Different families of bHLH proteins are responsible for recognising different E-box sequences, both Myc and Max are members of the phylogenetic group B of bHLH proteins, or III, IV by the classification according to Murre.[24,25]

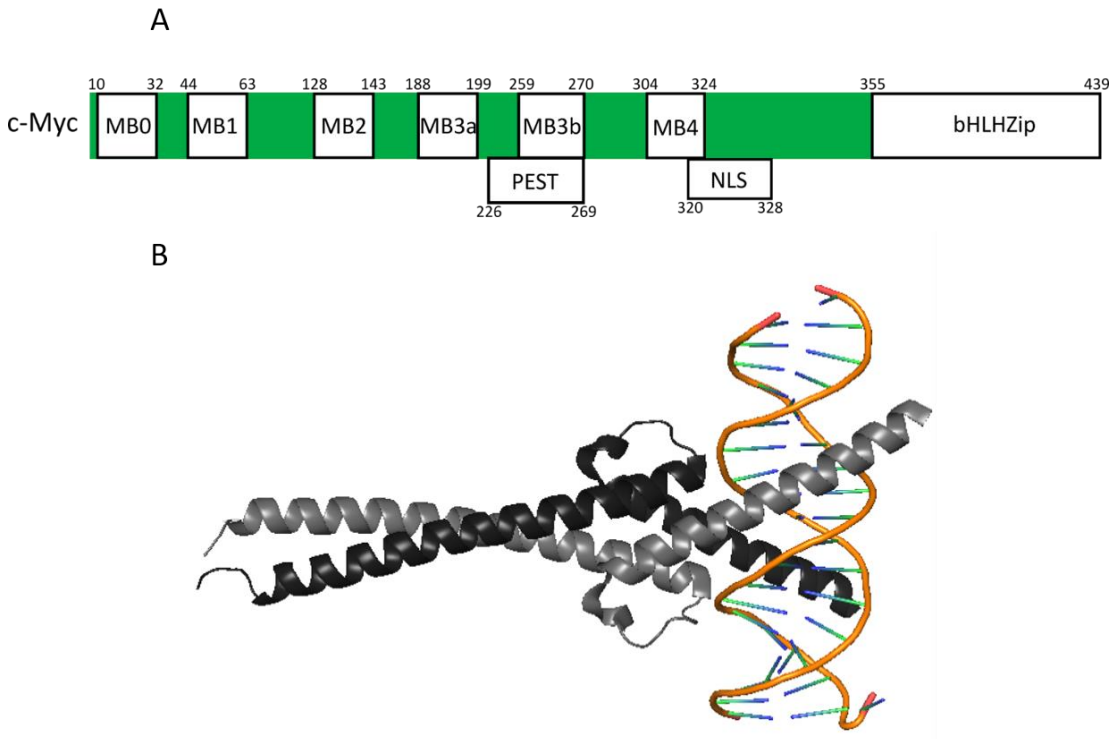

Figure 1.2: A) Gene map for the MYC family, highlighting Myc Box domains (MB0-MB4), the PEST domain, the nuclear localisation sequence (NLS) and the bHLHZip of c-Myc. B) The Myc-Max bHLHZip dimer (Myc grey, Max black) binding to E-box DNA (PDB: 1NKP).[26]

The Myc family have two highly homologous regions that lie within the transactivation domain (TAD) and have been termed Myc homology box 1 and 2 (MB1, MB2) (Figure 1.2A).[27]

In the early 1990s it was shown that Mycs' N-terminal region functions as a TAD and the C-terminal region possessed homology to the bHLHZip proteins. This led to a hypothesis that Myc formed homo or heterodimers in order to bind DNA.[28,29] However, Myc was shown to only form homodimers at high protein concentrations, but because of the tight regulation of Myc expression, was seen as unlikely.[30] Shortly afterwards, Myc-associated factor X (Max) was then discovered as a closely related bHLHZip protein which lacked a TAD region. Max was shown to form heterodimers with the Myc family, where the integrity of the HLH region was key for dimer formation (Figure 1.2B).[31]

The protein c-Myc is a 62 kDa protein comprising of the key TAD and bHLHZip regions mentioned previously (Figure 1.2A). Expression of c-Myc is tightly controlled in healthy cells, but becomes dysregulated and overexpressed in human cancers.[18] The c-Myc/Max dimer is a master regulator of gene transcription, controlling the expression of approximately 30% of the genes within the human genome.[32] c-Myc orchestrates a wide range of essential cellular processes, such as cell growth, apoptosis, RNA biogenesis and splicing, all of which when overexpressed attribute to cancer proliferation.[18]

The binding of the c-Myc/Max dimer to an E-box activates gene expression through the recruitment of the transformation/transcription domain-associated protein (TRRAP) and recruiting HAT complexes such as TIPS60, GCN5 and PCAF and ATP binding protein TIP48 to the vicinity of the E-box. This recruitment leads to the acetylation of histones H3 and H4, opening the chromatin structure, allowing the lead to transcription.[33] The interaction of c-Myc with additional cofactors such as WDR5 and PAF1 play roles in the direction of c-Myc to specific chromatin locations.[34,35]

Inhibitors targeting c-Myc have been investigated *in vitro*, however, to date there are no small molecule inhibitors within clinical trials for the direct inhibition of c-Myc.[36] This is likely due to target selectivity, rapid metabolism and low potency of the small molecules and peptides synthesised to date. One of the more successful modalities of modulating c-Myc activity is through the inhibition of upstream and downstream proteins that inhibit activity or target it for degradation.[36,37]

1.2.1 **Upstream targets of MYC**

1.2.1.1 BRD4

Bromodomain-containing proteins are referred to as epigenetic readers due to being responsible for reading lysine acetylation along histones, a process which impacts chromatin structure, function and subsequent control of gene regulation.[38] The bromodomain (BRD) is the only protein domain whose conserved activity is to exclusively function as an acetylated lysine (KAc) binding domain.[39] Bromodomains are present in a large number of proteins, with 46 diverse human proteins containing a total of 61 bromodomains as identified by Filippakopoulos and coworkers.[40] While 48 of these bromodomains have an Asn residue in the KAc binding site, the remaining 13 bromodomains instead have either a Tyr, Thr or Asp in its place and are referred to as atypical bromodomains.[41] The family of bromodomains can be divided into the eight sub-families (I-VIII) based on the sequence alignment of BRDs (Figure 1.3).[42]

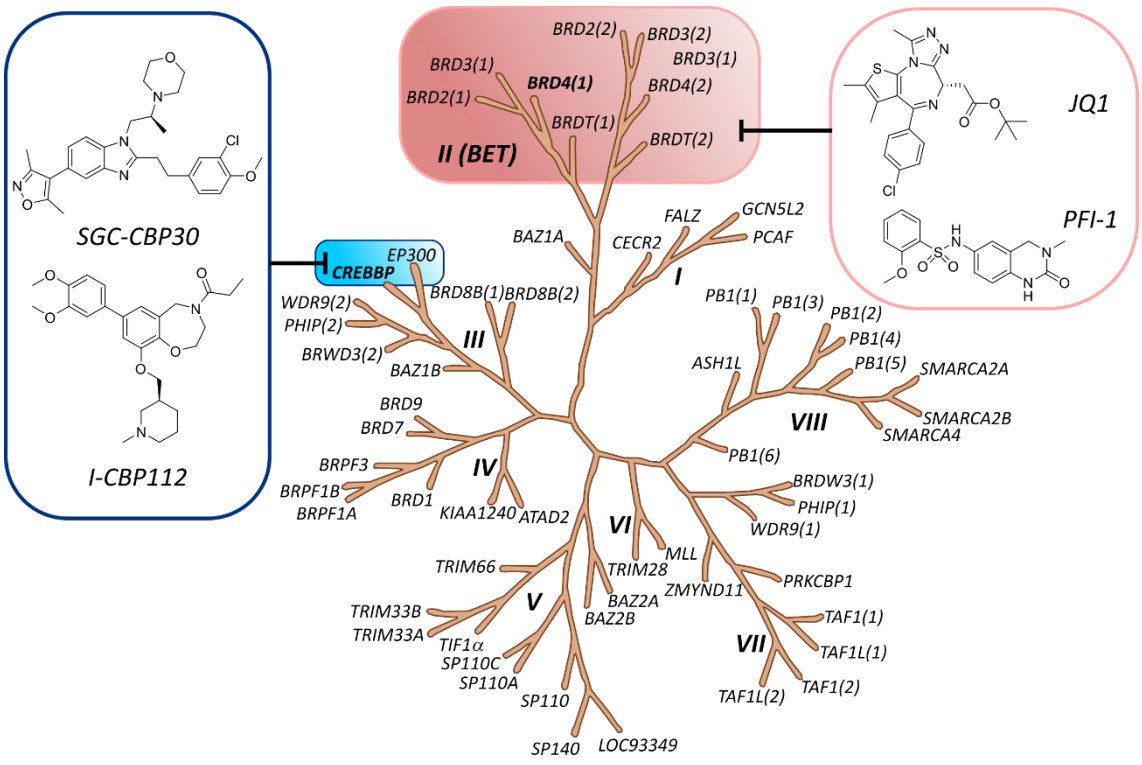

Figure 1.3: Bromodomain family tree with sub families (I-VIII) defined by literature.[40] BRDs focused within this project and SGC Chemical Probes highlighted. SGC-CBP30,[43] I-CBP112,[44] (+)-JQ1,[45] and PFI-1.[46]

Despite showing sequence similarity in terminal regions, BRDs are very similar across the board and can be separated into various families based on structure and function.[42] All BRDs share a conserved central hydrophobic pocket, for detecting acetylated lysine (KAc) residues. The characteristic structure of a BRD is comprised from 4 α-helices (αZ, αA, αB and αC) connected by interhelical loops (ZA and BC) (Figure 1.5).

The most notable and extensively researched family of BRDs is the Bromo- and Extra-terminal (BET) family of proteins which include ubiquitously expressed BRD2, BRD3, BRD4 and the testis-specific BRDT are a family of important proteins responsible for binding to KAc residues within histones and recruit other proteins to form complexes that stimulate transcription, initiation and elongation.[40,47,48] Common to all four proteins are two conserved N-terminal bromodomains BD1 and BD2 (Figure 1.4), which are the modules that recognise KAc residues on histone tails and other nuclear proteins. As the BET family have affinity for proteins with multiple acetylated sites, the proteins interact with hyper-acetylated histone regions along chromatin.[40,47–49]

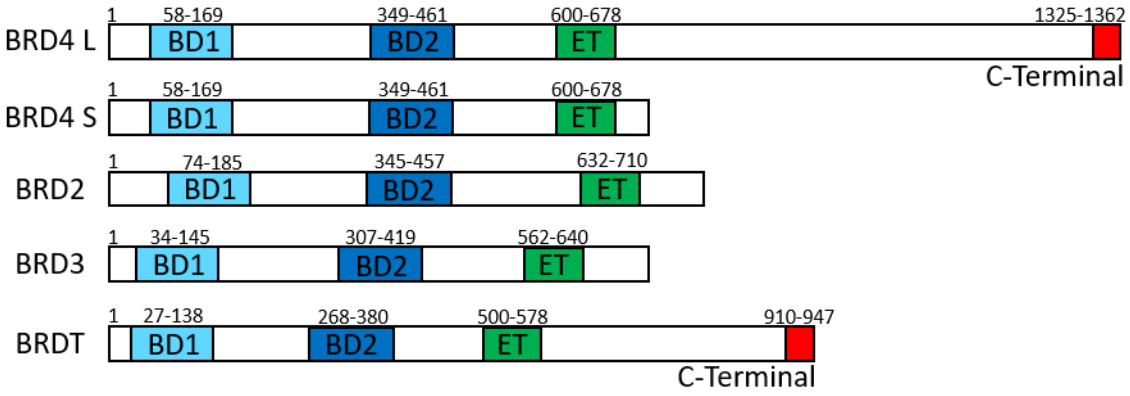

Figure 1.4: Domain architecture of human BET proteins, with short and long isoforms of BRD4 indicated.[50]

BRD4 is the most widely studied and understood member of the BET family of proteins. This is largely due to its known regulating expression of the oncogene MYC.[51,52] Other research has shown that BRD4 remains bound to transcriptional start sites of genes expressed during the M/G1 transition of the cell cycle, influencing mitotic progression.[53] The role of BRD4 in cancer aetiology, in particular, has resulted in research efforts to develop chemical probes and drugs for BRD4.[54] The binding of BRD4 to KAc domains within BD1 site occurs through the key interaction with the conserved asparagine residue Asn140 (Figure 1.5).[55]

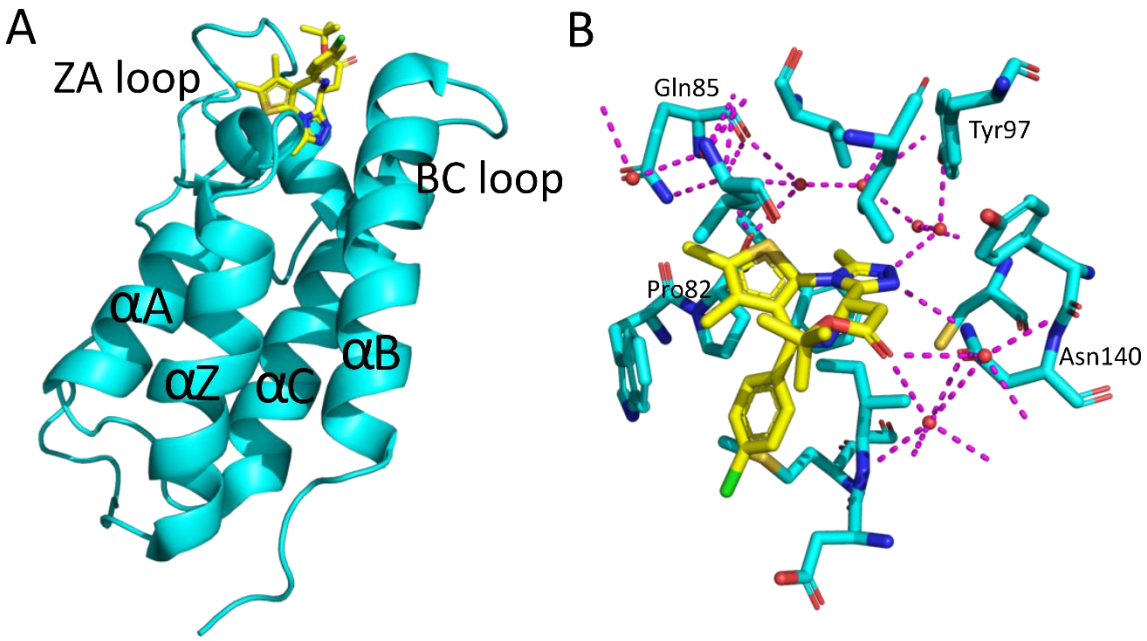

Figure 1.5: A) Structure of the BRD of BRD, highlighting the key structural components. B) Binding site of JQ1 within the first bromodomain of BRD4 (PDB: 3MXF), highlighting interactions to Asn140 and H-bonds to key residues Tyr97, Gln85 and Pro82.

Arguably the most famous example of a BRD4 inhibitor is (+)-JQ1, which is a selective and potent pan-BET inhibitor.[45] (+)-JQ1 (Figure 1.6) contains a privileged structure and binds to BD1 of BRD4 through the interaction between the 1,2,4-triazole ring, acting as a KAc mimic, and key residue Asn140. The binding is also driven by interaction of the carbonyl from the *tert*-butyl ester interacting with Asn140 *via* a water molecule. Binding of (+)-JQ1 significantly increases the thermal stability of all BET-BRDs. ITC studies illustrate that JQ1 binds to the first and second BRDs of BRD4 with K_d values of 50 nM and 90 nM respectively.[45] Usefully for this chemical probe, the opposite enantiomer ((-)-JQ1) displays no significant interaction with any bromodomain, and can act as a matched-pair negative control.[45]

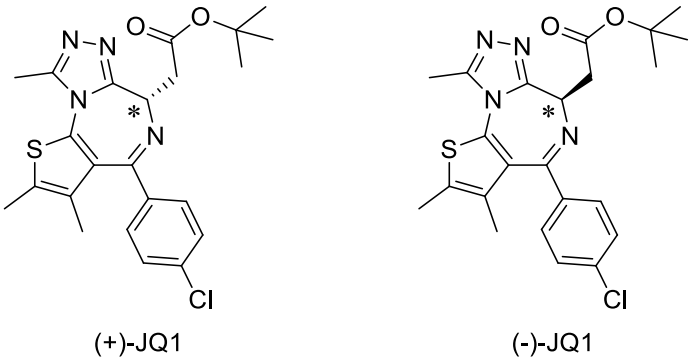

Figure 1.6: Structures for (+)-JQ1 and matched-pair negative control (-)-JQ1, with stereocenter highlighted.

Since the development of (+)-JQ1, research efforts have been applied to the clinical translation of BRD4 inhibitors, resulting in several chemical probes and clinical candidates, both with similar and different chemotypes to the prototypical BRD4 probe, (+)-JQ1. The compounds OTX015, TEN-010 and I-BET762 (Figure 1.7), are some examples of this research.

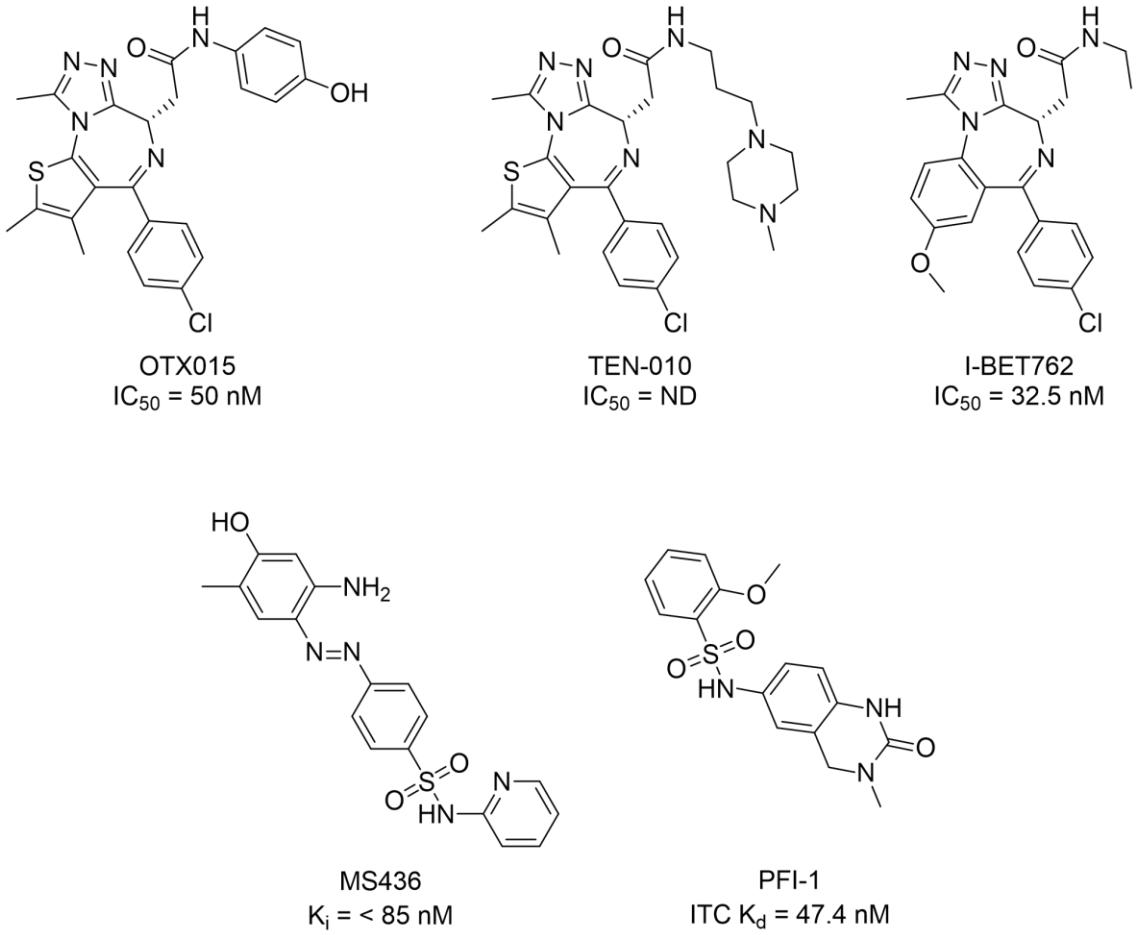

Figure 1.7: Structures and biochemical BRD4 binding values for a series of select potent inhibitors, based on information contained in ***Error! Reference source not found.*** *OTX015,*[56] *I-BET762,*[57] *MS436,*[58] *PFI-1.*[46,59]

The structural diversity of known BRD4 inhibitors is exemplified by the selected examples shown in Figure 1.7. The compounds are broadly similar in reported affinity/efficacy data but differ in selectivity profile and PK/PD characteristics. Pharmacokinetics (PK) is the study of the *in vitro* or *in vivo* effects of the body on the compound, for example; absorption, distribution metabolism and excretion (ADME), as well as off target toxicity. Whereas Pharmacodynamics (PD) refers to the study of how a drug binds to its target binding site and produces a pharmacological effect. PK is often referred to as "what the body does to the drug" and PD as what the drug does to the body.[60]

So far, no BRD targeting inhibitor has been approved by the FDA however, Table 1.1 provides a summary of selected clinical-stage BRD4 inhibitors with their salient structural features and trial identifier.[61]

Table 1.1: Clinical trial information for select BRD4 inhibitors.[61]

Name	Structure features	NCT Identifier	Reference
OTX015	Triazoloazepine	NCT02698189 NCT02698176 NCT01713582 NCT02259114	62–65
TEN-010	Triazoloazepine	NCT01987362 NCT02308761	66,67
I-BET762	Triazoloazepine	NCT01943851 NCT01587703 NCT02964507	68–70
CPI-0610	Isoxazole	NCT01949883 NCT02157636 NCT02158858	71
INCB0543294	Isoxazole	NCT02431260	72
I-BET151	Isoxazole	NCT02630251	73,74
PLX51107	Isoxazole	NCT02683395	75

Alongside pyrazoles and triazoles, another key bioisostere for KAc recognition is a 3,5-dimethylisoxazole moiety, through the MeC=N substituent. Substitution at the 4-position can alter both the selectivity profile and binding affinity (Figure 1.8).[76–78]

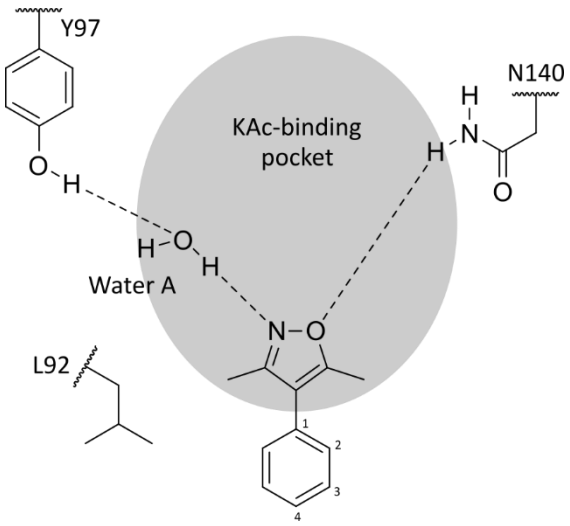

Figure 1.8: Binding mode of Isoxazoles within the KAc binding pocket of BRD4(1).

The isoxazole fragment has recently been incorporated into synthetic amino acids and these isoxazole containing peptides displayed comparable affinities to those of a hyper acetylated histone.[79] This isoxazole bioisostere has been incorporated into BRD inhibitors, with CPI-0610, INCB0543294, I-BET151 and PLX51107 being some examples of BRD4 targeting chemical probes containing isoxazoles, with nM activity vs BRD4 (Figure 1.9).

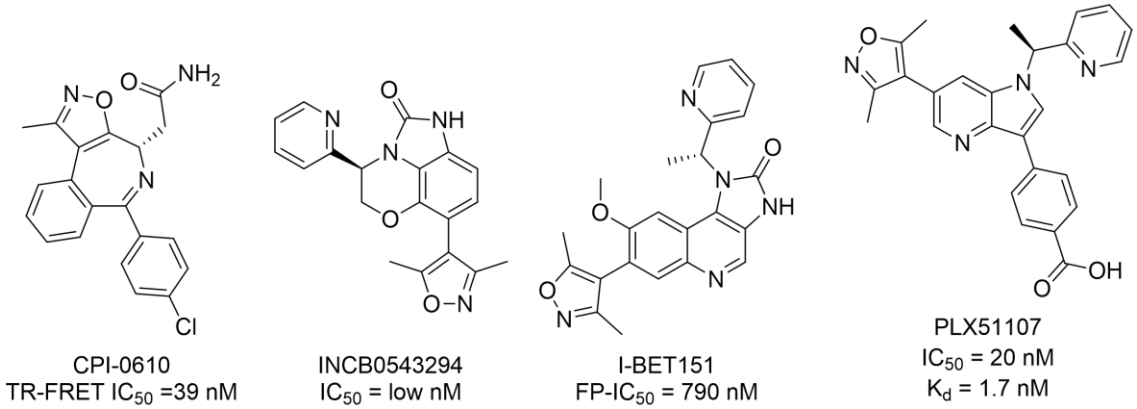

Figure 1.9: The biochemical BRD4 binding values and structures of select isoxazole containing BRD4 chemical probes: CPI0610,[71] INCBO543294,[72] I-BET151,[51] and PLX51107. [56,75]

In 2016, CPI-0610 was reported as a potent inhibitor of BRD4, which is a structurally similar core to (+)-JQ1, with an IC_{50} value of 39 nM.[71] The thiophene ring was replaced with a more stable phenyl ring with the goal of avoiding metabolic instabilities.[71]

The multivalent interaction between the BET family and chromatin, or other binding partners has been described as complex and context-dependent and because of this, remains poorly understood. The BET family of BRDs harbour two highly homologous BRDs and in recent years reports of selective BD2 inhibitors have emerged. Through the use of iBET-BD1 and iBET-BD2

(GSK778 and GSK046 respectively) have been shown to result in different effects.[80] For example, targeting BRD4(1) with iBET-BD1, as a BD1 specific probe, resulted in the anti-cancer characteristics observed with pan-BET inhibitor I-BET-151. Targeting BRD4(2), with iBET-BD2 as a BD2 selective inhibitor, has minimal effects at displacing chromatin-bound BET proteins.[81]

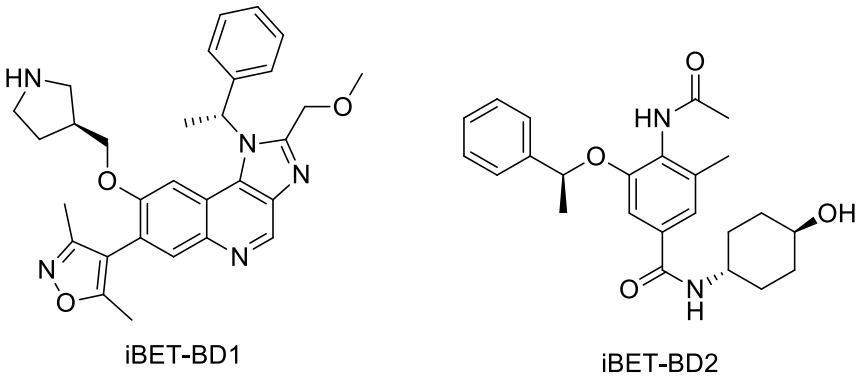

Figure 1.10: Structures of iBET-BD1 and iBET-BD2.

Many groups have investigated inhibitors specific to BRD4(2), with some examples of these inhibitors being BY27, RVX-297 and ABBV-744 (Figure 1.11).[81–85] BY27 is a 10 fold selective inhibitor to BRD4(2) with an IC_{50} value of 14.8 nM. In MV4-11 mouse xenograft models caused BY27 caused a 67% inhibition of tumour growth and was less toxic than I-BET762.[85] RVX-297 is a more selective BD2 inhibitor than BY27, being 58 times more selective to BD2 than BD1, with IC_{50} values of 1160 nM and 20 nM for BRD4(1) and BRD4(2) respectfully.[83] ABBV-744 which has cell-free IC_{50} values of 20,700 nM and 27.5 nM for BD1 and BD2 respectfully, being 753 times more selective to BD2 than BD1. ABBV-774 was shown to have potent anti-proliferative activity against AT-positive prostate cancer cells.[84]

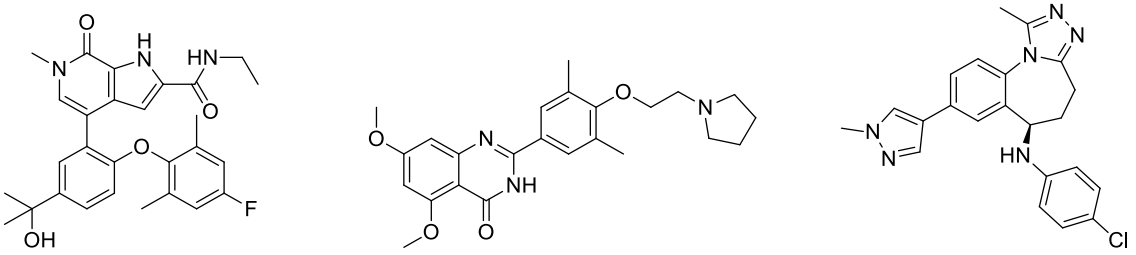

Figure 1.11: Structures of selective BRD4(2) inhibitors ABBV-744, RVX-297, and BY27 and their respective cell-free IC_{50} values.[83–85]

1.2.1.2 IRF4

An alternate upstream target of c-Myc is Interferon regulatory factor 4 (IRF4), which is a transcription factor belonging to the IRF family. IRF4 is expressed in the vast majority of cell types within the immune system and is induced in T-cells through T-cell receptor stimulation.[86] IRF4 binds weakly to DNA and interacts in T-cells with other transcription factors such as c-jun and basic leucine zipper transcription factors to both activate and repress the expression of genes.[87]

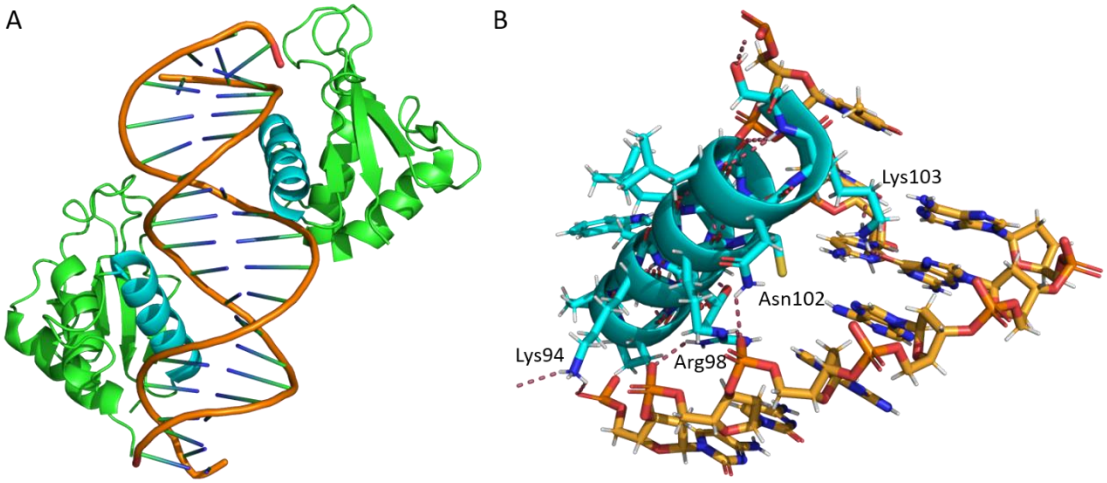

Figure 1.12: A) Overall structure of the IRF4/DNA Homodimer complex, with the key α3-recognition helix coloured in blue, adapted in Pymol from (PDB: 7JM4). B) Binding of the α3 helix to the groove of DNA.[88]

The α3 helix of IRF4 binds to DNA in the major groove, through a series of phosphate backbone contacts (Figure 1.12A). The key residues for binding include Arg98, Asn102 and Lys103 (Figure 1.12B), Arg98 interacts extensively with the first guanine base *via* a hydrogen bond. The contact with Asn102 is mediated by a hydrogen bond with the OP2 of the first base. Lys103, which is restricted to a few IRF family members, interacts with the fourth base of the recognition sequence through a van der Waals contact.[88]

B and T lymphocytes are involved in the antigen-specific immune response, given that they are the only cells to be able to recognise and respond to each antigenic type. B cells have the ability to transform into plasmocytes and are therefore responsible for producing antibodies.[89] In these lymphocytes, IRF4 is expressed at multiple stages of development, affecting cell differentiation, clonal expansion and the cellular outcome. Due to its crucial roles in these cells, IRF4 has been linked directly to immune-related diseases including chronic lymphocytic leukaemia (CLL) and multiple myeloma (MM). MM cells have been reported as having an addiction on IRF4 due to a direct target of IRF4 being MYC expression, and has been shown that IRF4 inhibition is cytotoxic to these cell types.[90] Originally, it was thought IRF4 was tissue

specific to immune response, however IRF4 has been reported as a critical transcription factor within the heart, kidney liver and brain.[91–93]

Knockdown of IRF4 reduced MYC mRNA levels by more than two fold in myeloma cell lines and caused a decrease in the levels of Myc-DNA binding activity.[90] Currently, there are no direct small molecule inhibitors of IRF4, however upstream targeting of IRF4 has been validated in the literature. Inhibition of the transcriptional co-activator CBP/p300, supresses IRF4 expression, which abrogates the viability of MM cells.[94,95]

1.2.1.3 CBP/p300

The cAMP response-element binding protein (CREB) binding protein (CBP/CREBBP) and p300 are ~300 kDa transcriptional cofactors which are highly homologous to each other, with a 63% homology at the amino acid level.[96–98]

These proteins contain various conserved protein binding domains (Figure 1.13), where the purposes of this section will focus on the BRD and the HAT capabilities of CBP/p300.[99]

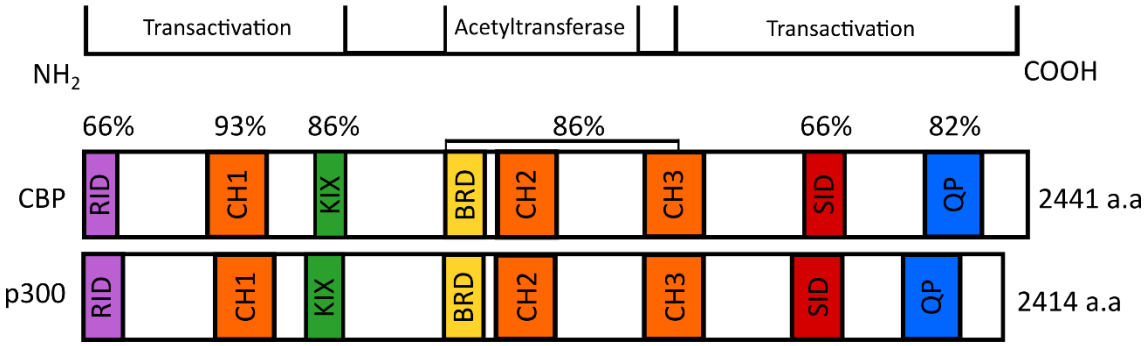

Figure 1.13: Schematic representation of CBP and p300 homologous regions and functional domains. RID, receptor-interacting domain; CH1-3, cysteine and histidine-rich regions 1-3; KIX, binding site of CREB; BRD, bromodomain; SID steroid receptor co-activator-1 interaction domain; QP, glutamine-and proline-rich domain.[99]

Despite the similarities of these proteins, the diverse phenotypes seen in knockout studies suggest that CBP and p300 have distinct biological functions. For example, homozygous removal of p300 results in embryonic lethality, with defects in heart development, neurulation and cell proliferation.[100] Deletion of CBP in mice is also lethal (in utero) and the mice exhibit retardation of development and delays in haematopoiesis.[101] CBP/p300 has also been reported to be critical in MYC/GATA1 regulatory axis in proliferation.[102]

As CBP/p300 contains both a BRD and HAT domain, this allows the proteins to function as both an epigenetic reader and writer (Figure 1.1). The BRD of CREBBP has also been found in various oncogenic fusions, where recently was shown to be fused to the SLX4 gene in lung cancer and RHBDF1 gene in small-cell lung cancer.[103,104]

1.2.1.3.1 CBP/p300 Histone Acetyltransferase Domain and Reported inhibitors

CBP/p300 function as transcriptional cofactors for many known targets in cancer therapy including c-MYC, c-MYB, p53, SMADS and BRCA1.[94,105–109] CBP/p300 have at least 400 described interacting partners making them among the most heavily connected nodes in the protein-protein interactome within mammals.[110] Application of these transcriptional cofactors to cancer therapy has shown that targeting p300 in CBP deficient cancers with either RNA interference or small molecules causes apoptosis due to the removal of MYC expression.[111]

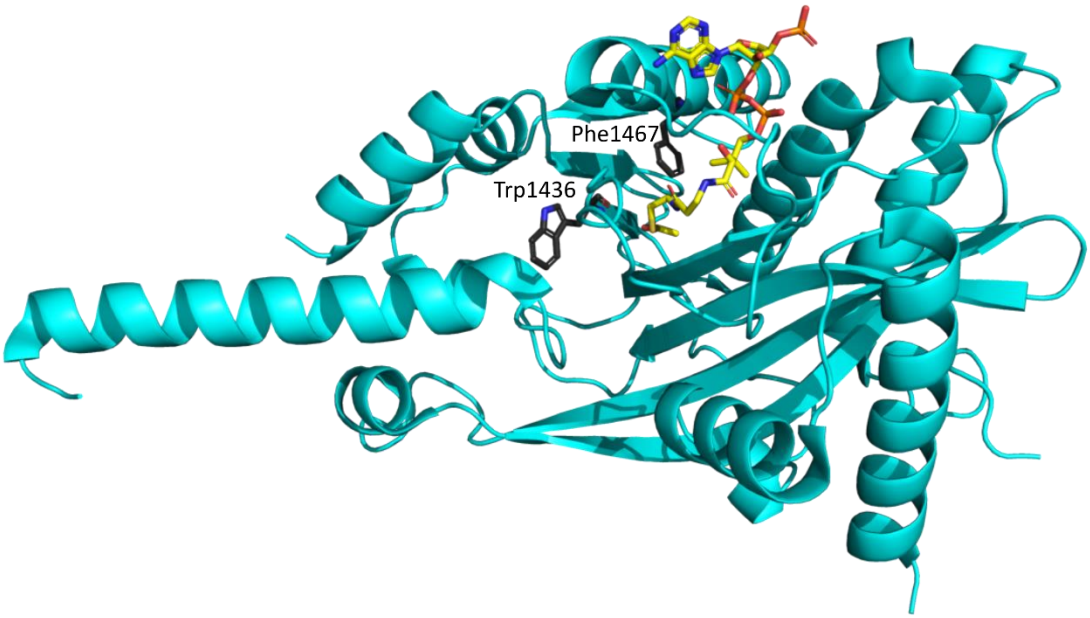

Figure 1.14: p300 HAT domain bound to AcCoA, with key residues Trp1436 and mutated Phe1467 coloured in black.[112]

Structural understanding of p300s HAT domain, led a proposed mechanism in which Trp1436 forms a hydrogen bond to the *N*-terminus of a histone lysine, orientating it for acetylation from AcCoA, which is held in place *via* a hydrogen bond to Tyr1467 (Scheme 1.1).[113] This proposed mechanism was confirmed through enzymatic and mutational studies. The structure of p300 with AcCoA is shown in Figure 1.14, with key residues Trp1436 and Phe1467 coloured in black.[112] Phe1467 has been classified as a key residue here due to being mutated from the functional Tyr residue.

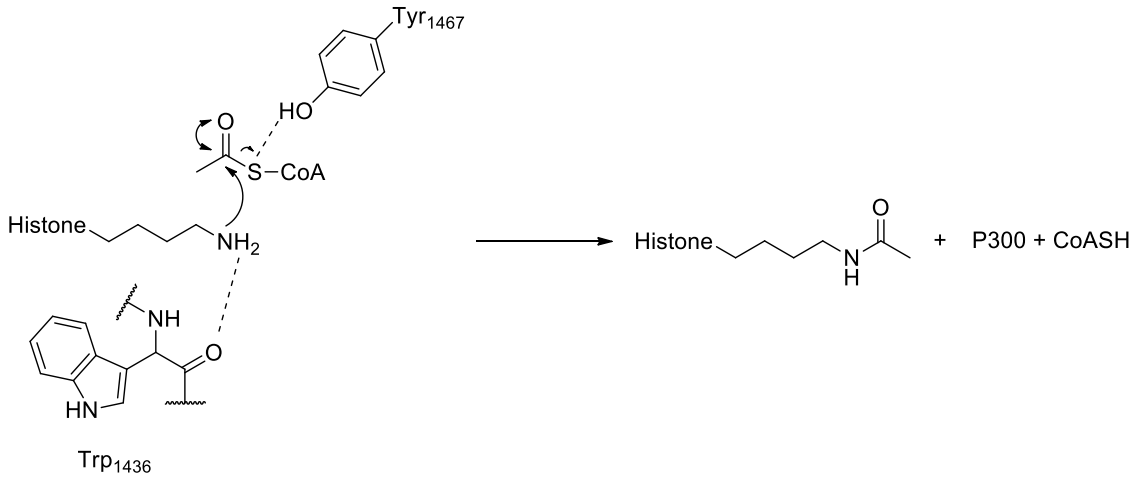

Scheme 1.1: A proposed mechanism for the acetylation of histone lysine within the HAT domain of p300.[113]

HATs can act as tumour-suppressors, due to their participation in cellular proliferation and cell cycle control but also as oncogenes, because abnormal acetylation of histones can activate downstream malignancies contributing to cancer, such as c-Myc.[96,114] There is increasing evidence linking abnormal acetylation to the development of cancers, for example Acute Myeloid Leukaemia (AML).[115–117] The first reported inhibitors to the HAT domain of p300/CBP involved bisubstrate inhibitor LysCoA, and natural products which had affinity against this target (Figure 1.15).

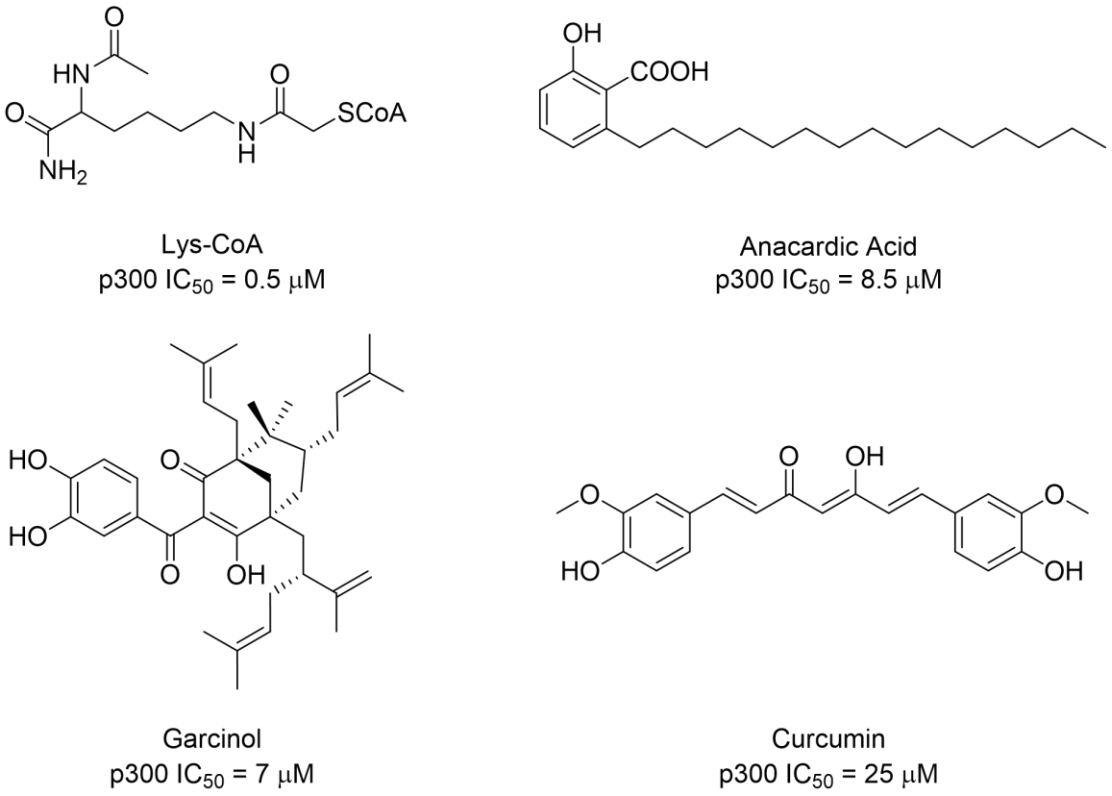

Figure 1.15: Bisubstrate inhibitor Lys-CoA and natural products targeting the p300 HAT domain. Lys-CoA.[118] *Anacardic Acid.*[119] *Garcinol.*[120] *Curcumin.*[121]

Lys-CoA was among the first p300 HAT inhibitor to be described in literature and was reported as a potent and selective inhibitor (0.5 μM). The potency of this compound can be credited to containing the CoA component of the natural substrate AcCoA. However, this compound had to be microinjected into the cells as the compound is not cell permeable.[118] However this showed that CBP/p300s HAT domain could be inhibited and sparked interest in the development of small molecule, cell permeable inhibitors.

Anacardic acid, a natural product from cashew nut shell liquid, is a potent inhibitor of both p300 (8.5 μM) and p300 and CBP-associated factor (PCAF) (5 μM). However, unlike the bisubstrate Lys-CoA, this compound was cell permeable and did not need microinjection.[119] Garcinol is a polyisoprenylated benzophenone derivative from kokum fruit rind and is a micromolar inhibitor of the HAT domain of p300 (7 μM), however is also a micromolar inhibitor to the HAT domain of the PCAF with equal affinity (5 μM).[120] Garcinol is also reported with to possess antioxidant and anti-inflammatory properties and has been explored with usage within the treatment of cocaine addiction.[122] This highlights that Garcinol hits a wide range of targets, which is sub-optimal for the investigation of specific inhibition.

Curcumin is the principal curcuminoid of turmeric and was found to bind to the HAT domain of CBP/p300 with an IC_{50} of 25 μM and was shown to inhibit the p300-mediated acetylation of p53 in vivo.[121] Curcumin to date has not been conclusively effective in randomised placebo-controlled clinical trial and has been labelled as 'pharmacodynamically fierce, yet pharmacokinetically feeble' - Meaning that it hits many targets yet does not get to its target.[123,124] Curcumin was reported to selectively inhibit the HAT domain of p300 over other related HATs, however curcumin is also a well-documented pan assay interference compound (PAIN) due to its ability to covalently label proteins, chelate metals, aggregates interferes with fluorescence, has redox reactivity and disrupts membranes.[125–132] Discovery of small molecule inhibitors (Figure 1.16) to the HAT domain of CBP/p300 began in 2010 with C646 through virtual ligand screening.[133]

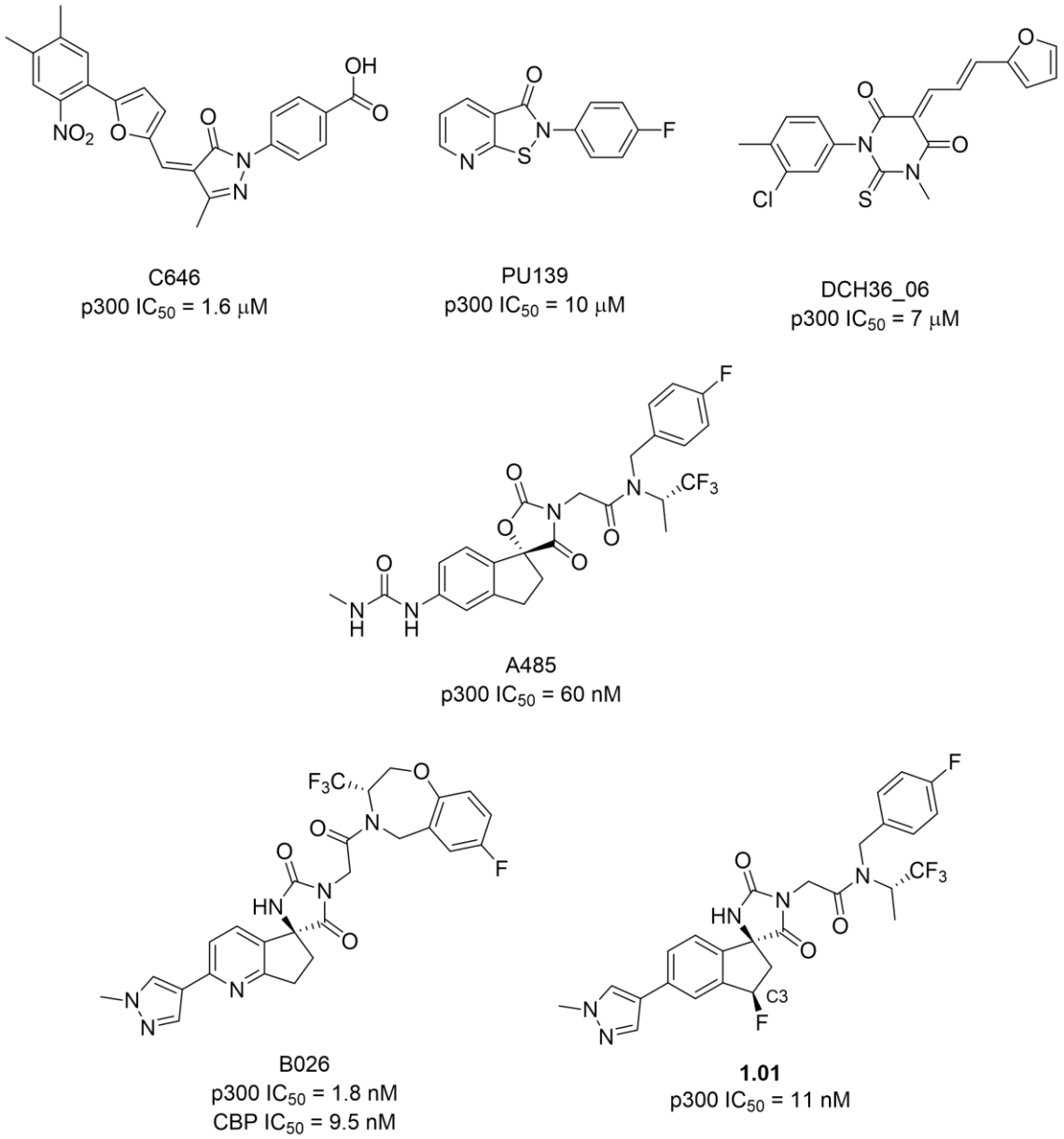

Figure 1.16: Reported synthetic small molecules cell-free IC_{50} values vs p300 HAT domain. C646.[133] *PU139.*[115] *DCH36_06.*[134] *A485.*[135] *B026.*[136] ***1.01***.[137]

C646 was originally reported as a selective competitive inhibitor with a K_i of 400 nM and an IC_{50} of 1.6 μM.[133,138] K_i is the inhibition constant and is reflective of the binding affinity rather than the strength (IC_{50}). In terms of medicinal chemistry, the nitro group of C646 could produce some toxic metabolites *in vivo* through conversion to an amine, followed by an acetamide.[139]

Since then, two other inhibitors have been described with similar affinities to C646, PU139 and DCH36_06. PU139 was reported as a pan-HAT inhibitor targeting CBP/p300, Gcn5 and PCAF, making it sub optimal for usage in biological systems due to its widespread targeting.[115]

DCH36_06 was initially reported as a potent CBP/p300 inhibitor, halting cell proliferation in several leukaemia cell lines.[134]

The problems facing HAT inhibitor development have been described over the last few years, with an example being a report from Dhalin and co-workers. Here they showed that out of 23 tested HAT inhibitors, 50% showed non-specific thiol reactivity or compound aggregation, with the inhibitors also acting as pan-HATs.[140] However, around this time the discovery of A485 was reported in 2017 with a low nanomolar affinity to the HAT domain of CBP/p300 (60 nM). A485 was CBP/p300 selective and did not significantly inhibit other HAT family members including PCAF, HAT1, MYST3, MYST4, TIP60 or GCN512 at 10 μM.[135] However in a CEREP screen, A485 was found to potently inhibit dopamine and serotonin receptors and so required modifications to minimalise these effects.[137]

This led into the development of two new HAT inhibitors based on the core structure of A485. These new inhibitors, B026 (p300 IC_{50} = 1.8 nM) and **1.01** (p300 IC_{50} = 11 nM) have a similar core unit to A485, with both compounds having switched the methyl urea to an *N*-methyl pyrazole to retain a hydrogen bond interaction between the spirocyclic carbonyl and Ser1400. The presence of the *N*-methyl pyrazole unit also boosted cell permeability.[137] Both compounds moved from a spiro-oxazolidinedione to a spirohydantoin scaffold. In B026 the tertiary amide was changed from two unique chains to a 7 membered fused phenyl ring. Having a substituent in the *R*-configuration on C3 of the hydantoin, gave a significant increase in affinity than other moieties tested. Both of these compounds gave reduced off-target inhibition of dopamine and serotonin transporters.[136,137]

A485 has been utilised in a co-treatment inhibition of p300 with I-CBP112 in LNCaP cells, hitting both the BRD and HAT domain. The co-treatment of the inhibitors caused a synergistic effect, resulting in the inhibition of proliferation prostate cancer cells. This was due to significant reduction in p300's presence on chromatin and therefore reduction in specific mRNAs including c-Myc.[141]

1.2.1.3.2 CBP/p300 Bromodomain and Reported Inhibitors

CBP and p300 are closely related proteins with their BRDs having a 96% sequence similarity.[142] Tyr residues in the ZA loop and the key Asn residue in the BC loop are responsible for direct KAc recognition through water mediated hydrogen bonding (Figure 1.17).[51,143–145]

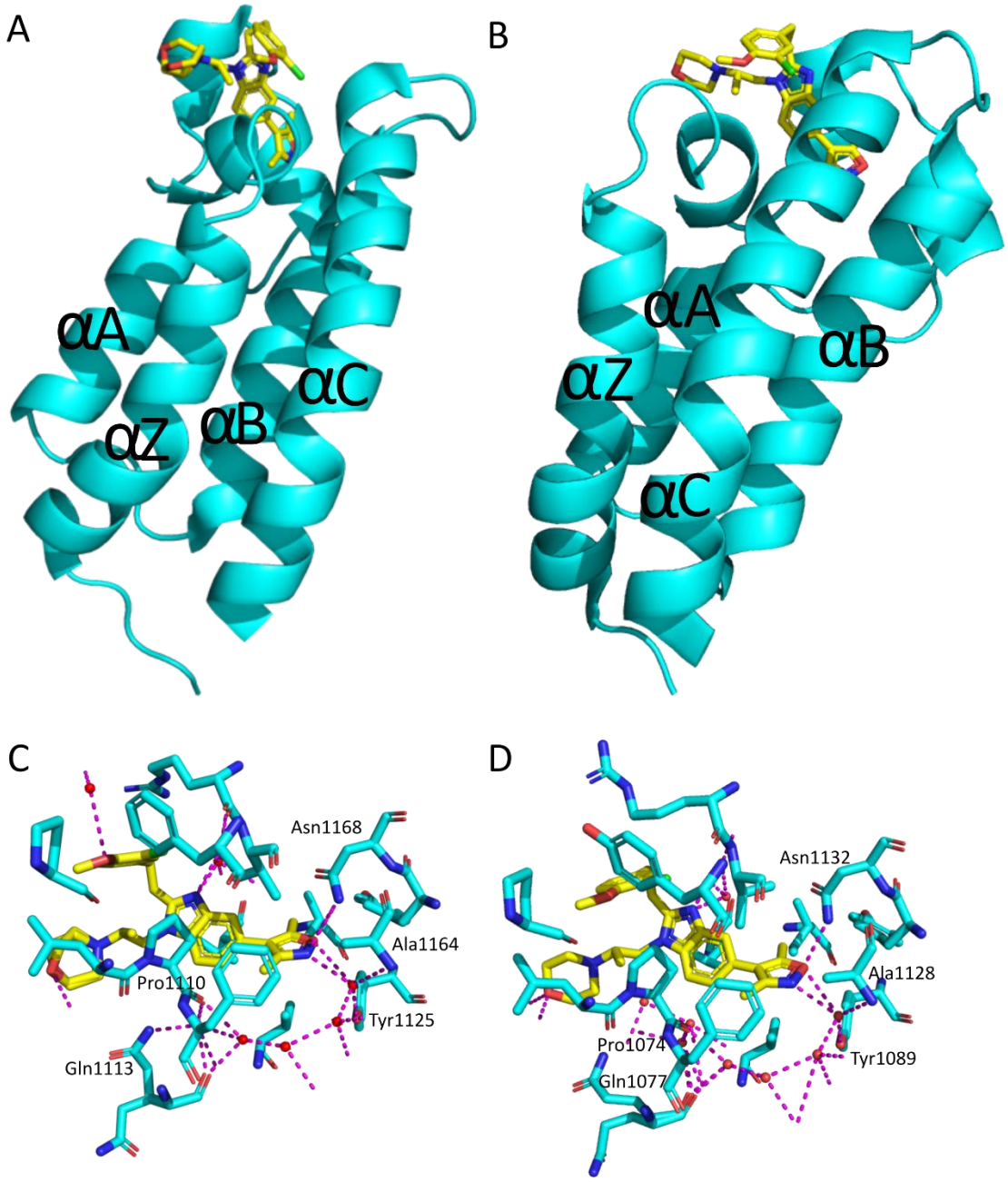

Figure 1.17: BRDs of CBP (5NR7) and p300 (5BT3), docked with chemical probe SGC-CBP30. A) Structure of the BRD of CBP showing structure of 4 α-Helices. B) Structure of the BRD of p300 showing structure of 4 α-Helices. C) Active site of the BRD of CBP, showing SGC-CBP30 bound to Asn1168. D) Active site of the BRD of CBP, showing SGC-CBP30 bound to Asn1132. The protein residues are coloured cyan, ligand yellow and water molecules red, with the respective interactions coloured in magenta.[43]

The binding KAc domains within BRDs of CBP (5NR7) and p300 (5BT3) occurs through the key H-bond interaction between the asparagine residues Asn1168/Asn1132 and the oxygen of the

isoxazole (Figure 1.17CD).[43] Additionally there is another H-bond interaction between the nitrogen of the isoxazole and a water molecule, which in itself is H-bonding to Ala, Tyr, and through a series of H-bonds with water molecules, to Gly and Pro.

After the reports of (+)-JQ1 in 2010, a druggability analysis of diverse members of BRD families using SiteMap had predicted CBP/p300 BRDs as potentially good therapeutic targets, however at that time there had not been any sub μM active inhibitors synthesised for these BRDs.[146] SiteMap is a computational program designed by Schrödinger, which highlights regions within the binding site suitable for occupancy of specific moieties. A key issue in the development of CBP/p300 inhibitors has not only been to develop probes which are potent and selective, but also ones that are devoid of BET activity. This is due to inhibition of BET BRDs producing profound phenotypes, which are related to the effects produced by CBP/p300 BRD inhibitors.[147,148] Having BRD inhibitors with a high degree of CBP/p300 selectivity over BET, allows for the understanding of CBP/p300 inhibition *in vivo*.

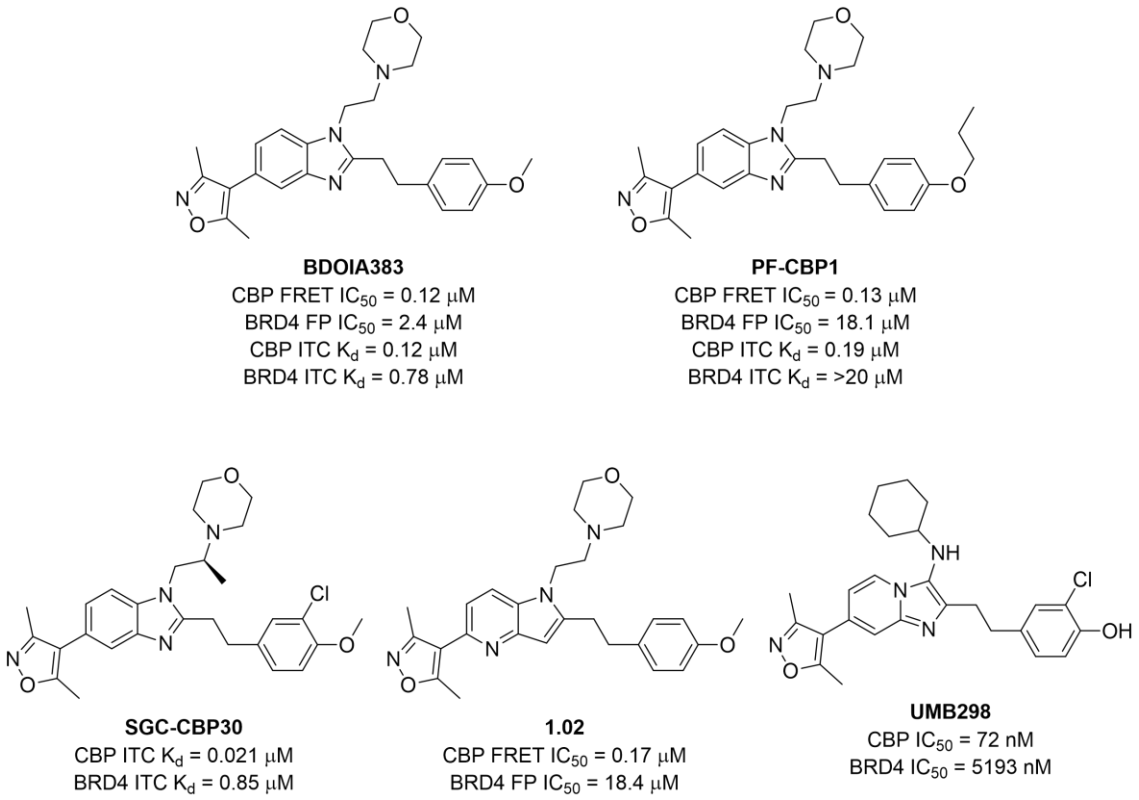

Figure 1.18: Isoxazole containing inhibitors for CBP/p300 BRD and their biochemical binding values.[43,149,150]

An investigation into achieving this resulted in a series of isoxazole containing CBP/p300 inhibitors. SGC-CBP30 was reported with an IC_{50} value of 0.12 μM and 2.4 μM for CBP and BRD4 respectively, and was the one of the first CBP selective inhibitors to be published.[43] Parallel work from the Jones group also demonstrated similar selectivity trends with inhibitor

BDOIA383 (Figure 1.18). Further tuning of BDOIA383 resulted in a more CBP selective probe (PF-CBP1).[2] Further work was performed to achieve **1.02**, through core modifications of BDOIA383 from a benzimidazole to a 4-azaindole, similar potencies to PF-CBP1 were obtained.[149] In the recent literature UMB298 has been reported as a potent selective BRD inhibitor of CBP/p300, which is 72-fold more selective to CBP/p300 (72 nM) than BRD4 (5193 nM).[150]

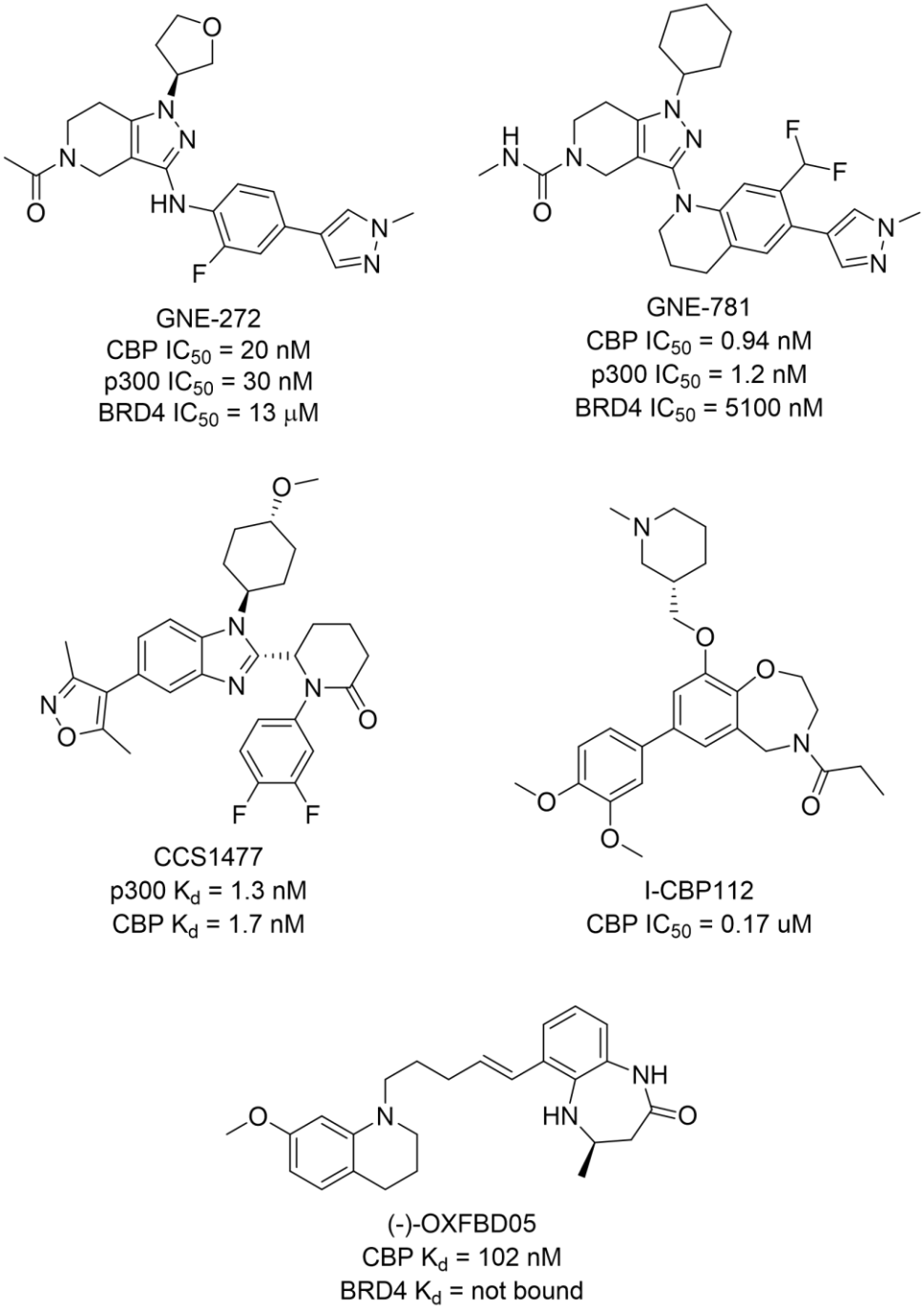

Figure 1.19: Example CBP/p300 BRD inhibitors. GNE-272.[151] GNE-781.[152] CCS1477.[153] I-CBP112.[44] (-)-OXFBD05.[154]

Alongside these inhibitors have been other groups publishing compounds that selectively bind to the BRDs of CBP/p300 (Figure 1.19). In 2015 I-CBP-112 was reported to bind to CBP/p300 with nanomolar affinity (170 nM) and in leukaemia cell lines impaired the disease-initiating self-renewal leukemic cells *in vitro* and *in vivo* without being significantly cytotoxic. I-CBP112 was also shown to synergise the efficacy of (+)-JQ1 when co-treated.[44]

A study published in 2016 that utilised structure-based design, resulted in GNE-272, which is a potent and selective BRD4 inhibitor, and was 650-fold more selective to the BRD of CBP than BRD4. When dosed in hematologic cells at 5 μM, GNE-272 caused an inhibition of MYC expression. An *in vivo* dose response study showed MYC repression with an EC_{50} value of 980 nM, and after 4 h of treatment significant repression of oncogenes.[151]

In an attempt to synthesise a more potent and selective CBP inhibitor, this group then went on to discover GNE-781, which is not just a more potent inhibitor, but 5425-fold more selective to CBP than BRD4. The selectivity difference in this inhibitor was explained by Trp81 in BRD4 from the WPF shelf serving as a lipophilic protrusion compared to CBP's wall, which as a result the tetrahydroisoquinoline of GNE-781 is rotated, making the van der Waals contacts with Leu92 unfavourable due to becoming solvent exposed. This ensures the complementarity of GNE-781 to BRD4 is less optimal than that for CBP. GNE-781 was also reported to possess greater cell potency than GNE-272, showing anti-tumour activity in AML lines and decreasing Foxp3 transcript levels. GNE-781 also showed MYC repression with an EC_{50} value of 6.6 nM, significantly lower than that for GNE-272.[152]

In recent years, reports of a potent CBP/p300 BRD inhibitor (CCS1477) CBP BRD inhibitor in Phase I/II clinical trials for treatment of prostate cancer (NCT03568656), and this is the only example of CBP/p300 inhibitors in clinical trials.[153,155]

In 2021, Conway *et al.* published a report on the development of a small molecule ligand for CBP/p300 through SAR guided by crystal structures and modelling, to result in OXFBD05, an inhibitor of CBP with a K_d value of 102 nM, with over >100 fold selectivity over BET bromodomains. Treatment of this compound in HCT116 cells also reduced c-Myc levels and caused a reduction in H3K18 and H3K27 acetylation.

While the inhibition of various proteins either upstream from, or oncogenic themselves has resulted in successful anticancer therapeutics, so far only a limited quantity of them have made a clinical impact in malignancies, where the most notable is MM. In recent years, a

number of groups have published methodologies to hijack the ubiquitin proteasome system in order to achieve greater therapeutic effects, through the targeted degradation of proteins.[156]

1.3 Targeted Protein Degradation

1.3.1 Ubiquitin Proteasome System

The turnover of proteins within cells is controlled by the ubiquitin/proteasome system (UPS), where ubiquitin (Ub) is a small protein only consisting of 76 amino acids, which can be attached to proteins as a common post-translational modification.[157] Ub contains seven lysine residues that together with the amine terminus, provide eight attachment sites for further Ub molecules (Figure 1.20).[158,159]

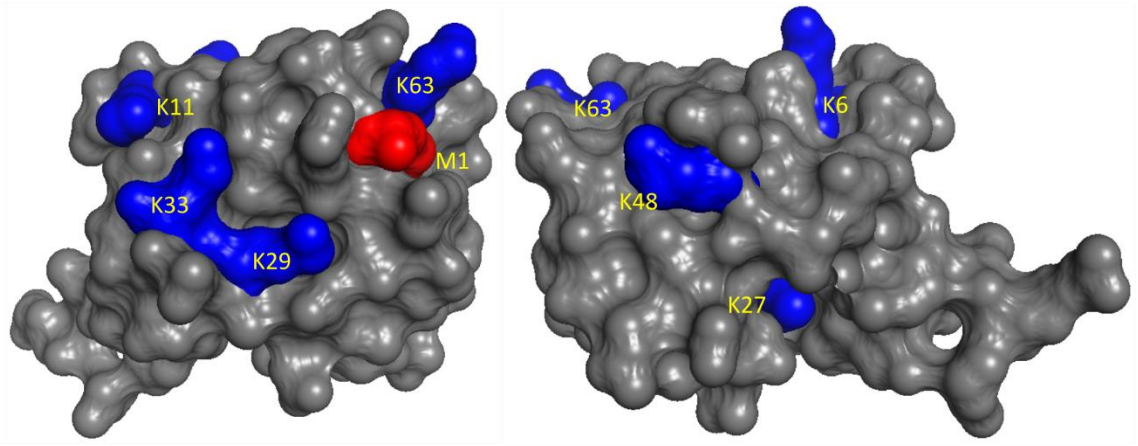

Figure 1.20: Structure of ubiquitin with the lysine residues highlighted in blue and the N-terminus highlighted in red. Adapted from known crystal 1UBQ in Pymol.[159]

Ubiquitylation arises through a cascade of three enzymes; an E1 ubiquitin activating enzyme, an E2 conjugation enzyme and an E3 ubiquitin protein ligase.[160–163] Ub is added to the amino group of lysine residues on the surface of target proteins, or to the lysine residues of other Ub molecules. This modification can occur in multiple ways, either through monoubiquitylation, multi-monoubiquitylation, polyubiquitylation and branched/forked ubiquitylation.[162] The quantity and positions of ubiquitin addition are read by varying ubiquitin receptors (UbR), which in turn dictate the biological outcome (Figure 1.21).[161]

The monoubiquitylation and multi-monoubiquitylation of a protein can recruit binding partners, inhibit interactions, change protein localisations and modulate protein activity.[164,165] For example, the E3 ligases MSL32, WWP1 or Mdm2 can monoubiquitylate p53 to induce nuclear export of the protein as a mechanism of controlling p53 activity. However, the polyubiquitylation of at least four ubiquitins, signals p53 for degradation by the 26S proteasome.[166–168] A20 has been shown to multi-monoubiquitylate Snail1, which promotes metastasis of aggressive breast cancers.[169]

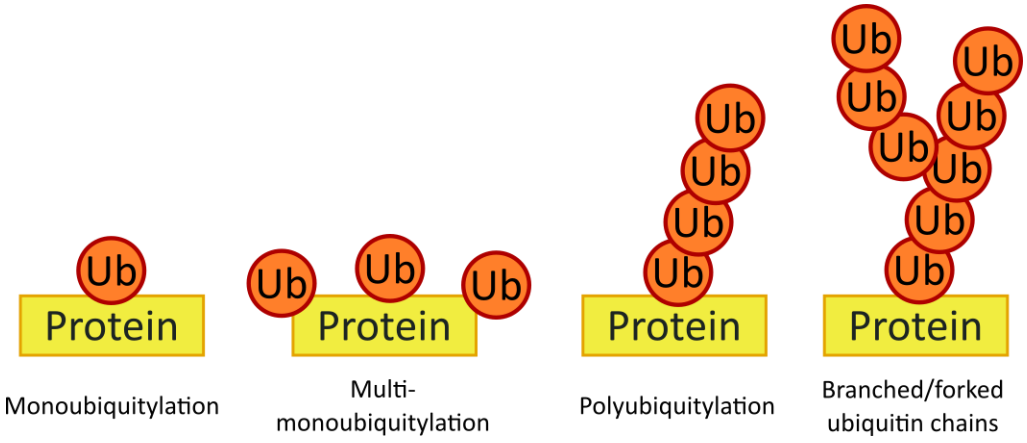

Figure 1.21: The classifications of ubiquitin modifications to proteins.[162]

Not all branched chains have their physiological functions fully understood, and research into the varying branches are still ongoing. Branched chains consisting of K11/K48, K29/K48 and K48/K63 linkages are shown to give enhanced proteasomal degradation in early mitosis and cell-cycle/protein quality control *via* proteasomal and autophagic degradation.[170–174]

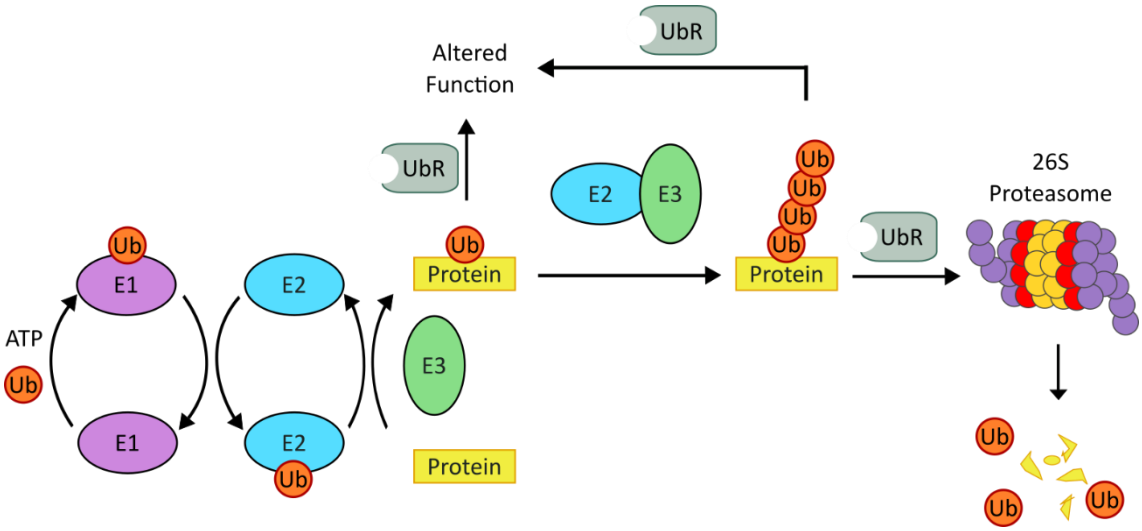

Figure 1.22: The ubiquitin system, showing the E1-E2 -E3 cascade of Ub to the protein and the biological outcome to result in either signalling or degradation by the 26S proteasome.

Ubiquitin is activated for transfer by an E1 activating enzyme with ATP, which is then in turn transferred in thioester linkage to the cysteine of an E2 conjugating enzyme (Figure 1.22). This then interacts with an E3 ubiquitin ligase, which directs transfer from the E2 enzyme to a lysine residue of the substrate protein. The substrate is then directed to an alternate function within the cell or continued through the E1-E2-E3 cascade to result in Ub chains. The straight chains assembled *via* K48 linkages on Ub typically direct the substrate to the proteasome for degradation.[161]

The human proteome contains the codes for more than 600 E3 ligases and there are two main types of E3 ligases; really interesting new gene (RING) and homologous to E6-AP carboxy terminus (HECT) which function *via* different modes of action (Fig).[175–177]

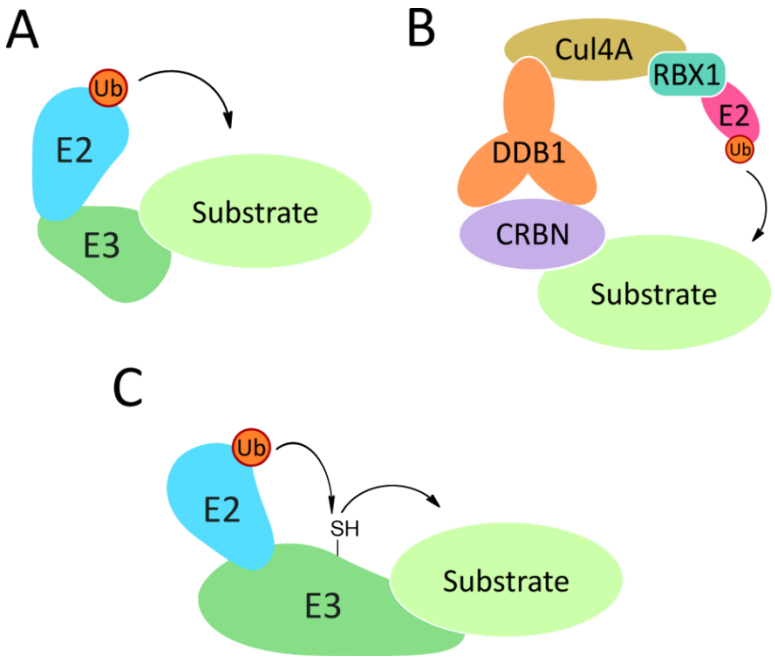

Figure 1.23: A) Mechanism of Ub transfer in RING E3 ligase. B) Mechanism of transfer in multicomplex CRL4^{CRBN} E3 ligase.[178] C) Mechanism of Ub transfer in HECT E3 ligase via the cysteine residue of the E3.

RING E3 ligases function as allosteric activators of the E2 and multicomponent scaffolds that bring the E2 into close proximity to the substrate. This type of E3 ligases can consist of a single protein (Figure 1.23A) or a multiprotein complex such as the CUL4-RBX1-DDB1-CRBN (CRL4^{CRBN}) E3 ligase, which consists of the RING-box protein 1 (RBX-1), which binds to Cullin-RING Ligase 4 (CUL4), which is bound to DNA-Damage Binding Protein 1 (DDB1) and subsequently Cereblon (CRBN) (Figure 1.23B).[178]

HECT E3 ligases catalyse substrate ubiquitylation in two steps, the first involves accepting Ub from the E2 in a trans-thiolation reaction onto their catalytic cysteine, and in the second step this Ub moiety is transferred to the substrate lysine (Figure 1.23C).[175,179]

Proteins are flagged for degradation *via* polyubiquitin chains under specific circumstances, some of which are abnormal proteins, short-lived proteins, ER-associated proteins and long-lived proteins.[180] Once flagged for degradation, these proteins are then sent to the proteasome. The 26S proteasome is a 2.5 MDa complex of proteins consisting of a 20S core and two 19S cap units. (Figure 1.24) The 19S cap units recognise proteins marked for degradation by their polyubiquitin chains, before de-ubiquitylation followed by unfolding for entering the channel.[181,182] The 20S core consists of two 7-membered β-subunits encased by 7

membered rings of α-subunits that produce a narrow tunnel down the centre of the unit.[183] These subunits possess the proteolytic capacity to break down proteins into their smaller peptide components.

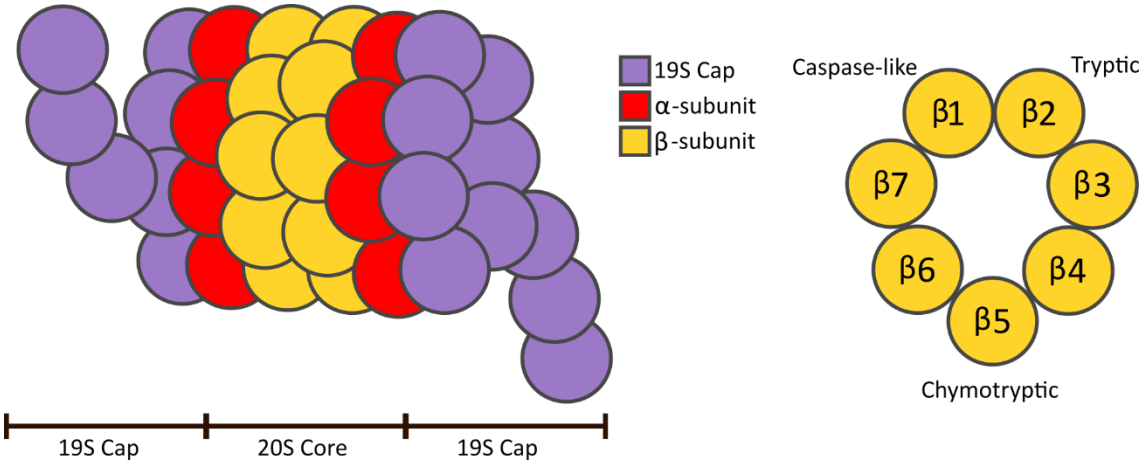

Figure 1.24: 26S Proteasome, highlighting the two 19S caps (purple) and the 20S core with α-subunits (red) encasing the β-subunits (yellow).

1.3.1.1 Inhibiting the Proteasome System

Inhibition of the proteasome is seen as the most therapeutically relevant method in inhibiting the UPS. The therapeutic relevance stems from cancer cells relying heavily on the proteasome to clear out the misfolded proteins and inhibiting the process of degradation, drives these cells to apoptosis.[184] Three β-subunits are responsible for the enzymatic activities of the proteasome, β1, β2 and β5.[185] Proteasome inhibitors mostly bind covalently to the catalytic Thr1 residue within the β5-subunit of the proteasome.[186] There are numerous examples of proteasome inhibitors within literature, a few are outlined in Figure 1.25.

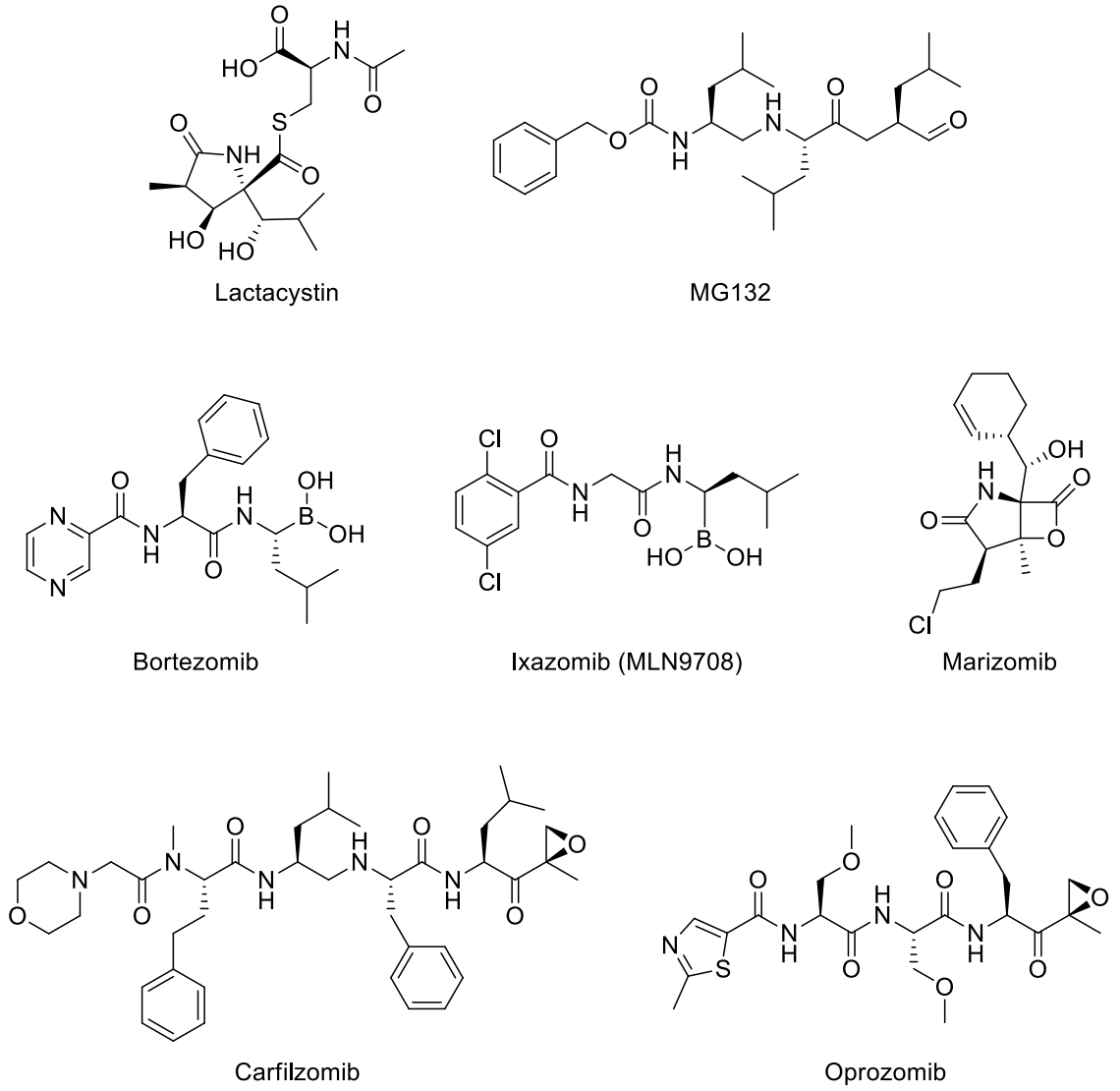

Figure 1.25: Examples of Proteasome inhibitors. Lactacystin.[187] MG132. Bortezomib.[188] Ixazomib.[189] Marizomib. Carfilzomib.[190] Oprozomib.

The first non-peptidic proteasome inhibitor was Lactacystin, which is a metabolite from *Streptomyces*.[187] Lactacystin inhibits the proteasome through irreversibly forming a covalent ester with the amino-terminal threonine on the β-subunit of the proteasome.[191] However the proteasome-lactacystin adduct is slowly hydrolysed with a $t_{1/2}$ of 20 hours, resulting the recovery of the proteasomes proteolytic activity.[192] MG132 belongs to a class of synthetic peptide aldehyde proteasome inhibitors and potent transition state inhibitors of chymotrypsin activity of the proteasome, with a low nM K_i for the chymostryptic activity of pure proteasomes and an IC_{50} of low μM in cultured cells.[180]

Bortezomib, first reported in 1998 as a promising anti-cancer therapeutic, was synthesised through investigating an increase in potency toward the proteasome with a boronic acid, than an aldehyde.[193] The boronic acid allows Bortezomib to form covalent and reversible complexes

with the proteasome, increasing its potency and selectivity compared to their corresponding aldehydes (2500 fold).[184,188,193,194] Ixazomib, which has a similar structure to Bortezomib, inhibits the proteasome in the same way as Bortezomib, and also displays the anti-multiple myeloma activity of other proteasome inhibitors.[189,195]

Marizomib is a β-lactone-γ-lactam proteasome inhibitor that acetylates Thr1 oxygen followed by Thr1-NH_2-catalysed nucleophilic displacement of the chloride by C-3O to give an irreversibly bound adduct (Scheme 1.2).[196]

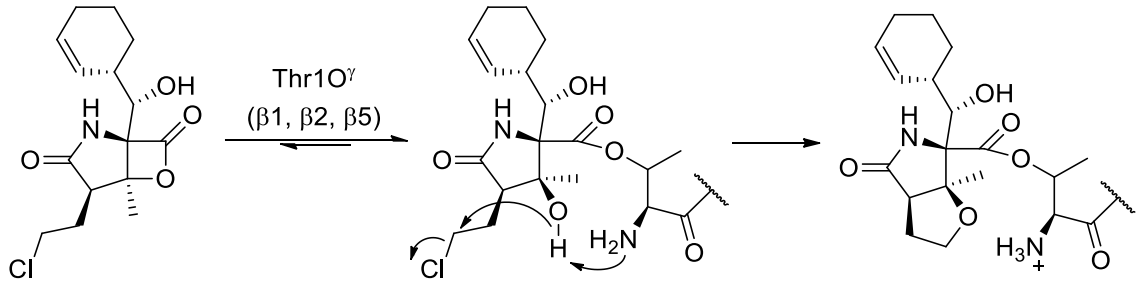

Scheme 1.2: Irreversible binding of Marizomib to Thr1.[196]

Carfilzomib, investigated as a combination therapy with lenalidomide and low dose dexamethasone has been authorised by the FDA for use on patients with relapsed multiple myeloma, where 78% of the trial patients reached complete response.[190,197,198] Both Carfilzomib and Oprozomib are irreversible inhibitors through Thr1 attack at the epoxide.[199]

1.3.2 Hijacking the UPS for Therapeutic Effects

1.3.2.1 Immunomodulatory Drugs

For many years, immunomodulatory drugs (IMiDs) have been used for the treatment of MM, alongside proteasome inhibitors.[195] However the full mode of action of IMiDs was not fully understood until recently, with a notorious example where thalidomide led to congenital malformations in phocomelia infants, a condition where the limbs being severely underdeveloped.[162] In 2010, it was shown that the E3 ligase CRBN was the target of thalidomide teratogenicity, a substrate receptor of CUL4.[201] Thalidomide can exist in two enantiomeric forms, *R* and *S*, where the *S*-enantiomer is teratogenic. However, the glutarimide ring within thalidomide can racemise between these two enantiomers at physiological pH, making it difficult to create a non-teratogenic form of thalidomide.[202]

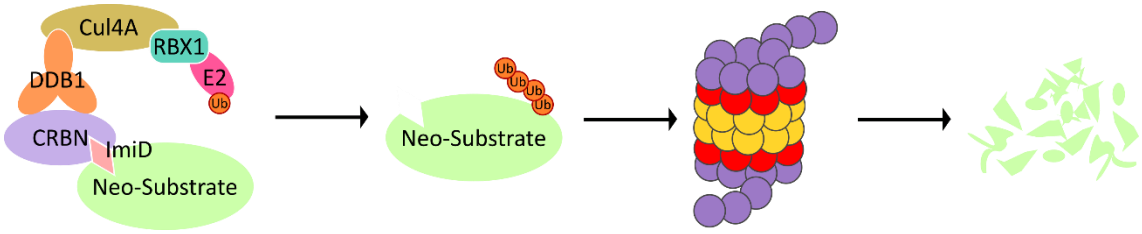

Figure 1.26: ImiD's act as molecular glue between CRBN and a neo-substrate, allowing for ubiquitylation and subsequent degradation.[203]

IMiDs target the $CRL4^{CRBN}$ E3 ligase to induce the degradation of Ikaros family zinc finger proteins, Ikaros (IKZF1) and Aiolos (IKZF3), two lymphoid transcription factors that are key for myeloma cell survival.[204–206] IMiDs bind CRBN through their conserved glutarimide ring, which interacts with a conserved hydrophobic pocket of CRBN. By acting as molecular glue, IMiDs can bind a neo-substrate to CRBN and induce ubiquitylation (Figure 1.26). There are multiple structures in this class of compounds (Figure 1.27), all CRBN recruiters must contain the key glutarimide ring where CC-122, CC-885 and CC-220 are new generation ImiDs.[203]

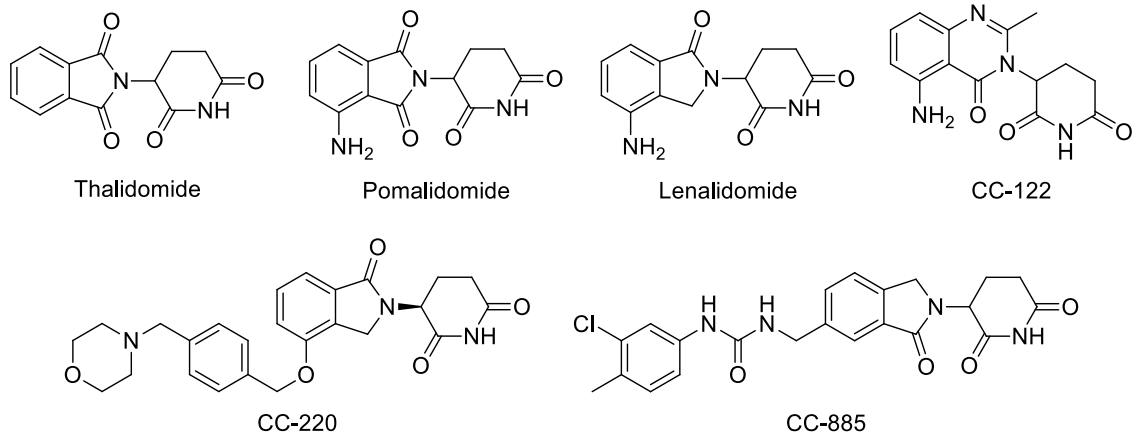

Figure 1.27: Chemical structure of thalidomide, lenalidomide, pomalidomide, CC-122, CC-885 and CC-220.[203]

The glutarimide ring binds into a tri-Trp pocket, inside the pocket the glutarimide ring, sandwiched between Trp383 and Trp389, makes non-polar contacts with Trp403. The ring also forms two hydrogen bonds with CRBN; one from the 6-carbonyl group to Trp383 and one from the glutarimide 1-imino group (NH) to the main-chain carbonyl group of His381.[207]

Lenalidomide and pomalidomide are FDA-approved drugs; the former has shown activities in many haematological malignancies, including myelodysplastic syndrome (MDS), mantle cell lymphoma (MCL) and CLL.[208–210] In primary effusion lymphoma (PEL), IMiDs are reported to supress IRF4 in a CRBN-dependant manner and rapidly degrade IKZF1. Co-treatment of lenalidomide and BRD4 inhibitors ((+)-JQ1, PFI-1 and IBET151) resulted in a synergistic cytotoxicity to PEL lines, *via* the suppressed expression of MYC.[211]

CC-122 binds $CRL4^{CRBN}$ in the same manner as lenalidomide, however, this results in a greater reduction of IKZF1 and IKZF3 in TMD8 cells, whilst also possessing broader cell autonomous activity than lenalidomide.[212] CC-122 is currently involved in a few clinical trials, including one for the safety, tolerability and effectiveness for patients with MM (NCT01421524).[203,213]

CC-220, picks up additional contacts on the surface of CRBN, which, through a TR-FRET binding assay showed CC-220 to have an IC_{50} value of 60 nM, significantly more potent than lenalidomide (1.5 μM).[214] CC-220 is currently in phase I/II clinical trials for MM (NCT02773030).[215] A screening of lenalidomide analogues in a cell-proliferation assay resulted in the identification of CC-885, which can induce $CRL4^{CRBN}$-dependant degradation of not just IKZF1, but also the translation termination factor GSPT1. This suggests a different substrate spectrum from lenalidomide or pomalidomide. CC-885 also had sub-nanomolar potency in AML cell lines, where lenalidomide and pomalidomide do not have significant activity, giving CC-885 potential for AML therapy.[216]

1.3.2.2 Proteolysis Targeting Chimeras

A recent methodology for inducing degradation of a specific protein is by using compounds called Proteolysis Targeting Chimeras (PROTACs), which is a term coined by Arvinas. PROTACs are heterobifunctional molecules containing a warhead ligand that binds to a protein of interest (POI) and an E3 ligase recruiter joined by a linker (Figure 1.28).

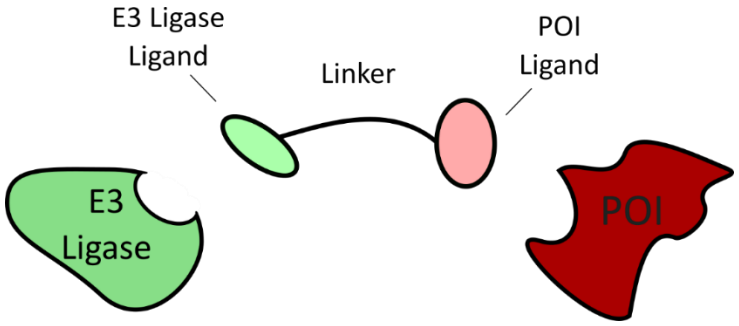

Figure 1.28: Cartoon diagram of a PROTAC and its components.

PROTACs function by bringing a POI and an E3 ligase into close proximity of each other, inducing ubiquitylation of a surface lysine on the POI, and once polyubiquitination has occurred, subsequent degradation via the proteasome (Figure 1.29).[217]

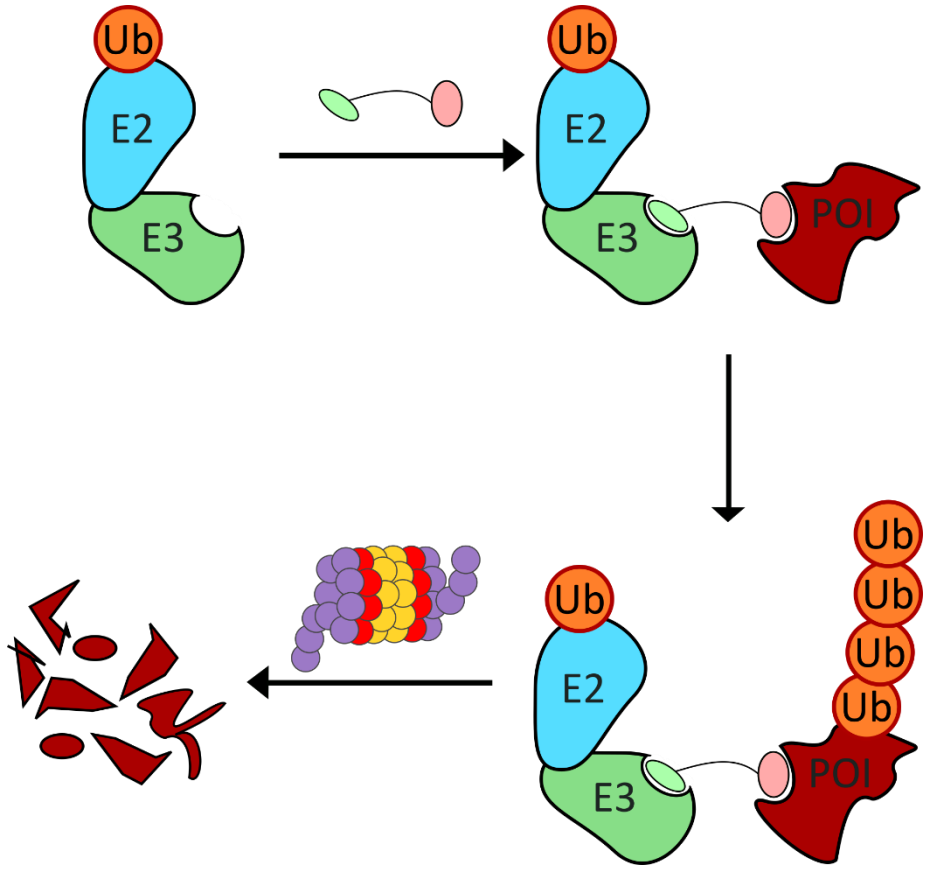

Figure 1.29: PROTAC-mediated ubiquitination and result and degradation via the 26S proteasome.

The first PROTAC to be reported was by the Crews group in 2001, dubbed PROTAC-1, consisted of a MetAP-2 inhibitor linked to a phospho-peptide derived from the recognition sequence of the F-box protein β-TRCP from its native substrate IκBα (Figure 1.30).[218] This PROTAC was shown to induce ubiquitination of MetAP-2, and in cell experiments revealed a rapid degradation time of 30 mins, albeit the concentration of PROTAC was high (analysed as a mixture of protein (4 µL of 9 µM) and 50 µM PROTAC).[218]

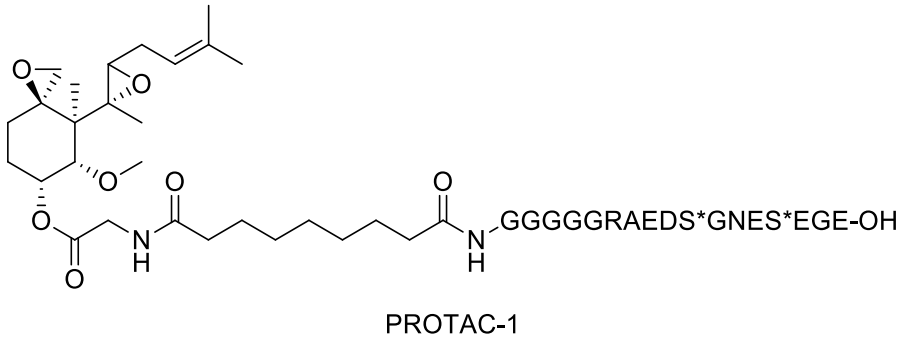

PROTAC-1

Figure 1.30: Structure of the first reported PROTAC. S = Serine phosphorylation.[218]*

The same research group then went on to create peptide containing PROTACs for both the estrogen receptor (ER) and the androgen receptor (AR) (Figure 1.31), which were shown to be ubiquitinated in a cell-free environment. The group also showed for the first time, that PROTACs can function within the context of cells. However, due to the poor cell permeability of peptides, these compounds were injected into cells. This study also elucidated that both ends of the chimeric molecule were required for the desired activity, rather than a synergistic dual treatment. The mechanism of degradation was confirmed to occur *via* the proteasome through the use of the proteasome inhibitor epoxomicin, which when co-treated, observed no degradation.[219]

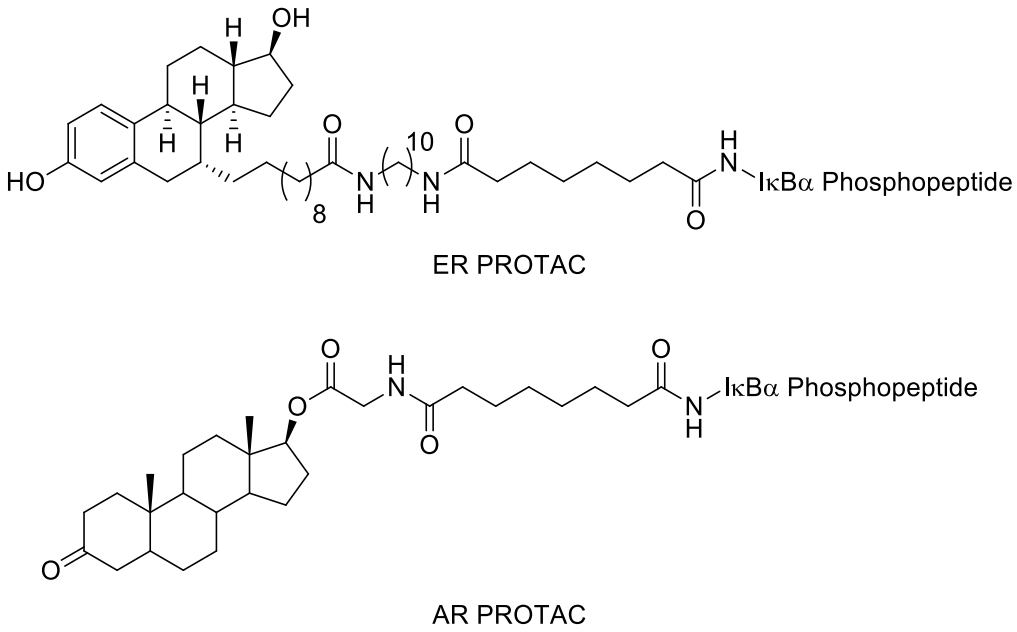

Figure 1.31: The first ER and AR PROTAC reported, comprising of the IκBα phosphopeptide and estradiol or dihydroxytestosterone respectively.[219]

The next generation of peptide based PROTACs contained a shorter peptide sequence, utilising the minimal recognition amino acid sequence for the von Hippel Lindau tumour-suppressor protein VHL (ALAPYIP), from its native substrate HIF-1α. In the presence of oxygen, VHL binds directly to HIF-1α subunits and targets them for degradation (Figure 1.32).[220,221] The polyarginine sequence was utilised here for its cell permeability. Attaching HIF-1α peptide sequence to an inhibitor of FKBP12 allowed degradation of a green fluorescent labelled FKBP by adding the compound to cell culture media.[222]

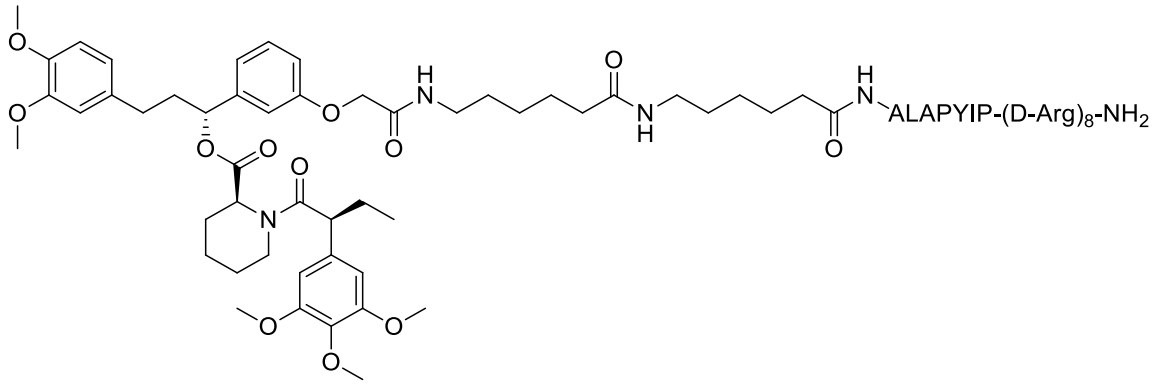

Figure 1.32: Structure of the first Hif-1α peptide PROTAC comprised the 7 amino acid sequence to recruit VHL and an inhibitor of FKBP12.[222]

More PROTACs containing this shorter VHL recognition sequence have been synthesised since the initial report, showing degradation of ER, the aryl hydrocarbon receptor, MetAP2, Smad3, Akt, Bcl-cL and tau.[223–229]

Peptide PROTACs are very useful for proof of principle studies for degradation of target proteins, however, overall have poor cell permeability due to the peptide chain attached to the warhead. Therefore work was performed in order to generate an all-small molecule PROTAC, and was first reported in 2008 (Figure 1.33). This PROTAC employed a nutlin derivative to recruit E3 ligase MDM2 and a non-steroidal androgen receptor (SARM) ligand connected *via* a PEG linker.[230] Degradation of SARM was observed after 7 hours of treatment with 10 μM of PROTAC. This however, was significantly less potent than the peptidic AR PROTAC mentioned previously. Still, this PROTAC was a notable step in the discovery of PROTAC libraries as it was shown to be a cell permeable, proteasome-dependant degrader of SARM.

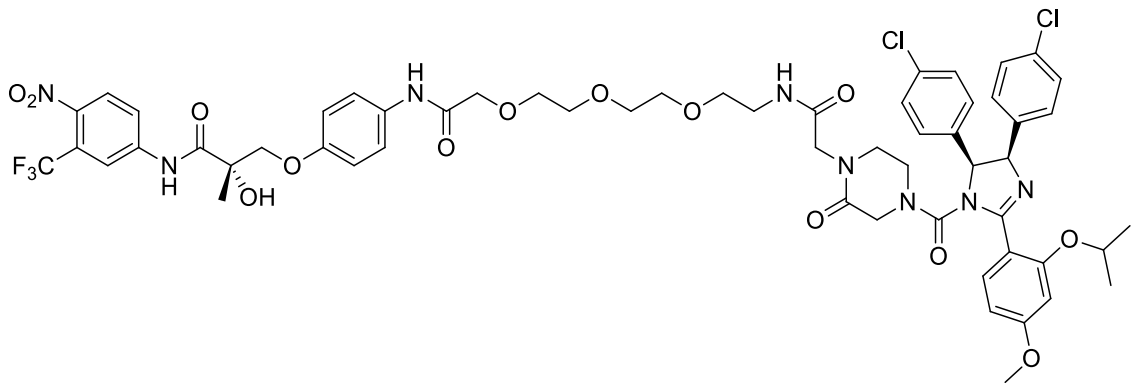

Figure 1.33: The first all small molecule PROTAC.[230]

To expand the potential E3s to recruit in this manner, the Crews and Ciulli groups had then focused on synthesising a small molecule ligand capable of binding to VHL, due to the success of recruiting this E3 ligase in peptide PROTACs. Structure-guided drug design led to the development of inhibitors of the HIF-1a/VHL protein-protein interaction, and further optimisation of these isoxazole inhibitors led to the eventual development of VHL032 (Figure 1.34).[231–233]

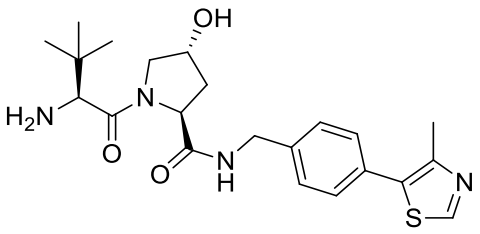

Figure 1.34: Structure of VHL ligand VHL032 developed by the Ciulli lab [233]

The discovery of small molecule ligands for VHL allowed for a new generation of PROTACs to be designed utilising this E3 ligase. The first example of PROTACs that contained VHL032, target RIPK2, and have been reported with DC_{50} (concentration at which 50% of maximum

degradation is observed) values of 1.4 nM (Figure 1.35).[234] This study, through *in vitro* ubiquitylation, demonstrated that PROTACs function catalytically through the recruitment of a physiological cascade of enzymes, rather than occupancy driven inhibition.

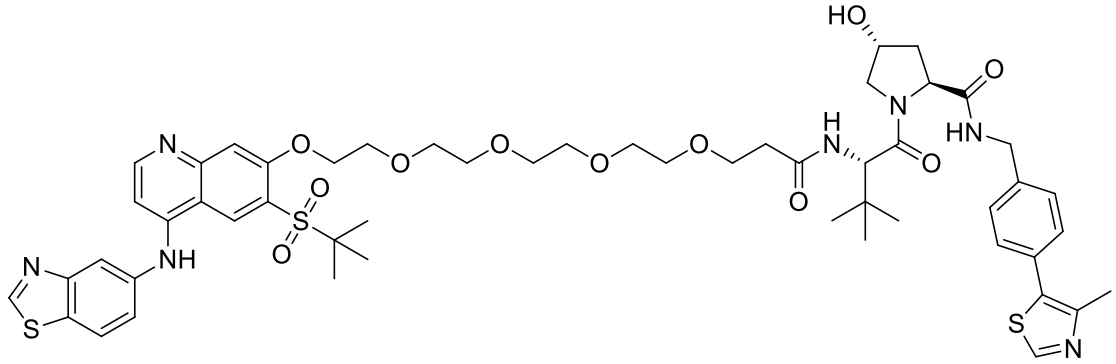

Figure 1.35: Structure of the first VHL ligand recruiting all small molecule PROTAC, targeting RIPK2.[234]

Since the mode of action for ImiD's was elucidated, these CRBN ligands were successfully incorporated into PROTACs, with two parallel reports in 2015 utilising a 4-hydroxy thalidomide and pomalidomide to result in PROTACs dBET1 and ARV-825 (Figure 1.36). These two PROTACs utilised (+)-JQ1 to target and successfully degrade BRD4, which subsequently caused a reduction in c-Myc levels.[235,236] dBET1 showed potent selectivity for BRD4 using BromoScan and complete degradation of BRD4 in MV4-11 cells after 2 hours of treatment.[235] However, due to the lack of selectivity of (+)-JQ1, degradation of BRD2 and BRD3 was also seen.

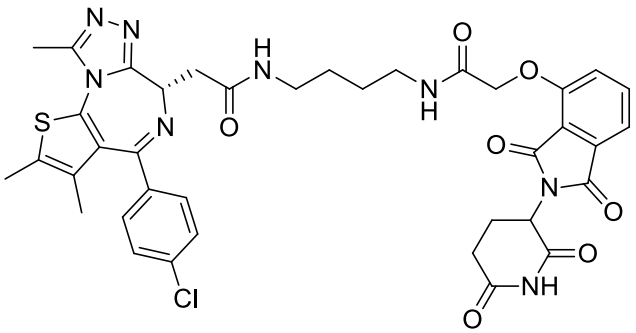

dBET1

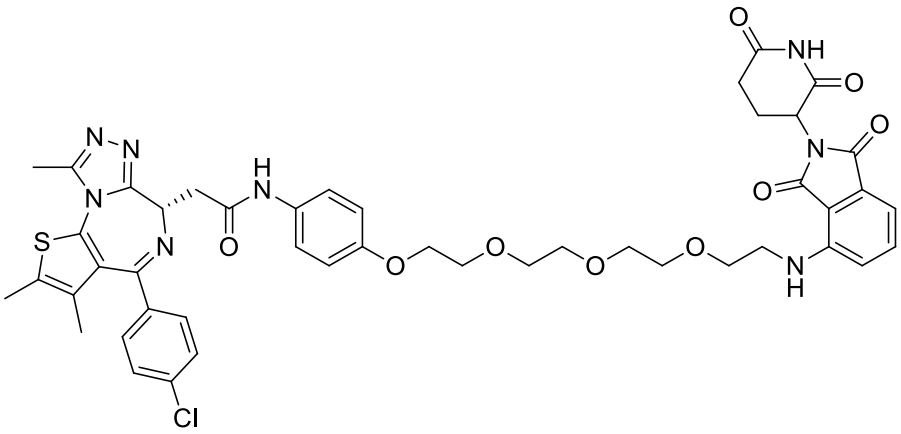

ARV-825

Figure 1.36: Structures of dBET1 and ARV-825, the first CRBN containing PROTACs published in 2015.[235,236]

The Crews group showed through ARV-825 that conjugation of a pomalidomide ligand resulted in dose-dependent BRD4 degradation, and a subsequent reduction in c-Myc levels. ARV-825 was reported to have a DC_{50} value of sub 1 nM in BL cell lines. The study also reported a dose dependence of BRD4 degradation with BRD4 remaining at high concentrations of the PROTAC. This led to the conclusion that high concentrations of PROTAC result in the formation of non-functional BRD4/PROTAC and PROTAC/CRBN dimers rather than the active trimer complex, resulting in a reduction of degradation. This phenomenon was dubbed the hook effect and was also seen with the RIPK2 PROTAC previously discussed.[234,236] Once PROTACs are added to a system, the observed degradation is proportional to the concentration of the PROTAC until the critical concentration of PROTAC has been exceeded, the dose-dependent degradation reverses itself with PROTAC increase. Dose dependency studies are required in order to understand where the critical concentration of the PROTAC lies, as this will differ from substrate to substrate.[234]

Traditional inhibition of BRD4 reduces c-Myc levels however, leads to an accumulation of the protein, through a cell resistance mechanism. PROTACs that target BRD4 cannot lead to this

effect due to the ubiquitylation and subsequent degradation of bound BRD4.[236] A direct comparison of dBET1 and ARV-825 showed ARV-825 to be more potent in 22Rv1 cells, which highlights the importance of linker chemistry for designing target degraders.[237]

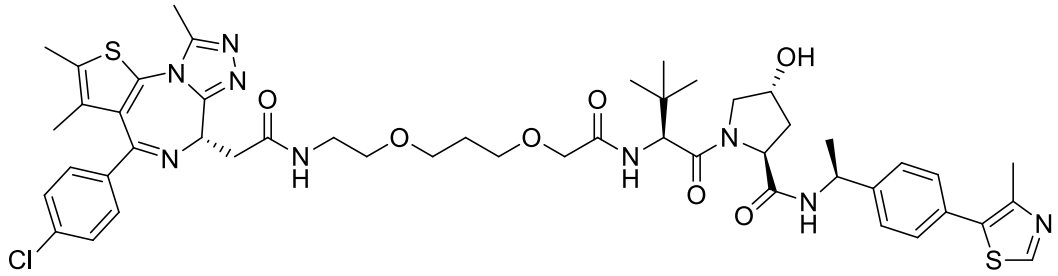

ARV-771

Figure 1.37: Structure of VHL recruiting BET PROTAC ARV-771.[237]

The same study reported the ARV-771 (Figure 1.37), a potent BET PROTAC with a DC_{50} <5 nM in 22Rv1 cells for castration resistant prostate cancer (CRPC). Treatment with ARV-771 resulted in depletion of c-Myc with an IC_{50} <1 nM, and has an antiproliferative effect of 10 – 500-fold more potent than either (+)-JQ1 or OTX015 on CRPC cell lines.[237]

In 2015 the Ciulli lab reported PROTAC MZ1 (Figure 1.38) as a potent, selective degrader of BRD4. HeLa cells were treated with varying concentrations of MZ1, and displayed BET removal >90% at concentrations down to 1 µM. When treated between 0.1-0.5 µM, MZ1 displayed preferential degradation of BRD4 over BRD2 and BRD3. This was the first example of a BET targeting PROTAC that showed preferential degradation to BRD4.[238] This gave the authors speculation about the position of lysine residues on the protein surface and the stability of ternary complexes.

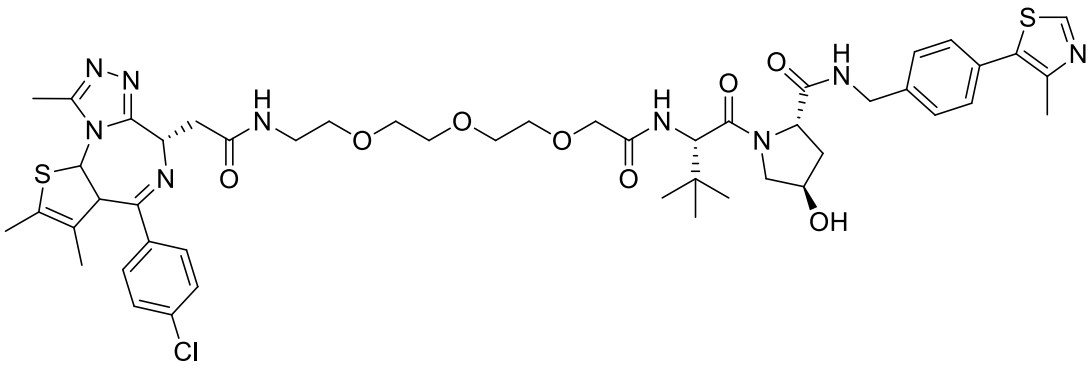

MZ1

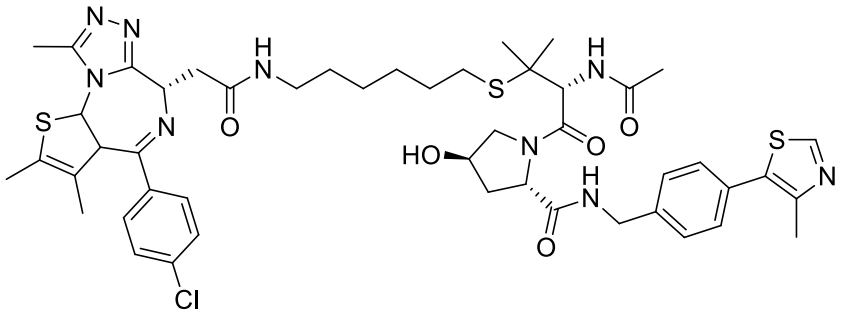

AT1

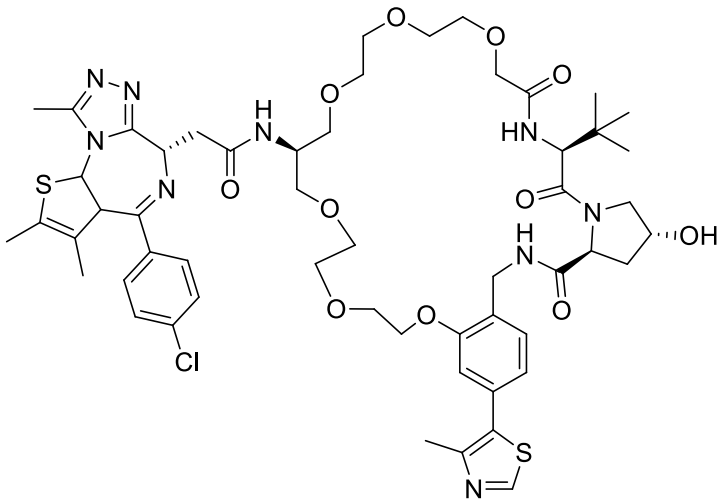

Macrocyclic PROTAC **1.03**

*Figure 1.38: Structures of MZ1, AT1 and the Macrocyclic PROTAC **1.03** from the Cuilli group.*[238–240]

Following this discovery, The Ciulli group managed to determine the ternary complex between VHL, BRD4 and MZ1 and therefore rationalise the selectivity for BRD4 over the other BET members. The determination of this crystal structure revealed new protein-protein and protein-ligand interactions of both hydrophobic and electrostatic nature. With this information to hand, the group were able to optimise the structure of the mediator of this ternary complex to result in PROTAC AT1, which resulted in BRD4 selective degradation across all

concentrations utilised. This study highlighted the importance of the PROTACs ability to fold on itself to be able to recruit the two components in such close proximity.[239]

Taking this phenomenon one step further in 2020 the group then reported the synthesis of a macrocyclic PROTAC (**1.03**), in order to lock the PROTAC conformation in the bound state. **1.03** was designed through a computational approach in order to retain key polar contacts and to best fit the MZ1 linker pose. This was thought to reduce any energetic penalty to adopt the bound state through conformational restriction. **1.03** was reported to have cooperativity with BD2 of BRD4, BRD2 and BRD3, whereas no cooperativity was observed with BD1, unlike MZ1 which showed cooperativity with all the BET BRDs. When treated in cells (HeLa, 22RV1 and MV4;11) **1.03** had similar cellular activity to MZ1, but was more selective to BRD4 at lower concentrations.[240]

The BAF complex is mutated in around 20% of human malignancies and is responsible for many cellular processes relating to chromatin. This complex contains one of the two mutually exclusive ATPases, SMARCA2 and SMARCA4, which are members of BRD family VIII.[241–243] In 2019, the Ciulli group reported the development of PROTAC degraders targeting these two BRDs. The initial degrader designed by the group as co-crystallised in the ternary complex with the SMARCA2 BRD and VHL. This allowed the group to use structure-based design of a more potent PROTAC through the optimisation of binding interactions within the ternary complex, as the group did previously with AT1. This methodology resulted in the discovery of ACBI1 (Figure 1.39), which was shown to exert anti proliferative effects in MV-4-11 cells with an IC_{50} of 28 nM, fitting in line with its DC_{50} value of 6 nM.[244]

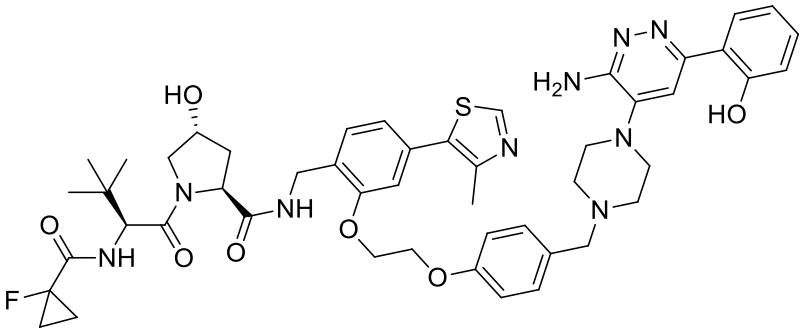

ACBI1

Figure 1.39: Structure of SMARCA2/4 degrader ACBI1.[244]

As examples for BRD4 degraders have shown to utilise both VHL and CRBN to allow for the polyubiquitylation and subsequent degradation of BRD4, it's important to know that this is not always the case. A report in 2015 from the Crews group synthesised degraders from two

potent tyrosine kinase inhibitors, bosutinib and dasatinib, through recruitment of CRBN or VHL E3 ligases, to degrade c-ABL and BCR-ABL. However, they found that the target for protein degradation was warhead and linker dependant and could be fine-tuned (Scheme 1.3).[245] This also served as a lesson for PROTAC design, as it highlights the importance of protein-protein interactions between the POI and the E3 ligase in the ternary complex.

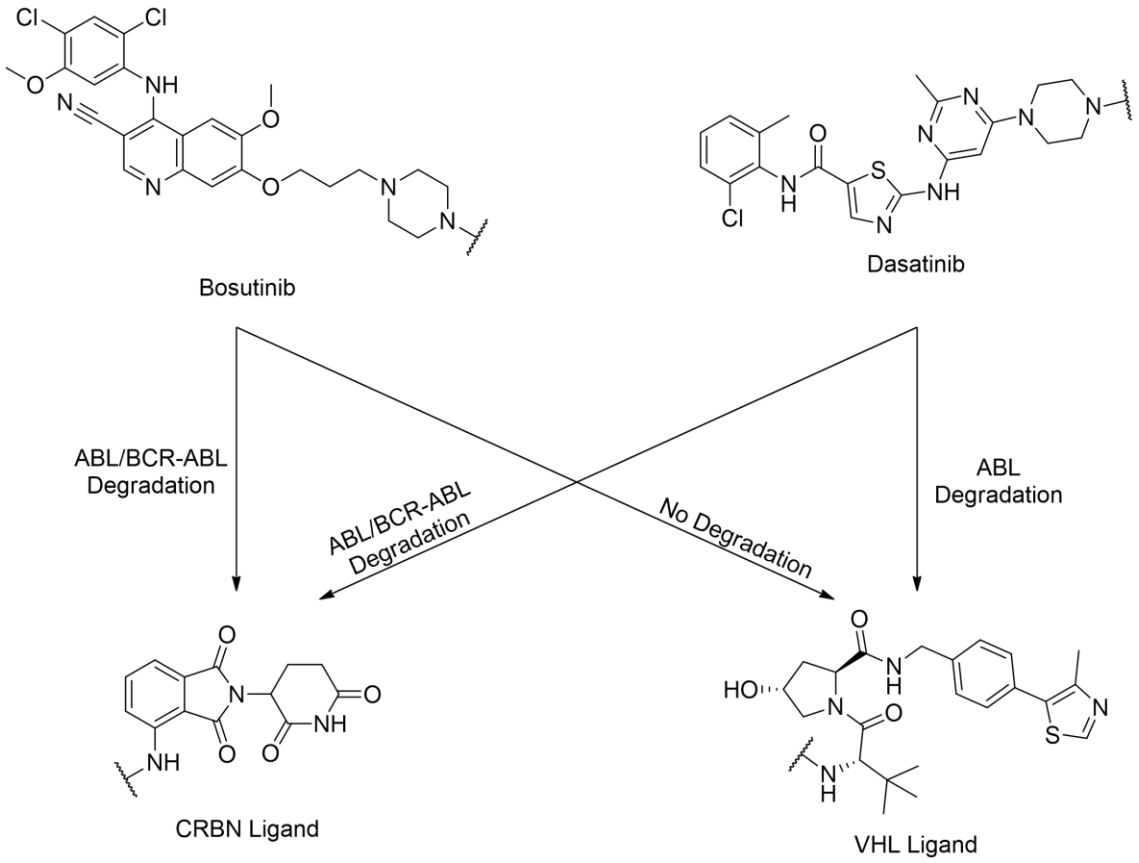

Scheme 1.3: Summary of ABL/BCR-ABL degradation depending on warhead and E3 ligands.[245]

In 2020, the first examples of CBP/p300 degraders were patented by the Dana Faber institute. These compounds were based on the structure of the HAT inhibitor A485, and showed that CPD 1 inhibited Kelly Neuroblastoma cell growth through selective degradation of p300 over CBP (Figure 1.40).[246] This further shows the importance of subtle protein-protein interaction changes in the ternary complex between proteins with similar binding sites.

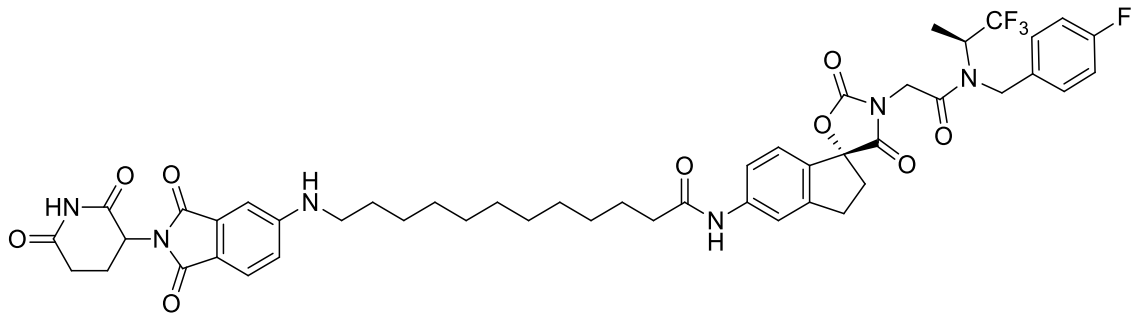

Figure 1.40: Structure of p300 selective degrader CPD 1.

In 2021, another example of a CBP/p300 degrader (dCBP-1) was published by the Ott croup, utilising GNE-781 as the warhead due to having a 4250 fold selectivity to CBP over BRD4 (Figure 1.41). This degrader was capable of almost complete degradation of CBP and p300 at 10 nM, where complete degradation of p300 was observed after 1 hour, and CBP 2 hours in HAP1 cells. Application of dCBP-1 to MM1S showed comparable effects to the HAP1 cells with CBP/p300 degradation and significant c-Myc loss was seen with 10 nM after 6 hours and almost complete loss was seen with 100 nM treatment.[247]

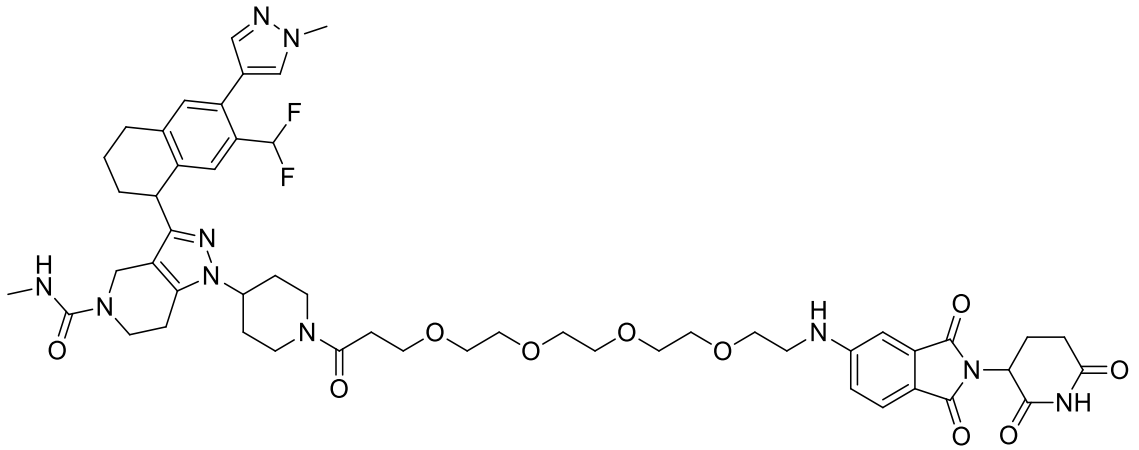

Figure 1.41: Structure of dCBP-1 reported by the Ott group in 2021.[247]

Currently, there are two PROTACs in clinical trials; ARV-110 for treatment of prostate cancer through targeted degradation of AR (NCT03888612) and ARV-471 for the treatment of breast cancer through targeted degradation of ERα (NCT04072952), with their structures disclosed in Figure 1.42.[248–250]

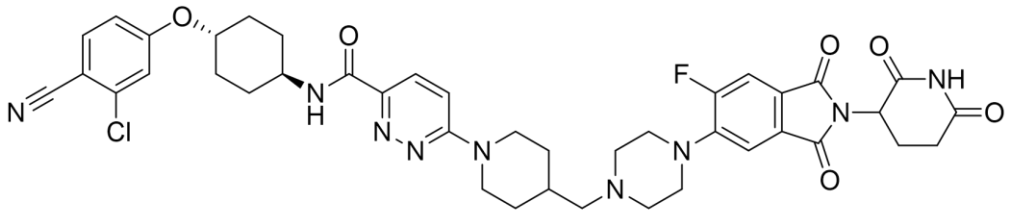

ARV-110

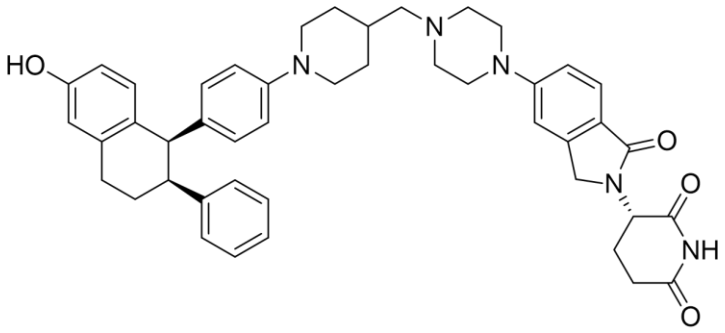

ARV-471

Figure 1.42: Structures of the two PROTACs within clinical trials, ARV-110 for the degradation of the AR and ARV-471 for the degradation of ERα.[248–250]

1.3.2.3 Specific and Non-genetic Inhibitors of Apoptosis Protein-Dependent Protein Erasers

Specific and Non-genetic Inhibitors of Apoptosis Protein-Dependent Protein Erasers (SNIPERs) are another small molecule strategy for targeted degradation. Inhibitor of apoptosis proteins (IAPs) are a family of proteins responsible for inhibiting the apoptosis pathway in cells when over expressed.[251,252]

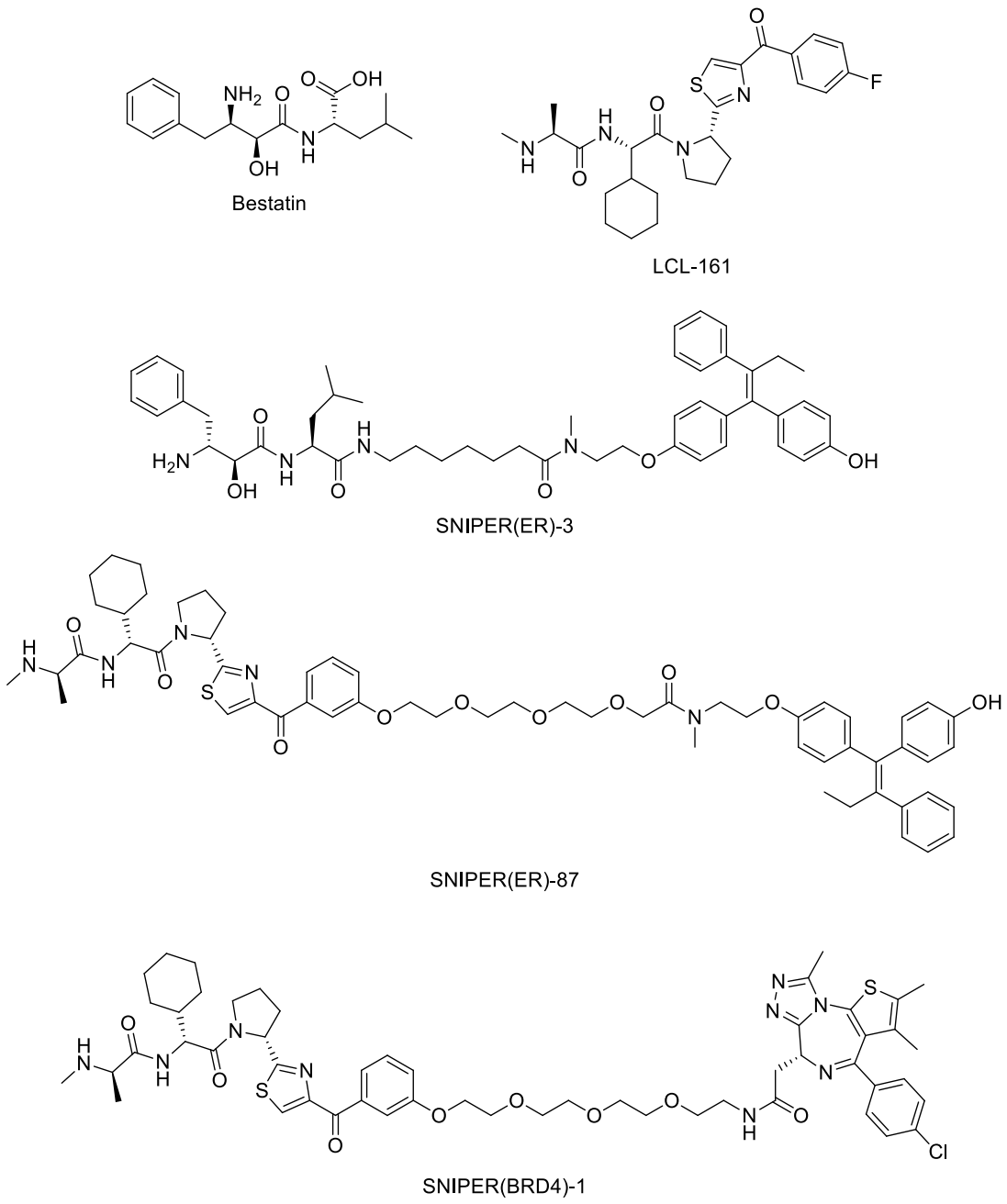

Figure 1.43: Structures of cIAP inhibitors Bestatin and LCL-161, example first generation SNIPER – SNIPER(ER)-3, and second generation SNIPERS SNIPER(ER)-87 and SNIPER(BRD4)-1.[253,254]

First generation SNIPERs were designed for a variety of targets, including ERα, utilising bestatin as a recruiter of cIAP1 and a target warhead for the POI (Figure 1.43).[251] Bestatin methyl esters are able to interact directly with cIAP and induce degradation through self-ubiquitylation dependant on its RING domain, and facilitates proteasomal degradation.[255] SNIPER(ER)-3, an ERα targeting SNIPER containing the ERα ligand 4-OHT and bestatin showed degradation of ERα following cIAP mediated ubiquitylation, which resulted in rapid cell death.[253] First generation SNIPERs which utilised bestatin were only able to induce degradation at concentrations of 10 μM or higher, which therefore sparked research into new SNIPER

compounds that could induce degradation at lower concentrations, becoming more therapeutically relevant.

Switching the cIAP ligand from bestatin to LCL-161 linked to ERα ligand 4-OHT *via* a PEG based linker, induced IAP-mediated ubiquitylation and subsequent degradation of ERα at nanomolar concentrations (SNIPER(ER)-87). This was 1000 times lower than the original reported ERα-SNIPER. Utilisation of this cIAP ligand has also resulted in a potent SNIPER has been made against BRD4 in which degradation of BRD4 can been observed as low as 3 nM, 75% degradation of BRD4 was observed at 30 nM.[254]

1.3.2.4 Hydrophobic Tagging, HaloPROTACs and dTAGs

HaloTags is a technology which utilises modified bacterial haloalkane dehalogenase that is designed to form a covalent bond with synthetic ligands through an ester bond between an aspartate in the enzyme and the hydrocarbon substrate. Halotag fusion proteins have been used to bioorthoginally label proteins *in vivo* and are the subsequent targets different types of tagging to track protein locations, understand cell pathways and protein-protein interactions. Tag based systems are advantageous to the understanding of protein functions *in vivo* due to the ability to selectively degrade any target, regardless of the presence of a small molecule ligand or not.[256]

In 2011, the Crews lab reported a methodology to degrade intracellular proteins through the use of hydrophobic tagging.[257] In the folding of proteins, a major driving force is the internalisation of hydrophobic residues with the proteins core. Any exposure of these hydrophobic residues is considered a hallmark of an unfolded protein.[258,259] Failure to fold a protein correctly, results in degradation *via* the UPS or Autophagic pathway.[260]

The Crews group synthesised 21 structurally distinct scaffolds designed to hydrophobically tag the HaloTag fusion proteins. After initial screening in HEK 293T cells expressing the luciferase-HaloTag fusion protein to determine the potency of this library, and on the basis of the high stability and cell permeability of adamantly groups, HyT13 (Figure 1.44) was the hydrophobic tag they continued through their investigation. The primary amine of HyT13 reacts to form a covalent bond with the HaloTag-fusion protein.[257]

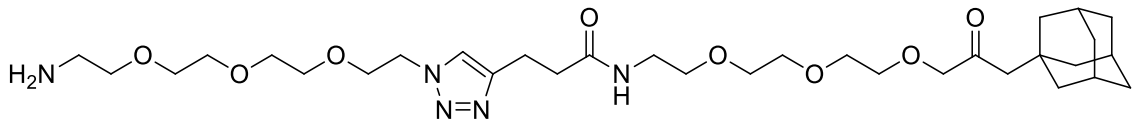

HyT13

Figure 1.44: Structure of hydrophobic tag HyT13.[257]

HyT13 was shown to efficiently degrade the fusion protein, with a maximal effect observed at 100 nM and a determined cellular IC_{50} of 21 nM. Treatment with proteasome inhibitor MG132 blocked HyT13 mediated degradation, confirming the mechanism of protein degradation. HyT13 was also shown to degrade fusion proteins within zebrafish embryos and reduced Hras1G12V tumour formation after 9 days.[257]

After the synthesis of the first small molecule VHL ligand from the Crews group, they applied this chemical probe to the HaloPROTACs, in order to be able to degrade HaloTag labelled proteins. [261] HaloPROTACs were first reported in 2015 and were comprised of VHL032 and a chloroalkane ligand for the HaloTag.[261] This study described the synthesis of a series of HaloPROTACs, where the most potent of these compounds was HaloPROTAC3 (Figure 1.45), which had a DC_{50} value of 19 nM to GFP-HaloTag7.[261] Linker length of these compounds was shown to be important here where reducing the number of PEG groups from 3 resulted in no significant degradation. This technology allows for the understanding of what occurs to intracellular signalling pathways when proteins are ubiquitinated and subsequently degraded by the proteasome.

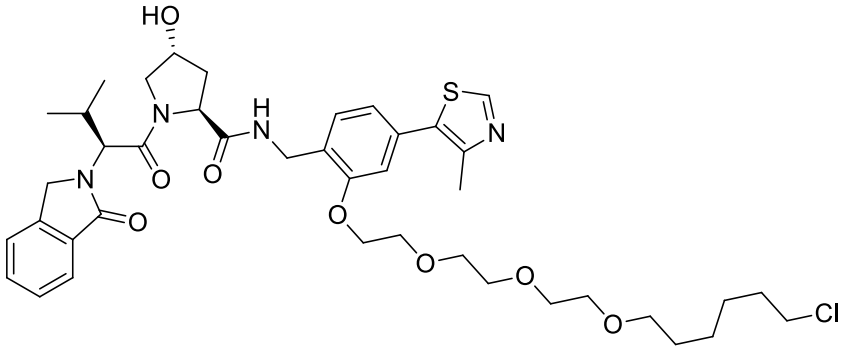

HaloPROTAC3

Figure 1.45: Structure of HaloPROTAC3.[261]

In 2018 reports from the Bradner group about a series of compounds that could result in a comparable loss-of-function to HaloPROTACs and hydrophobic tagging. Following on from their previous work with the reports of a CRBN recruiting FKBP12 degrader, the group synthesised a range of compounds dubbed dTAGs targeting an engineered variant of

$FKB12^{F36V}$.[235] $FKB12^{F36V}$ was chosen as the target for this experiment over $FKBP12^{WT}$ due to concerns about the confounding biological effects of endogenous $FKBP12^{WT}$ disruption. Use of the engineered variant allowed selective recognition of a synthetic ligand, API867. Initial assays reported dTAG-7 and dTAG-13 as selective heterodimerisers engaging and rapidly degrade $FKB12^{F36V}$ in $293FT^{WT}$ cells expressing $FKBP12^{F36V}$-Nluc.[262]

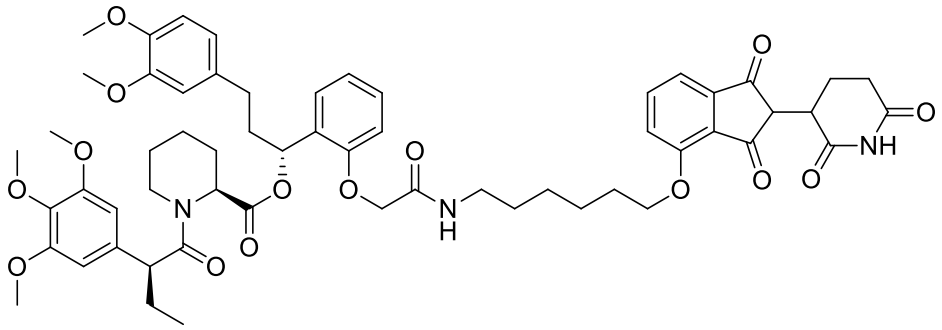

dTAG-13

Figure 1.46: Structure of dTAG-13.[262]

The group then expressed fusion chimera $FKBP12^{F36V}$-tagged BRD4, and treated the cells with dTAG13 (Figure 1.46), which led to rapid and potent degradation of the BRD4 fusion chimera, with no changes in BRD2 or BRD3 levels. The group had established a powerful chemical-genetic system to study BRD4 function, in isolation from the remaining BET members.[262]

1.3.3 **Intracellular Autophagy Machinery Mediated TPD**

Eukaryotic cells have two major degradation pathways, the proteasome (discussed previously) and the lysosome. Where proteasomal degradation is efficient at degrading abnormal soluble proteins, protein aggregates are typically targeted for degradation by autophagic vesicles. Autophagy is the major intracellular degradation system, ubiquitous in eukaryotic cells, in which material is delivered to and degraded in the lysosome. Lysosomes, often described as a "cellular garbage can" degrade extracellular material, plasma membrane proteins, cytosolic components and organelles.[263]

The Jentsch group, attempting to understand how the degradation pathway choice is made, took *Saccharomyces cerevisiae* as a model organism due to both pathways existing. They found proteasomal degradation was dependent on Dsk2, a polyubiquitination-binding domain; and autophagic degradation was dependant on Cue5, which functions as a ubiquitin-ATG8 adapter and thus mediates autophagic clearance of ubiquitin conjugates. Dsk2 had a 10-fold higher affinity to Ub than Cue5, allowing Dsk2 to rapidly mediate the degradation of soluble substrates. However, when the substrates aggregate, the oligomerisation of Cue5 confers a higher selectivity towards the substrate due to the bundling of Ub chains.[264]

Impairment of the autophagic degradation process has been reported in numerous pathological issues including the initiation and progression of cancer, attracting the attention for drug candidates.[265,266]

1.3.3.1 AUTACs

A study reported in 2019 had synthesised novel chimeric molecules names Autophagy-Targeting Chimeras (AUTACs), which consisted of a guanine tag and a specific binder to an intracellular target of interest. This group designed numerous AUTACs to provide proof of principle degradation of targets *via* lysosomal degradation. The group successfully decreased the levels of cytosolic MetAP2 and FKBP12 with AUTAC1 and AUTAC 2 respectively. An interesting AUTAC synthesised was AUTAC3, which comprised of (+)-JQ1 as the recruiting ligand to target the BET family of proteins linked *via* a PEG linker to a *p*-fluorobenzylguanine (FBnG) ligand (Figure 1.47). Unlike the other AUTACs developed here, BRD4 is a protein restricted to the nucleus, which made it a challenging target for autophagic degradation.[267] However the concepts of nuclear autophagy has been documented and work is being performed to understand the process.[268]

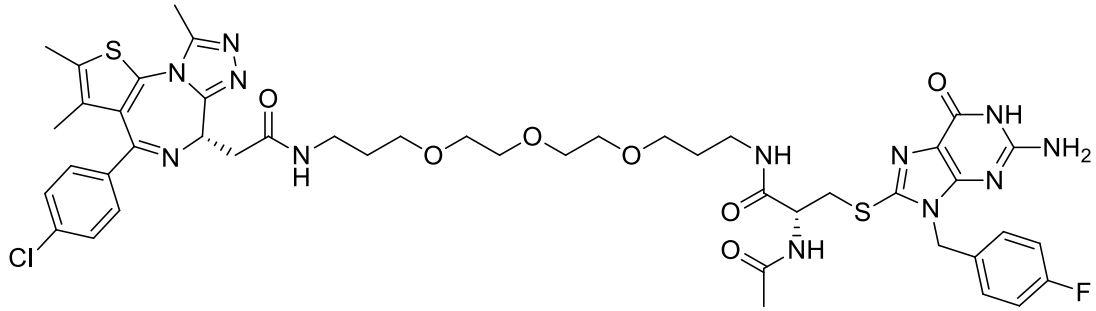

AUTAC3

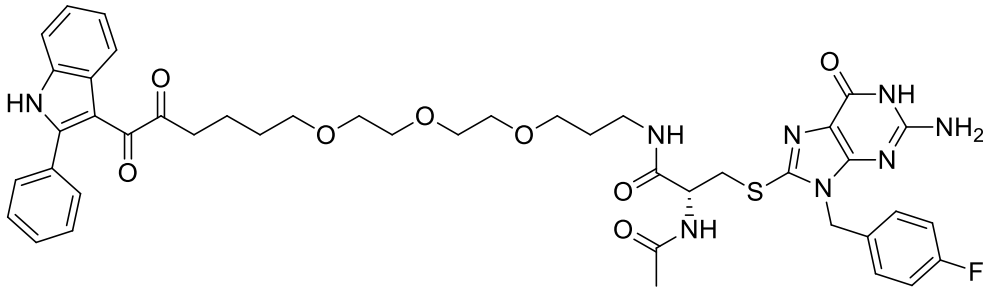

AUTAC4

Figure 1.47: Structures of AUTAC3 and AUTAC4.[267]

The study showed that AUTAC3 slightly reduced BRD4 levels in A549 cells, through the localisation of BRD4 with LC3B, a marker for autophagy, during the G2-to-G1 transition when the nuclear envelope is degraded, exposing the nuclear proteins to the cytoplasm.[267] Through the use of AUTAC 4 (Figure 1.47), which contained a phenylindole moiety, which binds non-covalently to the mitochondrial translocator protein TSPO. AUTAC4 was the first reported degrader that could target an entire organelle for degradation. AUTAC4 was shown to improve mitochondrial morphology and functions in Down syndrome-derived fibroblasts.[267]

1.3.3.2 Other Autophagic-Mediated Degraders

First published in 2019, the Lu group gave reports of a series of compounds called autophagosomes-tethering compounds (ATTECs). An ATTEC is a form of molecular glue that links the autophagosome protein microtubule-associated protein 1A/1B light chain 3 (LC3) and mutant huntingtin protein (mHTT).[269] It's likely thought that mHTT aggregation in the cytoplasm causes Huntington's disease, mHTT removal is a consensus strategy against this disease.[270] The ATTEC was able to successfully remove mHTT and not HTT in a mouse model. The great advantage of these ATTECs is that their molecular weight is significantly lower than heterobifunctional degraders (AUTACs, SNIPERs, and PROTACs) and fall back into small molecule territory for physiochemical properties.

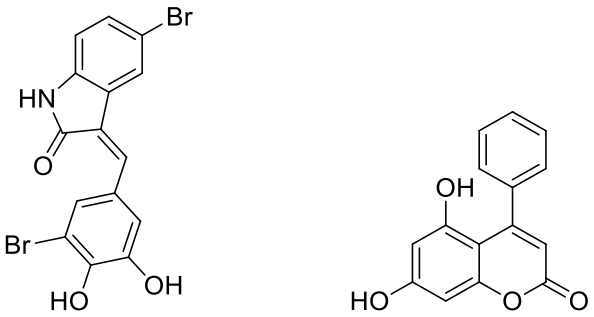

Figure 1.48: Structure of ATTECs first reported by Lu.[269,271]

A second approach to adapter-mediated selective autophagy is p62 binders, for example BMF-1-64 comprises of (+)-JQ1 to recruit BRD4 and p62 (Figure 1.49). As p62 is selectively degraded by autophagy by binding to the isolation membrane, this degrader can accelerate the degradation of BET proteins.[272,273]

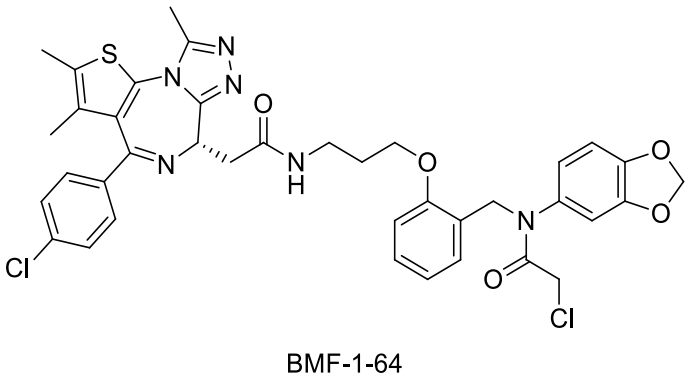

Figure 1.49: Reported structure of BMF-1-64.[272,273]

1.3.4 **Antibody-Conjugated Targeted Protein Degradation**

1.3.4.1 LYTACs

Extracellular and membrane-associated proteins encompass 40% of all protein-encoding genes, have been reported as having key roles in cancer, aging related diseases and autoimmune disorders.[274,275] Recently a new class of degraders was reported which utilises the lysosomal pathway for protein degradation. First reported in 2020 these compounds are dubbed Lysosome-Targeting Chimeras (LYTACs) and bind to a cell surface lysosome-targeting receptor (LTR) and an extracellular POI in order to degrade both secreted proteins and membrane-associated proteins with therapeutic interest (Figure 1.50).[276]

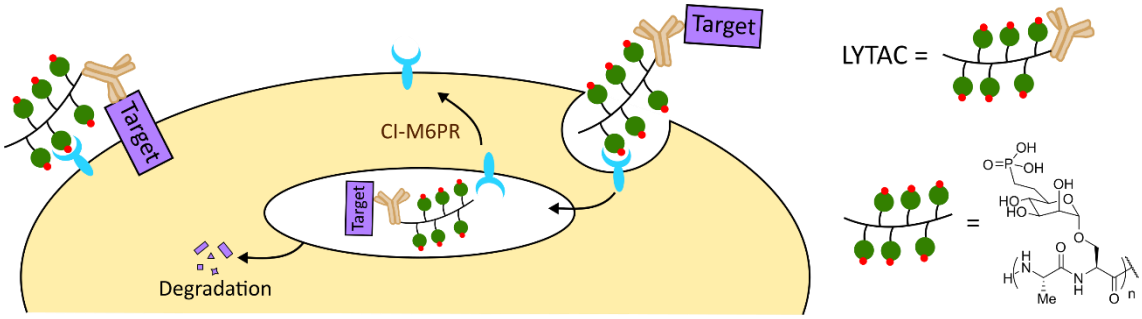

Figure 1.50: LYTAC mechanism of action.[276]

These LYTAC molecules are significantly larger than the before mentioned PROTACs with molecular weights in the KDa range. The structure of the LYTACs reported in this paper comprise *N*-carboxyanhydride-derived glycopeptides bearing multiple serine-*O*-mannose-6-phosphonate residues (Figure 1.50). The M6Pn component binds to CI-M6PR which is the targeted LTR, whereas the antibody binds to the POI. The recruited POI and LYTAC then gets transported for degradation *via* the lysosome. The report showed it was possible to target apoipoprotein E4, EGFR, CD71 and PD-L1 for degradation *via* the lysosome pathway.[276] Once proof of concept was performed, the Bertozzi group shifted away from M6PR in order to target a tissue specific receptor.

Another report from the Bertozzi group was for LYTAC targeting the Asialoglycoprotein receptor (ASGPR), which is a hepatocyte specific LTR, to degrade extra cellular proteins in the same manner shown in Figure 1.50. The synthesis of the LYTAC was performed through an 8 step synthesis before reacting with an azide on a non-specifically labelled antibody via a Cu-free strain-promoted azide-alkyne cycloaddition (Figure 1.51).[277]

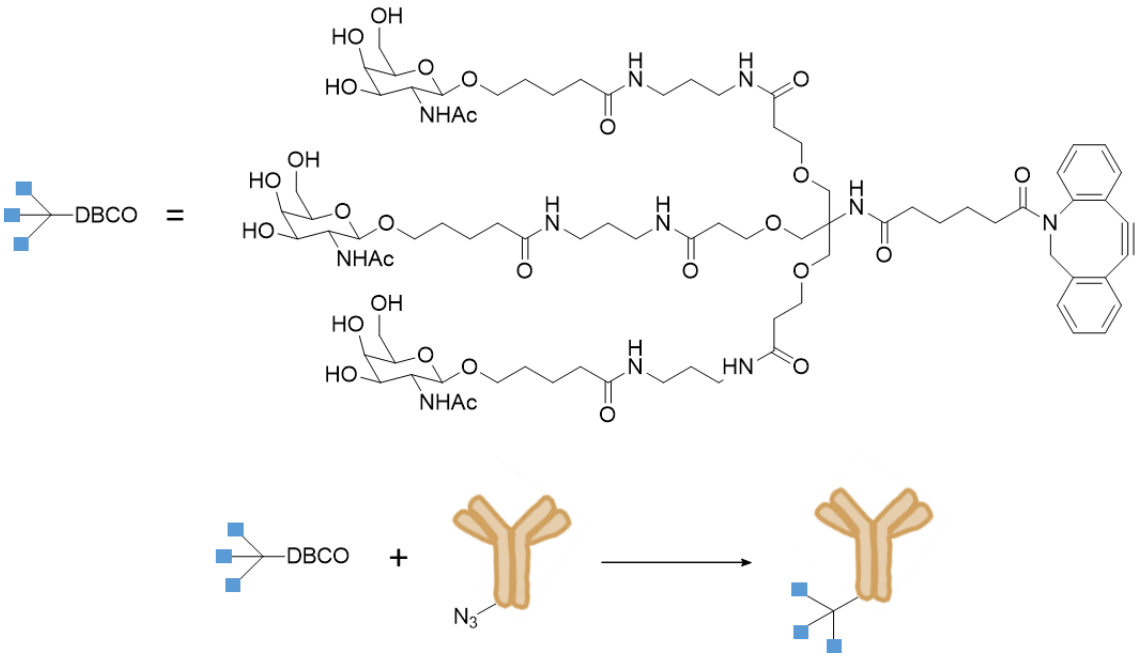

Figure 1.51: Structure of ASGPR targeting LYTAC, with its tri-GalNAc rings connected via linkers to DBCO.[277]

An advantage of LYTACs as a methodology for protein degradation is that it allows you to tune degradation to a specific cell type, through the targeting of a specific LTR. The tri-GalNHAc-LYTAC shown in Figure 1.51 degraded EGFR and HER2 in HCC cells, dependant on ASGPR. The report showed that conjugation of the ligand to the antibody was important through binding at three locations on Ptz, the c-terminus, the hinge domain and the CH1 heavy chain. Here conjugating at the hinge domain gave 70% degradation, whereas the CH1 domain gave 60%. However, as this technology is relatively new, further structure-function studies will be needed to further elucidate the structural understanding of degradation by LTRs.[277]

1.3.4.2 Antibody-conjugated PROTACs

Even though there have been numerous PROTACs reported showing efficient degradation of their targets, one of their main issues is that they are not tissue specific. This is due to recruiting elements that are broadly expressed across tissue types and, to date there has not been PROTACs recruiting E3 ligases with specific tissue locations.

Antibody-drug-conjugates (ADCs) are antibodies that target specific receptors found on cancer cells ensuring delivery of the chemotherapy drug to the right tissue, thereby reducing unwanted side effects of chemotherapy treatments.[278] A notable example is the ADC Trastuzumab emtansine (T-DM1), which is a human growth factor receptor 2 (HER2)-targeted antibody-drug conjugate. Once T-DM1 binds HER2, the HER2-T-DMI complex becomes internalised and degraded *via* the lysosome. This process releases the DM1 catabolites that bind to tubulin and begins the therapeutic effect.[279]

Only a handful of ADCs however have received FDA approval for treatment in the USA, due to failing in clinical trials by intrinsic uptake into normal cells.[280] There are many potential mechanisms that might explain why most ADCs failed during clinical trials, however a main concern was the dose limiting toxicity, which meant the ADCs were often used at sub-optimal therapeutic doses.[281]

However, reports in 2020 from the Tate group synthesised an antibody-PROTAC conjugate as a modality to deliver PROTACs to their specific targets, with multiple PROTACs conjugated to the antibody in order to overcome the need for high cytotoxic requirement in ACDs. The hypothesis from the group was that due to the catalytic nature of PROTACs, the need for the extremely high cytotoxicity of the drug could be circumvented. The PROTAC synthesised was dubbed Ab-PROTAC-3 and is portrayed in Figure 1.52.[280]

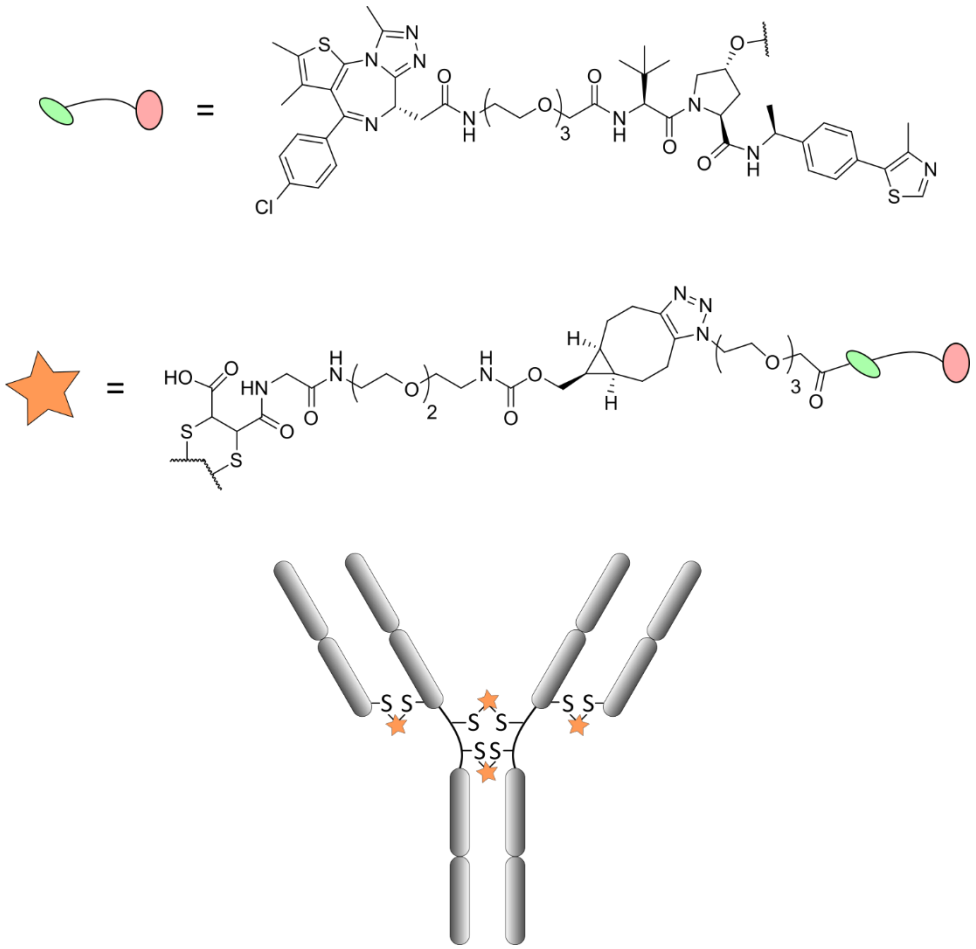

Figure 1.52: Structure of the antibody-conjugated PROTAC (PROTAC-3) from the Tate lab.[280]

The study utilised an analogue of MZ1 as a proof of concept study and showed that Ab-PROTAC-3 significantly degraded BRD4 only in HER2+ cells at 50 nM, while leaving BRD4 intact in HER2- cells at any concentration. The lack of degradation in HER2- cells confirmed the

degradation process of AB-PROTAC-3 was occurred after HER2 internalisation.[280] This modality has also been utilised by the Dragovich group, where they showed degradation of ERα *via* HER2 internalisation.[282]

1.4 Project Aims

As discussed within the literature review, there have been numerous studies investigating the degradation of BRD4 with the application to the reduction of c-myc for an oncogenic effect. At the time of starting the project in 2017, there were no reported CBP/p300 degraders and selective inhibitors to the BRD of CBP/p300 had only recently started to emerge. The aims of this project are to take ISOX-DUAL, which is a dual inhibitor of the bromodomains of both BRD4 and CBP/p300, to create dual action degraders.

This approach contained two novelties, the first being the potential to be one of the first reported CBP/p300 degraders, where the other being the dual action modality. This modality was chosen to be studied to see if a dual degradation approach of two upstream targets of c-Myc will synergise to have a higher therapeutic effect than single target degraders (Figure 1.53).

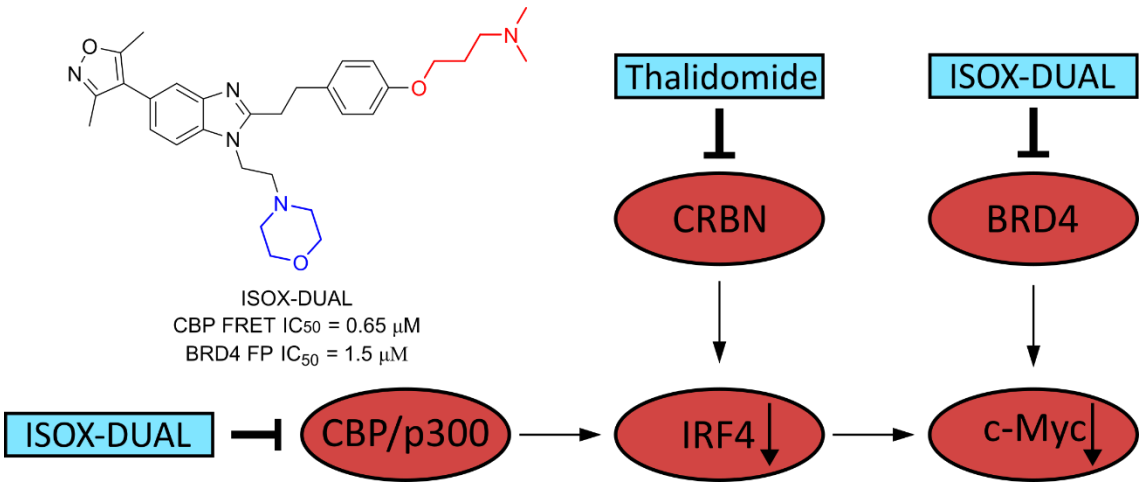

Figure 1.53: The structure of ISOX-DUAL, the cell-free IC_{50} values and the inhibition pathway for c-Myc.[2,204–206]

However, at the onset of this project, there were many issues that needed to be addressed before this could be considered a possibility.

- The reported low overall yield of ISOX-DUAL (1%), which is perfectly acceptable for a medicinal chemistry exercise, for a final compound merely for testing. However, this is not amenable to scale-up to allow for degrader synthesis and called for a synthesis re-evaluation.[2] Therefore the chemistry of ISOX-DUAL needed to be optimised to attempt to increase the overall synthetic yield to allow for improved mass transfer into the degrader synthesis (Chapter 2).
- Secondly, ISOX-DUAL has no available sites for linker attachment and so the structure of ISOX-DUAL needed to be modified to enable the synthesis of degraders. Analysis of reported co-crystal structures of BDOIA383 and SGC-CBP30 within the BRDs of BRD4

and CBP/p300 have identified two available positions for potential modifications (Figure 1.53), the phenol exit vector (red) and the morpholine ring (blue) (Chapter 3).[2,43]

Hence, this was a high-risk project with a need to address key issues in overall yield and linker chemistry. Once rectified, degraders could be synthesised from the ISOX-DUAL warhead and then analysed for their ability to degrade both BRD4 and CBP. Any lead like degraders would be measured for potential therapeutic effects on c-Myc (Chapter 4) to see if a dual degradation approach is more beneficial than a single degradation approach.

2 Chapter 2: Synthesis and Optimisation of ISOX-DUAL

2.1 Introduction

As discussed in Chapter 1, SGC-CBP30 is a CBP/p300 selective chemical probe with an IC_{50} value of 0.12 μM and 2.4 μM for CBP and BRD4 respectively, and was the one of the first CBP selective inhibitors to be published, with sub micromolar activity to CBP/p300 (Figure 2.1).[43] Parallel work from the Jones group also demonstrated similar selectivity trends with inhibitor BDOIA383.[2] Further tuning of BDOIA383 resulted in a more CBP selective probe (PF-CBP1) and also created a dual inhibitor of both BRD4 and CBP (ISOX-DUAL).[2] In the recent literature UMB298 has been reported as a potent selective BRD inhibitor of CBP/p300, which is 72-fold more selective to CBP/p300 (72 nM) than BRD4 (5193 nM).[150]

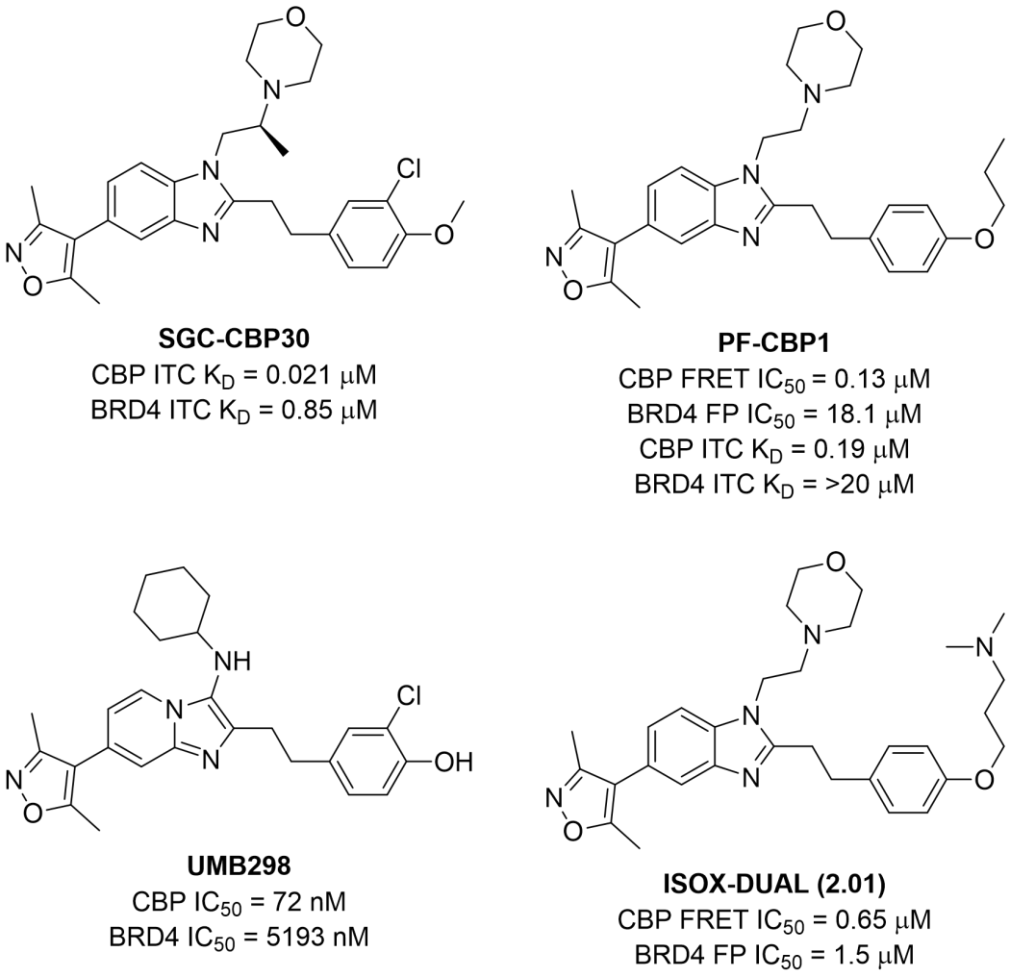

Figure 2.1: Isoxazole containing inhibitors for CBP/p300 BRD and their biochemical binding values.

ISOX-DUAL is a dual BRD inhibitor of BRD4 and CBP/p300 and this dual functionality comes from both the tertiary amine on the alkylated phenol and from the morpholine groups. The structure activity relationship (SAR) of compound SGC-CBP30 reported by Brennan and co-workers show that the affinity for CBP/P300 comes from the ethyl morpholine substituent.[43]

No BRD4 SAR was carried out for the isoxazole containing benzimidazole fragments but it is seen that the BRD4 efficacy lowers when the alkylated amine is varied or removed.[2] The Jones group demonstrated that ISOX-DUAL displays cytokine repressions of IL-6, IL-1βa and IFN-β at lower concentrations than PF-CBP1, thought to arise from the BET inhibitory component.[283] In the ISOX-DUAL studies a negative control was used, (ISOX-INACT), which introduced two methyl groups on the fused aromatic scaffold that, due to steric hindrance, force the isoxazole head group into an unfavourable angle within the binding pocket.

Part way into the project, reports of another dual inhibitor both BRD4 and CBP/p300 emerged. NEO2734 was described as a novel potent inhibitor of both BRD4 and CBP/p300 BRDs with IC_{50} values of <30 nM in cell-free assays (Figure 2.2).[284]

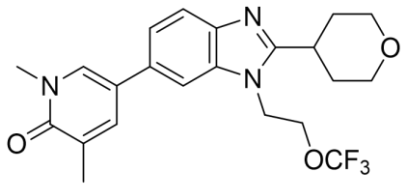

NEO2734
BRD4 IC_{50} = <30 nM
CBP/p300 IC_{50} = <30 nM

Figure 2.2: Structure and cell-free binding affinities of NEO2734 to the BRDs of BRD4 and CBP/p300.[284]

This inhibitor was shown to overcome (+)-JQ1 resistance in SPOP-mutated prostate cancer cells, and showed that a synergistic approach to targeting both BRD4 and CBP/p300 resulted in a higher therapeutic effect towards lymphoma cells that were exposed to either BET or CBP/p300 inhibitors alone.[285,286] There is pre-clinical evidence to support the notion that small molecule inhibitors targeting both BRD4 and CBP/p300 elicit antitumor activity.[94,135,151,153,287–289] Also combination treatment using both a BET inhibitor and a CBP/p300 inhibitor was also shown to provide a synergistic effect in AML cell lines.[44]

Our interest in ISOX-DUAL was for application to targeted degradation technology, to see if dual degradation of two upstream targets of c-Myc (BRD4 and CBP) will result in a more profound knockdown of c-Myc. To allow for degrader synthesis from ISOX-DUAL, the synthetic strategy needed to be modified to a feasible scalable route to allow for late-stage couplings and to carry more material through the synthesis. The literature synthetic strategy reported a 1% overall yield for ISOX-DUAL (Scheme 2.1), which was calculated through the linear transformations of **2.02** to ISOX-DUAL, considering **2.08** as a reagent.[2]

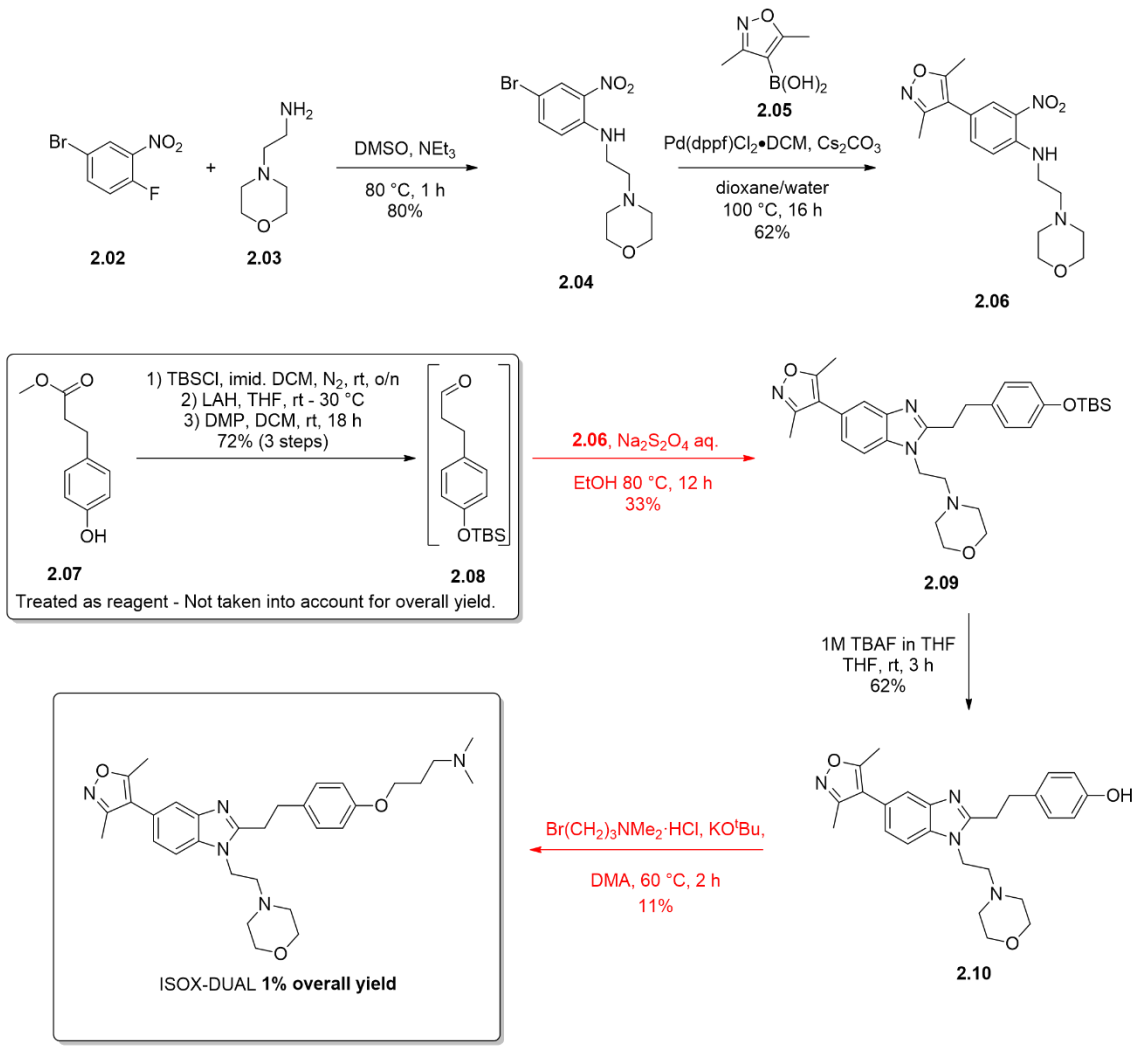

*Scheme 2.1: Published scheme for ISOX-DUAL from the Jones group showing each reaction and the yield obtained. The overall yield treated **2.08** as a reagent and was not a contributing factor to yield calculation.*

The route to improving the yield of ISOX-DUAL started from an improved protocol, proposed and utilised at Tocris Bio-Techne. Rather than cyclising intermediate **2.06** with **2.08**, here **2.06** is reduced with Pd/C and H_2 to **2.11**. This intermediate is then progressed into an amide formation with **2.13**. A condensation reaction to cyclise the benzimidazole, afforded ISOX-DUAL with an overall yield of 13% (Scheme 2.2). **2.13** was treated as a reagent here and not contributing to the yield. Performing the alkylation prior to benzimidazole formation led to a significant yield boost. The decision was made to investigate the steps of this scheme to enable the yield to be improved further, without much deviation from work already performed.

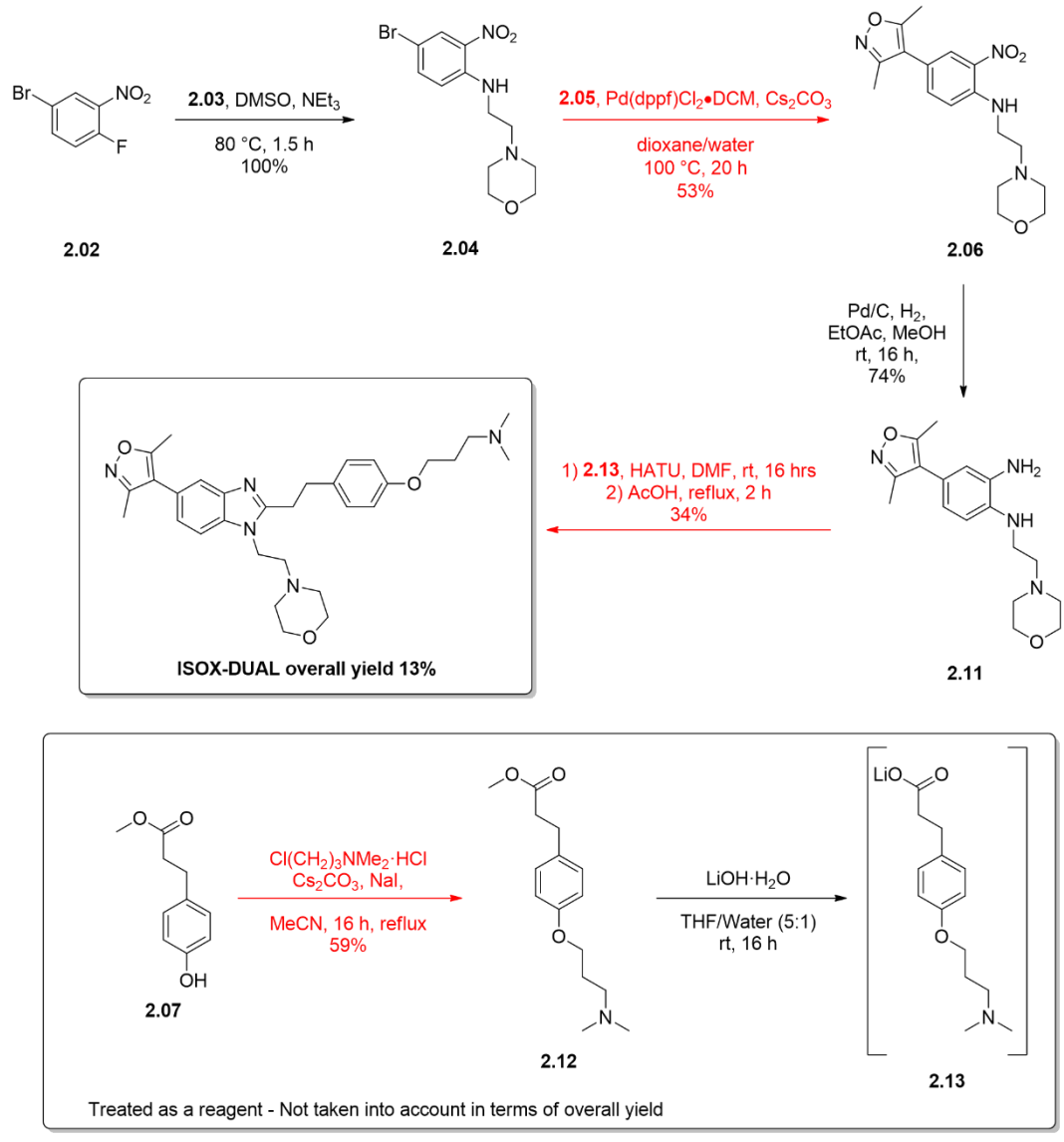

*Scheme 2.2: Synthesis scheme for ISOX-DUAL from Tocris showing each reaction and the yield obtained. The overall yield treated **2.13** as a reagent and was not a contributing factor to yield calculation.*

2.2 Results and Discussion

2.2.1 Nucleophilic Aromatic Substitution

2.2.1.1 Microwave Assisted Organic Synthesis

The use of microwaves in the synthesis of organic components has been a growing field in Chemistry since the late 1990s.[290] Conventional heating through mantles, oil baths and sand baths is a slow, energy inefficient process due to the heat energy being transferred to the surface of the vessel, which then heats the reaction (Figure 2.3). This means the reaction surface is a higher temperature than the reaction mixture, which can lead to local hot-spots and in some cases degradation of reaction components.[290] However, microwave assisted organic synthesis (MAOS) uses microwaves to generate heat within the material first, which then heats the volume. This is advantageous due to very rapid heating rates, considerably reduced reaction times, and reduced risk of dangerous hot spots forming.[291]

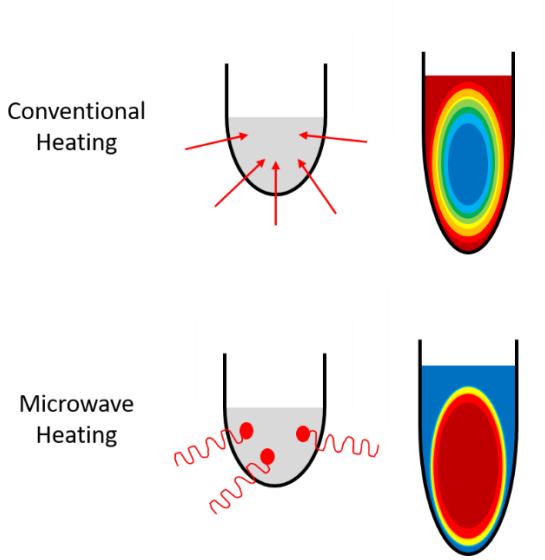

Figure 2.3: Illustration of heating conventional and microwave heating styles.

MAOS is based on the efficient heating of reaction components by the microwave dielectric heating effect, which is dependent on the ability of the reaction medium to absorb microwave energy and convert it to heat. This occurs through two mechanisms: dipolar polarisation and ionic conduction.[292]

Irradiating at microwave frequencies induces the dipoles and ions to move in the medium by interaction. Realignment with respect to an oscillating electric field loses energy in the form of heat through molecular friction and dielectric loss.[293] The interaction of solvent with microwave radiation has been described as complex, and depends on the viscosity and dielectric properties of the solvent. The best measurement for this is to compare their loss tangent values (tanδ). This is described as the loss angle (δ), which is the ratio between the

dielectric constant (ε) and the loss factor (ε"), which quantifies the solvents efficiency to convert the absorbed energy into heat.[294]

*2.2.1.2 Synthesis Scope of **2.04** via Microwave-Mediation.*

The initial step in the proposed synthesis of ISOX-DUAL involves an S_NAr reaction between 4-bromo-1-fluoro-2-nitrobenzene (**2.02**) and 4-(2-aminoethyl)morpholine (**2.03**). This methodology was replicated using literature conditions (Table 2.1, entry 1) and then modified to a microwave protocol to allow for the rapid synthesis of **2.04**.

*Table 2.1: Aromatic nucleophilic substitution of **2.02** to achieve compound **2.04**.*

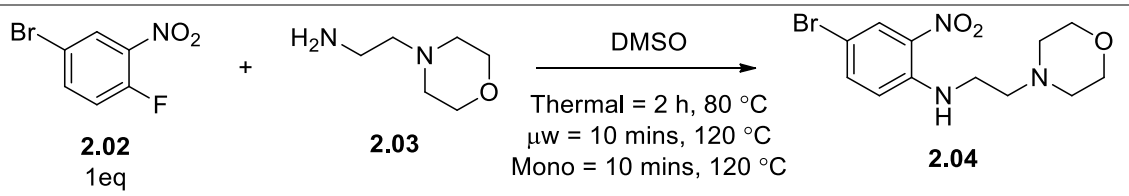

Entry	Method	2.02 (mmol)	2.03 (mmol)	Triethylamine (mmol)	Yield (%)	Purity[c] (%)
1[2]	Thermal	168 (1 eq.)	208 (1.24 eq.)	210 (1.25 eq.)	80	N/A
2[b]	Thermal	341 (1 eq.)	426 (1.25 eq.)	426 (1.25 eq.)	Quant	N/A
3	Thermal	0.5 (1 eq.)	0.625 (1.25 eq.)	0.625 (1.25 eq.)	88	75
4	μw[a]	1 (1 eq.)	1 (1 eq.)	1.2 (1.2 eq.)	quant	>99
5	μw[a]	1 (1 eq.)	2.5 (2.5 eq.)	0 (0 eq.)	quant	>99
6	Mono[d]	1 (1 eq.)	1 (1 eq.)	1.2 (1.2 eq.)	quant	>99
7	Mono[de]	1 (1 eq.)	2.5 (2.5 eq.)	0 (0 eq.)	quant	>99
8	μw[ae]	5 (1 eq.)	5.05 (1.01 eq.)	6 (1.2 eq.)	quant	>99
9	μw[ae]	25 (1 eq.)	25.25 (1.01 eq.)	100 (4 eq.)	>99	96

[a]μw = Microwave. [b] Industrial methodology. [c] Purity determined by LC-MS. [d]Mono = Anton Parr Monowave. [e] DMSO free.

Application to microwave-mediation was successful, giving high yields and high purities with no need for purification. The reduced reaction time and scale of 25 mmol in the microwave allows for automated large scale batch synthesis rather than a larger reaction vessel through conventional heating. The reaction also works well when removing DMSO as the solvent, and increasing the equivalents of the amine (Table 2.1, entries 7-9), which removes the potential for DMSO to degrade and explode the reaction vessel in higher temperature and pressure conditions.[295]

2.2.2 **Suzuki-Miyaura Cross-Coupling**

2.2.2.1 Suzuki-Miyaura Cross-Coupling

First reported in 1979, the Suzuki-Miyaura coupling described the palladium catalysed cross-coupling reaction of alkenylboranes with alkenyl or alkyl halides.[296] Through extensive research it had been shown that the coupling could incorporate aromatic, alkyl, alkenyl and alkynyl halides, and also pseudo halides such as triflates.[297] In recent years, research has been described and shown that nitro groups can also couple in this reaction.[298,299]

Akira Suzuki, along with Richard Heck and Ei-ichi Negishi was awarded 1/3 of the Nobel Prize in chemistry 2010 for palladium catalysed cross couplings in organic synthesis.[300] Over the years the Suzuki-Miyaura coupling has proven to be a highly used reaction within many drug discovery programs, allowing for the combination of complex or elaborated fragments together.[301] A general catalytic cycle for this cross-coupling mechanism is described in Scheme 2.3.

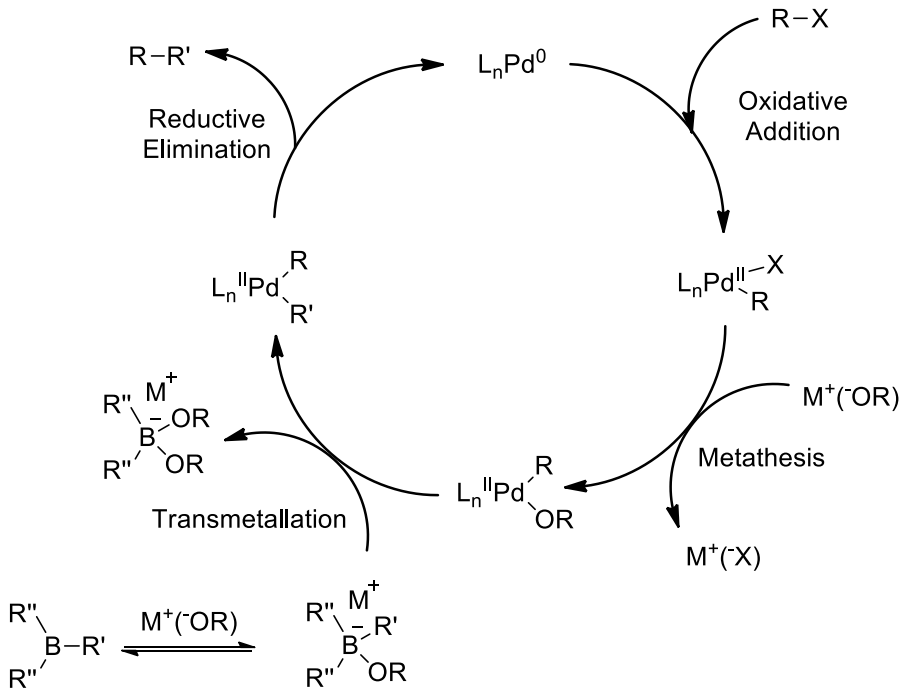

Scheme 2.3: A general catalytic cycle for the Suzuki-Miyaura coupling.[301]

2.2.2.1.1 Side Reactions of the Suzuki-Miyaura Cross-Coupling

As the Suzuki-Miyaura cross-coupling has been extensively researched since initial reports, understanding the mechanisms and potential side reactions that can occur during this cross-coupling has also been explored. The choice of solvent can play a key role in promoting or preventing these unwanted side reactions. The two main side reactions discussed here are dehalogenation and protodeboronation.

Dehalogenation is where the C-X halide bond is replaced with a C-H bond and is a frequent competing reaction. The aryl halides are prone to dehalogenation during the coupling reaction, thought to occur through displacement of the halide by the solvent of reaction and subsequent β-hydride elimination.[302] The hydrodehalogenation reaction described in Scheme 2.4, is promoted by the presence of strong bases, where deprotonated alcohol solvents in these circumstances act as alkoxide ligands. Combinations of π-acidic, back bonding ligands also result in significant quantities of hydrodehalogenated product.[303] Aqueous media can also be a contributing factor to hydrodehalognation.[304]

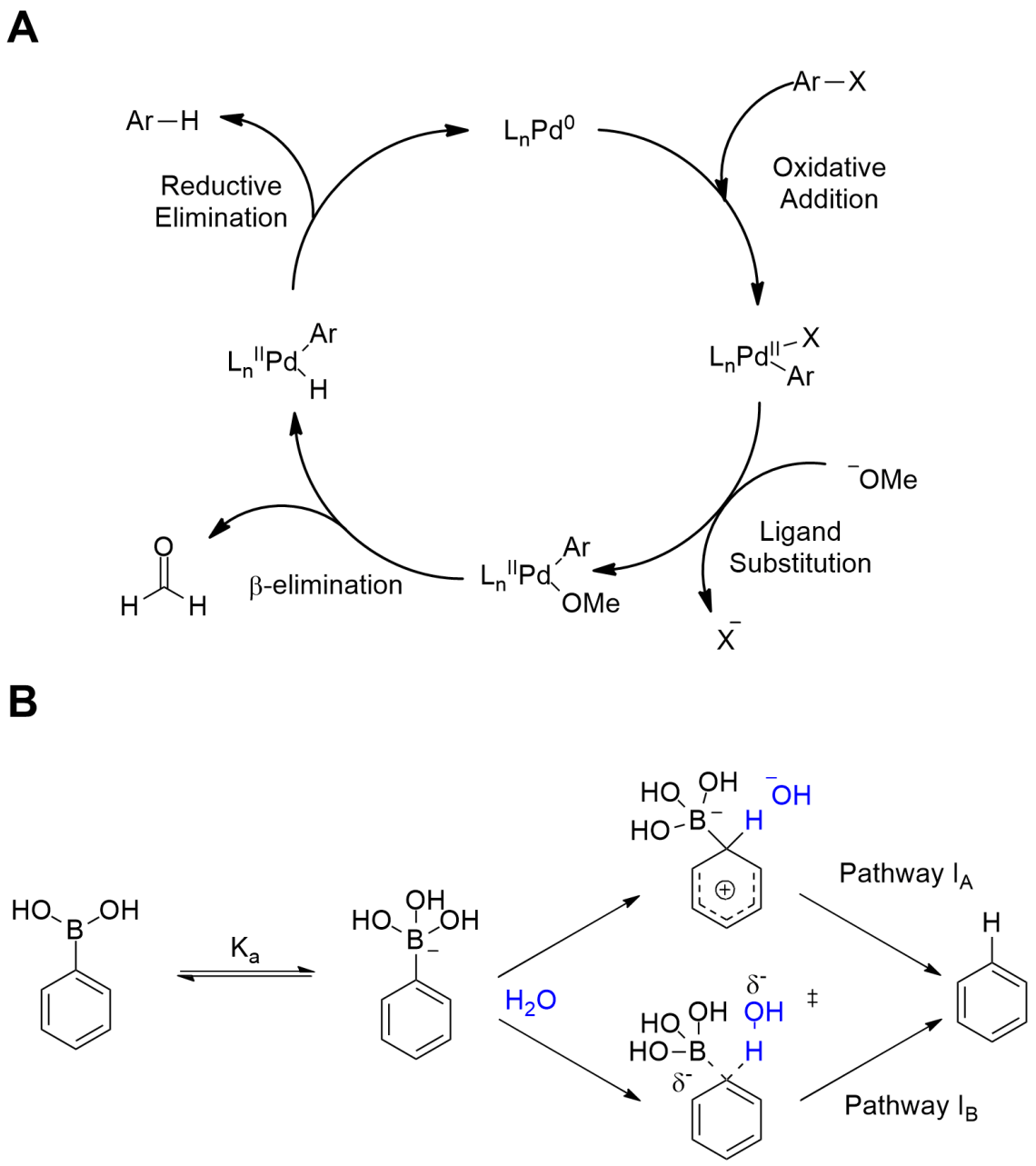

Scheme 2.4: A) A literature proposed catalytic cycle for hydrodehalogenation of the Aryl-halide component.[302] *B) A proposed mechanism for the protodeboronation of an aromatic species in basic media.*[305]

Protodeboronation (Scheme 2.4B) is where the C-B bond is converted to a C-H bond and is one of the most typical side reactions seen in Suzuki couplings. Substituents on or within the aromatic ring can either assist or help prevent this side reaction. The mechanism was proposed to go through a stepwise pathway (I_A) or a concerted (I_B) mechanism.[305] Alongside this, the boronate species are also prone to homo-coupling, and conversion to a phenol.[306]

Isoxazolyl boronic acid systems exhibit protodeboronation *via* a mechanism in which base catalyses the decomposition of the boronate. Computational analysis of this specific moiety has been calculated for the transition state in the protodeboronation mechanism. These

suggest that the heterocycle needs to be able to stabilise both the deprotonated boronate and the carbanion arising from C-B fragmentation. C-Nσ* and C-Oσ* orbitals are available in the 3,5-dimethylisoxazole boronic acid, and may explain why significant protodeboronation was observed in the substrate scope performed.[307] Typical alternatives to boronic acids as coupling reagents include boronic acid pinacol esters, MIDAs and organotrifluoroboronates.

MIDA boronates are a class of compounds developed by Burke and co-workers and are described as air stable and can be stored at room temperature with no degradation observed. These compounds also do not undergo Suzuki-Miyaura couplings under anhydrous conditions. While the hydrolysis of MIDA boronates can be rapid in aqueous hydroxide, this can be slowed down with weaker bases such as potassium phosphate to allow for slow release of the boronic acid at a rate slower than the catalytic turnover, which would reduce the quantity of protodeboronation observed.[308]

An alternative to MIDA boronates as a way of overcoming the undesirable protodeboronation is to use potassium organotrifluoroborates. These compounds can be easily synthesised from organoboron reagents by the addition of KHF_2 (Scheme 2.5). These compounds are described as air and moisture stable and have been demonstrated to give high isolated yields when applied into Suzuki-Miyaura cross-couplings.[309] Further examples of organofluoroborates can be seen with diazonium tetrafluoroborates.[310]

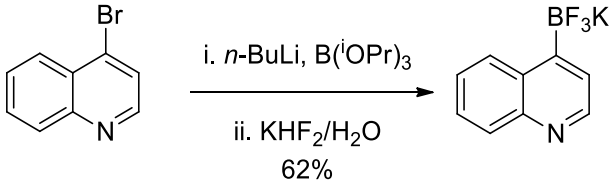

Scheme 2.5: Synthetic procedure for the synthesis of organotrifluoroborates.[309]

To provide an alternative to the two boronate species tried, a MIDA boronate was synthesised and trialled in the reaction scope. Previous work done by the Spencer group had optimised a series of conditions for synthesising these MIDA boronates *via* microwave-mediation (

Table 2.2).[311]

*Table 2.2: Temperature screen for the synthesis of MIDA boronate **2.14a**, with the optimal condition highlighted.*

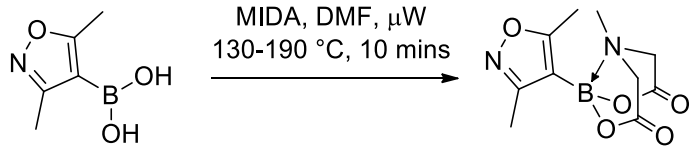

2.05 **2.14a**

Entry	Temperature[a] (˚C)	Yield[b] (%)
1	130	60
2	140	66
3	150	67
4	160	71
5	170	74
6	180	55
7	190	45

[a] Yield calculated from the isolated product following trituration.

The reaction screen highlighted 170 ˚C (

Table 2.2, entry 5) as the optimal temperature to synthesise this MIDA boronate, whereas the use of higher temperatures led to apparent degradation of the product, resulting in a lower isolated yield. The success of the reaction was confirmed by the presence of the doublets seen in the ^{1}H NMR at δ = 4.12 ppm and 4.32 ppm containing germinal couplings (17.3 Hz) at the between the two diastereotopic protons on the CH_2 of MIDA (Figure 2.4). The structure of the MIDA boronate was confirmed by crystallography from single crystals obtained by vapour diffusion from DMF/hexane.

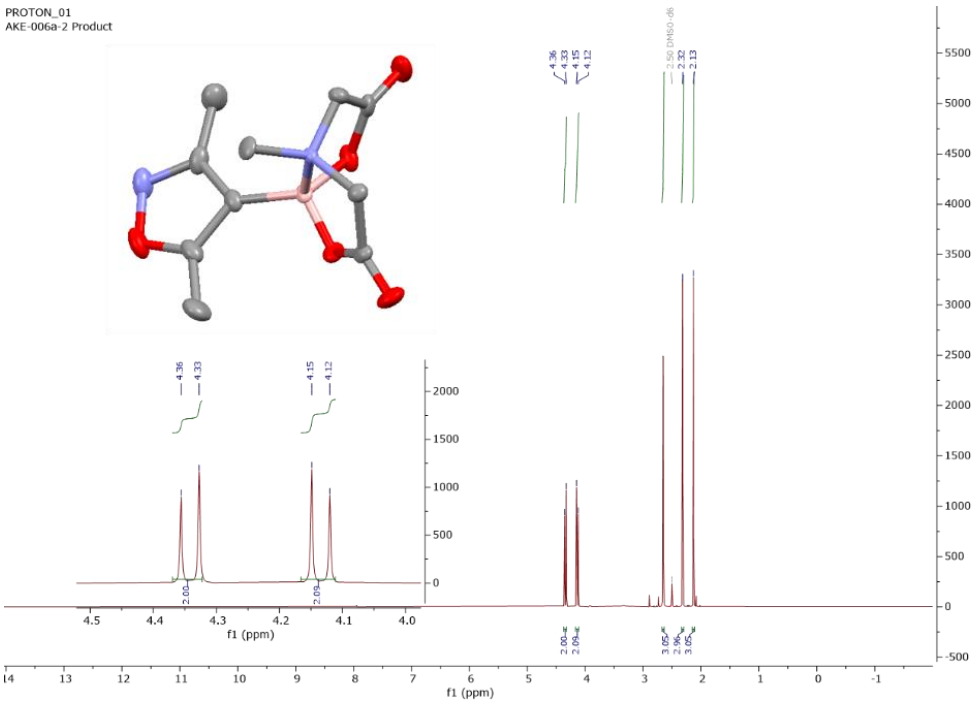

*Figure 2.4: ^{1}H NMR spectrum and crystal structure of MIDA boronate **2.14a**, highlighting the doublets at δ= 4.12 and 4.33 ppm, which display germinal couplings of 17.3 Hz.*

The next section will address the poor yielding Suzuki Miyaura reaction reported in Scheme 2.2 where a choice of boronic acid derivatives and coupling conditions will be considered.

2.2.2.2 Suzuki-Miyaura Reaction Screening and Optimisation

The next stage of the synthesis of the diamine intermediate (**2.11**) involved a Suzuki-Miyaura cross-coupling reaction between **2.04** and 3,5-dimethylisoxazole boronic acid. Table 2.3 describes the initial conditions tested; literature yields for this reaction were not ideal and are listed for comparison (Table 2.3, entries 1 & 2). The crude conversions calculated for each coupling were performed taking into account a de-halogenated product (**2.15**) formed from this reaction by subtracting the conversion of this compound from the product to afford a crude measurement.[311] The synthesis of **2.15** is described later as part of the reduction investigation. This species was proved to exist through an unequivocal synthesis from 1-fluoro-2-nitrobenzene and 4-(2-aminoethyl)morpholine and observing identical chemical shifts in both media.

*Table 2.3: Reaction screening for the Suzuki-Miyaura cross-coupling of compound **2.04**, using 5 mol% catalyst loading, 2.6 eq. base and 1.12 eq. boronate.*

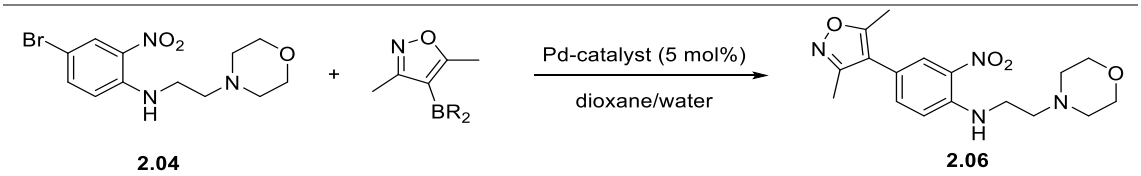

2.04 **2.06**

Entry	Pd-catalyst	BR_2	Base 2.6 eq.	Method	Time (h)	Temp (˚C)	Crude NMR Conversion[a] (%)	Yield[b] (%)
1[c]	$PdCl_2(dppf)\cdot DCM$	Acid	Cs_2CO_3	Thermal	20	100	N/A	53
2[2]	$PdCl_2(dppf)\cdot DCM$	Acid	Cs_2CO_3	Thermal	20	100	N/A	62
3	$PdCl_2(dppf)\cdot DCM$	Acid	Cs_2CO_3	Thermal	20	100	8	N/A
4	$PdCl_2(dppf)\cdot DCM$	PE[d]	Cs_2CO_3	Thermal	20	100	73	N/A
5	$PdCl_2(dppf)\cdot DCM$	Acid	Cs_2CO_3	Thermal	20	100	22	N/A
6	$PdCl_2(dppf)\cdot DCM$	PE	Cs_2CO_3	µw	3	150	73	N/A
7	$PdCl_2(dppf)\cdot DCM$	Acid	Cs_2CO_3	µw	3	150	54	N/A
8	$PdCl_2(dtbpf)$	PE	Cs_2CO_3	µw	3	150	71	N/A
9	$PdCl_2(dppf)\cdot DCM$	PE	CsF	µw	3	150	74	N/A
10	$PdCl_2(dtbpf)$	PE	CsF	µw	3	150	47	N/A
11	$PdCl_2(dppf)\cdot DCM$	PE	K_3PO_4	µw	3	150	72	N/A
12	$PdCl_2(dtbpf)$	PE	K_3PO_4	µw	3	150	82	N/A
13	$PdCl_2(dppf)\cdot DCM$	MIDA	K_3PO_4[e]	µw	3	150	51	N/A
14	$PdCl_2(dppf)\cdot DCM$	MIDA	K_3PO_4	µw	3	150	60	N/A

µw = Microwave. [a] Calculated from rough ^1H NMR integration of crude mixture, literature protocols did not calculate conversions. [b] Isolated yield reported for entries 1 and 2 and not obtained for reaction scoping. [c] Tocris methodology. [d] PE = Pinacol Ester [e] 7.5 eq. K_3PO_4 used.

Investigations into the Suzuki cross coupling began by replicating the methodology utilised by literature and industry, resulting low conversion rates (Table 2.3, entry 3) due to protodeboronation of the boronic acid. To ensure the reagent was not the issue the reaction was replicated with fresh reagent. However, the conversions were still not able to be matched (Table 2.3, entry 5). Switching the boron component to the pinacol ester (Table 2.3, entry 4) led to a significant boost to conversion, due to being more stable than their acid counterparts, resulting in less protodeboronation.[312]

To speed up reaction screening, the methodology was applied to a microwave reactor. The translation to a microwave protocol led to similar conversions for the pinacol ester (Table 2.3, entry 6) but increased the conversion for the boronic acid method (Table 2.3, entry 7),

suggesting that the increased the rate of catalytic turnover, reducing the effect of protodeboronation on conversion. Changing the precatalyst from (1,1'-bis(diphenylphosphino)ferrocene)palladium(II) dichloride ($PdCl_2$(dppf)·DCM) to 1,1'-bis(di-tert-butylphosphino)ferrocene-palladium dichloride ($PdCl_2$(dtbpf)) (Table 2.3, entry 8) led to no notable change in conversion (Table 2.3, entry 6). Utilising either CsF or K_3PO_4 as bases with $PdCl_2$(dppf)·DCM gave no significant changes to conversion (Table 2.3, entries 9, 11), however, using CsF with $PdCl_2$(dtbpf) lead to lower conversion (Table 2.3, entry 10) than K_3PO_4 (Table 2.3, entry 12).

Utilising MIDA boronate **2.14a** for the Suzuki-Miyaura coupling (Table 2.3, entries 13, 14) did not result in as high a conversion, to that which was observed with the pinacol ester. Varying the quantities of base for the coupling with the MIDA boronate was not fully explored due to the more successful coupling with the pinacol ester. The best conversions from the scope highlighted in green in Table 2.3 were performed on a 1 mmol scale to allow for the isolation of the product to record a yield, rather than the utilisation of crude NMR conversion; the best conditions within this series were highlighted in green within Table 2.4. All conditions in this screen utilised $PdCl_2$(dppf) as the precatalyst as these led to the best conversions overall in Table 2.3. The use of CsF and K_3PO_4 led to identical yields (Table 2.4, entries 3, 4), Cs_2CO_3 led to a reduced yield (Table 2.4, entry 2) and reducing the catalyst loading from 5 mol% to 1 mol% also led to a reduced yield (Table 2.4, entry 5).

Investigations using other catalysts were not performed at this stage due to the high conversions seen with highlighted entries in Table 2.2, and upon scaling this chemistry to 1 mmol scale, a 95% isolated yield was obtained (Table 2.4, entry 4).

Table 2.4: Scale up synthesis of the best conditions from Table 2.3.

Entry	Method[a]	Base	Yield[b] (%)
1	Thermal	CsF	74
2	µw[c]	Cs_2CO_3	79
3	µw	CsF	95
4	µw	K_3PO_4	95
5[d]	µw	K_3PO_4	66

[a] 1 mmol scale, all reactions used $PdCl_2$(dppf) as the catalyst and 1,4-dioxane as the solvent. Heated for 3 h in the microwave. [c] µw = microwave. [d] Isolated after purification [c]1mol% $PdCl_2$(dppf)

Using the optimised procedure identified (Table 2.4, entry 5), a series of analogues were synthesised (**2.16** – **2.21**) with varying heterocyclic boronic acid pinacol esters (Figure 2.5). The

yields for these analogues were all high, except for **2.17**. This shows that these reaction conditions have a broad reaction scope. It was thought that **2.17** had experienced thermal degradation within the reaction mixture, as no product, de-protected pyrazole or starting material could be isolated.[313] This compound was still included within the scope summary in order to show an observed limitation for the optimised conditions.

Performing these conditions on **2.06** with thermal conditions reduced the yield down to 76%, most likely due to degradation of the boronic acid starting material, and so future reactions on a larger scale should utilise microwave conditions with batches.

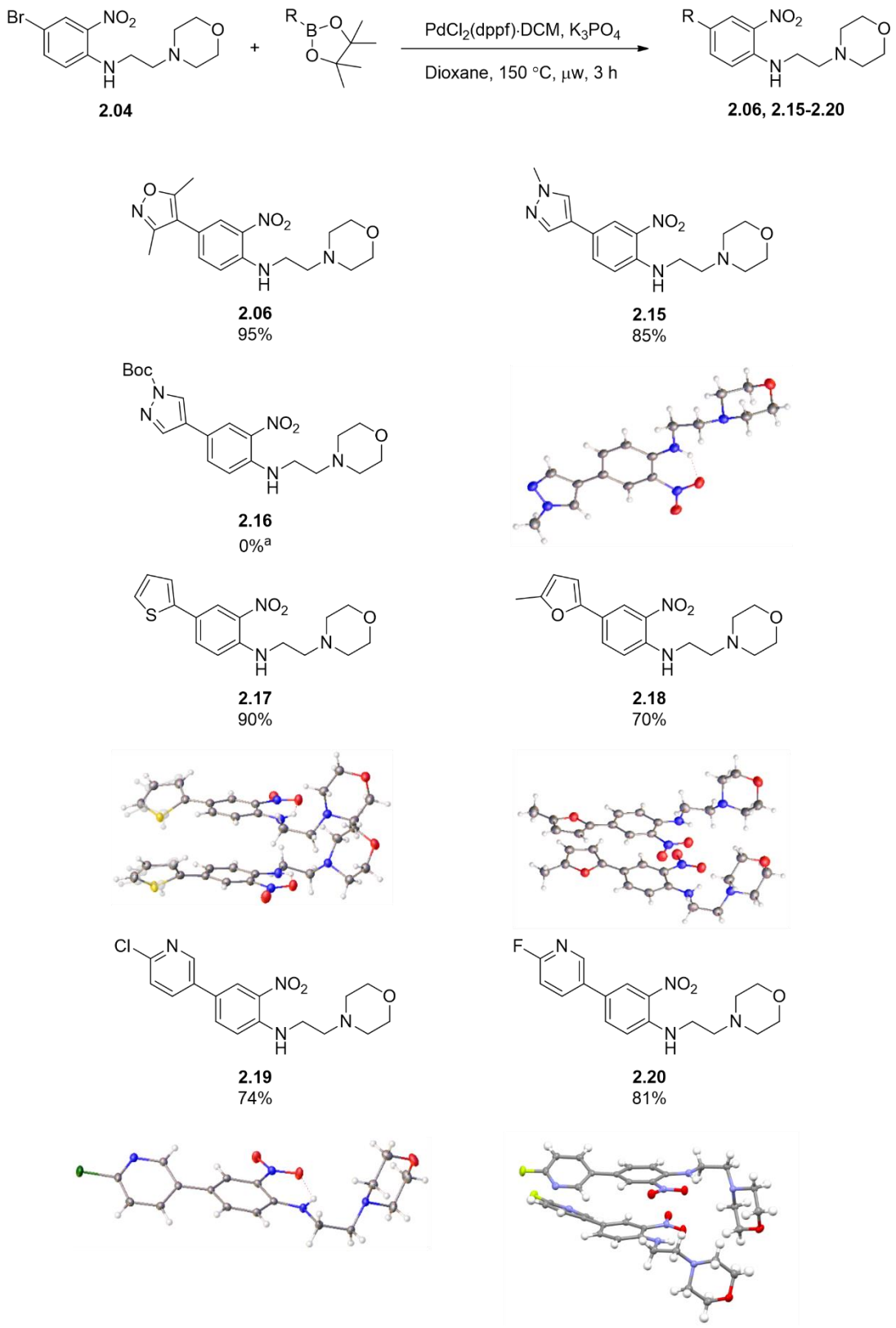

Figure 2.5: Suzuki-Miyaura analogues. [a] Thermal degradation of the Boc-group and no components could be isolated.

2.2.3 **Reduction of the Nitro Moiety**

The final reaction in the synthesis of the diamine intermediate (**2.11**) is a nitro reduction of the Suzuki-Miyaura product. A series of conditions were attempted to explore the potential to increase the yield of this reduction. The previously reported procedure was tested here alongside additional methodologies from the literature, and previous work in the group and conditions are given in Table 2.5. $Mo(CO)_6$ and a series of transfer hydrogenations were investigated initially due to the safety issues associated with use and storage of hydrogen.[314]

*Table 2.5: Conditions explored for the reduction of nitro-amine **2.06** to diamine **2.11***

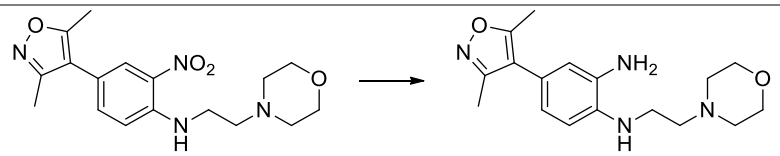

2.06 **2.11**

Entry	Methodology	Reaction Outcome
1[315]	$Mo(CO)_6$, DBU, EtOH, µw[a]	Complex mixture
2[316]	MoO_4, N_2H_4, EtOH	No Reduction
3[317]	CIP[b], TPGS-750-M, NH_4Cl	Complex mixture
4[318]	Zinc, Formic Acid	No Reduction
5	Pd/C Hydrogenation; 1 atm	Poor Yield/Complex Mixture
6[319]	Pd/C Hydrogenation; 4 atm[c]	Degradation
7[43]	1M $Na_2S_2O_4$, EtOH, 10% NH_3	Complete Conversion

[a] µw = microwave [b] CIP = Carbonyl Iron Powder. [c] 4 atm performed in COWare.

2.2.3.1 $Mo(CO)_6$ and Transfer Hydrogenations

Initial scoping of the reduction from **2.06** to **2.11** utilised a $Mo(CO)_6$ mediated nitro reduction. This was performed in the microwave following a literature procedure from previous work within the Spencer group and adapted utilising $Mo(CO)_6$ (1 eq.), DBU (3 eq.) and EtOH as the solvent, with a reaction time of 30 min.[315] The desired product could not be isolated from the crude mixture due to co-elution of another species. Analysis of this mixture *via* ^{1}H NMR suggests the fraction set contained both the product and a potential intermediate, which was thought to be a nitroso moiety, as the chemical shifts of the protons on the phenyl ring were in concordance with literature values for a similar substrate (Figure 2.6). However this theorised intermediate was not able to be isolated or characterised.[320–322] Increasing the equivalents of $Mo(CO)_6$ or DBU from 1 to 2 and 3 to 6 respectively did not drive the reaction toward completion. Neither reaction time nor temperature were investigated for this reduction.

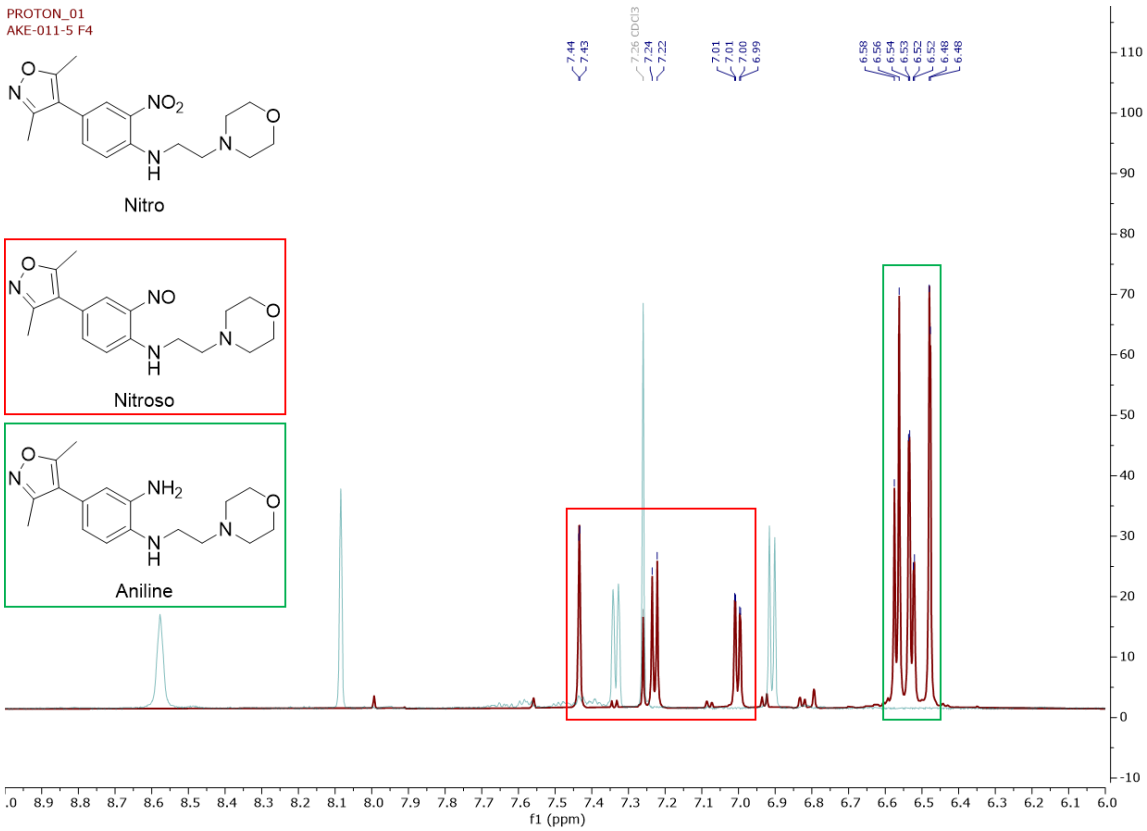

Figure 2.6: Structures of the species present during the $Mo(CO)_6$ mediated reduction. ^1H NMR spectrum displaying the nitro starting material (blue spectrum), nitroso intermediate (red spectrum δ=6.99 ppm – 7.44 ppm) and aniline product (red spectrum δ=6.48 ppm – 6.58 ppm).

Another molybdenum reagent was sourced to perform a transfer hydrogenation from hydrazine.[316] This reaction was trialled using 3 and 6 equivalents of hydrazine, monitoring the reaction after 30 minutes showed no product in the LC-MS trace, and leaving the reaction to react overnight yielded no additional conversion to the desired diamine **2.11**.

Moving away from molybdenum-mediated nitro reductions, an iron-mediated reduction was trialled using carbonyl iron powder (CIP). This is reported to be a safe, mild, efficient and environmentally responsible reduction of nitro compounds, due to the lack of organic solvent.[317] The procedure was reported to have good substrate scope, only seeing reduction of the nitro moiety, over other reducible moieties. This reaction was performed in a solution of TPGS-750-M (2% in water), a surfactant which has received attention in literature as an effective nanomicelle-forming species.[317]

Surfactants as amphiphilic molecules mediate between aqueous and organic species. Large quantities of water drive the formation of spontaneous micellar aggregates in the solution, with the hydrophobic components aggregating together. The use of surfactants allows for the achievement of catalysis or reactions in water, and are highly economical, due to their usage in day to day detergency.[323]

Applications of TPGS-750-M as a surfactant within aqueous media has been seen in reactions such as cross-couplings, radical reactions, and olefin metathesis; all reported with high yields.[323,324] The reduction of **2.06** to **2.11** was tested on a smaller scale than the literature protocol to remove the necessity of an overhead stirrer. Analysis led to the same observed issues with $Mo(CO)_6$ reduction, where the isolated compound was a mixture of the nitroso and aniline species. Addition of more equivalents of CIP and NH_4Cl did not drive the reaction to completion.

A zinc and formic acid combination was also trialled, however this reduction gave no conversion from the nitro starting material.[318]

2.2.3.2 Pd/C Hydrogenation

After testing alternative reductions with various heterogeneous metal reagents, and proton sources with little success, the focus was shifted back to hydrogenation. Pd/C is a robust and reliable reduction catalyst which is still being explored in uses such as nanoparticles and continuous flow, to avoid waste on industrial scale synthesis.[325–327] Pd/C has also been shown to reduce groups in aqueous media with TPGS-750-M.[327]

Replication of the industrial protocol showed the presence of the product after 16 hours of reaction and residual starting material *via* TLC. Purification with a gradient of 0 – 10% methanol in dichloromethane afforded the product as an impure white solid. The signals that were tentatively assigned to a nitroso derivative were also observed within the ^1H NMR spectrum. Increasing the reaction time, catalyst loading and repeatedly refilling the balloons with more H_2 did not convert any more of the mixture to the aniline product. This led to the hypothesis that either the reaction set up had leaks and/or these conditions were not enough to drive product formation.

A recent report from the Watson group performing a one pot synthesis of amino-azaheterocycles involved a Suzuki coupling followed by a ring reduction.[319] These conditions allow for certain reagents to be physically separated through the use of COWare, a multi-chamber reaction vessel capable of withstanding pressures up to 4 atmospheres. COWare was initially developed for generating lower molecular weight gases *in situ*, and has been used in many reductions and carbonylations.[328–333] For the purposes of this reduction, the reaction mixture was prepared in the right chamber and the left chamber had a mixture of Zn pellets and 7M HCl (Figure 2.7, A).

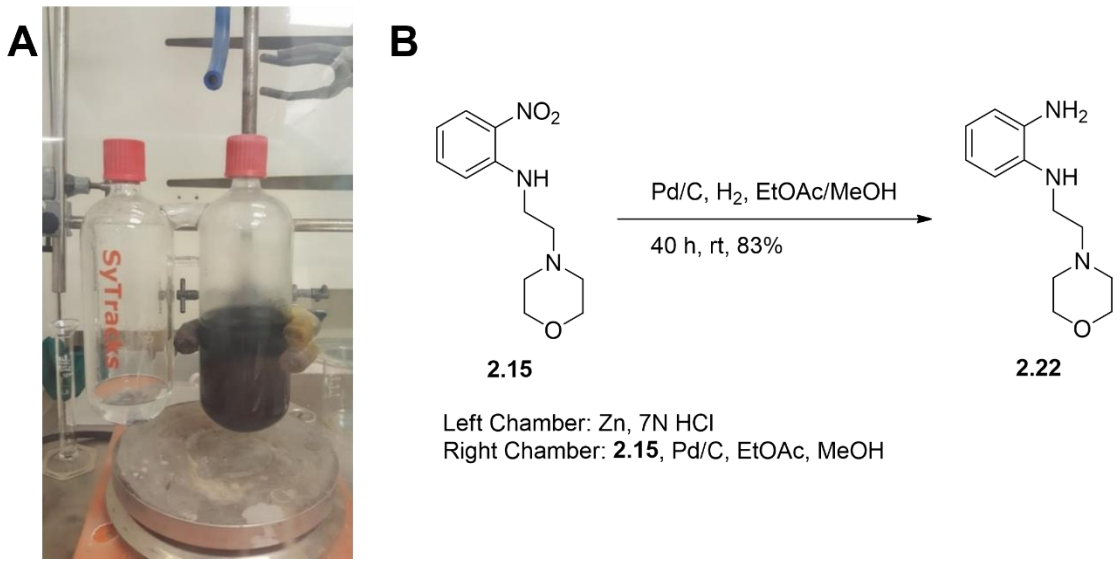

*Figure 2.7: A) Photo of the COware reaction set up to illustrate the bi-chamber reaction vessel with Zn/HCl in the left chamber and the Pd/C Hydrogenation in the right chamber. B) Scheme of reaction from **2.15** to **2.22**.*

The reduction conditions were initially performed on a similar substrate, **2.15** (Figure 2.7, B), which was cheaper to make, and allowing for methodology tests for benzimidazole formation (Table 2.6). Initial testing of this reaction did not immediately give full conversion to the product, due to the complete consumption of hydrogen. This was because of the maximum safety pressure of the reaction vessel and the generation of more H_2, through the addition of another aliquot of HCl, drove the reaction to the desired diamine (**2.22**) with an isolated yield of 83%.

As this reduction achieved full conversion to the desired product, the methodology was then applied to the synthesis of **2.11** (Scheme 2.6). This reduction went to completion, as no starting material was seen in the LC-MS, however the product signal had an ion with an m/z of 319, which was higher than expected (ca. m/z = 317).

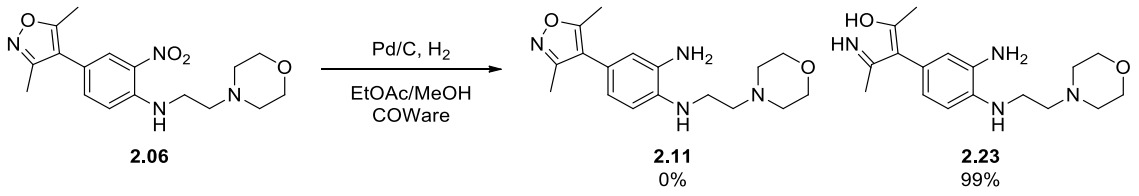

*Scheme 2.6: COWare reduction of **2.06** to attempt to synthesis **2.11**, showing observed imine enol product **2.23** instead.*

Analysis of the ^{1}H NMR spectrum of the product showed the dimethyl signals of the isoxazole ring had shifted up field from δ = 2.25 and 2.37 ppm to δ = 1.85 and 1.70 ppm (Figure 2.8). The movement of these signals indicated a loss of aromaticity, suggesting an opening of the

isoxazole ring to an imine enol product (**2.23**) as the likely cause for this shift, due to the lability of the N-O isoxazole bond.[334,335]

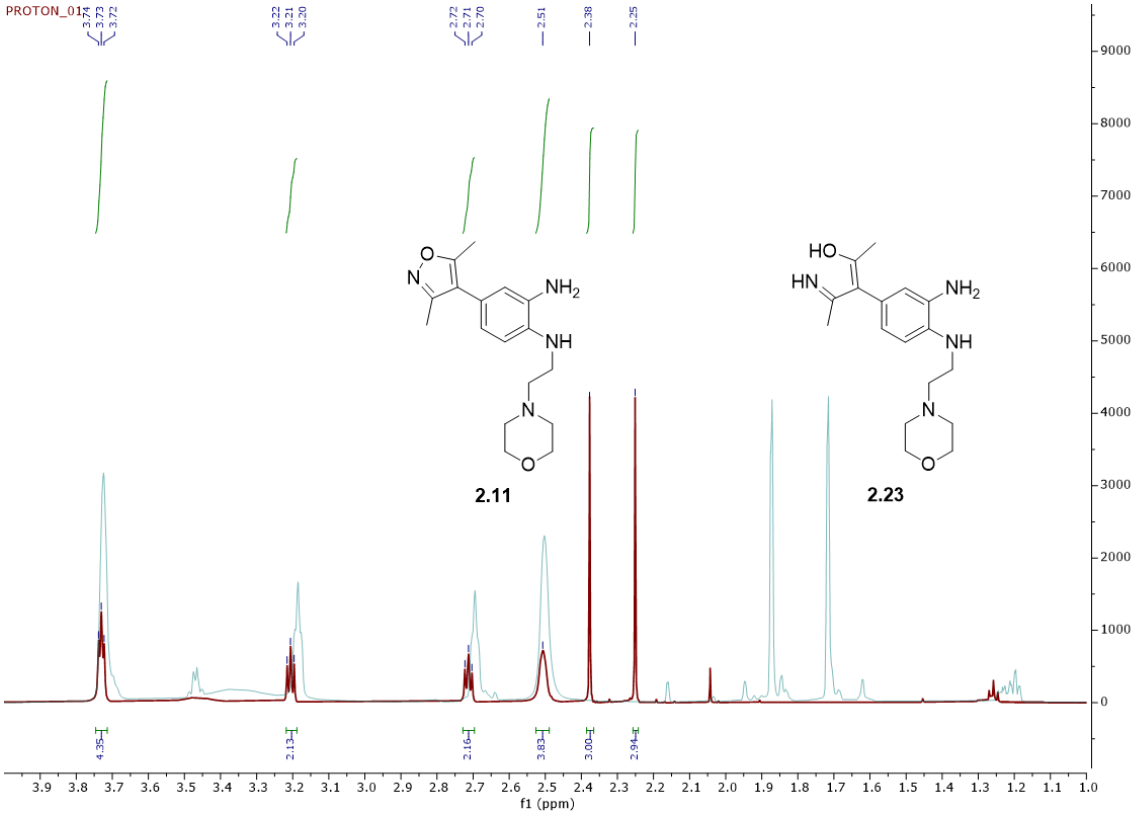

*Figure 2.8: Overlapped ^{1}H NMR spectra for the aniline product (**2.11**) and the imine-enol (**2.23**) product obtained from the reduction.*

2.2.3.3 $Na_2S_2O_4$ Reduction

As discussed previously in Section 2.1, Brennan and co-workers were investigating the synthesis of a novel CBP/p300 inhibitor (SGC-CBP30).[43] A key reaction utilised a reduction with sodium dithionite (Scheme 2.7), which is mild and compatible with polar protic solvents such as water and ethanol, making this an attractive methodology for scaling up.[30,31]

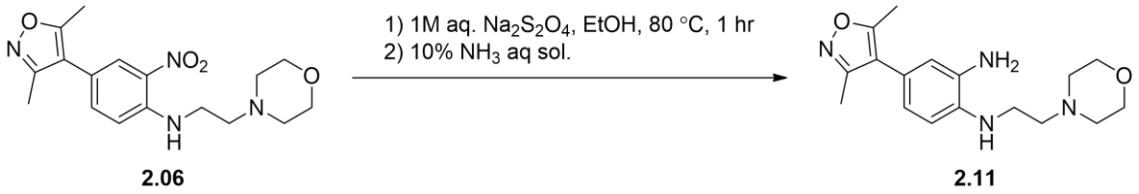

*Scheme 2.7: Scheme for the reduction of **2.06** to **2.11** as outlined by Brennan and co-workers.*

Replication of this protocol resulted in the successful reduction of **2.06** to **2.11**, affording a yellow gum with a yield of 81% (Scheme 2.7).[43] The chemical shifts observed in the ^{1}H NMR spectrum of the product were in agreement with those of an authentic sample of **2.11**. Further confirmation of the structure of **2.11** was by the correct mass observed by LC-MS.

2.2.4 **Synthesis of the Acid Precursor**

Initially, the reported protocol was repeated for the alkylation from **2.07** to **2.12** (Scheme 2.8), however a low yield of 18% was obtained, rather than the 59% reported.

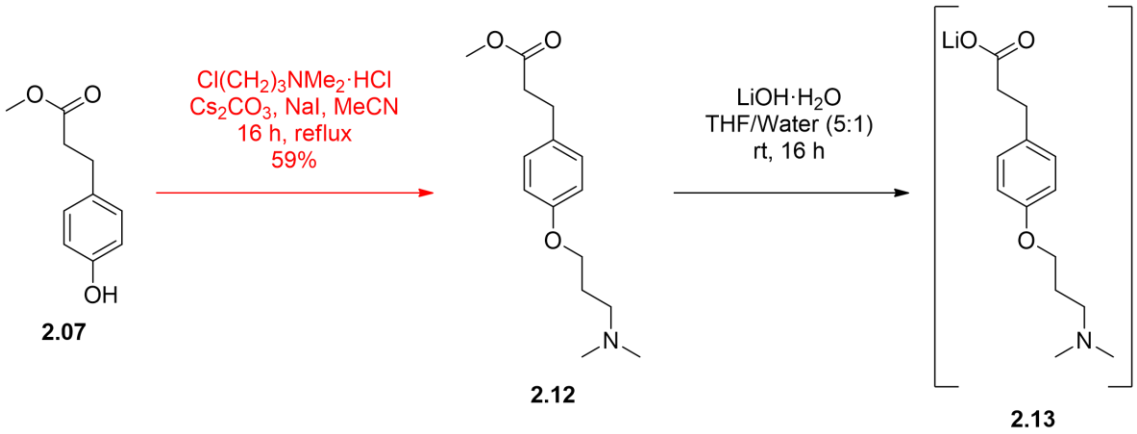

*Scheme 2.8: The industrial protocol from Scheme 2.2, to acid intermediate **2.13**.*

The reaction was trialled in a microwave using the same reagents and quantities but with heating at 130 ˚C for 7 minutes. However, no crude product was obtained after the work up, leading to suggest the reaction failed, as the starting material is removed in a NaOH wash. Next, the solvent was changed from MeCN to EtOH and the reaction was heated at 125 ˚C for 6 min in the microwave. This reaction, post work-up, gave a compound with a yield of 77%, however, the ^{1}H NMR spectrum showed two additional signals, a quartet at δ= 4.1 ppm which integrates for 2H and a triplet at δ= 1.22 ppm which integrates for 3H. This suggested that the product had also undergone a transesterification with the EtOH solvent (**2.24**). To avoid this the reaction was trialled in Methanol, ^{t}BuOH and dioxane, but did not result in a successful outcome.

As these tests yielded no product, the original methodology was reinvestigated. Initially, the equivalents of the alkyl chloride and base were increased from to 2.5 and 5 eq. respectively. The yield of this reaction increased to 87%. The alkylation conditions allow for an *in-situ* Finkelstein reaction of the alkyl chloride, as these conditions are usually performed with an excess of halogen salt, the quantities of NaI were doubled.[338] Adopting these conditions led to a similar yield to that obtained previously and varying the equivalents were not investigated anymore due to the yield increasing to a more acceptable level.

The ester hydrolysis step to form **2.13** from **2.12** (Scheme 2.8) was replicated from the reported procedure, stirring in a 50% THF/water solution in the presence of LiOH·H_2O (1.1 eq.). No aqueous work up was reported or performed on this reaction due to the product being a zwitterion.

2.2.5 **Amide Coupling and Benzimidazole Cyclisation**

Investigations into the final step in the formation of ISOX-DUAL initially utilised diamine fragment **2.22** from the reduction optimisation (Chapter 2.2.3.2), to spare the more expensive isoxazole moiety (**2.11**). Both 3-(4-hydroxyphenyl)propionic acid and **2.13** were utilised in this scope (Table 2.6). A small screen of amide coupling reagents was performed to see if the isolated yield could be increased from the initial reported 34% with HBTU (Scheme 2.2).

*Table 2.6: Reaction screening conditions for the amide coupling and benzimidazole cyclisation to synthesise compounds **2.25**, **2.26**, **2.27**, **2.10** and ISOX-DUAL.*

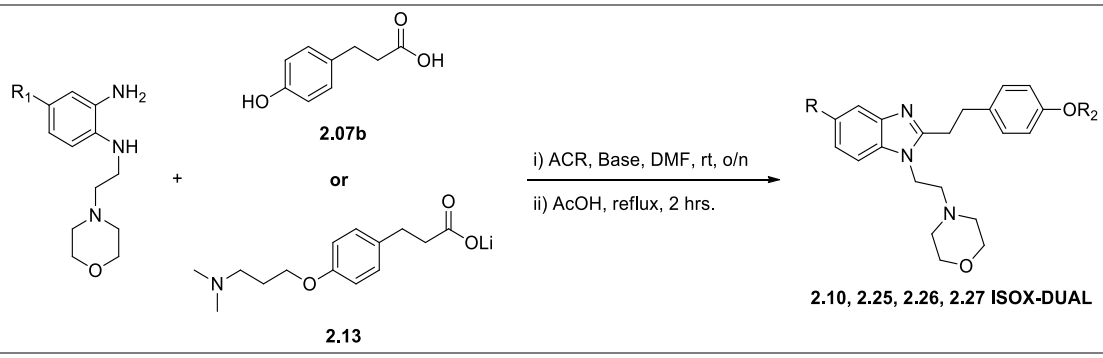

Entry	Product	R_1	R_2	Acid	Amide Coupling Reagent (ACR)	Yield[b] (%)
1	**2.25**	H	H	2.07b	HBTU	44
2	**2.25**	H	H	2.07b	HATU	74
3	**2.26**	H	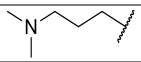	2.13	HBTU	70
4	**2.26**	H	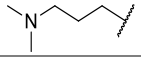	2.13	HATU	77
5	**2.26**	H	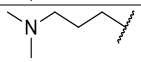	2.13	T3P[a]	30
6	**2.27**	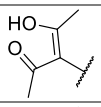	H	2.07b	HATU	51
7	**2.10**	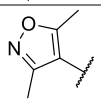	H	2.07b	HATU	30
8	**ISOX-DUAL**	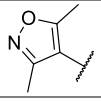	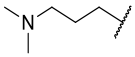	2.13	HATU	55

[a]T3P = Propanephosphonic acid anhydride. [b] Isolated yield after purification.

The synthesis of **2.25** and **2.26** was achieved with good yields (74% and 77% respectively) for the HATU conditions (Table 2.6 entries 2, 4). The increase in yield from HBTU to HATU was expected, due to the neighbouring group effect brought on by the nitrogen atom within the pyridine heterocycle, which is thought to occur through an internal base catalysed process implied by the 7-ring transition state (Figure 2.9).[339]

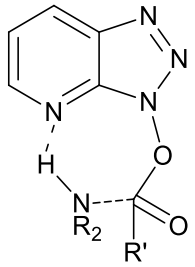

Figure 2.9: The internal 7-membered ring HATU can form between the activated acid, amine and the pyridine nitrogen.[339]

After the conditions had been investigated for diamine **2.21**, the HATU conditions were then applied to the synthesis of **2.10** and ISOX-DUAL (Table 2.6, entries 7, 8).

Compound **2.23** was utilised in this the amide formation and benzimidazole cyclisation (Table 2.6, entry 6) with 3-(4-hydroxyphenyl)propionic acid, and observed hydrolysis of the imine-enol, to a keto-enol moiety (**2.27**). A crystal structure of this compound was obtained from slow evaporation from $CHCl_3$, the keto enol was shown to exist as a pseudo-6 membered ring, with the proton being shared between both oxygen atoms due to tautomerism (Figure 2.10). Crystallography confirmed the hydrogen atoms bound to the keto-enol oxygen atoms were disordered with ratio ca. 43:57. The ^{1}H NMR spectrum shows the two methyl signals appearing as a 6H singlet, rather than the two 3H singlets observed in **2.23**, due to the methyl signals no longer being in different environments.

The low yield observed for **2.10** was attributed to polyesterification of the phenol occurring as a side reaction to the amide coupling (Scheme 2.9). Using HATU as the amide coupling reagent for the synthesis of ISOX-DUAL (Table 2.6, entry 8), gave a yield of 55%, and an overall synthetic yield of 42% (Scheme 2.10), significantly higher from that reported previously (Scheme 2.1, Scheme 2.2).

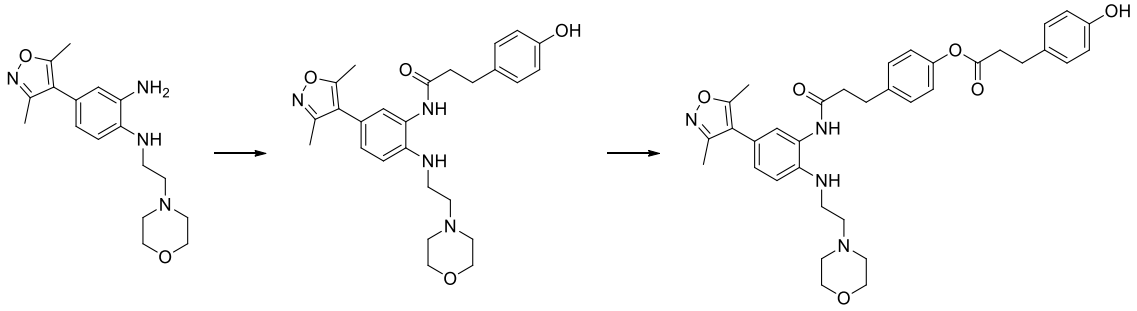

Scheme 2.9: Polyesterification side reaction observed by LC-MS from the amide coupling described in Table 2.6, entry 7.

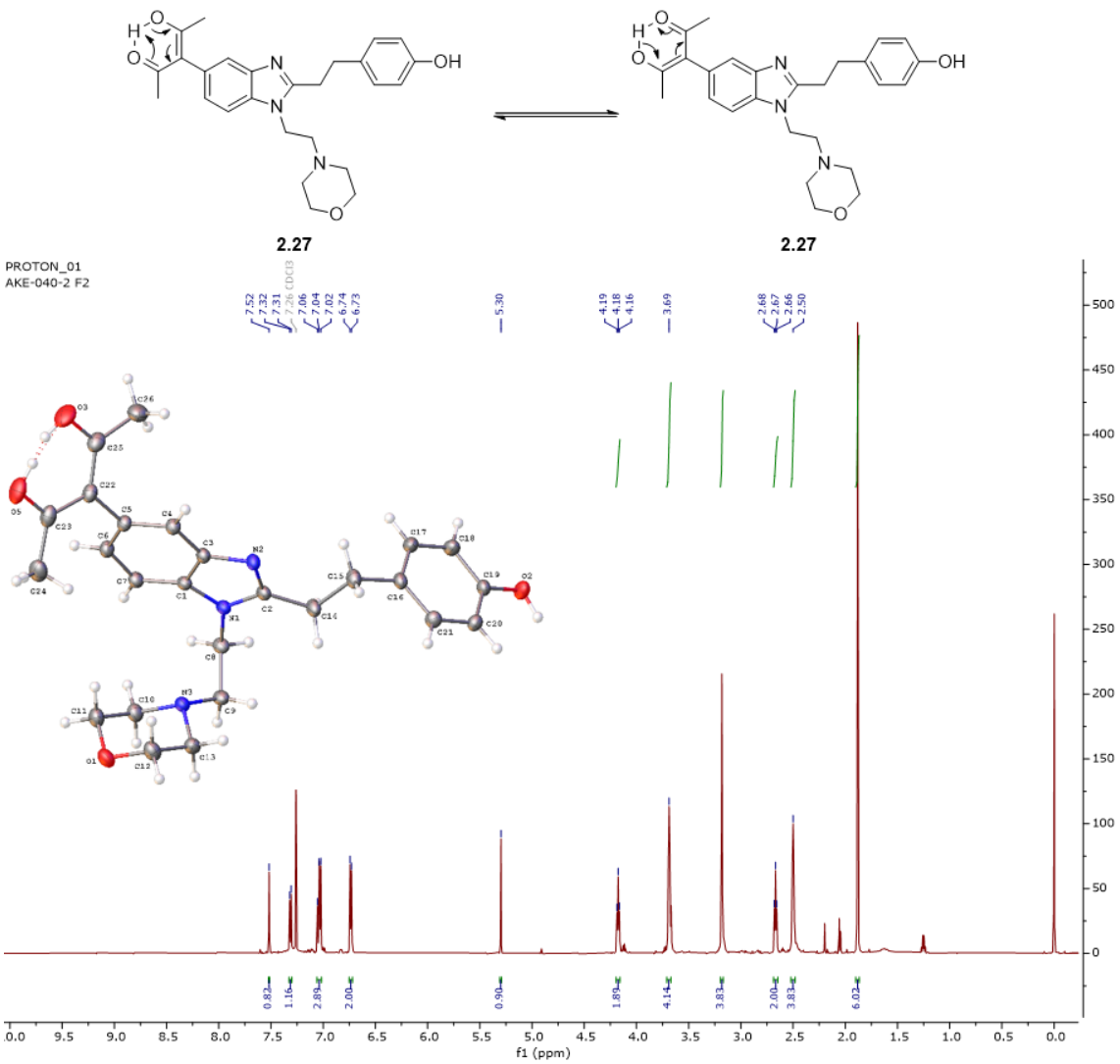

*Figure 2.10: ^{1}H NMR spectrum and crystal structure obtained for keto-enol product (**2.27**) from the benzimidazole formation from **2.23**. Schematic for the tautomerisation of the keto-enol to demonstrate the equivalence of the methyl signals.*

^{1}H NMR chemical shift analyses should serve, as with the isoxazole ring opening observations above, as a checkpoint for isoxazole maintenance or ring opened structures when working with these types of molecules.

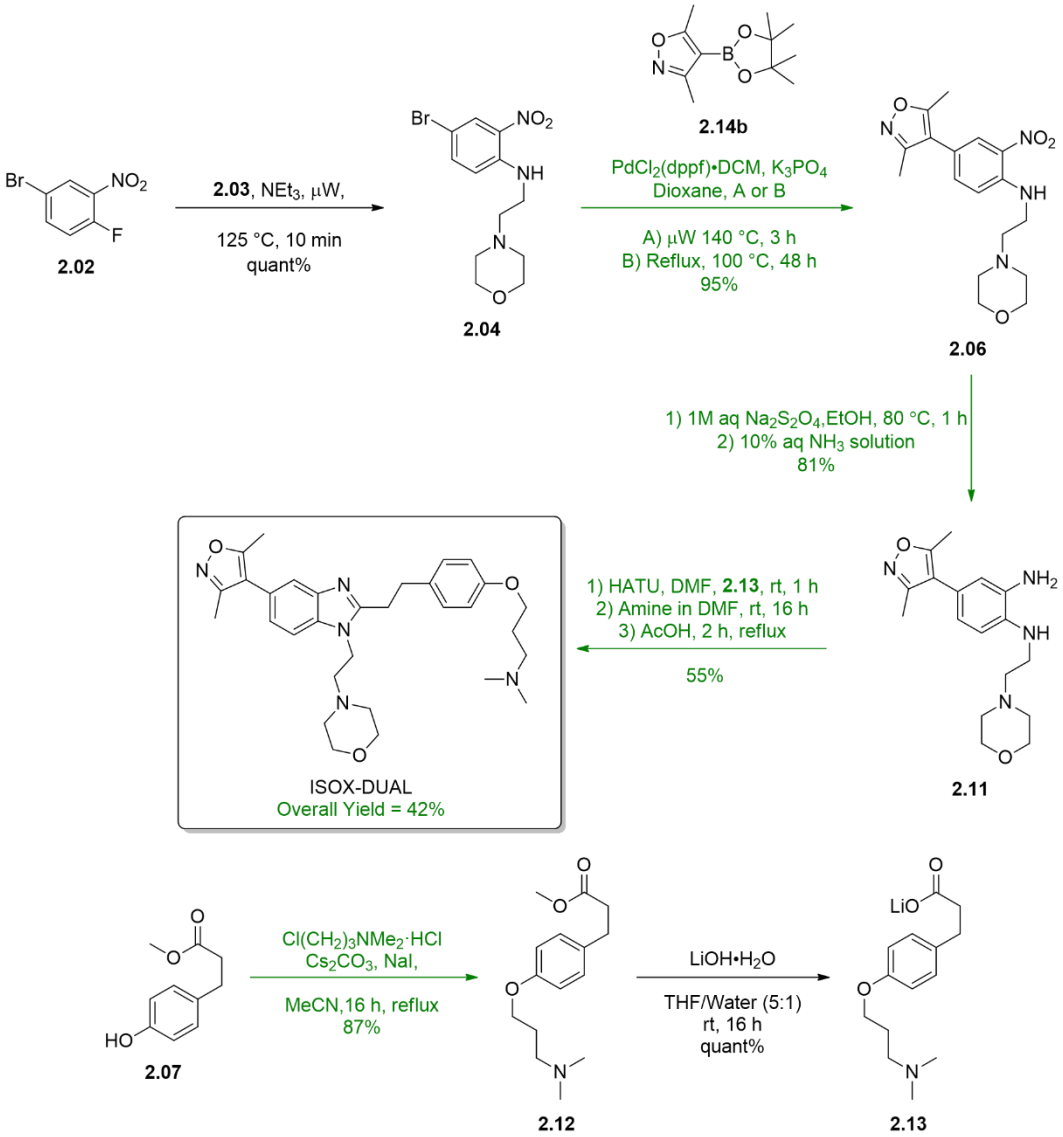

*Scheme 2.10: The optimised synthetic procedure for the synthesis of ISOX-DUAL with conditions and yields for each reaction. The overall yield treated **2.13** as a reagent and was not taken into account for overall yield calculation.*

2.3 Conclusions

In conclusion, this chapter has reported a simpler, higher yielding synthetic procedure for ISOX-DUAL as depicted in Scheme 2.10. The overall yield for isolation of this compound has increased from 1% (Scheme 2.1) and 13% (Scheme 2.2) to 42% and was performed on a 300 mg scale, in 98% purity by LC-MS.[2] The key findings of this study are outlined hereafter.

Modifying the Suzuki coupling to utilise a boronic acid pinacol ester (**2.28**), rather than the free acid, resulted in a yield boost (from 62% and 53% to 95%) due to a reduction in competing protodeboronation in the coupling reaction. This method is applicable to a range of other heterocycles and may be useful for late stage KAc bioisostere modification in these and similar scaffolds.

Switching the reduction protocol from the industrial hydrogenation protocol to the safer, milder $Na_2S_2O_4$ reduction, avoided ring opening of the isoxazole ring, and the resulting product **2.11** was obtained in 81% yield vs 74% *via* hydrogenation. Finally, through switching the ACR to HATU from HBTU, the yield for a combined amide formation and benzimidazole cyclisation was also increased (33% and 34% to 55%).

Table 2.7: Summary of yield improvements performed.

	ISOX-DUAL Protocol and Reaction Yield (%)		
Reaction	**Published**[2]	**Industrial**	**Optimised**
Suzuki-Miyaura	62	53	95
Nitro Reduction[a]	87	74	81
Benzimidazole formation	33	34	55
Alkylation	11	59	87

[a] Nitro reduction protocol taken from investigation into structurally similar compounds.[43]

3 Chapter 3: Synthesis of Modified ISOX-DUAL Compounds and Degrader Precursors

3.1 Introduction

As discussed in Chapter 1.3.2.2, PROTACs are heterobifunctional molecules that contain two ligands bound together by a linker (Figure 3.1). One of the ligands binds to a POI, while the other ligand binds to an E3 ubiquitin ligase protein. This brings the ligase and the target protein within close proximity, and allows for polyubiquitination of the target, which has surface lysine residues, and subsequent protein degradation.[238]

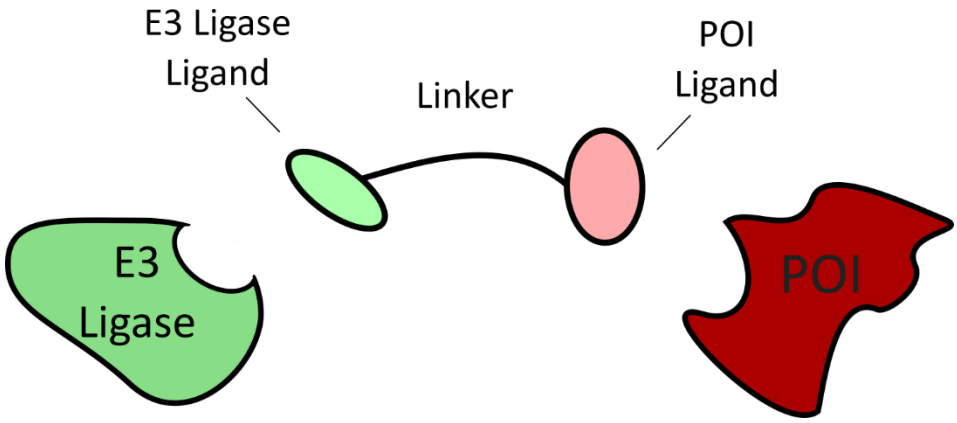

Figure 3.1: General cartoon of a PROTAC from Chapter 1.3.2.2.

In the development of novel PROTACs from known inhibitors, in some cases, the transition from an inhibitor to a PROTAC is relatively facile using standard chemistry, for example as with (+)-JQ1. As (+)-JQ1 is a potent inhibitor of BRD4, there has been significant research into PROTACs based on the structure of this compound. Some examples of these PROTACs include d-BET1, ARV-825, ARV-771, MZ1, AT1 and are discussed in more detail in Chapter 1.[235–239] These PROTACs are more trivially formed through the simple manipulation of ester hydrolysis, followed by amide coupling to the E3-linker component to result in the desired PROTACs (Scheme 3.1). MZ1 is given as an example of a PROTAC structure for (+)-JQ1-based PROTACs.

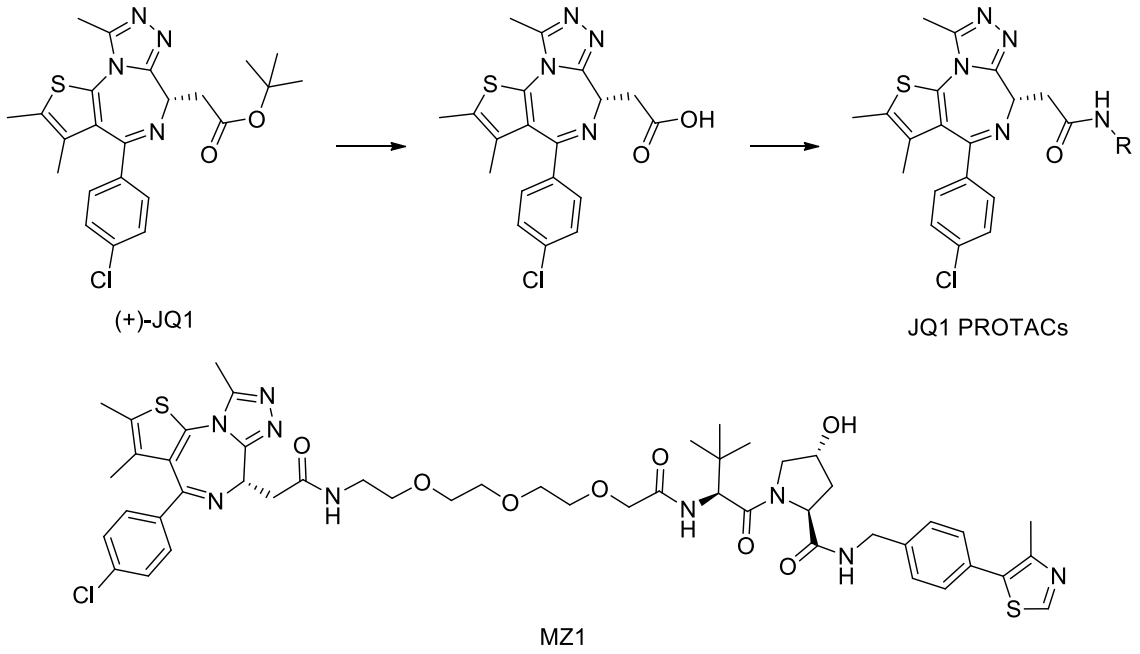

Scheme 3.1: Generic scheme for the synthesis of (+)-JQ1 PROTACs where R is a linker connected to an E3 ligand. The structure of MZ1 as an example.

Another example of an inhibitor which translates into degrader technology with minimal tweaks to the synthetic protocol is SHP2 Inhibitor 5 (Scheme 3.2).[340] With this compound they mad use of the aniline rather than the acetamide to convert through to SHP2 PROTAC 26.

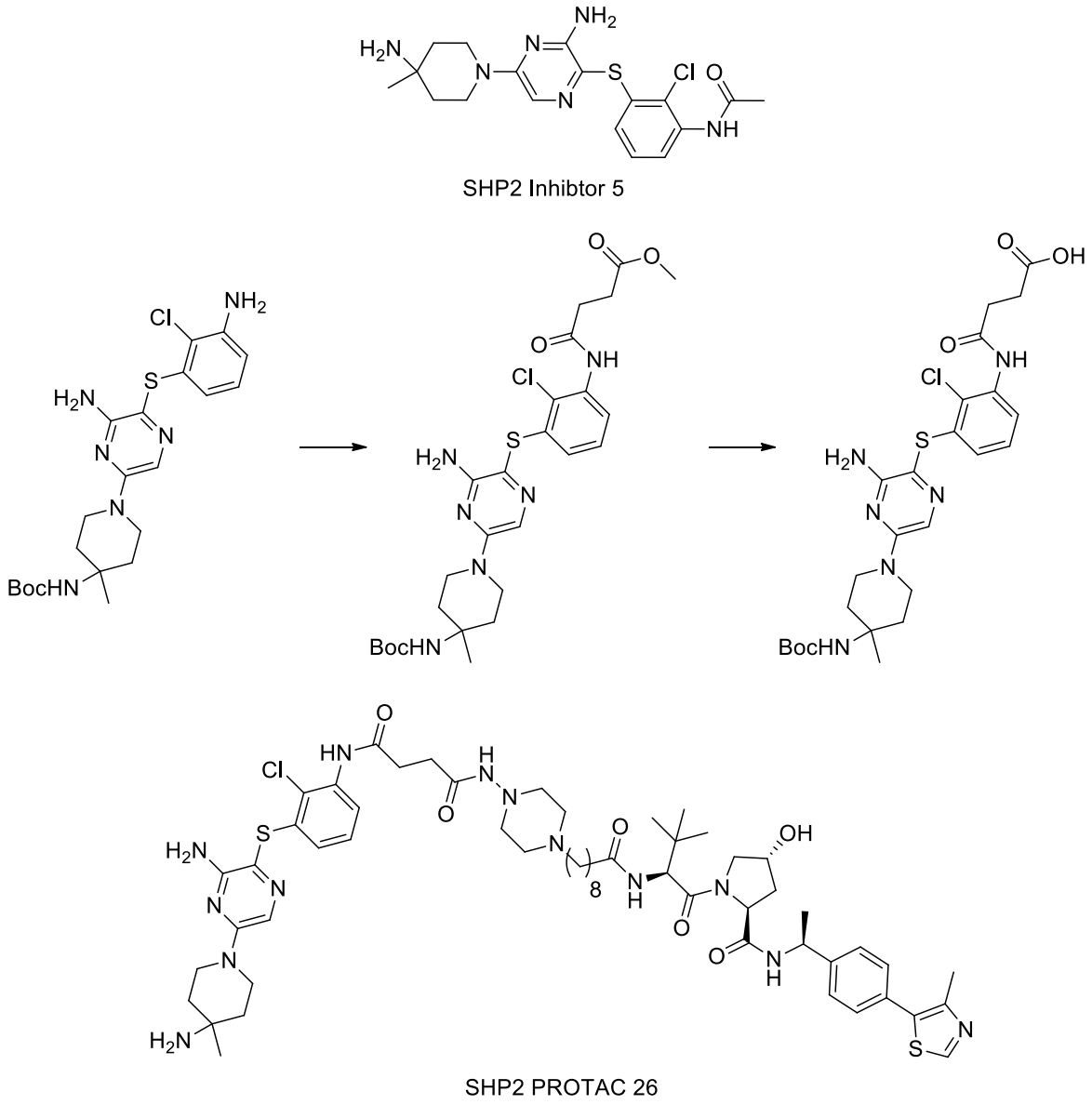

Scheme 3.2: Summary of the reported synthesis of SHP2 PROTAC, SHP2 PROTAC 26.[340]

A penultimate reaction in the synthesis of SHP2 inhibitor 5 is the acetylation of an intermediate followed by hydrolysis of the Boc-protecting group on the piperidine primary amine. Instead of acetylating at this location, an amide formation is performed with methyl malonyl chloride. This formation is followed by hydrolysis of the methyl ester before amide formation with the desired VHL linkers, before hydrolysing the Boc-protecting group.[340]

While in these examples, translation to PROTACs is minimalistic in terms of additional steps or modifications to the overall synthetic route, other reported PROTACs require significant modifications to their synthetic route to allow translation. This is due to the solvent exposed sites of the inhibitors lacking late stage modifiable sites within their structure. One example of this is a Napabucasin PROTAC, which is a degrader of the E3 ligase ZFP91.[341]

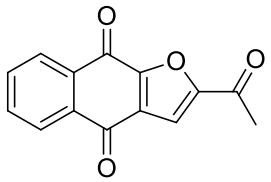

Napabucasin

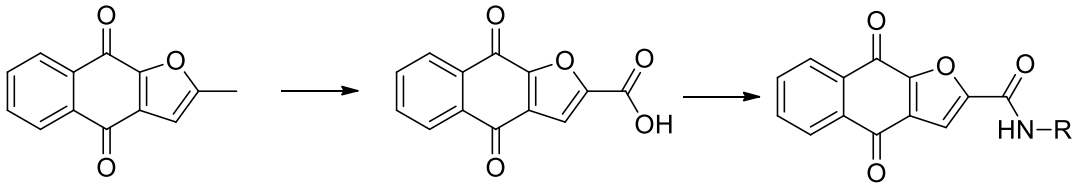

Scheme 3.3: Generic scheme for the synthesis of reported Napabucasin PROTACs.[341]

In the synthesis of these PROTACs, an intermediate containing a 2-methyl furan is oxidised to an aldehyde with SeO_2 and SiO_2 before oxidising again then to the acid with H_2O_2 before reacting with E3 linkers to make the desired PROTACs.

Another example where synthetic translation to PROTACs is more complex, is eEF2K inhibitor A484954 (Scheme 3.4). In order to synthesise PROTACs from this inhibitor, a complete re-synthesis of the compound is required, to replace the *N*-ethyl to an acetic acid. This group then allowed amide formation with their desired linkers to achieve eEF2K PROTACs. [342]

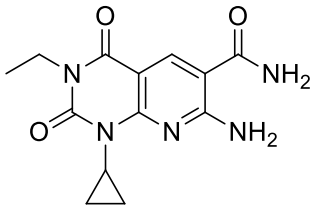

A484954

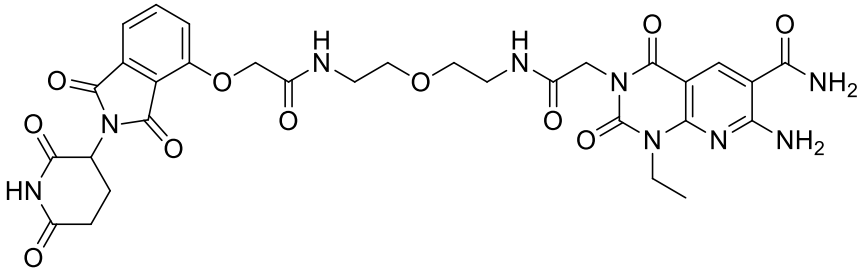

A484954 PROTAC 11l

Scheme 3.4: Inhibitor A484954 and PROTAC 11l for eEF2K.[342]

As discussed in Chapter 2, ISOX-DUAL is a dual inhibitor of BRD4 and CBP/p300 and the application of ISOX-DUAL to degrader technology had two initial issues. The first is the low overall published yield for ISOX-DUAL, which was rectified in Chapter 2. The yields for a few key steps were improved allowing the overall yield to increase from 1% and 13% to 42%. The second being is that ISOX-DUAL lacks sites for exit vector placement and therefore requires a synthesis rethink to create degraders.

As a means of ascertaining where the modifications would be needed to allow for linker attachment, analysis of the binding mode for BDOIA383 was performed (Figure 3.2 C), as no crystal structure for ISOX-DUAL is available in the literature. Analysis of the crystal structures identifies two sites within the inhibitor which are solvent exposed (BRD4: 5CFW, CBP: 5CGP).[2] As PROTAC is a registered trademark by Arvinas, when discussing the synthesis of small molecule degraders based on the structure of ISOX-DUAL, they will be referred to as “degraders”.

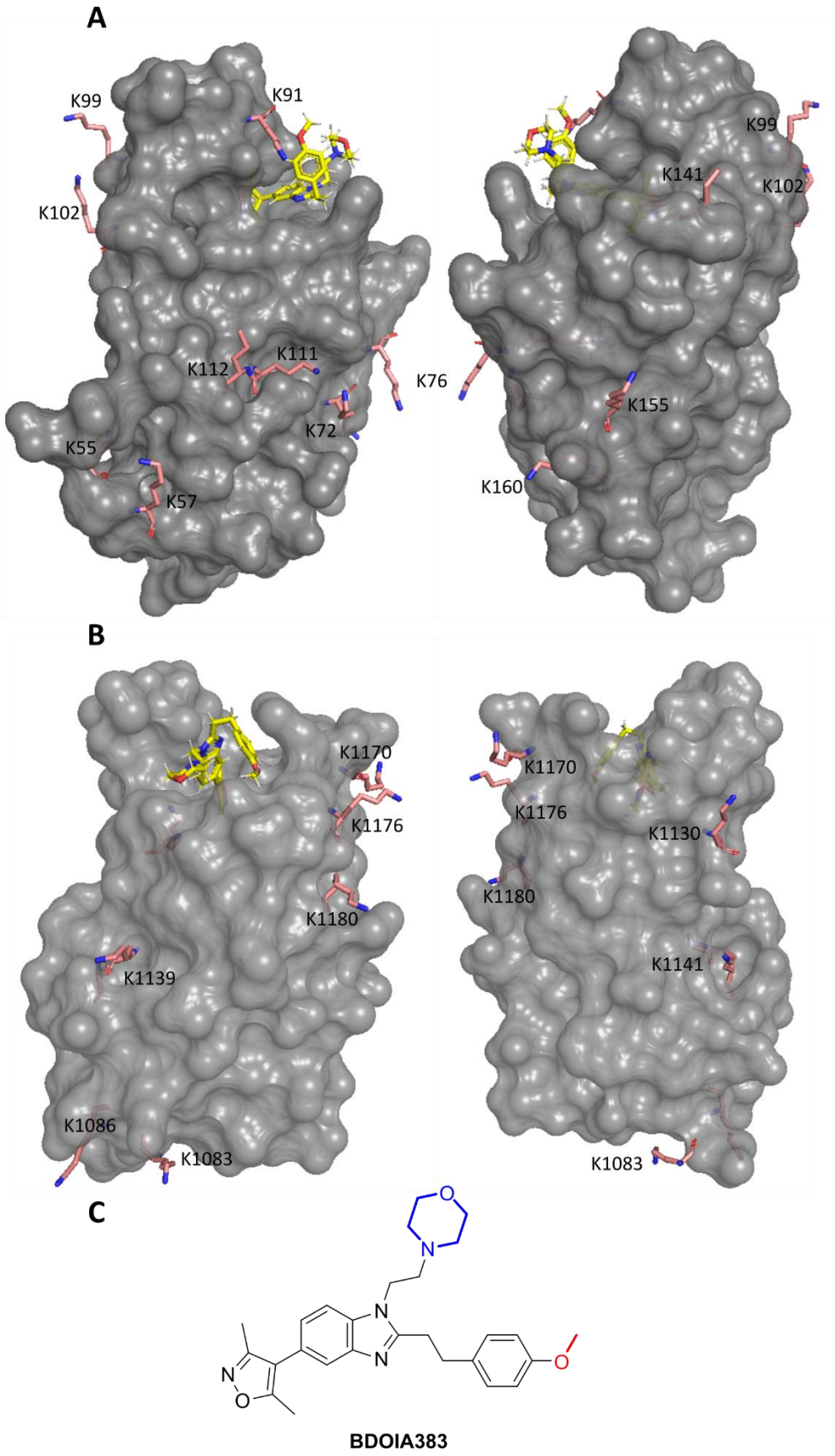

Figure 3.2: Crystal structures adapted from PDB structures using Pymol. A) Two angles for the crystal Structure of BRD4 with ligand BDOIA383 docked in the binding site, with lysine residues highlighted. B) Two angles for the crystal Structure of CBP with ligand BDOIA383 docked in the binding site, with lysine residues highlighted. C) Structure of BDOIA383, with solvent exposed moieties portrayed in blue and red.

Analysis of the co-crystal structures in BRD4 (Figure 3.2 A) and CBP (Figure 3.2 B) showed the orientation of BDOIA383 (Figure 3.2 C) within the bromodomains. Surface lysine residues were also confirmed to be near to the bromodomains KAc binding site, validating the targets for targeted protein degradation as ubiquitination sites.[2] Two modalities were identified and highlighted on BDOIA383 as solvent exposed sites (Figure 3.2, A). Translating this information across to ISOX-DUAL, the phenol can be alkylated at a late stage to result in a functionalisable site (Figure 3.3 B) and the morpholine can be switched out to a piperazine earlier in the synthesis (Figure 3.3 C).

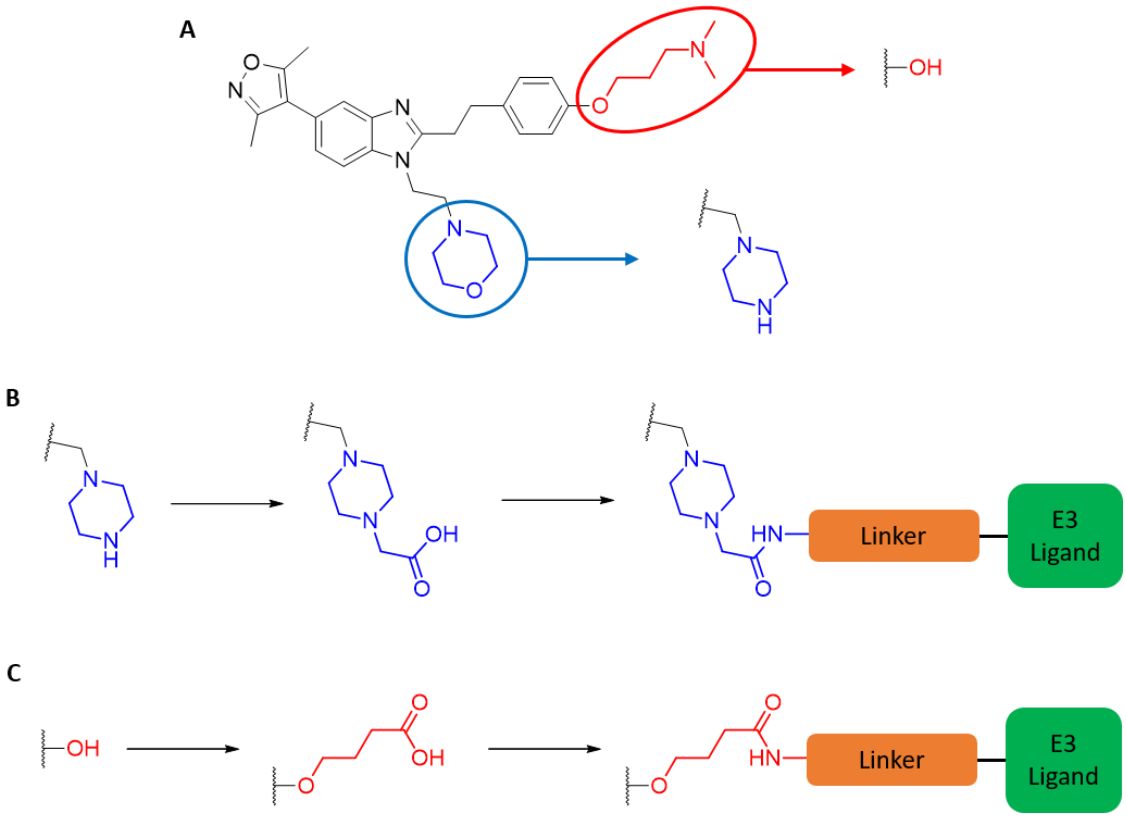

Figure 3.3: A) Structure of ISOX-DUAL, with solvent exposed sites highlighted in red and blue, showing changes in moieties to allow for conversion of ISOX-DUAL to degrader technology. B) Formation of degraders from piperazine site. C) Formation of degraders from modified ISOX-DUAL phenol site.

Substituting the morpholine moiety to a piperazine moiety was a similar modality used by the Ott group in the synthesis of dCBP-1 from GNE-781, where the solvent exposed tetrahydropyran was substituted for a piperidine, which allowed them to form amides with acid terminal linkers.[247]

The work in this chapter will focus on the manipulation of ISOX-DUAL into precursor compounds for degrader synthesis and discuss the changes made to our previously optimised synthetic strategy. Initial work was focused onto the route highlighted in red, due to the free

phenol compound **2.10** having already been synthesised (Chapter 2) and thus a more straightforward route to the precursor compound.

In order to check that the modifications to ISOX-DUAL did not negatively the binding to its dual targets BRD4 and CBP/p300, the binding affinities of these compounds were tested at each stage of the modifications.

3.2 Results and Discussion

3.2.1 Synthesis of Modified ISOX-DUAL Compounds

3.2.1.1 Synthesis of Phenol Modified Compounds

As highlighted in Figure 3.3, the phenol position of ISOX-DUAL can be manipulated into a compound which would allow connection to a series of E3-linkers, through benzimidazole **2.10** synthesised in Chapter 2.

As the synthesis of **2.10** resulted in polyesterification (Scheme 2.9), through the repeated ester coupling as a competitive side reaction, a small screen of protecting groups was trialled in order to increase the isolated yield of **2.10** (Scheme 3.5). The protected phenols would then be assessed for their stability under the hydrolysis conditions utilised in the synthesis of **2.13**.

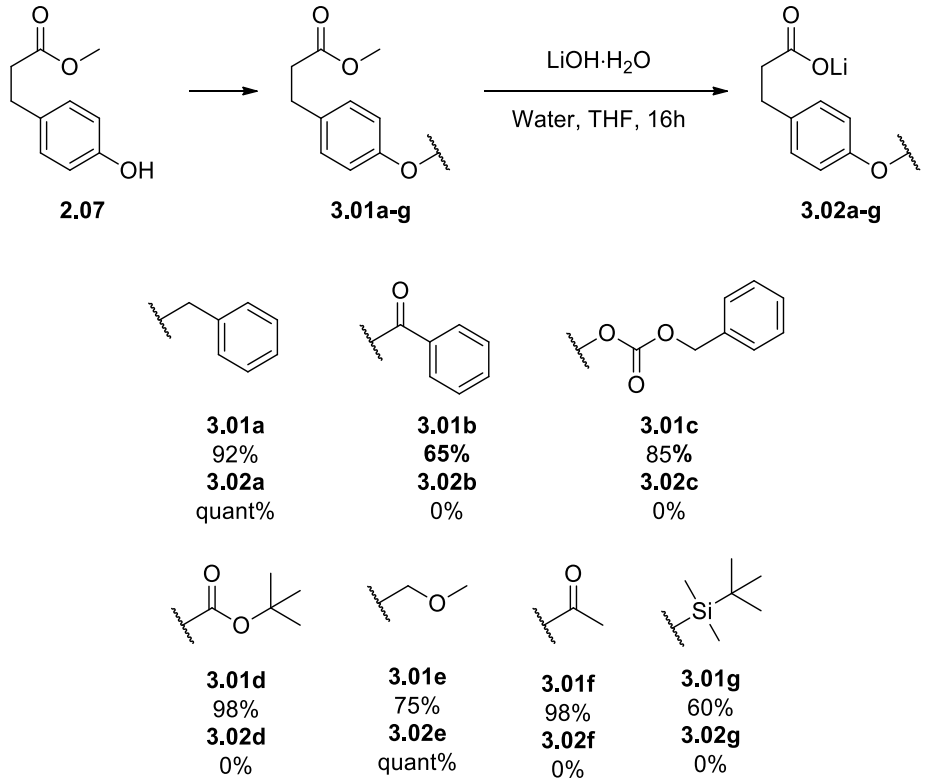

Scheme 3.5: Protecting group screen and obtained yields.

All protecting groups were attached in moderate to high yields, however, upon hydrolysing the methyl ester with LiOH, only **3.02a** and **3.02e** were isolated. Both of these compounds were carried through the benzimidazole synthesis in order to ascertain if the protecting group strategy would be successful in the synthesis of **2.10** or if a new route to the degrader precursors should be utilised. Both acids **3.02a** and **3.02e** were utilised in the combined amide formation and benzimidazole cyclisation reaction (Scheme 3.6).

*Scheme 3.6: The attempted amide coupling and benzimidazole cyclisation to synthesise compounds **3.03a** and **3.03e**.*

From this reaction, only **3.03a** was successful, which was isolated with a yield of 62% as a white solid. **3.03e** was partially de-protected during the AcOH reflux, and so was left overnight rather than 2 hours. Upon return to the reaction, it was determined that the reaction had then formed the acetyl ester rather than free phenol. Attempted de-protection of **3.03a** resulted in compound degradation.

Degrader synthesis utilising this position for linker attachments is a more trivial synthetic route compared to the piperazine counterpart. This is due to the requirement for no additional synthetic modifications from the synthesis of ISOX-DUAL, as **2.10** was synthesised identically, but with a commercially available acid rather than **2.13**. The synthesis of the phenol degrader precursor **3.07** was performed utilising Scheme 3.7.

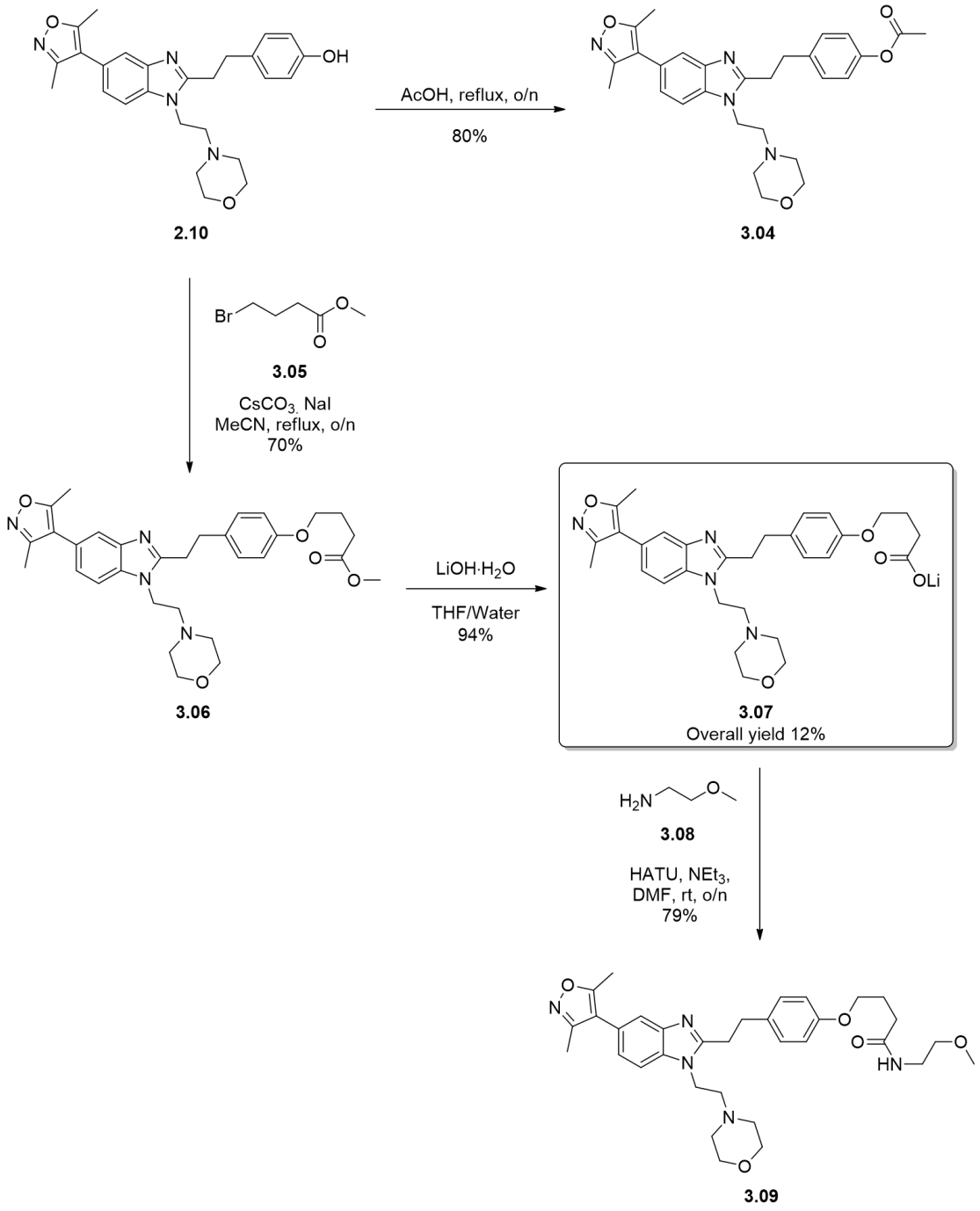

*Scheme 3.7: Synthetic route to afford **3.04**, the degrader precursor compound **3.07**, and the amide formation to create the degrader mimic **3.09**.*

Compound **2.01** was acetylated in good yield to result in **3.04**, which was synthesised in order to mimic direct modification of the phenol. In the synthesis towards degrader precursor **3.07**, **2.10** was alkylated with methyl 4-bromobutyrate (**3.05**) to afford **3.06**. In order to keep the structure of the degrader warhead as similar to ISOX-DUAL as possible, **3.05** was utilised as the alkylating agent in order to retain the propyl chain. The methyl ester was then hydrolysed to afford **3.07**, as a white solid at 94% yield, which will serve as the precursor to the degrader compounds.

To test the reaction to form the desired degraders from **3.07** and also to create a compound which can act as a degrader mimic, **3.09** was then synthesised through an amide formation with 2-methoxyethylamine. This amine was chosen due to its dual functions to act as a PEG linker mimic but also to give an easily identifiable handle by ^{1}H NMR spectroscopy.

After attempted protecting group chemistry had not succeeded, the synthetic procedure for **2.10** was scaled up and modified during an industrial placement at Tocris (Scheme 3.8). The modification of the synthetic procedure was performed to overcome the issues with ester polymerisation of the free phenol in **2.10** synthesis. The overall yield in the synthesis of **3.13** was 25%, which was a significant improvement from the overall yield of 12% for the lithium salt **3.07**.

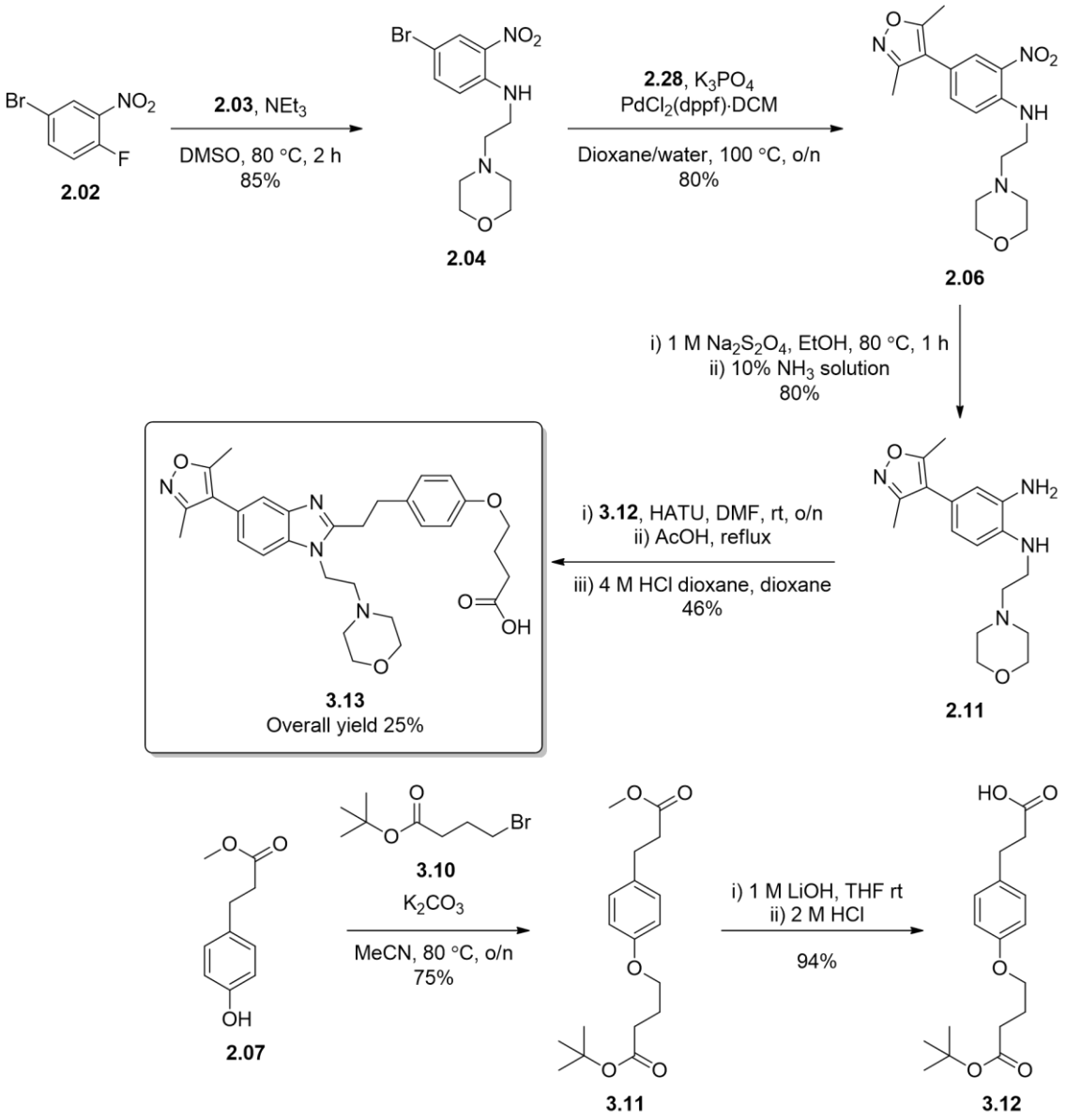

*Scheme 3.8: Scale up synthesis of **3.13**, with an overall yield of 25%. This yield calculation took **3.12** as a reagent and was not taken into consideration for yield calculation.*

The synthesis of acid **3.12** was successful, however upon acidification of the reaction mixture, partial hydrolysis of the *tert*-butyl ester was observed. This by-product wasn't removed before utilising in the synthesis of **3.13**, which will have contributed to yield loss. In order to prevent this from happening, future synthesis of **3.12** should be quenched with ammonium chloride.

The benzimidazole cyclisation towards **3.13** was carefully monitored and stopped before *tert*-butyl ester hydrolysis. This allowed purification at this stage, to ensure the compound was as pure as possible before hydrolysis. Hydrolysing the *tert*-butyl ester in 4 M HCl dioxane followed by MeCN trituration resulted in 10.5 g of **3.13** as a white solid (48%, overall yield 25%). This shows that the synthetic optimisations performed in Chapter 2, are applicable to the modified warhead ligands resulting in higher yielding and high purity degrader precursors.

3.2.1.2 Synthesis of Piperazine Modified Compounds

The synthesis of **3.17**, was originally performed matching the synthesis of ISOX-DUAL, as these reactions were optimised in Chapter 2. However, 4-(2-aminoethyl)-1-boc-piperazine (**3.14**) was used in the initial S_NAr reaction (Scheme 3.9).

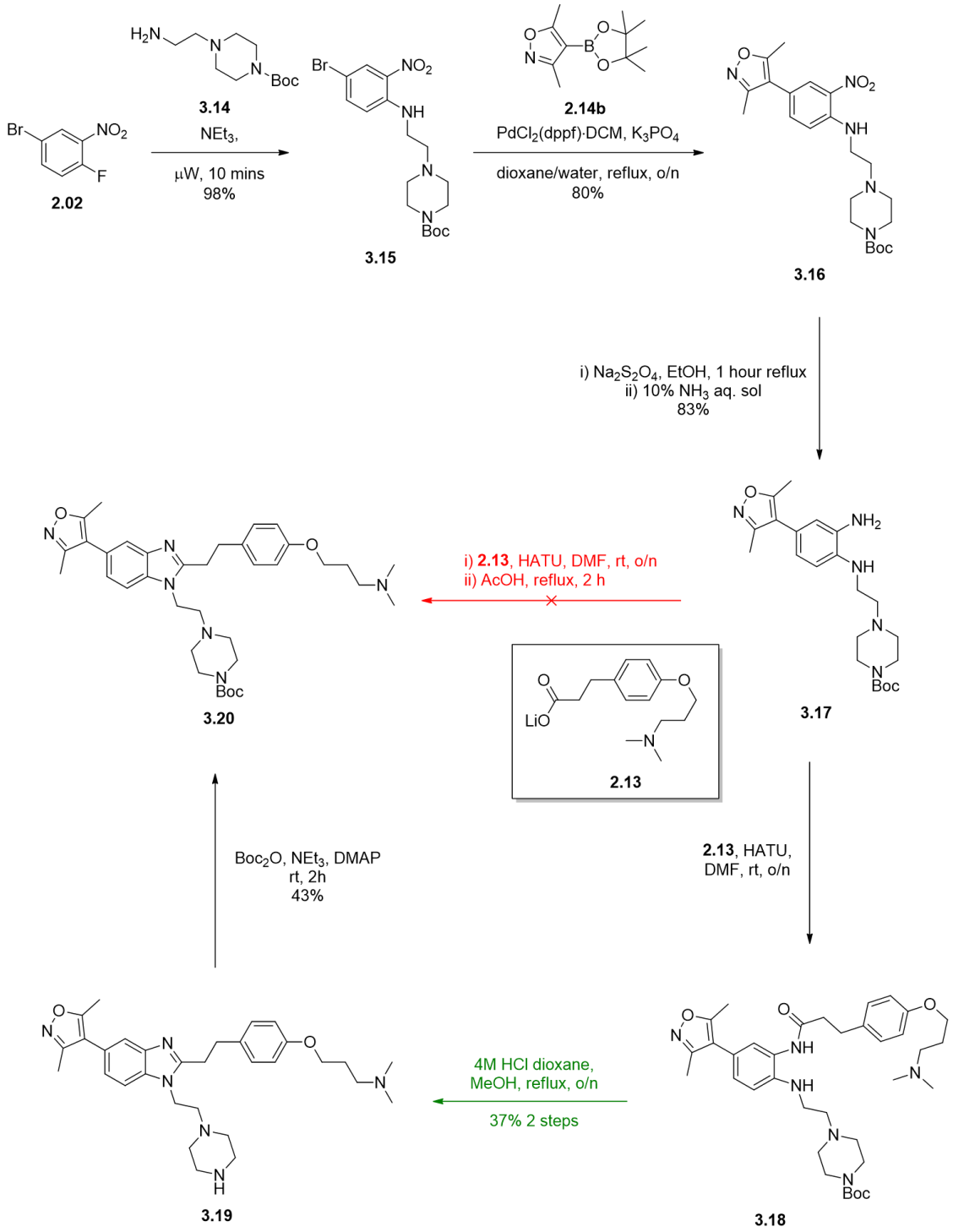

*Scheme 3.9: Original Synthetic route to obtain free piperazine **3.19** and Boc-piperazine **3.20**.*

The yields obtained from this synthesis route up to diamine **3.17** matched those observed in the synthesis of ISOX-DUAL. **3.15** was synthesised in near quantitative yield utilising the

microwave-mediated methodology used previously on the morpholine variant. Suzuki cross-coupling with **2.14b** resulted followed by reduction *via* sodium dithionite resulted in **3.17** in high yield. However, upon amide coupling and cyclisation the desired product **3.20** was not formed, instead a formyl (**3.21**) product was isolated in 46% yield (Scheme 3.10). This product was thought to have been synthesised through an acid-mediated formylation with DMF as the carbonyl source.[343,344]

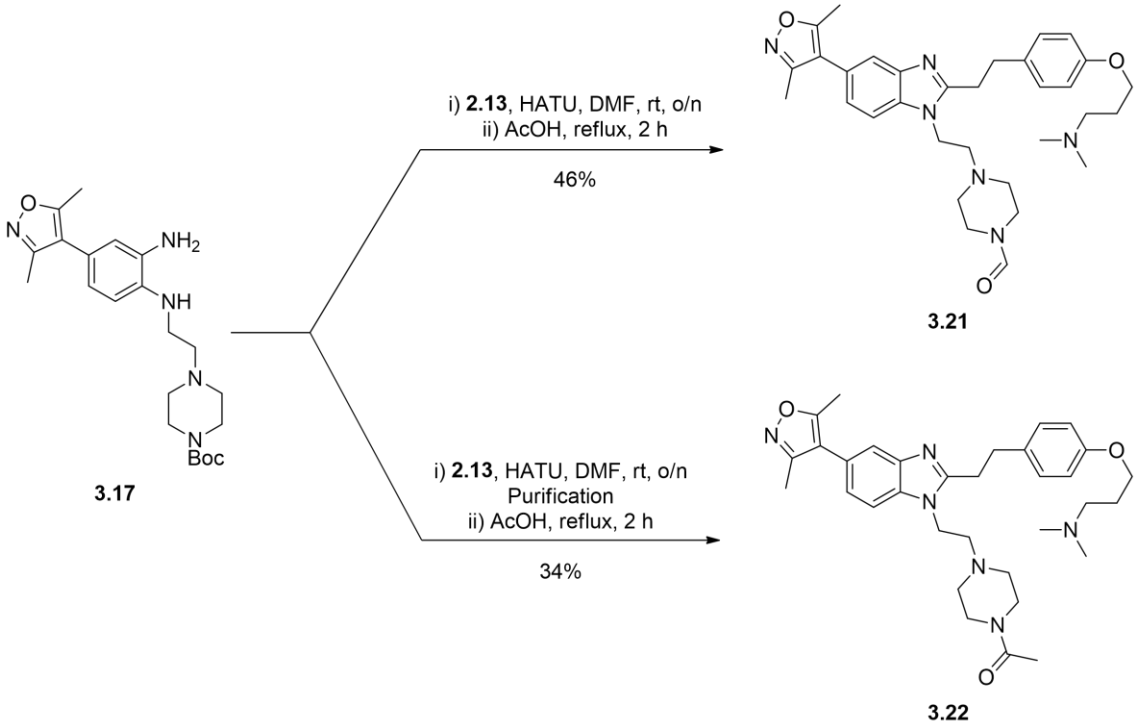

Scheme 3.10: Products obtained from the highlighted problematic reaction in Scheme 3.9.

Ensuring all DMF was removed from the crude mixture post amide formation through azeotropes with heptane and flash chromatography to afford **3.18** before AcOH reflux, still did not give desired product **3.20** or free amine **3.19**, rather an acetamide product (**3.22**). The formation of both compounds shows that diamine **3.17** is not viable in these conditions and a change in methodology was required.

In order to remove the issues with formylation and acetylation, purification was performed after the amide formation, to give **3.18** as an intermediate. Two alternative methodologies were trialled for the cyclisation of **3.18** to **3.19**, a $POCl_3$ reflux and a 4M HCl dioxane reflux.[345,346] The $POCl_3$ methodology only resulted in Boc-deprotection, with no cyclisation observed by LC-MS. The 4M HCl dioxane protocol afforded **3.19** after purification in 37% yield, as a beige solid; a small quantity of this was then Boc-protected using literature protocols (Scheme 3.9) to afford **3.20** in 43% yield as a clear oil.

Due to the synthetic issues and low yielding cyclisation to form **3.20**, and that **3.19** would need further reactions after these problematic steps, the synthesis route was re-evaluated. Instead of performing late-stage modifications of the piperazine to afford the precursor, the modifications were made prior to the nitro-reduction, which allowed for the successful synthesis of precursory **3.27** (Scheme 3.11).

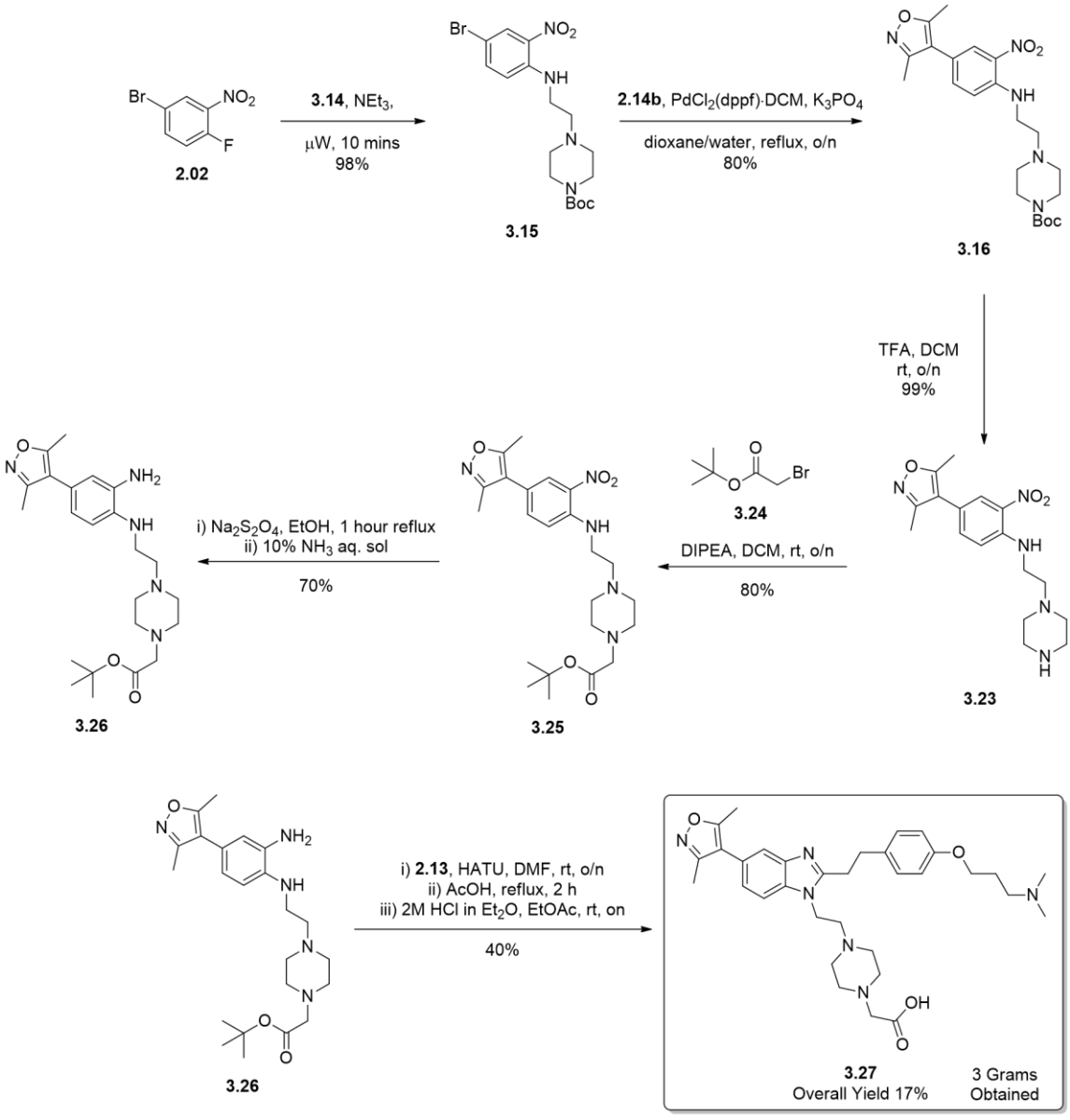

*Scheme 3.11: Synthetic route to obtain degrader precursor **3.27** with the adapted methodology.*

Within this synthetic route, intermediate **3.16** was de-protected with TFA to result in free amine **3.23** and then alkylated with *tert*-butylbromo acetate to afford **3.25** in high yield. Originally this reaction utilised methyl bromoacetate, but, after benzimidazole formation the product was poorly soluble, and it was decided to switch to a *tert*-butyl acetate as depicted in Scheme 3.11.

The switch from the carbamate of the Boc-group to an ester with a CH_2 spacer gave added stability through the amide coupling and cyclisation reactions. After cyclisation in acetic acid, the compound was dissolved in EtOAc and turned into the HCl salt by treatment with 2 M HCl in Et_2O, which resulted in 3 g of **3.27** as a white solid, in 40% yield, with an overall yield of 17%.

In order to mimic a future degrader structure, as done previously with **3.09**, **3.27** was reacted further to make two mimic compounds; methyl ester **3.28** and amide **3.29** (Scheme 3.12).

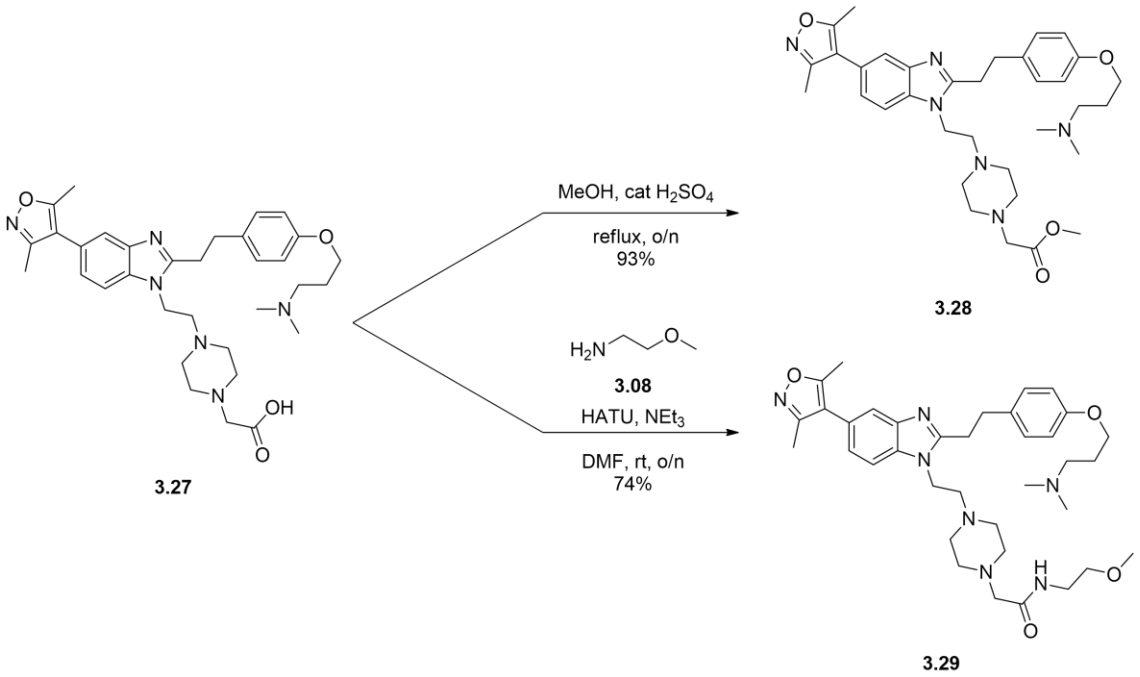

*Scheme 3.12: Synthesis of **3.28** and **3.29***

Both **3.28** and **3.29** were synthesised in high yields with purities >95%. In order to allow the compounds to be easily weighable for binding assays, these compounds were converted to HCl salts for storage and testing as described in the experimental.

3.2.1.3 Synthesis of ISOX-DUAL Precursor Intermediate for Future Degraders.

Towards the end of the project, focus was returned to the synthesis of ISOX-DUAL degrader intermediates, in order to create a common intermediate for future degrader research. Having two synthetic routes increases the quantity of work for the chemist, so having a common intermediate would be ideal in order to streamline the synthetic process to achieve the target compounds. Previous work performed by both Brennan and Jones utilised synthetic protocols that were applied to this route.[2,43] Scheme 3.13 contains a synthetic route in which results in aldehyde intermediate **3.35**.

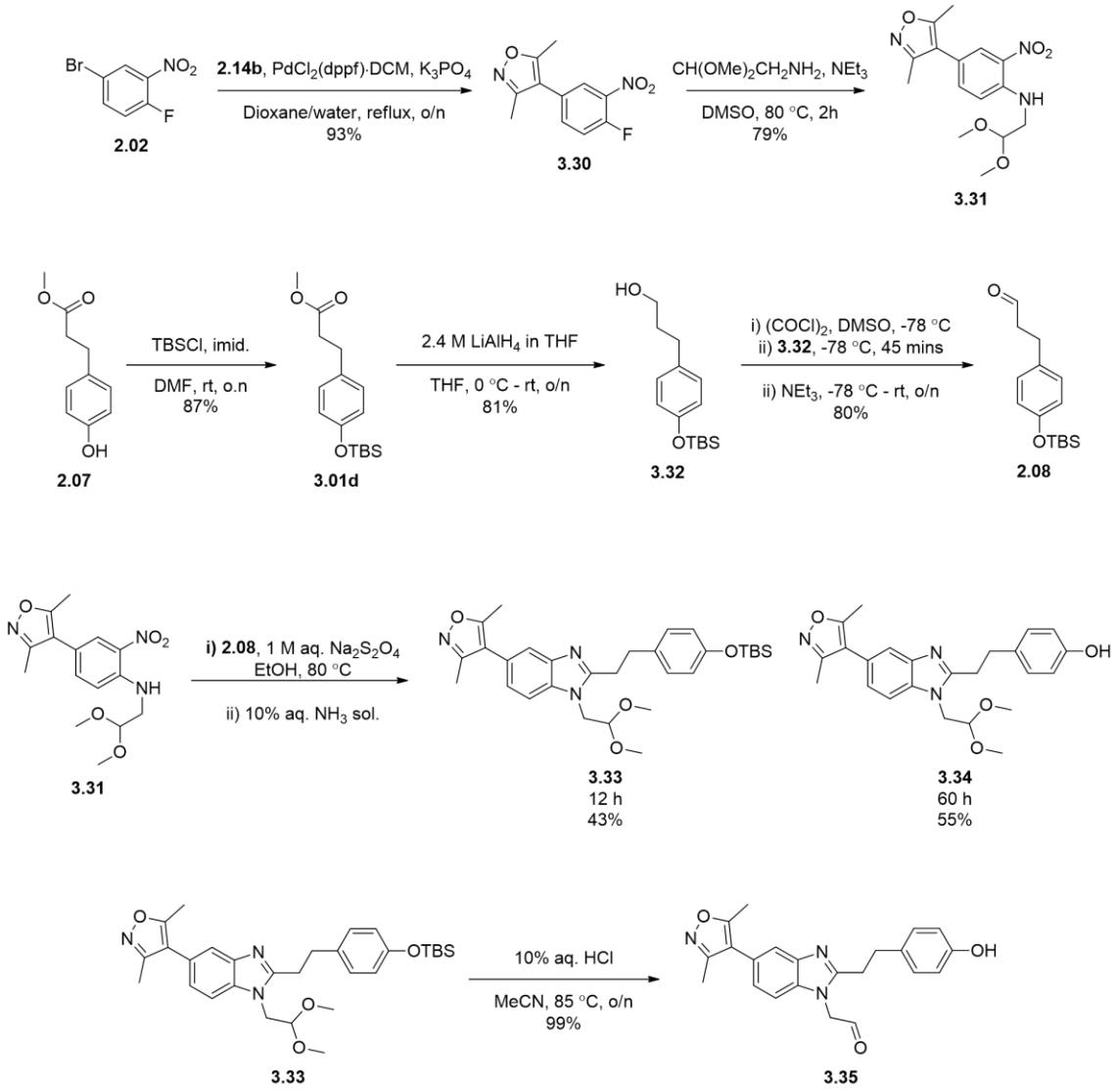

*Scheme 3.13: Synthesis of aldehyde intermediate **3.35**.*

Both compounds **3.31** and **2.08** were synthesised successfully as previously reported. **2.08**, however, was synthesised *via* a Swern Oxidation rather than through the use of Des-Martin Periodinane (DMP).[347] The product obtained from the cyclisation of **3.31** with **2.08** in aqueous dithionite solution was dependant on the reaction time. If the reaction was left to stir for 18

hours, **3.33** was formed, however if left to react over 66 hours, **3.34** was formed due to the additional reaction of TBS cleavage. This allows for modifications to the phenol to take place before conversion to the aldehyde if desired. Treating **3.33** with aqueous HCl results in the formation of **3.35**, monitored by LC-MS. Analysis of this compound proved difficult, the ^{1}H NMR spectrum for this sample was complex, however the LC-MS trace reported an m/z of 408.1. HR-MS also confirmed this m/z with an observed m/z of 408.1948. As the compound was only soluble in Methanol, it was theorised the solvent was interacting with the aldehyde and forming a hemiacetal (Figure 3.4). Attempts to analyse this compound in a solvent other than Methanol was unsuccessful due to solubility issues.

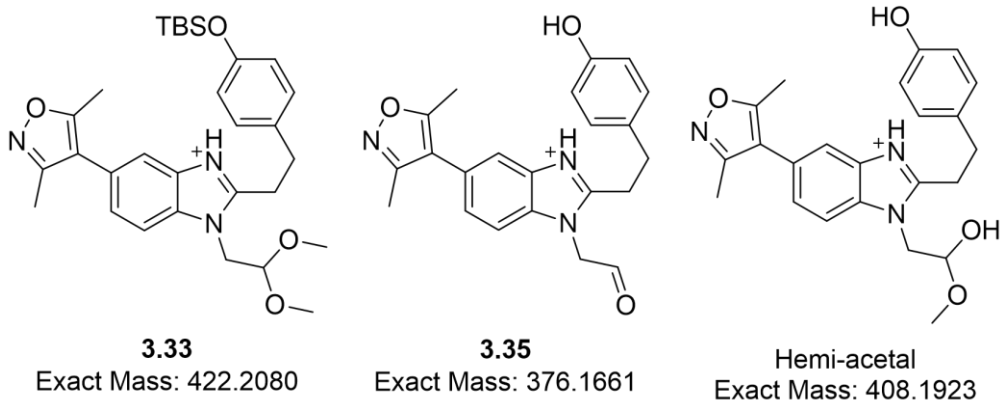

*Figure 3.4: Calculated $[M+H]^+$ masses for **3.33** the starting material of reaction, **3.35** the aldehyde product and the adduct of **3.35** responsible for the observed mass.*

To confirm the product was synthesised correctly and as pure as the LC-MS was suggesting, a small sample of **3.35** was reduced with $NaBH_4$ (Scheme 3.14). Upon purification alcohol **3.36** was isolated in almost quantitative yield and with excellent analytical data. This confirmed that the aldehyde **3.35** is likely to be in a complex mixture and that the reaction to synthesise **3.35** was successful.

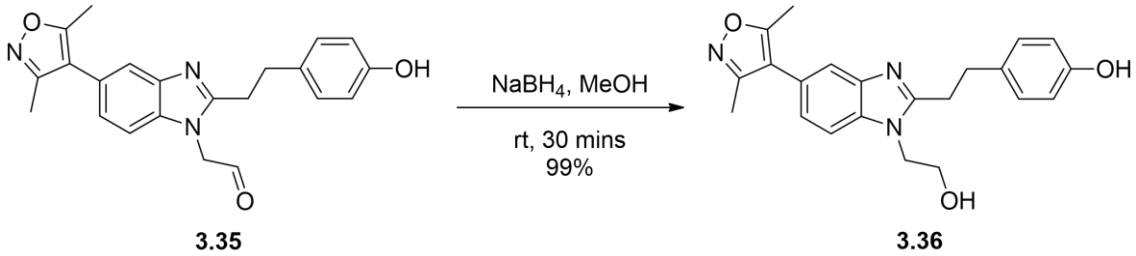

*Scheme 3.14: Reduction of **3.35** with $NaBH_4$ to check the aldehyde product was synthesised.*

However, attempting to perform a reductive amination with morpholine to afford **2.10**, TBS protecting the phenol or alkylating the phenol failed. Understanding why this was the case was not fully explored (due to time restraints from the Covid-19 lockdown), but it was thought that

the solubility issues of **3.35** due to the free phenol played a part. Instead, future work should investigate **3.34** as the synthetic intermediate for future degrader work. Using ISOX-DUAL as an example, you can alkylate the phenol position before converting to aldehyde **3.38** and finally performing a reductive amination to give ISOX-DUAL (Scheme 3.15).

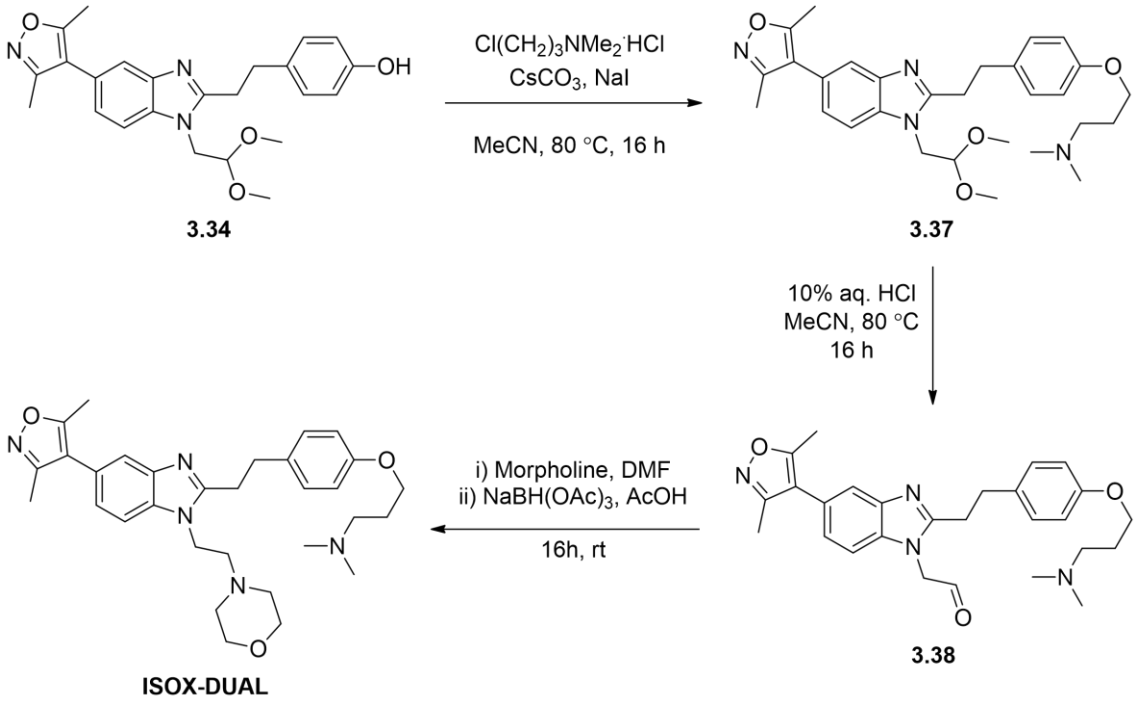

*Scheme 3.15: Example synthesis of ISOX-DUAL starting from intermediate **3.34**.*

3.2.2 Binding studies for the ISOX-DUAL Derivatives

The compounds synthesised in **Error! Reference source not found.**, Scheme 3.11 and Scheme 3.12 that were precursors to, or mimics of degraders, had their binding affinities measured against the bromodomains of both BRD4 and CBP/p300. This was to ensure that any modifications made to the structure had not disrupted binding and would be transferable, or not, thereafter to degrader modification. These results would be useful as a case study in degrader and degrader mimic design strategies. These binding assays were performed by Oleg Fedorov at the SGC using Alpha Screen assays reported previously.[43]

The binding studies for these two series were performed at different times with different repeats (due to the lockdown) and so have been separated into two tables, Table 3.1 for the phenolic compounds and Table 3.2 for the piperazine based compounds.

Table 3.1: Cell-free binding studies performed for the phenol compounds, with comparison to literature ISOX-DUAL, alongside controls (+)-JQ1, SGC-CBP30 and Bromosporine.

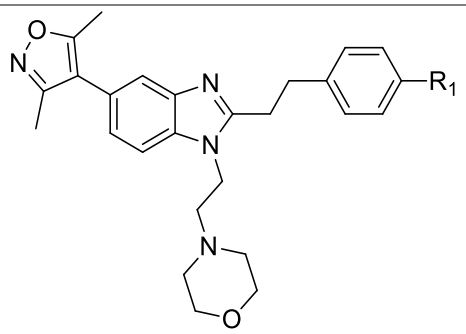

Entry	Compound	R_1	BRD4 IC_{50} (μM)[a]	CBP IC_{50} (μM)[a]
1	**2.10**		2.99 ± 0.086	0.265 ± 0.077
2	**3.04**	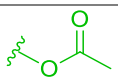	1.34 ± 0.072	0.168 ± 0.035
3	**3.06**	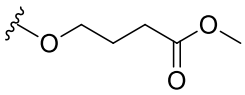	1.55 ± 0.011	0.523 ± 0.085
4	**3.09**	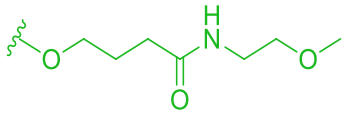	1.62 ± 0.009	0.328 ± 0.048
5	**2.10 (Lit)[b]**		4.40	0.240
6	**(+)-JQ1**	N/A	0.048 ± 0.001	N/A
7	**SGC-CBP30**	N/A	N/A	0.197 ± 0.021
8	**Bromosporine**	N/A	0.160 ± 0.004	2.94 ± 0.467

[b]assay n=3 data given as mean with SDs. [a]IC_{50} value calculated from FRET assay.[149]

ISOX-DUAL was ran in this assay as a control but had degraded and showed no observed binding to CBP so was not included. Instead the literature reporting IC_{50} value of **2.10** (Table 3.1, entry 5) was included as a comparable value to the IC_{50} values obtained.

The binding affinities of **2.10** was similar to that reported in literature for CBP and BRD4.[149] Investigations into the modifications at this site started though the acetylation of literature **2.10**. **3.04** had similar CBP affinity as literature probe SGC-CBP30 (Table 3.1, entry 2 vs entry 7) whilst retaining BRD4 binding. Compounds **3.06** and **3.09** contain a propyl chain, to mimic interactions that are present within ISOX-DUALs binding to the targets. **3.06** had a reduced affinity to CBP but not enough to warrant concern. **3.09** was synthesised as a mimic to potential degraders, and its affinities to BRD4/CBP match those of ISOX-DUAL (Table 3.2, entry 7). This confirms that this series of modifications are transferable to degrader design.

Table 3.2: Cell-free binding studies performed for the piperazine compounds, with comparison to ISOX-DUAL, alongside controls, SGC-CBP30, I-CBP112 and Bromosporine.

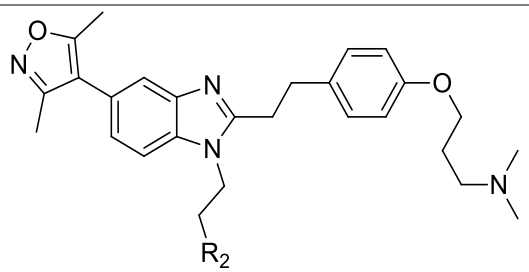

Entry	Compound	R_2	BRD4 IC_{50} (μM)[a]	CBP IC_{50} (μM)[a]
1	**ISOX-DUAL**	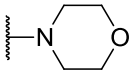	3.55	1.20
2	**3.19**	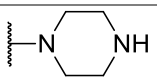	4.85	3.50
3	**3.22**	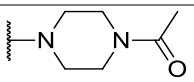	7.65	2.15
4	**3.20**	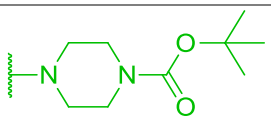	3.15	1.15
5	**3.28**	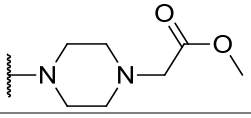	5.85	2.05
6	**3.29**	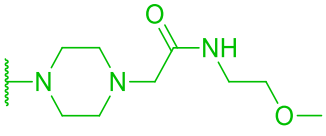	1.45	0.825
7	**ISOX-DUAL (Lit)**	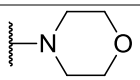	1.5	0.65
8	**(+)-JQ1**	N/A	0.061	N/A
9	**SGC-CBP30**	N/A	N/A	0.071
10	**Bromosporine**	N/A	0.35	3.1
11	**I-CBP112**	N/A	N/A	0.34

[a]assay n=2 data given is a mean.

Overall, none of the undertaken modifications resulted in a concerning loss of binding to the bromodomains. The IC_{50} values of ISOX-DUAL are double those reported in literature (Table 3.2, entry 1 vs entry 7). Switching from a morpholine to a piperazine (Table 3.2, entry 2) caused a slight reduction in CBP affinity. Expanding from the free amine with acetamide **3.22** (Table 3.2, entry 3) gave a reduction, but not significant enough to indicate binding affinity issues, whereas **3.20** matched the affinities of ISOX-DUAL (Table 3.2, entry 4). Alkylating the free amine to afford **3.28** gave similar affinities to ISOX-DUAL and **3.20** showing the CH_2 spacer, which was inserted for stability, did not reduce the binding affinities (Table 3.2, entry 5). Finally degrader mimic **3.29** (Table 3.2, entry 6) gave slighter more potent affinities to CBP than ISOX-DUAL and was validation for the binding of future degraders.

Both degrader mimics **3.09** and **3.29**, had retained their ISOX-DUAL like affinities for the bromodomains of both BRD4 and CBP, validating these precursor compounds for degrader synthesis (Chapter 4).

3.3 Conclusions

This chapter has reported the synthesis of novel modified ISOX-DUAL like structures in good yields, which allow manipulation to degrader technology. I also report the larger scale synthesis of degrader precursor compounds **3.10** (10 g) and **3.24** (3 g) synthesised, with overall yields of 25% and 17% respectively.

This chapter also describes the synthesis of an ISOX-DUAL and degrader intermediate (**3.34**) synthesised in good yield. This aldehyde containing compound provides the chemist the function to create desired degraders with modified linker sites able to do late stage degrader changes without having to constantly re-design the synthesis.

Finally, the data show that the modifications made to the degrader of ISOX-DUAL did not appear to remove binding affinities to either bromodomain. Degrader mimics **3.06** (1.62 µM for BRD4, 0.328 µM for CBP) and **3.26** (1.45 µM for BRD4, 0.825 µM for CBP) have not just retained their binding affinities to the target bromodomains, but also the dual properties of ISOX-DUAL. This should build confidence that degraders of ISOX-DUAL would still bind to their respective targets.

4 Chapter 4: Development and Analysis of ISOX-DUAL Degraders

4.1 Introduction

As discussed in Chapters 1 and 3, heterobifunctional degraders contain two ligands, one to a POI and the second to an E3 ligase, bound together by a linker. This allows the compound to bring together a POI and an E3 complex to induce ubiquitination on the target, and subsequent degradation.

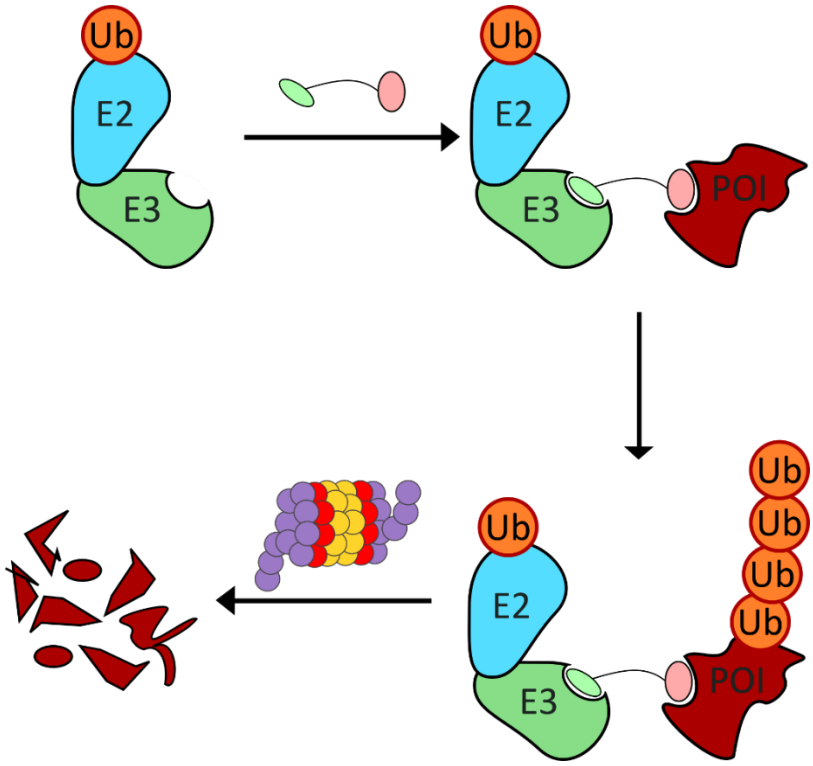

Figure 4.1: PROTAC-mediated ubiquitination and result and degradation via the 26S proteasome.

Small molecule inhibitors function in a competitive and occupancy-driven manner, while these heterobifunctional degraders induce ubiquitination of their target and subsequent degradation in a catalytic manner. This modality is less susceptible to increases in mutations, target expression, and does not incur the same resistance mechanism observed for small molecule inhibitors.[1,236]

In literature to date, there have been numerous degraders designed for BRD4, however only two publications have been found for CBP/p300 based degraders; a patent from the Dana Faber institute disclosing the structures of HAT domain recruiting A485 degraders, and another designed from HAT recruiting element GNE-781.[246,247] Currently, there are no BRD recruiting degraders for CBP/p300.

4.1.1 Aims of the Chapter

The aims of this chapter are to synthesise degraders from the precursors synthesised In Chapter 3 (**3.07** and **3.27**). These degraders will be initially screened against HeLa cells in order to check for their degradation potential before a streamlined selection of these are performed on other cell lines to check for their therapeutic effect against c-myc. By targeting both CBP/p300 and BRD4 (Figure 4.2), it is thought that a higher therapeutic effect against c-myc will be achieved due to degraders not relying upon potent binding to the POI like inhibitors do due to the catalytic nature of the degraders.

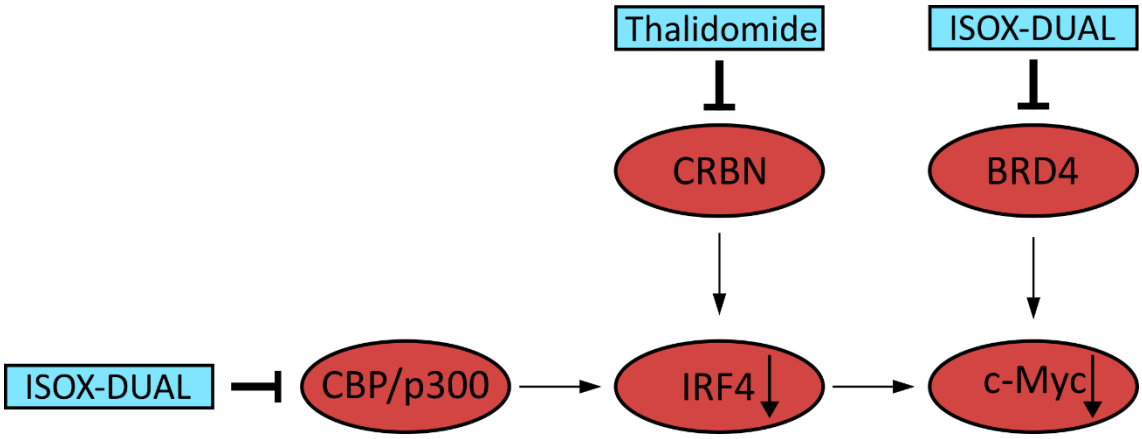

Figure 4.2: ISOX-DUALs inhibition pathway for c-Myc downregulation.[2,204–206]

Literature PROTACs have shown the incorporation of both CRBN/Cullin 4A and VHL/Cullin 2 ligands have successfully been incorporated into degrader compounds, and so therefore, this study utilised thalidomide analogues to recruit CRBN and VHL032 to recruit VHL in the design of our ISOX-DUAL degraders.[236,237] The design of these degraders followed a systematic strategy that included the optimisation of the linker length/composition, the position of the linker attachment to ISOX-DUAL (Figure 4.3), and the choice of the E3 ligase ligands. The phenol based degraders were synthesised initially as **3.07** was synthesised before **3.27**.

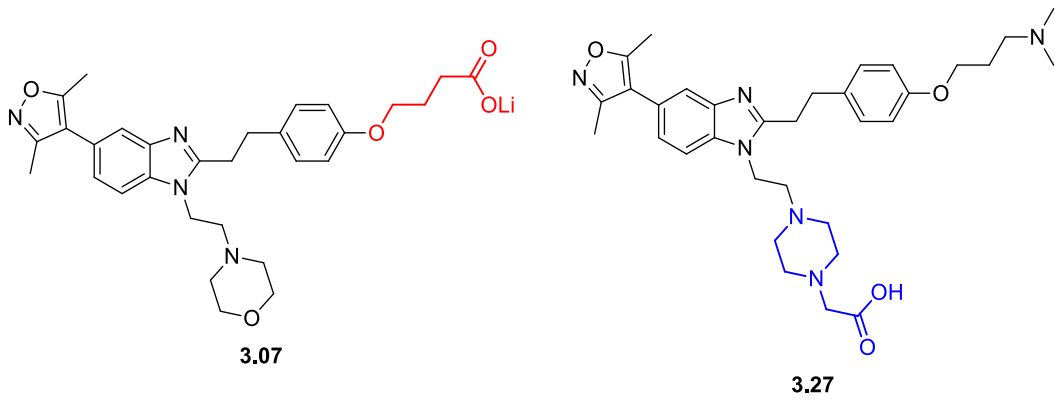

*Figure 4.3: Precursor compounds (Chapter 3) for the synthesis of degraders based on ISOX-DUAL, **3.07** for the phenol based degraders and **3.27** for the piperazine-based series.*

4.2 Results and Discussion

4.2.1 Synthesis of Phenol Modified Degraders

The first generation ISOX-DUAL degraders were synthesised through an amide formation reaction between precursor **3.07** and four E3 linker toolbox compounds (Figure 4.4).

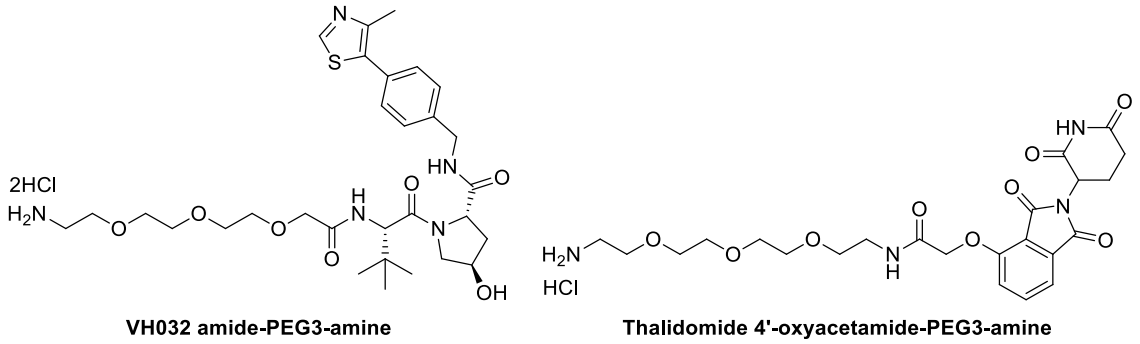

Figure 4.4: Example structures of the E3 linker toolbox compounds provided by Tocris.

During reaction work up, a base wash (saturated $NaHCO_3$) was utilised to remove any unreacted warhead ligand to assist with purification. The amide formations were achieved in moderate to high yields (55-75%) and isolated, after purification, with purities ≥95%. Once synthesised, the degrader compounds had their affinities determined against the BRDs of target proteins BRD4/CBP to assess SAR and target engagement. The yields, purities and IC_{50} values obtained for these degraders are contained in Table 4.1, alongside literature inhibitors and **2.10**.

Table 4.1: Yields, purities, and binding affinities of the first generation ISOX-DUAL degraders.

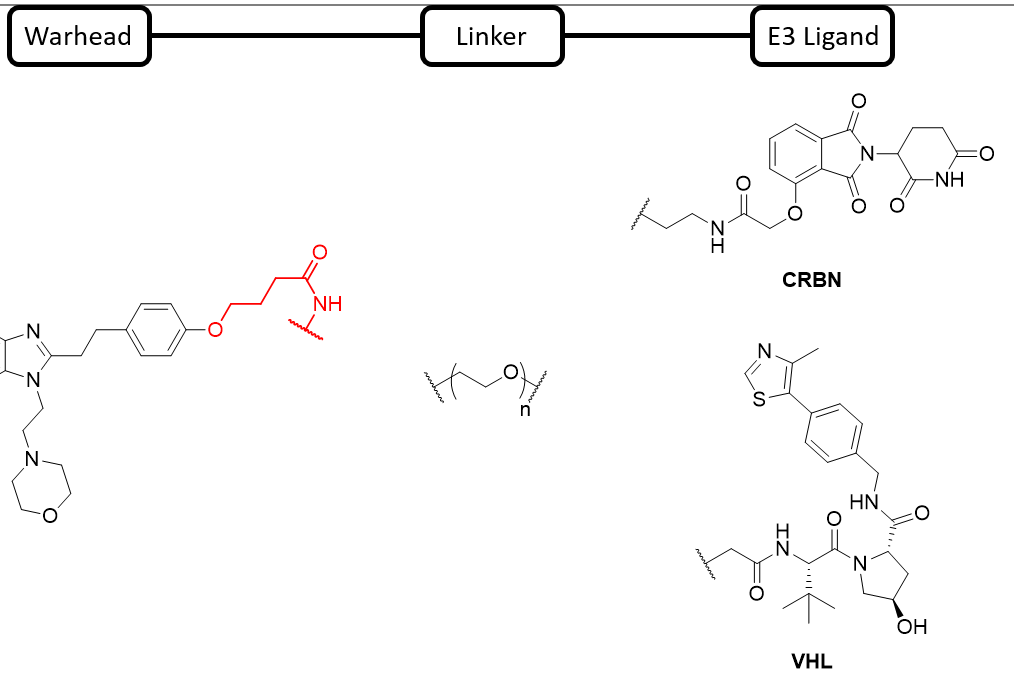

Entry	Compound	n	E3 Ligand	Yield (%)[a]	Purity (%)	BRD4 IC_{50} (μM)[b]	CBP IC_{50} (μM)[b]
1	**4.01**	3	CRBN	60	>99	2.002 ± 0.127	1.433 ± 0.081
2	**4.02**	4	CRBN	55	95	1.840 ± 0.042	1.468 ± 0.160
3	**4.03**	3	VHL	75	95	4.557 ± 0.137	3.367 ± 0.377
4	**4.04**	4	VHL	65	96	1.078 ± 0.029	1.473 ± 0.500
5	Bromosporine	-	-	-	-	0.048 ± 0.001	>20
6	SGC-CBP30	-	-	-	-	N/A	0.197 ± 0.021
7	(+)-JQ1	-	-	-	-	0.160 ± 0.004	N/A
8	**2.10**	-	-	-	-	2.99 ± 0.086	0.265 ± 0.077
9	**2.10** (lit)[149]	-	-	-	-	4.40	0.240
10	ISOX-DUAL (lit)[2]	-	-	-	-	1.5	0.65

[a]Isolated Yield. [b]assay n=3 data given as mean with SDs.

The binding affinities of the degraders had similar affinities to BRD4 as the literature precursor **2.10**, which as the free phenol compound synthesised in Chapter 2 and modified in Chapter 3. However, instead of being 10-20-fold more selective to BRD4 than CBP (Table 4.1, entry 8 and 9), they appear less selective, but more dual like. The loss in BRD4 affinity is not problematic, due to the aims of synthesising dual action degraders to observe any therapeutic benefit over single action degraders.

4.2.2 **Physiochemical Properties**

The size and nature of degrader compounds mean they fall into a chemical space beyond Lipinski's rule of five.[348,349] A recent report reviewed published literature on degrader compounds and found they exist within a differential physiochemical space.[350] Here they report some general principles for degrader design, which are that the hydrogen bond donor (HBD) count is kept ≤5, the total polar surface area (TPSA) does not exceed 250 Å^2 and that increased lipophilicity of degraders positively correlates with their degrader score, where the highest scorers have an average clogP of 6.[350]

With this information to hand, the physiochemical properties of the first generation degraders (Table 4.2, entries 3, 4, 7 and 8) were calculated along with theoretical compounds with various linkers and E3 ligands for phenol degraders (Table 4.2). Alongside these physiochemical properties were also calculated for the piperazine-based degraders (Table 4.3). This will allow the dictation of the synthesis of the degraders with ideal physiochemical properties, to ensure passive cellular permeability is not an issue. Chemdraw was used for the calculation of molecular weight and the online tool SwissADME was used for the calculation of HBA, HBD, TPSA, rotatable bonds and clogP.[351] Structures of these degraders are portrayed within Scheme 4.1

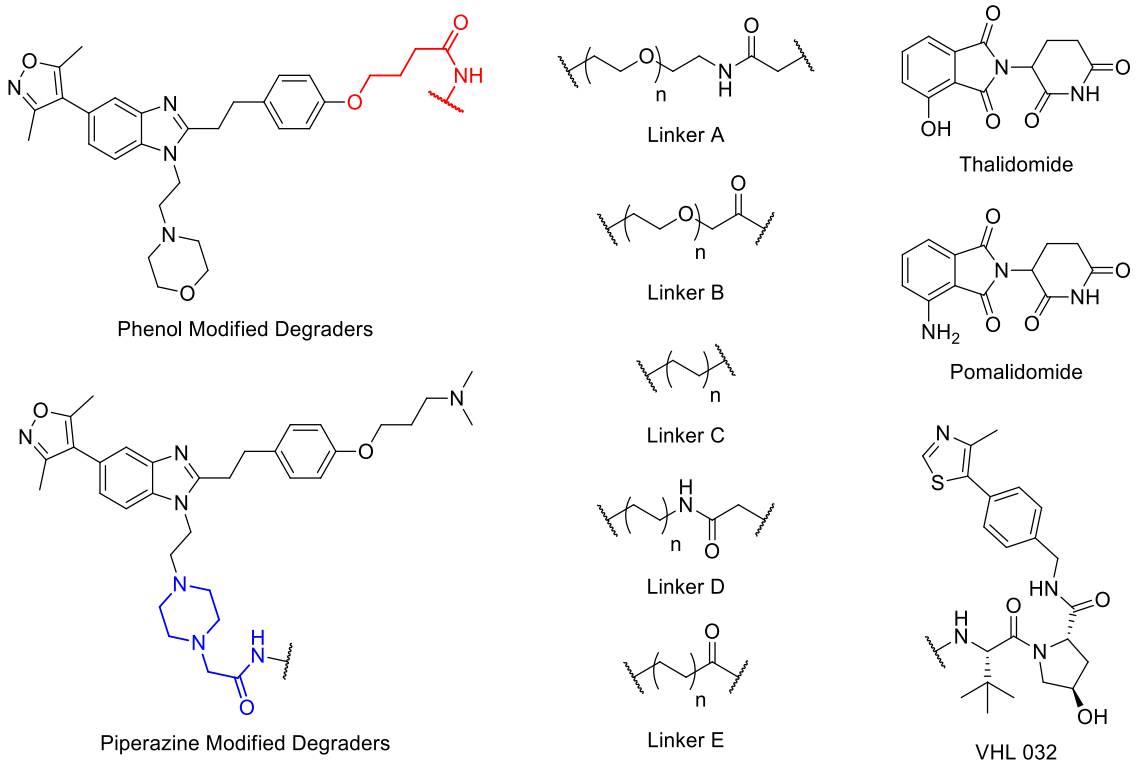

Scheme 4.1: Degraders which had physiochemical properties calculated in Table 4.2 for phenol modified degraders and Table 4.3 for piperazine modified degraders.

Table 4.2: Calculated properties of degrader compounds for the phenolic linker position. Structural information for the degraders is portrayed within Scheme 4.1.

Entry	Linker	n	Ligase Ligand	Exit Vector	Molecular Weight (g mol^{-1})	HBA[ac]	HBD[bc]	Rot Bonds[c] (Å^2)	TPSA[ce]	clogP[cde]
1	A	1	Thalidomide	Alkyl Amide	933.02	14	3	24	225.76	3.22
2	A	2	Thalidomide	Alkyl Amide	977.07	15	3	27	234.99	3.37
3	A	3	Thalidomide	Alkyl Amide	1021.12	16	3	30	244.22	3.40
4	A	4	Thalidomide	Alkyl Amide	1065.17	17	3	33	253.45	3.49
5	B	1	VHL 032	Amide	1046.28	13	4	28	243.75	5.34
6	B	2	VHL 032	Amide	1090.34	14	4	31	252.98	5.48
7	B	3	VHL 032	Amide	1134.39	15	4	34	262.21	5.47
8	B	4	VHL 032	Amide	1178.44	16	4	37	271.44	5.62
9	E	2	VHL 032	Amide	1016.26	12	4	26	234.52	5.65
10	E	4	VHL 032	Amide	1044.31	12	4	28	234.52	6.28
11	E	6	VHL 032	Amide	1072.36	12	4	30	234.52	6.83
12	E	8	VHL 032	Amide	1100.42	12	4	32	234.52	7.57
13	C	2	Thalidomide	Alkyl	831.91	12	2	18	187.43	3.88
14	C	4	Thalidomide	Alkyl	859.97	12	2	20	187.43	4.55
15	C	6	Thalidomide	Alkyl	888.02	12	2	22	187.43	5.20
16	C	8	Thalidomide	Alkyl	916.07	12	2	24	187.43	5.85
17	D	2	Thalidomide	Alkyl Amide	888.96	13	3	21	216.53	3.27
18	D	4	Thalidomide	Alkyl Amide	917.02	13	3	23	216.53	4.00
19	D	6	Thalidomide	Alkyl Amide	945.07	13	3	25	216.53	4.54
20	D	8	Thalidomide	Alkyl Amide	973.12	13	3	27	216.53	5.28
21	C	2	Pomalidomide	Alkyl	830.93	11	3	18	190.23	3.95
22	C	4	Pomalidomide	Alkyl	858.98	11	3	20	190.23	4.53
23	C	6	Pomalidomide	Alkyl	887.03	11	3	22	190.23	5.18
24	C	8	Pomalidomide	Alkyl	915.09	11	3	24	190.23	5.88

[a]HBA = Hydrogen Bond Acceptor. [b]HBD = Hydrogen Bond Donor. [c]Calculated properties were performed using swissADME. [d]Consensus clogP value was chosen. [e]TPSA/clogP flags were raised for 250 and 7 respectfully as described by literature.[350]

Table 4.3: Calculated properties of degrader compounds for the piperazine linker position. Structural information for the degraders is portrayed within Scheme 4.1.

Entry	Linker	n	Ligase Ligand	Exit Vector	Molecular Weight (g mol^{-1})	HBA[bd]	HBD[cd]	Rot Bonds[d] (Å^2)	TPSA[d]	clogP[de]
1	A	1	Thalidomide	Alkyl Amide	989.13	15	3	26	223.01	2.91
2	A	2	Thalidomide	Alkyl Amide	1033.18	16	3	29	232.24	2.93
3	A	3	Thalidomide	Alkyl Amide	1077.23	17	3	32	241.47	3.12
4	A	4	Thalidomide	Alkyl Amide	1121.28	18	3	35	250.70	3.29
5	B	1	VHL 032	Amide	1102.39	14	4	30	241.00	4.98
6	B	2	VHL 032	Amide	1146.45	15	4	33	250.23	5.38
7	B	3	VHL 032	Amide	1190.50	16	4	36	259.46	5.20
8	B	4	VHL 032	Amide	1234.55	17	4	39	268.69	5.36
9	E	2	VHL 032	Amide	1072.37	13	4	28	231.77	5.24
10	E	4	VHL 032	Amide	1100.42	13	4	30	231.77	6.01
11	E	6	VHL 032	Amide	1128.47	13	4	32	231.77	6.46
12	E	8	VHL 032	Amide	1156.53	13	4	32	231.77	7.24
13	C	2	Thalidomide	Alkyl	888.02	13	2	20	184.68	3.67
14	C	4	Thalidomide	Alkyl	916.07	13	2	22	184.68	4.34
15	C	6	Thalidomide	Alkyl	944.13	13	2	24	184.68	4.93
16	C	8	Thalidomide	Alkyl	972.18	13	2	26	184.68	5.67
17	D	2	Thalidomide	Alkyl Amide	945.07	14	3	23	213.78	3.03
18	D	4	Thalidomide	Alkyl Amide	973.13	14	3	25	213.78	3.71
19	D	6	Thalidomide	Alkyl Amide	1001.18	14	3	27	213.78	4.24
20	D	8	Thalidomide	Alkyl Amide	1029.23	14	3	29	213.78	5.00
21	C	2	Pomalidomide	Alkyl	887.04	12	3	20	187.48	3.67
22	C	4	Pomalidomide	Alkyl	915.09	12	3	22	187.48	4.29
23	C	6	Pomalidomide	Alkyl	943.14	12	3	24	187.48	4.99
24	C	8	Pomalidomide	Alkyl	971.20	12	3	26	187.48	5.57

[a]HBA = Hydrogen Bond Acceptor. [b]HBD = Hydrogen Bond Donor. [c]Calculated properties were performed using swissADME. [d]Consensus clogP value was chosen. [e]TPSA/clogP flags were raised for 250 and 7 respectfully as described by literature.[350]

The two thalidomide containing degraders had a low clogP (Table 4.2, entries 3, 4), whereas the two VHL032 containing degraders had clogP values closer to the average from the aforementioned study (Table 4.2, entries 7, 8). This was expected due to VHL032 having a higher clogP than any of the thalidomide analogues. Except for Table 4.2 entry 3 the synthesised degraders containing PEG linkers had a TPSA above 250 Å. The PEG linkers were originally chosen for the phenol degraders due to their usage within PROTAC literature.[234,236–238,240] This could be problematic for cell permeability, however, these compounds were still analysed *via* immunoblotting as physiochemical properties were calculated as a guideline rather than a series of rules.

Second generation synthesis of phenol degraders should look at the incorporation of alkyl linkers, due to the reduction in TPSA and an increase in clogP, which may be beneficial for passive cell permeability. However, no more phenol modified degraders were synthesised due to time restraints on the project (due to lockdown) and the immense workload that would be needed for immunoblotting.

As physiochemical property calculations were performed before the synthesis of the piperazine based degraders, these values allowed us to dictate the synthesis of this series and instead of synthesising a library of PEG linker degraders. This led to the synthesis of alkyl linkers with this series, due to overall significantly lower TPSA, and clogP values close to the aforementioned average of 6 from the literature review (Table 4.3, entries 9 – 24).[350] Some of these degraders, however, still retained relatively low clogP values (Table 4.3, entries 13, 17, 18, 19) and one had a clogP value above 7 (Table 4.3, entry 12). All the alkyl linked degraders were still made in order to check for observable degradation of the target proteins, even with unfavourable physiochemical properties.

4.2.3 **Synthesis of Piperazine Modified Degraders**

4.2.3.1 Synthesis of the Alkyl Linker Series

After calculating the physiochemical properties of a range of degraders, the synthesis of a series of E3 ligands and alkyl linkers was carried, to make degraders with a lower TPSA and higher clogP.

This work was initiated by the synthesis of 4-hydroxyl thalidomide (**4.09**) and was achieved through a one pot reaction (Scheme 4.2). This reaction was high yielding, and the product was pure by ^{1}H NMR spectroscopic analysis. A portion of compound **4.09** was alkylated with *tert*-butyl bromoacetate, followed by TFA deprotection of the *tert*-butyl ester group to afford **4.11** as a white solid in good yield. Compound **4.11** was then reacted with several *N*-Boc-diamines with varying alkyl lengths to afford intermediate amides **4.12**, **4.13**, **4.14** and **4.15**.

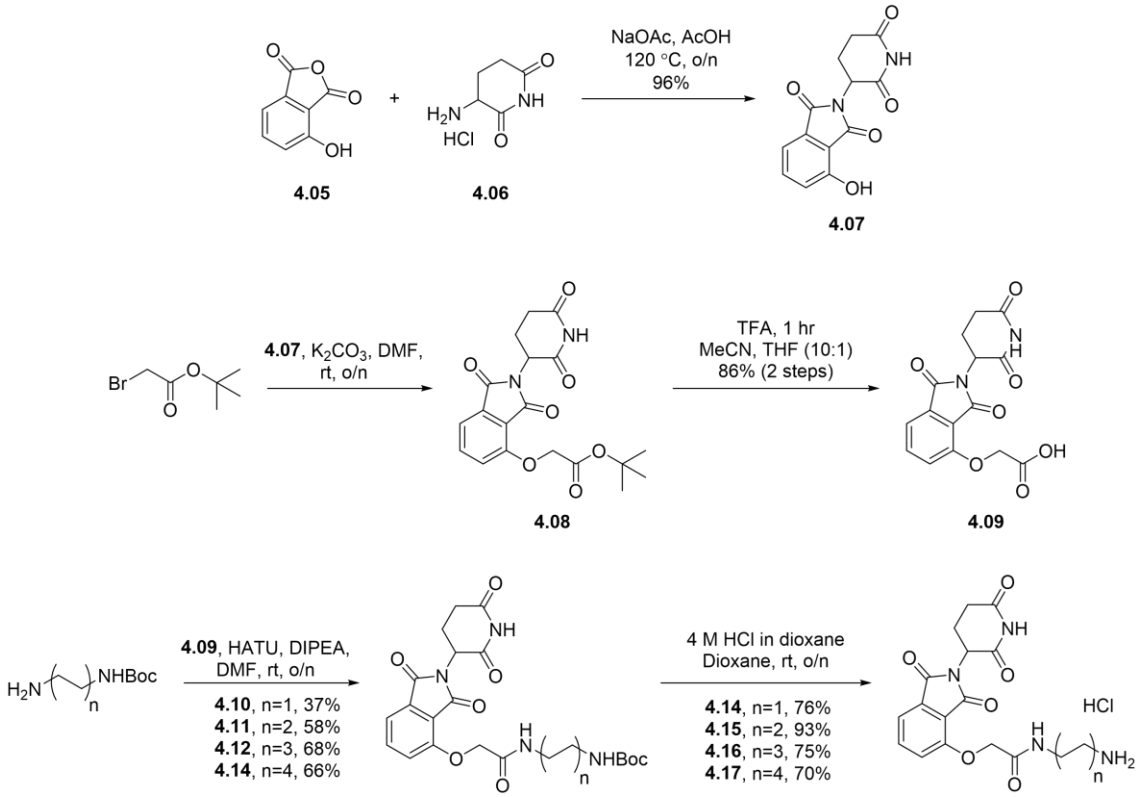

*Scheme 4.2: Synthesis of **4.09** and **4.11** and the respective thalidomide alkyl amide linkers **4.14, 4.15, 4.16, 4.17**.*

Amide formation and Boc-deprotection resulted in the target linkers (**4.14** – **4.17**) in good yields. The amide formation to achieve **4.10** resulted in a yield sub 50%, which was a significantly lower yield than the chain lengths. These 4 intermediates were then de-protected to result in the E3 linker as the HCl salt.

Compounds **4.18** – **4.21** were synthesised in high yields *via* an Appel reaction from varying length *N*-Boc-alkyl alcohols. These alkyl bromides were then used in an alkylation reaction with **4.07** and finally a Boc-deprotection to afford the target E3 linkers (Scheme 4.3).

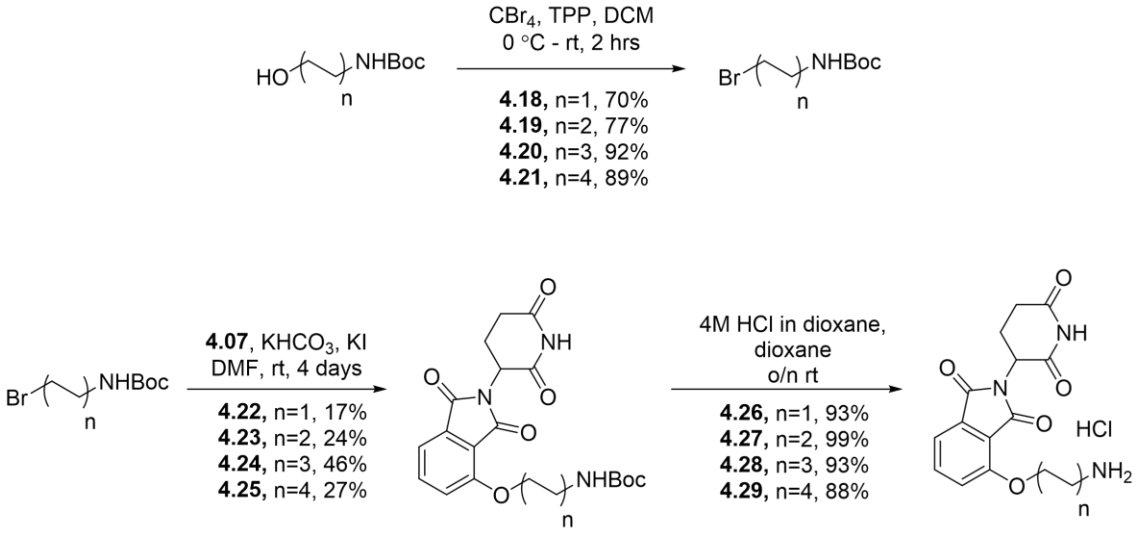

*Scheme 4.3: Synthetic sequence for the synthesis of thalidomide alkyl linkers **4.26**, **4.27**, **4.28**, **4.29**.*

Overall, the alkylation yields were low (**4.22** – **4.25**), hence, alkyl tosylates were also made and tested but did not achieve an increase in yield. Increasing temperature or reaction time did not increase the yield of this reaction either. Mitsunobu conditions were trialled with **4.07** with *N*-Boc-ethanolamine, however isolation of the product was not possible, as it was thought that both the NH and the OH were reacting in these conditions. Further investigations were not carried out.[352]

The final CRBN linker series was the pomalidomide one, which started with the synthesis of 4-fluorothalidomide (**4.31**), using the same one pot method as previously utilised for **4.07**, which resulted in **4.31** as a purple solid in high yield (Scheme 4.4).

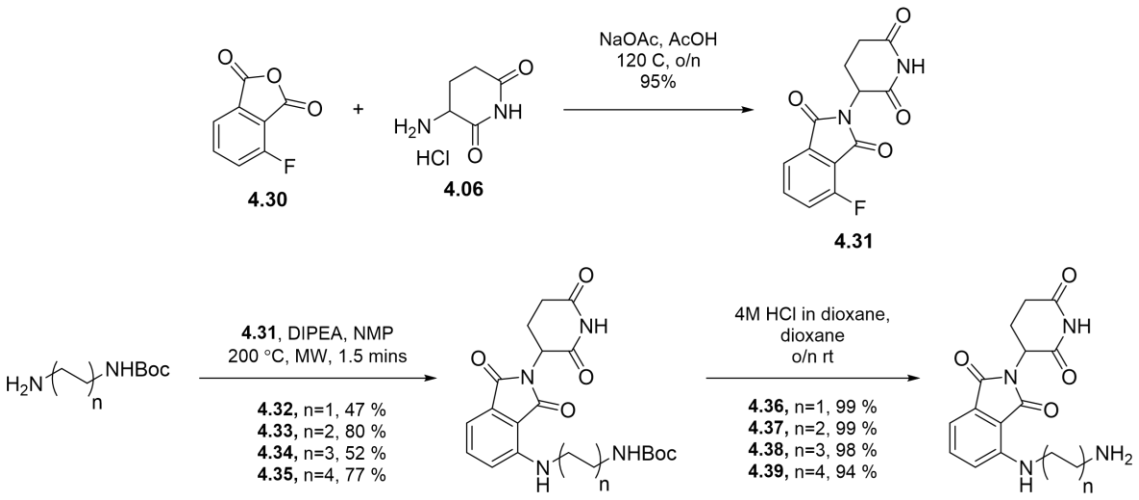

*Scheme 4.4: Synthetic sequence for the synthesis of pomalidomide alkyl linkers **4.35**, **4.36**, **4.37**, **4.39**.*

Previous research into the synthesis of ISOX-DUAL utilised microwave-mediated organic synthesis to synthesise (Chapter 2), these conditions were applied to these reactions but at a higher temperature, as NMP was the solvent here. The substitutions were achieved with mixed yields and inspecting the synthesis of **4.32** in an attempt to increase the yield resulted in no change. A future investigation into improving conversion of these compounds should investigate temperature and reaction time, as the other conditions are the same as literature, however this was not performed due to the lack of novelty in the compounds.[11] These amides were then converted to the HCl salt free amine in the same manner as previously in high yields to afford the desired E3 linkers (**4.36** – **4.39**) as yellow solids.

The final series of linkers to be utilised in the synthesis of the degrader library are based on VHL032. The methodologies utilised were adapted from literature (Scheme 4.5).[353] Original attempts to synthesise **4.42** tried to purify the methyl ester before hydrolysis, but resulted in significant compound loss, whereas carrying the material through crude did not seem to impact yield or purity of **4.42**.

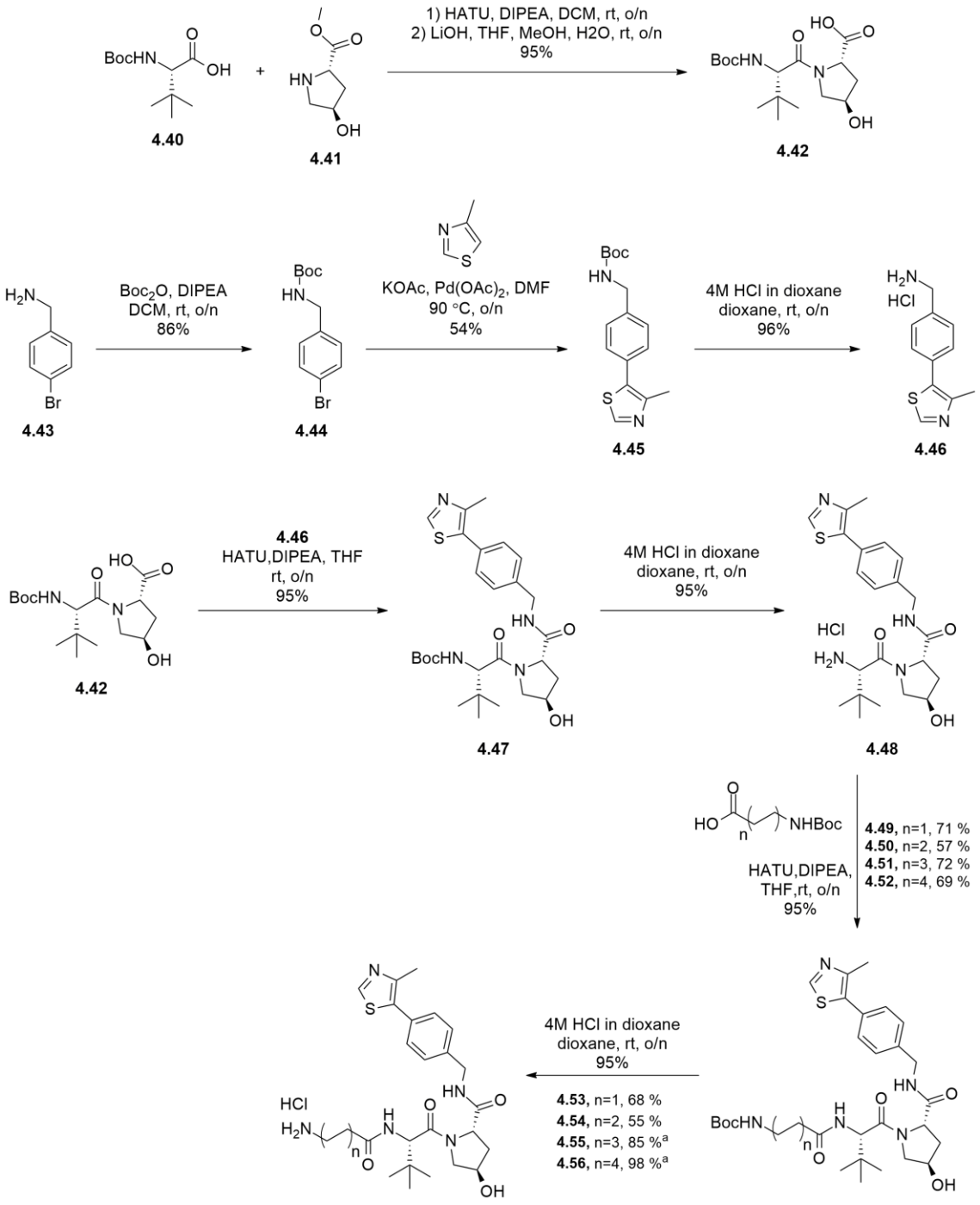

*Scheme 4.5: Synthetic scheme for the synthesis of VHL032 (**4.48**). [a]Reaction left for 2 hours due to degradation.*

Following literature precedents, **4.46** was synthesised through a Boc-protection (**4.44**), followed by a Heck coupling (**4.45**) and finally a Boc-deprotection to afford **4.46** as a yellow gum. Variances in the synthesis of **4.46** within the literature utilised a cyano moiety rather than an amine, however, this route was not utilised here.[232] Conversion to VHL032 (**4.48**) from **4.42** was performed in high yields through an amide coupling with **4.46** (95%) and Boc-deprotection to afford **4.48** as a yellow solid.

Amides **4.49** – **4.52** were achieved in mid to high yields before Boc-deprotection to afford E3 linkers **4.53** – **4.56**. These deprotections gave lower yields than the other linker series, this was found to be due to degradation of the material in the acidic conditions.

The Boc-deprotections were originally left overnight and resulted in the presence of a second peak in LC-MS, with an m/z of 318.2, which correlated with that of the cleaved pyrrolidine amide. To mitigate the amide cleavage in **4.55** and **4.56** a shorter reaction time was utilised, which resulted in a significant yield boost. To boost the yields of these linkers in future, it is crucial to monitor the progress of the hydrolysis.

4.2.3.2 Synthesis of Piperazine Modified Degraders

Initial reactions into synthesising the target degraders failed on test scales (0.079 mmol) and so were performed on a significantly higher scale than what was needed (0.227 mmol). Purification of these compounds was challenging, previously this was difficult to achieve due to the close running of a second compound with similar mass. In this iteration of reactions, mass was able to be sacrificed to obtain purer compounds *via* normal phase purification using 1-6% 7N NH_3 Methanol in DCM. Ideally prep HPLC would have been utilised to purify these compounds, however due to the legislation upon the ISOX-DUAL moiety, this was unable to be performed due to the unavailability at the site of the licence.

Manual column chromatography was utilised over flash chromatography to exert a higher control on the eluent's gradient, to get as much separation between the product and the impurity. Identification of the impurity was attempted, however was unachieved due to separation. This approach to the synthesis and purification resulted in high purities of the degraders (Table 4.4), full structures of the degraders can be found in the experimental.

Table 4.4: Synthesis of the Piperazine warhead degraders with various linker lengths, E3 ligase ligands and respective synthetic yields and purities.

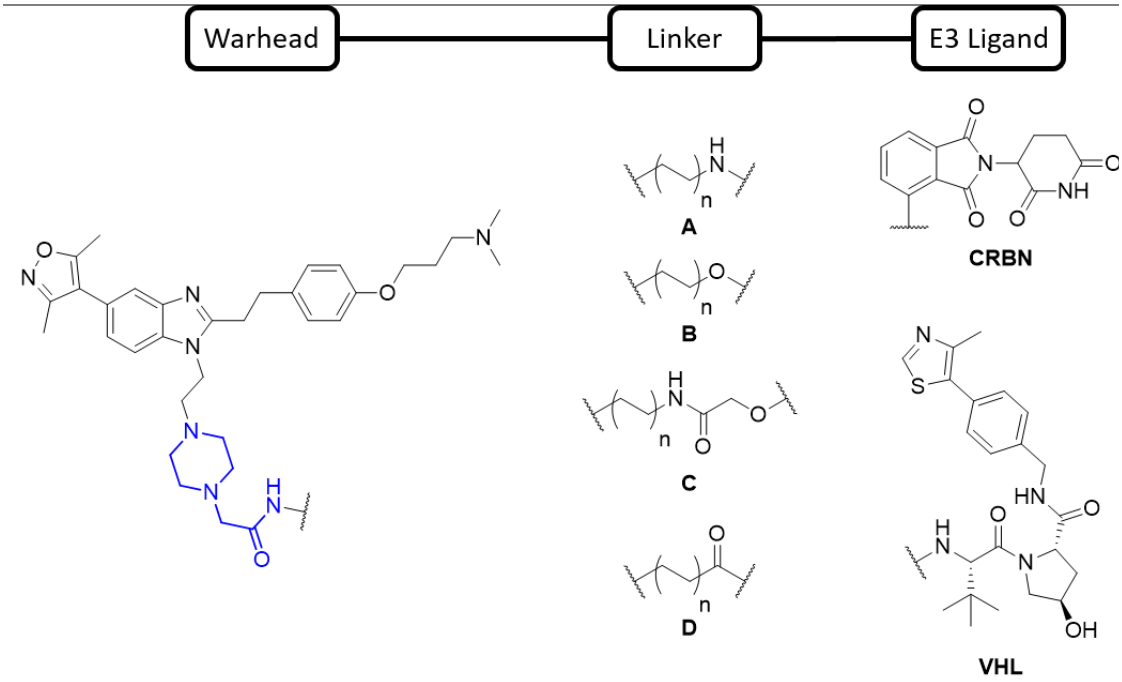

Entry	Compound	Linker	n	E3 Ligand	Yield (%)[a]	Purity (%)[b]
1	4.57	A	1	CRBN	49	98
2	4.58	A	2	CRBN	32	99
3	4.59	A	3	CRBN	46	98
4	4.60	A	4	CRBN	24	96
5	4.61	B	1	CRBN	35	>99
6	4.62	B	2	CRBN	37	96
7	4.63	B	3	CRBN	35	>99
8	4.64	B	4	CRBN	52	>99
9	4.65	C	1	CRBN	16	>99
10	4.66	C	2	CRBN	33	>99
11	4.67	C	3	CRBN	43	>99
12	4.68	C	4	CRBN	21	95
13	4.69	D	1	VHL	40	98
14	4.70	D	2	VHL	22	96
15	4.71	D	3	VHL	37	97
16	4.72	D	4	VHL	35	90

[a]Isolated Yield. [b]Determined by LC-MS.

4.2.3.3 Binding studies of Piperazine Modified Degraders

In order to ascertain if the binding affinities measured in Chapter 3 were maintained or lost in the translation from the piperazine based inhibitors to the degraders, the latter were subjected to their biochemical binding affinity assays against the two targets (Table 4.5). The affinities for ISOX-DUAL and **3.26** from Chapter 3 were included within Table 4.5 for comparison.

Table 4.5: Binding affinities of the Piperazine based degraders against BRD4 and CBP.

Entry	Compound	Linker	n	E3 Ligand	BRD4 IC_{50} (μM)[a]	CBP IC_{50} (μM)[a]	BRD4/CBP Selectivity
1	4.57	A	1	CRBN	0.157 ± 0.009	>20	>127
2	4.58	A	2	CRBN	0.117 ± 0.004	8.337 ± 2.098	71
3	4.59	A	3	CRBN	0.083 ± 0.003	4.513 ± 0.872	54
4	4.60	A	4	CRBN	0.081 ± 0.004	10.48 ± 0.358	123
5	4.61	B	1	CRBN	0.065 ± 0.006	6.742 ± 0.560	104
6	4.62	B	2	CRBN	0.088 ± 0.002	14.32 ± 0.106	163
7	4.63	B	3	CRBN	0.114 ± 0.004	>20	175
8	4.64	B	4	CRBN	0.088 ± 0.002	10.696 ± 1.14	121
9	4.65	C	1	CRBN	0.074 ± 0.004	6.039 ± 0.386	82
10	4.66	C	2	CRBN	0.109 ± 0.003	4.563 ± 1.478	42
11	4.67	C	3	CRBN	0.209 ± 0.006	8.799 ± 4.498	42
12	4.68	C	4	CRBN	0.119 ± 0.000	13.038 ± 1.534	110
13	4.69	D	1	VHL	0.161 ± 0.006	3.615 ± 0.126	22
14	4.70	D	2	VHL	0.127 ± 0.014	3.729 ± 0.003	29
15	4.71	D	3	VHL	0.101 ± 0.003	13.20 ± 0.338	131
16	4.72	D	4	VHL	0.131 ± 0.008	9.095 ± 1.550	70
17	3.26[b]	-	-	-	1.45	0.825	0.56
18	ISOX-DUAL[b]	-	-	-	1.5	0.65	0.43
19	(+)-JQ1	-	-	-	0.048 ± 0.001	>20	417
20	SGC-CBP30	-	-	-	N/A	0.197 ± 0.021	N/A
21	Bromosporine	-	-	-	0.160 ± 0.004	2.943 ± 0.467	18

[a]assay n=3 data given as mean with SDs. [b]assay n=2 data given as mean, taken from Chapter 3: Table 3.2.

Overall, the degrader compounds still engaged both BRD4 and CBP. However, affinity to BRD4 had improved significantly, with **4.61** having a similar binding affinity to (+)-JQ1 (Table 4.5, entry 5). Multiple degraders had their BRD4 affinities sub 100 nM (Table 4.5, entries 3 – 6, 8 and 9). This might be due to picking up additional interactions on the surface of the protein,

however at the time of submission for this document, no crystal structure of the degraders bound to BRD4 was obtained. However, work is in progress in this respect.

The CBP affinity of the degraders was reduced, with **4.61** being 104-fold more selective to BRD4 than CBP (Table 4.5, entry 5). This leads to suggest that modifications at the piperazine site reduces the dual-like affinity of the inhibitor and turns it into a BRD4 selective binder.

As binding affinity is only a measure of how well the compound binds to the target proteins and not a measure of ability to degrade, both series of degraders were carried on through the analysis, i.e. treated against cells, and the piperazine series was also sent for in vitro ubiquitylation assays to test their ability to ubiquitinate their targets outside of a cellular environment.

4.2.4 **Biochemical Analysis of Degraders**

The data discussed within this section was all carried out by collaborators within Bio-Techne, except for the data presented in Figure 4.11 which was carried out by myself, under the supervision of Professor Karim Malik and Dr Madhu Kollareddy at Bristol University.

4.2.4.1 Cell-Free Protein Ubiquitylation Assay

Cell-free ubiquitination assays provide a useful metric for evaluation of degrader libraries, by seeing if the degraders can engage the POI, E3 ligase and induce ubiquitination of the POI in a system with no complicating variables, such as off targets, cell permeability and metabolism. This will allow for a better understanding of the data received from Western blotting as if the degraders can induce ubiquitination here but not in the cells, it would suggest other factors are contributing to the observed reduced ubiquitination.

The *in vitro* assays contain all the components for analysis of the ternary complex; E1, UBE2D1, VHL ligase, BRD4, ubiquitin and buffer in deionised water, along with the degrader ligand. The addition of ATP sets the assay off, and analysis of any ubiquitination can be performed *via* Western blot.

Due to the covid-19 pandemic, only selected degraders, **4.69** – **4.72** (Figure 4.5) were investigated in this assay using house-bespoke procedures by Brad Brasher at Boston Biochem. However, currently degraders **4.59**, **4.62**, **4.67** and **4.68** along with control dBET-1, are currently being tested in this cell-free assay.

VHL032 containing degraders (**4.69** – **4.72**) were shown to engage both BRD4 and the VHL ligase to invoke ubiquitylation of BRD4 as seen by the change in mass of the protein. Each degrader also displays the dose response phenomenon, the *hook effect*, discussed in Chapter 1. At 40 µM, the concentration of the degrader is too high to generate ternary complexes, as the binding sites of both the POI and E3 recruiter will be saturated by ligands. At 0.87 nM the concentration of the degrader is too low to generate efficient ubiquitylation of the targets and so appears like the control (0 nM). At the summit of the curve, the concentration of degrader (e.g **4.71** 200 nM) is ideal for the generation of the maximum number of ternary complexes so all the BRD4 displays ubiquitylation.

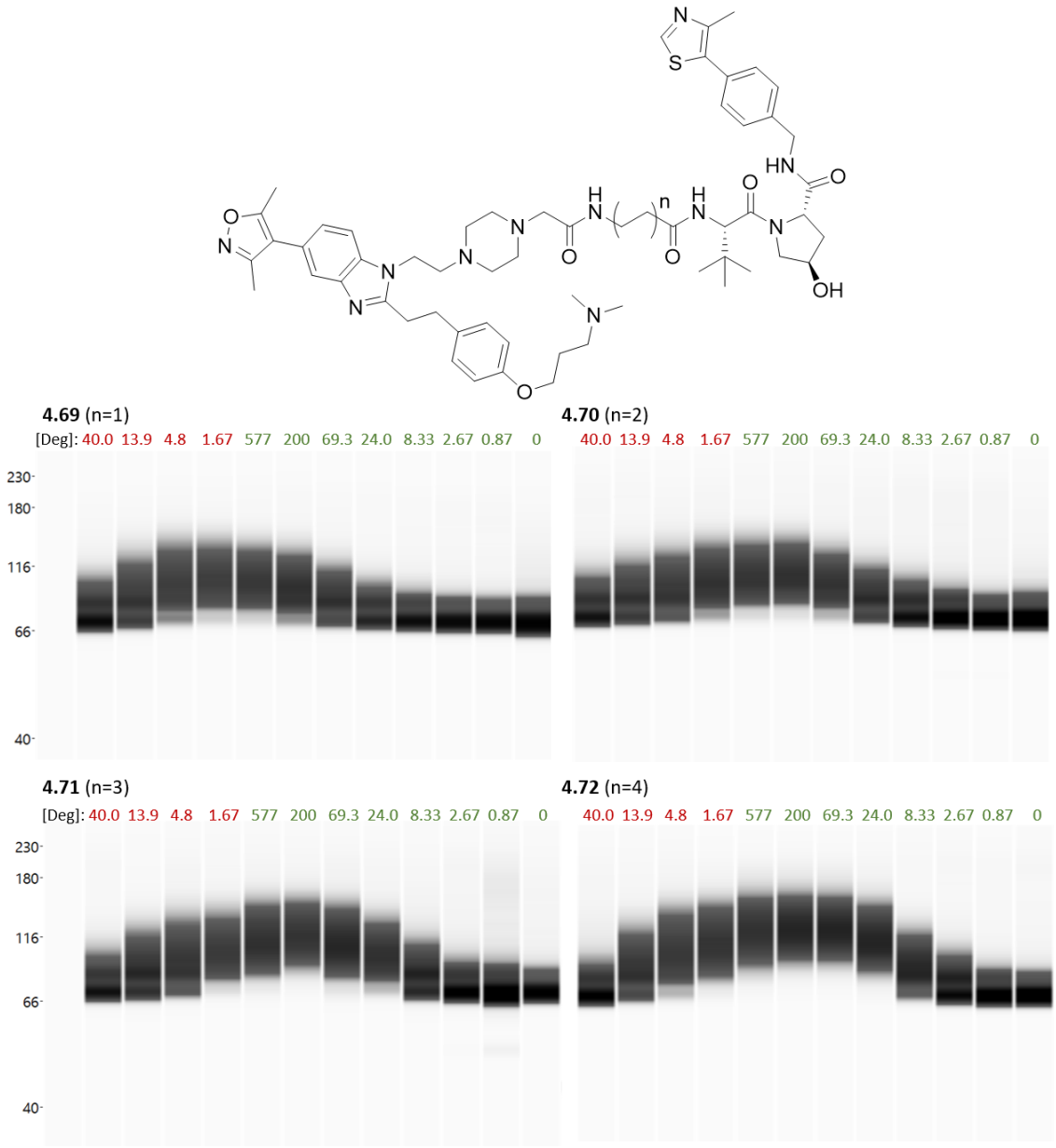

*Figure 4.5: In vitro BRD4-ubiquitylation assays for VHL032 containing degraders **4.69**, **4.70**, **4.71**, **4.72**. [Deg] concentrations given in μM (red) and nM (green). The observed hook effect is shown at lower concentrations as the linker length of the degrader gets longer.*

An interesting trend from Figure 4.5 is that as the length of the linker increases from n=1 in **4.69** to n=4 in **4.72**, the hook effect is shown to occur at lower concentrations of degrader. This suggests that the longer linker lengths create more stable ternary complexes than the shorter ones, most likely due to more favourable interactions being formed within the PPI. Degrader **4.72** displays slight ubiquitylation of BRD4 at 2.67 nM, and altogether this data suggests that the longer linker lengths in this series provide a more stable ternary complex.

4.2.4.2 Immunoassay Analysis of ISOX-DUAL Degrader Compounds

Treatment of HeLa cells with ISOX-DUAL degraders caused a reduction in BRD4 and CBP

Western blotting analysis of the degrader compounds was performed using Simple Western™, which, is a capillary electrophoresis immunoassay (CEI)-based methodology allowing for rapid and quantitative analysis on the relative abundance of a protein of interest. Utilisation of this modality will also allow for the capture and quantitation of high-molecular-weight proteins, such as BRD4 and CBP as well as eliminating run-to-run variability of Western blots by automation of the loading, transfer, incubation and wash times.[354]

Due to timings of the project, phenol-based degraders **4.01**-**4.04** were synthesised initially and their ability to degrade BRD4 and CBP/p300 was assessed by immunoassays using capillary-based electrophoresis. However, the initial experiments with these compounds revealed issues with HSP60 loading control level reduction, and issues with the integration of low peak signals. HSP60, in order to be retained on the same cartridge as BRD4 / CBP, appeared to be reduced in treatments with higher concentrations of compound. It was unclear as to why this was occurring.

Example data of this issue can be seen in the Western blots displayed in Figure 4.6, where HeLa cells were treated with the respective degrader for 4 or 24 hours at varying concentrations and their effect on the levels of CBP were measured. Both **4.02** and **4.04** appeared to give a reduction in CBP signals with increasing amounts of the degrader, with a higher reduction observed at 24-hour treatment times. However, treatment with the degraders caused a reduction or loss in HSP60, not caused by low protein loading as confirmed by the BCA assay. BRD4 assays to this extent appeared to show no significant degradation.

To ensure even protein was loaded into each line, lysates had BCA assays performed using conditions described in the experimental.

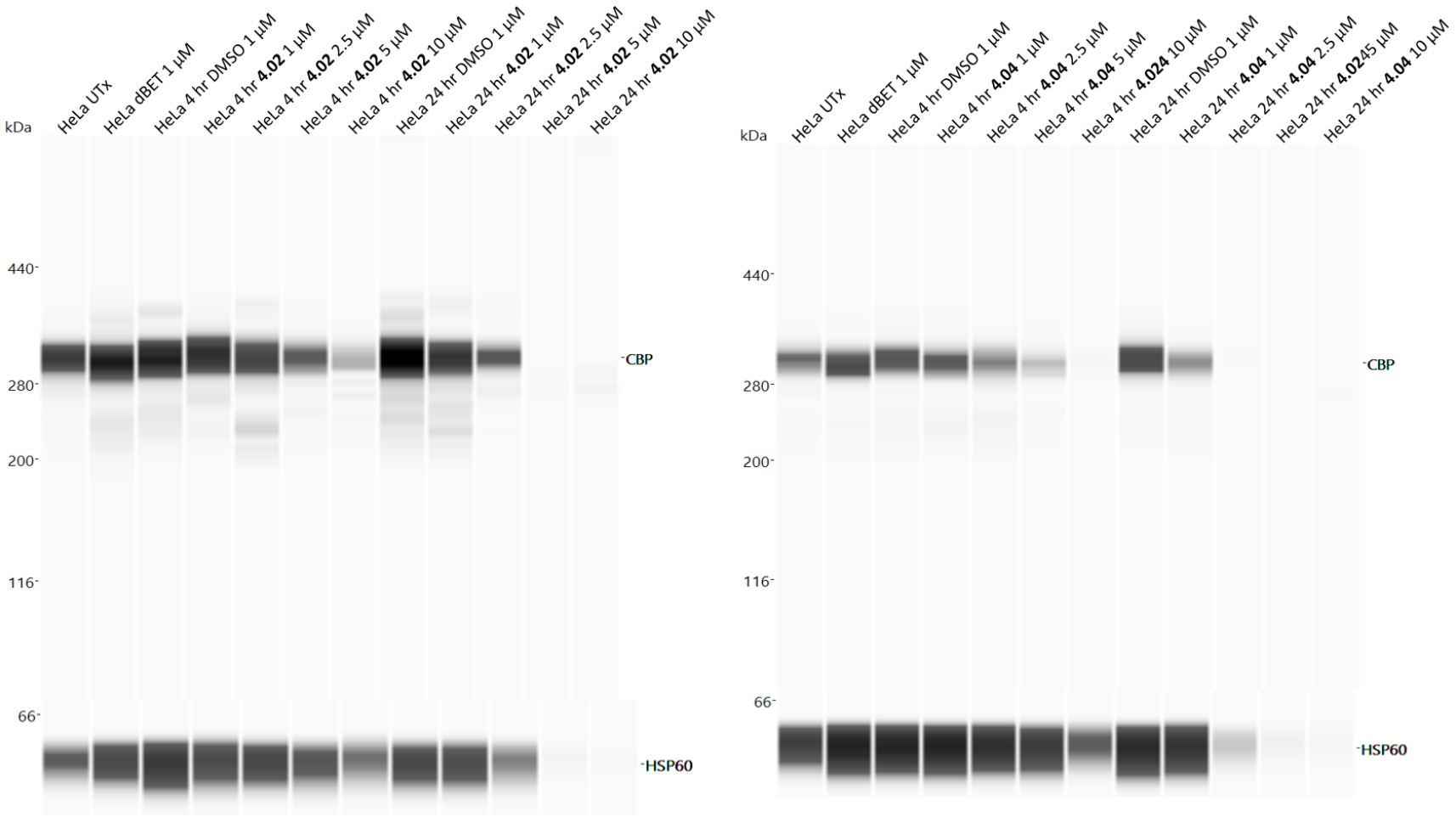

*Figure 4.6: Western blotting analysis of CBP with **4.02** (left WB) and **4.04** (right WB) in HeLa cells. Cells were treated for 4 or 24 h with each degrader at 1, 2.5, 5 and 10 µM. CBP was probed by Western blot on Simple Western with specific antibodies. HSP60 was used as the loading control. Western blot was computationally generated from peak areas integrated by the Simple Western™ software.*

Following the initial data on degraders **4.01**-**4.04**, these compounds were assessed alongside piperazine based degraders **4.57**-**4.72**. The biological activity of the synthesised degraders was once again assessed in HeLa cells. The degraders were treated at 2.5 μM for 24 hours before the cells were lysed and analysed *via* Simple Western^{TM+} (Graph 4.1). The individual samples were normalised to HSP60 and the overall result was normalised to DMSO.

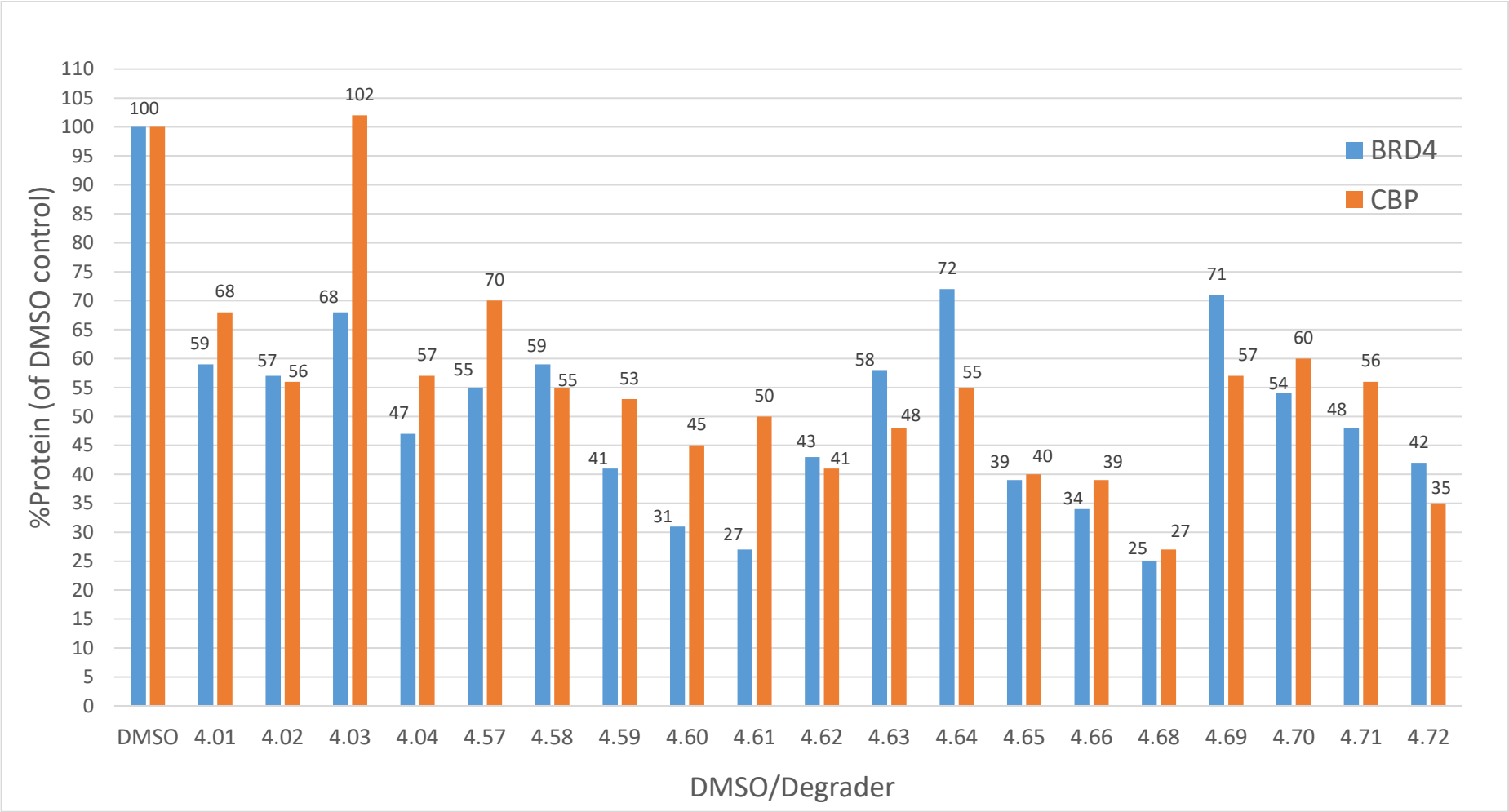

*Graph 4.1: Graphical representation for the protein levels of both BRD4 and CBP when treated with degraders **4.01** – **4.04** and **4.57** – **4.72** in HeLa cells. Each sample was normalised to HSP60 and then normalised to DMSO. Cells were treated for 24 hours with each individual degrader at 2.5 µM. BRD4 and CBP were probed by Western blot on Simple Western with specific antibodies. HSP60 was used as the loading control and had samples normalised to it.*

Overall, the synthesised degraders cause a reduction in BRD4 and CBP (except **4.03**) across the board, with varying potencies. Degrader **4.67** was omitted from the bar graph due to having BRD4 and CBP levels of 285% and 244% respectively, caused by an issue with software integration of the peak from the electropherogram. The graph including the peak for **4.67** is included within the ESI.

Within the phenol modified series of degraders (**4.01**-**4.04**), degrader **4.02** had the most dual like action in this series (43% BRD4 reduction and 44% CBP reduction). Degrader **4.04** gave the highest BRD4 reduction in the phenol series (53%), **4.03** gave a 32% reduction in BRD4 levels but gave no reduction in CBP levels.

Within the piperazine-modified pomalidomide degrader series (**4.57**-**4.60**), the longer linker length degraders gave a higher reduction of protein with **4.60** giving the best reduction of BRD4 (69%) and CBP (55%) levels.

Interestingly, in the piperazine-modified thalidomide degrader series (**4.61**-**4.64**), the longer length linkers appear to induce lower degradation of both target proteins. This was an unexpected trend as, structurally, the only difference between these degraders and **4.57**-**5.60** is the heteroatom (O vs NH) at the 4' position of thalidomide.

Both degraders, **4.66** and **4.67**, appear to give no significant differences in their degradation profiles, but both cause a reduction in >60% of both proteins. Degrader **4.68** gave the best reduction in BRD4 and CBP across the whole series (75% and 73%) whilst also retaining dual degradation of the targets.

Degrader **4.72** was the best degrader within the piperazine-modified VHL 032 degrader series (**4.69**-**4.72**) causing a 58% reduction of BRD4 and 65% reduction of CBP. This data point falls in line with the *in vitro* ubiquitination assay, where **4.72** gave the most potent action (Figure 4.5). This supports the hypothesis that the longer linker lengths in this series helps create a more stable ternary complex compared to the shorter linkers.

A streamlined selection of degraders from the initial assay ran were assessed using RePlex™ on Simple Western, in order to obtain BRD4 and CBP on the same scale as each other. The area of the proteins chemiluminescence was normalised to DMSO to give the protein levels of BRD4 and CBP as a percentage of the control. This allows for an easier comparison between the data sets to ascertain which compounds preferentially degrade CBP, BRD4 or have a dual action (Graph 4.2).

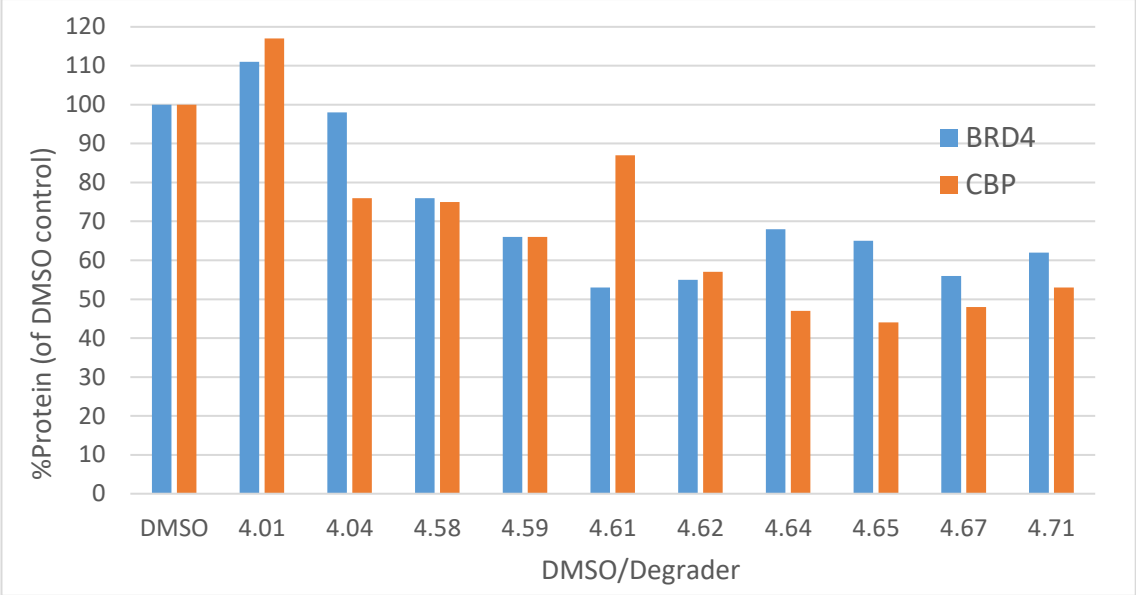

*Graph 4.2: Simple Western™ Replex™ analysis of BRD4 (blue) and CBP (orange) in HeLa cells treated with **4.01**, **4.04**, **4.58**, **4.59**, **4.61**, **4.62**, **4.64**, **4.65**, **4.71** and **4.67**. Cells were treated for 24 hours with 2.5 µM of compound. Data presented is normalised to DMSO to allow for comparison of degradation between BRD4 and CBP.*

Overall, the Replex data suggested the degraders were not working as well as initially thought, as exemplified with **4.01**, which appeared to promote CBP and BRD4 levels rather than reducing them. The degraders assessed here did not seem to give the same potency observed within the initial assay, for example compound **4.58** here reduced BRD4 and CBP by 41% and 45% respectively in Graph 4.1, whereas here only appeared to reduce the protein levels by 24% and 25%.

This series confirmed that the readout from treatment with **4.67** gave increased BRD4 and CBP was an outlier, as this degrader caused a reduction of BRD4 protein by 44% and CBP by 52%. **4.62** was the best "dual-like" degrader investigated in this series and compounds **4.64**, **4.65**, **4.67** and **4.71** degraded more CBP than BRD4.

From this data set the best dual-like degraders (**4.62**, **4.67** and **4.71**) were carried forward in the analysis, along with **4.68** due to being the best degrader from the initial series. Assessment of these 4 degraders maintains the variety of E3 ligands/exit vectors. These compounds were then treated in HeLa cells at 2.5 µM for 24 hours both with and without proteasome inhibitors Carfilzomib or MLN4924.

This assay gave no BRD4 or CBP degradation when treated with just the degraders (Figure 4.7), which suggested that something was amiss with the assay. Co-treated samples with Carfilzomib showed significantly less protein expression than other samples, even though the BCA values were comparable.

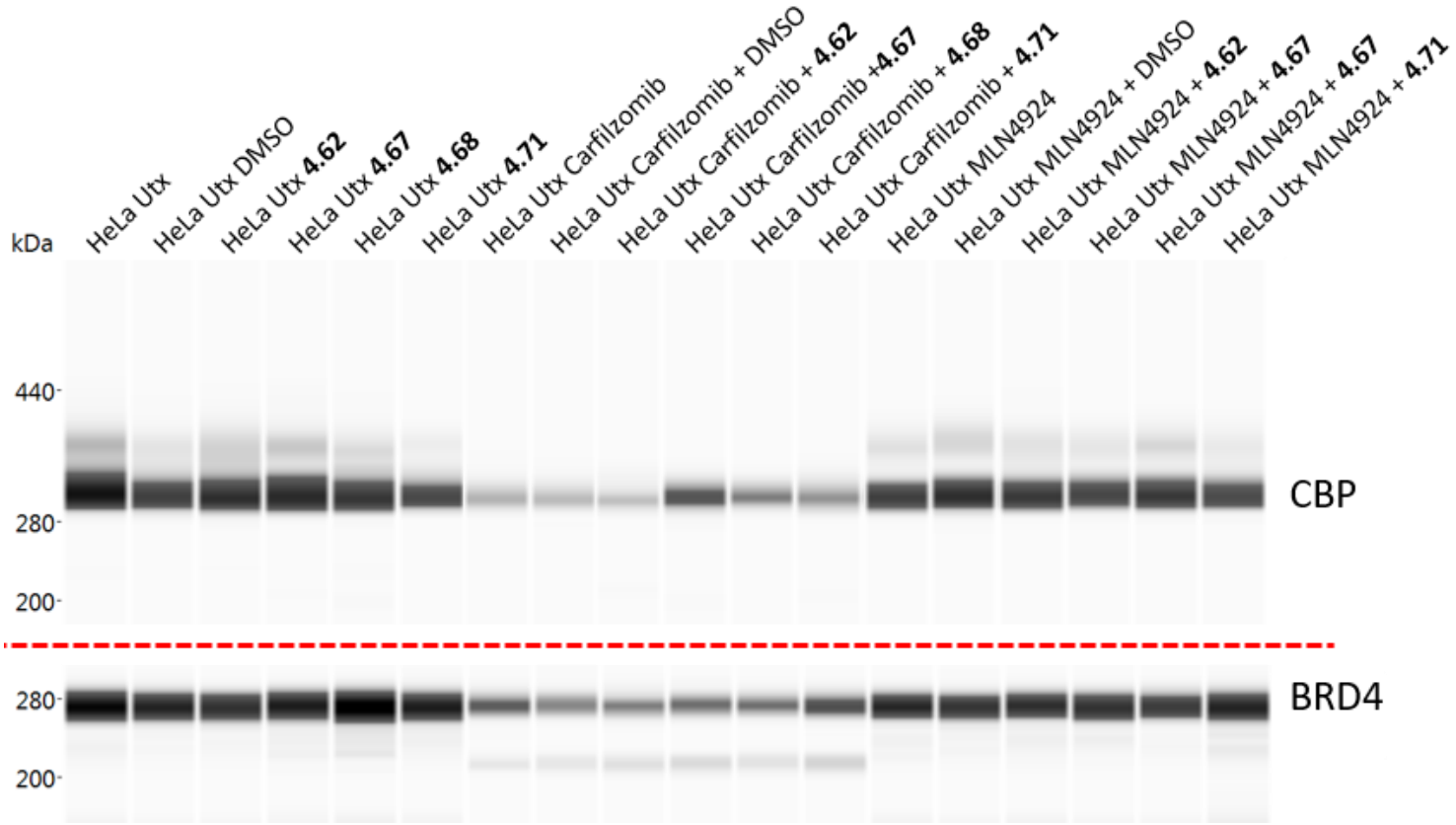

*Figure 4.7: Western blotting analysis of BRD4 and CBP in HeLa cells treated with **4.62**, **4.67**, **4.68** and **4.71**, both with and without proteasome inhibitor (Carfilzomib or MLN4924). Cells were treated for 24 h with each individual compound 2.5 µM. BRD4 and CBP were probed by Western blot with specific antibodies. Samples ran on Jess Replex™ (CBP and Total Protein) and WES (BRD4) total protein was used as the loading control and lanes were normalised to this prior to Western Blot generation.*

To assess the effectiveness of the pre-treatments, a step back was taken and dBET-1 (Chapter 1, Figure 1.36) was utilised in order to check BRD4 degradation within this assay. HeLa cells were pre-treated with the respective proteasome inhibitor for 2 hours before dBET-1 treatment at either 1 µM or 2 µM for 4 hours (Figure 4.8).

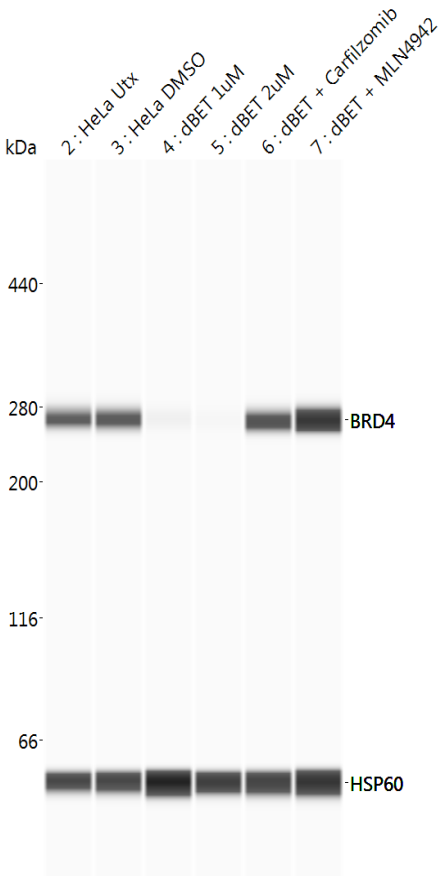

Figure 4.8: Assessment of pre-treatment effectiveness using dBET-1 and both proteasome inhibitors.

The conclusions from these assays were drawn to be that the pre-treatments protocols with either proteasome inhibitor can rescue BRD4 expression, however there is still the issue that the treatment with synthesised degraders here do not degrade BRD4 or CBP. It was thought that prolonged Carfilzomib treatment could be cytotoxic, after 26 hours incubation (2 hour pre-treatment followed by 24 with degrader) resulting in a partial suspension and showed slightly lower BCA values, whereas after a 6 hour incubation (2 hour pre-treatment followed by 4 with degrader) resulted in the cells being completely adherent and no difference in BCA values.

Attention was shifted to the cell line utilised to measure the degradation of the compounds, and it was thought that using a cell line more sensitive to CBP/p300 or BRD4 inhibition/degradation would assist in understanding the action of these compounds. Two cell

lines were initially trialled HDLM-2 (Hodgkin's Lymphoma) and HCT-116 (Colon Carcinoma), for this section of data, Tocris had provided our collaborators with a patented CBP/p300 degrader to probe the cell lines along with dBET-1. Treatment of HDLM-2 cells with 1 µM dBET-1 successfully degraded BRD4 and treatment with CBP degrader resulted in an accumulation of CBP protein (Figure 4.9). The electropherogram was showed a chemiluminescence 12,000 higher for the CBP degrader treatment than DMSO, suggesting either CBP is resulting in accumulation of protein, a resistance pathway reported for BRD4 inhibitor (+)-JQ1, or the treatment concentration was too high for this degrader and is being utilised at a sub-optimal concentration due to the hook effect.[236] Treatments with both dBET-1 and CBP degrader resulted in decreased c-Myc levels, showing the efficacy of individual treatments. This leads to suggest, that the CBP degrader could be acting as an inhibitor rather than a degrader here.

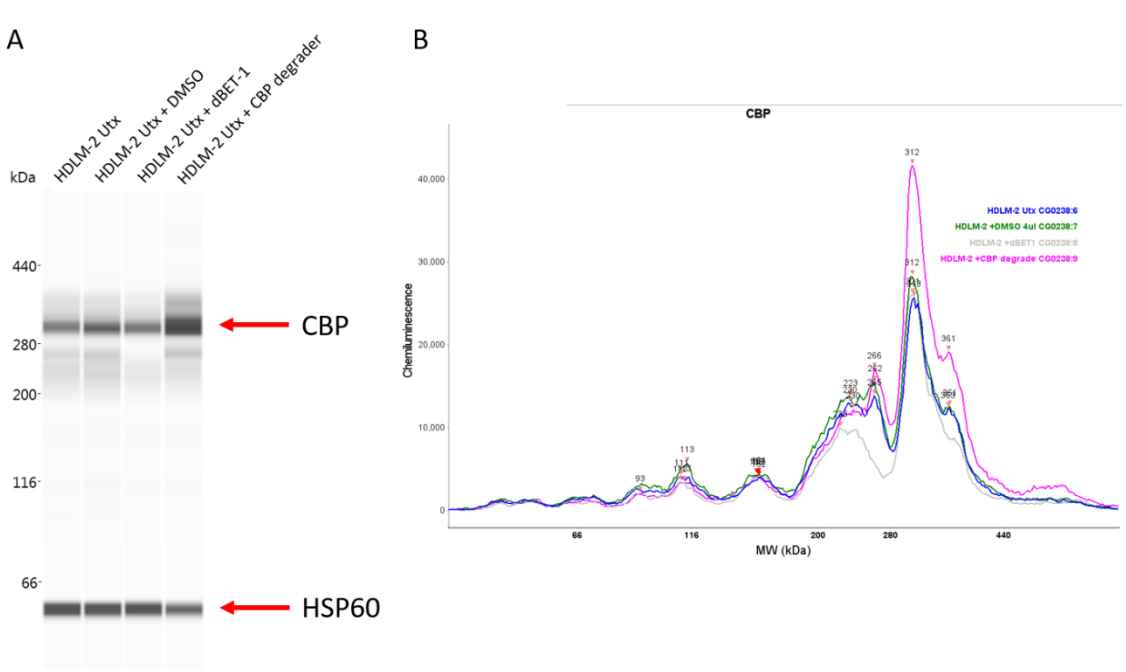

Figure 4.9: A) Western blot of CBP and HSP60 in HDLM-2 cells treated with dBET-1 or CBP degrader. Cells were treated for 6 h with each individual compound 2.5 µM. CBP and HSP60 were probed by Western blot with specific antibodies. B) Electropherogram obtained from Compass software, showing the upregulation of CBP (pink) compared to DMSO (green).

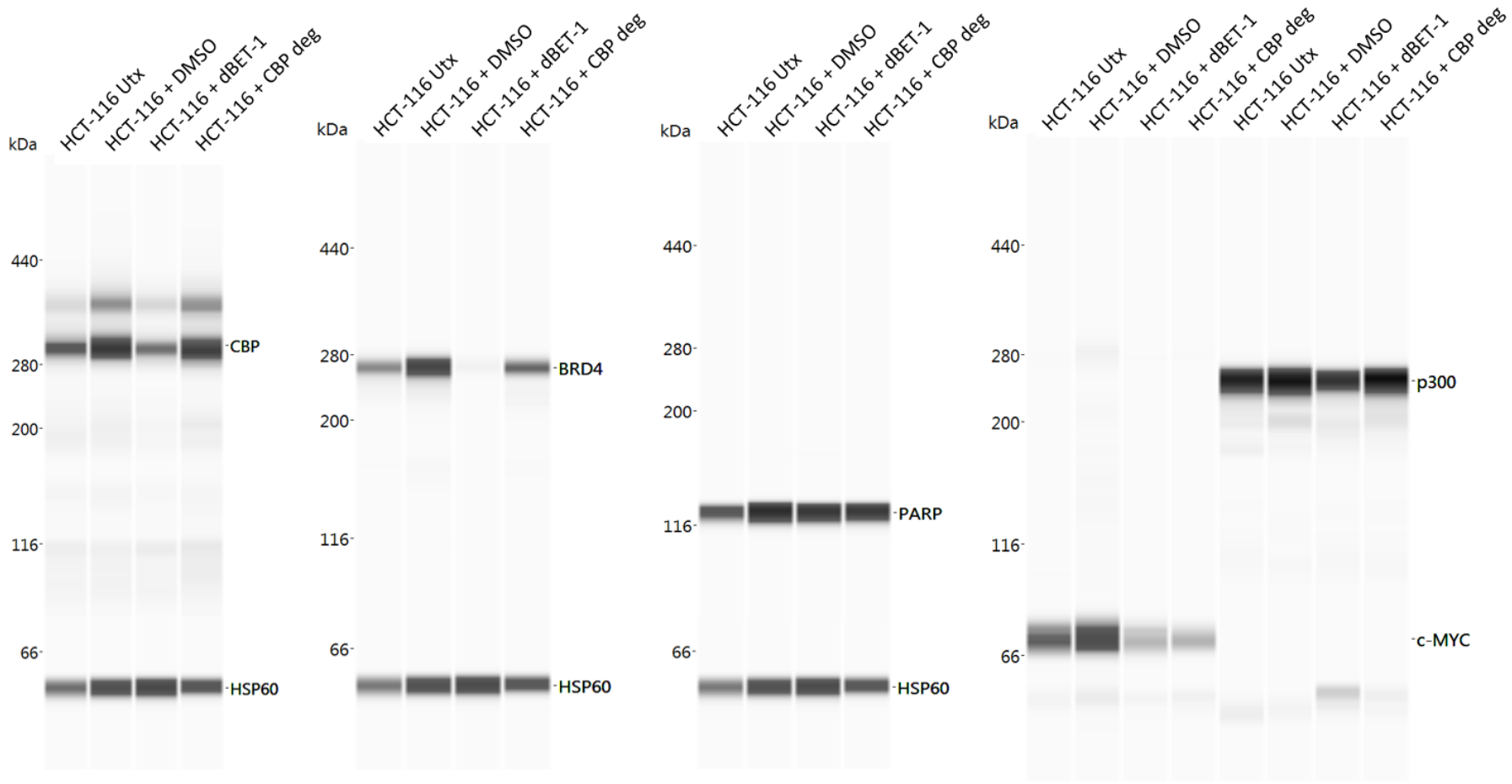

Figure 4.10: Western blotting analysis of CBP, BRD4 p300 and c-myc in HCT-116 cells treated with dBET-1 and CBP degrader. Cells were treated for 6 h with each individual compound 1 µM for dBET-1 and 9 µM for CBP degrader. BRD4, CBP, p300, c-myc and PARP were probed by Western blot with specific antibodies. HSP60 was used as the loading control.

Treatment of dBET-1 in HCT-116 cells successfully decreased BRD4 expression, whereas CBP degrader did not induce degradation of either CBP or p300, however in HCT-116 cells, did not result in an accumulation of protein. Both treatments resulted in a decrease of c-Myc, suggesting that dBET-1 is affecting c-Myc levels through degradation of BRD4, whereas CBP degrader is affecting the levels of c-Myc through inhibition of CBP/p300.

Two conclusions can be formed from this data, treatment of these cell lines with CBP degraders are either being performed at a concentration too high for this degrader and we are observing the hook effect at work, or that these cell lines are not suitable for CBP degradation. Due to the covid-19 pandemic, the collection and analysis of this data was delayed, and this work is still on-going, once a suitable cell line is found which does not appear to upregulate CBP expression, the degraders will be re-assessed for their ability to degrade the target proteins.

At the beginning of 2020, whilst the initial triage assay was being performed by collaborates at Bio-Techne, I undertook a 1-week placement at Bristol University working with the Malik group. During this time, -select ISOX-DUAL degraders were treated in two different neuroblastoma cell lines, one N-Myc driven (Be2c) and the other c-Myc driven (SK-N-AS). These lines were selected due to their Myc protein expression being heavily dependent on BET.[355]

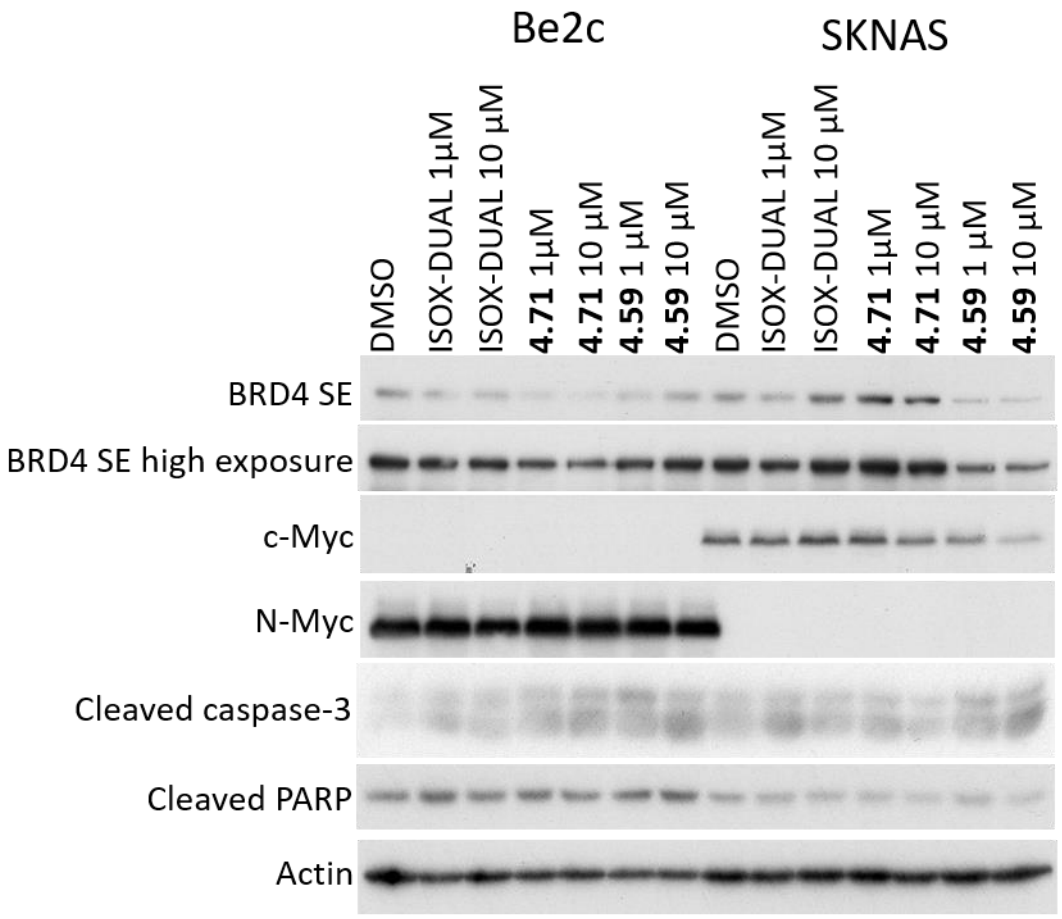

*Figure 4.11: Traditional Western blotting analysis of BRD4 in Be2c and SK-N-AS cells treated with ISOX-DUAL, **4.59** and **4.71**. Cells were treated for 48 h with each individual compound at the indicated concentration. BRD4, c-Myc, N-Myc, Cleaved Caspase-3, and Cleaved PARP were probed by Western blot with specific antibodies. Actin was used as the loading control.*

Here two degraders, one CRBN (**4.59**) and one VHL (**4.71**) recruiting degrader were evaluated for their ability to induce BRD4 degradation in Be2c cells and SK-N-AS cells (Figure 4.11). The Western blotting data showed that **4.71** could induce significant BRD4 degradation at both 1 µM and 10 µM in Be2c cells with no discernible difference between concentrations. **4.59** only induced significant degradation of BRD4 at 1 µM, where 10 µM appears to be near control levels, suggesting the concentration of **4.59** may be too high, as described by the hook effect. In order to confirm this is the case, more concentrations would need to be utilised, however, due to timings and the covid-19 pandemic this was not possible. Treatment with both degraders in Be2c cells caused no reduction in N-Myc levels.

Where **4.71** resulted in degradation of BRD4 within Be2c cells, dosing at the same concentrations in SK-N-AS cells appeared to cause an accumulation, rather than degradation, a response seen as a cellular resistance mechanism to BET inhibition.[236] Treatment of **4.59** in SK-N-AS cells, induced BRD4 degradation at both concentrations, where 10 µM caused a significant decrease in c-Myc.

4.3 Conclusions

In conclusion, this chapter has described the synthesis of a series of novel dual-targeting degraders for the BRDs of BRD4 and CBP/p300.

Degraders **4.69**-**4.72** were shown to successfully induce ubiquitination of BRD4 in a cell-free environment in a dose dependant manner. Longer length degrader **4.72** was able to induce ubiquitylation at lower concentrations, highlighting the importance of linker length variance in degrader design studies.

In initial assessments, the degraders showed their ability to reduce the protein levels of both BRD4 and CBP to varying potencies, however as the assays went forwards, the potencies appeared to occur to less of an effect. The ^{1}H NMR spectra of the degraders in d^{6}-DMSO did not show signs of degradation.

The data collected for the degraders to date highlights the importance in the choice of cell line for treatment with synthesised degraders. These data align with reports in the literature; Ottis and co-workers reported dBET6s efficient induction of BRD4 degradation in both MV4-11 and HL60 cells, but this showed low efficacy in SK-N-AS and HCT-116 cells. This observation was also shown to occur with MZ1 too. Taken together this further confirms that the amenability of TPD can vary significantly depending on the cell model.[356]

From the combined data obtained so far for this degrader series, degraders **4.68** and **4.72** (structures contained within Figure 4.5) were the most promising due to **4.68** causing a profound reduction of BRD4 (75%) and CBP (73%) in HeLa cells (Graph 4.1). Degrader **4.72** was also included here due to the observed ubiquitination of BRD4 at 2.67 nM (Figure 4.5). From this it appears that the longer alkyl linker lengths achieve a more profound affect at ubiquitylating the target proteins.

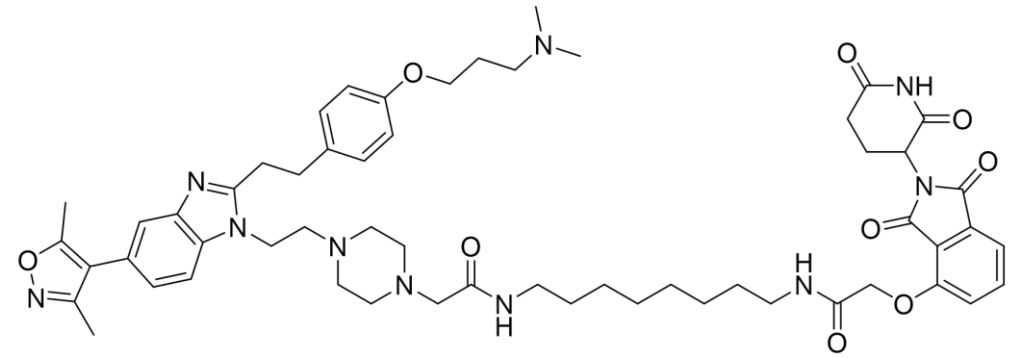

4.68

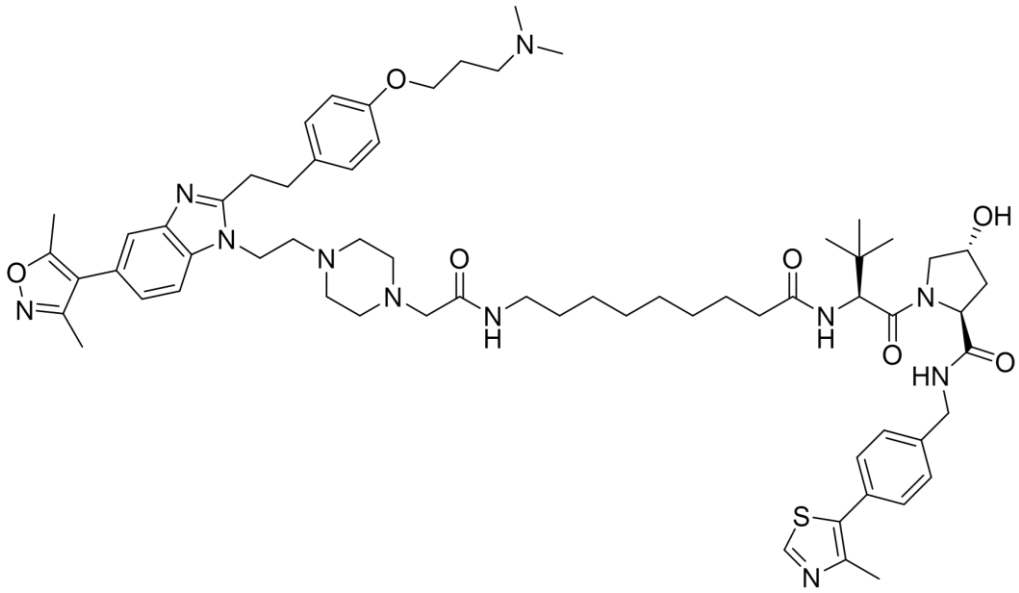

4.72

Figure 4.12: Structures of the two promising degraders from the initial HeLa screen (Graph 4.1) and the ubiquitination assay (Figure 4.5).

Table 4.6 contains a small series of degraders, mostly targeting BRD4 or CBP/p300, the cell lines utilised, treatment durations and incubation times. From this, and as reported in literature for inhibitors and degraders, future work on these degrader compounds should be focused on cell lines that are sensitive to BRD4 and/or CBP/p300 inhibition. This would enable a better understanding of the compounds activities and can tailor the therapeutic to a specific cancer.

Following the issues observed with the proteasome inhibitor assay on selected compounds, collaborators are currently attempting the dBET-1 and CBP degrader treatment on MM cell lines U266 and RPMI-8226 to ascertain the mode of action of the degraders in a better suited cell line. If these cell lines result in the same observations as seen previously, attention needs to be shifted to the concentration of CBP degrader the cells are being treated with. MV4-11

cells also appear to be susceptible to PROTAC modality against BRD4 and would be a good candidate for future assay work.

Table 4.6: Example cell lines from PROTAC studies, with their respective target, treatment concentrations and incubation times reported. References for the experiments are given with entry numbers.

Entry	Cell line	PROTAC	Target	Treatment Concentration (nM)	Incubation time (h)
1[357]	TPC-1	ARV-825	BRD4	5, 25, 100, 250	24
2[236]	Namalwa	ARV-825	BRD4	100, 300, 1000	16
3[236]	Ramos	ARV-825	BRD4	100, 300, 1000	16
4[237]	22Rv1	ARV-771	BRD4	0, 1, 4, 11, 34	16
5[237]	VCap	ARV-771	BRD4	0, 1, 4, 11, 34	16
6[237]	LnCaP95	ARV-771	BRD4	0, 1, 4, 11, 34	16
7[358]	HCT116	PROTAC 3	CDK9	2500, 5000, 10000, 20000	6
8[359]	HCT116	A1874	BRD4	25, 100, 250, 1000, 2500, 10000	24
9[360]	MV4-11	HBL-4	BRD4/PLK1	5, 10, 20, 40, 80	24
10[361]	THP-1	Compound 21	BRD4	1000	3
11[362]	MV4-11	15	BRD4	1, 10, 50, 100, 500	18
12[363]	Saos-2 (Osteosarcoma)	BETd-360	BRD4	3, 10, 30	24
13[363]	MNNG-HOS (Osteosarcoma)	BETd-360	BRD4	3, 10, 30	24
15[364]	RS4;11	Compound 23	BRD4	0.03, 0.1, 1, 3, 10	24
16[365]	MV4-11	dBET6	BRD4	50	3
17[365]	MOLT4^{WT}	dBET6	BRD4	5, 10, 50, 100, 500	3
18[247]	HAP1	dCBP-1	CBP/p300	10, 100, 250, 500, 1000	6
19[247]	MM1S	dCBP-1	CBP/p300	10, 100, 250, 500, 1000	6
20[366]	MV4-11	FLT-3 PROTAC	FLT-3	5, 10, 50, 100, 500	24
21[366]	MOLM4	FLT-3 PROTAC	FLT-3	1, 5, 10, 50, 100	24
22[367]	MM1S	Compound 12d	HDAC6	10, 100	6
23[367]	OPM2	dMCL1-2	MCL1	25, 100, 250, 500, 1000	48

5 Chapter 5: Conclusions, Preliminary Studies and Future Directions

5.1 Conclusions

The overall aims of this project were to design heterobifunctional degraders from ISOX-DUAL. However, as mentioned in the project aims, before this was possible two major issues had to be rectified with the chemistry of ISOX-DUAL.

- Firstly, the initial synthesis of ISOX-DUAL reported a very low overall yield (1%). However, this was not amenable to scale-up to allow for degrader synthesis and called for a synthesis re-evaluation.[2]
- Secondly, is that ISOX-DUAL had no available sites for linker attachment and so the structure of ISOX-DUAL needed to be modified to be able to synthesise degraders.

Chapter 2 describes the investigation into the optimisation of ISOX-DUAL, and was shown to be successful, with the overall yield for isolation of this compound being increased from 1% (Scheme 2.1) and 13% (Scheme 2.2) to 42%.[2] Modifying the Suzuki coupling to utilise a boronic acid pinacol ester (**2.14b**), rather than the free acid, resulted in a yield boost (from 62% and 53% to 75%) due to a reduction in competing protodeboronation in the coupling reaction. The yield for the combined amide formation and benzimidazole cyclisation was also increased (33% and 34% to 55%).

Table 5.1: Summary of yield improvements performed.

	ISOX-DUAL Protocol and Reaction Yield (%)		
Reaction	**Published**[2]	**Industrial**	**Optimised**
Suzuki-Miyaura	62	53	75
Nitro Reduction[a]	87	74	81
Benzimidazole formation	33	34	55
Alkylation	11	59	87

[a] Nitro reduction protocol taken from investigation into structurally similar compounds.[43]

Chapter 3 then discusses the application of the optimised chemistry route to obtain ISOX-DUAL and applies it to the synthesis for two degrader precursor compounds, **3.07** and **3.27**. Synthesis of a series of phenol modified compounds were designed to probe the SAR of this exit vector (Figure 5.1). The synthesised compounds from this vector retained the dual-like affinities observed for ISOX-DUAL matched the values obtained for literature compound **2.10**, confirming this exit vectors compatibility for degrader synthesis.

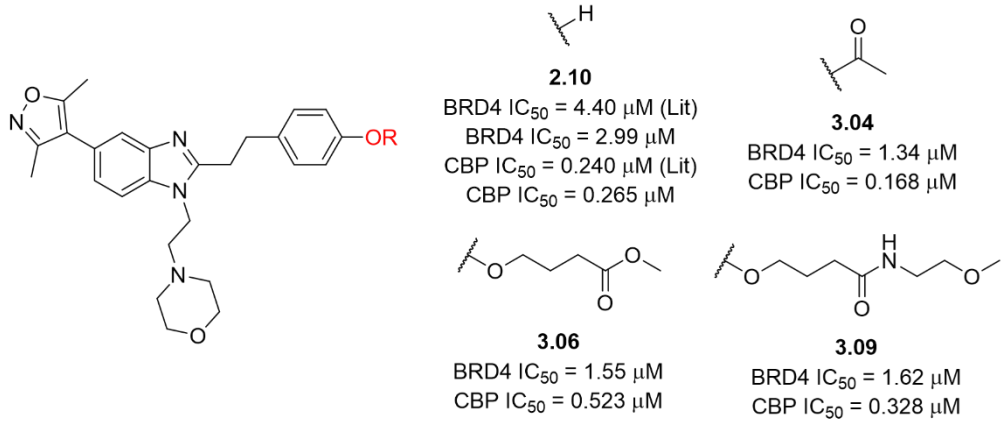

*Figure 5.1: The structures of phenol modified compounds **2.10**, **3.04**, **3.06** and degrader mimic **3.09** and their respective cell-free binding IC_{50} values.*

Investigations into the synthesis of the piperazine modified precursors encountered issues with regards to the stability of the Boc-protecting group during the synthesis of **3.20** and resulted in the de-protection and subsequent formylation (**3.21**) or acetylation (**3.22**) of the piperazine. To circumvent this, the synthetic procedure was modified removing the Boc-group prior to nitro-reduction, and the free piperazine was alkylated with *tert*-butyl bromoacetate.

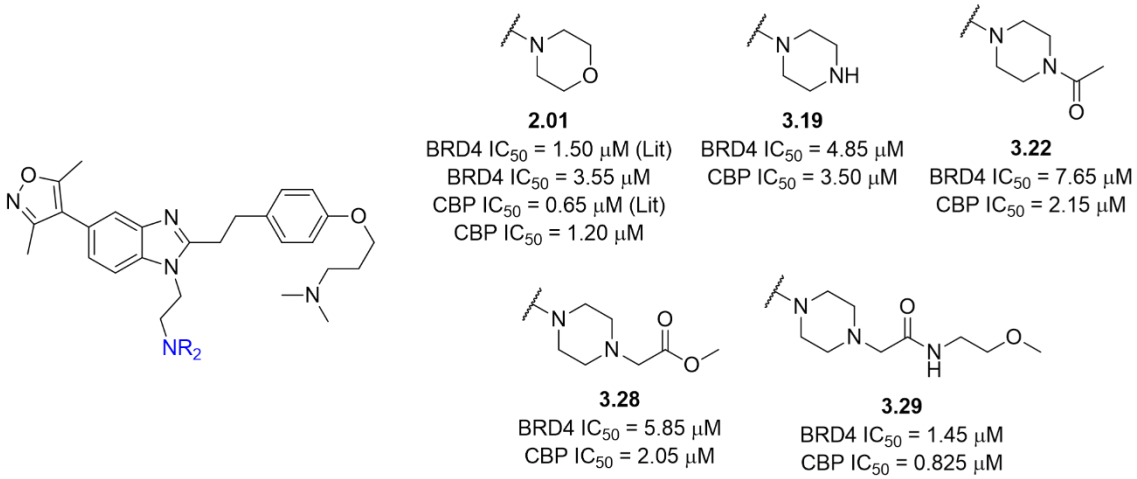

*Figure 5.2: The structures of piperazine-modified compounds **3.19**, **3.22**, **3.28** and degrader mimic **3.29** and their respective cell-free binding IC_{50} values.*

This modification allowed for the successful synthesis of precursor **3.27**. Following this, a series of piperazine-modified compounds were synthesised from **3.27** to probe the SAR of this exit vector (Figure 5.1). Modifications from this vector also maintained affinities to both targets, validating this exit vectors compatibility to degrader synthesis.

To consolidate the synthesis of ISOX-DUAL degraders, Chapter 3 also describes two potential intermediates (**3.29** & **3.30**) in good yield, which gives a streamlined synthesis for future target degraders designed from both vectors. Intermediate **3.29** allows for the modification of the phenol or alkylation to the *N*,*N*-dimethylpropylamine moiety before hydrolysis to the aldehyde.

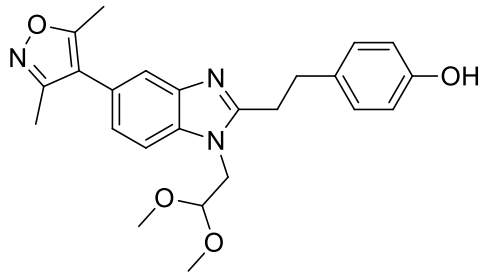

3.29

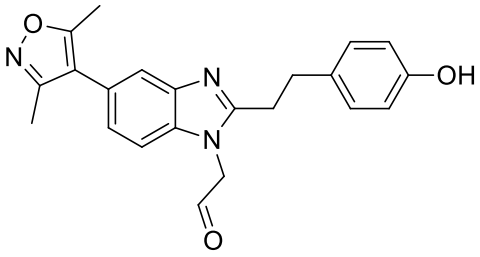

3.30

*Scheme 5.1: Structures of intermediates **3.29** and **3.30**.*

Finally, Chapter 4 describes the synthesis of 20 novel degrader compounds based on the structure of ISOX-DUAL. These degraders include 4 PEG linked degraders to either CRBN or VHL from the phenol exit-vector and 16 alkyl-linked from the piperazine vector, to either recruit CRBN or VHL (Figure 5.3, Table 5.2)

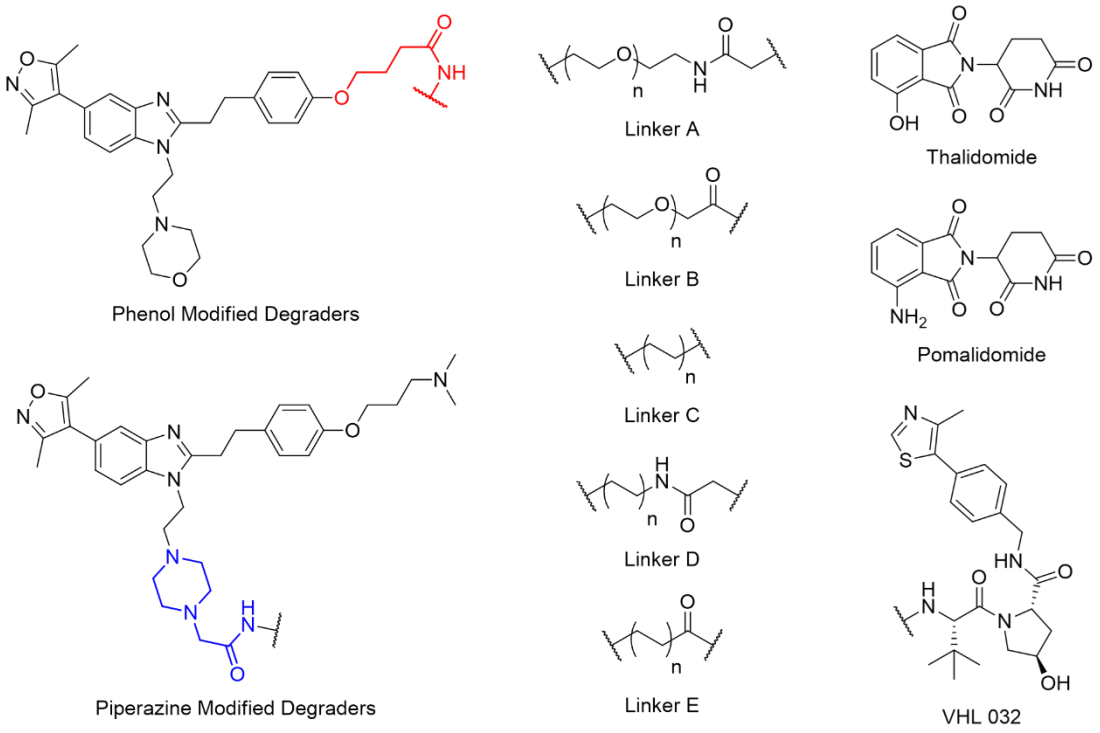

Figure 5.3: Summary of the Degraders which had both the physiochemical properties calculated (Table 4.2, Table 4.3) and were synthesised for biological analysis (Table 4.1, Table 4.4).

Table 5.2: Summary of the Degraders shown in Figure 5.3

Exit Vector	Linker	n	E3 Recruiter	Number of Degraders
Phenol	A	3, 4	Thalidomide	2
Phenol	B	3, 4	VHL 032	2
Piperazine	C	1,2,3,4	Pomalidomide	4
Piperazine	C	1,2,3,4	Thalidomide	4
Piperazine	D	1,2,3,4	Thalidomide	4
Piperazine	E	1,2,3,4	VHL 032	4

Initial triage analysis of these compounds in HeLa cells resulted in **4.68** as the best degrader the assay, degrading 75% of BRD4 and 73% of CBP, with a dual-like ratio. To further understand the data obtained from the Western blot experiments described within Chapter 4, additional assays on these degraders are being currently being performed by collaborators, including cell line variations, qPCR studies, dose dependencies and proteasome inhibitor assays.

5.2 Preliminary Studies

5.2.1 Expansion of the ISOX-DUAL core fragment

Late-stage work was performed on the synthesis of degraders for BRD4/CBP and this section will highlight the preliminary work performed and where the work would lead to. Firstly, there were numerous issues with the synthesis of ISOX-DUAL as detailed within Chapter 2. An alternative strategy was trialled with the synthesis of the bromo-benzimidazole of ISOX-DUAL, as a means of applying the isoxazole moiety, or another KAc mimic near the final stages of synthesis (Scheme 5.2). An example of how this would assist with these degraders or degrader precursor compounds would be for the use of benzyl protecting groups in the synthesis of phenol-modified degraders (Chapter 3), without cleaving the N-O isoxazole bond (Chapter 2).

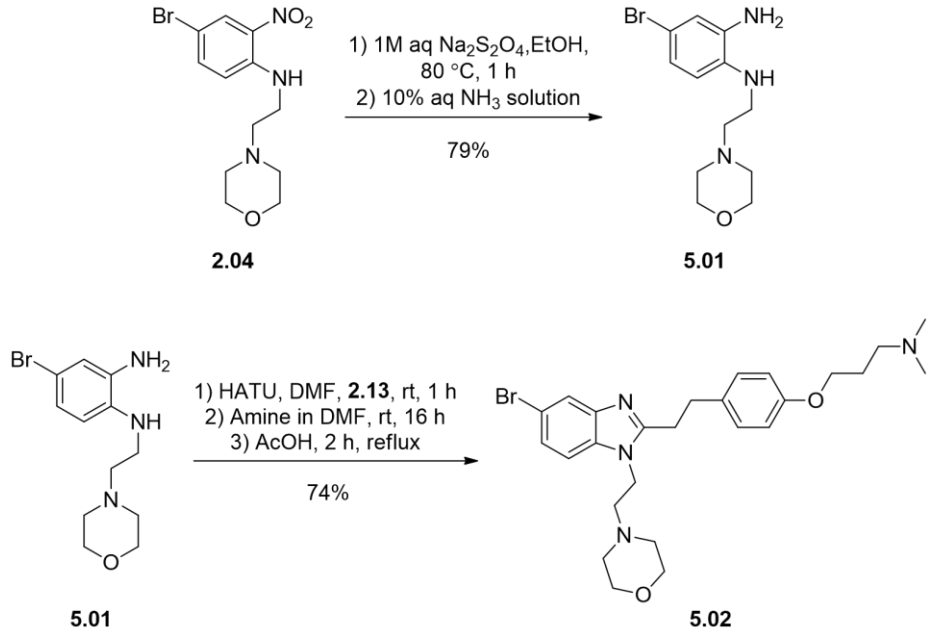

*Scheme 5.2: Synthesis of **5.02** for the application to late stage KAc mimic couplings.*

5.2.2 **Preliminary Work Toward the Development of Degraders for the HAT Domain of CBP/p300**

During the Covid-19 pandemic, and with collaborators at Tocris and SGC Oxford, a small library of degraders was synthesised targeting the HAT domain of CBP/p300 for TPD. The degraders utilised diastereomer (*S*)-(*S*)-A485 (**5.03**) as our warhead component, which was isolated from the racemic mixture during the synthesis of A485 by Tocris (#6387). This compound was discussed in section 1.2.1.3.1. Target engagement of (*S*)-(*S*)-A485 with a propylamine-urea gave an IC_{50} value of 50 nM against the HAT domain, highlighting that changing confirmation of the spiro-oxazolidinedione, only slightly weakened affinity and did not remove it. This was further confirmed in literature when looking at compound **21** vs **22** in the report of A485 (

Figure 5.4).[368]

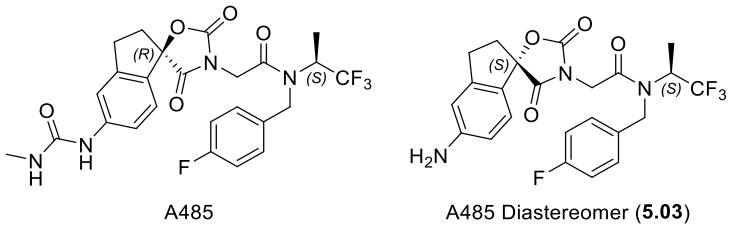

*Figure 5.4: Structures of (R,S)-A485, (S,S)-A485 (**5.03**).*

Two series of degraders for this compound were designed based on their physiochemical properties (Table 5.3), an amide series (**5.04**-**5.06**) and a urea series (**5.07**-**5.09**), both containing an alkyl linker to pomalidomide to recruit CRBN (Scheme 5.3).

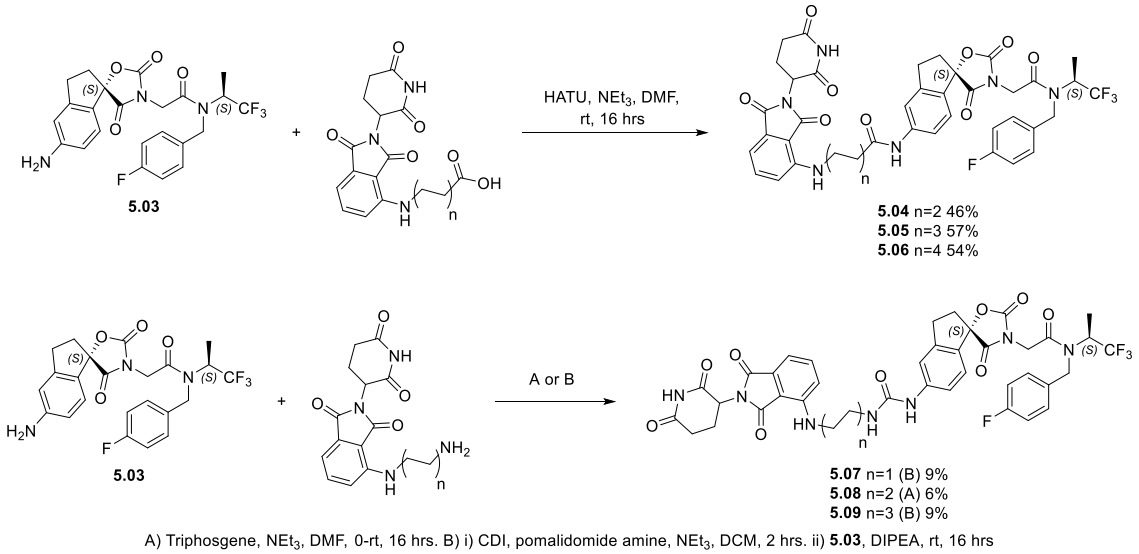

*Scheme 5.3: Reaction schemes for both the amide series (**5.04**-**5.06**) and the urea series (**5.07**-**5.09**) for the A485 degrader series.*

The rationality for designing degraders from this exit vector was because the methyl urea as seen in literature co-crystal (PDB: 5KJ2) is pointing into solvent, minimising our impact on the binding affinity of A485 to the HAT domains. The synthesis of the amide series was successful with moderate yields, whereas the amide series were synthesised with low yields (5-10%). Two methodologies were trialled in making the urea series, a triphosgene-mediated method which was utilised for the synthesis of A485, and a CDI-mediated method.

Analysis of the reaction mixtures for the triphosgene-mediated urea synthesis suggested (*S*)-(*S*)-A485 was forming the isocyanate then reacting with another molecule of itself, prior to the addition of the second amine.[368] This issue could have been influenced by the poor solubility of the E3-linker-amine HCl salt utilised in the coupling, but detailed investigations were not performed due to time restraints from the Covid-19 pandemic. This work is currently still ongoing, with biological analysis being performed in the USA within the Ott lab.

Table 5.3: Calculated properties of degrader compounds for the phenolic linker position. Structural information for the degraders is portrayed within

Figure 5.4.

Compound	Molecular Weight (g mol^{-1})	HBA[ac]	HBD[bc]	No. Rot Bonds[c]	TPSA[ce] (Å^2)	clogP[cde]
5.04	834.77	13	3	16	191.60	3.85
5.05	862.82	13	3	18	191.60	4.54
5.06	890.88	13	3	20	191.60	5.29
5.07	821.73	13	4	15	203.63	3.11
5.08	849.78	13	4	17	203.63	3.62
5.09	877.84	13	4	19	203.63	4.31

[a]HBA = Hydrogen Bond Acceptor. [b]HBD = Hydrogen Bond Donor. [c]Calculated properties were performed using swissADME. [d]Consensus clogP value was chosen. [e]TPSA/clogP flags were raised for 250 and 7 respectfully.

At the same time these compounds were synthesised, a patent from the Dana Faber institute was released, disclosing the structures of (*R*,*S*)-A-485 PROTACs, which was included and discussed in Chapter 1.[246]

5.3 Future Directions

5.3.1 Reversal of the Amide Linkage in Phenol-based Degraders.

The current design of degraders from ISOX-DUAL from the phenol exit vector had moved the nitrogen atom an extra carbon away from the core structure of phenol. As a way of flipping around the amide bond, future work can look at improving degrader design on this compound through alkylation of the phenol, either on **2.07** or **2.10** then once the benzimidazole has been formed, the nitrile can be reduced and reacted with an acid or amine terminal-linker to generate an amide or urea linkage.

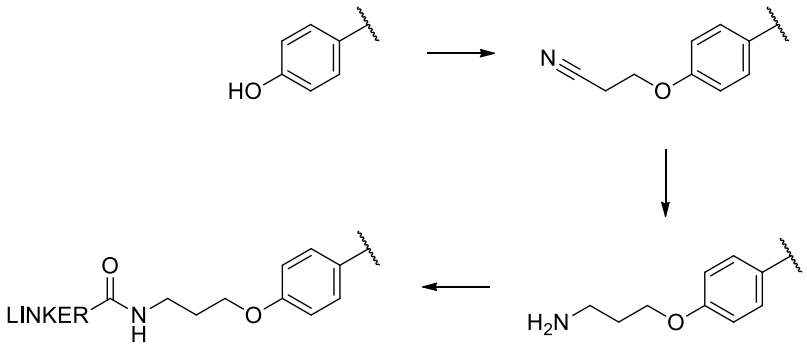

Scheme 5.4: Proposed scheme for the synthesis of phenol degraders with the amide bond flipped around.

5.3.2 **In-Depth Analysis of First-Generation Degraders**

Based on the data obtained on the current synthesised degraders to date I propose the following investigations.

- Cell-free ubiquitination assays for all degraders synthesised against both BRD4 and CBP/p300, to confirm that the degraders do successfully engage ubiquitination to both targets.
- The degraders should have their cell-viabilities checked in more useful cell lines such as MV4-11 or MMS1, as both cell lines have been widely used for BRD4 and CBP inhibition/degradation before taking into triage assays, dosing at either 2.5 µM or both 0.5 µM and 2.5 µM.
- The most potent degraders from this series (4 – 6) should be re-assessed with dose dependencies across 5 or 6 concentrations.
- The best degrader from the dose-dependency investigation should be assessed in its ability to reduce c-Myc levels in MV4-11 or MMS1 cells, and have its DC_{50} and D_{max} calculated for BRD4, CBP and p300, but also the EC_{50} for c-Myc.

Obtaining a co-crystal structure of this degrader within the ternary complex would allow for a detailed understanding of how this compound binds to the two sites and allow for the direction of the second-generation degraders to design a more potent dual degrader.

Currently the 16 piperazine-modified degraders are being tested for their ability to degrade BRD4, CBP and p300 within the Ott laboratory at Harvard University as ongoing work.

5.3.3 **Second Generation degraders of ISOX-DUAL**

Intermediate **3.30** can allow for various chemistry to be performed to create significantly different degraders in the optimisation of the ternary complex and maximisation of the degradation profile (Scheme 5.5).

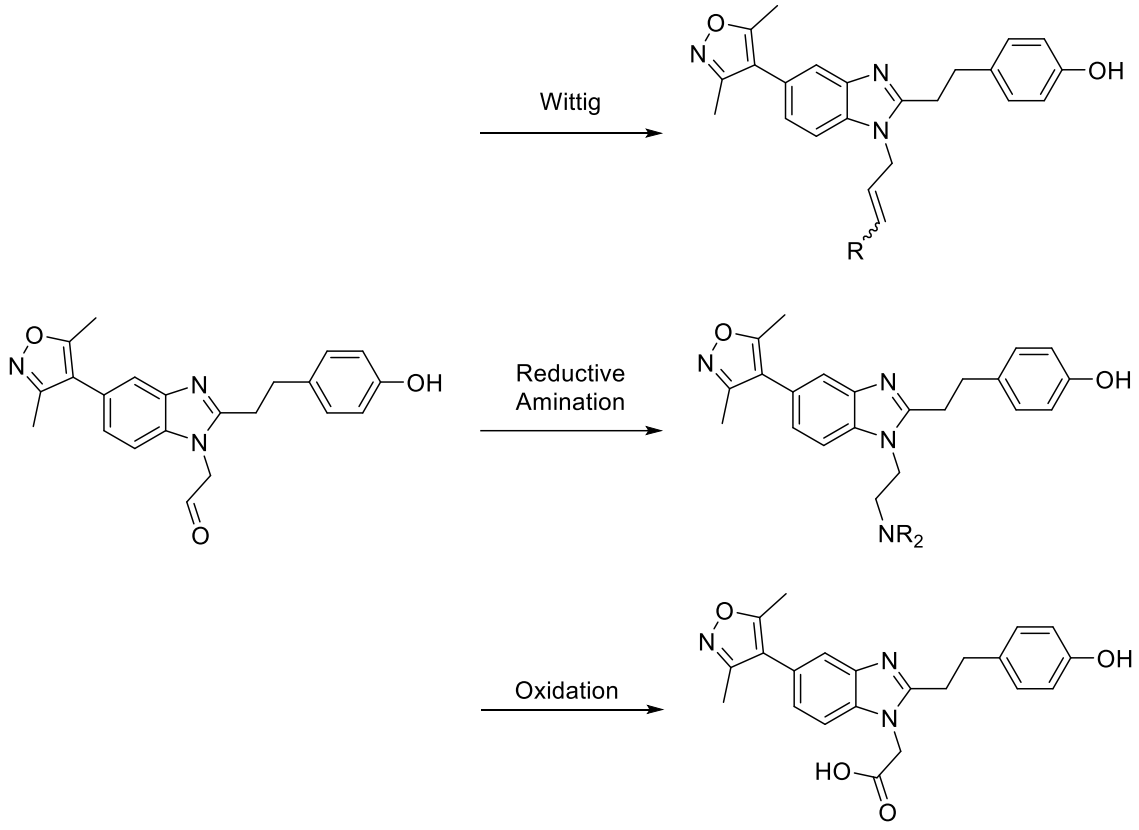

*Scheme 5.5: Example reactions that can be performed on intermediate **3.30** to generate new degraders.*

A future series should investigate alkyl linkers to reduce the high TPSA generated from the PEG linker (Table 4.2) in the phenol degrader series, which may increase cell permeability and thus potentially increasing observed degradation. This approach should be coupled with the use of computer aided PROTAC design, in which a co-crystal of an ISOX-DUAL based degrader can show the interactions between the proteins which can be optimised through placing heteroatoms or other moieties at key positions for picking up additional interactions. This methodology has been shown to be efficient and successful in the Ciulli group.[238–240]

Two degraders that performed well in the initial assays performed on this series, **4.68** which caused a profound reduction of BRD4 (75%) and CBP (73%) in HeLa cells (Graph 4.1). Also, degrader **4.72** which resulted in an observed ubiquitination of BRD4 at 2.67 nM (Figure 4.5). From this it appears that the longer alkyl linker lengths achieve a more profound affect at ubiquitylating the target proteins and warrants an investigation into longer length alkyl

degraders to ascertain if we currently have optimised ternary complex formations with the alkyl linker series. Examples of this would be to design alkyl C9-C12 linkers for these degraders, as this would allow the analysis to investigate whether longer linkers than C8, affect the amount of observed BRD4 or CBP degradation (example structures Figure 5.5).

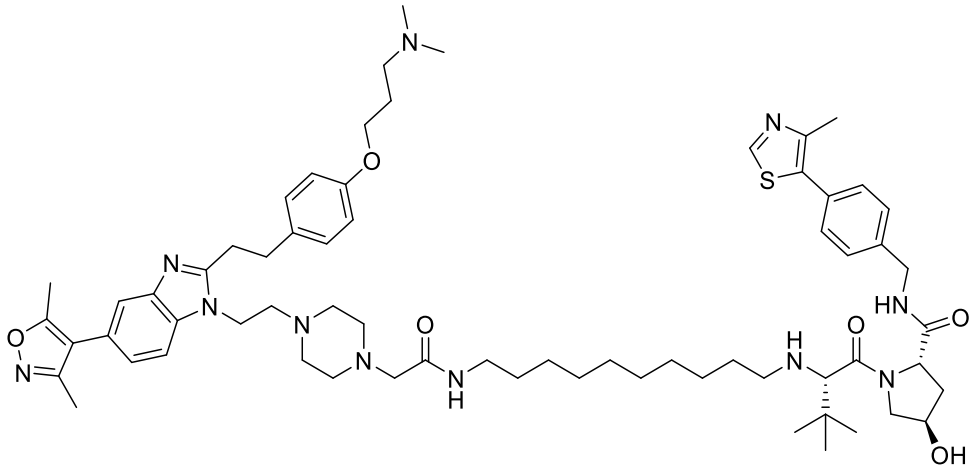

Alkyl C10 VHL degrader

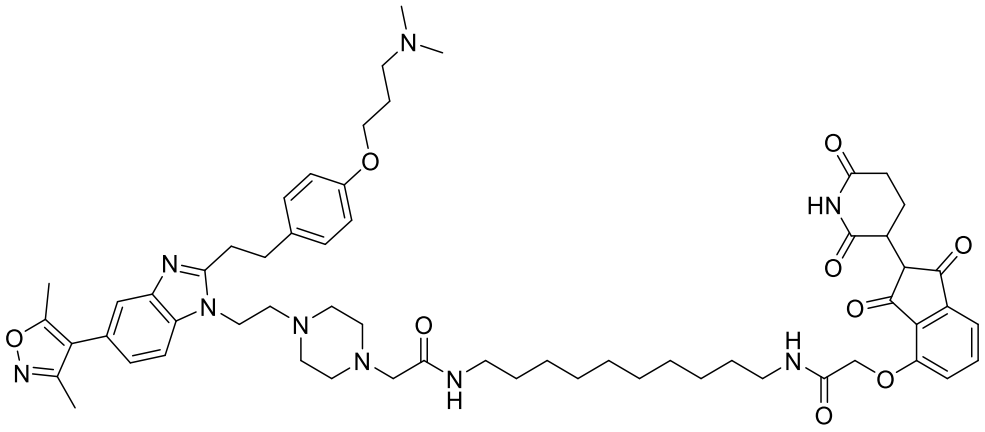

Alkyl C10 Thalidomide alkyl amide degrader

Figure 5.5: Example structures of proposed future synthesis of degraders, utilising a C10 linker with either a VHL ligand or a thalidomide, bound by an alkyl amide bridge between the linker and the ligand of the E3 recruiter.

With the use of programmes such as PRosettaC, the co-crystal structures of ISOX-DUAL or the PROTAC mimics, with the key moieties already changed, can be used to model linkers, and predict novel PPIs, which would further help to stabilise the ternary complex. The top hits from *in silico* design can be synthesised and tested, allowing the creation of a dual action degrader that forms tight interactions with the ternary complexes formed for both target bromodomains.[369–371]

6 Chapter 6: Experimental

All reactions were carried out under air at room temperature unless otherwise stated, using commercial grade reagents and solvents. Unless otherwise stated, reactions were either heated using a Radley's hotplate or *via* a CEM discovery microwave fitted with an explorer unit within a ventilated fume hood, with the sash lowered, as these reactions are under high pressure and temperature. COWare was purchased from Sigma Aldrich. The progress of all reactions was monitored by LC-MS (5 µm C18 110 Å column) and TLC using commercially available silica gel plates (60 Å, F254), with visualisation under UV or by $KMnO_4$ staining. All NMR samples were ran using a Varian NMR 600, 500 or 400 MHz spectrometer stated per sample. Chemical shifts are reported in parts per million (ppm), with δ relative to the residual solvent peak of the solution for ^{1}H and ^{13}C. Purifications were carried out using a Teledyne ISCO purification unit, either Combi Flash RF 75 PSI or Combi Flash RF 150 PSI, using either Teledyne or Biotage silica gel columns. LC-MS were performed on a Shimadzu 2020 Mass Directed Automated Purification (MDAP) system using a 30-minute method in water/acetonitrile with 0.1% formic acid (5 min at 5%, 5-95% over 20 min, 5 min at 95% or 5 min at 30%, 30-95% over 20 min, 5 min at 95%) with the UV set to 254 nm. All mass spectrometry was conducted by Dr. Alaa Abdul-Sada at the University of Sussex. Calculations of compound m/z were performed using Chemdraw Ultra 12.0.2.1076. X-ray crystallography was carried out by the UK National Crystallography Service by Graham Tizzard.[372]

Alpha screen assays were carried out by Oleg Fedorov at the SGC using methodologies previously utilised in literature.[43,373]

The scale up synthesis route to afford **3.10** was performed at Tocris and NMR samples were ran using a Bruker 400 MHz spectrometer and LC-MS were performed on an Agilent HPLC system using an 8-minute method in water/acetonitrile with 0.1% formic acid (1.5 min at 5%, 5 – 95% over 5 min and 1.5 min at 95%) with the UV set to 254 nm.

6.1 Chapter 2

4-Bromo-N-(2-morpholinoethyl)-2-nitroaniline (**2.04**)

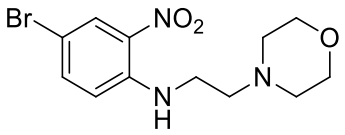

Original Thermal Method

A round bottomed flask was equipped with a magnetic flea before the addition of 4-bromo-1-fluoro-2-nitrobenzene (62 µL, 0.5 mmol, 1 eq.) and DMSO (1.8 mL). Triethylamine (100 µL, 0.625 mmol, 1.25 eq.) was added before the steady addition of 4-(2-aminoethyl)morpholine (82 µL, 0.625 mmol, 1.25 eq.). The reaction mixture was then heated to 80 °C and left for 2 hours. Upon completion by TLC, the cooled reaction mixture was partitioned between EtOAc (10 mL) and water (15 mL). The organic layer was collected and the aqueous was extracted with EtOAc (4 × 10 mL). The organic fractions were combined and washed successively with $NaHCO_3$, brine, dried over $MgSO_4$ and concentrated *in vacuo* to give the product as an orange solid (145.3 mg, 0.44 mmol, 88%). ^{1}H NMR (500 MHz, $CDCl_3$) δ_{ppm} 2.52 (s, 4H), 2.72 (t, *J* = 6.3 Hz, 2H), 3.34 (q, *J* = 5.8 Hz, 2H), 3.76 (s, 4H), 6.73 (d, *J* = 9.2 Hz, 1H), 7.49 (dd, *J* = 8.6, 1.6 Hz, 1H), 8.33 (d, *J* = 2.2 Hz, 1H), 8.53 (s, 1H). Data matched those observed in literature.[2]

Microwave Scale

A CEM Explorer vial was equipped with a magnetic flea and 4-bromo-1-fluoro-2-nitrobenzene (3.10 mL, 25 mmol, 1 eq.). This was then followed by the successive addition of triethylamine (4.2 mL, 30 mmol, 1.2 eq.) and 4-(2-aminoethyl)morpholine (3.34 mL, 25.25 mmol, 1.01 eq.). The vessel was sealed and heated using the dynamic heating method, with max power set to 300 W, max pressure 300 psi, max temperature 120 °C, high stirring throughout and power max turned off. This method was used to hold the method at 120 °C for 10 min. After cooling, the reaction mixture was partitioned between EtOAc (250 mL) and water (300 mL). The organic layer was collected and the aqueous was extracted with EtOAc (4 × 150 mL). The organic fractions were combined and washed with $NaHCO_3$ (300 mL), brine (300 mL), dried over $MgSO_4$ and concentrated *in vacuo* to give the product as an orange solid (8.23 g, 24.93 mmol, 99%). Data matched those observed in literature.[2]

4-(3,5-Dimethylisoxazol-4-yl)-N-(2-morpholinoethyl)-2-nitroaniline (**2.06**)

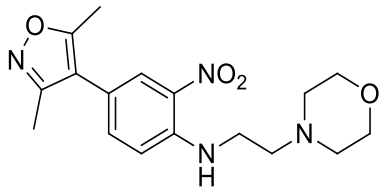

Microwave Reaction – Reaction Scoping (Table 2.3, entry 11)

To a 35 mL microwave vessel were added, **2.04** (165.1 mg, 0.5 mmol, 1 eq.), 3,5-dimethylisoxazole-4-boronic acid pinacol ester (125 mg, 0.56 mmol, 1.12 eq.), $PdCl_2$(dppf) (16.3 mg, 0.025 mmol, 0.05 eq.), potassium phosphate (276 mg, 1.30 mmol, 2.6 eq) as a 1 M solution in water, and 1,4-dioxane. The vessel was sealed, degassed by evacuating and refilling with argon (×3). The vessel was then heated using the dynamic heating method, with max power set to 300 W, max pressure 300 psi, max temperature 150 °C, high stirring throughout and power max turned off. This method was used to hold the method at 150 °C for 3 hours. The reaction mixture was cooled, filtered over Celite, which was washed with EtOAc (3 × 50 mL) before concentrating the filtrate *in vacuo*. Percentage conversion was calculated from crude ^{1}H NMR spectrum based on relative integrations of signals.

Microwave Reaction - Optimised Conditions

To a 35 mL microwave vessel were added, **2.04** (310 mg, 1 mmol, 1 eq.), 3,5-dimethylisoxazole-4-boronic acid pinacol ester (250 mg, 1.12 mmol, 1.12 eq.), $PdCl_2$(dppf)·DCM (40.8 mg, 0.05 mmol, 0.05 eq.), potassium phosphate (552 mg, 2.60 mmol, 2.6 eq.) as a 1 M solution in water and 1,4-dioxane. The vessel was sealed, degassed by evacuating and refilling with argon (×3). The vessel was then heated using the dynamic heating method, with max power set to 300 W, max pressure 300 psi, max temperature 150 °C, high stirring throughout and power max turned off. This method was used to hold the method at 150 °C for 3 hours. The reaction mixture was cooled, filtered over Celite, which was washed with EtOAc (3 × 50 mL) before concentrating the filtrate *in vacuo*. The crude component was then purified *via* flash chromatography using 0 – 100% EtOAc in hexane to afford the product as an orange solid (328.7 mg, 0.95 mmol, 95%).^{1}H NMR (600 MHz, $CDCl_3$) δ_{ppm} 2.25 (s, 3H), 2.39 (s, 3H), 2.53 (s, 4H), 2.74 (t, *J* = 6.1 Hz, 2H), 3.76 (t, *J* = 4.6 Hz, 4H), 6.90 (d, *J* = 8.8 Hz, 1H), 7.33 (dd, *J* = 8.8, 2.2 Hz, 1H), 8.08 (d, *J* = 2.1 Hz, 1H), 8.57 (s, 1H). Data matched those observed in literature.[2,43]

4-(2-(5-(3,5-dimethylisoxazol-4-yl)-1-(2-morpholinoethyl)-1*H*-benzo[*d*]imidazol-2-yl)ethyl)phenol (**2.10**)

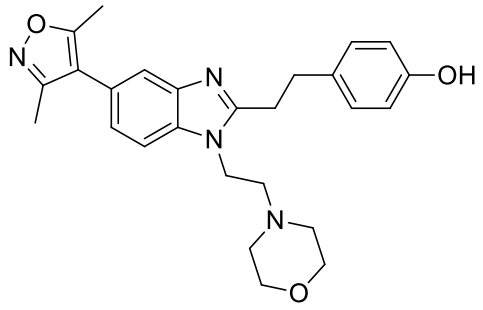

To a solution of 4-hydroxyphenyl propionic acid (686 mg, 4.13 mmol, 1.1 eq.) and HATU (1.99 g, 5.25 mmol, 1.2 eq.) in DMF (30 mL) was added triethylamine (1.6 mL, 11.3 mmol, 3 eq.) followed by a solution of **2.11** (1.3 g, 3.75 mmol, 1 eq.) in DMF (5 mL). The stirring solution was left to stir overnight at room temperature. The reaction mixture was partitioned between Dichloromethane (100 mL) and water (100 mL). The aqueous phase was then extracted with Dichloromethane (3 × 25 mL). The combined organic phases were washed with saturated aqueous $NaHCO_3$ (150 mL), brine (200 mL), dried over $MgSO_4$, filtered, and concentrated *in vacuo*. The crude component was dissolved in AcOH (50 mL) and heated to reflux for 2 hours. The reaction mixture was then cooled, concentrated *in vacuo* and dichloromethane (50 mL) was added before neutralisation with saturated aqueous $NaHCO_3$. The organic phase was collected, and the aqueous phase was extracted with Dichloromethane (4 × 50 mL), before being combined and washed with brine (200 mL) dried over $MgSO_4$, filtered, and concentrated *in vacuo*. The resultant crude product was purified *via* flash chromatography using 0 – 20% methanol (with 0.5% NH_4OH) in dichloromethane to give the product as a white solid. (502.36 mg, 1.125 mmol, 30%). ^{1}H NMR (600 MHz, $CDCl_3$) δ_{ppm} 2.26 (s, 3H), 2.39 (s, 3H), 2.49 (s, 4H), 2.65 (t, *J* = 7.0 Hz, 2H), 3.18 (m, 4H), 3.69 (s, 4H), 4.14 – 4.18 (m, 2H), 6.73 (d, *J* = 7.9 Hz, 2H), 7.00 (d, *J* = 7.8 Hz, 2H), 7.13 (d, *J* = 8.2 Hz, 1H), 7.36 (d, *J* = 8.2 Hz, 1H), 7.58 (s, 1H), 8.07 (s, 1H). ^{13}C NMR (151 MHz, $CDCl_3$) δ_{ppm} 11.0, 11.7, 29.9, 33.3, 41.7, 54.2, 57.7, 66.9, 109.7, 115.9, 117.1, 119.8, 123.7, 124.6, 129.5, 131.8, 134.2, 142.6, 155.4, 155.6, 159.1, 165.2. LC-MS (5-95 MeCN in 20 mins) ^{t}R = 3.23 min, Purity = 97%, m/z = 447.05. HR-MS-ESI (m/z): $[M+H]^+$ calculated for $C_{29}H_{31}N_4O_3$, 447.2391; found, 447.2367.

4-(3,5-Dimethylisoxazol-4-yl)-N1-(2-morpholinoethyl)benzene-1,2-diamine (**2.11**)

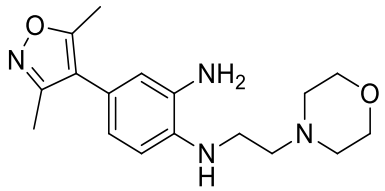

To a stirring suspension of **2.06** (3.31 g, 9.75 mmol, 1 eq.) in EtOH (75 mL), was added 1.0 M aq. $Na_2S_2O_4$ (70 mL) before heating to 80 ˚C for 1 hour. The reaction mixture was then cooled and partitioned between 10% aqueous ammonia (75 mL), and EtOAc (75 mL). The phases were separated then the aqueous phase was extracted with EtOAc (4 × 50mL). The combined organic phases were washed with brine (2 × 200 mL), dried over $MgSO_4$, filtered, and concentrated *in vacuo* to yield the product as a yellow gum (2.5 g, 7.9 mmol, 81%). ^{1}H NMR (600 MHz; $CDCl_3$) δ_{ppm} 2.25 (s, 3H), 2.38 (s, 3H), 2.50 (s, 4H), 2.71 (t, *J* = 5.9 Hz, 2H), 3.20 (t, *J* = 5.9 Hz, 2H), 3.47 (s, 2H), 3.73 (s, 4H), 6.59 (s, 1H), 6.68 (s, 2H). LC-MS (5-95 MeCN in 20 mins) ^{t}R = 8.66 min, Purity = 95%, m/z = $[M+H]^+$ 316.95. Data matched those observed in literature.[43]

Methyl 3-(4-(3-(dimethylamino)propoxy)phenyl)propanoate (**2.12**)

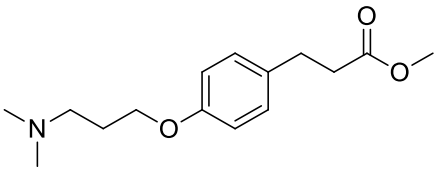

To a stirring solution of methyl 3-(4-hydroxyphenyl)propanoate (9.00 g, 50 mmol, 1 eq.) in MeCN (200 mL) was added caesium carbonate (48.9 g, 150 mmol, 3 eq.), followed by sodium iodide (3.75 g, 25 mmol 0.5 eq.), and 3-chloro-*N*,*N*-dimethylpropan-1-amine hydrochloride (9.3 g, 60 mmol 1.2 eq.). The reaction mixture was placed under argon and heated to reflux over for 48 h. Upon reaction cooling, the mixture was concentrated *in vacuo* before partitioning between dichloromethane (300 mL) and water (300 mL). The organic was collected and washed with 1M NaOH (300 mL), brine (300 mL) and dried over $MgSO_4$ before concentration *in vacuo* to result in a clear oil (11.6 g, 43 mmol, 87%). ^{1}H NMR (600 MHz, $CDCl_3$) δ_{ppm} 1.93 (p, *J* = 6.4 Hz, 2H), 2.24 (s, 6H), 2.43 (t, *J* = 7.3 Hz, 2H), 2.59 (t, *J* = 7.8 Hz, 2H), 2.88 (t, *J* = 7.8 Hz, 2H), 3.66 (s, 3H), 3.98 (t, *J* = 6.4 Hz, 2H), 6.82 (d, *J* = 8.7 Hz, 4H), 7.09 (d, *J* = 8.3 Hz, 4H).

Lithium 3-(4-(3-(dimethylamino)propoxy)phenyl)propanoate (**2.13**)

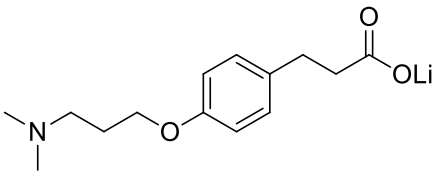

To a stirring solution of **2.12** (11.6 g, 43 mmol, 1 eq.) in a mixture of THF: water (5:1, 250 mL), was added LiOH·H_2O (2.22 g, 52.8 mmol, 1.1 eq.) and left to stir overnight at room temperature. The reaction mixture was concentrated *in vacuo* and was azeotroped with THF (5 × 50 mL) to afford the product as the lithium salt, which was used crude without characterisation (11.06 g, 43 mmol, quant.).

2-(3,5-Dimethylisoxazol-4-yl)-6-methyl-1,3,6,2-dioxazaborocane-4,8-dione (**2.14a**)

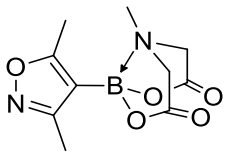

3,5-Dimethylisoxazol-4-yl-4-boronic acid (143.2 mg, 1.02 mmol, 1 eq.) was added to a 10 mL microwave vial equipped with a magnetic stirrer, followed by methylaminodiacetic acid (150 mg, 1.02 mmol, 1 eq.) and dry DMF (1 mL). The tube was sealed with a Teflon cap and the reaction mixture was heated using a dynamic heating method, with max power set to 300 W, max pressure set to 300 psi, max temperature set to 170 °C, high stirring throughout and power max off. This method was used to hold the reaction mixture at 170 °C for 10 mins. After cooling, the reaction mixture was concentrated *in vacuo* resulting in a white precipitate, which was triturated *via* sonification with H_2O (5 mL), cooled in an ice-bath, filtered, and washed with cold H_2O (5 mL). The white solid was then triturated again with Et_2O (5 mL), cooled in an ice-bath, filtered, and washed with cold Et_2O (5 mL). The product was then air dried to result in a white solid (153 mg, 0.605 mmol, 74%). ^{1}H NMR (600 MHz, d^6-DMSO) δ_{ppm} 2.12 (s, 3H), 2.31 (s, 3H), 2.64 (s, 3H), 4.13 (d, *J* = 17.3 Hz, 2H), 4.34 (d, *J* = 17.3 Hz, 2H). ^{13}C NMR (600 MHz d^6-DMSO) δ_{ppm} 12.2, 12.9, 47.5, 62.3, 162.3, 162.7, 169.4, 173.7, C-B carbon missing from NMR.[374] LC-MS (30-95% MeCN in 20 mins) ^{t}R = 11.74 min, Purity = >99%, m/z = no ionisation. HR-MS-EI; m/z = $[M]^+$ 252.[311]

N-(2-Morpholinoethyl)-2-nitroaniline (**2.15**)

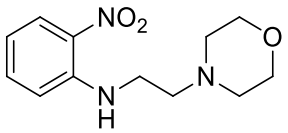

A microwave vial was equipped with a magnetic flea and flushed with argon. 4-(2-aminoethyl)morpholine (2.86 g, 22 mmol, 1.1 eq.), followed by triethylamine (14 mL, 100 mmol, 5 eq.) were added. This was stirred for 3 min before the addition of the 2-fluoronitrobenzene (2.82 g, 20 mmol, 1 eq.), following which the vial was sealed and heated using the dynamic heating method, with max power set to 300 W, max pressure 300 psi, max temperature 125 °C, high stirring throughout and power max turned off. This method was used to hold the temperature at 125 °C for 10 min. After cooling, the reaction mixture was transferred to a separating funnel where it was partitioned between water and EtOAc. The organic layer was collected and the aqueous was extracted with EtOAc. The organics were then collected and combined, washed with sat $NaHCO_3$, brine and dried over anhydrous $MgSO_4$ before concentration *in vacuo* to yield the product as an orange oil with yield (5.05 g, 20.1 mmol, 99%). ^{1}H NMR (600 MHz, $CDCl_3$) δ_{ppm} 2.53 (s, 4H), 2.72 (t, *J* = 5.6 Hz, 2H), 3.37 (q, *J* = 5.6 Hz, 2H), 3.76 (s, 4H), 6.64 (t, *J* = 8.0 Hz, 1H), 6.82 (d, *J* = 8.6 Hz, 1H), 7.43 (t, *J* = 8.0 Hz, 1H), 8.18 (d, *J* = 8.6 Hz, 1H), 8.49 (s, 1H). LC-MS (30-95 MeCN in 20 mins) ^{t}R = 3.35 min, Purity = 98%, m/z = 252.05 $[M + H]^+$.

4-(1-Methyl-1*H*-pyrazol-4-yl)-*N*-(2-morpholinoethyl)-2-nitroaniline (**2.16**)

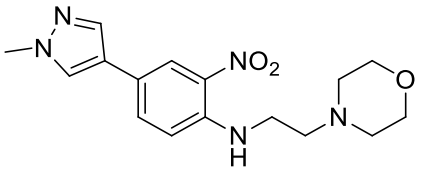

Compound **2.16** was synthesised using the microwave conditions for **2.06**, using 0.5 mmol of **2.04**. The crude component was then purified *via* flash chromatography using 0 – 10% methanol in EtOAc to result in the product as a red solid (113 mg, 0.414 mmol, 85%). ^{1}H NMR (600 MHz, $CDCl_3$) δ_{ppm} 2.53 (s, 4H), 2.74 (t, *J* = 6.1 Hz, 2H), 3.40 (q, *J* = 5.8 Hz, 2H), 3.79 – 3.74 (m, 4H), 3.94 (s, 3H), 6.85 (d, *J* = 8.9 Hz, 1H), 7.57 (dd, *J* = 8.8, 2.1 Hz, 1H), 7.71 (s, 1H), 7.58 (s, 1H), 8.27 (d, *J* = 2.1 Hz, 1H), 8.50 (s, 1H). ^{13}C NMR (151 MHz, $CDCl_3$) δ_{ppm} 39.3, 39.7, 53.4, 56.3, 67.2, 77.2, 114.7, 120.8, 121.7, 122.9, 126.6, 132.2, 134. 1, 136.4, 144.1. LC-MS (30-95 MeCN

in 20 mins) ^{t}R = 3.29 min, Purity = >99%, m/z = 332.00 $[M + H]^+$. HR-MS (m/z): $[M + H]^+$ calculated for $C_{16}H_{22}N_5O_3$, 332.1723; found, 332.1714.

tert-butyl 4-(4-((2-Morpholinoethyl)amino)-3-nitrophenyl)-1*H*-pyrazole-1-carboxylate (**2.17**)

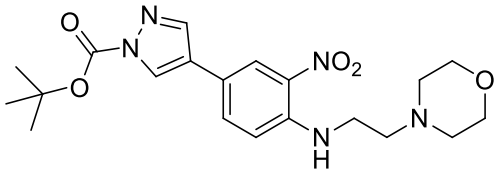

Compound synthesised was attempted using microwave conditions for **2.06** using 0.5 mmol of **2.04**, however decomposition occurred *in situ* and no product was obtained.

N-(2-Morpholinoethyl)-2-nitro-4-(thiophen-2-yl)aniline (**2.18**)

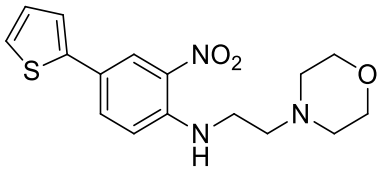

Compound **2.18** was synthesised using microwave conditions for **2.06**, using 0.5 mmol of **2.04**. The crude component was then purified *via* flash chromatography using 0 – 100% EtOAc in hexane to result in the product as an orange solid (150 mg, 0.450 mmol, 90%). ^{1}H NMR (600 MHz, $CDCl_3$) δ_{ppm} 2.56 (t, *J* = 4.5 Hz, 4H), 2.76 (t, *J* = 6.1 Hz, 2H), 3.42 (q, *J* = 5.6 Hz, 2H), 3.79 (s, 4H), 6.88 (d, *J* = 8.9 Hz, 1H), 7.07 – 7.10 (m, 1H), 7.25 (m, 2H), 7.71 (d, *J* = 10.4 Hz, 1H), 8.44 (d, *J* = 1.7 Hz, 1H), 8.60 (s, 1H). ^{13}C NMR (151 MHz, $CDCl_3$) δ_{ppm} 25.1, 53. 4, 56.2, 67.2, 114.7, 122.4, 122.5, 123.5, 124.3, 128.2, 132.0, 134.2, 142.7, 144.5. LC-MS (30-95 MeCN in 20 mins) ^{t}R = 5.52 min, Purity = 95% – one peak, m/z = 334.35[M + H]. HR-MS (m/z): $[M + H]^+$ calculated for $C_{16}H_{20}N_3O_3S$, 334.1225; found, 334.1214.

4-(5-Methylfuran-2-yl)-*N*-(2-morpholinoethyl)-2-nitroaniline (**2.19**)

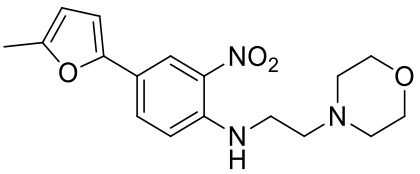

Compound **2.19** was synthesised using microwave conditions for **2.06**, using 0.5 mmol of **2.04**. The crude component was then purified *via* flash chromatography using a C18 reverse phase column with 5-95% acetonitrile in water with 0.5% formic acid over 20 mins, to result in the product as a red solid (132 mg, 0.400 mmol, 80%). ^{1}H NMR (600 MHz, $CDCl_3$) δ_{ppm} 2.36 (s, 3H),

2.53 (s, 4H), 2.73 (t, *J* = 6.0 Hz, 2H), 3.39 (q, *J* = 5.4 Hz, 2H), 3.76 (s, 4H), 6.03 (s, 1H), 6.42 (s, 1H), 6.83 (d, *J* = 8.9 Hz, 1H), 7.69 (d, *J* = 8.8 Hz, 1H), 8.42 (s, 1H), 8.56 (s, 1H). ^{13}C NMR (151 MHz, $CDCl_3$) δ_{ppm} 13.8, 39.6, 53.3, 56.2, 67.1, 104.9, 107.8, 114.5, 119.6, 121.0, 131.9, 132.0, 144.2, 150.7, 151.8. LC-MS (30-95 MeCN in 20 mins) ^{t}R = 5.86 min, Purity = >99%, m/z = 332.05 $[M + H]^+$. HR-MS (m/z): $[M + H]^+$ calculated for $C_{17}H_{22}N_3O_4$, 332.1610; found, 332.1605.

4-(6-chloropyridin-3-yl)-*N*-(2-morpholinoethyl)-2-nitroaniline (**2.20**)

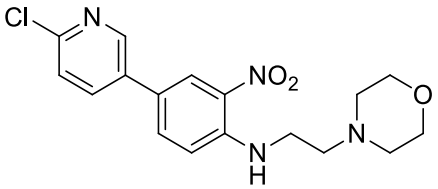

Compound **2.20** was synthesised using microwave conditions for **2.06**, using 0.5 mmol of **2.04**. The crude component was then purified *via* flash chromatography using 0 – 10% methanol in EtOAc to result in the product as an orange solid (134.2 mg, 0.370 mmol, 74%). ^{1}H NMR (600 MHz, $CDCl_3$) δ_{ppm} 2.54 (s, 4H), 2.75 (t, *J* = 6.1 Hz, 2H), 3.42 (q, *J* = 5.6 Hz, 2H), 3.77 (t, *J* = 4.6 Hz, 4H), 6.95 (d, *J* = 8.9 Hz, 1H), 7.38 (d, *J* = 8.3 Hz, 1H), 7.66 (dd, *J* = 8.9, 2.2 Hz, 1H), 7.81 (dd, *J* = 8.3, 2.6 Hz, 1H), 8.41 (d, *J* = 2.2 Hz, 1H), 8.57 (d, *J* = 2.5 Hz, 1H), 8.64 (t, *J* = 4.5 Hz, 1H). ^{13}C NMR (151 MHz, $CDCl_3$) δ_{ppm} 39.6, 53.3, 56.1, 67.1, 115.3, 123.5, 124.5, 125.0, 132.4, 133.7, 134.7, 136.4, 136.3, 145.1, 147.2, 150.2. LC-MS (30-95 MeCN in 20 mins) ^{t}R = 4.08 min, Purity = 94% - one peak, m/z = 363. $[M + H]^+$. HR-MS (m/z): $[M + H]^+$ calculated for $C_{17}H_{20}ClN_4O_3$, 363.1224; found, 363.1221.

4-(6-Fluoropyridin-3-yl)-*N*-(2-morpholinoethyl)-2-nitroaniline (**2.21**)

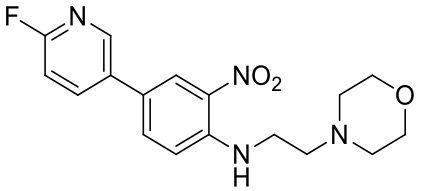

Compound **2.21** was synthesised using microwave conditions for **2.06**, using 0.5 mmol of **2.04**. The crude component was then purified *via* flash chromatography using 0 – 100% EtOAc in hexane to afford the product as an orange oil (138 mg, 0.398 mmol, 81%).^{1}H NMR (600 MHz, $CDCl_3$) δ_{ppm} 2.55 (s, 4H), 2.76 (t, *J* = 6.1 Hz, 2H), 3.43 (q, *J* = 5.7 Hz, 2H), 3.77 (t, *J* = 4.6 Hz, 4H), 6.95 (d, *J* = 8.8 Hz, 1H), 7.00 (dd, *J* = 8.5, 2.9 Hz, 1H), 7.65 (d, *J* = 8.8 Hz, 1H), 7.94 (td, *J* = 8.0, 2.5

Hz, 1H), 8.39 (s, 2H), 8.61 (s, 1H). ^{13}C NMR (151 MHz, $CDCl_3$) δ_{ppm} 39.6, 53.3, 56.1, 67.1, 109.7, 109.9, 115.3, 123.8, 125.0, 132.4, 132.9, 134.6, 139.0, 139.0, 144.9, 145.1, 145.2, 162.3, 163.9. LC-MS (30-95 MeCN in 20 mins) ^{t}R = 6.98 min, Purity = 96%, m/z = 347.20 $[M + H]^+$. HR-MS (m/z): $[M + H]^+$ calculated for $C_{17}H_{20}FN_4O_3$, 347.1519; found, 347.1501.

N-(2-Morpholinoethyl)benzene-1,2-diamine (**2.22**)

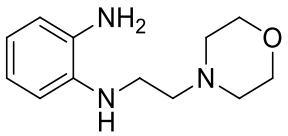

A COware vessel was equipped with a magnetic flea in one chamber and flushed with argon. Pd/C 10 wt% (4.26 g, 4 mmol, 0.2 eq.), and **2.14** (5.03 g, 20 mmol, 1 eq.) were added to the same chamber and dissolved in EtOAc: methanol (5:1, 20 mL). Zinc (10 g) was added to the other chamber and the vessel was flushed with argon for a further 5 mins before sealing. 7M HCl (14.22 mL, 99.5 mmol) was then added to the zinc chamber. The reaction mixture was left to stir at room temperature overnight behind a blast shield, with the addition of more 7N HCl after 16 h (14.22 mL, 99.5 mmol). The reaction vessel was carefully vented, and the organic component was filtered over Celite, washing with EtOAc (3 × 50 mL) and the filtrate was concentrated *in vacuo*. The resultant crude product was purified *via* flash chromatography using 0-10% methanol in dichloromethane to afford the product as a clear oil (3.69 g, 16.7 mmol, 83%). ^{1}H NMR (600 MHz, $CDCl_3$) δ_{ppm} 2.49 (s, 4H), 2.68 (t, *J* = 5.9 Hz, 2H), 3.18 (t, *J* = 5.9 Hz, 2H), 3.72 (t, *J* = 4.7 Hz, 4H), 6.73 – 6.64 (m, 3H), 6.81 (t, *J* = 7.5 Hz, 1H). LC-MS (30-95 MeCN in 20 mins) ^{t}R = 3.05 min, Purity = >99%, m/z = 222.00 $[M + H]^+$.

(*Z*)-3-(3-Amino-4-((2-morpholinoethyl)amino)phenyl)-4-iminopent-2-en-2-ol (**2.23**)

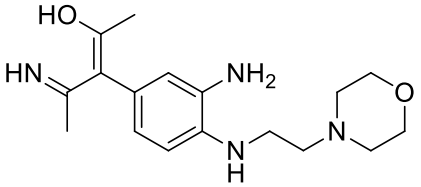

A COware vessel was equipped with a magnetic flea in one chamber and flushed with argon. Pd/C 10 wt% (5.02 g, 4.72 mmol, 0.2 eq.), and **2.06** (8.17 g, 23.6 mmol, 1 eq.) were added to the same chamber and dissolved in EtOAc: methanol (5:1, 20 mL). Zinc (10 g) was added to the other chamber and the vessel was flushed with argon for a further 5 mins before sealing. 7M HCl (14.22 mL, 99.5 mmol) was then added to the zinc chamber. The reaction mixture was left

to stir at room temperature overnight behind a blast shield, with the addition of more 7N HCl after 16 h (14.2 mL, 99.5 mmol). The reaction vessel was carefully vented, and the organic component was filtered over Celite, washing with EtOAc (3 × 50 mL) and the filtrate was concentrated *in vacuo* to afford the crude product as a brown oil (7.5 g, 23.6 mmol, 99%). The compound was used crude. ^{1}H NMR (600 MHz, $CDCl_3$) δ_{ppm} 1.72 (s, 3H), 1.87 (s, 3H), 2.51 (s, 4H), 2.70 (t, *J* = 5.7 Hz, 2H), 3.19 (t, *J* = 5.7 Hz, 2H), 6.51 (s, 1H), 3.73 (s, 4H), 6.62 – 6.53 (m, 2H), 10.45 (s, 1H). LC-MS (30-95 MeCN in 20 mins) ^{t}R = 3.05 min, Purity = 90%, m/z = 319.00 $[M + H]^{+}$.

Ethyl 3-(4-(3-(dimethylamino)propoxy)phenyl)propanoate (**2.24**)

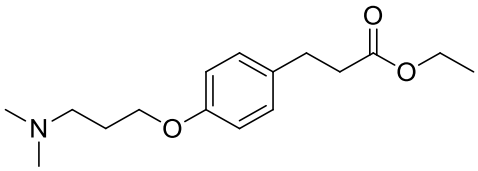

A microwave vial was equipped with a magnetic flea, methyl 3-(4-hydroxyphenhyl)propionate (90.1 mg, 0.5 mmol, 1 eq.) and EtOH (5 mL). potassium carbonate (691.1 mg, 5 mmol, 10 eq.) and 3-dimethyl-1-propylchloride hydrochloride (205.5 mg, 1.3 mmol, 2.6 eq) was successively added before the reaction mixture was sealed and heated using the dynamic heating method, with max power set to 300 W, max pressure 300 psi, max temperature 125 °C, high stirring throughout and power max turned off. This method was used to hold the method at 125 °C for 10 min. After cooling, the reaction mixture was concentrated *in vacuo* before partitioning between water (25 mL) and EtOAc (20 mL). The organic layer was extracted and washed with saturated $NaHCO_3$ (20 mL), brine (20 mL), dried over MgSO4, filtered, and concentrated *in vacuo* to afford the product as a clear oil (116.5 mg, 0.417 mmol, 73%). ^{1}H NMR (600 MHz, $CDCl_3$) δ_{ppm} 1.23 (t, *J* = 7.2 Hz, 3H), 1.93 (p, *J* = 6.7 Hz, 2H), 2.44 (t, *J* = 7.3 Hz, 2H), 2.57 (t, *J* = 7.9 Hz, 2H), 2.88 (t, *J* = 7.8 Hz, 2H), 3.98 (t, *J* = 6.5 Hz, 2H), 4.12 (q, *J* = 7.1 Hz, 2H), 6.82 (d, *J* = 8.5 Hz, 4H), 7.09 (d, *J* = 8.5 Hz, 4H).

4-(2-(1-(2-Morpholinoethyl)-1H-benzo[d]imidazol-2-yl)ethyl)phenol (**2.25**)

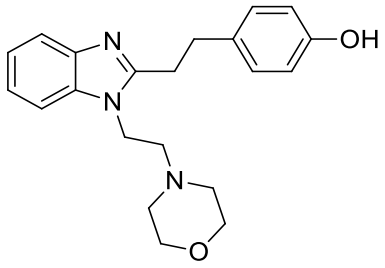

To a solution of 4-hydroxyphenyl propionic acid (166.18 mg, 2 mmol, 1 eq.) and HATU (912.6 mg, 2.4 mmol, 1.2 eq.) in DMF (5 mL) was added triethylamine (557 µL, 4 mmol, 2 eq.) followed by a solution of **2.22** (442.6 mg, 2 mmol, 1 eq.) in DMF (3 mL). The stirring solution was left to stir overnight at room temperature. The reaction mixture was partitioned between dichloromethane (50 mL) and water (50 mL). The aqueous phase was then extracted with dichloromethane (3 × 25 mL). The combined organic phases were washed with saturated aqueous $NaHCO_3$ (100 mL), brine (100 mL), dried over $MgSO_4$, filtered, and concentrated *in vacuo*. The crude component was dissolved in AcOH (50 mL) and heated to reflux for 2 hours. The reaction mixture was then cooled, concentrated *in vacuo* and Dichloromethane (50 mL) was added before neutralisation with saturated aqueous $NaHCO_3$. The organic phase was collected, and the aqueous phase was extracted with dichloromethane (4 × 50 mL), before being combined and washed with brine (200 mL) dried over $MgSO_4$, filtered, and concentrated *in vacuo*. The resultant crude product was purified *via* flash chromatography using 0-10% methanol in dichloromethane with 0.5% NH_4OH to afford the product as a yellow oil (497 mg, 1.40 mmol, 74%).^{1}H NMR (600 MHz, $CDCl_3$) δ_{ppm} 2.47 (s, 4H), 2.61 (t, *J* = 7.0 Hz, 2H), 3.15 (dq, *J* = 14.1, 7.1 Hz, 4H), 3.71 – 3.64 (m, 4H), 4.13 (t, *J* = 6.9 Hz, 2H), 6.71 (d, *J* = 8.1 Hz, 2H), 6.96 (d, *J* = 8.2 Hz, 2H), 7.26 (s, 3H), 7.33 – 7.28 (m, 1H), 7.72 (d, *J* = 8.3 Hz, 1H) 8.21 (s, 1H). ^{13}C NMR (151 MHz, $CDCl_3$) δ_{ppm} 29.8, 33.5, 41.4, 54.1, 57.6, 66.9, 109.4, 116.0, 119.1, 122.4, 122.5, 129.5, 131.4, 134.6, 142.0, 154.7, 156.0. LC-MS (30-95 MeCN in 20 mins) ^{t}R = 3.06 min, Purity = >99%, m/z = 352.00. $[M + H]^+$. HR-MS-EI; m/z = $[M]^+$ 351.

N,*N*-Dimethyl-3-(4-(2-(1-(2-morpholinoethyl)-1H-benzo[d]imidazol-2-yl)ethyl)phenoxy)propan-1-amine (**2.26**)

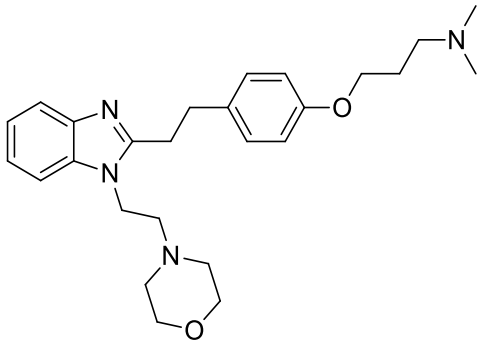

2.13 (514.6 mg, 2 mmol, 1 eq.) was suspended in DMF (5 mL) before the addition of HATU (912.6 mg, 2.4 mmol, 1.2 eq.) and was left to stir at room temperature for 1 hour. A solution of **2.22** (442.6 mg, 2 mmol, 1 eq.) in DMF (3 mL) was added to the stirring mixture before leaving overnight at room temperature. The reaction mixture was partitioned between dichloromethane (50 mL) and water (50 mL). The aqueous phase was then extracted with dichloromethane (3 × 25 mL). The combined organic phases were washed with saturated aqueous $NaHCO_3$ (100 mL), brine (100 mL), dried over $MgSO_4$, filtered, and concentrated *in vacuo*. The crude component was dissolved in AcOH (50 mL) and heated to reflux for 2 hours. The reaction mixture was then cooled, concentrated *in vacuo* and Dichloromethane (50 mL) was added before neutralisation with saturated aqueous $NaHCO_3$. The organic phase was collected, and the aqueous phase was extracted with dichloromethane (4 × 50 mL), before being combined and washed with brine (200 mL), dried over $MgSO_4$, filtered, and concentrated *in vacuo*. The resultant crude product was purified *via* flash chromatography using 0-10% methanol in dichloromethane with 0.5% NH_4OH to afford the product as a yellow oil (671 mg, 1.54 mmol, 77%). ^{1}H NMR (600 MHz, $CDCl_3$) δ_{ppm} 1.95 (dt, *J* = 13.3, 7.1 Hz, 2H), 2.27 (s, 6H), 2.40 (s, 4H), 2.48 (t, *J* = 7.3 Hz, 2H), 2.53 (t, *J* = 6.8 Hz, 2H), 3.15 – 3.09 (m, 2H), 3.21 – 3.15 (m, 2H), 3.63 (s, 4H), 3.96 (t, *J* = 6.3 Hz, 2H), 4.05 (t, *J* = 6.8 Hz, 2H), 6.80 (d, *J* = 8.2 Hz, 2H), 7.09 (d, *J* = 8.1 Hz, 2H), 7.28 – 7.19 (m, 3H), 7.73 (d, *J* = 6.6 Hz, 1H). ^{13}C NMR (151 MHz, $CDCl_3$) δ_{ppm} 27.3, 29.9, 33.2, 41.3, 45.3, 54.0, 56.3, 57.5, 66.1, 66.8, 109.1, 114.3, 119.3, 121.9, 122.1, 129.3, 133.0, 134.8, 142.7, 154.5, 157.6. LC-MS (30-95 MeCN in 20 mins) ^{t}R = 2.95 min, A% = 100, m/z = 437.15. [M + H]. HR-MS (m/z): $[M + H]^+$ calculated for $C_{26}H_{37}N_4O_2$, 437.2917; found, 437.2902.

(*Z*)-4-Hydroxy-3-(2-(4-hydroxyphenethyl)-1-(2-morpholinoethyl)-1H-benzo[d]imidazol-5-yl)pent-3-en-2-one (**2.27**)

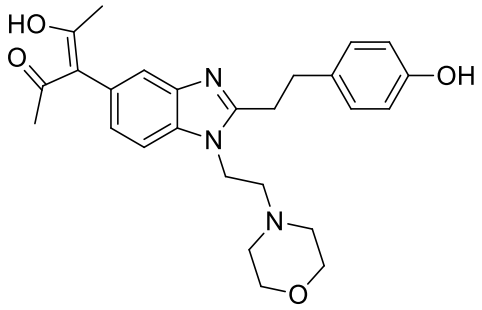

To a solution of 4-hydroxyphenyl propionic acid (914 mg, 5.05 mmol, 1.01 eq.) and HATU (2.47 g, 6.5 mmol, 1.3 eq.) in DMF (15 mL) was added triethylamine (1.4 mL, 10 mmol, 2 eq.) followed by a solution of **2.23** (1.732 g, 5 mmol, 1 eq.) in DMF (15 mL). The stirring solution was left to stir overnight at room temperature. The reaction mixture was partitioned between dichloromethane (50 mL) and water (50 mL). The aqueous phase was then extracted with dichloromethane (3 × 25 mL). The combined organic phases were washed with saturated aqueous $NaHCO_3$ (100 mL), brine (100 mL), dried over $MgSO_4$, filtered, and concentrated *in vacuo*. The crude component was dissolved in AcOH (50 mL) and heated to reflux for 2 hours. The reaction mixture was then cooled, concentrated *in vacuo* and dichloromethane (50 mL) was added before neutralisation with saturated aqueous $NaHCO_3$. The organic phase was collected, and the aqueous phase was extracted with dichloromethane (4 × 50 mL), before being combined and washed with brine (250 mL), dried over $MgSO_4$, filtered and concentrated *in vacuo*. The resultant crude product was purified *via* flash chromatography using 0-15% Methanol in Dichloromethane with 0.5% NH_4OH to afford the product as a yellow oil (1.14 g, 2.50 mmol, 51%). ^{1}H NMR (600 MHz, $CDCl_3$) δ_{ppm} 1.87 (s, 6H). 2.50 (s, 4H), 2.67 (t, *J* = 7.1 Hz, 2H), 3.21 – 3.11 (m, 5H), 3.69 (s, 4H), 4.18 (t, *J* = 7.1 Hz, 2H), 6.74 (d, *J* = 8.0 Hz, 2H), 7.00 (d, *J* = 8.1 Hz, 2H), 7.05 (d, *J* = 8.2 Hz, 1H), 7.32 (d, *J* = 8.2 Hz, 1H), 7.51 (s, 1H). ^{13}C NMR (151 MHz, $CDCl_3$) δ_{ppm} 24.3, 29.7, 33.1, 41.5, 54.0, 57.6, 66.7, 109.5, 115.3, 115.8, 121.4, 125.5, 129.3, 131.0, 131.5, 134.0, 142.4, 155.3, 155.4, 191.20. LC-MS (30-95 MeCN in 20 mins) ^{t}R = 3.36 min, Purity = 99%, m/z = 450.10. $[M + H]^+$. HR-MS (m/z): $[M + H]^+$ calculated for $C_{26}H_{32}N_3O_4$, 450.2393; found, 450.2397.

3-(4-(2-(5-(3,5-dimethylisoxazol-4-yl)-1-(2-morpholinoethyl)-1H-benzo[d]imidazol-2-yl)ethyl)phenoxy)-N,N-dimethylpropan-1-amine (**ISOX-DUAL**)

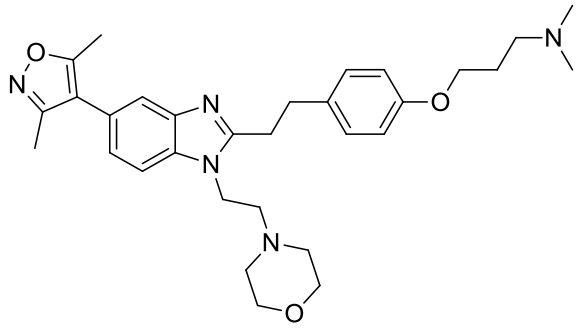

Compound **2.13** (283 mg, 1.1 mmol, 1.1 eq.) was suspended in DMF (5 mL) before the addition of HATU (494.3 mg, 1.3 mmol, 1.3 eq.) and DIPEA (179 µL, 1.5 mmol, 1.5 eq.) before leaving to stir at room temperature for 1 hour. A solution of **2.11** (316.4 mg, 1.0 mmol, 1 eq.) in DMF (3 mL) was added to the stirring mixture before leaving overnight at room temperature. The reaction mixture was partitioned between dichloromethane (50 mL) and water (50 mL). The aqueous phase was then extracted with dichloromethane (3 × 25 mL). The combined organic phases were washed with saturated aqueous $NaHCO_3$ (100 mL), brine (100 mL), dried over $MgSO_4$, filtered, and concentrated *in vacuo*. The crude component was dissolved in AcOH (50 mL) and heated to reflux for 2 hours. The reaction mixture was then cooled, concentrated *in vacuo* and dichloromethane (50 mL) was added before neutralisation with saturated aqueous $NaHCO_3$. The organic phase was collected, and the aqueous phase was extracted with dichloromethane (4 × 50 mL), before being combined and washed with brine (250 mL), dried over $MgSO_4$, filtered, and concentrated *in vacuo*. The resultant crude product was purified *via* flash chromatography using 0 – 10% methanol in dichloromethane with 0.5% NH_4OH to afford the product as a yellow oil (292.7 mg, 0.55 mmol, 55%).[1]H NMR (600 MHz, $CDCl_3$) δ_{ppm} 1.98 (p, *J* = 6.6 Hz, 2H). 2.29 (s, 9H), 2.42 (s, 3H), 2.45 (s, 4H), 2.50 (t, *J* = 7.0 Hz, 2H), 2.59 (t, *J* = 6.8 Hz, 2H), 3.19 – 3.14 (m, 2H), 3.25 – 3.20 (m, 2H), 3.67 (s, 4H), 3.99 (t, *J* = 6.3 Hz, 2H), 4.11 (t, *J* = 6.8 Hz, 2H), 6.84 (d, *J* = 8.1 Hz, 2H), 7.12 (t, *J* = 8.3 Hz, 3H), 7.34 (d, *J* = 8.2 Hz, 1H), 7.62 (s, 1H). [13]C NMR (151 MHz, $CDCl_3$) δ_{ppm} 11.0, 11.7, 27.5, 30.1, 33.2, 41.6, 45.5, 54.2, 57.8, 66.3, 67.0, 109.5, 114.8, 117.3, 120.1, 123.5, 124.3, 129.4, 133.0, 134.4, 143.2, 155.6, 157.8, 159.2, 165.2, LC-MS (5-95 MeCN in 20 mins) ^tR = 3.09 min, Purity = 98%, m/z = 532.30. Data matched those in literature.[2]

6.2 Chapter 3

6.2.1 Synthesis of Compounds

Methyl 3-(4-(benzyloxy)phenyl)propanoate (**3.01a**)[375]

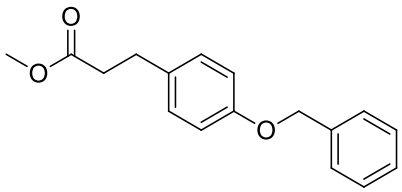

To a solution of **2.07** (1.0 g, 5.6 mmol, 1 eq.) in MeCN (75 mL) was added potassium carbonate (2.0 g, 14 mmol, 2.5 eq.) followed by benzyl bromide (1.67 mL, 14 mmol, 2.5 eq.). The reaction mixture was then heated to reflux and left to stir for 16 h. Once cooled, the mixture was diluted with water (100 mL) and extracted with EtOAc (3 × 100 mL). The combined organics were washed with 1 M NaOH (100 mL), brine (100 mL), dried over MgSO4, filtered, and concentrated *in vacuo*. The resultant crude product was purified *via* flash chromatography using 0 – 20% EtOAc in hexane to afford the product as a white solid (1.39 g, 5.15 mmol, 92%). ^{1}H NMR (600 MHz, $CDCl_3$) δ_{ppm} 2.60 (t, *J* = 8.3 Hz, 2H), 2.89 (t, *J* = 7.8 Hz, 2H), 3.66 (s, 3H), 5.04 (s, 2H), 6.90 (d, *J* = 7.7 Hz, 2H), 7.11 (d, *J* = 8.5 Hz, 2H), 7.31 – 7.34 (m, 1H), 7.38 (t, *J* = 7.5 Hz, 2H), 7.43 (d, *J* = 7.4 Hz, 2H). ^{13}C NMR (151 MHz, $CDCl_3$) δ_{ppm} 30.3, 36.1, 51.7, 70.2, 115.0, 127.6, 128.1, 128.7, 129.4, 133.0, 137.3, 157.5, 173.6. HR-MS-ESI (m/z): $[M+Na]^+$ calculated for $C_{17}H_{18}NaO_3$, 293.1154; found, 293.1146.

4-(3-Methoxy-3-oxopropyl)phenyl benzoate (**3.01b**)[376]

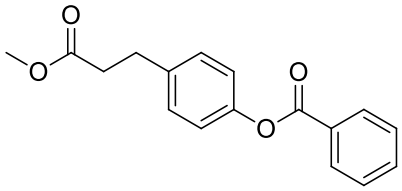

To a solution of **2.07** (1.0 g, 5.5 mmol, 1 eq.) in Dichloromethane (20 mL) was degassed and placed under an argon atmosphere before the addition of pyridine (0.89 mL, 11 mmol, 2 eq.) and benzoyl chloride (0.97 mL, 8.32 mmol, 1.5 eq.). The reaction mixture was left to stir for 3 h at room temperature, before concentrating *in vacuo*. The resultant crude product was purified *via* flash chromatography using 0 – 40% EtOAc in hexane to afford the product as a white solid (1.02 g, 3.6 mmol, 65%). ^{1}H NMR (600 MHz, $CDCl_3$) δ_{ppm} 2.65 (t, *J* = 7.9 Hz, 2H), 2.98 (t, *J* = 7.8 Hz, 2H), 3.69 (s, 3H), 7.12 – 7.15 (m, 2H), 7.25 – 7.26 (m, 2H), 7.49 – 7.53 (m, 2H), 7.63 (ddt, *J* = 7.8, 6.9, 1.3 Hz, 1H), 8.18 – 8.21 (m, 2H). ^{13}C NMR (151 MHz, $CDCl_3$) δ_{ppm} 30.5, 35.8, 51.8, 121.8,

128.7, 129.5, 129.8, 130.3, 133.7, 138.3, 149.5, 165.4, 173.4. HR-MS-ESI (m/z): $[M+Na]^+$ calculated for $C_{17}H_{16}NaO_4$, 307.0946; found, 307.0944.

Methyl 3-(4-(((benzyloxy)carbonyl)oxy)phenyl)propanoate (**3.01c**)[377]

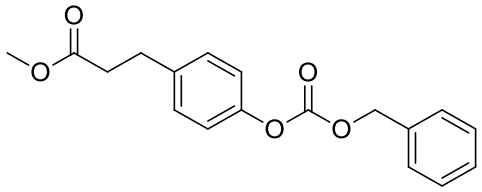

To a solution of **2.07** (1 g, 5.5 mmol, 1 eq.) in Dichloromethane (15 mL) was added DMAP (222 mg, 0.55 mmol, 0.1 eq.) and triethylamine (1.083 mL, 7.78 mmol, 1.5 eq.). The reaction mixture was cooled to 0 ˚C before the addition of CbzCl (1.14 g, 6.06, 1.2 eq.), the reaction mixture was left to stir at 0 ˚C for 30 mins before slowly warming to room temperature and left to stir for 16 h. The reaction mixture was quenched with water (15 mL). The organic layer was collected, and aqueous layer extracted with DCM (3 × 15 mL). The combined organics were washed with brine (100 mL), dried over $MgSO_4$, filtered, and concentrated *in vacuo*. The resultant crude product was purified *via* flash chromatography using 0 – 40% EtOAc in hexane to afford the product as a white solid (1.49 g, 4.7 mmol, 85%). ^{1}H NMR (600 MHz, $CDCl_3$) δ_{ppm} 2.63 (t, *J* = 7.8 Hz, 2H), 2.95 (t, *J* = 7.8 Hz, 2H), 3.67 (s, 3H), 5.27 (s, 2H), 7.09 – 7.12 (m, 2H), 7.19 – 7.22 (m, 2H), 7.35 – 7.42 (m, 3H), 7.44 (d, *J* = 7.8 Hz, 2H). ^{13}C NMR (151 MHz, $CDCl_3$) δ_{ppm} 30.3, 35.7, 51.7, 70.4, 121.1, 128.6, 128.8, 128.8, 129.4, 134.9, 138.5, 149.7, 153.8, 173.2. HR-MS-ESI (m/z): $[M+Na]^+$ calculated for $C_{18}H_{18}NaO_5$, 337.1052; found, 337.1045.

Methyl 3-(4-((tert-butoxycarbonyl)oxy)phenyl)propanoate (**3.01d**)[378]

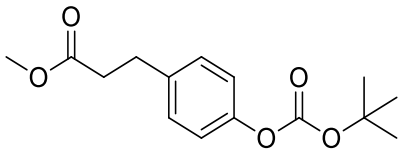

To a solution of **2.07** (1.0 g, 5.5 mmol, 1 eq.) in Dichloromethane (20 mL) was added DMAP (0.067 g, 0.55 mmol 0.1 eq), triethylamine (1.54 mL, 11 mmol, 2 eq.) and Boc-anhydride (2.4 g, 11 mmol, 2 eq.) before leaving to stir overnight at room temperature. The reaction mixture was diluted with water (50 mL), the organic layer was collected, and the aqueous layer was and extracted with dichloromethane (2 × 20 mL). The combined organics were washed with 1 M NaOH (50 mL), brine (100 mL), dried over MgSO4, filtered, and concentrated *in vacuo*. The resultant crude product was purified *via* flash chromatography using 0 – 20% EtOAc in hexane to afford the product as a white solid (1.51 g, 5.39 mmol, 98%). ^{1}H NMR (600 MHz, $CDCl_3$) δ_{ppm}

1.55 (s, 10H), 2.61 (t, *J* = 7.8 Hz, 2H), 2.94 (t, *J* = 7.8 Hz, 2H), 3.67 (s, 3H), 7.08 (d, *J* = 8.5 Hz, 2H), 7.19 (d, *J* = 8.2 Hz, 2H). ^{13}C NMR (151 MHz, $CDCl_3$) δ_{ppm} 27.8, 30.4, 35.8, 51.8, 83.6, 121.4, 129.3, 138.2, 149.7, 152.2, 173.3. HR-MS-ESI (m/z): $[M+Na]^+$ calculated for $C_{15}H_{20}NaO_5$, 303.1208; found, 303.1201.

Methyl 3-(4-(methoxymethoxy)phenyl)propanoate (**3.01e**)[379]

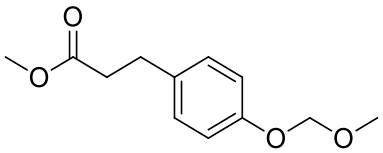

60% Sodium hydride in mineral oil (576 mg, 24 mmol, 1.2 eq.) was added in three portions to a stirred solution of **2.07** (3.61 g, 20 mmol, 1 eq.) in DMF (80 mL) at 0 ˚C. This was stirred for 30 mins before the addition of methyl chloromethoxy ether (1.67 mL, 22 mmol, 1.1 eq.) added dropwise. The reaction was stirred for 16 h and then diluted with water (100 mL) and extracted with EtOAc (3 × 50 mL). The combined organic fractions were washed with 1 M NaOH (50 mL), brine solution (50 mL), dried over MgSO4, filtered, and concentrated *in vacuo*. The resultant crude product was purified *via* flash chromatography using 0 – 60% EtOAc in hexane to afford the product as a white solid (3.36 g, 15 mmol, 75%). ^{1}H NMR (600 MHz, $CDCl_3$) δ_{ppm} 2.60 (t, *J* = 7.8 Hz, 2H), 2.90 (t, *J* = 7.8 Hz, 2H), 3.47 (s, 3H), 3.66 (s, 3H), 5.15 (s, 2H), 6.96 (d, *J* = 8.6 Hz, 2H), 7.11 (d, *J* = 8.6 Hz, 2H). ^{13}C NMR (151 MHz, $CDCl_3$) δ_{ppm} 30.3, 36.1, 51.7, 56.1, 94.7, 116.5, 129.4, 134.1, 155.9, 173.5. HR-MS-ESI (m/z): $[M+Na]^+$ calculated for $C_{12}H_{16}NaO_4$, 247.0946; found, 247.0941.

Methyl 3-(4-acetoxyphenyl)propanoate (**3.01f**)

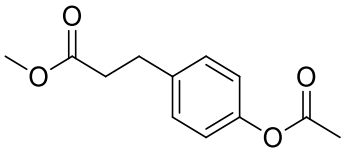

To a stirring solution of methyl-3-(4-hydroxyphenyl)propanoate (1 g, 5.55 mmol, 1 eq.) in Dichloromethane (10 mL) was successively added pyridine (0.67 mL, 8.32 mmol, 1.5 eq.) and acetic anhydride (0.7 mL, 8.32 mmol, 1.5 eq.), the reaction mixture was left to stir overnight at room temperature. The reaction mixture was poured into water (25 mL) and stirred vigorously for 30 mins. The organic layer was then collected and washed with saturated aqueous $NaHCO_3$ (25 mL), brine (25 mL), dried over $MgSO_4$, filtered, and concentrated *in vacuo* (1.2 g, 5.4 mmol, 98%). ^{1}H NMR (600 MHz, $CDCl_3$) δ_{ppm} 2.28 (s, 3H), 2.62 (t, *J* = 7.8 Hz, 2H), 2.94 (t, *J* = 7.8 Hz, 2H),

3.67 (s, 3H), 7.00 (d, *J* = 8.4 Hz, 2H), 7.20 (d, *J* = 8.4 Hz, 2H). HR-MS-ESI (m/z): $[M+Na]^+$ calculated for $C_{12}H_{14}NaO_4$, 245.0790; found, 245.0783.

Methyl 3-(4-((tert-butyldimethylsilyl)oxy)phenyl)propanoate (**3.01g**)[2]

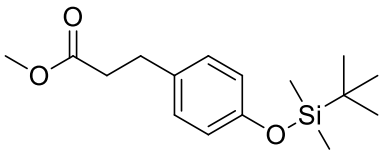

To a mixture of methyl 3-(4-hydroxyphenyl)propionate (5 g, 27.7 mmol, 1 eq) in DMF (50 mL) was added TBSCl (4.6 g, 30.5 mmol, 1.1 eq) and imidazole (2.8 g, 41.6 mmol, 1.5 eq) under an argon atmosphere. This mixture was left to stir overnight at room temperature. Upon completion the reaction mixture was concentrated then partitioned between EtOAc (50 mL) and water (50 mL). The organic layer was collected, and the aqueous phase was extracted with EtOAc (3 × 50 mL). The organic collections were combined and washed with brine (200 mL), dried over $MgSO_4$, filtered, and concentred *in vacuo*. The resultant crude oil was purified *via* flash chromatography using 0-70% EtOAc in hexane to afford the product as a clear oil (7.12g, 24.2 mmol, 87%). ^{1}H NMR (600 MHz, $CDCl_3$) δ_{ppm} 0.18 (s, 6H), 0.97 (s, 9H), 2.59 (t, *J* = 8.0, 7.5 Hz, 2H), 2.87 (t, *J* = 8.0 Hz, 2H), 3.66 (s, 3H), 6.75 (d, *J* = 8.5 Hz, 2H), 7.04 (d, *J* = 8.5 Hz, 2H). Data matched those observed in literature.[2]

Lithium 3-(4-(benzyloxy)phenyl)propanoate (**3.02a**)

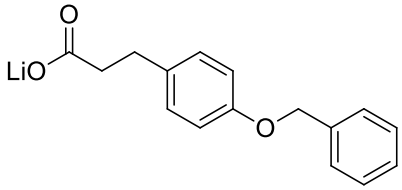

To a stirring solution of **3.01a** (1.39 g, 5.15 mmol, 1 eq.) in a mixture of THF: water (5:1, 250 mL), was added $LiOH{\cdot}H_2O$ (2.22 g, 52.8 mmol, 1.1 eq.) and left to stir overnight at room temperature. The reaction mixture was concentrated *in vacuo* and was azeotroped with THF (5 × 50 mL) to afford the product as the lithium salt, which was used crude (1.35 g, 5.15 mmol, quant.). LC-MS (5-95 MeCN in 20 mins) ^{t}R = 19.80 min, Purity = 90%, m/z = 254.90 $[M-H]^-$.

Lithium 3-(4-(methoxymethoxy)phenyl)propanoate (**3.02e**)

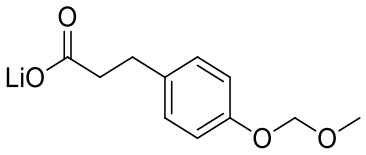

To a stirring solution of **3.01a** (3.36 g, 15 mmol, 1 eq.) in a mixture of THF: water (5:1, 250 mL), was added $LiOH{\cdot}H_2O$ (2.22 g, 52.8 mmol, 1.1 eq.) and left to stir overnight at room temperature. The reaction mixture was concentrated *in vacuo* and was azeotroped with THF (5 × 50 mL) to afford the product as the lithium salt, which was used crude (3.20 g, 15 mmol, quant.). LC-MS (5-95 MeCN in 20 mins) ^{t}R = 16.71 min, Purity = 95%, m/z = 208.85 $[M-H]^-$.

4-(2-(2-(4-(benzyloxy)phenethyl)-5-(3,5-dimethylisoxazol-4-yl)-1*H*-benzo[*d*]imidazol-1-yl)ethyl)morpholine (**3.03a**)

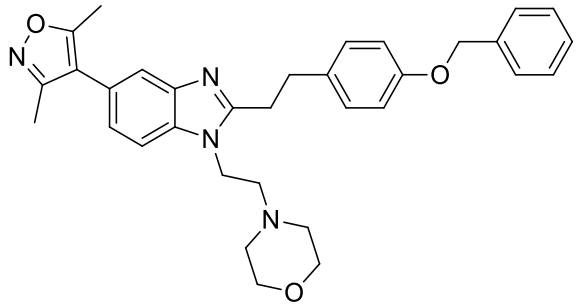

Compound **3.02a** (1.24 g, 4.74 mmol, 1.1 eq.) was suspended in DMF (25 mL) before the addition of HATU (1.95 g, 5.14 mmol, 1.3 eq.) and was left to stir at room temperature for 1 hour. A solution of **2.11** (1.25 g, 3.65 mmol, 1 eq.) in DMF (25 mL) was added to the stirring mixture before leaving overnight at room temperature. The reaction mixture was partitioned between dichloromethane (150 mL) and water (150 mL). The aqueous phase was then extracted with dichloromethane (3 × 50 mL). The combined organic phases were washed with saturated aqueous $NaHCO_3$ (100 mL), brine (100 mL), dried over $MgSO_4$, filtered, and concentrated *in vacuo*. The crude component was dissolved in AcOH (150 mL) and heated to reflux for 2 hours. The reaction mixture was then cooled, concentrated *in vacuo* and dichloromethane (150 mL) was added before neutralisation with saturated aqueous $NaHCO_3$. The organic phase was collected, and the aqueous phase was extracted with dichloromethane (4 × 100 mL), before being combined and washed with brine (250 mL), dried over $MgSO_4$, filtered, and concentrated *in vacuo*. The resultant crude product was purified *via* flash chromatography using 0 – 10% methanol (with 0.5% NH_4OH) in dichloromethane to afford the product as a white solid (1.31 g, 2.44 mmol, 62%). ^{1}H NMR (600 MHz, $CDCl_3$) δ_{ppm} 2.30 (s, 3H), 2.43 (s, 3H), 2.45 (t, *J* = 4.6 Hz, 4H), 2.60 (t, *J* = 6.9 Hz, 2H), 3.15 – 3.19 (m, 2H), 3.23 (t, *J* = 6.9 Hz, 2H), 3.67 (t, *J* = 4.6 Hz, 4H), 4.09 (t, *J* = 6.9 Hz, 2H), 5.05 (s, 2H), 6.90 – 6.93 (m, 2H), 7.11 – 7.16 (m, 3H), 7.33 (dd, *J* = 7.9, 5.3 Hz, 2H), 7.38 (dd, *J* = 8.1, 7.0 Hz, 2H), 7.42 (d, *J* = 7.2 Hz, 2H), 7.63 (t, *J* = 1.2 Hz, 1H). ^{13}C NMR (151 MHz, $CDCl_3$) δ_{ppm} 11.0, 11.7, 30.0, 33.2, 41.6, 54.2, 57.7, 67.0, 70.2, 109.5, 115.2, 117.2, 120.1, 123.5, 124.4, 127.6, 128.1, 128.7, 129.5, 133.4, 134.4, 137.2, 143.2, 155.6, 157.6, 159.1, 165.2. LC-MS (5-95 MeCN in 20 mins) ^{t}R = 13.91 min, Purity = 96%, m/z = 537.20 $[M+H]^+$. HR-MS-ESI (m/z): $[M+H]^+$ calculated for $C_{33}H_{37}N_4O_3$, 537.2866; found, 537.2863.

4-(2-(5-(3,5-Dimethylisoxazol-4-yl)-1-(2-morpholinoethyl)-1*H*-benzo[*d*]imidazol-2-yl)ethyl)phenyl acetate (**3.04**)

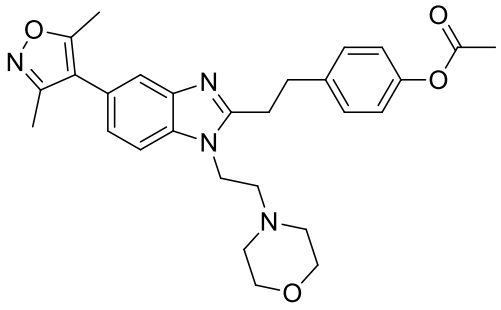

To a stirred solution of **2.10** (87 mg, 0.195 mmol, 1 eq.) in Dichloromethane (5 mL), were added pyridine (0.032 mL, 0.39 mmol, 2 eq.) and acetic anhydride (0.037 mL, 0.39 mmol, 2 eq.) at room temperature, and the mixture was left to stir for 1 hour. The reaction mixture was then quenched with saturated aqueous NH_4Cl (10 mL) and extracted with DCM (10 mL). The organic layer was collected, washed with brine (10 mL), dried over $MgSO_4$, and concentrated *in vacuo* before flash chromatography using 0 – 10% methanol (with 0.5% NH_4OH) in dichloromethane to afford the product as a clear oil. (76.2 mg, 0.156 mmol, 80%).^{1}H NMR (600 MHz, $CDCl_3$) δ_{ppm} 1.92 (s, 6H), 2.05 (s, 3H), 2.09 (s, 4H), 2.25 (t, *J* = 6.8 Hz, 2H), 2.79 – 2.85 (m, 2H), 2.90 – 2.95 (m, 2H), 3.30 (s, 4H), 3.74 (t, *J* = 6.8 Hz, 2H), 6.64 (d, *J* = 7.8 Hz, 2H), 6.75 (d, *J* = 8.2 Hz, 1H), 6.86 – 6.90 (m, 2H), 6.98 (d, *J* = 8.2 Hz, 1H). ^{13}C NMR (600 MHz, $CDCl_3$) δ_{ppm} 11.0, 11.7, 21.2, 29.7, 33.3, 41.6, 54.1, 57.7, 66.9, 109.5, 117.2, 120.0, 121.9, 123.6, 124.4, 129.5, 134.4, 138.3, 143.1, 149.4, 155.2, 159.1, 165.1, 169.7. LC-MS (5-95 MeCN in 20 mins) ^{t}R = 4.10 min, Purity = 92%, m/z = 489.05 $[M+H]^+$. HR-MS-ESI (m/z): $[M+H]^+$ calculated for $C_{28}H_{33}N_4O_4$, 489.2496; found, 489.2477.

Methyl 4-(4-(2-(5-(3,5-dimethylisoxazol-4-yl)-1-(2-morpholinoethyl)-1*H*-benzo[*d*]imidazol-2-yl)ethyl)phenoxy)butanoate (**3.06**)

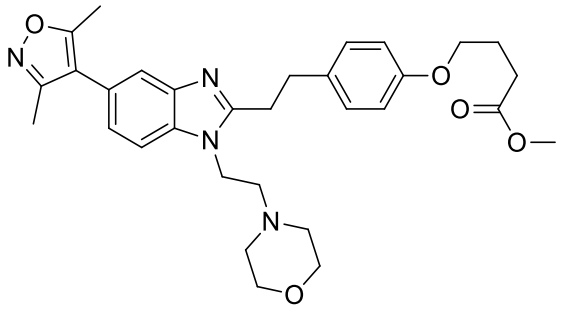

To a stirring solution of **2.10** (1.4 g, 3.1 mmol, 1 eq.) in MeCN (50 mL) was added K_2CO_3 (0.857 g, 6.2 mmol, 2 eq.), followed by methyl 4-bromobutyrate (1.1224 g, 6.2 mmol, 2 eq.) before leaving to stir overnight at reflux. The reaction was cooled and partitioned between EtOAc (50 mL) and water (50 mL). The organic phase was collected, and the aqueous layer was extracted with EtOAc (3 × 25 mL). The organics were combined and washed with brine (100 mL), dried over $MgSO_4$, and concentrated *in vacuo.* The resultant crude product was purified *via* flash chromatography using 0 – 5% methanol in dichloromethane with 0.5% NH_4OH to afford the product as a clear oil (1.12 g, 2.0 mmol, 70%). ^{1}H NMR (500 MHz, $CDCl_3$) δ_{ppm} 2.07 – 2.13 (m, 2H), 2.30 (s, 3H), 2.43 (s, 3H), 2.46 (t, *J* = 4.6 Hz, 4H), 2.52 (t, *J* = 7.3 Hz, 2H), 2.59 (t, *J* = 6.9 Hz, 2H), 3.14 – 3.18 (m, 2H), 3.22 (t, *J* = 6.9 Hz, 2H), 3.68 (d, *J* = 7.9 Hz, 7H), 3.98 (t, *J* = 6.1 Hz, 2H), 4.11 (t, *J* = 6.9 Hz, 2H), 6.82 (d, *J* = 8.6 Hz, 2H), 7.10 – 7.15 (m, 3H), 7.34 (d, *J* = 8.3 Hz, 1H), 7.62 (d, *J* = 1.5 Hz, 1H). ^{13}C NMR (126 MHz, $CDCl_3$) δ_{ppm} 11.0, 11.7, 15.4, 24.7, 30.1, 30.7, 33.2, 41.6, 51.8, 54.2, 57.7, 66.8, 67.0, 109.5, 110.1, 114.8, 117.2, 120.0, 123.5, 124.3, 129.5, 133.1, 134.4, 143.2, 155.6, 157.6, 159.2, 165.2, 173.8. LC-MS (5-95 MeCN in 20 mins) ^{t}R = 12.30 min, Purity = 96%, m/z = 547.20 $[M+H]^+$. HR-MS-ESI (m/z): $[M+H]^+$ calculated for $C_{31}H_{39}N_4O_5$, 547.2915; found, 547.2892.

Lithium 4-(4-(2-(5-(3,5-dimethylisoxazol-4-yl)-1-(2-morpholinoethyl)-1*H*-benzo[*d*]imidazol-2-yl)ethyl)phenoxy)butanoate (**3.07**)

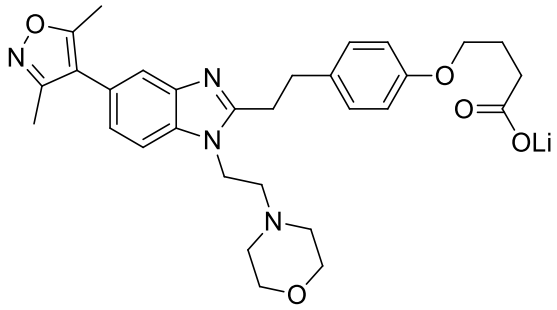

To a stirring solution of **3.06** (1.1 g, 2.5 mmol, 1 eq.) in THF (100 mL) and water (20 mL) was added $LiOH{\cdot}H_2O$ (0.115 g, 2.75 mmol, 1.1 eq.) and was left to stir at room temperature overnight. Upon reaction completion, the resultant solution was concentrated *in vacuo* and was azeotroped with THF (5 × 50 mL) to result in **3.07** as a white solid. (1.0 g, 1.86 mmol, 94%). LC-MS (5-95 MeCN in 20 mins) ^{t}R = 11.04, Purity = 95%, m/z = 531.15.

4-(4-(2-(5-(3,5-Dimethylisoxazol-4-yl)-1-(2-morpholinoethyl)-1*H*-benzo[*d*]imidazol-2-yl)ethyl)phenoxy)-N-(2-methoxyethyl)butanamide (**3.09**)

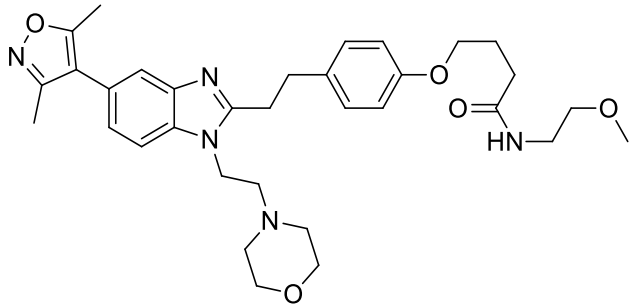

To a stirring solution of **3.07** (100 mg, 0.19 mmol, 1 eq.) and HATU (83.7 mg, 0.22 mmol, 1.2 eq.) in DMF (mL) was added triethylamine (26.5 µL, 0.19 mmol, 1.2 eq.) followed by 2-methoxyethylamine (14.3 mg, 0.19 mmol, 1 eq.) before leaving the reaction to stir at room temperature overnight. The mixture was partitioned between Dichloromethane (25 mL) and water (25 mL). Organic collected and washed with sat. $NaHCO_3$ (25 mL), brine (3 × 10 mL), dried over $MgSO_4$ and filtered before concentrating *in vacuo*. The product was purified with flash chromatography using 0 – 10% Methanol in Dichloromethane with 0.5% NH_4OH to afford **3.09** as a clear oil (88.4 mg, 0.15 mmol, 79%). ^1H NMR (500 MHz, $CDCl_3$) δ_{ppm} 1.89 (s, 1H), 2.08 – 2.15 (m, 2H), 2.29 (s, 3H), 2.39 (t, *J* = 7.3 Hz, 2H), 2.42 (s, 3H), 2.45 (t, *J* = 4.5 Hz, 4H), 2.59 (t, *J* = 6.9 Hz, 2H), 3.14 – 3.18 (m, 2H), 3.22 (dd, *J* = 8.8, 6.4 Hz, 2H), 3.32 (s, 3H), 3.43 (s, 4H), 3.66

(d, *J* = 4.6 Hz, 4H), 3.98 (t, *J* = 6.0 Hz, 2H), 4.11 (t, *J* = 6.9 Hz, 2H), 5.94 (s, 1H), 6.82 (d, *J* = 8.6 Hz, 2H), 7.10 – 7.15 (m, 3H), 7.34 (d, *J* = 9.0 Hz, 1H), 7.62 (s, 1H).^{13}C NMR 11.0, 11.7, 30.0, 33.0, 33.1, 39.3, 41.6, 54.1, 57.7, 58.9, 66.9, 67.0, 71.3, 109.5, 114.8, 117.2, 120.0, 123.5, 124.3, 129.5, 133.1, 134.4, 143.1, 155.5, 157.6, 159.1, 165.2, 172.4. LC-MS (5-95 MeCN in 20 mins) ^{t}R = 11.08 min, Purity = 99%, m/z = 590.20. HR-MS-ESI (m/z): $[M+H]^+$ calculated for $C_{33}H_{43}N_5O_5Na$, 612.3156; found, 612.3143.

4-Bromo-*N*-(2-morpholinoethyl)-2-nitroaniline (**2.04**)

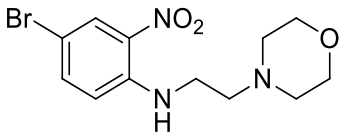

4-bromo-2-fluoro-1-nitrobenzene (27g, 123 mmol, 1 eq.) was dissolved in DMSO (100 mL) before the sequential addition of triethylamine (51.3 mL, 368 mmol, 3 eq.) and 4-(2-aminoethyl)morpholine (16.9 mL, 129 mmol, 1.05 eq.). The reaction mixture was then heated to 80 °C for 1 hour. The reaction mixture was partitioned between EtOAc (500 mL) and water (500 mL). The organic layer was collected and the aqueous extracted with EtOAc (3 × 250 mL). The combined organics were then washed with brine (1 L), dried over $MgSO_4$, filtered, and concentrated *in vacuo* to afford an orange solid. This solid was then triturated in Et_2O for an hour before being filtered and transferred to a vacuum oven to dry at 40 ˚C overnight, resulting in the product as an orange solid (40.6 g, 123 mmol, Quant%). ^{1}H NMR (400 MHz, $CDCl_3$) δ_{ppm} 2.52 (d, *J* = 2.1 Hz, 4H), 2.69 – 2.74 (m, 2H), 3.31 – 3.37 (m, 2H), 3.73 – 3.77 (m, 4H), 6.73 (d, *J* = 9.2 Hz, 1H), 7.49 (dd, *J* = 8.8, 2.1 Hz, 1H), 8.32 (d, *J* = 2.4 Hz, 1H), 8.51 (s, 1H). LC-MS (5-95 MeCN in 5 mins) ^{t}R = 3.178, Purity = >99%, m/z = 332.1 $[M + H]^+$.

4-(3,5-Dimethylisoxazol-4-yl)-*N*-(2-morpholinoethyl)-2-nitroaniline (**2.06**)

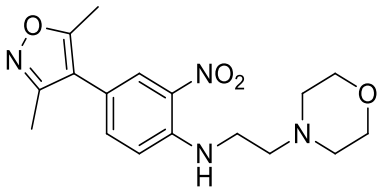

Compound **2.04** (38 g, 115 mmol, 1 eq.), potassium phosphate (63.5 g, 299 mmol, 2.6 eq.), 3,5-dimethylisoxazole boronic acid pinacol ester (25.6 g, 115 mmol, 1 eq.) were dissolved In 1,4-dioxane (1.2L) and water (120 mL). The mixture was degassed and refilled with argon three times before the addition of $PdCl_2$(dppf)·DCM (4.7 g, 5.75 mmol, 0.05 eq.). The reaction

mixture was then degassed and refilled with argon once, heated to 110 °C and left overnight under a stream of N_2. Reaction was then cooled to room temperature and filtered through a pad of Celite before concentrating *in vacuo* to approximately 300 mL. Crude mixture was then partitioned between water (600 mL) and EtOAc (600 mL), the organic phase was collected, and the aqueous phase extracted with EtOAc (3 × 250 mL). The organic extracts were then combined and washed with brine (3 × 400 mL), dried over $MgSO_4$, filtered, and concentrated *in vacuo* to result in a dark brown solid. This solid was then purified *via* flash chromatography using 0 – 80% EtOAc in hexane to afford the product as an orange solid (37.4 g, 108 mmol, 94%). ^{1}H NMR (400 MHz, $CDCl_3$) δ_{ppm} 2.26 (s, 3H), 2.40 (s, 3H), 2.55 (d, *J* = 4.6 Hz, 3H), 2.75 (t, *J* = 6.1 Hz, 2H), 3.38 – 3.44 (m, 2H), 3.78 (d, *J* = 4.6 Hz, 4H), 6.91 (d, *J* = 8.8 Hz, 1H), 7.34 (dd, *J* = 8.8, 2.2 Hz, 1H), 8.09 (d, *J* = 2.2 Hz, 1H), 8.58 (s, 1H). LC-MS (5-95 MeCN in 5 mins) ^{t}R = 3.266, Purity = >99%, m/z = 347.2 $[M + H]^+$.

4-(3,5-Dimethylisoxazol-4-yl)-*N*^{1}-(2-morpholinoethyl)benzene-1,2-diamine (**2.11**)

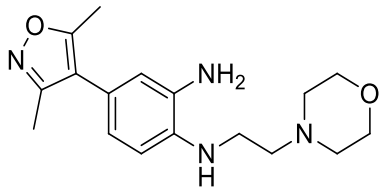

Compound **2.06** (17.4 g, 50 mmol, eq.) was suspended in EtOH (800 mL) before the addition of 1 M $Na_2S_2O_4$ (800 mL) and heated to reflux for 1 hour. Upon cooling the reation mixture was quenched with 10% NH_3 solution (800 mL) and extracted with EtOAc (4 × 300 mL). The organic phases were combined, successively washed with water (500 mL) and brine (3 × 500 mL), dried over $MgSO_4$, and filtered before concentrating *in vacuo* to result in a beige oil. This oil was then triturated in petrol 40-60 and Et_2O (1:1) for 16 hours before concentrating to afford the product as a beige solid (12.70 g, 40.14 mmol, 80%). ^{1}H NMR (400 MHz, $CDCl_3$) δ_{ppm} 2.25 (s, 3H), 2.38 (s, 3H), 2.50 (s, 4H), 2.71 (t, *J* = 5.9 Hz, 2H), 3.21 (d, *J* = 5.8 Hz, 2H), 3.45 (s, 2H), 3.69 – 3.76 (m, 4H), 4.08 (s, 1H), 6.59 (s, 1H), 6.68 (s, 2H). LC-MS (5-95 MeCN in 5 mins) ^{t}R = 2.364, Purity = >99%, m/z = 317.2 $[M + H]^+$.

tert-Butyl 4-(4-(3-methoxy-3-oxopropyl)phenoxy)butanoate (**3.11**)

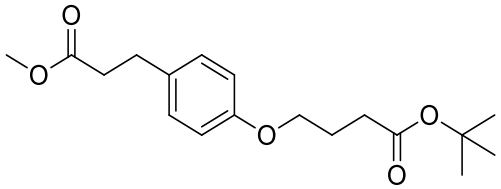

To a solution of methyl 3-(4-hydroxyphenyl)propionate (20 g, 111 mmol, 1 eq.) in MeCN (200 mL) was added potassium carbonate (30.6 g, 222 mmol, 2 eq.). The reaction was then fitted with a dropping funnel containing a solution of tert-butyl 4-bromobutanoate (25 g, 111 mmol, 1 eq.) in MeCN (100 mL). The reaction mixture was then heated to reflux overnight. Upon cooling the reaction mixture was filtered and transferred to a separating funnel and partitioned between dichloromethane (700 mL) and water (500 mL). The organic phase was collected and washed with 1M K_2CO_3 solution (10 × 250 mL), brine (2 × 300 mL) and dried over $MgSO_4$ before concentration *in vacuo*. The crude mixture was then purified by column chromatography using 5% - 10% - 15% - 20% EtOAc in petroleum ether 40 – 60, to give the product as a clear oil which crystallised over time (27 g, 83.8 mmol, 75%). ^{1}H NMR (400 MHz, $CDCl_3$) δ_{ppm} 1.45 (s, 9H), 2.01 – 2.08 (m, 2H), 2.41 (t, *J* = 7.3 Hz, 2H), 2.59 (t, *J* = 7.8 Hz, 2H), 2.88 (t, *J* = 7.8 Hz, 2H), 3.66 (s, 3H), 3.96 (t, *J* = 6.2 Hz, 2H), 6.81 (d, *J* = 8.7 Hz, 2H), 7.10 (d, *J* = 8.6 Hz, 2H). LC-MS (5-95 MeCN in 5 mins) ^{t}R = 5.879, Purity = 96%, m/z = 289.2.

4-(4-(3-Methoxy-3-oxopropyl)phenoxy)butanoic acid (**3.12**)

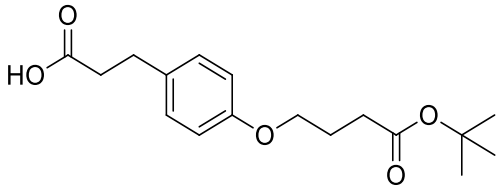

3.11 (27 g, 87.7 mmol, 1 eq.) was dissolved in THF (200 mL), before the addition of a 1M LiOH solution (200 mL, 2.4 eq.). The reaction mixture was left to stir until completion by TLC. The reaction was then acidified to pH 2 with 2 M HCl and extracted with EtOAc (4 × 200 mL), organics were combined and washed with brine, dried over $MgSO_4$, and concentrated *in vacuo* to result in the product as a white solid (24.3 g, mmol, 94%). ^{1}H NMR (400 MHz, $CDCl_3$) δ_{ppm} 1.40 (s, 9H), 1.87 – 1.93 (m, 2H), 2.46 (d, *J* = 7.5 Hz, 2H), 2.74 (t, *J* = 7.6 Hz, 2H), 3.90 – 3.94 (m, 2H), 6.81 (d, *J* = 8.7 Hz, 2H), 7.11 (d, *J* = 8.6 Hz, 2H).

4-(4-(2-(5-(3,5-Dimethylisoxazol-4-yl)-1-(2-morpholinoethyl)-1*H*-benzo[d]imidazol-2-yl)ethyl)phenoxy)butanoic acid (**3.13**)

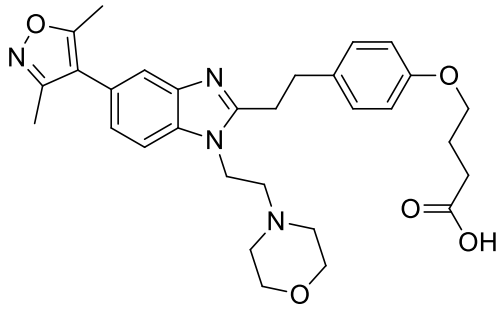

To a suspension of Compound **3.12** (12.38 g, 40.14 mmol, 1 eq.) in DMF (200 mL), was added triethylamine (16.8 mL, 120 mmol, 3 eq.) and HATU (19.84 g, 15.1 mmol, 1.3 eq.). The Reaction vessel was flushed with argon and left to stir for 1 hour before the addition of Compound **2.11** (12.7 g, 40.14 mmol, 1 eq.) in DMF (150 mL). The reaction was then left to stir at room temperature overnight. The reaction mixture was then partitioned between EtOAc (500 mL) and water (2 L). The organic layer was collected, and the aqueous layer was extracted with EtOAc (3 × 300 mL). The organic extracts were combined and successively washed with saturated aqueous $NaHCO_3$ (150 mL), brine (150 mL), dried over $MgSO_4$, filtered, and concentrated *in vacuo* to result in the crude intermediate. This intermediate was purified *via* column chromatography using 1% 7N NH_3 methanol for 1 L, 2% 7N NH_3 methanol for 1 L, 3% 7N NH_3 methanol for 500 mL and finally 4% 7N NH_3 methanol in dichloromethane resulted in the product as a pale brown solid. This solid was dissolved in AcOH and heated to reflux for 2 hours, after which the reaction mixture was cooled and concentrated *in vacuo* and azeotroped with EtOAc (100 mL) and heptane (300 mL) three times. The crude component was dissolved in EtOAc (300 mL) and poured into saturated aqueous $NaHCO_3$ (400 mL). The organic layer was collected and washed with brine (500 mL), dried over $MgSO_4$, filtered, and concentrated *in vacuo*. This intermediate was purified using 3% - 5% - 7% 7N NH_3 Methanol in Dichloromethane to afford the product as a beige solid. This solid was dissolved in dioxane (100 mL) and HCl as a 4 M solution in dioxane (50 mL, 200 mmol, 10 eq.) was added before leaving to stir for 4 hours, after which the reaction mixture was concentrated and triturated overnight in MeCN which resulted in a white precipitate. This precipitate was filtered and washed with Et_2O and dried under vacuum under an N_2 atmosphere to afford the product as a white solid (10.5 g, 18 mmol, 46%). ^{1}H NMR (600 MHz, d^6-DMSO) δ_{ppm} 1.91 (q, *J* = 6.8 Hz, 2H), 2.24 (s, 3H), 2.37 (t, *J* = 7.3 Hz, 2H), 2.43 (s, 3H), 3.19 (t, *J* = 8.0 Hz, 4H), 3.48 – 3.57 (m, 6H), 3.88 (d, *J* = 12.3 Hz, 2H), 3.95 (t, *J* = 6.4 Hz, 2H), 4.02 (d, *J* = 12.8 Hz, 2H), 5.02 (t, *J* = 8.2 Hz, 2H), 6.88 (d, *J* = 8.6 Hz, 2H), 7.32 (d, *J* = 8.6 Hz, 2H), 7.60 (dd, *J* = 8.5, 1.6 Hz, 1H), 7.81 (s, 1H), 8.30

(d, *J* = 8.6 Hz, 1H), 12.59 (s, 1H). ^{13}C NMR (151 MHz, d^6-DMSO) δ_{ppm} 10.5, 11.3, 24.3, 27.4, 30.1, 31.3, 38.5, 51.1, 51.9, 63.2, 66.4, 66.6, 113.4, 114.5, 114.7, 115.5, 126.5, 127.7, 129.7, 131.0, 131.2, 155.0, 157.3, 158.3, 165.7, 174.1. LC-MS (30-95 MeCN in 20 mins) ^{t}R = 7.27 min, Purity = 95%, m/z = 533.55 $[M + H]^+$. HR-MS (m/z): $[M + H]^+$ calculated for $C_{30}H_{37}N_4O_5$, 533.2764; found, 533.2785.

tert-Butyl 4-(2-((4-bromo-2-nitrophenyl)amino)ethyl)piperazine-1-carboxylate (**3.15**)

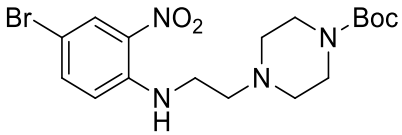

A microwave vial was equipped with a magnetic flea and flushed with argon. 4-(2-Aminoethyl)-1-boc-piperazine (5.05 g, 22 mmol, 1.1 eq.), followed by triethylamine (15 mL). This was stirred for 3 min before the addition of the aryl fluoride (4.40 g, 20 mmol, 1 eq.), following addition the vial was sealed and heated using the dynamic heating method, with max power set to 300 W, max pressure 300 psi, max temperature 125 °C, high stirring throughout and power max turned off. This method was used to hold the method at 125 °C for 10 min. After cooling, the reaction mixture was transferred to a separating funnel where it was partitioned between water (250 mL) and EtOAc (200 mL). The organic was collected and the aqueous was extracted with EtOAc (3 × 75 mL). The combined organic layers were then washed with saturated aqueous $NaHCO_3$ (200 mL), brine (200 mL) and then dried over anhydrous $MgSO_4$ before concentration *in vacuo* to yield **3.15** as an orange solid (8.40 g, 19.6 mmol, 98%). ^{1}H NMR (600 MHz, $CDCl_3$) δ_{ppm} 1.46 (s, 9H), 2.46 (s, 4H), 2.73 (t, *J* = 6.1 Hz, 2H), 3.34 (q, *J* = 5.6 Hz, 2H), 3.50 – 3.45 (m, 4H), 6.73 (d, *J* = 9.1 Hz, 1H), 7.49 (dd, *J* = 9.1, 2.3 Hz, 1H), 8.32 (d, *J* = 2.2 Hz, 1H), 8.51 (s, 1H). ^{13}C NMR (151 MHz; $CDCl_3$; Me_4Si) δ 28.6, 39. 8, 52.7, 55.6, 79.9, 106.4, 115.9, 129.1, 132.5, 139.0, 144.3, 154.9. LC-MS (5-95 MeCN in 20 mins) ^{t}R = 7.94 min, Purity = 99%, m/z = 429.00. HR-MS-ESI (m/z): $[M+H]^+$ calculated for $C_{17}H_{26}BrN_4O_4$, 429.1132; found, 429.1132.

tert-Butyl 4-(2-((4-(3,5-dimethylisoxazol-4-yl)-2-nitrophenyl)amino)ethyl)piperazine-1-carboxylate (**3.16)**

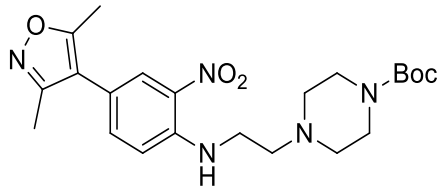

A round bottom flask was equipped with a magnetic flea and flushed with argon. Compound **3.15** (8.40 g, 19.60 mmol, 1 eq.), potassium phosphate (10.82 g, 50.96 mmol, 2.6 eq.), $PdCl_2$(dppf)·DCM (0.80 g, 0.98 mmol, 5 mol%), and boronic acid pinacol ester (4.90 g, 21.95 mmol, 1.12 eq.) were added. The mixture was flushed with argon before the addition of 1,4-dioxane (200 mL). The reaction was then heated to reflux and left overnight under an atmosphere of argon. After cooling, the reaction mixture was filtered through Celite and concentrated *in vacuo*. Purification using 0-100% EtOAc in hexane, resulted in **3.16** as an orange oil (6.99 g, 15.68 mmol, 80%).^{1}H NMR (600 MHz, $CDCl_3$) δ_{ppm} 1.47 (s, 9H), 2.26 (s, 3H), 2.40 (s, 3H), 2.52 – 2.45 (m, 4H), 2.76 (t, *J* = 6.1 Hz, 2H), 3.41 (q, *J* = 5.8 Hz, 2H), 3.52 – 3.46 (m, 4H), 6.91 (d, *J* = 8.8 Hz, 1H), 7.34 (dd, *J* = 8.8, 2.0 Hz, 1H), 8.08 (d, *J* = 2.1 Hz, 1H), 8.58 (s, 1H). ^{13}C NMR (151 MHz; $CDCl_3$) δ_{ppm} 10.9, 11.7, 28.6, 39. 8, 43.4, 44.4, 52.7, 55.7, 79.9, 114.9, 115.1, 117.5, 127.2, 132.1, 136.9, 144.6, 154. 9, 158.7, 165.5. LC-MS (5-95 MeCN in 20 mins) ^{t}R = 7.61 min, Purity = 99%, m/z = 446.50 $[M+H]^+$. HR-MS-ESI (m/z): $[M+H]^+$ calculated for $C_{22}H_{32}N_5O_5$, 446.2398; found, 446.2421.

tert-Butyl 4-(2-((2-amino-4-(3,5-dimethylisoxazol-4-yl)phenyl)amino)ethyl)piperazine-1-carboxylate (**3.17**)

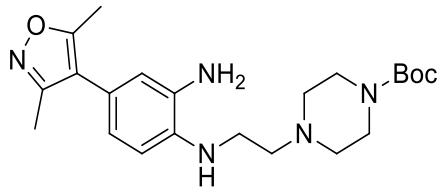

To a solution of **3.16** (1.50 g, 3.47 mmol, 1 eq.) in EtOH (55 mL) was added 1 M aqueous $Na_2S_2O_4$ solution (55 mL) and the reaction was heated to 80 °C for 1 hour. Upon cooling the reaction mixture was extracted with 10% ammonia solution (55 mL) and EtOAc (75 mL), the organic layer was collected and then the aqueous layer was re-extracted with EtOAc (3 × 30 mL). The organics were combined and washed with brine (3 × 100 mL), dried over $MgSO_4$,

and concentrated *in vacuo* to give the product as a yellow oil, which was used crude in the next step. (1.20 g, 2.89 mmol, 83%). ^{1}H NMR (600 MHz, $CDCl_3$) δ_{ppm} 1.46 (s, 9H), 2.25 (s, 3H), 2.38 (s, 3H), 2.45 (s, 4H), 2.72 (t, *J* = 5.8 Hz, 2H), 3.20 (d, *J* = 11.7 Hz, 2H), 3.45 (s, 4H), 6.59 (s, 1H), 6.68 (s, 2H). LC-MS (5-95 MeCN in 20 mins) ^{t}R = 7.39 min, m/z = 416.30 $[M+H]^+$.

3-(4-(2-(5-(3,5-Dimethylisoxazol-4-yl)-1-(2-(piperazin-1-yl)ethyl)-1*H*-benzo[*d*]imidazol-2-yl)ethyl)phenoxy)-*N*,*N*-dimethylpropan-1-amine (**3.19**)

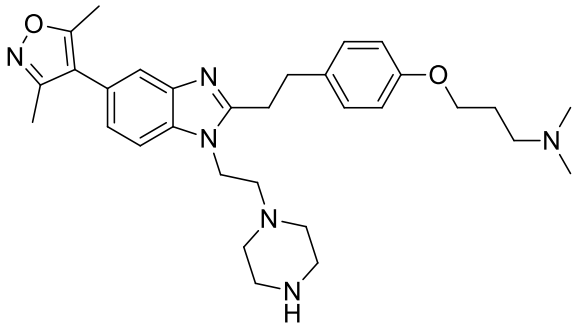

To a suspension of Compound **2.13** (0.818 g, 3.18 mmol, 1.1 eq.) in DMF (10 mL), was added Triethylamine (0.8 mL, 5.78 mmol, 2 eq.) and HATU (1.43 g, 3.76 mmol, 1.3 eq.). The reaction vessel was flushed with argon and left to stir for 1 hour before the addition of compound **3.17** (1.20 g, 3.76 mmol, 1 eq.) in DMF (10 mL). The reaction was then left to stir at room temperature overnight. The reaction mixture was then partitioned between EtOAc (50 mL) and water (50 mL). The organic layer was collected and washed with water (4 × 150 mL) saturated aqueous $NaHCO_3$ (100 mL), brine (100 mL), dried over anhydrous $MgSO_4$ and concentrated *in vacuo* to afford the crude product. Purification *via* column chromatography using *via* flash chromatography using 0 – 20% 7N NH_3 methanol in dichloromethane afforded intermediate **3.18**. The latter was then dissolved in methanol (20 mL) before the addition of HCl as a 4 M solution in dioxane (2.6 mL, 10.5 mmol, 10 eq.), the reaction was then heated to reflux overnight. The reaction mixture was cooled and concentrated *in vacuo* before addition of Dichloromethane (50 mL) and sat $NaHCO_3$ (50 mL) solution and left to vigorously stir for 10 min. The organic layer was collected, and the aqueous layer was extracted with dichloromethane (3 × 50 mL). The combined organics were washed with brine, dried over $MgSO_4$, filtered, and concentrated *in vacuo*. The crude product was purified *via* flash chromatography using 0 – 20% 7N NH_3 methanol in dichloromethane to afford the product as a beige solid (564 mg, 1.064 mmol, 37%). ^{1}H NMR (600 MHz, $CDCl_3$) δ_{ppm} 1.95 (q, *J* = 6.8 Hz, 2H), 2.27 (s, 6H), 2.29 (s, 3H), 2.41 – 2.48 (m, 9H), 2.59 (t, *J* = 7.0 Hz, 2H), 2.86 (t, *J* = 4.8 Hz, 4H), 3.15 – 3.19 (m, 2H), 3.21 (d, *J* = 8.6 Hz, 2H), 3.99 (d, *J* = 6.5 Hz, 2H), 4.11 (t, *J* = 7.0 Hz, 2H), 6.84 (d, *J* = 8.1 Hz, 2H), 7.12 (dd, *J* = 14.3, 8.2 Hz, 3H), 7.34 (d, *J* = 8.2 Hz, 1H), 7.62 (s, 1H). ^{13}C NMR

(151 MHz, $CDCl_3$) δ_{ppm} 11.0, 11.7, 30.1, 33.2, 41.7, 45.5, 46.1, 55.0, 56.5, 58.0, 66.4, 109.6, 114.8, 117.3, 120.0, 123.5, 124.3, 129.4, 133.0, 134.5, 143.2, 155.7, 157.8, 159.2, 165.1. LC-MS (5-95 MeCN in 20 mins) ^tR = 7.344 min, Purity = 97%, m/z = 531.4 $[M+H]^+$. HR-MS-ESI (m/z): $[M+H]^+$ calculated for $C_{31}H_{43}N_6O_2$, 531.3447; found, 531.3443.

tert-Butyl 4-(2-(2-(4-(3-(dimethylamino)propoxy)phenethyl)-5-(3,5-dimethylisoxazol-4-yl)-1*H*-benzo[*d*]imidazol-1-yl)ethyl)piperazine-1-carboxylate (**3.20**)

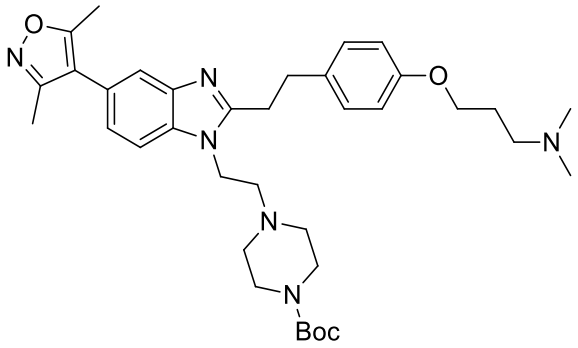

To a solution of di-*tert*-butyl dicarbonate (58 mg, 0.265 mmol, 1.4 eq.) and DMAP (4.6 mg, 0.038 mmol, 0.2 eq.) in dichloromethane (5 mL) was added a dropwise a solution of **3.17** (100 mg, 0.189 mmol, 1 eq.) in dichloromethane (3 mL) and triethylamine (0.131 mL, 0.945 mmol, 5 eq.). The resulting mixture was stirred overnight. After this time, water (10 mL) was added. The organic phase was collected, and the aqueous phase was extracted with dichloromethane (5 × 10 mL). The combined organic layers were washed with brine (100 mL), dried over $MgSO_4$, filtered, and concentrated *in vacuo*. The crude product was then purified *via* flash chromatography using 0 – 10% 7N NH_3 Methanol in Dichloromethane to afford the product as a clear oil (52 mg, 0.082 mmol, 43%). ^1H NMR (600 MHz, $CDCl_3$) δ_{ppm} 1.44 (s, 9H), 2.07 (q, *J* = 6.9 Hz, 2H), 2.29 (s, 3H), 2.41 (d, *J* = 8.1 Hz, 13H), 2.61 (d, *J* = 6.9 Hz, 2H), 2.65 (s, 2H), 3.13 – 3.18 (m, 2H), 3.19 – 3.24 (m, 2H), 3.38 (s, 4H), 4.00 (t, *J* = 6.2 Hz, 2H), 4.11 (d, *J* = 13.7 Hz, 2H), 6.83 (d, *J* = 8.5 Hz, 2H), 7.12 (dd, *J* = 12.4, 8.4 Hz, 3H), 7.33 (d, *J* = 8.2 Hz, 1H), 7.62 (s, 1H). ^{13}C NMR (151 MHz; $CDCl_3$) δ_{ppm} 11.0, 11.7, 27.7, 28.5, 29.8, 30.1, 30.4, 33.2, 41.8, 45.6, 53.6, 56.5, 57.3, 66.4, 80.0, 109.5, 114.8, 117.2, 120.1, 123.5, 124.3, 129.4, 132.9, 134.4, 143.2, 154.7, 155.6, 157.8, 159.1, 165.1. LC-MS (5-95 MeCN in 20 mins) ^tR = 7.38 min, Purity = 92% - one peak, m/z = 631.45 $[M+H]^+$. HR-MS-ESI (m/z): $[M+H]^+$ calculated for $C_{36}H_{51}N_6O_4$, 631.3972; found, 631.3998.

4-(2-(2-(4-(3-(Dimethylamino)propoxy)phenethyl)-5-(3,5-dimethylisoxazol-4-yl)-1*H*-benzo[*d*]imidazol-1-yl)ethyl)piperazine-1-carbaldehyde (**3.21**)

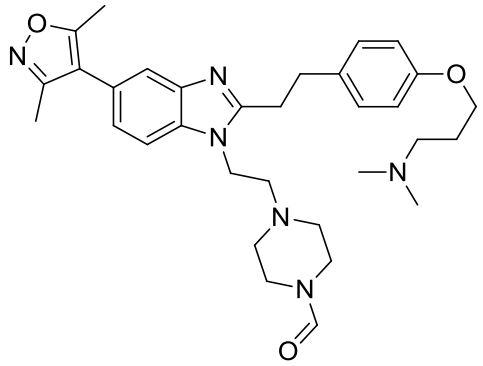

To a suspension of **2.13** (0.746 g, 2.90 mmol, 1.1 eq.) in DMF (30 mL), was added HATU (1.346 g, 3.54, 1.3 eq.). The reaction vessel was flushed with argon and left to stir for 1 hour before the addition of **3.17** (1.1 g, 2.64 mmol, 1 eq.) in DMF (30 mL). The reaction was then left to stir at room temperature overnight. The reaction mixture was then partitioned between DCM (50 mL) and water (50 mL). The organic layer was collected and washed with water (4 × 150 mL) saturated aqueous $NaHCO_3$ (100 mL), brine (100 mL), dried over anhydrous $MgSO_4$ and concentrated *in vacuo*. The latter was dissolved in AcOH and heated to reflux for 2 hours. The reaction mixture was cooled to room temperature and concentrated *in vacuo* before purification *via* flash chromatography using 0 – 10% methanol (with 0.5% NH_4OH) in dichloromethane to afford **3.21** as a brown oil. (685 mg, 1.2 mmol, 46%). ^{1}H NMR (600 MHz, $CDCl_3$) δ_{ppm} 2.0 – 2.1 (m, 4H), 2.3 (s, 3H), 2.4 (d, *J* = 22.2 Hz, 14H), 2.6 – 2.7 (m, 4H), 3.2 (t, *J* = 7.7 Hz, 2H), 3.2 – 3.2 (m, 2H), 3.3 (t, *J* = 5.0 Hz, 1H), 3.4 – 3.4 (m, 1H), 3.5 (t, *J* = 5.1 Hz, 1H), 3.6 (t, *J* = 5.0 Hz, 1H), 4.0 (t, *J* = 6.2 Hz, 2H), 4.1 (t, *J* = 6.7 Hz, 2H), 6.8 (d, *J* = 8.2 Hz, 2H), 7.1 – 7.1 (m, 3H), 7.3 (d, *J* = 8.2 Hz, 1H), 7.6 (s, 1H), 8.0 (s, 1H). ^{13}C NMR (151 MHz; $CDCl_3$) δ_{ppm} 11.0, 11.7, 21.4, 27.0, 30.1, 33.2, 39.9, 41.4, 41.8, 45.1, 45.6, 46.3, 52.9, 53.3, 54.0, 54.3, 56.4, 57.2, 66.1, 109.5, 114.8, 117.2, 120.1, 123.6, 124.4, 129.4, 133.1, 134.4, 143.2, 155.5, 157.7, 159.1, 160.8, 165.2, 169.0. LC-MS (5-95 MeCN in 20 mins) ^{t}R = 9.35 min, Purity = 94%, m/z = 559.20. HR-MS-ESI (m/z): $[M+H]^+$ calculated for $C_{32}H_{43}N_6O_4$, 559.3397; found, 559.3351.

1-(4-(2-(2-(4-(3-(Dimethylamino)propoxy)phenethyl)-5-(3,5-dimethylisoxazol-4-yl)-1*H*-benzo[*d*]imidazol-1-yl)ethyl)piperazin-1-yl)ethanone (**3.22**)

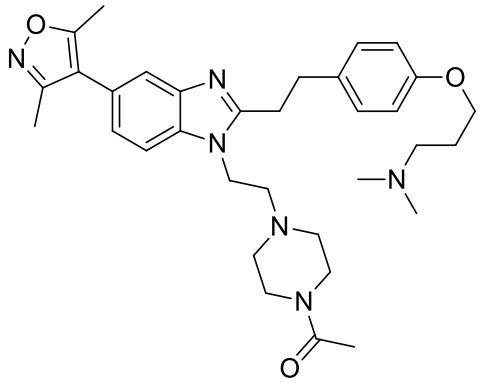

To a suspension of **2.13** (0.918 g, 3.57 mmol, 1.1 eq.) in DMF (20 mL), was added Triethylamine (1.36 mL, 9.75 mmol, 3 eq.) and HATU (1.61 g, 4.23 mmol, 1.3 eq.). The reaction vessel was flushed with argon and left to stir for 1 hour before the addition of **3.17** (1.35 g, 3.25 mmol, 1 eq.) in DMF (30 mL). The reaction was then left to stir at room temperature overnight. The reaction mixture was then partitioned between EtOAc (50 mL) and water (50 mL). The organic layer was collected and washed with water (4 × 150 mL) saturated aqueous $NaHCO_3$ (100 mL), brine (100 mL), dried over anhydrous $MgSO_4$ and concentrated *in vacuo* to result in the crude product. Purification *via* column chromatography using *via* flash chromatography using 0 – 20% 7N NH_3 methanol in dichloromethane to afford intermediate **3.18**. The latter was then dissolved in AcOH and heated to reflux overnight. The reaction mixture was cooled, concentrated, and suspended in dichloromethane before neutralising with saturated $NaHCO_3$ solution. The organic phase was collected, and the aqueous phase was extracted with DCM (4 × 50 mL). The combined organics were washed with brine, dried over $MgSO_4$, filtered, and concentrated *in vacuo*. The crude product was purified *via* flash chromatography using 0 – 20% (7N NH_3 methanol) in dichloromethane to afford the product as a pale brown oil (640 mg, 1.12 mmol, 34%). ^{1}H NMR (600 MHz, $CDCl_3$) δ_{ppm} 1.94 (p, *J* = 6.7 Hz, 2H), 2.06 (s, 3H), 2.24 (d, *J* = 2.3 Hz, 7H), 2.29 (s, 3H), 2.39 – 2.45 (m, 9H), 2.62 (t, *J* = 6.8 Hz, 2H), 3.15 (ddd, *J* = 8.5, 7.1, 2.2 Hz, 2H), 3.18 – 3.24 (m, 2H), 3.37 – 3.40 (m, 2H), 3.58 (t, *J* = 5.0 Hz, 2H), 3.98 (t, *J* = 6.4 Hz, 2H), 4.10 (t, *J* = 6.8 Hz, 2H), 6.83 (d, *J* = 8.5 Hz, 2H), 7.11 (dd, *J* = 8.4, 4.4 Hz, 3H), 7.33 (d, *J* = 8.2 Hz, 1H), 7.62 (s, 1H). ^{13}C NMR (151 MHz, $CDCl_3$) δ_{ppm} 11.1, 11.8, 27.4, 30.2, 33.2, 39.9, 41.8, 45.4, 45.6, 52.9, 54.3, 56.4, 57.2, 66.3, 109.5, 114.6, 114.8, 117.2, 120.1, 123.6, 124.4, 129.4, 129.5, 133.0, 134.3, 143.2, 155.5, 159.2, 160.8, 165.2. LC-MS (5-95 MeCN in 20 mins) ^{t}R = 6.97 min, Purity = 96% - one peak, m/z = 573.55 $[M+H]^+$. HR-MS-ESI (m/z): $[M+H]^+$ calculated for $C_{33}H_{45}N_6O_4$, 573.3553; found, 573.3546.

4-(3,5-Dimethylisoxazol-4-yl)-2-nitro-N-(2-(piperazin-1-yl)ethyl)aniline (**3.23**)

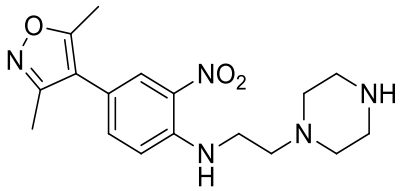

To a stirring solution of Compound **3.16** (2.8 g, 6.3 mmol, 1 eq.) in Dichloromethane (200 mL) was added TFA (20 mL, 26.2 mmol), and the reaction was left to stir at room temperature overnight. The reaction mixture was concentrated *in vacuo*, flask had dichloromethane (5 × 50 mL) added and removed to result in the product as the TFA salt. The latter was suspended in dichloromethane (50 mL) and neutralised with saturated $NaHCO_3$. The organic layer was collected, and the aqueous layer was extracted with dichloromethane (5 × 50 mL). The organic layers were combined and washed with brine (2 × 100 mL), dried over MgSO4, filtered, and concentrated *in vacuo* to result in **3.23** as a red oil (2.2 g, 6.2 mmol, 99%). ^{1}H NMR (600 MHz, $CDCl_3$) δ_{ppm} 2.26 (s, 3H), 2.40 (s, 3H), 2.55 (s, 4H), 2.75 (s, 2H), 2.98 (s, 4H), 3.40 (q, *J* = 5.6 Hz, 2H), 6.91 (d, *J* = 8.8 Hz, 1H), 7.34 (d, *J* = 8.6 Hz, 1H), 8.09 (s, 1H), 8.58 (s, 1H). ^{13}C NMR (151 MHz, $CDCl_3$) δ_{ppm} 10.9, 11.7, 39.7, 46.1, 53.8, 56.2, 114.9, 115.1, 117.4, 132.1, 136.9, 144.6, 158.7, 165.5. LC-MS (5-95 MeCN in 20 mins) ^{t}R = 10.56 min, Purity = 99%, m/z = 345.95 $[M+H]^+$. HR-MS-ESI (m/z): $[M+H]^+$ calculated for $C_{17}H_{24}N_5O_3$, 346.1874; found, 346.1859.

tert-Butyl 2-(4-(2-((4-(3,5-dimethylisoxazol-4-yl)-2-nitrophenyl)amino)ethyl)piperazin-1-yl)acetate (**3.25**)

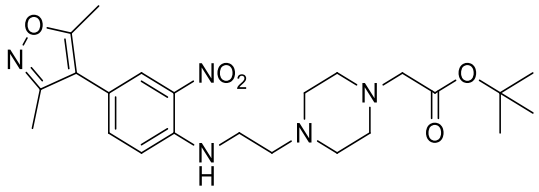

A solution of **3.23** (2.1 g, 6.3 mmol, 1 eq.) in Dichloromethane (100 mL) was flushed with argon before addition of DIPEA (4.40 mL, 25.2 mmol, 4 eq.) to the flask. To the mixture was added *tert*-butyl bromoacetate (1.11 mL, 7.56 mmol, 1.2 eq.), and it was then left to stir overnight at room temperature. The reaction was then transferred to a separating funnel and washed with water (50 mL), saturated aqueous $NaHCO_3$ solution (50 mL), brine (100 mL) and dried over anhydrous $MgSO_4$ before concentration *in vacuo*. Purification using 0-100% EtOAc in hexane resulted in the product as an orange oil (2.31 g, 5.04 mmol, 80%). ^{1}H NMR (600 MHz, $CDCl_3$) δ_{ppm} 1.47 (s, 8H), 2.26 (s, 3H), 2.40 (s, 3H), 2.62 (s, 7H), 2.76 (t, *J* = 6.1 Hz, 2H), 3.13 (s, 2H), 3.39 (q, *J* = 5.6 Hz, 2H), 6.91 (d, *J* = 8.8 Hz, 1H), 7.33 (d, *J* = 8.8 Hz, 1H), 8.57 (s, 1H), 8.08 (s, 1H). ^{13}C

NMR (151 MHz; $CDCl_3$; Me_4Si) δ 10. 8, 11.6, 28.2, 39.7, 52.5, 53.1, 55.5, 59.9, 81.1, 114.7, 115.0, 117.2, 127.0, 131.9, 136.7, 144.5, 158.6, 165.3, 169.6. LC-MS (5-95 MeCN in 20 mins) ^{t}R = 12.59 min, Purity = >99%, m/z = 460.10 $[M+H]^+$. HR-MS-ESI (m/z): $[M+H]^+$ calculated for $C_{23}H_{34}N_5O_5^+$, 460.2554; found, 460.2542.

tert-Butyl 2-(4-(2-((2-amino-4-(3,5-dimethylisoxazol-4-yl)phenyl)amino)ethyl)piperazin-1-yl)acetate (**3.26**)

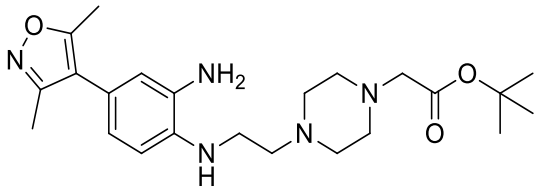

To a suspension of **3.21** (2.30 g, 5.01 mmol) in EtOH (75 mL) was added 1M aqueous $Na_2S_2O_4$ solution (75 mL) and the reaction was heated to 80 °C for 1 hour. Upon cooling the reaction mixture was extracted with 10% NH_3 solution (75 mL) and EtOAc (75 mL), the organic layer was collected and then the aqueous layer was re-extracted with EtOAc (3 × 25 mL). The organics were combined and washed with brine (100 mL), dried over $MgSO_4$, and concentrated *in vacuo* to give the product as a yellow oil, which was used crude in the next step. (1.36 g, 3.51 mmol, 70%). ^1H NMR (600 MHz, $CDCl_3$) δ_{ppm} 1.47 (s, 9H), 2.25 (s, 3H), 2.37 (s, 3H), 2.60 (d, *J* = 22.6 Hz, 8H), 2.71 (t, *J* = 5.8 Hz, 2H), 3.12 (s, 2H), 3.20 (t, *J* = 5.8 Hz, 2H), 3.48 (s, 2H), 6.58 (s, 1H), 6.68 (s, 2H). ^{13}C NMR (151 MHz; $CDCl_3$) δ_{ppm} 10.8, 11.5, 28.1, 40.6, 52.8, 53.00, 56.7, 59.6, 81.1, 111.6, 116.5, 116.8, 120.2, 121.2, 134.6, 137.1, 159.0, 164.4, 169.5. LC-MS (30-95 MeCN in 20 mins) ^{t}R = 17.02 min, Purity = 95%, m/z = 430.05 $[M+H]^+$. HR-MS-ESI (m/z): $[M+Na]^+$ calculated for $C_{23}H_{35}N_5NaO_3^+$, 452.2632; found, 452.2638.

2-(4-(2-(2-(4-(3-(dimethylamino)propoxy)phenethyl)-5-(3,5-dimethylisoxazol-4-yl)-1*H*-benzo[*d*]imidazol-1-yl)ethyl)piperazin-1-yl)acetic acid hydrochloride (**3.27**)

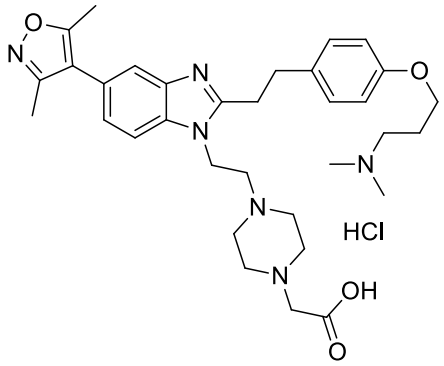

To a suspension of Compound **2.13** (3.3 g, 12.8 mmol, 1.1 eq.) in DMF (30 mL), was added triethylamine (3.23 mL, 23.2 mmol, 2 eq.) and HATU (5.7 g, 15.1 mmol, 1.3 eq.). The reaction vessel was flushed with argon and left to stir for 1 hour before the addition of **3.26** (5 g, 11.6 mmol, 1 eq.) in DMF (30 mL). The reaction was then left to stir at room temperature overnight. The reaction mixture was then partitioned between dichloromethane (150 mL) and water (150 mL). The organic layer was collected and washed with water (4 × 150 mL) saturated aqueous $NaHCO_3$ (150 mL), brine (150 mL), dried over anhydrous $MgSO_4$ and concentrated *in vacuo* to result in the crude product. Purification *via* column chromatography using 3% methanol (with 0.1% NH_3) for 2 L, 3% methanol (with 0.2% NH_3) for 1 L and finally 5% methanol (with 0.5% NH_3) in dichloromethane resulted in the product as a pale brown gum (2.59 g, 3.908 mmol). The purified product was then dissolved in AcOH (50 mL) and heated to reflux for 1.5 hours. Upon cooling the reaction mixture was concentrated *in vacuo* and was stripped with heptane (5 × 75 mL). The brown gum was dissolved in anhydrous EtOAc (60 mL) and purged with N_2. To this stirring solution was added 2M HCl in Et_2O (6 mL, 11.72 mmol, 3 eq), a solid immediately formed and excess Et_2O was added, and the solution was left to stir overnight at room temperature. The precipitate was then filtered under *vacuo* under an atmosphere of N_2. After drying in a vacuum oven for one hour the product was then freeze dried overnight to result in the product as an off-white solid (3.04 g, 4.60 mmol, 40%). ^{1}H NMR (600 MHz, d^6-DMSO) δ_{ppm} 2.10 – 2.17 (m, 2H), 2.24 (s, 3H), 2.42 (s, 3H), 2.74 (d, *J* = 4.8 Hz, 6H), 3.16 – 3.22 (m, 4H), 3.36 (s, 8H), 3.57 (t, *J* = 8.0 Hz, 2H), 3.97 (s, 2H), 4.02 (t, *J* = 6.2 Hz, 2H), 4.85 (s, 2H), 6.89 (d, *J* = 8.7 Hz, 2H), 7.33 (d, *J* = 8.5 Hz, 2H), 7.57 (d, *J* = 8.5 Hz, 1H), 7.79 (s, 1H), 8.22 (d, *J* = 8.6 Hz, 1H), 11.03 (s, 1H). ^{13}C NMR (151 MHz, d^6-DMSO) δ_{ppm} 10.5, 11.4, 23.9, 27.3, 31.3, 42.0, 53.9, 55.0, 64.9, 113.5, 114.6, 115.5, 126.5, 127.6, 129.7, 131.1, 131.6, 154.8, 157.1, 158.3, 165.7. LC-MS (30-95 MeCN in 20 mins) ^{t}R = 7.36 min, Purity = 95% - one peak, m/z = 589.25 $[M + H]^+$.HR-MS (m/z): $[M + H]^+$ calculated for $C_{33}H_{45}N_6O_4$, 589.3502; found, 589.3577.

Methyl 2-(4-(2-(2-(4-(3-(dimethylamino)propoxy)phenethyl)-5-(3,5-dimethylisoxazol-4-yl)-1*H*-benzo[*d*]imidazol-1-yl)ethyl)piperazin-1-yl)acetate (**3.28**)

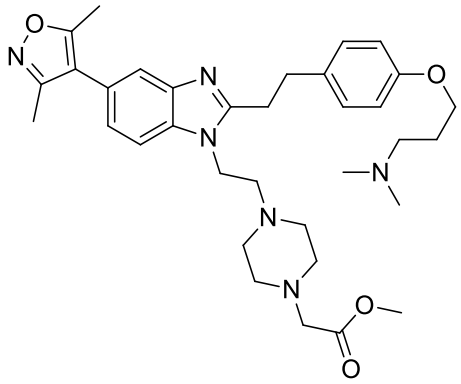

A solution of **3.27** (100 mg, 0.151 mmol, 1 eq.) and H_2SO_4 (1 drop) in Methanol (5 mL) was heated to reflux overnight. The reaction mixture was concentrated *in vacuo* and suspended in EtOAc (10 mL) and water (10 mL) and the biphasic mixture was neutralised with saturated $NaHCO_3$ (10 mL). The organic layer was collected and washed with brine, dried over $MgSO_4$, filtered, and concentrated *in vacuo*. The crude product was purified *via* flash chromatography using 0 – 20% Methanol in Dichloromethane to result in the product as a clear oil. The clear oil was dissolved in anhydrous EtOAc (10 mL) and purged with N_2. To this stirring solution was added 2M HCl in Et_2O (0.132 mL, 0.27 mmol, 2 eq.), a solid immediately formed and excess Et_2O was added and the solution was left to stir overnight at room temperature. The precipitate was then filtered under *vacuo* under an atmosphere of N_2 to result in **3.28** as a beige solid (85 mg, 0.141, 93%). ^{1}H NMR (600 MHz, $CDCl_3$) δ_{ppm} 2.01 (q, *J* = 6.9 Hz, 3H), 2.30 (s, 3H), 2.33 (s, 6H), 2.43 (s, 3H), 2.56 (s, 8H), 2.62 (d, *J* = 7.0 Hz, 3H), 3.14 – 3.18 (m, 2H), 3.21 (s, 4H), 3.72 (s, 3H), 4.00 (t, *J* = 6.3 Hz, 2H), 4.10 (t, *J* = 7.0 Hz, 2H), 6.83 (d, *J* = 8.6 Hz, 2H), 7.10 – 7.15 (m, 3H), 7.34 (d, *J* = 8.2 Hz, 1H), 7.62 (d, *J* = 1.5 Hz, 1H). ^{13}C NMR (151 MHz; $CDCl_3$) δ_{ppm} 11.1, 11.8, 30.1, 33.2, 41.7, 45.4, 51.9, 53.0, 53.5, 56.5, 57.3, 59.4, 66.2, 109.6, 114.8, 117.3, 120.0, 123.5, 124.3, 129.5, 133.1, 134.4, 143.2, 155.6, 157.7, 159.2, 165.2, 170.8. LC-MS (30-95 MeCN in 20 mins) ^{t}R = 7.03 min, Purity = 91% - one peak, m/z = 603.25 $[M + H]^+$.HR-MS (m/z): $[M + H]^+$ calculated for $C_{34}H_{47}N_6O_4$, 603.3659; found, 603.3651.

2-(4-(2-(2-(4-(3-(Dimethylamino)propoxy)phenethyl)-5-(3,5-dimethylisoxazol-4-yl)-1*H*-benzo[*d*]imidazol-1-yl)ethyl)piperazin-1-yl)-*N*-(2-methoxyethyl)acetamide (**3.29**)

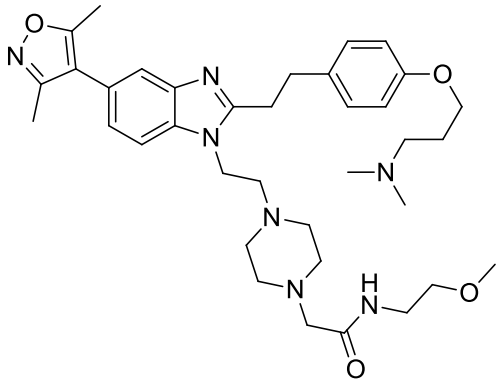

To a stirring solution of **3.27** (150 mg, 0.227 mmol, 1 eq.) and HATU (112.2 mg, 0.295 mmol, 1.3 eq.) in DMF (5 mL) was added triethylamine (95 µL, 0.681 mmol, 3 eq.) followed by 2-methoxyethylamine (40 µL, 0.453 mmol, 2 eq.) before leaving the reaction to stir at room temperature overnight. The mixture was then partitioned between Dichloromethane (25 mL) and water (25 mL). The organic layer was collected and washed with saturated $NaHCO_3$ (25 mL), brine (3 × 10 mL), dried over $MgSO_4$ and filtered before concentrating *in vacuo*. The product was purified with flash chromatography using 0 – 10% 7N NH_3 Methanol in Dichloromethane to result in the product as a clear oil. The clear oil was dissolved in anhydrous EtOAc (10 mL) and purged with N_2. To this stirring solution was added 2M HCl in Et_2O (0.17 mL, 0.33 mmol, 2 eq.), a solid immediately formed and excess Et_2O was added, and the solution was left to stir overnight at room temperature. The precipitate was then filtered under *vacuo* under an atmosphere of N_2 to result in **3.29** as a white solid (120 mg, 0.167, 74%). ^{1}H NMR (600 MHz, $CDCl_3$) δ_{ppm} 2.16 (dd, *J* = 15.3, 5.8 Hz, 2H), 2.29 (s, 3H), 2.42 (s, 3H), 2.49 (s, 8H), 2.57 (s, 7H), 2.64 (t, *J* = 6.8 Hz, 2H), 2.87 (s, 2H), 2.98 (s, 2H), 3.15 – 3.19 (m, 2H), 3.23 (t, *J* = 7.0 Hz, 2H), 3.34 (s, 3H), 3.45 (d, *J* = 1.0 Hz, 4H), 4.04 (t, *J* = 6.0 Hz, 2H), 4.11 (t, *J* = 6.7 Hz, 2H), 6.83 (d, *J* = 8.6 Hz, 2H), 7.10 – 7.12 (m, 1H), 7.15 (d, *J* = 8.6 Hz, 2H), 7.34 (d, *J* = 8.2 Hz, 2H), 7.62 (d, *J* = 1.5 Hz, 1H). ^{13}C NMR (600 MHz, $CDCl_3$) δ_{ppm} 10.9, 11.6, 22.6, 26.0, 29.8, 32.8, 38.6, 41.7, 44.3, 53.2, 53.6, 56.1, 57.1, 58.7, 61.4, 65.4, 71.3, 109.3, 114.6, 117.1, 119.9, 123.4, 124.2, 129.4, 133.4, 134.3, 143.1, 155.5, 157.2, 159.0, 165.0, 170.0. LC-MS (5-95 MeCN in 20 mins) ^{t}R = 8.69 min, Purity = 96%, m/z = 646.30 $[M + H]^+$. HR-MS (m/z): $[M + H]^+$ calculated for $C_{36}H_{52}N_7O_4$, 646.4081; found, 646.4094.

4-(4-Fluoro-3-nitrophenyl)-3,5-dimethylisoxazole (**3.30**)[43]

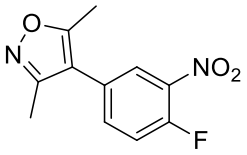

$Pd(dppf)Cl_2$ (0.988 g, 1.21 mmol, 0.05 eq.) was added to a solution of 4-bromo-1-fluoro-2-nitrobenzene (5.3 g, 24.1 mmol, 1 eq.), potassium phosphate (13.3 g, 62.7 mmol, 2.6 eq.) and 3,5-dimethylisoxazole-4-boronic acid pinacol ester (6.1 g, 27 mmol, 1.12 eq.) in 1,4-dioxane and water (9:1) (190 mL). The mixture of was degassed by evacuating and refilling with argon (×3) then heated at 100 ˚C overnight. The reaction mixture was cooled, filtered through a pad of Celite, washed with EtOAc (4 × 50 mL) and the filtrate was concentrated *in vacuo*. The crude component was then purified *via* flash chromatography using 0 – 70% EtOAc in hexane to afford the product as a yellow solid. (5.3 g, 22.5 mmol, 93%). ^{1}H NMR (600 MHz, $CDCl_3$) δ_{ppm} 7.95 (dd, *J* = 7.0, 2.3 Hz, 1H), 7.54 – 7.51 (m, 1H), 7.40 (t, *J* = 8.8 Hz, 1H), 2.44 (s, 3H), 2.29 (s, 3H). Data matched those previously.[43]

N-(2,2-Dimethoxyethyl)-4-(3,5-dimethylisoxazol-4-yl)-2-nitroaniline (**3.31**)[43]

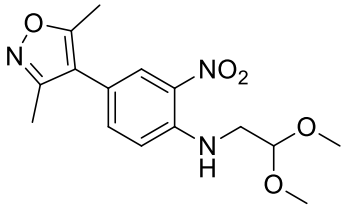

To a stirring solution of **3.30** (3.6 g, 15.2 mmol, 1 eq.) in DMSO (20 mL) was added aminoacetaladehyde dimethyl acetal (1.99 mL, 18.3 mmol, 1.2 eq.) and triethylamine (4.3 mL, 30.4 mmol, 3 eq.) The reaction was heated to 80 C for 2 hours, after which the reaction was cooled and partitioned between EtOAc (200 mL) and water (200 mL). The organic phase was collected and the aqueous was extracted with EtOAc (4 × 50 mL). The organic extracts were combined and washed with brine, dried over $MgSO_4$, filtered, and concentrated *in vacuo*. The crude oil was then purified *via* flash chromatography using 0 – 100% EtOAc in hexane to afford the product as an orange solid (3.841 g, 11.95 mmol, 79%). ^{1}H NMR (600 MHz, $CDCl_3$) δ_{ppm} 2.26 (s, 3H), 2.40 (s, 3H), 3.47 (s, 6H), 3.49 (t, *J* = 5.4 Hz, 2H), 4.66 (t, *J* = 5.5 Hz, 1H), 6.96 (d, *J* = 8.8 Hz, 1H), 7.34 (dd, *J* = 8.8, 2.1 Hz, 1H), 8.08 (d, *J* = 2.0 Hz, 1H), 8.19 (t, *J* = 5.4 Hz, 1H). LC-MS (30-95 MeCN in 20 mins) ^{t}R = 19.24 min, Purity = 98%, m/z = 322.00 $[M + H]^+$.

3-(4-((*tert*-Butyldimethylsilyl)oxy)phenyl)propan-1-ol (**3.32**)[2]

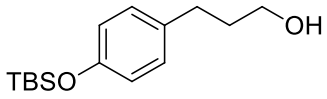

3.01g (7.73 g, 26.3 mmol, 1 eq.) was dissolved in THF (50 mL) and the reaction vessel was purged with argon. The solution was cooled to 0 ˚C before the slow addition of 2.4 M $LiAlH_4$ in THF (17.5 mL, 42 mmol, 1.6 eq.). Once complete the reaction was slowly warmed to room temperature and left to stir overnight. The reaction mixture was then concentrated *in vacuo* and the crude residue was suspended in EtOAc (100 mL). Water was added until no more solid had formed, then the precipitate was filtered through a pad of celite. The filtrate was transferred to a separating funnel and the organic phase was collected, washed with brine (100 mL), dried over $MgSO_4$, and concentrated *in vacuo*. The resultant crude oil was purified *via* flash chromatography using 0-70% EtOAc in hexane to afford the product as a clear oil (5.65 g, 21.2 mmol, 81%). ^{1}H NMR (600 MHz, $CDCl_3$) δ_{ppm} 0.18 (s, 6H), 0.97 (s, 9H), 2.66 – 2.62 (m, 2H), 1.89 – 1.82 (m, 2H), 3.66 (q, *J* = 6.3 Hz, 2H), 6.75 (d, *J* = 8.4 Hz, 2H), 7.04 (d, *J* = 8.4 Hz, 2H).[2]

3-(4-((*tert*-Butyldimethylsilyl)oxy)phenyl)propanal (**2.08**)[347]

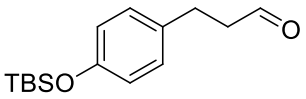

To a dry 250 mL RBF containing dichloromethane (50 mL) was added 2 M Oxalyl chloride in dichloromethane (12.72 mL, 25.44 mmol, 1.2 eq.) The stirring solution was cooled to –78 ˚C, after which DMSO (7.8 mL, 50.9 mmol, 2.4 eq.) was added dropwise. After the evolution of gas had ceased, a solution of **3.32** (5.65 g, 21.2 mmol, 1 eq.) in dichloromethane (25 mL) was added slowly and once added, the reaction was left to stir for 45 mins before the addition of Triethylamine (14.77 mL, 106 mmol, 5 eq.). The reaction mixture was left to stir at –78 ˚C to room temperature overnight. Saturated $NaHCO_3$ (100 mL) was added to quench the reaction. The reaction mixture was washed with Et_2O (250 mL), and the organic extract was washed with water (200 mL), brine (200 mL), dried over $MgSO_4$, filtered, and concentrated *in vacuo* within a fume hood. The resultant oil was purified *via* flash chromatography using 0 – 70% EtOAc in hexane to afford the product as a clear oil (4.46 g, 16.8 mmol, 80%). ^{1}H NMR (600 MHz, $CDCl_3$) δ_{ppm} 0.18 (s, 6H), 0.97 (s, 9H), 0.97 (s, 9H), 2.74 (td, *J* = 7.6, 1.5 Hz, 2H), 2.89 (t, *J* = 7.5 Hz, 2H), 6.76 (d, *J* = 8.4 Hz, 2H), 7.04 (d, *J* = 8.5 Hz, 2H), 9.81 (s, 1H).[347]

4-(2-(4-((*tert*-Butyldimethylsilyl)oxy)phenethyl)-1-(2,2-dimethoxyethyl)-1H-benzo[d]imidazol-5-yl)-3,5-dimethylisoxazole (**3.33**)[2,43]

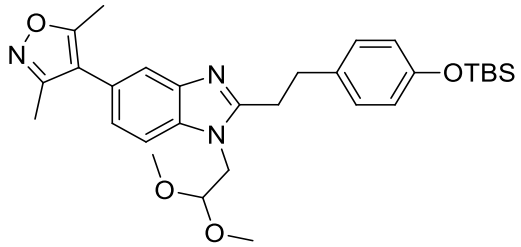

To a stirring solution of **3.31** (3.84 g, 11.95 mmol, 1 eq.) and **2.08** (3.16 g, 11.95 mmol. 1 eq.) in methanol (60 mL) was added 1M aqueous solution of $Na_2S_2O_4$ (60 mL). The resulting suspension was heated to 80 ˚C overnight. The reaction mixture was then cooled and partitioned between EtOAc (200 mL) and 10% aqueous NH_3 (60 mL). The organic phase was collected and the aqueous was extracted with EtOAc (3 × 50 mL). The organic phase was combined and washed with brine (3 × 100 mL), dried over MgSO4, filtered, and concentrated *in vacuo*. The crude product was then purified *via* flash chromatography using 0 – 100% Et_2O in hexane to afford the product as a white solid (2.73 g, 5.10 mmol, 43%). ^{1}H NMR (600 MHz, $CDCl_3$) δ_{ppm} 0.18 (s, 6H), 0.98 (s, 9H), 2.30 (s, 3H), 2.43 (s, 3H), 3.18 (s, 4H), 3.35 (s, 6H), 4.09 (d, *J* = 5.2 Hz, 2H), 4.49 (t, *J* = 5.2 Hz, 1H), 6.77 (d, *J* = 8.4 Hz, 2H), 7.09 (d, *J* = 8.4 Hz, 2H), 7.12 (dd, *J* = 8.2, 1.6 Hz, 1H), 7.38 (d, *J* = 8.2 Hz, 1H), 7.62 (s, 1H). ^{13}C NMR (151 MHz, $CDCl_3$) δ_{ppm} 11.1, 11.8, 25.8, 29.9, 33.4, 46.6, 55.7, 103.3, 109. 8, 120.0, 120.3, 123.6, 124.4, 129.5, 133.8, 134.8, 143.1, 154.3, 156.3, 159.2, 165.2. HR-MS (m/z): $[M + H]^+$ calculated for $C_{30}H_{42}N_3O_4Si$, 536.2945; found, 536.2944.[2,43]

4-(2-(1-(2,2-Dimethoxyethyl)-5-(3,5-dimethylisoxazol-4-yl)-1*H*-benzo[*d*]imidazol-2-yl)ethyl)phenol (**3.34**)[2,43]

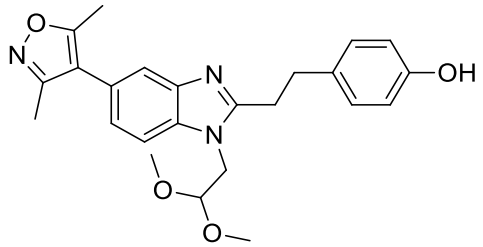

To a stirring solution of **3.31** (1.59 g, 4.95 mmol, 1 eq.) and **2.08** (1.31 g, 4.95 mmol. 1 eq.) in methanol (30 mL) was added 1M aqueous solution of $Na_2S_2O_4$ (20 mL). The resulting suspension was heated to 80 ˚C for 72 hrs. The reaction mixture was then cooled and partitioned between EtOAc (100 mL) and 10% aqueous NH_3 (50 mL). The organic phase was collected and the aqueous was extracted with EtOAc (3 × 25 mL). The organic phase was combined and washed with brine (3 × 50 mL), dried over $MgSO_4$, filtered, and concentrated *in vacuo*. The crude product was then purified *via* flash chromatography using 0 – 100% Et_2O in hexane to afford the product as a white solid (1.16 g, 2.74 mmol, 55%). ^{1}H NMR (600 MHz, d^6-DMSO) δ_{ppm} 2.20 (s, 3H), 2.37 (s, 3H), 3.00 (t, *J* = 8.0 Hz, 2H), 3.09 (t, *J* = 8.0 Hz, 2H), 3.25 (s, 6H), 4.23 (d, *J* = 5.0 Hz, 2H), 4.52 (t, *J* = 5.1 Hz, 1H), 6.65 (d, *J* = 8.4 Hz, 2H), 7.05 (d, *J* = 8.5 Hz, 2H), 7.13 (dd, *J* = 8.3, 1.6 Hz, 1H), 7.56 – 7.52 (m, 2H), 9.18 (s, 1H). ^{13}C NMR (151 MHz d^6-DMSO) δ_{ppm} 10.6, 11.4, 28.9, 32.0, 45.4, 55.0, 102.8, 110.7, 115.1, 116.7, 118.8, 122.7, 122.9, 129.3, 131.4, 134.9, 142.5, 155.6, 156.0, 158.4, 164.6. LC-MS (30-95 MeCN in 20 mins) ^{t}R = 8.74 min, Purity = 95%, m/z = 422.10 $[M + H]^+$. HR-MS (m/z): $[M + H]^+$ calculated for $C_{24}H_{28}N_3O_4$, 422.2080; found, 422.2062.[2,43]

2-(5-(3,5-Dimethylisoxazol-4-yl)-2-(4-hydroxyphenethyl)-1*H*-benzo[*d*]imidazol-1-yl)acetaldehyde (**3.35**)[380]

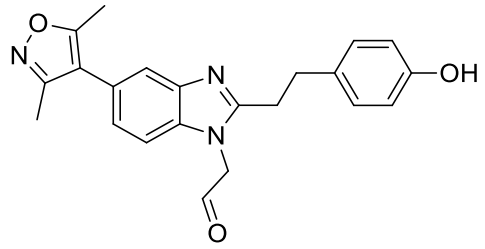

To a stirring solution of **3.33** (2.7g, 5.04 mmol, 1 eq.) in MeCN (32 mL) was added 10% aqueous HCl (32 mL), the stirring solution was heated to 85 ˚C overnight. The reaction mixture was concentrated *in vacuo*. The resultant gum was re-suspended in 9:1 dichloromethane: methanol (100 mL) and water (100 mL). The biphasic mixture was neutralised with saturated $NaHCO_3$, and the organic phase was collected. The aqueous phase was extracted with 9:1 dichloromethane: methanol (5 x 30 mL), and the organic phases were combined. The combined organic phases were then washed with brine (200 mL), dried over $MgSO_4$, filtered, and concentrated *in vacuo* to result in **3.27** as a white solid (1.88 g, 5.01 mmol, 99%). LC-MS (30-95 MeCN in 20 mins) ^tR = 7.44 min, Purity = 88% single peak, m/z = 408.1 [M + H]. HR-MS (m/z): $[M + H]^+$ calculated for $C_{22}H_{22}N_3O_3$, 376.1661; found, 408.1948.

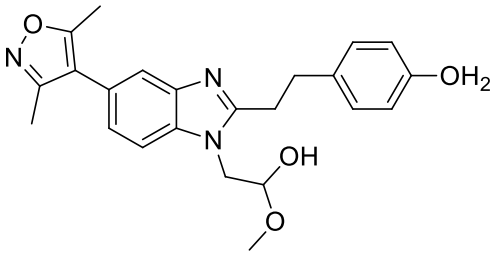

Chemical Formula: $C_{23}H_{26}N_3O_4$
Exact Mass: 408.1923

HR-MS (m/z): $[M + H]^+$ calculated for $C_{23}H_{26}N_3O_4$, 408.1923; found, 408.1948.

4-(2-(5-(3,5-Dimethylisoxazol-4-yl)-1-(2-hydroxyethyl)-1*H*-benzo[*d*]imidazol-2-yl)ethyl)phenol (**3.36**)

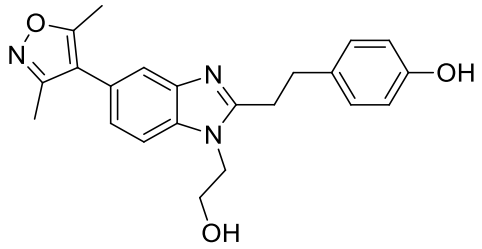

$NaBH_4$ (20 mg, 0.529 mmol, 4 eq.) was added to a stirring solution of **3.35** (50 mg, 0.133 mmol, 1 eq.) in methanol (5 mL), and left was for 30 mins. The reaction mixture was partitioned between dichloromethane (20 mL) and water (20 mL). The organic phase was collected, and the aqueous phase was extracted with dichloromethane (2 × 10 mL). The organic phases were combined and washed with brine (50 mL), dried over $MgSO_4$, filtered, and concentrated *in vacuo*. The crude product was then purified *via* flash chromatograph using 0 – 5% methanol in EtOAc to afford the product as a white solid (50 mg, 0.131 mmol, 99%). ^{1}H NMR (600 MHz, d^6-DMSO) δ_{ppm} 2.20 (s, 3H), 2.37 (s, 3H), 3.00 (t, *J* = 7.8 Hz, 2H), 3.11 (t, *J* = 7.8 Hz, 2H), 3.14 (d, *J* = 5.2 Hz, 1H), 3.66 (q, *J* = 5.4 Hz, 2H), 4.20 (t, *J* = 5.4 Hz, 2H), 4.95 (t, *J* = 5.4 Hz, 1H), 6.66 (d, *J* = 8.5 Hz, 2H), 7.07 (d, *J* = 8.5 Hz, 2H), 7.13 (dd, *J* = 8.3, 1.6 Hz, 1H), 7.56 – 7.52 (m, 2H), 9.18 (s, 1H). ^{13}C NMR (151 MHz, d^6-DMSO) δ_{ppm} 10.6, 11.3, 29.0, 32.1, 45.7, 59.7, 110.5, 115.1, 116.8, 118.8, 122.5, 122.6, 129.3, 131.4, 134.7, 142.7, 155.6, 156.0, 158.4, 164.6. LC-MS (30-95 MeCN in 20 mins) ^{t}R = 7.79 min, Purity = 91%, m/z = 378.10 $[M + H]^+$, 399.9 $[M + Na]^+$. HR-MS (m/z): $[M + H]^+$ calculated for $C_{22}H_{23}N_3O_3$, 378.1818; found, 378.1773.

6.2.2 **AlphaScreen Assays for Benzimidazole and Degrader Compounds**

AlphaScreen assays were performed by Oleg Fedorov at SGC Oxford, with minor modifications from the manufacturers protocol (PerkinElmer, USA). Briefly, all reagents were diluted in the recommended buffer (50 mM HEPES, 100 mM NaCl, 0.1% BSA; pH = 7.4) supplemented with 0.05% CHAPS and allowed to equilibrate to room temperature prior to addition to plates. Concentrations of the various proteins, peptides, solvents, and compounds are given in the relevant results sections and are expressed as the final concentrations after the addition of all assay components. 4 ml of HIS-tagged protein was added to low-volume 384-well plates (ProxiPlatet-384 Plus, PerkinElmer, USA), followed by 4 ml of either buffer, non-biotinylated peptide, solvent, or compound. Plates were sealed and incubated at room temperature for 30 min, before the addition of 4 ml biotinylated peptide, resealing and incubation for a further 30 min. 4 ml of streptavidin-coated donor beads (25 mg ml^{-1}) and 4 µl of nickel chelate acceptor beads (25 µg/ml) were then added under low light conditions. Plates were foil sealed to protect from light, incubated at room temperature for 60 min and read on a PHERAstar FS plate reader (BMG Labtech, Germany) using an AlphaScreen 680 excitation/570 emission filter set. IC_{50}s were calculated in GraphPad Prism 5 (GraphPad Software, USA). Results for compounds dissolved in DMSO were normalised against corresponding DMSO controls prior to IC_{50} determination, which are given as the final concentration of compound in the 20 µl reaction volume.

6.3 Chapter 4

6.3.1 Additional General Comments

The phenol degraders utilised Toolbox amine linkers obtained from Tocris, with catalogue numbers listed for each case. The piperazine degraders were performed at Tocris and NMR samples were ran using a Bruker 400 MHz spectrometer and LC-MS were performed on an Agilent HPLC system using an 8 minute method in water/acetonitrile with 0.1% formic acid (1.5 min at 5%, 5 – 95% over 5 min and 1.5 min at 95%) with the UV set to 254 nm.

6.3.2 Chemistry

6.3.2.1 Synthesis of Phenol Modified Degraders

General Procedure A

To a RBF equipped with a magnetic flea and was flushed with argon before the addition of **3.07** (1 eq.), Tocris toolbox amines (25 mg, 1 eq.), amide coupling reagent (1.3 eq.) and Triethylamine (3 eq.). DMF (5 mL) was added to the flask and the mixture was left to overnight at room. The reaction mixture was then partitioned between dichloromethane (25 mL) and water (50 mL), the organic layer was collected, and the aqueous layer was extracted with Dichloromethane (4 × 10 mL). The combined organic collections were washed with saturated $NaHCO_3$ (50 mL), brine (2 × 50 mL), dried over $MgSO_4$, filtered, and concentrated *in vacuo*.

4-(4-(2-(5-(3,5-dimethylisoxazol-4-yl)-1-(2-morpholinoethyl)-1*H*-benzo[*d*]imidazol-2-yl)ethyl)phenoxy)-*N*-(1-((2-(2,6-dioxopiperidin-3-yl)-1,3-dioxoisoindolin-4-yl)oxy)-2-oxo-6,9,12-trioxa-3-azatetradecan-14-yl)butanamide (**4.01**)

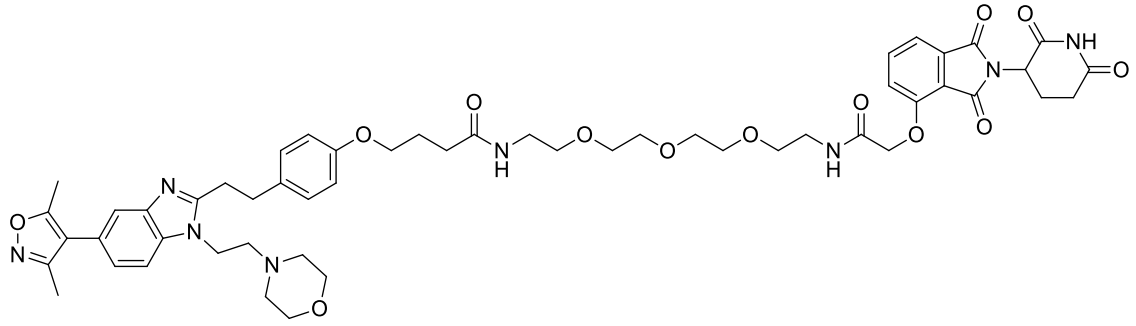

Compound **4.01** was synthesised according to General Procedure A, using thalidomide 4'-oxyacetamide-PEG3-amine (#6467) and purified *via* Flash Chromatography using 0-20% methanol (with 0.5% NH_4OH) in dichloromethane over 20 cvs to give **4.01** as a clear oil. (29.6 mg, 0.029 mmol, 60%) ^{1}H NMR (500 MHz, $CDCl_3$) δ_{ppm} 2.10 (dt, *J* = 22.7, 7.2 Hz, 6H), 2.29 (s, 4H), 2.37 (t, *J* = 7.3 Hz, 3H), 2.42 (s, 3H), 2.47 (s, 4H), 2.60 (t, *J* = 6.9 Hz, 2H), 2.65 – 2.81 (m, 3H), 2.85 (d, *J* = 15.7 Hz, 1H), 2.97 (s, 1H), 3.18 (s, 4H), 3.43 (ddq, *J* = 14.3, 9.6, 5.2, 4.8 Hz, 3H), 3.50 – 3.70 (m, 23H), 3.95 (t, *J* = 6.1 Hz, 2H), 4.13 (t, *J* = 7.0 Hz, 2H), 4.62 (s, 2H), 4.94 (t, *J* = 6.2 Hz, 1H), 6.70 (s, 1H), 6.79 (d, *J* = 8.6 Hz, 2H), 7.10 – 7.13 (m, 3H), 7.17 (s, 1H), 7.37 (s, 1H), 7.54 (s, 1H), 7.63 (s, 1H), 7.67 – 7.74 (m, 2H), 9.64 (s, 1H). ^{13}C NMR (126 MHz, $CDCl_3$) δ 11.0, 11.7, 22.9, 25.3, 29.9, 31.5, 32.8, 33.2, 39.1, 49.3, 54.1, 57.6, 66.8, 67.2, 67.9, 69.6, 70.2, 70.3, 70.3, 109.7, 114.8, 117.1, 117.4, 118.1, 119.4, 119.8, 123.7, 124.6, 129.5, 132.9, 133.7, 134.2, 137.2, 154.5, 155.5, 157.7, 159.1, 165.2, 166.0, 166.7, 166.9, 168.7, 171.8, 172.8. LCMS (5-95 MeCN in 20 mins) ^{t}R = 11.77, Purity = >99%, m/z = 511.30, 1021.35, 1043.40. HRMS (m/z): $[M + Na]^+$ calculated for $C_{53}H_{64}N_8NaO_{13}$, 1043.45; found, 1043.4453.

4-(4-(2-(5-(3,5-dimethylisoxazol-4-yl)-1-(2-morpholinoethyl)-1*H*-benzo[*d*]imidazol-2-yl)ethyl)phenoxy)-*N*-(1-((2-(2,6-dioxopiperidin-3-yl)-1,3-dioxoisoindolin-4-yl)oxy)-2-oxo-6,9,12,15-tetraoxa-3-azaheptadecan-17-yl)butanamide (**4.02**)

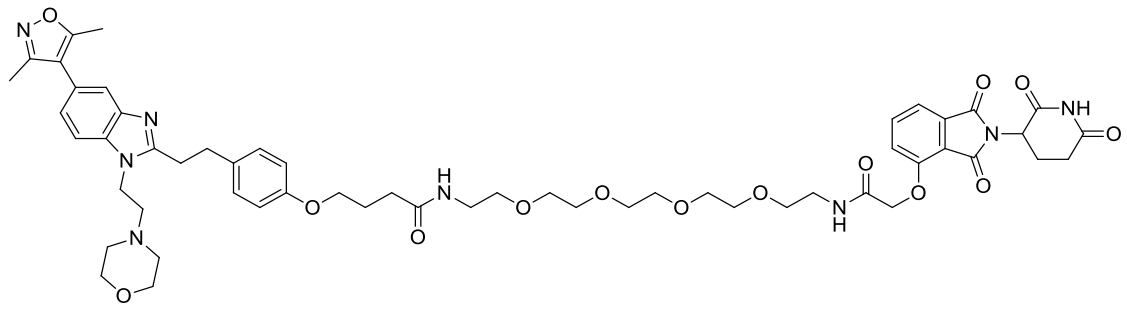

Compound **4.02** was synthesised according to General Procedure A, using thalidomide 4'-oxyacetamide-PEG4-amine (#6468), and purified *via* Flash Chromatography using 0-20% methanol (with 0.5% NH_4OH) in dichloromethane over 20 cvs to give **4.02** as a clear oil (25 mg, 0.023 mmol, 55%). ^{1}H NMR (600 MHz; $CDCl_3$) δ_{ppm} 2.01 (s, 2H), 2.03 – 2.17 (m, 5H), 2.29 (s, 3H), 2.37 (t, *J* = 7.3 Hz, 2H), 2.42 (s, 3H), 2.48 (s, 4H), 2.61 (t, *J* = 6.9 Hz, 2H), 2.68 – 2.89 (m, 4H), 3.19 (d, *J* = 4.4 Hz, 4H), 3.43 (q, *J* = 5.3 Hz, 2H), 3.52 – 3.71 (m, 27H), 3.95 (t, *J* = 6.2 Hz, 2H), 4.14 (d, *J* = 7.0 Hz, 2H), 4.62 (s, 2H), 4.93 – 4.97 (m, 1H), 6.63 (s, 1H), 6.79 (d, *J* = 8.1 Hz, 2H), 7.09 – 7.13 (m, 3H), 7.17 (s, 1H), 7.36 (d, *J* = 8.2 Hz, 1H), 7.53 (s, 1H), 7.64 (s, 1H), 7.67 (s, 1H), 7.72 (d, *J* = 15.7 Hz, 1H), 9.51 (s, 1H). ^{13}C NMR (151 MHz, $CDCl_3$) δ_{ppm} 11.0, 11.7, 22.8, 25.3, 29.9, 31.6, 32.8, 33.2, 39.2, 39.3, 49.5, 54.1, 66.8, 67.3, 68.0, 69.6, 70.1, 70.4, 70.4, 70.5, 70.6, 109.7, 114.9, 117.2, 117.4, 118.2, 119.5, 129.5, 132.9, 133.8, 137.1, 154.6, 155.5, 157.7, 159.1, 165.2, 166.0, 167.0, 168.6, 171.6, 172.8.LCMS (5-95 MeCN in 20 mins) ^{t}R = 11.92, Purity = 95%, m/z = 533.40, 1065.30, 1087.35. HRMS (m/z): $[M + Na]^+$ calculated for $C_{55}H_{68}N_8NaO_{14}$, 1087.47; found, 1087.4664.

(2S,4R)-1-((S)-2-(tert-butyl)-19-(4-(2-(5-(3,5-Dimethylisoxazol-4-yl)-1-(2-morpholinoethyl)-1*H*-benzo[*d*]imidazol-2-yl)ethyl)phenoxy)-4,16-dioxo-6,9,12-trioxa-3,15-diazanonadecan-1-oyl)-4-hydroxy-*N*-(4-(4-methylthiazol-5-yl)benzyl)pyrrolidine-2-carboxamide (**4.03**)

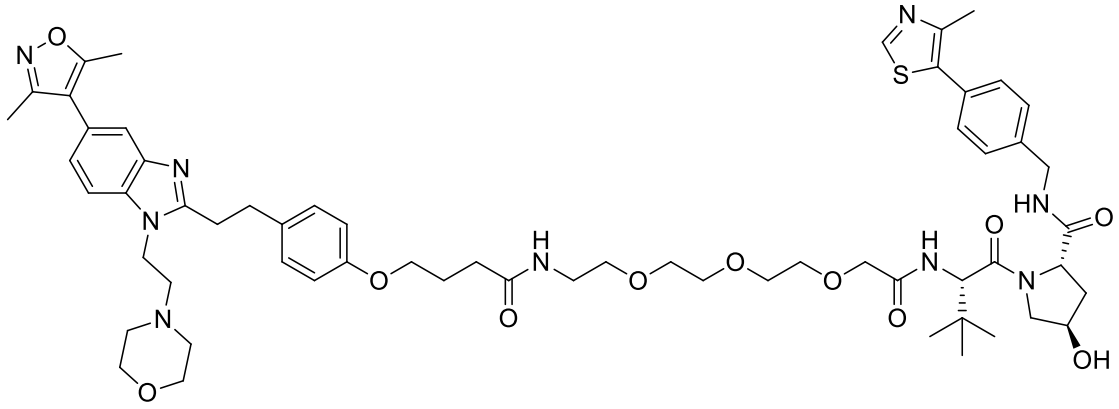

Compound **4.03** was synthesised according to General Procedure A, using VH 032 amide-PEG3-amine (#6463) and purified *via* Flash Chromatography using 0-20% methanol (with 0.5% NH_4OH) in dichloromethane over 20 cvs to give **23** as a clear oil (34 mg, 0.030 mmol, 75%). ^{1}H NMR (600 MHz; $CDCl_3$) δ_{ppm} 0.95 (s, 9H), 1.19 (t, *J* = 7.1 Hz, 2H), 2.09 (dp, *J* = 27.2, 7.7, 6.9 Hz, 3H), 2.28 (s, 4H), 2.35 (t, *J* = 7.4 Hz, 2H), 2.41 (s, 3H), 2.44 (s, 5H), 2.49 (s, 3H), 2.59 (t, *J* = 6.9 Hz, 2H), 3.13 – 3.21 (m, 4H), 3.39 (s, 2H), 3.44 – 3.50 (m, 3H), 3.57 (d, *J* = 9.4 Hz, 4H), 3.64 (d, *J* = 6.7 Hz, 9H), 3.95 (t, *J* = 6.0 Hz, 2H), 3.97 – 4.05 (m, 3H), 4.11 (t, *J* = 7.0 Hz, 2H), 4.31 – 4.36 (m, 1H), 4.51 – 4.58 (m, 3H), 4.67 (t, *J* = 7.9 Hz, 1H), 6.55 (d, *J* = 5.7 Hz, 1H), 6.80 (d, *J* = 8.0 Hz, 2H), 7.09 – 7.13 (m, 3H), 7.29 (d, *J* = 9.0 Hz, 1H), 7.34 (s, 5H), 7.44 (d, *J* = 6.0 Hz, 1H), 7.60 (s, 1H), 8.65 (s, 1H). ^{13}C NMR (151 MHz, $CDCl_3$) δ_{ppm} 11.0, 11.7, 15.4, 16.1, 25.3, 26.5, 30.0, 32.8, 33.1, 35.5, 36.5, 39.4, 41.6, 43.3, 54.1, 56.9, 57.0, 57.7, 58.8, 65.9, 66.9, 67.2, 70.0, 70.1, 70.5, 70.6, 70.9, 109.6, 114.8, 117.2, 120.0, 123.5, 124.3, 128.2, 129.4, 129.6, 131.0, 131.7, 133.1, 134.4, 138.3, 143.1, 148.5, 150.4, 155.5, 157.6, 159.1, 165.1, 170.3, 171.1, 172.8. LCMS (5-95 MeCN in 20 mins) ^{t}R = 7.18, Purity = 95%, m/z = 568.05, 817.35, 1134.50. HRMS (m/z): $[M + Na]^+$ calculated for $C_{60}H_{79}N_9NaO_{11}$, 1156.55; found, 1156.5388.

(2S,4R)-1-((S)-2-(tert-butyl)-22-(4-(2-(5-(3,5-Dimethylisoxazol-4-yl)-1-(2-morpholinoethyl)-1*H*-benzo[*d*]imidazol-2-yl)ethyl)phenoxy)-4,19-dioxo-6,9,12,15-tetraoxa-3,18-diazadocosan-1-oyl)-4-hydroxy-*N*-(4-(4-methylthiazol-5-yl)benzyl)pyrrolidine-2-carboxamide (**4.04**)

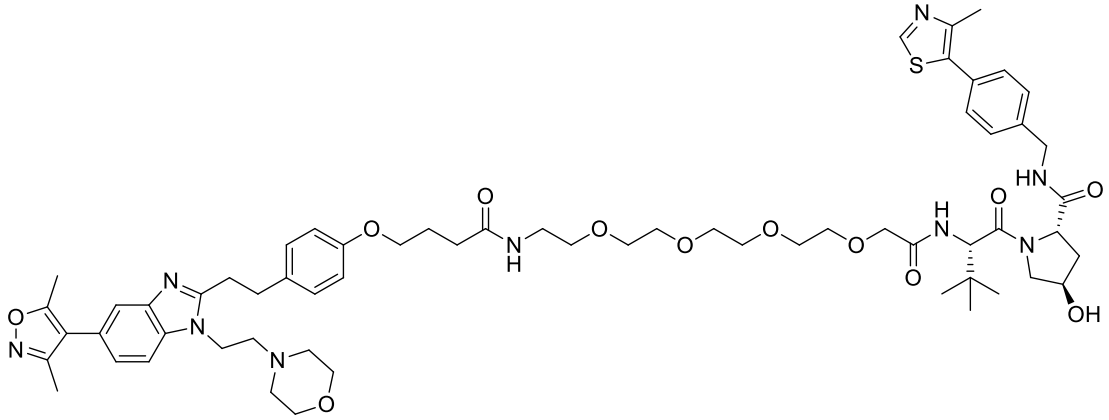

Compound **4.04** was synthesised according to General Procedure A, using VH 032 amide-PEG4-amine (#6464) and purified *via* Flash Chromatography using 0-20% methanol (with 0.5% NH_4OH) in dichloromethane over 20 cvs to give **4.04** as a clear oil (28 mg, 0.024 mmol, 65%). ^{1}H NMR (600 MHz; $CDCl_3$) δ_{ppm} 0.94 (s, 9H), 2.28 (s, 3H), 2.36 (t, *J* = 7.4 Hz, 2H), 2.41 (s, 3H), 2.44 (s, 5H), 2.49 (s, 3H), 2.59 (t, *J* = 6.9 Hz, 2H), 3.15 (d, *J* = 8.3 Hz, 2H), 3.19 (d, *J* = 8.3 Hz, 2H), 3.41 (t, *J* = 5.3 Hz, 2H), 3.51 (t, *J* = 5.1 Hz, 2H), 3.56 (s, 4H), 3.63 (d, *J* = 20.6 Hz, 14H), 3.93 – 3.97 (m, 3H), 3.98 – 4.03 (m, 2H), 4.12 (d, *J* = 6.9 Hz, 2H), 4.34 (dd, *J* = 15.0, 5.4 Hz, 1H), 4.50 – 4.55 (m, 3H), 4.70 (t, *J* = 7.9 Hz, 1H), 6.50 (d, *J* = 5.4 Hz, 1H), 6.80 (d, *J* = 8.2 Hz, 2H), 7.09 – 7.13 (m, 3H), 7.26 (s, 2H), 7.34 (d, *J* = 4.5 Hz, 5H), 7.39 (t, *J* = 6.1 Hz, 1H), 7.60 (s, 1H), 8.65 (s, 1H). ^{13}C NMR (600 MHz, $CDCl_3$) δ_{ppm} 11.0, 11.7, 16.1, 25.3, 26.5, 30.0, 32.8, 33.1, 35.4, 36.3, 39.3, 41.6, 43.3, 54.1, 56.9, 57.1, 57.7, 58.7, 66.9, 67.2, 70.0, 70.1, 70.2, 70.5, 70.6, 70.6, 71.0, 109.6, 114.8, 117.2, 120.0, 123.5, 124.3, 128.2, 129.4, 129.6, 131.0, 131.7, 133.1, 134.4, 138.3, 143.1, 148.5, 150.4, 155.5, 157.6, 159.1, 165.1, 170.2, 171.1, 171.3, 172.7. LCMS (5-95 MeCN in 20 mins) ^{t}R = 7.16, A% = 96, m/z = 590.00, 861.35, 1178.55. HRMS (m/z): $[M + Na]^+$ calculated for $C_{62}H_{83}N_9NaO_{12}S^+$, 1200.58; found, 1200.5796.

6.3.2.2 Synthesis of E3-ligands and Linkers

4-Hydroxythalidomide (**4.07**)

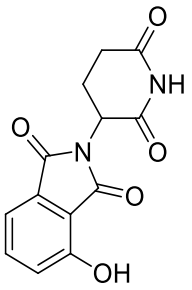

A suspension of 3-hydroxyphthalic anhydride (25 g, 152 mmol, 1 eq.) and 3-aminopiperidine-2,6-dione hydrochloride (25 g, 152 mmol, 1 eq.) in AcOH (300 mL) was treated with sodium acetate (27.5 g, 335 mmol, 2.2 eq.) and the resulting mixture was heated to 120 °C and left to stir overnight. The reaction mixture was then cooled and concentrated *in vacuo*, followed by azeotroping with heptane (5 × 200 mL). The crude solid was suspended in water and triturated for 1 hour before filtering and washing with water. The solid was then triturated in Methanol (300 mL), cooled in ice, filtered, and washed with methanol to result in the product as a beige solid (39.90 g, 145 mmol, 96%). ^{1}H NMR (600 MHz, d^{6}-DMSO) δ_{ppm} 2.02 (dtd, *J* = 13.0, 5.4, 2.3 Hz, 1H), 2.62 – 2.48 (m, 3H), 2.88 (ddd, *J* = 17.0, 13.9, 5.4 Hz, 1H), 5.07 (dd, *J* = 12.9, 5.5 Hz, 1H), 7.26 (d, *J* = 8.3 Hz, 1H), 7.32 (d, *J* = 7.1 Hz, 1H), 7.67 – 7.63 (m, 1H), 11.08 (s, 1H), 11.18 (s, 1H). ^{13}C NMR (151 MHz d^{6}-DMSO) δ_{ppm} 22.0, 31.0, 48.6, 114.3, 114.4, 123.6, 133.1, 136.4, 155.5, 165.8, 167.0, 170.0, 172.8. LC-MS (5-95 MeCN in 20 mins) ^{t}R = 13.12 min, m/z = 273 (-ve). HR-MS (m/z): $[M + Na]^{+}$ calculated for $C_{13}H_{10}N_2O_5Na$, 297.0487; found, 297.0482.

2-((2-(2,6-Dioxopiperidin-3-yl)-1,3-dioxoisoindolin-4-yl)oxy)acetic acid (**4.09**)

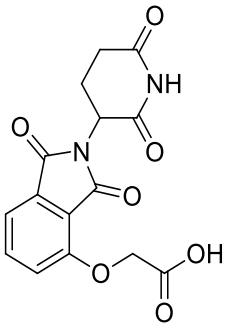

4-hydroxythalidomide (25 g, 91.2 mmol, 1 eq.) and potassium carbonate (18.91 g, 137 mmol, 1.5 eq.) were stirred in DMF (200 mL) before the slow addition of *tert*-butlbromoacetate (17.8 g, 91.2 mmol, 1 eq.), and the reaction mixture was left to stir overnight at room temperature. The reaction was then poured into water (1.2 L) and extracted with EtOAc (3 × 200 mL). The combined extracts were then washed with $NaHCO_3$ (400 mL), brine (3 × 300 mL),

dried over MgSO4 and concentrated *in vacuo*. The resulting solid was recrystallized from EtOH to give the product, which was carried forward without any further characterisation.

To a round bottom flask charged with the product was added TFA (250 mL) and stirred at room temperature for 1 hour. The reaction mixture was then concentrated before re-concentrating from MeCN (3 × 300 mL). The resultant solid was then heated to reflux in MeCN:THF for 1 hour before allowing to cool and stir at room temperature for 72 hours. The resultant solid was collected by filtration and washed with MeCN to result in the product as a white solid (26.0 g, 78.2 mmol, 86%). ^{1}H NMR (600 MHz, d^{6}-DMSO) δ_{ppm} 2.04 (dt, *J* = 12.9, 2.8 Hz, 1H), 2.62 – 2.48 (m, 4H), 2.93 – 2.85 (m, 1H), 4.99 (s, 2H), 5.10 (dd, *J* = 12.9, 5.4 Hz, 1H), 7.39 (d, *J* = 8.6 Hz, 1H), 7.48 (d, *J* = 7.3 Hz, 1H), 7.79 (dd, *J* = 8.5, 7.3 Hz, 1H), 11.10 (s, 1H), 13.23 (s, 1H). ^{13}C NMR (151 MHz d^{6}-DMSO) δ_{ppm} 21.96, 30.94, 48.78, 64.99, 115.76, 116.32, 119.87, 133.25, 136.75, 155.12, 165.16, 166.73, 169.48, 169.90, 172.77. LC-MS (5-95 MeCN in 20 mins) ^{t}R = 14.68, m/z = 333. HR-MS (m/z): $[M + H]^{+}$ calculated for $C_{15}H_{13}N_2O_7$, 333.0723; found, 333.0717.

General Procedure B

Thalidomide 4'-oxyacetic acid (1.5 g, 4.51 mmol, 1 eq.) and HATU (1.89 g, 4.96 mmol, 1.1 eq.) were dissolved in DMF (20 mL). *N*-Boc-diamine (1.1 eq.), and DIPEA (2.46 mL, 13.53 mmol, 3 eq.) were then added sequentially to the stirring mixture. The reaction was left to stir at room temperature overnight. Upon depletion of the starting material, the reaction mixture was diluted with water (200 mL) and extracted with EtOAc (3 × 100 mL). Organic collections were combined and washed with saturated $NaHCO_3$ (200 mL), brine (3 × 150 mL), dried over $MgSO_4$, filtered, and concentrated *in vacuo* before purification.

General Procedure C

Boc-protected linker intermediates (1 eq.) were dissolved in anhydrous dioxane (12 mL) before the slow addition of 4 M HCl in dioxane (10 eq.), the reaction was then left to stir at room temperature overnight. The reaction mixture was then filtered under an inert atmosphere and washed with dioxane (2 × 5 mL), followed by Et_2O (3 × 5 mL) to afford the linkers as the HCl salt.

tert-Butyl (2-(2-((2-(2,6-Dioxopiperidin-3-yl)-1,3-dioxoisoindolin-4-yl)oxy)acetamido)ethyl)carbamate (**4.10**)

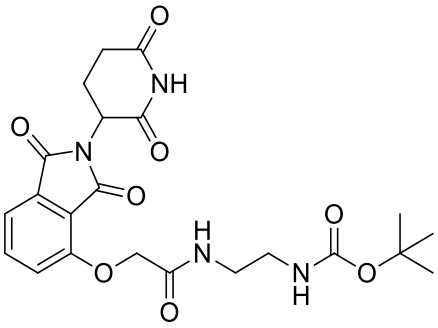

Compound **4.10** was synthesised according to general procedure B. The crude mixture was purified by Flash Chromatography using 0-5% methanol in dichloromethane to afford the product as a white foam (800 mg, 1.68 mmol, 37%). ^{1}H NMR (600 MHz, d^{6}-DMSO) δ_{ppm} 1.36 (s, 9H), 2.01 – 2.07 (m, 1H), 2.51 – 2.62 (m, 2H), 2.90 (ddd, *J* = 17.0, 13.9, 5.5 Hz, 1H), 3.01 (q, *J* = 6.3 Hz, 2H), 3.17 (q, *J* = 6.4 Hz, 2H), 4.76 (s, 2H), 5.12 (dd, *J* = 12.9, 5.5 Hz, 1H), 6.84 (t, *J* = 5.8 Hz, 1H), 7.39 (d, *J* = 8.6 Hz, 1H), 7.50 (d, *J* = 7.2 Hz, 1H), 7.81 (dd, *J* = 8.5, 7.3 Hz, 1H), 8.03 (t, *J* = 5.9 Hz, 1H), 11.10 (s, 1H).

tert-Butyl (4-(2-((2-(2,6-dioxopiperidin-3-yl)-1,3-dioxoisoindolin-4-yl)oxy)acetamido)butyl)carbamate (**4.11**)

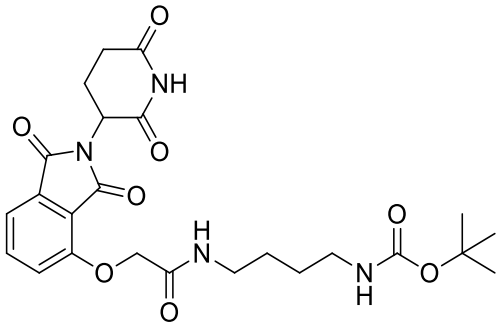

Compound **4.11** was synthesised according to general procedure B. The crude mixture was purified by Flash Chromatography using 0-5% methanol in dichloromethane to afford the product as a white foam (1.32 g, 2.62 mmol, 58%). ^{1}H NMR (600 MHz, d^{6}-DMSO) δ_{ppm} 1.34 (s, 12H), 2.02 (ddd, *J* = 12.8, 5.3, 2.2 Hz, 1H), 2.48 – 2.58 (m, 2H), 2.87 (tt, *J* = 11.3, 5.6 Hz, 4H), 3.11 (q, *J* = 6.4 Hz, 2H), 4.74 (s, 2H), 5.09 (dd, *J* = 12.9, 5.4 Hz, 1H), 6.74 (t, *J* = 5.4 Hz, 1H), 7.36 (d, *J* = 8.5 Hz, 1H), 7.47 (d, *J* = 7.2 Hz, 1H), 7.79 (dd, *J* = 8.5, 7.3 Hz, 1H), 7.92 (t, *J* = 5.8 Hz, 1H), 11.07 (s, 1H).

tert-Butyl (6-(2-((2-(2,6-dioxopiperidin-3-yl)-1,3-dioxoisoindolin-4-yl)oxy)acetamido)hexyl)carbamate (**4.12**)

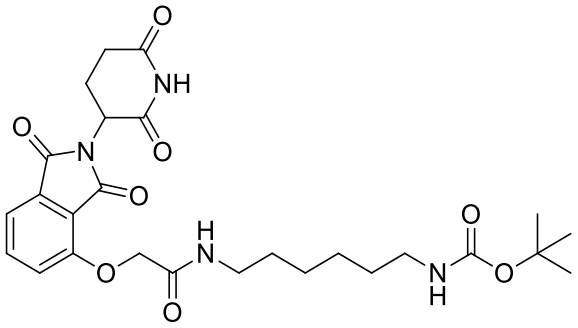

Compound **4.12** was synthesised according to general procedure B. The crude mixture was purified by Flash Chromatography using 0-5% methanol in dichloromethane to afford the product as a white foam (1.62 g, 3.06 mmol, 68%). ^{1}H NMR (600 MHz, d^{6}-DMSO) δ_{ppm} 1.27 (s, 2H), 1.39 (s, 12H), 1.45 (t, *J* = 7.1 Hz, 2H), 2.04 – 2.09 (m, 1H), 2.54 – 2.65 (m, 2H), 2.91 (d, *J* = 6.4 Hz, 4H), 3.16 (q, *J* = 6.6 Hz, 2H), 4.79 (s, 2H), 5.14 (dd, *J* = 12.9, 5.4 Hz, 1H), 6.73 – 6.77 (m, 1H), 7.42 (d, *J* = 8.5 Hz, 1H), 7.52 (d, *J* = 7.2 Hz, 1H), 7.84 (dd, *J* = 8.5, 7.3 Hz, 1H), 7.94 (t, *J* = 5.8 Hz, 1H), 11.12 (s, 1H).

tert-Butyl (8-(2-((2-(2,6-dioxopiperidin-3-yl)-1,3-dioxoisoindolin-4-yl)oxy)acetamido)octyl)carbamate (**4.13**)

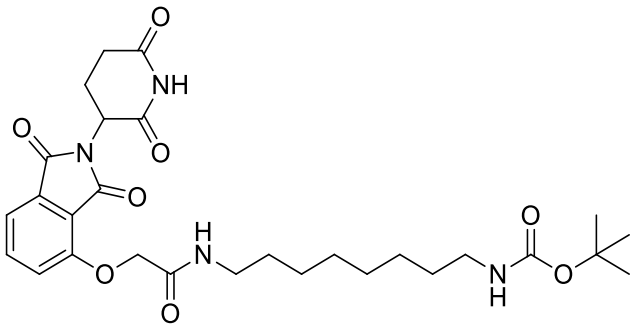

Compound **4.13** was synthesised according to general procedure B. The crude mixture was purified by Flash Chromatography using 0-5% methanol in dichloromethane to afford the product as a white foam (1.67 g, 2.98 mmol, 66%). ^{1}H NMR (600 MHz, d^{6}-DMSO) δ_{ppm} 1.23 (d, *J* = 9.3 Hz, 8H), 1.34 (d, *J* = 6.8 Hz, 14H), 1.42 (t, *J* = 6.9 Hz, 2H), 2.01 – 2.06 (m, 1H), 2.51 – 2.62 (m, 2H), 2.88 (q, *J* = 6.4, 5.6 Hz, 4H), 3.13 (q, *J* = 7.0, 6.2 Hz, 2H), 4.76 (s, 2H), 5.12 (dd, *J* = 12.9, 5.5 Hz, 1H), 6.73 (t, *J* = 5.9 Hz, 1H), 7.39 (d, *J* = 8.5 Hz, 1H), 7.50 (d, *J* = 7.3 Hz, 1H), 7.81 (dd, *J* = 8.5, 7.3 Hz, 1H), 7.91 (t, *J* = 5.8 Hz, 1H), 11.10 (s, 1H).

N-(2-Aminoethyl)-2-((2-(2,6-dioxopiperidin-3-yl)-1,3-dioxoisoindolin-4-yl)oxy)acetamide hydrochloride (**4.14**)

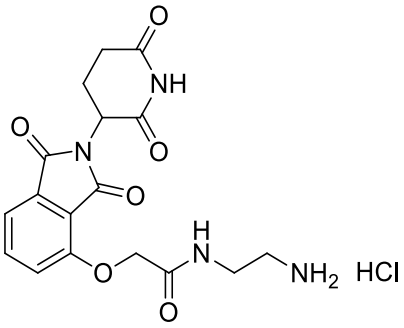

Compound **4.14** was synthesised according to general procedure C to afford the product as a beige solid (530 mg, 1.69 mmol, 76%). ^{1}H NMR (600 MHz, d^{6}-DMSO) δ_{ppm} 2.01 – 2.06 (m, 1H), 2.51 – 2.63 (m, 2H), 2.85 – 2.91 (m, 3H), 3.40 (q, *J* = 6.1 Hz, 2H), 4.83 (s, 2H), 5.12 (dd, *J* = 12.9, 5.4 Hz, 1H), 7.45 (s, 1H), 7.50 (d, *J* = 7.2 Hz, 1H), 7.81 (dd, *J* = 8.5, 7.3 Hz, 1H), 8.04 (s, 3H), 8.30 (t, *J* = 5.8 Hz, 1H), 11.11 (s, 1H). LC-MS (30-95 MeCN in 20 mins) ^{t}R = 9.27, Purity = 98%, m/z = 375.10 $[M + H]^{+}$.

N-(4-Aminobutyl)-2-((2-(2,6-dioxopiperidin-3-yl)-1,3-dioxoisoindolin-4-yl)oxy)acetamide hydrochloride (**4.15**)

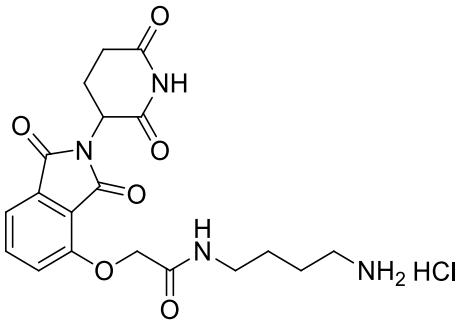

Compound **4.15** was synthesised according to general procedure C to afford the product as a beige solid (958 mg, 2.18 mmol, 93%). ^{1}H NMR (600 MHz, d^{6}-DMSO) δ_{ppm} 1.47 – 1.61 (m, 5H), 2.01 – 2.06 (m, 1H), 2.51 – 2.63 (m, 2H), 2.77 (t, *J* = 6.4 Hz, 2H), 2.90 (dd, *J* = 7.2, 4.9 Hz, 2H), 3.16 (q, *J* = 6.5 Hz, 2H), 4.79 (s, 2H), 5.12 (dd, *J* = 12.9, 5.4 Hz, 1H), 7.41 (d, *J* = 8.5 Hz, 1H), 7.50 (d, *J* = 7.2 Hz, 1H), 7.83 (dd, *J* = 8.5, 7.3 Hz, 1H), 7.97 (s, 3H), 8.11 (t, *J* = 5.9 Hz, 1H), 11.12 (s, 1H). LCMS (5-95 Ana in 20 mins) ^{t}R = 10.24, Purity = >99%, m/z = 403.15 $[M + H]^{+}$.

N-(6-Aminohexyl)-2-((2-(2,6-dioxopiperidin-3-yl)-1,3-dioxoisoindolin-4-yl)oxy)acetamide hydrochloride (**4.16**)

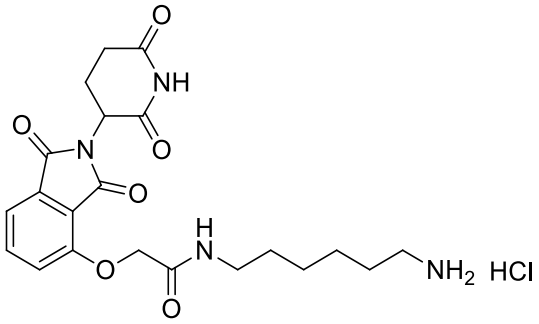

Compound **4.16** was synthesised according to general procedure C to afford the product as a white solid (993 mg, 2.13 mmol, 75%). ^{1}H NMR (600 MHz, d^{6}-DMSO) δ_{ppm} 1.25 – 1.32 (m, 4H), 1.44 (p, *J* = 7.1 Hz, 2H), 1.53 (p, *J* = 7.4 Hz, 2H), 2.02 – 2.07 (m, 1H), 2.51 – 2.63 (m, 2H), 2.74 (t, *J* = 7.5 Hz, 2H), 2.90 (ddd, *J* = 17.1, 13.9, 5.5 Hz, 1H), 3.14 (q, *J* = 6.6 Hz, 2H), 4.78 (s, 2H), 5.12 (dd, *J* = 12.9, 5.4 Hz, 1H), 7.40 (d, *J* = 8.5 Hz, 1H), 7.50 (d, *J* = 7.2 Hz, 1H), 7.82 (dd, *J* = 8.5, 7.2 Hz, 1H), 7.92 (s, 2H), 8.02 (t, *J* = 5.8 Hz, 1H), 11.12 (s, 1H). LCMS (5-95 Ana in 20 mins) ^{t}R = 10.24, Purity = 86%, m/z = 431.20 $[M + H]^{+}$.

N-(9-Aminononyl)-2-((2-(2,6-dioxopiperidin-3-yl)-1,3-dioxoisoindolin-4-yl)oxy)acetamide hydrochloride (**4.17**)

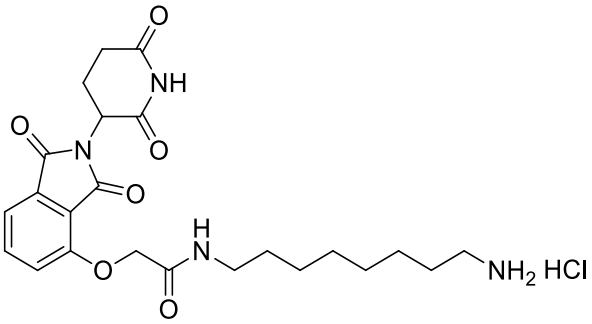

Compound **4.17** was synthesised according to general procedure C to afford the product as a white solid (1.04 g, 2.09 mmol, 70%). ^{1}H NMR (600 MHz, d^{6}-DMSO) δ_{ppm} 1.23 (s, 10H), 1.40 (t, *J* = 6.9 Hz, 2H), 1.51 (p, *J* = 7.5 Hz, 2H), 1.99 – 2.04 (m, 1H), 2.49 – 2.60 (m, 2H), 2.67 – 2.73 (m, 2H), 2.87 (ddd, *J* = 17.1, 13.9, 5.4 Hz, 1H), 3.11 (q, *J* = 7.0 Hz, 2H), 4.75 (s, 2H), 5.09 (dd, *J* = 12.9, 5.4 Hz, 1H), 7.37 (d, *J* = 8.5 Hz, 1H), 7.47 (d, *J* = 7.2 Hz, 1H), 7.78 (dd, *J* = 8.5, 7.3 Hz, 1H), 7.93 (s, 3H), 7.98 (t, *J* = 5.8 Hz, 1H), 11.09 (s, 1H). LCMS (5-95 Ana in 20 mins) ^{t}R = 11.42, Purity = 87%, m/z = 459.25 $[M + H]^{+}$.

General Procedure D

N-boc-alcoholamines (1 eq.) were dissolved in Dichloromethane (100 mL) before the addition of CBr_4 (1.1 eq.). The reaction mixture was then cooled to 0 ˚C and triphenylphosphine (1.1 eq.) was added in portions. The reaction was then left to warm to room temperature and was stirred overnight.

tert-Butyl (2-bromoethyl)carbamate (**4.18**)

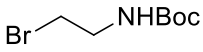

4.18 was synthesised according to general procedure D. Reaction mixture was concentrated and purified *via* flash chromatography (0 – 40% EtOAc in hexane) to afford the product as a clear oil (1.94 g, 8.65 mmol, 70%). ^{1}H NMR (600 MHz, $CDCl_3$) δ_{ppm} 1.45 (s, 9H), 3.45 (t, *J* = 5.9 Hz, 2H), 3.53 (t, *J* = 6.0 Hz, 2H), 4.95 (s, 1H).

tert-Butyl (4-bromobutyl)carbamate (**4.19**)

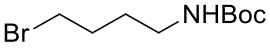

4.19 was synthesised according to general procedure D. Reaction mixture was concentrated and purified *via* flash chromatography (0 – 40% EtOAc in hexane) to afford the product as a clear oil (2.06 g, 8.16 mmol, 77%). ^{1}H NMR (600 MHz, $CDCl_3$) δ_{ppm} 1.44 (s, 9H), 1.64 (q, *J* = 7.3 Hz, 2H), 1.86 – 1.91 (m, 2H), 3.15 (q, *J* = 6.9 Hz, 2H), 3.42 (t, *J* = 6.7 Hz, 2H).

tert-Butyl (6-bromohexyl)carbamate (**4.20**)

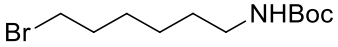

4.20 was synthesised according to general procedure D. Reaction mixture was concentrated and purified *via* flash chromatography (0 – 40% EtOAc in hexane) to afford the products as a clear oil (2.15 g, 7.67 mmol, 92%). ^{1}H NMR (600 MHz, $CDCl_3$) δ_{ppm} 1.34 (q, *J* = 8.9, 8.2 Hz, 2H), 1.44 (s, 13H), 1.83 – 1.89 (m, 2H), 3.09 – 3.14 (m, 2H), 3.40 (t, *J* = 6.8 Hz, 2H).

tert-Butyl (8-bromooctyl)carbamate (**4.21**)

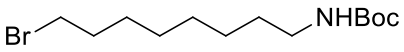

4.21 was synthesised according to general procedure D. Reaction mixture was concentrated and purified *via* flash chromatography (0 – 40% EtOAc in hexane) to afford the products as a clear oil (2.19 g, 7.10 mmol, 89%). ^{1}H NMR (600 MHz, $CDCl_3$) δ_{ppm} 1.31 (s, 6H), 1.44 (s, 13H), 1.84 (p, *J* = 7.0 Hz, 2H), 3.10 (q, *J* = 6.9 Hz, 2H), 3.40 (t, *J* = 6.8 Hz, 2H).

tert-Butyl (2-((2-(2,6-dioxopiperidin-3-yl)-1,3-dioxoisoindolin-4-yl)oxy)ethyl)carbamate (**4.22**)

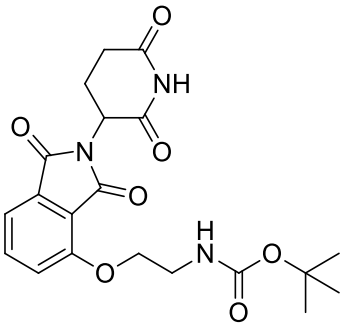

A solution of **4.07** (2.4 g, 8.65 mmol, 1 eq.) and *tert*-butyl-(2-bromoethyl)carbamate (1.94 g, 8.65 mmol, 1 eq.) in DMF (50 mL) was treated with potassium bicarbonate (1.43 g, 12.98 mmol, 1.5 eq.) and potassium iodide (0.143 g, 0.865 mmol, 0.1 eq.) sequentially. The reaction was then left to stir for 4 days at room temperature. Upon completion, the reaction mixture was poured into water (300 mL) and extracted with EtOAc (3 × 75 mL), the organic collections were then combined and washed with 1 M K_2CO_3 (200 mL), brine (3 × 100 mL), dried over $MgSO_4$ and concentrated *in vacuo*. The crude mixture was then purified *via* column chromatography (1% - 2% - 3% 7N NH_3 methanol in dichloromethane) to result in the product as a white foam (632.7 mg, 1.514 mmol, 17%). ^{1}H NMR (400 MHz, $CDCl_3$) δ_{ppm} 1.45 (s, 9H), 2.10 – 2.17 (m, 1H), 2.69 – 2.96 (m, 4H), 3.61 (q, *J* = 5.5 Hz, 2H), 4.24 (t, *J* = 5.1 Hz, 2H), 4.96 (dd, *J* = 12.3, 5.3 Hz, 1H), 5.18 (s, 1H), 7.24 (d, *J* = 8.4 Hz, 1H), 7.49 (d, *J* = 6.7 Hz, 1H), 7.69 (dd, *J* = 8.5, 7.3 Hz, 1H), 7.96 (s, 1H). LCMS (5-95 MeCN in 5 mins) ^{t}R = 4.17 min, Purity = 95%, m/z = 440 $[M + Na]^{+}$.

tert-Butyl (4-((2-(2,6-dioxopiperidin-3-yl)-1,3-dioxoisoindolin-4-yl)oxy)butyl)carbamate (**4.23**)

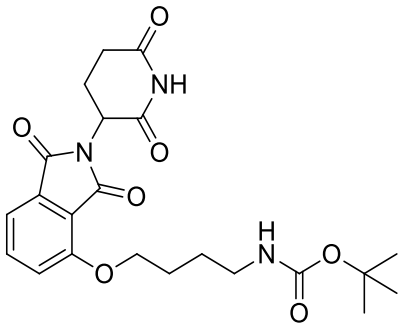

A solution of **4.07** (2.24 g, 8.17 mmol, 1 eq.) *tert*-butyl-(4-bromobutyl)carbamate (2.24 g, 8.17 mmol, 1 eq.) in DMF (50 mL) was treated with potassium bicarbonate (1.35 g, 12.26 mmol, 1.5 eq.) and potassium iodide (0.136 g, 0.817 mmol, 0.1 eq.) sequentially. The reaction was then left to stir for 4 days at room temperature. Upon completion, the reaction mixture was poured into water (300 mL) and extracted with EtOAc (3 × 75 mL), the organic collections were then combined and washed with 1 M K_2CO_3 (200 mL), brine (3 × 100 mL), dried over $MgSO_4$ and concentrated *in vacuo*. The crude mixture was then purified *via* column chromatography (0.5% - 1% - 1.5% 7N NH_3 methanol in dichloromethane) to result in the product as a white foam (859 mg, 1.92 mmol, 24%). ^{1}H NMR (400 MHz, $CDCl_3$) δ_{ppm} 1.44 (s, 9H), 1.74 (p, *J* = 7.0 Hz, 2H), 1.89 – 1.97 (m, 2H), 2.10 – 2.17 (m, 1H), 2.67 – 2.93 (m, 4H), 3.22 (q, *J* = 6.7 Hz, 2H), 4.20 (t, *J* = 6.1 Hz, 2H), 4.85 (s, 1H), 4.95 (dd, *J* = 12.3, 5.3 Hz, 1H), 7.21 (d, *J* = 8.5 Hz, 1H), 7.46 (d, *J* = 7.2 Hz, 1H), 7.68 (dd, *J* = 8.5, 7.3 Hz, 1H), 7.94 (s, 1H).LCMS (5-95 MeCN in 5 mins) ^{t}R = 4.505 min, Purity = 95%, m/z = 468 $[M + Na]^+$.

tert-Butyl (6-((2-(2,6-dioxopiperidin-3-yl)-1,3-dioxoisoindolin-4-yl)oxy)hexyl)carbamate (**4.24**)

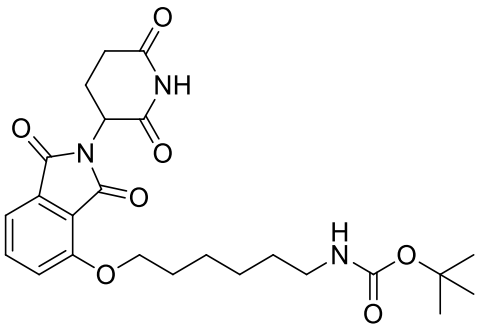

A solution of **4.07** (2.10 g, 7.66 mmol, 1 eq.) *tert-butyl*-(6-bromohexyl)carbamate (2.15 g, 7.66 mmol, 1 eq.) in DMF (50 mL) was treated with potassium bicarbonate (1.27 g, 11.50 mmol, 1.5 eq.) and potassium iodide (0.127 g, 0.766 mmol, 0.1 eq.) sequentially. The reaction was then left to stir for 4 days at room temperature. Upon completion, the reaction mixture was poured into water (300 mL) and extracted with EtOAc (3 × 75 mL), the organic

collections were then combined and washed with 1 M K_2CO_3 (200 mL), brine (3 × 100 mL), dried over $MgSO_4$ and concentrated *in vacuo*. The crude mixture was then purified *via* column chromatography (0.5% - 1% - 1.5% 7N NH_3 methanol in dichloromethane) to result in the product as a white foam (1.022 g, 2.16 mmol, 46%). ^{1}H NMR (400 MHz, $CDCl_3$) δ_{ppm} 1.44 (s, 11H), 1.53 (h, *J* = 7.3 Hz, 5H), 1.84 – 1.92 (m, 2H), 2.09 – 2.16 (m, 1H), 2.66 – 2.95 (m, 4H), 3.12 (d, *J* = 6.5 Hz, 2H), 4.17 (t, *J* = 6.4 Hz, 2H), 4.54 (s, 1H), 4.95 (dd, *J* = 12.2, 5.3 Hz, 1H), 7.21 (d, *J* = 8.4 Hz, 1H), 7.45 (d, *J* = 7.3 Hz, 1H), 7.67 (dd, *J* = 8.5, 7.3 Hz, 1H), 8.00 (s, 1H). LCMS (5-95 MeCN in 5 mins) ^{t}R = 4.91 min, Purity = 97%, m/z = 496 $[M + Na]^+$.

tert-Butyl (8-((2-(2,6-dioxopiperidin-3-yl)-1,3-dioxoisoindolin-4-yl)oxy)octyl)carbamate (**4.25**)

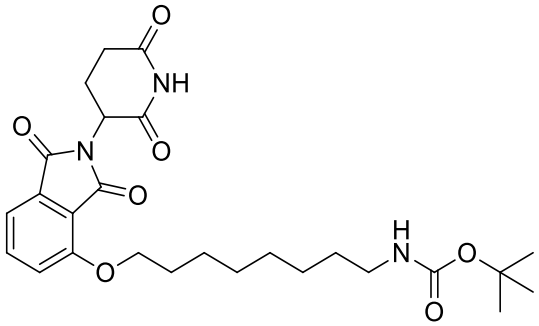

A solution of **4.07** (1.95 g, 7.10 mmol, 1 eq.) *tert-butyl*-(6-bromohexyl)carbamate (2.19 g, 7.10 mmol, 1 eq.) in DMF (50 mL) was treated with potassium bicarbonate (1.17 g, 10.65 mmol, 1.5 eq.) and potassium iodide (0.117 g, 0.710 mmol, 0.1 eq.) sequentially. The reaction was then left to stir for 4 days at room temperature. Upon completion, the reaction mixture was poured into water (300 mL) and extracted with EtOAc (3 × 75 mL), the organic collections were then combined and washed with 1 M K_2CO_3 (200 mL), brine (3 × 100 mL), dried over $MgSO_4$ and concentrated *in vacuo*. The crude mixture was then purified *via* column chromatography (0.5% - 1% - 1.5% 7N NH_3 methanol in dichloromethane) to result in the product as a white foam (949.9 mg, 1.89 mmol, 27%). ^{1}H NMR (400 MHz, d^6-DMSO) δ_{ppm} 1.36 (s, 17H), 1.45 (p, *J* = 7.3 Hz, 2H), 1.75 (p, *J* = 6.6 Hz, 2H), 1.98 – 2.05 (m, 1H), 2.52 – 2.62 (m, 2H), 2.83 – 2.93 (m, 3H), 4.20 (t, *J* = 6.4 Hz, 2H), 5.08 (dd, *J* = 12.8, 5.4 Hz, 1H), 6.75 (d, *J* = 4.9 Hz, 1H), 7.44 (d, *J* = 7.2 Hz, 1H), 7.51 (d, *J* = 8.5 Hz, 1H), 7.77 – 7.83 (m, 1H), 11.09 (s, 1H). LCMS (5-95 MeCN in 5 mins) ^{t}R = 5.40 min, Purity = 90%, m/z = 524 $[M + Na]^+$.

4-(2-Aminoethoxy)-2-(2,6-dioxopiperidin-3-yl)isoindoline-1,3-dione hydrochloride (**4.26**)

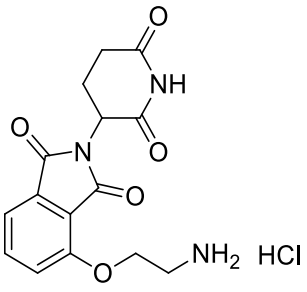

Compound **4.26** was synthesised according to general procedure C to afford the product as a white solid (494 mg, 1.40 mmol, 92.7%). ^{1}H NMR (400 MHz, d^{6}-DMSO) δ_{ppm} 1.99 – 2.07 (m, 1H), 2.53 – 2.68 (m, 2H), 2.84 – 2.95 (m, 1H), 3.26 (d, *J* = 10.5 Hz, 2H), 4.44 (t, *J* = 5.3 Hz, 2H), 5.08 – 5.14 (m, 1H), 7.56 (dd, *J* = 14.9, 7.8 Hz, 2H), 7.86 (dd, *J* = 8.5, 7.3 Hz, 1H), 7.97 (s, 2H), 11.11 (s, 1H). LCMS (5-95 MeCN in 5 mins) ^{t}R = 1.52 min, Purity = >99%, m/z = 318.2 $[M + H]^{+}$.

4-(4-Aminobutoxy)-2-(2,6-dioxopiperidin-3-yl)isoindoline-1,3-dione hydrochloride (**4.27**)

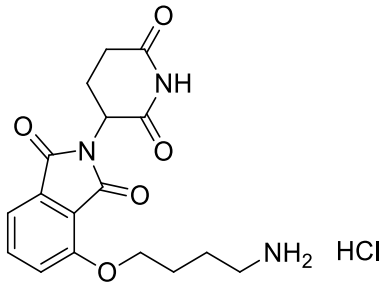

Compound **4.27** was synthesised according to general procedure C to afford the product as a white solid (721 mg, 1.89 mmol, 99%). ^{1}H NMR (400 MHz, d^{6}-DMSO) δ_{ppm} 1.71 – 1.88 (m, 4H), 1.99 – 2.07 (m, 1H), 2.60 (dd, *J* = 20.7, 3.5 Hz, 1H), 2.83 – 2.94 (m, 3H), 4.24 (t, *J* = 5.9 Hz, 2H), 5.08 (dd, *J* = 12.7, 5.4 Hz, 1H), 7.47 (d, *J* = 7.2 Hz, 1H), 7.53 (d, *J* = 8.6 Hz, 1H), 7.74 – 7.86 (m, 3H), 11.09 (s, 1H). LCMS (5-95 MeCN in 5 mins) ^{t}R = 2.72 min, Purity = 99%, m/z = 346 $[M + H]^{+}$.

4-((6-Aminohexyl)oxy)-2-(2,6-dioxopiperidin-3-yl)isoindoline-1,3-dione hydrochloride (**4.28**)

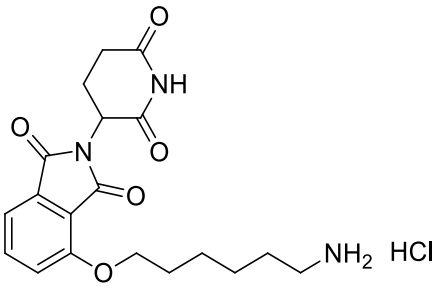

Compound **4.28** was synthesised according to general procedure C to afford the product as a white solid (93%, 807 mg, 1.97 mmol). ^{1}H NMR (400 MHz, d^{6}-DMSO) δ_{ppm} 1.38 (p, *J* = 8.1 Hz, 2H), 1.47 (p, *J* = 7.2 Hz, 2H), 1.58 (p, *J* = 7.6 Hz, 2H), 1.76 (p, *J* = 6.5 Hz, 2H), 2.00 – 2.05 (m, 1H), 2.45 – 2.54 (m, 2H), 2.59 (dd, *J* = 15.1, 2.3 Hz, 1H), 2.76 (s, 2H), 2.84 – 2.92 (m, 1H), 4.21 (t, *J* = 6.4 Hz, 2H), 5.08 (dd, *J* = 12.9, 5.4 Hz, 1H), 7.44 (d, *J* = 7.3 Hz, 1H), 7.52 (d, *J* = 8.6 Hz, 1H), 7.81 (dd, *J* = 8.5, 7.3 Hz, 1H), 7.96 (s, 3H), 11.09 (s, 1H). LCMS (5-95 MeCN in 5 mins) ^{t}R = 3.049 min, Purity = 99%, m/z = 374 $[M + H]^{+}$.

4-((8-Aminooctyl)oxy)-2-(2,6-dioxopiperidin-3-yl)isoindoline-1,3-dione hydrochloride (**4.29**)

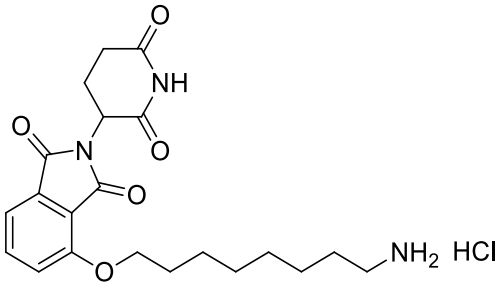

Compound **4.29** was synthesised according to general procedure C to afford the product as a white solid (720 mg, 1.64 mmol, 88%). ^{1}H NMR (400 MHz, d^{6}-DMSO) δ_{ppm} 1.25 – 1.38 (m, 8H), 1.45 (q, *J* = 7.8, 7.3 Hz, 2H), 1.51 – 1.57 (m, 2H), 1.73 – 1.78 (m, 2H), 2.02 (dtd, *J* = 12.9, 5.4, 2.4 Hz, 1H), 2.46 – 2.54 (m, 2H), 2.59 (d, *J* = 15.2 Hz, 1H), 2.71 – 2.76 (m, 2H), 2.88 (ddd, *J* = 17.1, 14.0, 5.4 Hz, 1H), 4.18 (s, 2H), 5.08 (dd, *J* = 12.9, 5.4 Hz, 1H), 7.45 (s, 1H), 7.52 (d, *J* = 8.5 Hz, 1H), 7.79 – 7.82 (m, 1H), 7.94 (s, 2H), 11.09 (s, 1H). LCMS (5-95 MeCN in 5 mins) ^{t}R = 3.456 min, Purity = 99%, m/z = 402.9 $[M + H]^{+}$.

4-Fluorothalidomide (**4.31**)

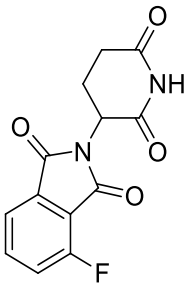

A suspension of 3-fluoropthalic anhydride (15.13 g, 91.1 mmol, 1 eq.) and 3-aminopiperidine-2,6-dione hydrochloride (15 g, 91.1 mmol, 1 eq.) in AcOH (200 mL) was treated with sodium acetate (16.44 g, 200.42 mmol, 2.2 eq.). The reaction mixture was then left to stir overnight at 120 °C. Upon completion the reaction mixture was then cooled and concentrated *in vacuo*, using heptane to azeotrope (4 × 150 mL). The crude mixture was then suspended in water for 1 hour before filtering. The filter cake was washed with water (50 mL), then petroleum ether 40 – 60 (3 × 50 mL) and vacuum dried to give the product as a purple solid (95%, 23.9 g, 86.54 mmol). ^{1}H NMR (600 MHz, *d*^{6}-DMSO) δ_{ppm} 2.07 (dtd, *J* = 13.0, 5.4, 2.4 Hz, 1H), 2.55 (dd, *J* = 13.1, 4.4 Hz, 1H), 2.62 (dt, *J* = 17.3, 3.4 Hz, 1H), 2.90 (ddd, *J* = 17.1, 13.9, 5.4 Hz, 1H), 5.17 (dd, *J* = 13.0, 5.4 Hz, 1H), 7.74 (t, *J* = 8.8 Hz, 1H), 7.79 (d, *J* = 7.3 Hz, 1H), 7.95 (td, *J* = 7.9, 4.3 Hz, 1H), 11.15 (s, 1H). ^{13}C NMR (151 MHz, *d*^{6}-DMSO) δ_{ppm} 21.8, 30. 9, 49.1, 117.1 (d), 120.0, 123.1 (d), 133. 4, 138.1 (d), 155.9, 157.7, 164.0, 166.1 (d), 169.7, 172.7. LCMS (5-95 MeCN in 20 mins) ^{t}R = 16.02 min, Purity = 90% - one peak, m/z = 274 (-ve).

General Procedure E

A solution of **4.31** (1.5 g, 5.4 mmol, 1 eq.), *N*-boc-ethylenediamine (7.02 mmol, 1.3 eq.) and DIPEA (2.83 mL, 16.02 mmol, 3 eq.) in NMP (10 mL) was heated to 200 °C in the microwave for 15 mins using the dynamic heating method, with max power set to 300 W, max pressure 300 psi, max temperature 200 °C, high stirring throughout and power max turned off. After cooling, the reaction mixture was transferred to a separating funnel and partitioned between water (100 mL) and ethyl acetate (50 mL), the organic layer was collected, and the aqueous layer extracted with ethyl acetate (2 × 50 mL). The organic collections were combined, washed with saturated $NaHCO_3$ (150 mL), brine (150 mL), dried over $MgSO_4$, filtered, and concentrated *in vacuo*.

tert-Butyl (2-((2-(2,6-dioxopiperidin-3-yl)-1,3-dioxoisoindolin-4-yl)amino)ethyl)carbamate (**4.32**)

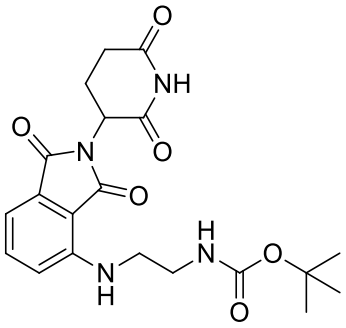

Compound **4.32** was synthesised according to general procedure E and then purified *via* flash chromatography using 0 – 100% EtOAc in hexane to afford the product as a yellow foam (1.062 g, 2.55 mmol, 47%,). ^{1}H NMR (600 MHz, $CDCl_3$) δ_{ppm} 1.44 (s, 9H), 2.12 (ddd, *J* = 13.0, 6.5, 4.0 Hz, 1H), 2.70 – 2.83 (m, 2H), 2.86 – 2.91 (m, 1H), 3.36 (q, *J* = 6.2 Hz, 2H), 3.44 (t, *J* = 6.2 Hz, 2H), 4.88 (s, 1H), 4.92 (dd, *J* = 12.4, 5.3 Hz, 1H), 6.39 (t, *J* = 6.2 Hz, 1H), 6.98 (d, *J* = 8.5 Hz, 1H), 7.11 (d, *J* = 7.1 Hz, 1H), 7.50 (dd, *J* = 8.5, 7.1 Hz, 1H), 8.21 (s, 1H). LCMS (5-95 MeCN in 20 mins) ^{t}R = 19.75 min, Purity = 96%, m/z = 439 $[M + Na]^+$.

tert-Butyl (4-((2-(2,6-dioxopiperidin-3-yl)-1,3-dioxoisoindolin-4-yl)amino)butyl)carbamate (**4.33**)

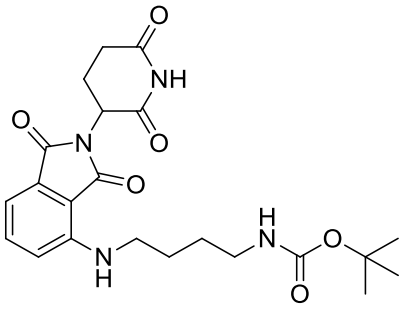

Compound **4.33** was synthesised according to general procedure E and then purified *via* flash chromatography using 0 – 100% EtOAc in hexane to afford the product as a yellow foam (1.91 g, 4.30 mmol, 80%). ^{1}H NMR (600 MHz, $CDCl_3$) δ_{ppm} 1.44 (s, 9H), 1.59 (dd, *J* = 15.3, 6.8 Hz, 2H), 1.66 – 1.72 (m, 2H), 2.10 – 2.15 (m, 1H), 2.70 – 2.83 (m, 2H), 2.88 (dd, *J* = 16.3, 3.4 Hz, 1H), 3.17 (q, *J* = 6.7 Hz, 2H), 3.30 (q, *J* = 6.6 Hz, 2H), 4.58 (s, 1H), 4.91 (dd, *J* = 12.5, 5.4 Hz, 1H), 6.23 (t, *J* = 5.8 Hz, 1H), 6.88 (d, *J* = 8.5 Hz, 1H), 7.09 (d, *J* = 7.0 Hz, 1H), 7.48 (dd, *J* = 8.5, 7.1 Hz, 1H), 8.15 (s, 1H).LCMS (5-95 MeCN in 20 mins) ^{t}R = 20.95 min, Purity = 95%, m/z = 467.15 $[M + Na]^+$.

tert-Butyl (6-((2-(2,6-dioxopiperidin-3-yl)-1,3-dioxoisoindolin-4-yl)amino)hexyl)carbamate (**4.34**)

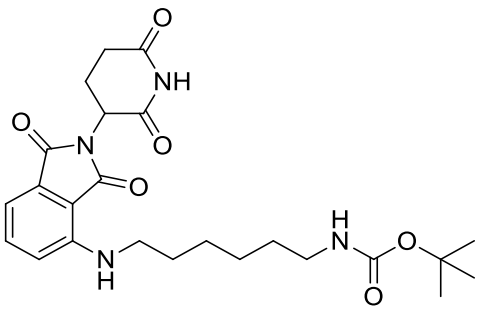

Compound **4.34** was synthesised according to general procedure E and then purified *via* flash chromatography using 0 – 100% EtOAc in hexane to afford the product as a yellow foam (1.321 g, 2.80 mmol, 52%). ^{1}H NMR (600 MHz, $CDCl_3$) δ_{ppm} 1.26 (t, *J* = 7.2 Hz, 2H), 1.44 (s, 9H), 1.61 (q, *J* = 7.3 Hz, 2H), 1.69 (p, *J* = 7.0 Hz, 2H), 2.10 – 2.15 (m, 1H), 2.70 – 2.84 (m, 2H), 2.89 (dt, *J* = 17.0, 2.8 Hz, 1H), 3.18 (d, *J* = 7.4 Hz, 2H), 3.30 (q, *J* = 6.6 Hz, 2H), 4.12 (q, *J* = 7.2 Hz, 1H), 4.56 (s, 1H), 4.91 (dd, *J* = 12.3, 5.3 Hz, 1H), 6.21 – 6.25 (m, 1H), 6.89 (d, *J* = 8.5 Hz, 1H), 7.09 (d, *J* = 7.0 Hz, 1H), 7.49 (dd, *J* = 8.5, 7.1 Hz, 1H), 8.01 (s, 1H). LCMS (5-95 MeCN in 20 mins) ^{t}R = 22.43 min, Purity = 89%, m/z = 472 $[M + H]^+$.

tert-Butyl (8-((2-(2,6-dioxopiperidin-3-yl)-1,3-dioxoisoindolin-4-yl)amino)octyl)carbamate (**4.35**)

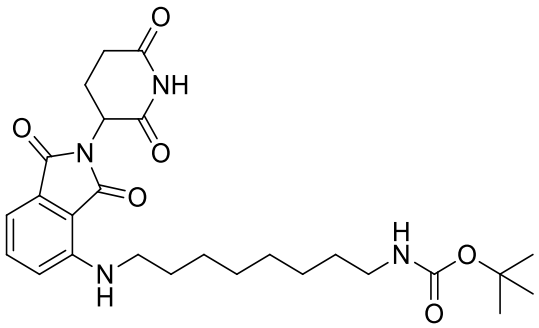

Compound **4.35** was synthesised according to general procedure E and then purified *via* flash chromatography using 0 – 100% EtOAc in hexane to afford the product as a yellow foam (2.09 g, 4.18 mmol, 77%). ^{1}H NMR (600 MHz, $CDCl_3$) δ_{ppm} 8.19 (s, 1H), 1.27 – 1.34 (m, 8H), 1.43 (s, 16H), 1.65 (d, *J* = 7.4 Hz, 2H), 2.09 – 2.14 (m, 1H), 2.68 – 2.82 (m, 3H), 2.87 (dd, *J* = 16.5, 3.9 Hz, 1H), 3.09 (q, *J* = 6.9 Hz, 2H), 3.22 – 3.26 (m, 2H), 4.52 (s, 1H), 4.88 – 4.92 (m, 1H), 6.22 (t, *J* = 5.6 Hz, 1H), 6.86 (d, *J* = 8.5 Hz, 1H), 7.07 (d, *J* = 7.1 Hz, 1H), 7.47 (dd, *J* = 8.5, 7.1 Hz, 1H), 8.19 (s, 1H). LCMS (5-95 MeCN in 20 mins) ^{t}R = 11.82 min, Purity = 88%, m/z = 373.1 $[M + H]^+$.

4-((2-Aminoethyl)amino)-2-(2,6-dioxopiperidin-3-yl)isoindoline-1,3-dione hydrochloride (**4.36**)

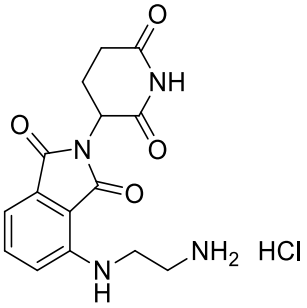

Compound **4.36** was synthesised according to general procedure C to afford the product as a yellow solid (890 mg, 2.52 mmol, 99%). ^{1}H NMR (400 MHz, d^{6}-DMSO) δ_{ppm} 1.99 – 2.06 (m, 1H), 2.53 – 2.63 (m, 2H), 2.84 – 3.01 (m, 3H), 3.61 (q, *J* = 6.5 Hz, 2H), 5.07 (dd, *J* = 12.8, 5.4 Hz, 1H), 6.83 (t, *J* = 6.5 Hz, 1H), 7.09 (d, *J* = 7.1 Hz, 1H), 7.23 (d, *J* = 8.4 Hz, 1H), 7.62 (dd, *J* = 8.5, 7.1 Hz, 1H), 8.00 (s, 3H), 11.10 (s, 1H). LCMS (5-95 MeCN in 5 mins) ^{t}R = 1.87 min, Purity = 99%, m/z = 339.2 $[M + Na]^{+}$.

4-((4-Aminobutyl)amino)-2-(2,6-dioxopiperidin-3-yl)isoindoline-1,3-dione hydrochloride (**4.37**)

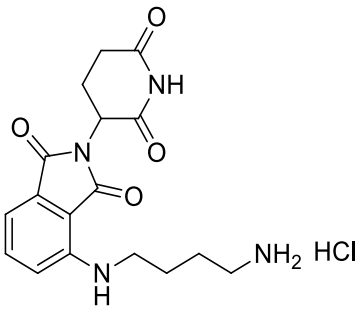

Compound **4.37** was synthesised according to general procedure C to afford the product as a yellow solid (890 mg, 2.52 mmol, 99%). ^{1}H NMR (600 MHz, d^{6}-DMSO) δ_{ppm} 1.62 (s, 4H), 2.02 (dd, *J* = 8.9, 3.9 Hz, 1H), 2.50 – 2.61 (m, 2H), 2.79 (q, *J* = 6.6 Hz, 2H), 2.88 (ddd, *J* = 17.1, 13.9, 5.4 Hz, 1H), 3.30 – 3.35 (m, 2H), 5.04 (dd, *J* = 12.9, 5.5 Hz, 1H), 7.02 (d, *J* = 7.0 Hz, 1H), 7.12 (d, *J* = 8.6 Hz, 1H), 8.09 (s, 3H), 11.09 (s, 1H).. LCMS (5-95 MeCN in 20 mins) ^{t}R = 10.78 min, Purity = 94%, m/z = 345.10 $[M + H]^{+}$.

4-((6-aminohexyl)amino)-2-(2,6-dioxopiperidin-3-yl)isoindoline-1,3-dione hydrochloride (**4.38**)

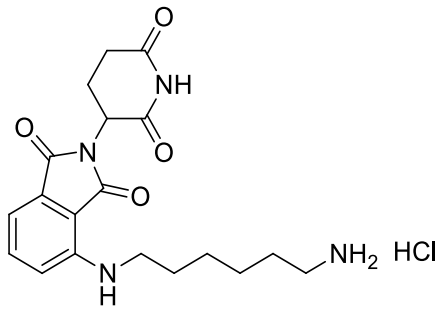

Compound **4.38** was synthesised according to general procedure C to afford the product as a yellow solid (1.125 g, 2.75 mmol, 98%). ^{1}H NMR (600 MHz, d^{6}-DMSO) δ_{ppm} 1.32 (s, 4H), 1.54 (p, *J* = 6.7, 5.9 Hz, 4H), 2.00 (ddd, *J* = 12.8, 7.8, 5.3 Hz, 1H), 2.51 (dd, *J* = 13.0, 4.4 Hz, 1H), 2.56 (d, *J* = 17.1 Hz, 1H), 2.72 (h, *J* = 5.9 Hz, 2H), 2.82 – 2.89 (m, 1H), 3.27 (q, *J* = 6.7 Hz, 2H), 5.03 (d, *J* = 12.9 Hz, 1H), 6.51 (t, *J* = 6.0 Hz, 1H), 6.99 (d, *J* = 7.0 Hz, 1H), 7.07 (d, *J* = 8.6 Hz, 1H), 7.56 (dd, *J* = 8.6, 7.0 Hz, 1H), 7.96 (s, 3H), 11.06 (s, 1H). LCMS (5-95 MeCN in 20 mins) ^{t}R = 11.82 min, Purity = 88%, m/z = 373.1 $[M + H]^{+}$.

4-((8-Aminooctyl)amino)-2-(2,6-dioxopiperidin-3-yl)isoindoline-1,3-dione hydrochloride (**4.39**)

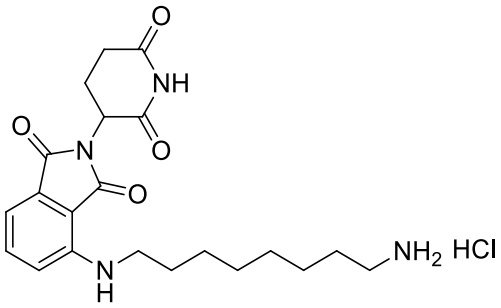

Compound **4.39** was synthesised according to general procedure C to afford the product as a yellow solid (1.7 g, 3.94 mmol, 94%). ^{1}H NMR (600 MHz, d^{6}-DMSO) δ_{ppm} 1.26 – 1.37 (m, 9H), 1.55 (dp, *J* = 22.6, 7.3 Hz, 5H), 2.00 – 2.05 (m, 1H), 2.54 (dd, *J* = 13.1, 4.4 Hz, 1H), 2.59 (d, *J* = 17.3 Hz, 1H), 2.70 – 2.77 (m, 2H), 2.88 (ddd, *J* = 17.1, 13.9, 5.4 Hz, 1H), 3.29 (q, *J* = 6.6, 6.1 Hz, 2H), 5.05 (dd, *J* = 12.8, 5.4 Hz, 1H), 6.52 (s, 1H), 7.02 (d, *J* = 7.0 Hz, 1H), 7.09 (d, *J* = 8.6 Hz, 1H), 7.58 (dd, *J* = 8.6, 7.1 Hz, 1H), 7.90 (s, 3H), 11.09 (s, 1H). LCMS (5-95 MeCN in 20 mins) ^{t}R = 12.96 min, Purity = 94%, m/z = 401.20 $[M + H]^{+}$.

(2*S*,4*R*)-1-((*S*)-2-((*tert*-Butoxycarbonyl)amino)-3,3-dimethylbutanoyl)-4-hydroxypyrrolidine-2-carboxylic acid (**4.42**)

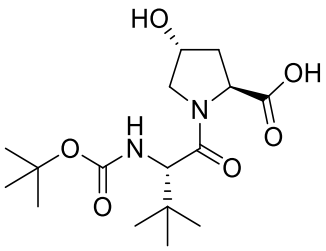

To a slurry of L-4-Hydroxyproline methyl ester hydrochloride (10 g, 55 mmol, 1eq.), Boc-L-tert-leucine (12.7 g, 55 mmol, 1 eq.) and HATU (31.4 g, 82.6 mmol, 1.5 eq.) In DMF (200 mL) was added DIPEA (47.9 mL, 275 mmol, 5 eq.) slowly at 0 °C. The reaction was allowed to warm to room temperature and left to stir overnight. Upon completion, the reaction mixture was quenched with water (500 mL). The aqueous was then extracted with EtOAc (3 × 300 mL), the organics were combined and successively washed with 5% (w/w) citric acid solution (2 × 100 mL), saturated $NaHCO_3$ (2 × 100 mL), brine (3 × 250 mL), dried over $MgSO_4$, filtered, and concentrated *in vacuo* to give a thick red oil which was used in the next step without further purification.

To a solution of (2*S*,4*R*)-methyl 1-((*S*)-2-((tert-butoxycarbonyl)amino)-3,3-dimethylbutanoyl)-4-hydroxypyrrolidine-2-carboxylate (55 mmol, 1 eq.) in a mixture of THF (180 mL) and Methanol (180 mL), was added LiOH monohydrate (5.4 g, 225 mmol, 5 eq.) and the resulting solution was left to stir overnight at room temperature. The reaction mixture was concentrated *in vacuo* and the residue was acidified with 1M HCl to pH 2, followed by extraction with EtOAc (3 × 100 mL). The combined organics were then washed with 5% (w/w) citric acid solution (200 mL), brine (2 × 200 mL), dried over $MgSO_4$ and concentrated *in vacuo* to give the product as a white solid (18.06 g, 52 mmol, 95%). ^{1}H NMR (600 MHz, d^6-DMSO) δ_{ppm} 0.93 (s, 9H), 1.38 (s, 9H), 1.88 (td, *J* = 8.9, 4.5 Hz, 1H), 2.06 – 2.13 (m, 1H), 2.69 (s, 1H), 3.57 – 3.67 (m, 2H), 4.16 (d, *J* = 9.4 Hz, 1H), 4.26 (t, *J* = 8.4 Hz, 1H), 4.32 (s, 1H), 5.17 (d, *J* = 3.8 Hz, 1H), 6.47 (d, *J* = 9.3 Hz, 1H), 12.39 (s, 1H).

tert-Butyl 4-Bromobenzylcarbamate (**4.44**)

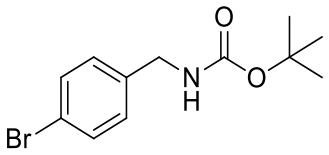

A solution of di-*tert*-butyl dicarbonate (37.6 g, 172.5 mmol 1.15 eq.) in dichloromethane (200 mL) was added slowly to a stirring solution of 4-bromobenzylamine (27.9 g, 150 mmol, 1 eq.) and DIPEA (30 mL, 172.5 mmol, 1.15 eq.) in dichloromethane (200 mL), the reaction was then left to stir at room temperature overnight. Upon completion, the reaction mixture was poured into water (400 mL) and Organic collected. The aqueous layer was extracted with dichloromethane (2 × 100 mL) before combining the organics. The organic was then successively washed with saturated $NaHCO_3$ (250 mL), brine (300 mL), dried over $MgSO_4$ and concentrated *in vacuo*. The crude product was purified *via* flash chromatography (0 – 15% EtOAc in hexane) to afford the product as a white solid (36.78 g, 129 mmol, 86%). ^{1}H NMR (600 MHz, $CDCl_3$) δ_{ppm} 1.45 (s, 9H), 4.26 (d, *J* = 6.1 Hz, 2H), 4.86 (s, 1H), 7.15 (d, *J* = 8.1 Hz, 2H), 7.44 (d, *J* = 8.4 Hz, 2H). Data matched those in literature.

tert-Butyl 4-(4-Methylthiazol-5-yl)benzylcarbamate (**4.45**)

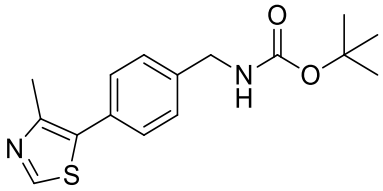

tert-Butyl 4-bromobenzylcarbamate (25.0 g, 134 mmol, 1 eq.), KOAc (26.4 g, 269 mmol, 2 eq.) and $Pd(OAc)_2$ (0.302 g, 1.34 mmol, 10 mol%) were dissolved in DMF (150 mL) before the addition of 4-methylthiazole (26.65 g, 269 mmol, 2 eq.). The reaction mixture was heated to 90 °C and left overnight. The reaction mixture was diluted with water (1 L) and extracted with EtOAc (3 × 250 mL). The organic collections were combined and washed with brine (3 × 300 mL), dried over $MgSO_4$, filtered, and concentrated *in vacuo*. The crude oil was purified *via* flash chromatography (0 – 50% EtOAc in Hexane) to afford the product as an off-white solid (54%, 9.67 g, 31.7 mmol). ^{1}H NMR (600 MHz, $CDCl_3$) δ_{ppm} 1.47 (s, 9H), 2.52 (s, 3H), 4.36 (d, *J* = 6.1 Hz, 2H), 4.93 (s, 1H), 7.34 (d, *J* = 7.9 Hz, 2H), 7.40 (d, *J* = 8.2 Hz, 2H), 8.67 (s, 1H). LCMS (5-95 MeCN in 20 mins) ^{t}R = 21.71 min, Purity = 93%, m/z = 305 $[M + H]^+$.

(4-(4-Methylthiazol-5-yl)phenyl)methanamine hydrochloride (**4.46**)

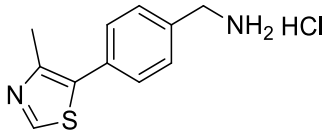

tert-butyl 4-(4-methylthiazol-5-yl)benzylcarbamate (18.73 g, 61.5 mmol, 1 eq.) was dissolved in dichloromethane (200 mL) before the slow addition of TFA (20 mL, 308 mmol, 5 eq.), the reaction was then left to stir at room temperature overnight. The reaction mixture was then concentrated *in vacuo* and azeotroped with a dichloromethane/heptane mix (5 × 200 mL) to result in a yellow gum (96%, 8.51 g, 30.6 mmol). ^{1}H NMR (600 MHz, *d*^{6}-DMSO) δ_{ppm} 2.47 (s, 3H), 4.06 (q, *J* = 5.9 Hz, 2H), 7.55 (d, *J* = 8.3 Hz, 2H), 7.62 (d, *J* = 8.4 Hz, 2H), 8.62 (s, 3H), 9.12 (s, 1H).

tert-Butyl ((*S*)-1-((2*S*,4*R*)-4-Hydroxy-2-((4-(4-methylthiazol-5-yl)benzyl)carbamoyl)pyrrolidin-1-yl)-3,3-dimethyl-1-oxobutan-2-yl)carbamate (**4.47**)

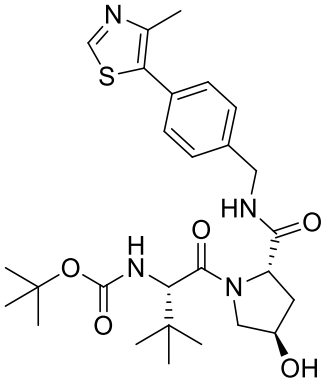

To a stirring suspension of **4.42** (18.1 g, 53 mmol, 1 eq.), **4.46** (14.6 g, 53 mmol, 1 eq.) and HATU (24.2 g, 63.6 mmol, 1.2 eq.) in THF (300 mL) was added DIPEA slowly (46 mL, 265 mmol, 5 eq.). The reaction was then left to stir at room temperature overnight. Upon completion the reaction mixture was concentrated, and the residue was suspended in EtOAc (500 mL) and successively washed with water (1 L), sat $NaHCO_3$ (500 mL), brine (3 × 500 mL), dried over $MgSO_4$, filtered, and concentrated *in vacuo*. The crude product was purified *via* flash chromatography (0 – 100% Et_2O in hexane) to afford the product as a white solid (21.7 g, 40.8 mmol, 77%). ^{1}H NMR (600 MHz, $CDCl_3$) δ_{ppm} 0.91 (s, 9H), 1.40 (s, 9H), 1.97 (s, 1H), 2.09 – 2.14 (m, 1H), 2.50 (s, 4H), 3.27 (d, *J* = 4.2 Hz, 1H), 3.58 (dd, *J* = 11.3, 3.6 Hz, 1H), 4.06 (d, *J* = 11.4 Hz, 1H), 4.15 (d, *J* = 9.1 Hz, 1H), 4.30 (d, *J* = 20.1 Hz, 1H), 4.51 (s, 1H), 4.53 – 4.59 (m, 1H), 4.75 (t, *J*

= 7.9 Hz, 1H), 5.19 (d, *J* = 9.0 Hz, 1H), 7.34 (q, *J* = 8.2 Hz, 4H), 7.45 (t, *J* = 6.0 Hz, 1H), 8.67 (s, 1H). ^{13}C NMR (600 MHz, $CDCl_3$) δ_{ppm} 16.2, 26.5, 28.4, 34.9, 35.8, 43.4, 43.9, 56.0, 56.6, 58.4, 59.0, 70.2, 80.6, 128.2, 129.6, 131.0, 131.7, 138.2, 148.6, 150.5, 156.6, 170.7, 172.8. LCMS (30-95 MeCN in 20 mins) ^{t}R = 16.25 min, Purity = 96%, m/z = 531.15 $[M + H]^+$.

(2*S*,4*R*)-1-((*S*)-2-Amino-3,3-dimethylbutanoyl)-4-hydroxy-N-(4-(4-methylthiazol-5-yl)benzyl)pyrrolidine-2-carboxamide dihydrochloride (**4.48**)

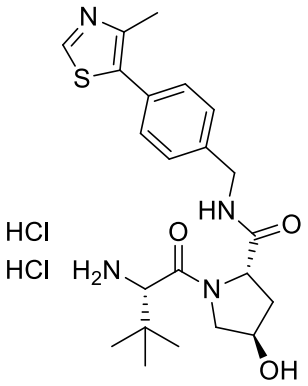

To a stirring solution of **4.47** (13.4 g, 25 mmol, 1 eq.) was dissolved in anhydrous dioxane (150 mL) before the slow addition of 4 M HCl in dioxane (32 mL, 126 mmol, 5 eq.), the reaction was then left to stir at room temperature overnight. The reaction mixture was then filtered under a nitrogen atmosphere and washed with dioxane (50 mL), Et_2O (4 × 200 mL) and left to dry for 1 hour to result in the product as a yellow solid (95%, 12.70 g, 25 mmol). ^{1}H NMR (600 MHz, *d*^{6}-DMSO) δ_{ppm} 1.02 (s, 9H), 1.38 (s, 1H), 1.86 – 1.91 (m, 1H), 2.12 (dd, *J* = 11.8, 8.6 Hz, 1H), 2.45 (s, 3H), 3.54 – 3.58 (m, 1H), 3.79 (d, *J* = 13.0 Hz, 1H), 3.89 (q, *J* = 5.6 Hz, 1H), 4.24 (dd, *J* = 15.8, 5.7 Hz, 1H), 4.36 (s, 1H), 4.42 (dd, *J* = 15.8, 6.5 Hz, 1H), 4.59 – 4.51 (m, 1H), 6.55 (s, 2H), 7.40 (s, 4H), 8.19 (d, *J* = 5.5 Hz, 3H), 8.76 (s, 1H), 9.12 (s, 1H). LCMS (5-95 MeCN in 20 mins) ^{t}R = 10.67 min, Purity = 93%, m/z = 431.15 $[M + H]^+$.

tert-Butyl (3-(((*S*)-1-((2*S*,4*R*)-4-Hydroxy-2-((4-(4-methylthiazol-5-yl)benzyl)carbamoyl)pyrrolidin-1-yl)-3,3-dimethyl-1-oxobutan-2-yl)amino)-3-oxopropyl)carbamate (**4.49**)

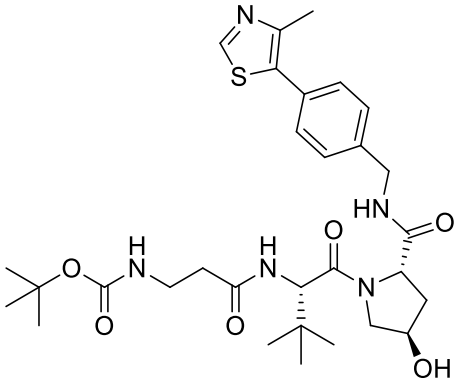

Compound **4.48** (1.5 g, 2.98 mmol, 1 eq.), 3-(boc-amino)propanoic acid (564 mg, 2.98 mmol, 1 eq.) and HATU (1.89 g, 4.96 mmol, 1.6 eq.) were dissolved in DMF (20 mL). DIPEA (3 mL, 17.88 mmol, 6 eq.) was then added to the stirring mixture. The reaction was left to stir at room temperature overnight. Upon depletion of the starting material, the reaction mixture was diluted with water (200 mL) and extracted with EtOAc (3 × 100 mL). Organic collections were combined and washed with saturated $NaHCO_3$ (200 mL), brine (3 × 150 mL), dried over $MgSO_4$ and concentrated *in vacuo* before purification. The crude mixture was purified by Flash chromatography (0 – 5% methanol in dichloromethane) to give the product as a white foam (71%, 1.27 g, 2.11 mmol). ^{1}H NMR (600 MHz, $CDCl_3$) δ_{ppm} 0.93 (s, 9H), 1.41 (s, 9H), 2.16 (t, *J* = 11.2 Hz, 1H), 2.35 (d, *J* = 11.3 Hz, 1H), 2.45 (d, *J* = 30.8 Hz, 1H), 2.51 (s, 2H), 3.29 – 3.39 (m, 2H), 3.61 (dd, *J* = 11.4, 3.5 Hz, 1H), 4.07 (d, *J* = 11.4 Hz, 1H), 4.33 (dd, *J* = 14.8, 4.9 Hz, 1H), 4.47 – 4.58 (m, 3H), 4.72 (t, *J* = 8.1 Hz, 1H), 5.21 (s, 1H), 6.56 (s, 1H), 7.34 (q, *J* = 8.3 Hz, 4H), 8.67 (s, 1H). LCMS (5-95 MeCN in 20 mins) ^{t}R = 17.99 min, Purity = 95%, m/z = 602.45 $[M + H]^+$.

tert-Butyl (5-(((*S*)-1-((2*S*,4*R*)-4-Hydroxy-2-((4-(4-methylthiazol-5-yl)benzyl)carbamoyl)pyrrolidin-1-yl)-3,3-dimethyl-1-oxobutan-2-yl)amino)-5-oxopentyl)carbamate (**4.50**)

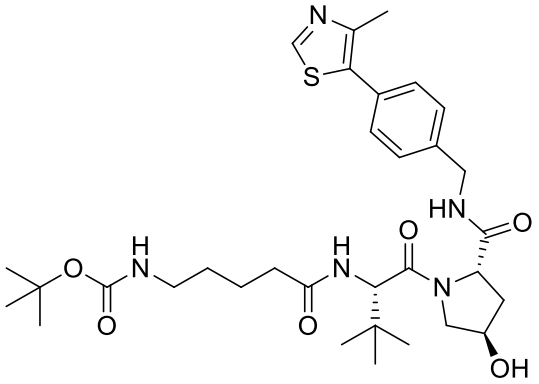

Compound **4.48** (1.5 g, 2.98 mmol, 1 eq.), 3-(boc-amino)pentanoic acid (647 mg, 2.98 mmol, 1 eq.) and HATU (1.89 g, 4.96 mmol, 1.6 eq.) were dissolved in DMF (20 mL). DIPEA (3 mL, 17.88 mmol, 6 eq.) was then added to the stirring mixture. The reaction was left to stir at room temperature overnight. Upon depletion of the starting material, the reaction mixture was diluted with water (200 mL) and extracted with EtOAc (3 × 100 mL). Organic collections were combined and washed with saturated $NaHCO_3$ (200 mL), brine (3 × 150 mL), dried over $MgSO_4$ and concentrated *in vacuo* before purification. The crude mixture was purified by Flash chromatography (0 – 5% methanol in dichloromethane) to give the product as a white foam (57%, 1.1 g, 1.7 mmol). ^{1}H NMR (600 MHz, $CDCl_3$) δ_{ppm} 0.93 (s, 8H), 1.41 (s, 9H), 1.74 (s, 2H), 2.15 (s, 1H), 2.36 (s, 1H), 2.43 (s, 1H), 2.51 (s, 3H), 3.35 (s, 2H), 3.58 – 3.62 (m, 1H), 4.07 (d, *J* = 11.4 Hz, 1H), 4.33 (dd, *J* = 14.8, 4.8 Hz, 1H), 4.48 – 4.59 (m, 3H), 4.74 (t, *J* = 8.1 Hz, 1H), 5.20 (s, 1H), 6.47 (d, *J* = 8.6 Hz, 1H), 7.35 (q, *J* = 8.3 Hz, 4H), 8.67 (s, 1H). LCMS (5-95 MeCN in 20 mins) ^{t}R = 18.61 min, Purity = 98%, m/z = 630.45 $[M + H]^+$.

tert-Butyl (7-(((*S*)-1-((2*S*,4*R*)-4-Hydroxy-2-((4-(4-methylthiazol-5-yl)benzyl)carbamoyl)pyrrolidin-1-yl)-3,3-dimethyl-1-oxobutan-2-yl)amino)-7-oxoheptyl)carbamate (**4.51**)

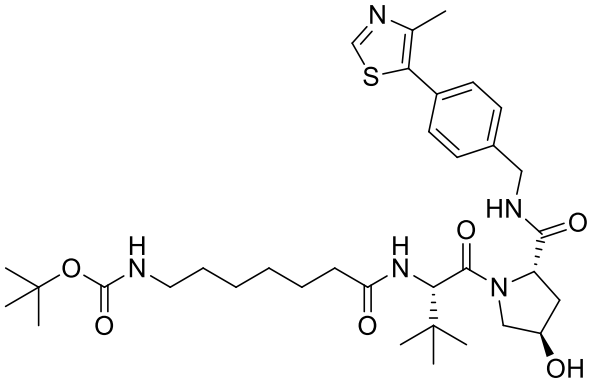

Compound **4.48** (750 mg, 1.49 mmol, 1 eq.), 3-(boc-amino)heptanoic acid (385 mg, 1.49 mmol, 1 eq.) and HATU (735 mg, 1.94 mmol, 1.5 eq.) were dissolved in DMF (20 mL). DIPEA (1 mL, 7.44 mmol, 4 eq.) was then added to the stirring mixture. The reaction was left to stir at room temperature overnight. Upon depletion of the starting material, the reaction mixture was diluted with water (200 mL) and extracted with EtOAc (3 × 100 mL). Organic collections were combined and washed with saturated $NaHCO_3$ (200 mL), brine (3 × 150 mL), dried over $MgSO_4$ and concentrated *in vacuo* before purification. The crude mixture was purified by Flash chromatography (0 – 5% 7N NH_3 methanol in dichloromethane) to give the product as a white foam (700 mg, 1.06 mmol, 71.5%). ^{1}H NMR (400 MHz, $CDCl_3$) δ_{ppm} 0.94 (s, 9H), 1.28 (s, 4H), 1.42 (s, 11H), 1.61 (d, *J* = 17.9 Hz, 2H), 2.12 – 2.27 (m, 3H), 2.52 (s, 3H), 2.89 (s, 1H), 3.07 (d, *J* = 7.1 Hz, 2H), 3.59 (d, *J* = 10.9 Hz, 1H), 4.15 (d, *J* = 11.4 Hz, 1H), 4.34 (d, *J* = 12.2 Hz, 1H), 4.54 (td, *J* = 23.3, 22.3, 11.6 Hz, 4H), 4.75 (t, *J* = 8.0 Hz, 1H), 6.06 (d, *J* = 8.6 Hz, 1H), 7.33 – 7.38 (m, 4H), 8.68 (s, 1H). LCMS (5-95 MeCN in 5 mins) ^{t}R = 4.91 min, Purity = 98%, m/z = 558.4 [M + H - boc]$^+$.

tert-Butyl (9-(((*S*)-1-((2*S*,4*R*)-4-Hydroxy-2-((4-(4-methylthiazol-5-yl)benzyl)carbamoyl)pyrrolidin-1-yl)-3,3-dimethyl-1-oxobutan-2-yl)amino)-9-oxononyl)carbamate (**4.52**)

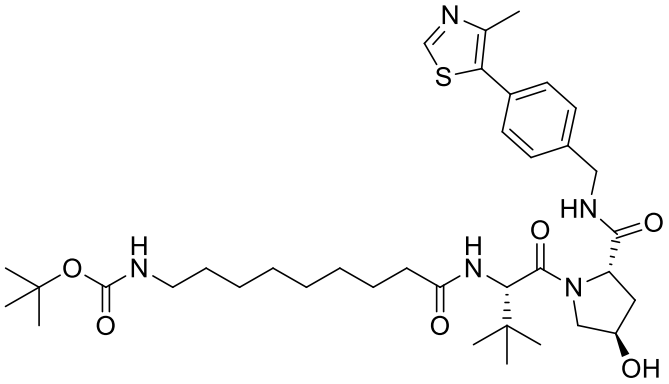

Compound **4.48** (750 mg, 1.49 mmol, 1 eq.), 3-(boc-amino)nonanoic acid (407 mg, 1.49 mmol, 1 eq.) and HATU (735 mg, 1.94 mmol, 1.5 eq.) were dissolved in DMF (20 mL). DIPEA (1 mL, 7.44 mmol, 4 eq.) was then added to the stirring mixture. The reaction was left to stir at room temperature overnight. Upon depletion of the starting material, the reaction mixture was diluted with water (200 mL) and extracted with EtOAc (3 × 100 mL). Organic collections were combined and washed with saturated $NaHCO_3$ (200 mL), brine (3 × 150 mL), dried over $MgSO_4$ and concentrated *in vacuo* before purification. The crude mixture was purified by Flash chromatography (0 – 5% 7N NH_3 methanol in dichloromethane) to give the product as a white foam (700 mg, 0.685 mmol, 69%). ^{1}H NMR (400 MHz, $CDCl_3$) δ_{ppm} 0.93 (s, 10H), 1.27 (s, 9H), 1.43 (s, 11H), 2.10 – 2.21 (m, 3H), 2.52 (s, 3H), 2.55 – 2.62 (m, 1H), 2.75 (s, 1H), 3.08 (d, *J* = 7.2 Hz, 2H), 3.56 – 3.62 (m, 1H), 4.14 (d, *J* = 11.3 Hz, 1H), 4.33 (dd, *J* = 14.9, 5.2 Hz, 1H), 4.45 – 4.61 (m, 5H), 4.75 (d, *J* = 7.9 Hz, 2H), 6.02 (d, *J* = 7.7 Hz, 1H), 7.32 – 7.39 (m, 5H), 8.68 (s, 1H). 0.93 (s, 10H), 1.27 (s, 9H), 1.43 (s, 11H), 2.10 – 2.21 (m, 3H), 2.52 (s, 3H), 2.55 – 2.62 (m, 1H), 2.75 (s, 1H), 3.08 (d, *J* = 7.2 Hz, 2H), 3.56 – 3.62 (m, 1H), 4.14 (d, *J* = 11.3 Hz, 1H), 4.33 (dd, *J* = 14.9, 5.2 Hz, 1H), 4.45 – 4.61 (m, 5H), 4.75 (d, *J* = 7.9 Hz, 2H), 6.02 (d, *J* = 7.7 Hz, 1H), 7.32 – 7.39 (m, 5H), 8.68 (s, 1H). LCMS (5-95 MeCN in 5 mins) ^{t}R = 5.25 min, Purity = 96%, m/z = 586.4 $[M + H - boc]^+$.

(2*S*,4*R*)-1-((*S*)-2-(3-Aminopropanamido)-3,3-dimethylbutanoyl)-4-hydroxy-N-(4-(4-methylthiazol-5-yl)benzyl)pyrrolidine-2-carboxamide dihydrochloride (**4.53**)

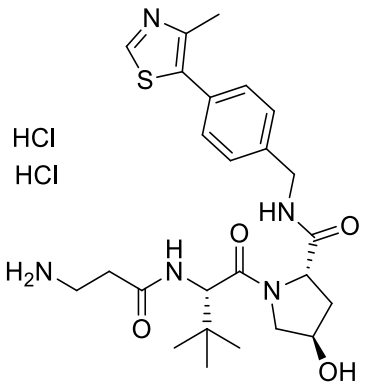

Compound **4.53** was synthesised according to General Procedure C to afford the product as a white solid (784 mg, 1.36 mmol, 68%). ^{1}H NMR (600 MHz, d^{6}-DMSO) δ_{ppm} 0.94 (s, 9H), 1.89 (t, *J* = 12.9 Hz, 1H), 2.05 (t, *J* = 11.7 Hz, 1H), 2.46 (d, *J* = 2.5 Hz, 3H), 2.63 (s, 2H), 2.94 (q, *J* = 6.1, 5.5 Hz, 2H), 3.16 (d, *J* = 2.2 Hz, 2H), 3.60 – 3.69 (m, 2H), 4.22 (dd, *J* = 15.9, 5.4 Hz, 1H), 4.35 (s, 1H), 4.40 – 4.46 (m, 2H), 4.54 (d, *J* = 10.7 Hz, 1H), 7.38 – 7.45 (m, 4H), 8.09 (s, 3H), 8.26 (d, *J* = 9.2 Hz, 1H), 8.65 (q, *J* = 5.1, 4.1 Hz, 1H), 9.23 (s, 1H). LCMS (5-95 MeCN in 20 mins) ^{t}R = 11.40 min, Purity = 97%, m/z = 502.20 $[M + H]^{+}$.

(2*S*,4*R*)-1-((*S*)-2-(5-aminopentanamido)-3,3-dimethylbutanoyl)-4-hydroxy-N-(4-(4-methylthiazol-5-yl)benzyl)pyrrolidine-2-carboxamide dihydrochloride (**4.54**)

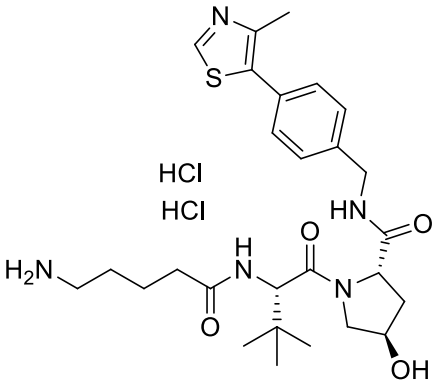

Compound **4.54** was synthesised according to General Procedure C to afford the product as a white solid (796 mg, 0.97 mmol, 55%). ^{1}H NMR (600 MHz, d^{6}-DMSO) δ_{ppm} 0.94 (s, 9H), 1.54 (s, 4H), 1.90 (ddd, *J* = 12.9, 8.6, 4.6 Hz, 1H), 2.01 – 2.06 (m, 1H), 2.13 – 2.19 (m, 1H), 2.28 (dd, *J* = 14.1, 6.7 Hz, 1H), 2.45 (s, 3H), 2.75 (d, *J* = 6.5 Hz, 2H), 3.62 (d, *J* = 11.2 Hz, 1H), 3.67 (dd, *J* = 10.5, 4.1 Hz, 1H), 4.19 – 4.24 (m, 1H), 4.35 (s, 1H), 4.41 – 4.45 (m, 2H), 4.54 (d, *J* = 9.3 Hz, 1H),

7.38 – 7.44 (m, 4H), 7.90 – 7.96 (m, 4H), 8.59 (d, *J* = 12.3 Hz, 1H), 9.06 (s, 1H). LCMS (5-95 MeCN in 20 mins) ^{t}R = 11.77 min, Purity = 90%, m/z = 530.30 $[M + H]^+$.

(2*S*,4*R*)-1-((*S*)-2-(7-aminoheptanamido)-3,3-dimethylbutanoyl)-4-hydroxy-N-(4-(4-methylthiazol-5-yl)benzyl)pyrrolidine-2-carboxamide dihydrochloride (**4.55**)

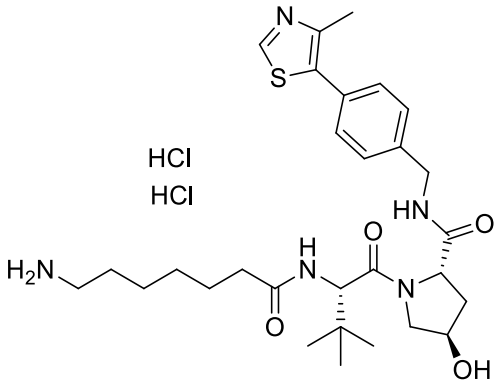

Compound **4.51** (700 mg, 1.06 mmol, 1 eq.) was dissolved in anhydrous dioxane (10 mL) before the slow addition of 4 M HCl in dioxane (2.65 mL, 10.6 mmol, 10 eq.), the reaction was then left to stir at room temperature for 3 h. The reaction mixture was then filtered under a nitrogen atmosphere and washed with dioxane (20 mL), Et_2O (4 × 20 mL) and left to dry for 1 hour to result in the product as a yellow gum, which was freeze dried from water overnight to give the product as yellow crystals (570 mg, 0.904 mmol, 85%). ^{1}H NMR (400 MHz, d^6-DMSO) δ_{ppm} 0.93 (s, 9H), 1.19 – 1.33 (m, 6H), 1.50 (q, *J* = 9.1, 8.1 Hz, 5H), 1.85 – 1.94 (m, 1H), 1.99 – 2.33 (m, 5H), 2.44 (s, 3H), 2.70 – 2.77 (m, 2H), 3.60 – 3.69 (m, 2H), 4.21 (dd, *J* = 15.9, 5.5 Hz, 1H), 4.35 (s, 1H), 4.39 – 4.46 (m, 2H), 4.54 (d, *J* = 9.4 Hz, 1H), 7.40 (q, *J* = 8.3 Hz, 4H), 7.75 (s, 2H), 7.85 (d, *J* = 9.3 Hz, 1H), 8.57 (d, *J* = 5.8 Hz, 1H), 9.00 (d, *J* = 5.4 Hz, 1H). LCMS (5-95 MeCN in 5 mins) ^{t}R = 3.48 min, Purity = 98%, m/z = 558.4 $[M + H]^+$.

(2*S*,4*R*)-1-((*S*)-2-(9-aminononanamido)-3,3-dimethylbutanoyl)-4-hydroxy-N-(4-(4-methylthiazol-5-yl)benzyl)pyrrolidine-2-carboxamide dihydrochloride (**4.56**)

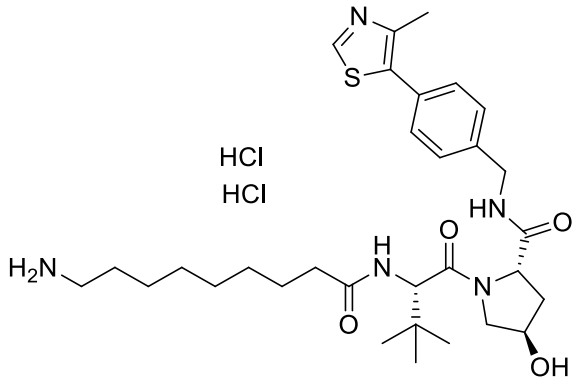

Compound **4.52** (700 mg, 1.02 mmol, 1 eq.) was dissolved in anhydrous dioxane (10 mL) before the slow addition of 4 M HCl in dioxane (2.55 mL, 10.2 mmol, 10 eq.), the reaction was then left to stir at room temperature for 3 h. The reaction mixture was then filtered under a nitrogen atmosphere and washed with dioxane (20 mL), Et_2O (4 × 20 mL) and left to dry for 1 hour to result in the product as a yellow gum, which was freeze dried from water overnight to give the product as yellow crystals (666 mg, 1.01 mmol, 99%).^{1}H NMR (400 MHz, d^6-DMSO) δ_{ppm} 1.04 (s, 9H), 1.37 (s, 9H), 1.64 (q, *J* = 7.1 Hz, 4H), 2.03 – 2.11 (m, 1H), 2.19 – 2.36 (m, 3H), 2.61 (s, 3H), 2.91 (t, *J* = 7.7 Hz, 2H), 3.81 (dd, *J* = 11.0, 3.9 Hz, 1H), 3.91 (d, *J* = 11.0 Hz, 1H), 4.42 (d, *J* = 15.8 Hz, 1H), 4.50 (s, 1H), 4.56 (dd, *J* = 16.2, 6.9 Hz, 2H), 4.64 (s, 1H), 7.52 – 7.59 (m, 4H), 10.02 (s, 1H). LCMS (5-95 MeCN in 5 mins) ^{t}R = 3.72 min, Purity = 95%, m/z = 586.4 $[M + H]^+$.

6.3.2.3 Synthesis of Piperazine Modified Degraders

General Procedure F

To a suspension of **3.27** (150 mg, 0.227 mmol, 1 eq.) and HATU (112 mg, 0.295 mmol, 1.3 eq.) in DMF (10 mL) was added Triethylamine (221 µL, 1.587 mmol, 7 eq.) and the E3 toolbox amine (0.227 mmol, 1 eq.). The reaction was left to stir overnight. The reaction was then diluted with water (100 mL) and extracted with EtOAc (3 × 25 mL). Organic extracts were combined and washed with brine (50 mL), saturated aqueous $NaHCO_3$ (50 mL), brine (2 × 50 mL), dried over $MgSO_4$ and filtered before concentration *in vacuo*.

2-(4-(2-(2-(4-(3-(Dimethylamino)propoxy)phenethyl)-5-(3,5-dimethylisoxazol-4-yl)-1*H*-benzo[d]imidazol-1-yl)ethyl)piperazin-1-yl)-*N*-(2-((2-(2,6-dioxopiperidin-3-yl)-1,3-dioxoisoindolin-4-yl)amino)ethyl)acetamide (**4.57**)

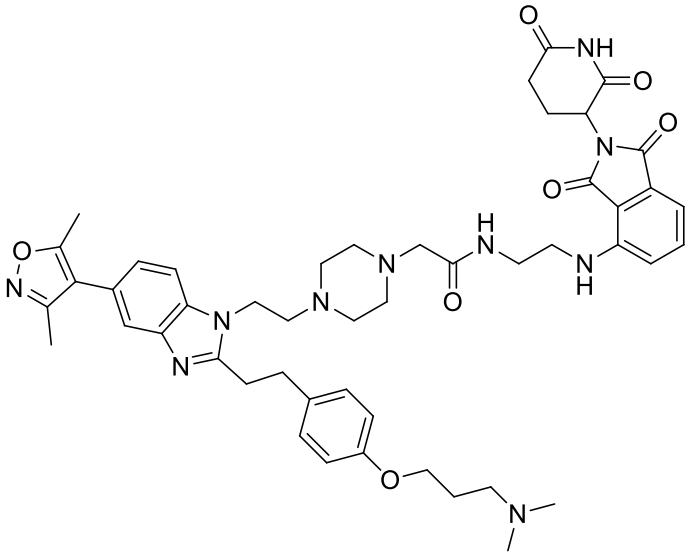

Degrader **4.57** was synthesised according to General Procedure F and the crude material was then purified using column chromatography (300 mm × 25 mm, using 120 mm × 25 mm silica) using 250 mL (2% 7N NH_3 methanol, to 6% 7N NH_3 methanol) in dichloromethane increasing by 1% per 250 mL. The yellow foam was then freeze dried overnight to result in **4.57** as a yellow solid (72 mg, 0.081 mmol, 36%). ^{1}H NMR (600 MHz, d^{6}-DMSO) δ_{ppm} 1.80 (p, *J* = 6.7 Hz, 2H), 1.97 – 2.01 (m, 1H), 2.12 (s, 6H), 2.23 (s, 3H), 2.32 (t, *J* = 7.1 Hz, 4H), 2.40 (s, 4H), 2.51 – 2.59 (m, 5H), 2.85 (s, 3H), 3.11 (d, *J* = 8.1 Hz, 2H), 3.14 – 3.18 (m, 2H), 3.29 (q, *J* = 6.4 Hz, 4H), 3.39 (d, *J* = 6.3 Hz, 4H), 3.93 (t, *J* = 6.4 Hz, 2H), 4.24 (t, *J* = 6.4 Hz, 2H), 5.05 (dd, *J* = 12.8, 5.4 Hz, 1H), 6.70 (s, 1H), 6.84 (d, *J* = 8.6 Hz, 2H), 7.02 (d, *J* = 7.0 Hz, 1H), 7.16 (dd, *J* = 8.2, 1.6 Hz, 1H), 7.21 (d, *J* = 8.7 Hz, 3H), 7.54 – 7.58 (m, 3H), 7.90 (t, *J* = 5.9 Hz, 1H), 11.11 (s, 1H). ^{13}C NMR (151 MHz, d^{6}-DMSO) δ_{ppm} 11.0, 11.8, 22.6, 27.4, 29.0, 31.4, 32.2, 41.1, 45.6, 56.1, 61.7, 66.1, 109.6, 110.7, 114.7, 117.1, 119.3, 123.0, 123.1, 129.8, 132.6, 133.5, 134.9, 136.6, 143.0, 146.8, 156.0, 157.5, 158.8, 165.0, 167.7, 170.2, 170.5, 173.3, 1 Carbon Missing. LCMS (5-95 MeCN in 5 mins) ^{t}R = 3.212 min, Purity= 99%, m/z = 887.40 $[M + H]^{+}$. HR-MS (m/z): $[M + H]^{+}$ calculated for $C_{48}H_{59}N_{10}O_{7}$, 887.4568; found, 887.4599.

2-(4-(2-(2-(4-(3-(dimethylamino)propoxy)phenethyl)-5-(3,5-dimethylisoxazol-4-yl)-1*H*-benzo[d]imidazol-1-yl)ethyl)piperazin-1-yl)-*N*-(4-((2-(2,6-dioxopiperidin-3-yl)-1,3-dioxoisoindolin-4-yl)amino)butyl)acetamide (**4.58**)

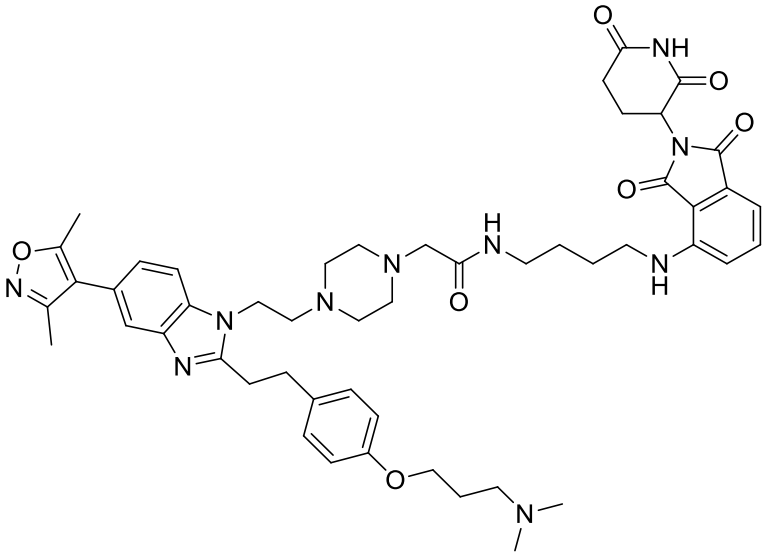

Degrader **4.58** was synthesised according to General Procedure F and the crude material was then purified using column chromatography (300 mm × 25 mm, using 120 mm × 25 mm silica) using 250 mL (2% 7N NH_3 methanol, to 6% 7N NH_3 methanol) in dichloromethane increasing by 1% per 250 mL. The yellow foam was then freeze dried overnight to result in **4.58** as a yellow solid (65 mg, 0.071 mmol, 31%). ^{1}H NMR (600 MHz, d^6-DMSO) δ_{ppm} 1.45 – 1.52 (m, 4H), 1.81 (p, *J* = 6.7 Hz, 2H), 1.97 – 2.02 (m, 1H), 2.13 (s, 6H), 2.23 (s, 3H), 2.33 (t, *J* = 7.2 Hz, 6H), 2.40 (s, 3H), 2.51 – 2.59 (m, 4H), 2.84 (s, 4H), 3.09 – 3.19 (m, 8H), 3.30 (q, *J* = 6.7 Hz, 4H), 3.94 (t, *J* = 6.4 Hz, 2H), 4.24 (t, *J* = 6.3 Hz, 2H), 5.04 (dd, *J* = 12.9, 5.5 Hz, 1H), 6.57 (t, *J* = 6.1 Hz, 1H), 6.84 (d, *J* = 8.6 Hz, 2H), 7.00 (d, *J* = 7.0 Hz, 1H), 7.08 (d, *J* = 8.6 Hz, 1H), 7.16 (dd, *J* = 8.1, 1.7 Hz, 1H), 7.21 (d, *J* = 8.6 Hz, 2H), 7.53 – 7.57 (m, 3H), 7.69 (t, *J* = 6.1 Hz, 1H), 11.11 (s, 1H). ^{13}C NMR (151 MHz, d^6-DMSO) δ_{ppm} 10.6, 11.3, 22.2, 26.2, 26.7, 26.9, 28.6, 31.0, 31.8, 37.8, 40.1, 41.5, 45.2, 48.5, 52.8, 52.9, 55.7, 57.1, 61.3, 65.7, 109.0, 110.3, 110.4, 114.3, 116.7, 117.2, 118.9, 122.6, 122.7, 129.4, 132.2, 133.1, 134.5, 136.3, 142.6, 146.4, 155.6, 157.0, 158.4, 164.6, 167.3, 169.0, 170.1, 172.9. LCMS (5-95 MeCN in 5 mins) ^{t}R = 3.212 min, Purity = 99%, m/z = 915.5 $[M + H]^+$. HR-MS (m/z): $[M + H]^+$ calculated for $C_{50}H_{63}N_{10}O_7$, 915.4881; found, 915.4950.

2-(4-(2-(2-(4-(3-(dimethylamino)propoxy)phenethyl)-5-(3,5-dimethylisoxazol-4-yl)-1*H*-benzo[d]imidazol-1-yl)ethyl)piperazin-1-yl)-*N*-(6-((2-(2,6-dioxopiperidin-3-yl)-1,3-dioxoisoindolin-4-yl)amino)hexyl)acetamide (**4.59**)

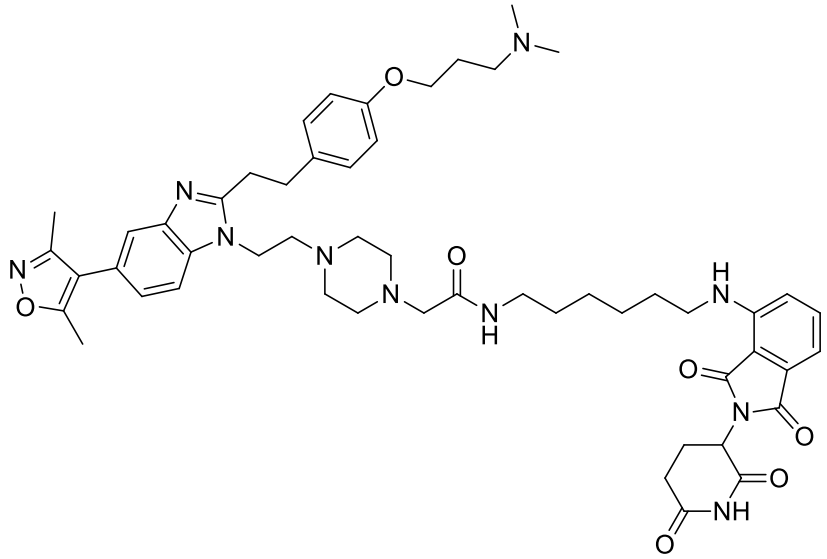

Degrader **4.59** was synthesised according to General Procedure F and the crude material was then purified using column chromatography (300 mm × 25 mm, using 120 mm × 25 mm silica) using 250 mL (2% 7N NH_3 methanol, to 6% 7N NH_3 methanol) in dichloromethane increasing by 1% per 250 mL. The yellow foam was then freeze dried overnight to result in **4.59** as a yellow solid (95 mg, 0.101 mmol, 44%). ^{1}H NMR (600 MHz, d^6-DMSO) δ_{ppm} 1.27 (t, *J* = 7.5 Hz, 2H), 1.31 – 1.35 (m, 2H), 1.38 – 1.43 (m, 2H), 1.54 (q, *J* = 7.3 Hz, 2H), 1.80 (p, *J* = 6.7 Hz, 2H), 2.01 (td, *J* = 7.7, 6.6, 4.3 Hz, 1H), 2.12 (s, 6H), 2.23 (s, 3H), 2.31 (d, *J* = 7.1 Hz, 3H), 2.40 (s, 4H), 2.51 – 2.62 (m, 5H), 2.82 – 2.89 (m, 3H), 3.04 – 3.08 (m, 2H), 3.11 (d, *J* = 8.3 Hz, 2H), 3.13 – 3.17 (m, 2H), 3.27 (q, *J* = 6.7 Hz, 3H), 3.93 (t, *J* = 6.4 Hz, 2H), 4.24 (t, *J* = 6.4 Hz, 2H), 5.04 (dd, *J* = 12.9, 5.5 Hz, 1H), 6.53 (t, *J* = 6.0 Hz, 1H), 6.83 (d, *J* = 8.6 Hz, 2H), 6.99 (d, *J* = 7.0 Hz, 1H), 7.07 (d, *J* = 8.6 Hz, 1H), 7.16 (dd, *J* = 8.1, 1.7 Hz, 1H), 7.20 (d, *J* = 8.6 Hz, 2H), 7.53 – 7.57 (m, 3H), 7.63 (t, *J* = 5.9 Hz, 1H), 11.11 (s, 1H).^{13}C NMR (151 MHz, d^6-DMSO) δ_{ppm} 10.6, 11.3, 22.2, 26.0, 26.1, 27.0, 28.6, 29.2, 31.8, 38.1, 41.8, 45.2, 48.5, 52.8, 53.0, 55.7, 57.1, 61.3, 65.7, 114.3, 116.7, 117.2, 122.6, 122.7, 129.4, 132.2, 133.1, 134.5, 142.6, 146.4, 155.6, 157.1, 158.4, 164.6, 167.3, 168.9, 170.1, 172.9, 5 carbons missing. LCMS (5-95 MeCN in 5 mins) ^{t}R = 3.681 min, Purity = 97%, m/z = 943.6 $[M + H]^+$. HR-MS (m/z): $[M + H]^+$ calculated for $C_{52}H_{67}N_{10}O_7$, 943.5194; found, 943.5203.

2-(4-(2-(2-(4-(3-(dimethylamino)propoxy)phenethyl)-5-(3,5-dimethylisoxazol-4-yl)-1*H*-benzo[d]imidazol-1-yl)ethyl)piperazin-1-yl)-*N*-(8-((2-(2,6-dioxopiperidin-3-yl)-1,3-dioxoisoindolin-4-yl)amino)octyl)acetamide (**4.60**)

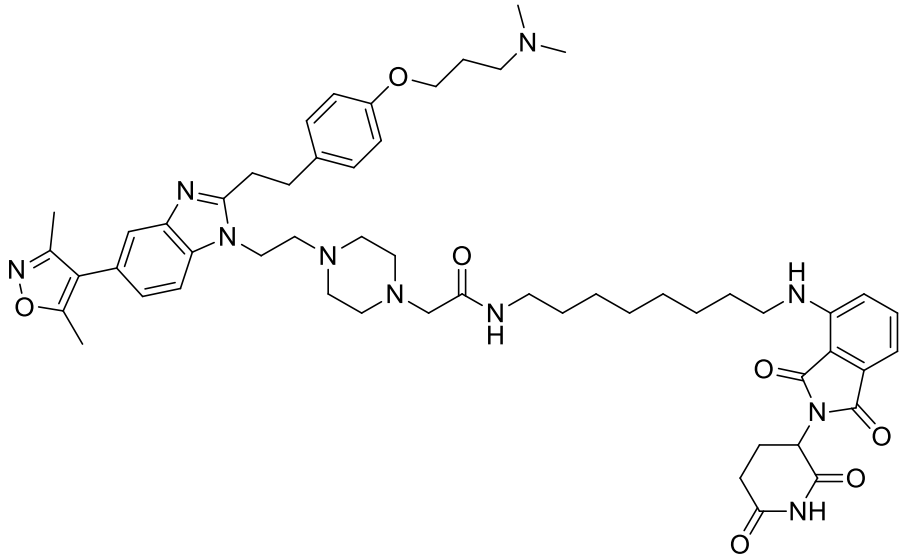

Degrader **4.60** was synthesised according to General Procedure F and the crude material was then purified using column chromatography (300 mm × 25 mm, using 120 mm × 25 mm silica) using 250 mL (2% 7N NH_3 methanol, to 6% 7N NH_3 methanol) in dichloromethane increasing by 1% per 250 mL. The yellow foam was then freeze dried overnight to result in **4.60** as a yellow solid (53 mg, 0.055 mmol, 24%). ^{1}H NMR (600 MHz, d^6-DMSO) δ_{ppm} 1.20 – 1.33 (m, 12H), 1.36 – 1.39 (m, 2H), 1.55 (t, *J* = 7.3 Hz, 2H), 1.80 (d, *J* = 6.8 Hz, 2H), 1.99 – 2.03 (m, 1H), 2.12 (s, 6H), 2.23 (s, 3H), 2.31 (s, 2H), 2.40 (s, 3H), 2.51 – 2.62 (m, 6H), 2.82 – 2.90 (m, 4H), 3.05 (d, *J* = 6.6 Hz, 2H), 3.09 – 3.12 (m, 2H), 3.14 – 3.17 (m, 2H), 3.27 (d, *J* = 6.7 Hz, 2H), 3.32 (s, 1H), 3.93 (d, *J* = 6.5 Hz, 2H), 4.24 (t, *J* = 6.5 Hz, 2H), 5.04 (dd, *J* = 12.9, 5.5 Hz, 1H), 6.52 (t, *J* = 5.9 Hz, 1H), 6.83 (d, *J* = 8.6 Hz, 2H), 7.00 (d, *J* = 7.0 Hz, 1H), 7.07 (d, *J* = 8.6 Hz, 1H), 7.16 (dd, *J* = 8.1, 1.7 Hz, 1H), 7.20 (d, *J* = 8.6 Hz, 2H), 7.53 – 7.56 (m, 3H), 7.61 (t, *J* = 6.0 Hz, 1H), 11.11 (s, 1H). ^{13}C NMR (151 MHz, d^6-DMSO) δ_{ppm} 10.6, 11.3, 22.2, 26.3, 26.3, 27.0, 28.7, 28.7, 29.2, 31.0, 31.8, 38.1, 40.1, 41.8, 45.3, 48.5, 52.8, 53.0, 55.7, 57.1, 61.3, 65.7, 110.3, 110.4, 114.3, 116.7, 117.2, 118.9, 122.6, 122.7, 129.4, 132.2, 133.1, 134.5, 136.3, 142.6, 146.4, 155.6, 157.1, 158.4, 164.6, 167.3, 168.8, 170.2, 172.9. LCMS (5-95 MeCN in 5 mins) ^{t}R = 3.94 min, Purity= 97%, m/z = 971.5 [M + H]$^+$. HR-MS (m/z): [M + H]$^+$ calculated for $C_{54}H_{71}N_{10}O_7$, 971.5507; found, 971.5601.

2-(4-(2-(2-(4-(3-(dimethylamino)propoxy)phenethyl)-5-(3,5-dimethylisoxazol-4-yl)-1*H*-benzo[d]imidazol-1-yl)ethyl)piperazin-1-yl)-*N*-(2-((2-(2,6-dioxopiperidin-3-yl)-1,3-dioxoisoindolin-4-yl)oxy)ethyl)acetamide (**4.61**)

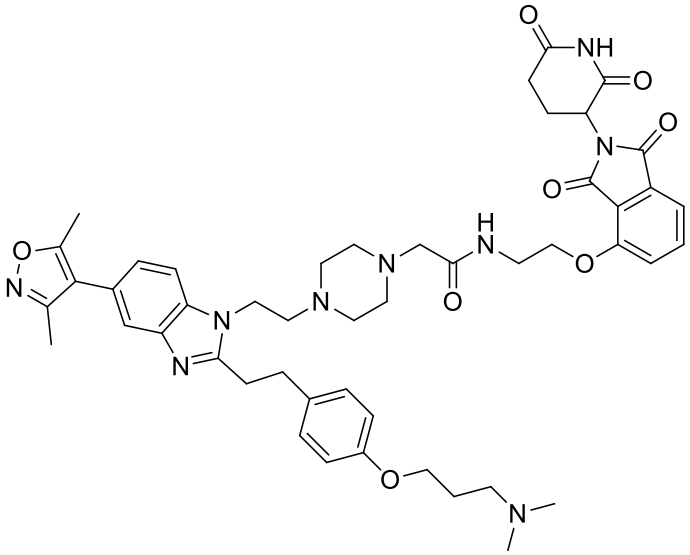

Degrader **4.61** was synthesised according to General Procedure F and the crude material was then purified using column chromatography (300 mm × 25 mm, using 120 mm × 25 mm silica) using 250 mL (2% 7N NH_3 methanol, to 6% 7N NH_3 methanol) in dichloromethane increasing by 1% per 250 mL. The white foam was then freeze dried overnight to result in **4.61** as a white solid (70 mg, 0.07 mmol, 35%). ^{1}H NMR (600 MHz, d^{6}-DMSO) δ_{ppm} 1.79 (p, *J* = 6.7 Hz, 2H), 1.92 – 1.97 (m, 1H), 2.11 (s, 6H), 2.21 (s, 3H), 2.31 (t, *J* = 7.2 Hz, 4H), 2.38 (s, 8H), 2.77 – 2.87 (m, 3H), 3.05 – 3.15 (m, 5H), 3.49 (q, *J* = 5.8 Hz, 2H), 3.91 (t, *J* = 6.4 Hz, 2H), 4.22 (dt, *J* = 20.6, 6.1 Hz, 4H), 5.05 (dd, *J* = 12.6, 5.5 Hz, 1H), 6.81 (d, *J* = 8.6 Hz, 2H), 7.14 (dd, *J* = 8.2, 1.6 Hz, 1H), 7.17 (d, *J* = 8.6 Hz, 2H), 7.43 (d, *J* = 7.2 Hz, 1H), 7.51 – 7.54 (m, 3H), 7.78 (dd, *J* = 8.5, 7.2 Hz, 1H), 7.82 (t, *J* = 5.8 Hz, 1H), 11.11 (s, 1H).^{13}C NMR (151 MHz, d^{6}-DMSO) δ_{ppm} 10.6, 11.4, 22.1, 26.9, 28.6, 30.9, 31.8, 37.5, 40.1, 45.2, 48.8, 52.8, 52.9, 55.7, 57.2, 61.1, 65.7, 67.3, 110.3, 114.3, 115.6, 116.4, 116.7, 118.9, 120.0, 122.6, 122.7, 129.4, 133.1, 133.3, 134.5, 137.1, 142.6, 155.6, 155.6, 157.0, 158.4, 164.6, 165.2, 166.8, 169.6, 169.9, 172.8. LCMS (5-95 MeCN in 5 mins) ^{t}R = 3.15 min, Purity = 99%, m/z = 888.4 $[M + H]^{+}$. HR-MS (m/z): $[M + H]^{+}$ calculated for $C_{48}H_{58}N_9O_8$, 888.4408; found, 888.4467.

2-(4-(2-(2-(4-(3-(dimethylamino)propoxy)phenethyl)-5-(3,5-dimethylisoxazol-4-yl)-1*H*-benzo[d]imidazol-1-yl)ethyl)piperazin-1-yl)-*N*-(4-((2-(2,6-dioxopiperidin-3-yl)-1,3-dioxoisoindolin-4-yl)oxy)butyl)acetamide (**4.62**)

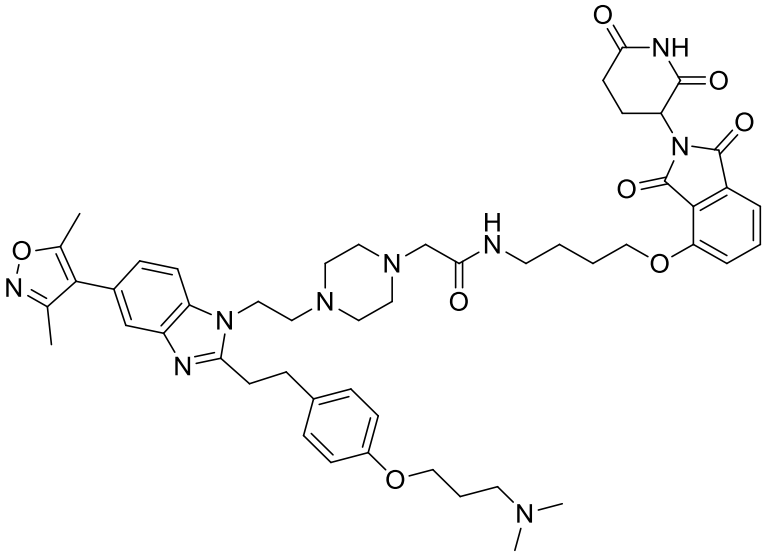

Degrader **4.62** was synthesised according to General Procedure F and the crude material was then purified using column chromatography (300 mm × 25 mm, using 120 mm × 25 mm silica) using 250 mL (2% 7N NH_3 methanol, to 6% 7N NH_3 methanol) in dichloromethane increasing by 1% per 250 mL. The white foam was then freeze dried overnight to result in **4.62** as a white solid (75 mg, 0.082 mmol, 37%). ^{1}H NMR (600 MHz, d^6-DMSO) δ_{ppm} 1.57 (p, *J* = 7.0 Hz, 2H), 1.70 (p, *J* = 6.6 Hz, 2H), 1.78 (p, *J* = 6.7 Hz, 2H), 1.97 (ddd, *J* = 12.8, 6.5, 4.1 Hz, 1H), 2.11 (s, 6H), 2.20 (s, 3H), 2.31 (t, *J* = 7.2 Hz, 5H), 2.38 (s, 3H), 2.38 – 2.44 (m, 3H), 2.48 – 2.56 (m, 5H), 2.81 – 2.87 (m, 3H), 3.06 – 3.09 (m, 2H), 3.14 (dd, *J* = 8.1, 4.6 Hz, 4H), 3.91 (t, *J* = 6.4 Hz, 2H), 4.17 – 4.23 (m, 4H), 5.04 (dd, *J* = 12.9, 5.5 Hz, 1H), 6.81 (d, *J* = 8.6 Hz, 2H), 7.13 (dd, *J* = 8.2, 1.7 Hz, 1H), 7.18 (d, *J* = 8.6 Hz, 2H), 7.40 (d, *J* = 7.2 Hz, 1H), 7.47 (d, *J* = 8.6 Hz, 1H), 7.53 (d, *J* = 8.4 Hz, 2H), 7.71 (t, *J* = 6.1 Hz, 1H), 7.77 (dd, *J* = 8.6, 7.3 Hz, 1H), 11.10 (s, 1H). ^{13}C NMR (151 MHz, d^6-DMSO) δ_{ppm} 10.6, 11.3, 22.0, 25.8, 25.9, 26.9, 28.6, 31.0, 31.8, 37.7, 40.1, 45.2, 48.7, 52.9, 52.9, 55.7, 57.1, 61.3, 65.7, 68.5, 110.3, 114.3, 115.2, 116.2, 116.7, 118.9, 119.8, 122.6, 122.7, 129.4, 133.1, 133.3, 134.5, 137.1, 142.6, 155.6, 155.9, 157.0, 158.4, 164.6, 165.4, 166.9, 169.0, 170.0, 172.8. LCMS (5-95 MeCN in 5 mins) ^{t}R = 3.19 min, Purity = 96%, m/z = 916.4 $[M + H]^+$. HR-MS (m/z): $[M + H]^+$ calculated for $C_{50}H_{62}N_9O_8$, 916.4721; found, 916.4725.

2-(4-(2-(2-(4-(3-(dimethylamino)propoxy)phenethyl)-5-(3,5-dimethylisoxazol-4-yl)-1*H*-benzo[d]imidazol-1-yl)ethyl)piperazin-1-yl)-*N*-(6-((2-(2,6-dioxopiperidin-3-yl)-1,3-dioxoisoindolin-4-yl)oxy)hexyl)acetamide (**4.63**)

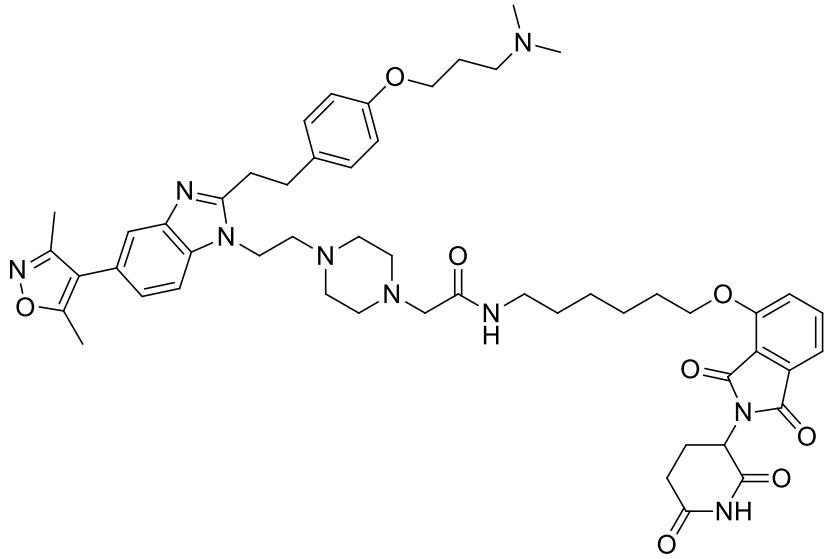

Degrader **4.63** was synthesised according to General Procedure F and the crude material was then purified using column chromatography (300 mm × 25 mm, using 120 mm × 25 mm silica) using 250 mL (2% 7N NH_3 methanol, to 6% 7N NH_3 methanol) in dichloromethane increasing by 1% per 250 mL. The white foam was then freeze dried overnight to result in **4.63** as a white solid (74 mg, 0.078 mmol, 35%). ^{1}H NMR (600 MHz, d^{6}-DMSO) δ_{ppm} 1.19 – 1.34 (m, 8H), 1.35 – 1.42 (m, 4H), 2.11 (s, 6H), 2.21 (s, 3H), 2.31 (t, *J* = 7.2 Hz, 3H), 2.39 (s, 3H), 2.50 – 2.59 (m, 4H), 2.81 – 2.88 (m, 3H), 3.04 (q, *J* = 6.7 Hz, 2H), 3.07 – 3.11 (m, 2H), 3.12 – 3.16 (m, 2H), 3.92 (t, *J* = 6.4 Hz, 2H), 4.16 (t, *J* = 6.4 Hz, 2H), 4.23 (t, *J* = 6.4 Hz, 2H), 5.06 (dd, *J* = 12.9, 5.4 Hz, 1H), 6.82 (d, *J* = 8.6 Hz, 2H), 7.14 (dd, *J* = 8.1, 1.7 Hz, 1H), 7.19 (d, *J* = 8.6 Hz, 2H), 7.40 (d, *J* = 7.3 Hz, 1H), 7.47 (d, *J* = 8.5 Hz, 1H), 7.54 (d, *J* = 8.0 Hz, 2H), 7.60 (t, *J* = 6.0 Hz, 1H), 7.76 (dd, *J* = 8.5, 7.2 Hz, 1H), 11.11 (s, 1H). ^{13}C NMR (151 MHz, d^{6}-DMSO) δ_{ppm} 10.6, 11.3, 22.0, 25.3, 26.3, 26.9, 28.4, 28.7, 29.2, 31.0, 31.8, 38.1, 40.1, 45.2, 48.7, 53.0, 55.7, 57.1, 61.3, 65.7, 68.8, 110.3, 114.3, 115.2, 116.2, 116.7, 118.9, 119.8, 122.6, 122.7, 129.4, 133.1, 133.3, 134.5, 137.1, 142.6, 155.6, 156.0, 157.1, 158.4, 164.6, 165.3, 166.9, 168.8, 170.0, 172.8. LCMS (5-95 MeCN in 5 mins) ^{t}R = 3.42 min, Purity = 99%, m/z = 944.5 $[M + H]^+$. HR-MS (m/z): $[M + H]^+$ calculated for $C_{52}H_{66}N_9O_8$, 944.5034; found, 944.5126.

2-(4-(2-(2-(4-(3-(dimethylamino)propoxy)phenethyl)-5-(3,5-dimethylisoxazol-4-yl)-1*H*-benzo[d]imidazol-1-yl)ethyl)piperazin-1-yl)-*N*-(8-((2-(2,6-dioxopiperidin-3-yl)-1,3-dioxoisoindolin-4-yl)oxy)octyl)acetamide (**4.64**)

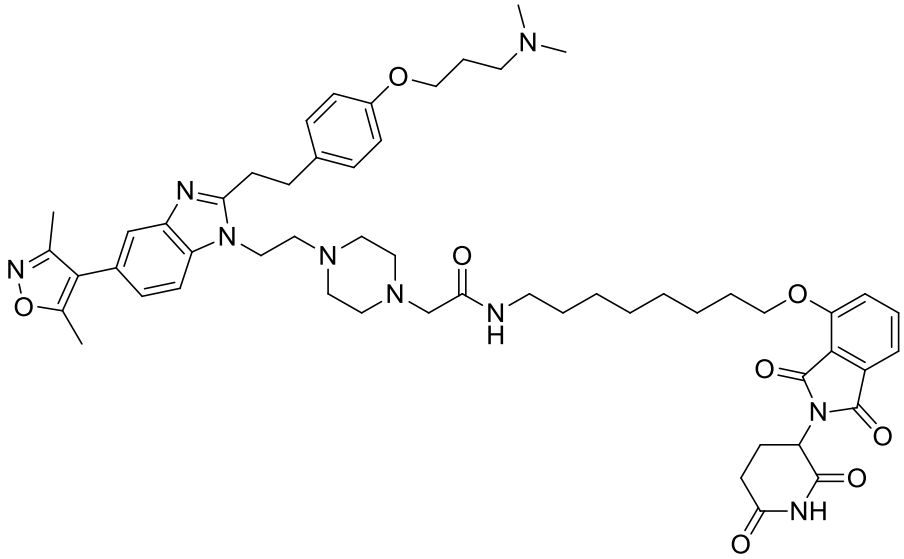

Degrader **4.64** was synthesised according to General Procedure F and the crude material was then purified using column chromatography (300 mm × 25 mm, using 120 mm × 25 mm silica) using 250 mL (2% 7N NH_3 methanol, to 6% 7N NH_3 methanol) in dichloromethane increasing by 1% per 250 mL. The white foam was then freeze dried overnight to result in **4.64** as a white solid (114 mg, 0.117 mmol, 52%). ^{1}H NMR (600 MHz, d^{6}-DMSO) δ_{ppm} 1.27 – 1.33 (m, 2H), 1.40 – 1.46 (m, 4H), 1.74 (q, *J* = 7.7, 7.1 Hz, 2H), 1.80 (p, *J* = 6.7 Hz, 2H), 2.12 (s, 7H), 2.23 (s, 3H), 2.32 (t, *J* = 7.1 Hz, 6H), 2.40 (s, 4H), 2.51 – 2.59 (m, 4H), 2.84 (s, 3H), 3.06 – 3.12 (m, 4H), 3.16 (t, *J* = 6.7 Hz, 2H), 3.93 (t, *J* = 6.4 Hz, 2H), 4.18 (t, *J* = 6.4 Hz, 2H), 4.24 (t, *J* = 6.4 Hz, 2H), 5.07 (dd, *J* = 12.9, 5.4 Hz, 1H), 6.84 (d, *J* = 8.6 Hz, 2H), 7.16 (dd, *J* = 8.1, 1.7 Hz, 1H), 7.20 (d, *J* = 8.6 Hz, 2H), 7.42 (d, *J* = 7.3 Hz, 1H), 7.49 (d, *J* = 8.6 Hz, 1H), 7.56 (d, *J* = 8.5 Hz, 2H), 7.64 (t, *J* = 6.0 Hz, 1H), 7.77 (dd, *J* = 8.5, 7.3 Hz, 1H), 11.12 (s, 1H). ^{13}C NMR (151 MHz, d^{6}-DMSO) δ_{ppm} 10.6, 11.3, 22.0, 25.0, 26.1, 27.0, 28.4, 28.6, 29.2, 31.0, 31.8, 38.1, 40.1, 45.2, 48.7, 52.8, 52.9, 55.7, 57.1, 61.3, 65.7, 68.7, 110.3, 114.3, 115.2, 116.2, 116.7, 118.9, 119.8, 122.6, 122.7, 129.4, 133.1, 133.3, 134.5, 137.1, 155.6, 156.0, 157.1, 158.4, 164.6, 165.3, 166.9, 168.9, 170.0, 172.8. LCMS (5-95 MeCN in 5 mins) ^{t}R = 3.69 min, Purity = 97%, m/z = 972.5 $[M + H]^+$. HR-MS (m/z): $[M + H]^+$ calculated for $C_{54}H_{70}N_9O_8$, 972.5347; found, 972.5416.

2-(4-(2-(2-(4-(3-(dimethylamino)propoxy)phenethyl)-5-(3,5-dimethylisoxazol-4-yl)-1*H*-benzo[d]imidazol-1-yl)ethyl)piperazin-1-yl)-*N*-(2-(2-((2-(2,6-dioxopiperidin-3-yl)-1,3-dioxoisoindolin-4-yl)oxy)acetamido)ethyl)acetamide (**4.65**)

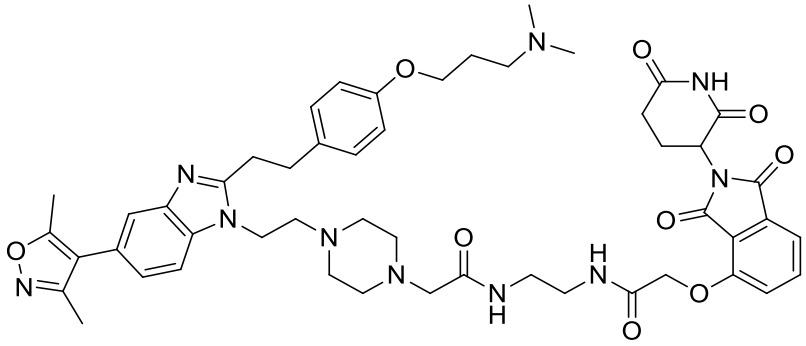

Degrader **4.65** was synthesised according to General Procedure F and the crude material was then purified using column chromatography (300 mm × 25 mm, using 120 mm × 25 mm silica) using 250 mL (2% 7N NH_3 methanol, to 6% 7N NH_3 methanol) in dichloromethane increasing by 1% per 250 mL. The white foam was then freeze dried overnight to result in **4.65** as a white solid (34 mg, 0.036 mmol, 16%). ^{1}H NMR (600 MHz, d^6-DMSO) δ_{ppm} 1.84 (p, *J* = 6.6 Hz, 2H), 1.90 – 2.03 (m, 2H), 2.22 (d, *J* = 13.6 Hz, 8H), 2.40 (s, 11H), 2.53 – 2.62 (m, 2H), 2.78 – 2.91 (m, 4H), 3.08 – 3.24 (m, 12H), 3.94 (t, *J* = 6.4 Hz, 2H), 4.20 – 4.25 (m, 2H), 4.75 (s, 2H), 5.11 (dd, *J* = 12.9, 5.5 Hz, 1H), 6.84 (d, *J* = 8.5 Hz, 2H), 7.14 – 7.23 (m, 4H), 7.37 (d, *J* = 8.6 Hz, 1H), 7.47 (d, *J* = 7.3 Hz, 1H), 7.53 – 7.57 (m, 2H), 7.76 – 7.80 (m, 1H), 8.05 (t, *J* = 5.6 Hz, 1H), 11.14 (s, 1H). ^{13}C NMR (151 MHz, d^6-DMSO) δ_{ppm} 10.6, 11.4, 22.0, 28.6, 31.0, 31.8, 38.1, 38.3, 40.1, 44.9, 48.8, 52.9, 52.9, 55.5, 57.1, 61.2, 65.4, 65.6, 67.6, 110.3, 114.3, 114.4, 116.1, 116.7, 116.8, 118.9, 122.6, 122.7, 129.4, 129.5, 133.1, 133.1, 134.5, 137.0, 142.6, 155.1, 155.6, 157.0, 158.4, 164.6, 165.5, 166.8, 167.2, 169.5, 169.9, 172.8. LCMS (5-95 MeCN in 5 mins) ^{t}R = 3.17 min, Purity = >99%, m/z = 945.4 $[M + H]^+$. HR-MS (m/z): $[M + H]^+$ calculated for $C_{50}H_{61}N_{10}O_9$, 945.4623; found, 945.4614.

2-(4-(2-(2-(4-(3-(dimethylamino)propoxy)phenethyl)-5-(3,5-dimethylisoxazol-4-yl)-1*H*-benzo[d]imidazol-1-yl)ethyl)piperazin-1-yl)-*N*-(4-(2-((2-(2,6-dioxopiperidin-3-yl)-1,3-dioxoisoindolin-4-yl)oxy)acetamido)butyl)acetamide (**4.66**)

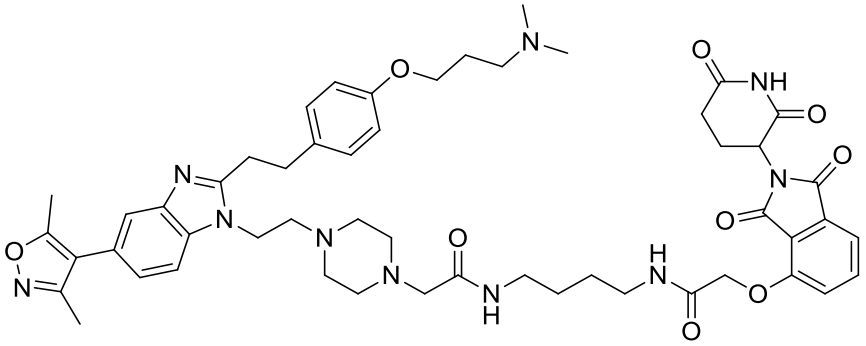

Degrader **4.66** was synthesised according to General Procedure F and the crude material was then purified using column chromatography (300 mm × 25 mm, using 120 mm × 25 mm silica) using 250 mL (2% 7N NH_3 methanol, to 6% 7N NH_3 methanol) in dichloromethane increasing by 1% per 250 mL. The white foam was then freeze dried overnight to result in **4.66** as a white solid (72 mg, 0.074 mmol, 32%). ^{1}H NMR (600 MHz, d^6-DMSO) δ_{ppm} 1.37 (d, *J* = 3.5 Hz, 4H), 1.80 – 1.85 (m, 2H), 1.92 – 2.02 (m, 2H), 2.20 (d, *J* = 8.3 Hz, 9H), 2.38 (s, 5H), 2.43 (d, *J* = 12.9 Hz, 6H), 2.49 – 2.58 (m, 5H), 2.79 – 2.89 (m, 4H), 2.94 – 3.17 (m, 13H), 3.92 (t, *J* = 6.4 Hz, 2H), 4.23 (d, *J* = 6.5 Hz, 2H), 4.51 – 4.67 (m, 1H), 4.74 (s, 2H), 5.09 (dd, *J* = 12.9, 5.5 Hz, 1H), 6.82 (d, *J* = 8.6 Hz, 2H), 7.14 (d, *J* = 8.3 Hz, 1H), 7.19 (t, *J* = 8.3 Hz, 3H), 7.34 (d, *J* = 8.6 Hz, 1H), 7.45 (d, *J* = 7.3 Hz, 1H), 7.53 (dd, *J* = 4.9, 3.2 Hz, 2H), 7.63 (t, *J* = 5.9 Hz, 1H), 7.75 – 7.79 (m, 1H), 7.96 (t, *J* = 5.7 Hz, 1H), 11.12 (s, 1H). ^{13}C NMR (151 MHz, d^6-DMSO) δ_{ppm} 10.6, 11.4, 22.0, 26.5, 26.7, 28.6, 31.0, 31.8, 37.9, 38.1, 40.1, 44.8, 48.8, 52.9, 52.9, 55.5, 57.1, 61.3, 65.6, 67.6, 110.3, 114.3, 116.1, 116.7, 116.8, 118.9, 120.4, 122.6, 122.7, 129.4, 133.1, 133.1, 134.5, 137.0, 142.6, 155.1, 155.6, 157.0, 158.4, 164.6, 165.5, 166.7, 166.8, 169.0, 169.9, 172.8, 173.0. LCMS (5-95 MeCN in 5 mins) ^{t}R = 3.262 min, Purity = >99.9%, m/z = 973.5 $[M + H]^+$. HR-MS (m/z): $[M + H]^+$ calculated for $C_{52}H_{65}N_{10}O_9$, 973.4936; found, 973.5108.

2-(4-(2-(2-(4-(3-(dimethylamino)propoxy)phenethyl)-5-(3,5-dimethylisoxazol-4-yl)-1H-benzo[d]imidazol-1-yl)ethyl)piperazin-1-yl)-*i*-(6-(2-((2-(2,6-dioxopiperidin-3-yl)-1,3-dioxoisoindolin-4-yl)oxy)acetamido)hexyl)acetamide (**4.67**)

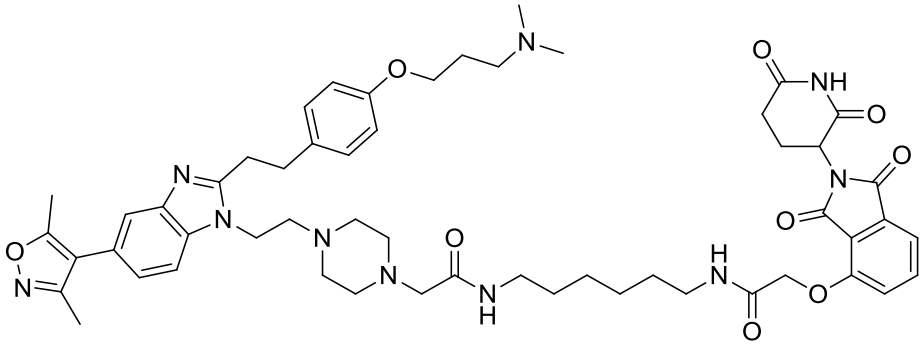

Degrader **4.67** was synthesised according to General Procedure F and the crude material was then purified using column chromatography (300 mm × 25 mm, using 120 mm × 25 mm silica) using 250 mL (2% 7N NH_3 methanol, to 6% 7N NH_3 methanol) in dichloromethane increasing by 1% per 250 mL. The white foam was then freeze dried overnight to result in **4.67** as a white solid (97 mg, 0.097 mmol, 43%). ^{1}H NMR (600 MHz, d^6-DMSO) δ_{ppm} 1.18 – 1.27 (m, 5H), 1.39 (dt, *J* = 23.4, 7.0 Hz, 5H), 1.82 (p, *J* = 6.7 Hz, 2H), 2.02 (dd, *J* = 12.7, 5.5 Hz, 1H), 2.16 (s, 6H), 2.23 (s, 3H), 2.32 – 2.39 (m, 6H), 2.40 (s, 3H), 2.53 (t, *J* = 7.1 Hz, 4H), 2.58 (dd, *J* = 17.1, 4.4 Hz, 2H), 3.94 (t, *J* = 6.4 Hz, 2H), 4.25 (t, *J* = 6.4 Hz, 2H), 4.76 (s, 2H), 5.09 – 5.14 (m, 1H), 6.84 (d, *J* = 8.6 Hz, 2H), 7.16 (dd, *J* = 8.3, 1.6 Hz, 1H), 7.21 (d, *J* = 8.6 Hz, 2H), 7.37 (d, *J* = 8.5 Hz, 1H), 7.48 (d, *J* = 7.3 Hz, 1H), 7.56 (dd, *J* = 5.0, 3.2 Hz, 2H), 7.63 (t, *J* = 6.0 Hz, 1H), 7.78 – 7.81 (m, 1H), 7.94 (t, *J* = 5.8 Hz, 1H), 11.14 (s, 1H). ^{13}C NMR (151 MHz, d^6-DMSO) δ_{ppm} 10.6, 11.3, 22.0, 26.0, 26.1, 26.8, 28.6, 29.0, 29.2, 31.0, 31.8, 38.1, 38.2, 40.1, 45.0, 48.8, 52.8, 52.9, 55.6, 57.1, 61.3, 65.6, 67.6, 110.3, 114.3, 116.1, 116.7, 116.8, 118.9, 120.4, 122.6, 122.7, 129.4, 133.0, 133.1, 134.5, 137.0, 142.6, 155.1, 157.0, 158.4, 164.6, 165.5, 166.6, 166.8, 168.9, 169.9, 172.8. LCMS (5-95 MeCN in 5 mins) ^{t}R = 3.341 min, Purity = >99.9%, m/z = 1001.2 $[M + H]^+$. HR-MS (m/z): $[M + H]^+$ calculated for $C_{54}H_{69}N_{10}O_9$, 1001.5249; found, 1001.5238.

2-(4-(2-(2-(4-(3-(dimethylamino)propoxy)phenethyl)-5-(3,5-dimethylisoxazol-4-yl)-1H-benzo[*d*]imidazol-1-yl)ethyl)piperazin-1-yl)-*N*-(8-(2-((2-(2,6-dioxopiperidin-3-yl)-1,3-dioxoisoindolin-4-yl)oxy)acetamido)octyl)acetamide (**4.68**)

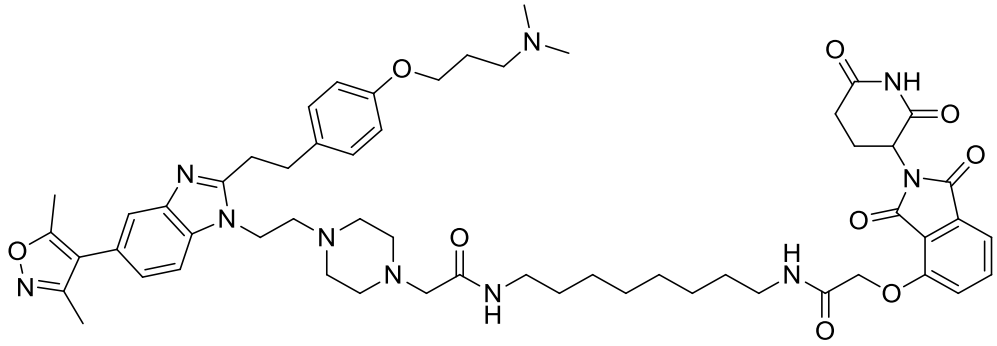

Degrader **4.68** was synthesised according to General Procedure F and the crude material was then purified using column chromatography (300 mm × 25 mm, using 120 mm × 25 mm silica) using 250 mL (2% 7N NH_3 methanol, to 6% 7N NH_3 methanol) in dichloromethane increasing by 1% per 250 mL. The white foam was then freeze dried overnight to result in **4.68** as a white solid (48 mg, 0.047 mmol, 20%). ^{1}H NMR (600 MHz, d^6-DMSO) δ_{ppm} 1.20 (s, 10H), 1.37 (dt, *J* = 24.3, 6.4 Hz, 4H), 1.81 (p, *J* = 6.6 Hz, 2H), 1.98 – 2.03 (m, 1H), 2.16 (s, 6H), 2.21 (s, 4H), 2.38 (s, 10H), 2.50 – 2.59 (m, 6H), 2.82 (s, 2H), 2.84 – 2.91 (m, 1H), 3.02 – 3.05 (m, 2H), 3.11 (dq, *J* = 27.6, 6.7 Hz, 8H), 3.92 (t, *J* = 6.4 Hz, 2H), 4.23 (t, *J* = 6.4 Hz, 2H), 5.10 (dd, *J* = 12.9, 5.5 Hz, 1H), 6.82 (d, *J* = 8.5 Hz, 2H), 7.14 (dd, *J* = 8.3, 1.6 Hz, 1H), 7.19 (d, *J* = 8.6 Hz, 2H), 7.36 (d, *J* = 8.5 Hz, 1H), 7.47 (d, *J* = 7.2 Hz, 1H), 7.54 (dd, *J* = 5.0, 3.2 Hz, 2H), 7.60 (t, *J* = 5.9 Hz, 1H), 7.78 (dd, *J* = 8.5, 7.3 Hz, 1H), 7.92 (t, *J* = 5.8 Hz, 1H), 11.12 (s, 1H). ^{13}C NMR (151 MHz, d^6-DMSO) δ_{ppm} 10.6, 11.3, 22.0, 26.3, 26.7, 28.6, 28.7, 29.0, 29.2, 31.0, 31.8, 38.1, 38.3, 40.1, 45.0, 48.8, 52.8, 53.0, 55.6, 57.1, 61.3, 65.6, 67.6, 110.3, 114.3, 116.1, 116.7, 116.8, 118.9, 120.4, 122.6, 122.7, 129.4, 133.0, 133.1, 134.5, 136.9, 142.6, 155.1, 155.6, 157.0, 158.4, 164.6, 165.5, 166.6, 166.8, 168.8, 169.9, 172.8. LCMS (5-95 MeCN in 5 mins) ^{t}R = 3.478 min, Purity = 95%, m/z = 1029.5 $[M + H]^+$. HR-MS (m/z): $[M + H]^+$ calculated for $C_{56}H_{73}N_{10}O_9$, 1029.5562; found, 1029.5603.

(2*S*,4*R*)-1-((*S*)-2-(3-(2-(4-(2-(2-(4-(3-(Dimethylamino)propoxy)phenethyl)-5-(3,5-dimethylisoxazol-4-yl)-1*H*-benzo[d]imidazol-1-yl)ethyl)piperazin-1-yl)acetamido)propanamido)-3,3-dimethylbutanoyl)-4-hydroxy-*N*-(4-(4-methylthiazol-5-yl)benzyl)pyrrolidine-2-carboxamide (**4.69**)

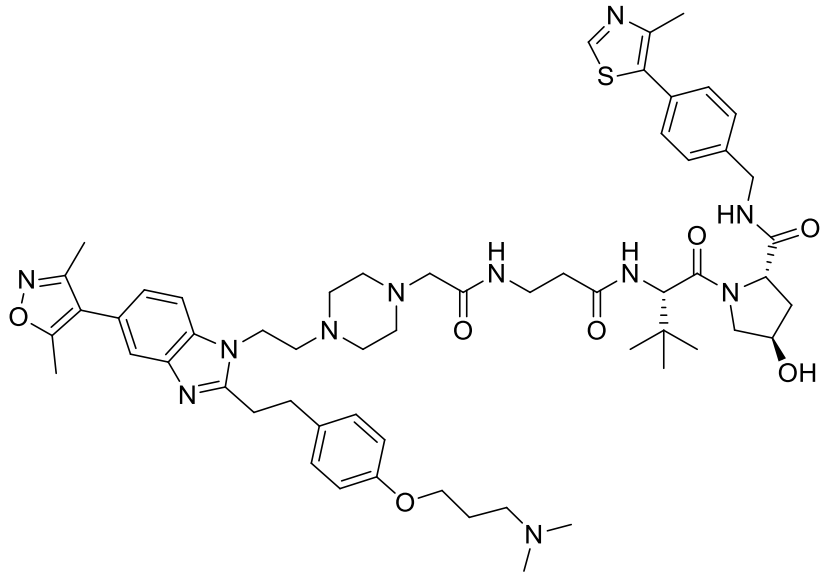

Degrader **4.69** was synthesised according to General Procedure F and the crude material was then purified using column chromatography (300 mm × 25 mm, using 120 mm × 25 mm silica) using 250 mL (3% 7N NH_3 methanol, to 7% 7N NH_3 methanol) in dichloromethane increasing by 1% per 250 mL. The white foam was then freeze dried overnight to result in **4.69** as a white solid (96 mg, 0.090 mmol, 39%). ^{1}H NMR (600 MHz, d^6-DMSO) δ_{ppm} 0.90 (s, 9H), 1.79 (p, *J* = 6.7 Hz, 2H), 1.85 – 1.90 (m, 1H), 2.11 (s, 6H), 2.21 (s, 3H), 2.31 (d, *J* = 7.1 Hz, 3H), 2.40 (d, *J* = 21.0 Hz, 10H), 2.52 – 2.55 (m, 2H), 2.77 – 2.85 (m, 2H), 3.07 – 3.11 (m, 2H), 3.15 (t, *J* = 6.9 Hz, 2H), 3.22 – 3.29 (m, 2H), 3.60 (d, *J* = 10.6 Hz, 1H), 3.64 (dd, *J* = 10.5, 4.1 Hz, 1H), 3.92 (t, *J* = 6.4 Hz, 2H), 4.19 (dd, *J* = 15.9, 5.5 Hz, 1H), 4.24 (t, *J* = 6.4 Hz, 2H), 4.32 (s, 1H), 4.39 – 4.44 (m, 2H), 4.52 (d, *J* = 9.3 Hz, 1H), 5.14 (d, *J* = 3.6 Hz, 1H), 6.82 (d, *J* = 8.6 Hz, 2H), 7.14 (dd, *J* = 8.2, 1.6 Hz, 1H), 7.19 (d, *J* = 8.5 Hz, 2H), 7.36 (d, *J* = 8.2 Hz, 2H), 7.40 (d, *J* = 8.2 Hz, 2H), 7.54 (dd, *J* = 4.9, 3.2 Hz, 2H), 7.62 (t, *J* = 6.0 Hz, 1H), 8.00 (d, *J* = 9.3 Hz, 1H), 8.57 (t, *J* = 6.1 Hz, 1H), 8.96 (s, 1H). ^{13}C NMR (151 MHz, d^6-DMSO) δ_{ppm} 10.6, 11.4, 16.0, 26.4, 27.0, 28.6, 31.8, 34.7, 35.0, 35.3, 38.0, 40.1, 40.8, 41.7, 45.2, 52.9, 53.0, 55.7, 56.4, 57.1, 61.2, 65.7, 68.9, 110.3, 114.3, 116.7, 118.9, 122.6, 122.7, 127.4, 128.7, 129.4, 129.7, 131.2, 133.1, 134.5, 139.5, 142.6, 147.7, 151.5, 155.6, 157.1, 158.4, 164.6, 168.9, 169.5, 170.5, 172.0. LCMS (5-95 MeCN in 5 mins) ^{t}R = 3.405 min, Purity = 98%, m/z = 1072.6 $[M + H]^+$. HR-MS (m/z): $[M + H]^+$ calculated for $C_{58}H_{78}N_{11}O_7S$, 1072.5806; found, 1072.5883.

(2*S*,4*R*)-1-((*S*)-2-(5-(2-(4-(2-(2-(4-(3-(Dimethylamino)propoxy)phenethyl)-5-(3,5-dimethylisoxazol-4-yl)-1*H*-benzo[d]imidazol-1-yl)ethyl)piperazin-1-yl)acetamido)pentanamido)-3,3-dimethylbutanoyl)-4-hydroxy-*N*-(4-(4-methylthiazol-5-yl)benzyl)pyrrolidine-2-carboxamide (**4.70**)

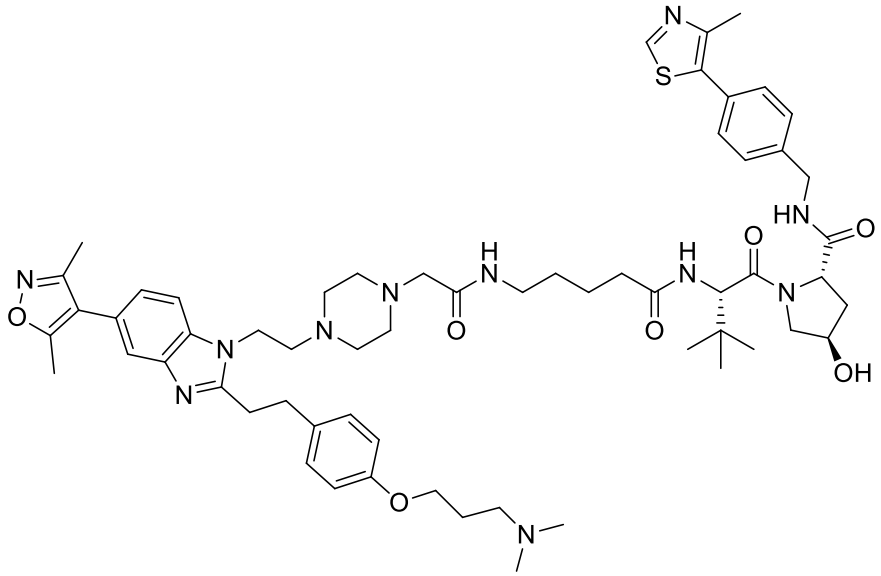

Degrader **4.70** was synthesised according to General Procedure F and the crude material was then purified using column chromatography (300 mm × 25 mm, using 120 mm × 25 mm silica) using 250 mL (3% 7N NH_3 methanol, to 7% 7N NH_3 methanol) in dichloromethane increasing by 1% per 250 mL. The white foam was then freeze dried overnight to result in **4.70** as a white solid (55 mg, 0.050 mmol, 22%). ^{1}H NMR (600 MHz, d^6-DMSO) δ_{ppm} 0.90 (s, 9H), 1.40 (dq, *J* = 52.0, 7.1 Hz, 4H), 1.80 (q, *J* = 6.8 Hz, 2H), 1.85 – 1.90 (m, 1H), 2.01 (t, *J* = 10.6 Hz, 1H), 2.05 – 2.09 (m, 1H), 2.10 (s, 6H), 2.21 (s, 3H), 2.26 (dd, *J* = 14.3, 7.2 Hz, 2H), 2.30 (t, *J* = 7.1 Hz, 2H), 2.38 (s, 3H), 2.42 (s, 3H), 2.53 (t, *J* = 6.4 Hz, 2H), 2.82 (s, 2H), 3.04 (q, *J* = 6.6 Hz, 2H), 3.10 (d, *J* = 8.4 Hz, 2H), 3.15 (t, *J* = 6.9 Hz, 2H), 3.59 – 3.66 (m, 2H), 3.92 (t, *J* = 6.4 Hz, 2H), 4.19 (dd, *J* = 15.9, 5.4 Hz, 1H), 4.23 (t, *J* = 6.5 Hz, 2H), 4.32 (s, 1H), 4.41 (dt, *J* = 16.1, 7.2 Hz, 2H), 4.52 (d, *J* = 9.4 Hz, 1H), 5.13 (d, *J* = 3.6 Hz, 1H), 6.82 (d, *J* = 8.6 Hz, 2H), 7.14 (dd, *J* = 8.3, 1.5 Hz, 1H), 7.19 (d, *J* = 8.6 Hz, 2H), 7.36 (d, *J* = 8.2 Hz, 2H), 7.40 (d, *J* = 8.2 Hz, 2H), 7.53 – 7.55 (m, 2H), 7.64 (t, *J* = 6.0 Hz, 1H), 7.86 (d, *J* = 9.4 Hz, 1H), 8.57 (t, *J* = 6.1 Hz, 1H), 8.96 (s, 1H). ^{13}C NMR (151 MHz, d^6-DMSO) δ_{ppm} 10.6, 11.3, 16.0, 22.9, 26.4, 27.0, 28.6, 29.0, 31.8, 34.6, 35.3, 37.9, 38.0, 40.1, 41.6, 45.3, 52.9, 53.0, 55.7, 56.3, 56.4, 57.1, 58.7, 61.3, 65.7, 68.9, 110.3, 114.3, 116.7, 118.9, 122.6, 122.7, 127.4, 128.7, 129.4, 129.6, 131.2, 133.1, 134.5, 139.5, 142.6, 147.7, 151.5, 155.6, 157.1, 158.4, 164.6, 168.9, 169.7, 172.0. LCMS (5-95 MeCN in 5 mins) ^{t}R = 3.562 min, Purity = 96%, m/z = 1100.6 $[M + H]^+$. HR-MS (m/z): $[M + H]^+$ calculated for $C_{60}H_{82}N_{11}O_7S$, 1100.6119; found, 1100.6189.

(2*S*,4*R*)-1-((S)-2-(7-(2-(4-(2-(2-(4-(3-(dimethylamino)propoxy)phenethyl)-5-(3,5-dimethylisoxazol-4-yl)-1*H*-benzo[d]imidazol-1-yl)ethyl)piperazin-1-yl)acetamido)heptanamido)-3,3-dimethylbutanoyl)-4-hydroxy-*N*-(4-(4-methylthiazol-5-yl)benzyl)pyrrolidine-2-carboxamide (**4.71**)

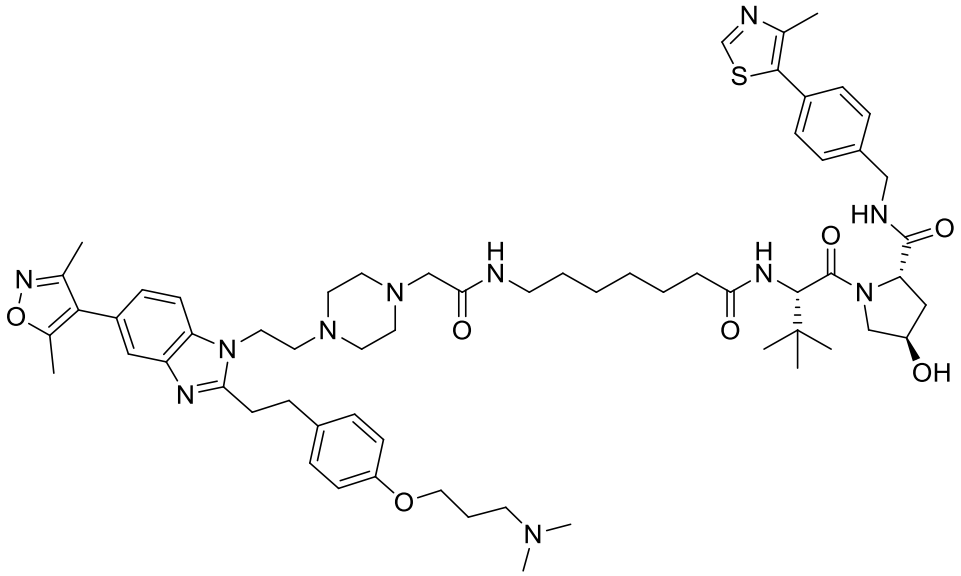

Degrader **4.71** was synthesised according to General Procedure F and the crude material was then purified using column chromatography (300 mm × 25 mm, using 120 mm × 25 mm silica) using 250 mL (3% 7N NH_3 methanol, to 7% 7N NH_3 methanol) in dichloromethane increasing by 1% per 250 mL. The white foam was then freeze dried overnight to result in **4.71** as a white solid (93 mg, 0.082 mmol, 36%). ^{1}H NMR (600 MHz, d^6-DMSO) δ_{ppm} 0.90 (s, 9H), 1.20 (d, *J* = 3.8 Hz, 4H), 1.35 (t, *J* = 7.0 Hz, 2H), 1.39 – 1.49 (m, 2H), 1.79 (p, *J* = 6.7 Hz, 2H), 1.85 – 1.89 (m, 1H), 1.99 (d, *J* = 8.2 Hz, 1H), 2.05 – 2.09 (m, 1H), 2.10 (s, 6H), 2.21 (s, 3H), 2.23 (t, *J* = 7.2 Hz, 1H), 2.30 (t, *J* = 7.1 Hz, 3H), 2.38 (s, 3H), 2.42 (s, 3H), 2.52 (t, *J* = 6.5 Hz, 2H), 2.82 (s, 2H), 3.02 (q, *J* = 6.7 Hz, 2H), 3.09 (t, *J* = 7.3 Hz, 2H), 3.13 – 3.16 (m, 2H), 3.59 – 3.66 (m, 2H), 3.92 (t, *J* = 6.4 Hz, 2H), 4.19 (dd, *J* = 15.9, 5.5 Hz, 1H), 4.24 (t, *J* = 6.4 Hz, 2H), 4.32 (s, 1H), 4.41 (dt, *J* = 16.2, 7.2 Hz, 2H), 4.52 (d, *J* = 9.4 Hz, 1H), 5.12 (s, 1H), 6.82 (d, *J* = 8.6 Hz, 2H), 7.14 (dd, *J* = 8.4, 1.5 Hz, 1H), 7.19 (d, *J* = 8.6 Hz, 2H), 7.36 (d, *J* = 8.3 Hz, 2H), 7.40 (d, *J* = 8.0 Hz, 2H), 7.54 (dd, *J* = 4.9, 3.2 Hz, 2H), 7.61 (t, *J* = 6.0 Hz, 1H), 7.85 (d, *J* = 9.4 Hz, 1H), 8.57 (t, *J* = 6.1 Hz, 1H), 8.96 (s, 1H). ^{13}C NMR (151 MHz, d^6-DMSO) δ_{ppm} 10.6, 11.3, 16.0, 25.4, 26.2, 26.4, 27.0, 28.4, 28.6, 29.1, 31.8, 34.8, 35.2, 38.0, 38.2, 40.1, 41.7, 45.3, 52.8, 53.0, 55.7, 56.3, 56.4, 57.1, 58.7, 61.3, 65.7, 68.9, 110.3, 114.3, 116.7, 118.9, 122.6, 122.7, 127.4, 128.7, 129.4, 129.6, 131.2, 133.1, 134.5, 139.5, 142.6, 147.7, 151.5, 155.6, 157.1, 158.4, 164.6, 168.9, 169.7, 172.0, 172.1. LCMS (5-95 MeCN in 5 mins) ^{t}R = 3.930 min, Purity= 97%, m/z = 1128.6 $[M + H]^+$. HR-MS (m/z): $[M + H]^+$ calculated for $C_{62}H_{86}N_{11}O_7S$, 1128.6432; found, 1128.6401.

(2*S*,4*R*)-1-((S)-2-(9-(2-(4-(2-(2-(4-(3-(dimethylamino)propoxy)phenethyl)-5-(3,5-dimethylisoxazol-4-yl)-1*H*-benzo[d]imidazol-1-yl)ethyl)piperazin-1-yl)acetamido)nonanamido)-3,3-dimethylbutanoyl)-4-hydroxy-*N*-(4-(4-methylthiazol-5-yl)benzyl)pyrrolidine-2-carboxamide (**4.72**)

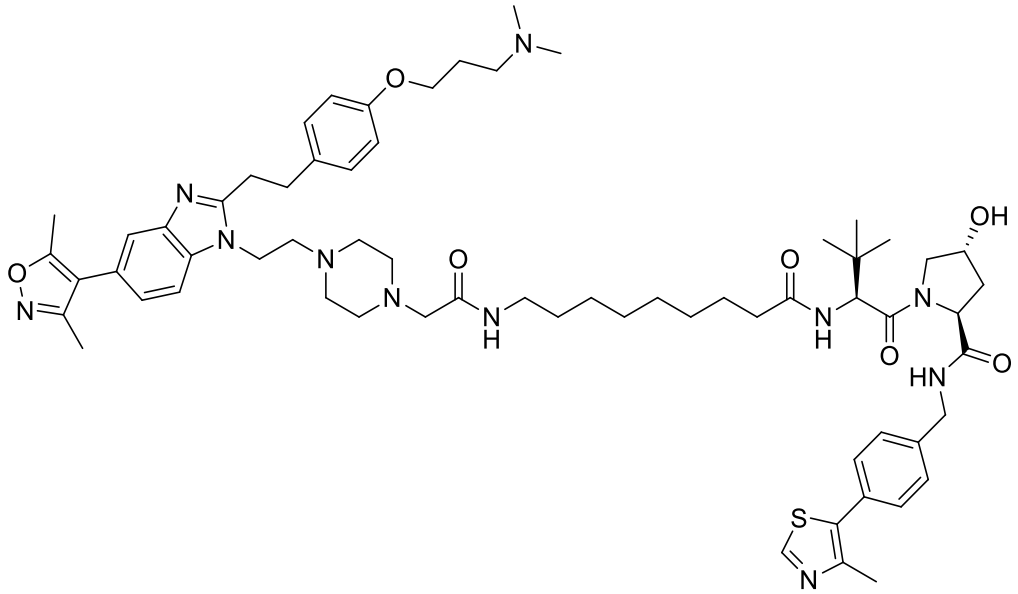

Degrader **4.72** was synthesised according to General Procedure F and the crude material was then purified using column chromatography (300 mm × 25 mm, using 120 mm × 25 mm silica) using 250 mL (3% 7N NH_3 methanol, to 7% 7N NH_3 methanol) in dichloromethane increasing by 1% per 250 mL. The white foam was then freeze dried overnight to result in **4.74** as a white solid (91 mg, 0.079 mmol, 35%). ^{1}H NMR (600 MHz, d^6-DMSO) δ_{ppm} 0.92 (s, 9H), 1.22 (s, 9H), 1.35 – 1.52 (m, 5H), 1.81 (p, *J* = 6.7 Hz, 2H), 1.89 (dd, *J* = 21.4, 4.6 Hz, 1H), 2.00 – 2.04 (m, 1H), 2.12 (s, 6H), 2.23 (s, 4H), 2.32 (t, *J* = 7.1 Hz, 6H), 2.40 (s, 3H), 2.44 (s, 3H), 2.45 (s, 2H), 2.54 (t, *J* = 6.4 Hz, 3H), 2.83 (s, 2H), 3.04 (q, *J* = 6.7 Hz, 2H), 3.11 (d, *J* = 9.0 Hz, 2H), 3.16 (t, *J* = 7.8 Hz, 2H), 3.61 – 3.67 (m, 2H), 3.94 (t, *J* = 6.4 Hz, 2H), 4.18 – 4.27 (m, 4H), 4.34 (s, 1H), 4.39 – 4.45 (m, 2H), 4.53 (d, *J* = 9.4 Hz, 1H), 5.14 (d, *J* = 3.5 Hz, 1H), 6.84 (d, *J* = 8.6 Hz, 2H), 7.16 (d, *J* = 8.3 Hz, 1H), 7.20 (d, *J* = 8.5 Hz, 2H), 7.38 (d, *J* = 8.3 Hz, 2H), 7.41 (d, *J* = 8.0 Hz, 2H), 7.54 – 7.57 (m, 2H), 7.62 (t, *J* = 6.0 Hz, 1H), 7.86 (d, *J* = 9.4 Hz, 1H), 8.58 (t, *J* = 6.2 Hz, 1H), 8.98 (s, 1H). ^{13}C NMR (151 MHz, d^6-DMSO) δ_{ppm} 10.6, 11.3, 16.0, 25.5, 26.4, 27.0, 28.7, 28.7, 29.2, 31.8, 34.9, 35.2, 38.0, 38.2, 40.1, 41.6, 45.3, 52.8, 53.0, 55.7, 56.3, 56.4, 57.1, 58.7, 61.3, 65.7, 68.9, 110.3, 114.3, 116.7, 118.9, 122.6, 122.7, 127.4, 128.7, 129.4, 129.6, 131.2, 133.1, 134.5, 139.5, 142.6, 147.7, 151.5, 155.6, 157.1, 158.4, 164.6, 168.8, 169.7, 172.0, 172.1. LCMS (5-95 MeCN in 5 mins) ^{t}R = 4.271 min, Purity = 87%, m/z = 1156.6 $[M + H]^+$. HR-MS (m/z): $[M + H]^+$ calculated for $C_{64}H_{90}N_{11}O_7S$, 1156.6745; found, 1156.6660.

6.3.3 **Cell Culture and Immunoblotting**

Experimental 6.3.3.1 and 6.3.3.2 were performed by collaborators within Bio-Techne.

6.3.3.1 Cell Culture

HeLa cells (ATCC CCL-2) were obtained from the ATCC and cultured in EMEM medium with 10% FBS per supplier recommendation. HCT-116 cells (ATCC CCL-247) were obtained from the ATCC and cultured in McCoy's 5a Medium Modified with 10% FBS per supplier recommendation. HDLM-2 cells (#ACC 17) were obtained from DSMZ and cultured per supplier recommendation. All cell lines were cultured at 37 ˚C with 5% CO_2.

6.3.3.2 Immunoassays (R&D Systems)

For immunoassays, cells were plated into 6-well plates, followed by overnight incubation before treatment with compounds. Cells were harvested using either RIPA buffer (R&D Systems in-house) with Halt Protease and phosphatase cocktail (Thermo Scientific #78440) or by boiling in 1% SDS (R&D Systems in-house).

Using the RIPA method, the media was aspirated and washed twice with 1x PBS (Gibco 14190144). This was aspirated before the addition of 100-200 µL of RIPA buffer with inhibitors. Cells were then scraped and transferred to 1.5 mL centrifuge tubes and incubated on ice for 15 mins. The lysates were centrifuged at 13,000 g for 20 mins at 4 ˚C, before the supernatant was collected into new micro-centrifuge tubes. Protein concentration was determined by BCA protein assay (Thermo Fischer Kit; 4PL standard curve). Lysates were stored at – 20 ˚C until immunoblotting.

Using the 1% SDS method, the media was aspirated and washed twice with 1x PBS. This was aspirated before the addition of 100-200 µL of boiling 1% SDS (diluted in 1x PBS) directly onto cells. Cells were then scraped and transferred to 1.5 mL centrifuge tubes before sonicating for 3 seconds until homogenous. Protein concentration was determines by BCA protein assay (Thermo Fischer Kit; 4PL standard curve). Lysates were stored at – 20 ˚C until immunoblotting.

Capillary-based immunoassays were performed using a standard WES (Simple Western) or JESS (Replex™, Simple Western). Lysates were loaded onto plates at 0.2 mg/mL total protein. Staining was performed using the following antibodies: BRD4 (CST #13440, 1:25 or Novus BRB4 for Replex™ runs), CBP (CST #7389, 1:25), p300 (CST #54062S, 1:25), c-Myc (AF3696, 20 µg/mL), PARP (AF600, 10 µg/mL) and HSP60 (R&D AF1800, 5 or 10 µg/mL), which was used as the loading control in certain assays. Total protein was used as the loading control when not HSP60.

6.3.3.3 Cell lines and Immunoblotting for Bristol placement

Neuroblastoma cell lines Be2c and SK-N-AS were obtained from ATCC and cultured as described by the vendor. The cell lines were cultured in Dulbecco's modified Eagle's medium (DMEM) mixture F12-HAM (Sigma) supplemented with 10% fetal bovine serum (FBS) (Life Technologies), 200 mM L- Glutamine (Sigma), 100 units/ml penicillin, 0.1 mg/mL streptomycin (Sigma) and 1% (v/v) non-essential amino acids (Life technologies). Be2c and SK-N-AS cells were processed separately in all steps of cell culturing. Cells were grown adherently in standard T-25 flasks at 37 ˚C with 5.0% CO_2 and passaged by trypsinization at ~75% confluency.

Whole cell lysates were prepared using RIPA lysis buffer (25mMTris-HCl pH 8.0, 150 mM NaCl, 1 mM EDTA, 0.2% SDS, 0.5% NP40 and 0.2% sodium deoxycholate) supplemented with protease and phosphatase inhibitors (Roche). Cells while in media were collected in 15 mL tubes, centrifuged at 2000 rpm for 5 min at 4 ˚C, media aspirated and cells washed with PBS. Lysis buffer was added and samples were sonicated (Diagenode bioruptor) and clarified at maximum speed at 4 ˚C for 20 min. Protein quantification was performed using the Micro BCA kit (Thermo Fischer Scientific) and proteins were resolved by SDS-PAGE and transferred to PVDF membranes (Millipore). Blots were developed using KPL LumiGLO Peroxidase Chemiluminescent substrate. Antibodies used were BRD4 (12183), cleaved caspase-3 (9664), c-Myc (18583), N-Myc (84406) from Cell Signalling Technology, cleaved PARP (ab32064) from Abcam and Actin (A3854) from Sigma.[381]

6.4 Chapter 5

6.4.1 General Comments

The amide HAT degraders (**5.04**-**5.06**) utilised Toolbox acid linkers obtained from Tocris, with catalogue numbers listed for each case. The diasteromer (*S*,*S*)-A485 (**5.03**) was obtained from Tocris, and used without further purification.

4-bromo-N^1-(2-morpholinoethyl)benzene-1,2-diamine (**5.01**)

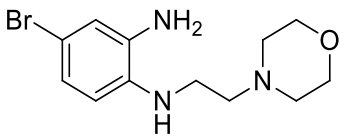

To a stirring suspension of **2.04** (1.7 g, 5.15 mmol, 1 eq.) in EtOH (100 mL), was added 1.0 M aq. $Na_2S_2O_4$ (100 mL) before heating to 80 ˚C for 1 hour. The reaction mixture was then cooled and partitioned between 10% aqueous NH_3 (100 mL), and EtOAc (100 mL). The phases were separated then the aqueous phase was extracted with EtOAc (4 × 50mL). The combined organic phases were washed with brine (2 × 200 mL), dried over $MgSO_4$, filtered and concentrated *in vacuo* to yield the product as a yellow gum (1.22 g, 4.07 mmol, 79%). ^{1}H NMR (600 MHz, $CDCl_3$) δ_{ppm} 2.48 (s, 4H), 2.67 (t, *J* = 5.9 Hz, 2H), 3.13 (t, *J* = 5.9 Hz, 2H), 3.45 (s, 2H), 3.72 (s, 4H), 6.49 (d, *J* = 8.4 Hz, 1H), 6.83 (s, 1H), 6.89 (d, *J* = 8.4 Hz, 1H).

3-(4-(2-(5-bromo-1-(2-morpholinoethyl)-1*H*-benzo[*d*]imidazol-2-yl)ethyl)phenoxy)-*N*,*N*-dimethylpropan-1-amine (**5.02**)

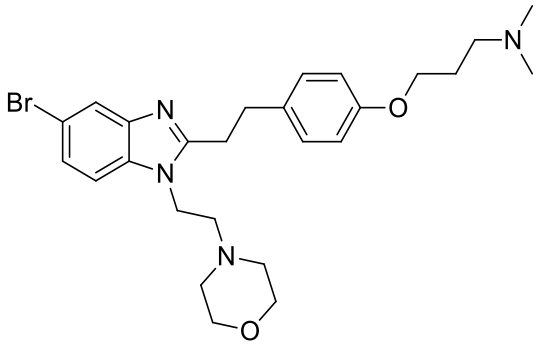

Compound **2.13** (1.16 g, 4.5 mmol, 1.1 eq.) was suspended in DMF (25 mL) before the addition of HATU (2.03 mg, 5.33 mmol, 1.3 eq.) and was left to stir at room temperature for 1 hour. A solution of **5.01** (1.22 g, 4.1 mmol, 1 eq.) in DMF (25 mL) was added to the stirring mixture before leaving overnight at room temperature. The reaction mixture was partitioned between dichloromethane (250 mL) and water (250 mL). The aqueous phase was then extracted with dichloromethane (3 × 50 mL). The combined organic phases were washed with saturated aqueous $NaHCO_3$ (100 mL), brine (100 mL), dried over $MgSO_4$, filtered, and concentrated *in vacuo*. The crude component was dissolved in AcOH (50 mL) and heated to reflux for 2 hours. The reaction mixture was then cooled, concentrated *in vacuo* and dichloromethane (50 mL) was added before neutralisation with saturated aqueous $NaHCO_3$. The organic phase was collected, and the aqueous phase was extracted with dichloromethane (4 × 50 mL), before being combined and washed with brine (250 mL), dried over $MgSO_4$, filtered, and concentrated *in vacuo*. The resultant crude product was purified *via* flash chromatography using 0 – 10% methanol (with 0.5% NH_4OH) in dichloromethane to afford the product as a yellow oil (1.55 g, 3 mmol, 74%).^{1}H NMR (600 MHz, $CDCl_3$) δ_{ppm} 2.10 (p, *J* = 6.3 Hz, 2H), 2.40 (s, 4H), 2.51 (s, 8H), 2.79 (t, *J* = 7.7 Hz, 2H), 3.10 – 3.20 (m, 4H), 3.63 (s, 4H), 4.01 (dt, *J* = 12.9, 6.4 Hz, 4H), 6.79 (d, *J* = 8.1 Hz, 2H), 7.09 (d, *J* = 8.0 Hz, 2H), 7.15 (d, *J* = 8.4 Hz, 1H), 7.33 (d, *J* = 8.5 Hz, 1H), 7.87 (s, 1H). ^{13}C NMR (151 MHz, $CDCl_3$) δ_{ppm} 15.4, 26.3, 30.0, 33.2, 41.7, 44.5, 54.1, 56.2, 57.6, 65.6, 66.0, 66.9, 110.5, 114.8, 115.1, 122.3, 125.2, 129.5, 133.3, 134.0, 144.2, 155.8, 157.4. HR-MS-ESI (m/z): $[M+H]^+$ calculated for $C_{26}H_{36}BrN_4O_2$, 515.2022; found, 515.2016.

6.4.2 **Synthesis of Degraders for the HAT Domain of CBP/p300**

5-((2-(2,6-dioxopiperidin-3-yl)-1,3-dioxoisoindolin-4-yl)amino)-N-((S)-3'-(2-((4-fluorobenzyl)((S)-1,1,1-trifluoropropan-2-yl)amino)-2-oxoethyl)-2',4'-dioxo-2,3-dihydrospiro[indene-1,5'-oxazolidin]-5-yl)pentanamide (**5.04**)

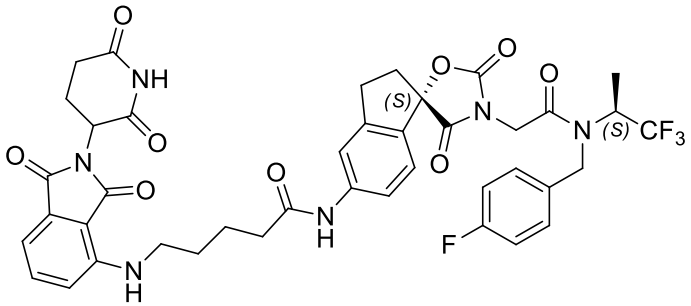

A solution of pomalidomide 4'-alkylC4-acid (#7209) (25 mg, 0.067 mmol, 1 eq.), HATU (33 mg, 0.087 mmol, 1.3 eq.), triethylamine (56 µL, 0.402 mmol, 6 eq.) and **5.03** (32 mg, 0.067 mmol, 1 eq.) in DMF (5 mL) was stirred overnight at room temperature. The reaction mixture was diluted with water (50 mL) and extracted with EtOAc (4 × 25 mL). The combined organic collections were washed with saturated $NaHCO_3$ (50 mL), brine (2 × 50 mL), dried over $MgSO_4$, filtered, and concentrated *in vacuo*. The crude product was then purified *via* Flash Chromatography using 0 – 5% methanol in dichloromethane to result in the product as a yellow solid (25 mg, 0.030 mmol, 45%).^{1}H NMR (600 MHz, $CDCl_3$) δ_{ppm} 0.88 (t, *J* = 6.9 Hz, 1H), 1.25 (s, 5H), 1.32 (d, *J* = 7.2 Hz, 4H), 1.41 (s, 1H), 1.72 (d, *J* = 7.7 Hz, 3H), 1.83 (t, *J* = 7.8 Hz, 3H), 2.08 – 2.15 (m, 1H), 2.39 (t, *J* = 7.4 Hz, 3H), 2.54 (d, *J* = 9.8 Hz, 1H), 2.80 (s, 10H), 2.88 (d, *J* = 14.9 Hz, 2H), 3.04 – 3.12 (m, 1H), 3.20 (dt, *J* = 15.3, 7.3 Hz, 1H), 3.30 (d, *J* = 6.7 Hz, 3H), 4.19 (d, *J* = 16.4 Hz, 1H), 4.43 (d, *J* = 16.4 Hz, 1H), 4.68 (q, *J* = 18.4 Hz, 2H), 4.88 – 4.93 (m, 1H), 5.49 (t, *J* = 7.9 Hz, 1H), 6.23 (s, 1H), 6.86 (d, *J* = 8.5 Hz, 1H), 7.06 (d, *J* = 7.1 Hz, 1H), 7.09 – 7.18 (m, 4H), 7.29 (t, *J* = 6.9 Hz, 2H), 7.37 (d, *J* = 8.4 Hz, 1H), 7.47 (t, *J* = 7.9 Hz, 1H), 7.57 (s, 1H), 7.78 (s, 1H), 8.23 (s, 1H). ^{13}C NMR (151 MHz, $CDCl_3$) δ_{ppm} 11.7, 22.9 (d, *J* = 8.8 Hz), 28.7, 29.8, 30.5, 31.5, 31.7, 35.6, 37.2, 38.8, 41.8, 42.4, 46.2, 49.0, 50.6 (d, *J* = 31.8 Hz), 94.7, 110.0, 111.7, 116.0, 116.5 (d, *J* = 21.8 Hz), 116.8, 119.2, 125.0, 127.3 (d, *J* = 8.0 Hz), 131.5, 132.5, 136.4, 140.7, 146.8, 146.9, 154.5, 161.6, 163.3, 167.1, 167.7, 168.8, 169.7, 171.1, 171.3, 174.2. LC-MS (5-95 MeCN in 20 mins) ^tR = 21.01 min, Purity = 96%, m/z = 857.35 $[M + Na]^+$. HR-MS-ESI (m/z): $[M+H]^+$ calculated for $C_{41}H_{39}F_4N_6O_9$, 835.2715; found, 835.2714.

7-((2-(2,6-dioxopiperidin-3-yl)-1,3-dioxoisoindolin-4-yl)amino)-N-((S)-3'-(2-((4-fluorobenzyl)((S)-1,1,1-trifluoropropan-2-yl)amino)-2-oxoethyl)-2',4'-dioxo-2,3-dihydrospiro[indene-1,5'-oxazolidin]-5-yl)heptanamide (**5.05**)

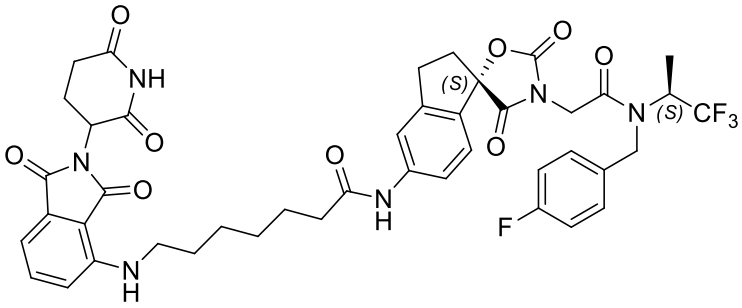

A solution of pomalidomide 4'-alkylC6-acid (#7210) (25 mg, 0.061 mmol, 1 eq.), HATU (30 mg, 0.079 mmol, 1.3 eq.), triethylamine (51 µL, 0.365 mmol, 6 eq.) and **5.03** (29 mg, 0.061 mmol, 1 eq.) in DMF (5 mL) was stirred overnight at room temperature. The reaction mixture was diluted with water (50 mL) and extracted with EtOAc (4 × 25 mL). The combined organic collections were washed with saturated $NaHCO_3$ (50 mL), brine (2 × 50 mL), dried over $MgSO_4$, filtered and concentrated *in vacuo*. The crude product was then purified *via* Flash Chromatography using 0 – 5% methanol in dichloromethane to result in the product as a yellow solid (30 mg, 0.034 mmol, 57%).^{1}H NMR (600 MHz, $CDCl_3$) δ_{ppm} 0.87 (t, *J* = 7.0 Hz, 2H), 1.23 – 1.33 (m, 7H), 1.39 – 1.48 (m, 5H), 1.70 (dq, *J* = 45.0, 7.2 Hz, 4H), 2.11 (dd, *J* = 13.5, 3.9 Hz, 1H), 2.34 (t, *J* = 7.4 Hz, 2H), 2.49 – 2.55 (m, 1H), 2.68 – 2.83 (m, 3H), 2.87 (d, *J* = 16.5 Hz, 1H), 3.06 – 3.12 (m, 1H), 3.18 – 3.29 (m, 3H), 4.19 (d, *J* = 16.4 Hz, 1H), 4.42 (d, *J* = 16.5 Hz, 1H), 4.67 (q, *J* = 18.5 Hz, 2H), 4.89 (dd, *J* = 12.8, 4.9 Hz, 1H), 5.48 (p, *J* = 7.6 Hz, 1H), 6.21 (t, *J* = 5.6 Hz, 1H), 6.86 (d, *J* = 8.5 Hz, 1H), 7.06 (d, *J* = 7.1 Hz, 1H), 7.09 – 7.16 (m, 3H), 7.29 (dd, *J* = 8.5, 5.0 Hz, 2H), 7.37 (d, *J* = 8.4 Hz, 1H), 7.42 – 7.48 (m, 2H), 7.79 (s, 1H), 8.09 (s, 1H).^{13}C NMR (151 MHz, $CDCl_3$) δ_{ppm} 11.7, 14.3, 22.8, 22.9, 25.2, 26.6, 28.8 (d, *J* = 20.3 Hz), 29.8, 30.5, 31.5, 31.7, 35.6, 37.5, 41.8, 42.6, 46.2, 49.0, 50.6 (d, *J* = 30.6 Hz), 94.7, 109.8, 111.6, 116.1, 116.5 (d, *J* = 21.8 Hz), 116.9, 119.2, 124.4, 125.0, 126.3, 127.3 (d, *J* = 8.1 Hz), 131.5, 132.5, 136.3, 140.7, 146.8, 147.1, 154.5, 161.6, 163.3, 167.1, 167.7, 168.8, 169.7, 171.2, 171.6, 174.2. LC-MS (5-95 MeCN in 20 mins) ^{t}R = 1.63 min, Purity = 94%, m/z = 863.25. HR-MS-ESI (m/z): $[M+H]^+$ calculated for $C_{43}H_{43}F_4N_6O_9$, 863.3028; found, 863.3048.

9-((2-(2,6-dioxopiperidin-3-yl)-1,3-dioxoisoindolin-4-yl)amino)-N-((S)-3'-(2-((4-fluorobenzyl)((S)-1,1,1-trifluoropropan-2-yl)amino)-2-oxoethyl)-2',4'-dioxo-2,3-dihydrospiro[indene-1,5'-oxazolidin]-5-yl)nonanamide (**5.06**)

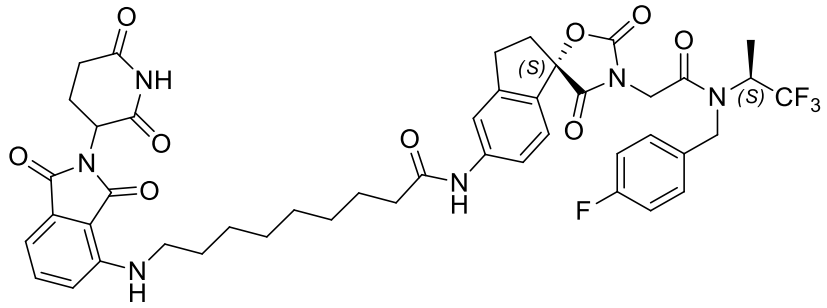

A solution of pomalidomide 4'-alkylC8-acid (#7211) (25 mg, 0.058 mmol, 1 eq.), HATU (29 mg, 0.076 mmol, 1.3 eq.), triethylamine (49 µL, 0.348 mmol, 6 eq.) and **5.03** (28 mg, 0.058 mmol, 1 eq.) in DMF (5 mL) was stirred overnight at room temperature. The reaction mixture was diluted with water (50 mL) and extracted with EtOAc (4 × 25 mL). The combined organic collections were washed with saturated $NaHCO_3$ (50 mL), brine (2 × 50 mL), dried over $MgSO_4$, filtered and concentrated *in vacuo*. The crude product was then purified *via* Flash Chromatography using 0 – 5% methanol in dichloromethane to result in the product as a yellow solid (28 mg, 0.031 mmol, 54%).^{1}H NMR (600 MHz, $CDCl_3$) δ_{ppm} 0.88 (t, *J* = 7.0 Hz, 2H), 1.23 – 1.45 (m, 18H), 1.59 (s, 2H), 1.61 – 1.73 (m, 5H), 2.08 – 2.15 (m, 1H), 2.35 (d, *J* = 7.4 Hz, 2H), 2.54 (q, *J* = 4.7 Hz, 1H), 2.67 – 2.84 (m, 4H), 2.84 – 2.91 (m, 1H), 3.11 (d, *J* = 8.9 Hz, 1H), 3.18 – 3.27 (m, 3H), 4.19 (d, *J* = 16.5 Hz, 1H), 4.43 (d, *J* = 16.4 Hz, 1H), 4.63 – 4.74 (m, 2H), 4.90 (dd, *J* = 12.5, 5.3 Hz, 1H), 5.49 (t, *J* = 7.8 Hz, 1H), 6.22 (t, *J* = 5.6 Hz, 1H), 6.87 (d, *J* = 8.5 Hz, 1H), 7.07 (d, *J* = 7.0 Hz, 1H), 7.09 – 7.18 (m, 3H), 7.29 (t, *J* = 6.8 Hz, 2H), 7.32 – 7.40 (m, 2H), 7.49 (d, *J* = 7.9 Hz, 1H), 7.81 (s, 1H), 8.07 (d, *J* = 24.9 Hz, 1H). ^{13}C NMR (151 MHz, $CDCl_3$) δ_{ppm} 11.7, 14.2, 14.3, 22.8, 22.9, 25.5, 26.8, 29.1 (d, *J* = 5.5 Hz), 29.2 (d, *J* = 12.4 Hz), 29.8, 30.5, 31.5, 31.7, 35.7, 37.9, 41.8, 42.7, 46.2, 49.0, 50.6 (d, *J* = 30.3 Hz), 94.7, 109.9, 111.5, 116.0, 116.5 (d, *J* = 21.7 Hz), 116.8, 119.1, 125.1, 127.3 (d, *J* = 7.5 Hz), 131.5, 132.5, 132.6, 136.3, 140.7, 146.9, 147.1, 154.5, 161.7, 167.0, 167.8, 168.5, 169.7, 171.1, 171.6, 174.2. LC-MS (5-95 MeCN in 20 mins) ^{t}R = 23.30 min, Purity = 97%, m/z = 891.20. HR-MS-ESI (m/z): $[M+H]^+$ calculated for $C_{45}H_{47}F_4N_6O_9$, 891.3341; found, 891.3310.

2-((1S)-5-(3-(2-((2-(2,6-dioxopiperidin-3-yl)-1,3-dioxoisoindolin-4-yl)amino)ethyl)ureido)-2',4'-dioxo-2,3-dihydrospiro[indene-1,5'-oxazolidin]-3'-yl)-N-(4-fluorobenzyl)-N-((S)-1,1,1-trifluoropropan-2-yl)acetamide (**5.07**)

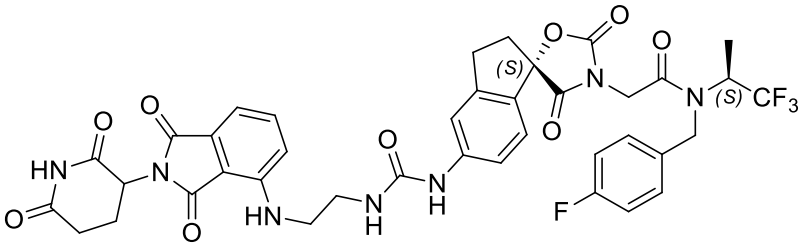

A mixture of **4.36** (73.4 mg, 0.208 mmol, 2 eq.), CDI (69 mg, 0.416 mmol, 4 eq.) and triethylamine (60 µL, 0.416 mmol, 4 eq.) in dichloromethane (10 mL) was stirred at room temperature for 2 hours. **5.03** (50 mg, 0.104 mmol, 1 eq.) and DIPEA (20 µL, 0.208 mmol, 2 eq.) was successively added to the stirring solution before leaving to stir for 16 hours. The reaction mixture was quenched with saturated NH_4Cl (25 mL) and transferred to a separating funnel. The organic layer was collected, and the aqueous layer was extracted with dichloromethane (4 × 25 mL). The combined organic layers were washed with water (50 mL), brine (100 mL), dried over $MgSO_4$, filtered, and concentrated *in vacuo*. The crude component was then purified *via* Flash Chromatography using 0 – 5% methanol in dichloromethane to result in the product as yellow solid (7.3 mg, 0.009 mmol, 9%). ^{1}H NMR (600 MHz, $CDCl_3$) δ_{ppm} 1.25 (s, 1H), 1.31 (d, *J* = 7.3 Hz, 3H), 1.41 (t, *J* = 7.3 Hz, 1H), 2.04 – 2.10 (m, 1H), 2.44 – 2.51 (m, 1H), 2.66 – 2.77 (m, 4H), 2.82 (d, *J* = 14.2 Hz, 1H), 2.93 – 3.01 (m, 1H), 3.09 (dt, *J* = 15.2, 7.4 Hz, 1H), 3.32 (d, *J* = 43.6 Hz, 5H), 4.19 (d, *J* = 16.5 Hz, 1H), 4.43 (d, *J* = 16.2 Hz, 1H), 4.62 – 4.74 (m, 2H), 4.91 (t, *J* = 8.7 Hz, 1H), 5.44 – 5.51 (m, 1H), 5.80 (s, 1H), 6.33 (d, *J* = 7.3 Hz, 1H), 6.82 (s, 1H), 6.91 (s, 1H), 6.96 (t, *J* = 6.3 Hz, 1H), 7.11 (d, *J* = 16.4 Hz, 2H), 7.22 (d, *J* = 8.3 Hz, 1H), 7.26 – 7.31 (m, 2H), 7.36 (dd, *J* = 15.7, 4.0 Hz, 1H), 7.45 (d, *J* = 16.8 Hz, 1H), 7.53 (s, 1H), 9.08 (s, 1H). LC-MS (5-95 MeCN in 20 mins) ^{t}R = 19.38 min, Purity = 89%, m/z = 822.35. Insufficient material for ^{13}C NMR.

2-((1S)-5-(3-(4-((2-(2,6-dioxopiperidin-3-yl)-1,3-dioxoisoindolin-4-yl)amino)butyl)ureido)-2',4'-dioxo-2,3-dihydrospiro[indene-1,5'-oxazolidin]-3'-yl)-N-(4-fluorobenzyl)-N-((S)-1,1,1-trifluoropropan-2-yl)acetamide (**5.08**)

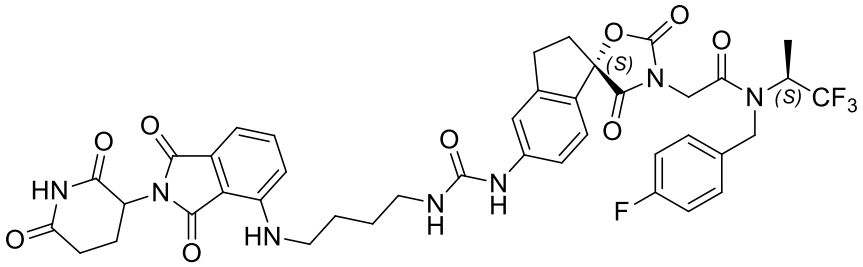

5.03 (50 mg, 0.104 mmol, 1 eq.) was dissolved in DMF (5 mL) and flushed with argon triethylamine (87 µL, 0.624 mmol, 6 eq.) was added and the reaction mixture was cooled to 0 ˚C. Triphosgene (15 mg, 0.052 mmol, 0.5 eq.) was added in one portion and the reaction mixture was left to stir for 30 mins before the addition of **4.37** (91 mg, 0.208 mmol, 2 eq.) in DMF (2 mL). The reaction mixture was left to stir at room temperature for 16 hours. The reaction mixture was partitioned between water (30 mL) and EtOAc (30 mL). The organic layer was collected, and the aqueous layer was extracted with EtOAc (3 × 15 mL). The combined organic layers were washed with brine (3 × 50 mL), dried over MgSO4, filtered, and concentrated *in vacuo*. The crude product was purified *via* Flash Chromatography using 0 – 5% methanol in dichloromethane to afford the product as a yellow solid (5 mg, 0.006 mmol, 6%). ^{1}H NMR (600 MHz, $CDCl_3$) δ_{ppm} 1.22 – 1.27 (m, 3H), 1.32 (d, *J* = 7.3 Hz, 3H), 1.41 (s, 1H), 1.57 – 1.70 (m, 6H), 2.12 (d, *J* = 4.9 Hz, 1H), 2.47 – 2.55 (m, 1H), 2.71 – 2.83 (m, 4H), 2.88 (s, 1H), 3.05 (d, *J* = 17.8 Hz, 1H), 3.16 (d, *J* = 15.4 Hz, 2H), 3.23 – 3.31 (m, 5H), 4.09 – 4.22 (m, 2H), 4.40 – 4.47 (m, 1H), 4.63 – 4.75 (m, 2H), 4.90 – 5.01 (m, 3H), 5.49 (d, *J* = 7.3 Hz, 1H), 6.20 (t, *J* = 5.5 Hz, 1H), 6.74 (s, 1H), 6.86 (d, *J* = 8.6 Hz, 1H), 6.99 (d, *J* = 8.4 Hz, 1H), 7.05 (dd, *J* = 7.0, 3.0 Hz, 1H), 7.13 (d, *J* = 8.4 Hz, 2H), 7.27 – 7.34 (m, 3H), 7.42 – 7.49 (m, 2H), 8.31 (s, 1H). LC-MS (5-95 MeCN in 20 mins) ^{t}R = 20.36 min, Purity = 92%, m/z = 850.35. Insufficient material for ^{13}C NMR.

2-((1S)-5-(3-(6-((2-(2,6-dioxopiperidin-3-yl)-1,3-dioxoisoindolin-4-yl)amino)hexyl)ureido)-2',4'-dioxo-2,3-dihydrospiro[indene-1,5'-oxazolidin]-3'-yl)-N-(4-fluorobenzyl)-N-((S)-1,1,1-trifluoropropan-2-yl)acetamide (**5.09**)

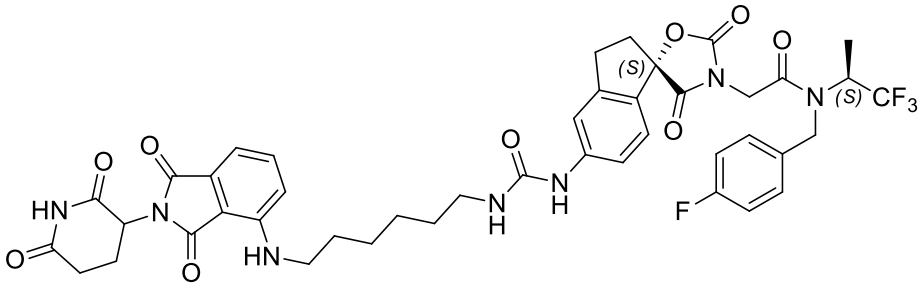

A mixture of **4.38** (85.1 mg, 0.208 mmol, 2 eq.), CDI (69 mg, 0.416 mmol, 4 eq.) and triethylamine (60 µL, 0.416 mmol, 4 eq.) in dichloromethane (10 mL) was stirred at room temperature for 2 hours. **5.03** (50 mg, 0.104 mmol, 1 eq.) and DIPEA (20 µL, 0.208 mmol, 2 eq.) was successively added to the stirring solution before leaving to stir for 16 hours. The reaction mixture was quenched with saturated NH_4Cl (25 mL) and transferred to a separating funnel. The organic layer was collected, and the aqueous layer was extracted with dichloromethane (4 × 25 mL). The combined organic layers were washed with water (50 mL), brine (100 mL), dried over $MgSO_4$, filtered, and concentrated *in vacuo*. The crude component was then purified *via* Flash Chromatography using 0 – 5% methanol in dichloromethane to result in the product as yellow solid (9 mg, 0.010 mmol, 9%).^{1}H NMR (600 MHz, $CDCl_3$) δ_{ppm} 0.88 (t, *J* = 7.0 Hz, 2H), 1.24 – 1.30 (m, 4H), 1.32 (d, *J* = 7.3 Hz, 3H), 1.37 – 1.49 (m, 7H), 1.53 (s, 2H), 1.68 (t, *J* = 7.1 Hz, 3H), 2.13 (t, *J* = 7.5 Hz, 1H), 2.54 (d, *J* = 5.2 Hz, 1H), 2.70 – 2.80 (m, 4H), 2.89 (d, *J* = 16.0 Hz, 1H), 3.09 (s, 1H), 3.28 (q, *J* = 6.4 Hz, 7H), 4.20 (d, *J* = 16.4 Hz, 1H), 4.43 (d, *J* = 16.4 Hz, 1H), 4.68 (q, *J* = 18.0 Hz, 4H), 4.91 (s, 1H), 5.49 (s, 1H), 6.23 (s, 1H), 6.49 (s, 1H), 6.87 (d, *J* = 8.5 Hz, 1H), 7.03 (s, 1H), 7.05 (d, *J* = 7.1 Hz, 1H), 7.13 (t, *J* = 8.4 Hz, 2H), 7.30 (t, *J* = 6.7 Hz, 2H), 7.35 (d, *J* = 8.3 Hz, 1H), 7.47 (d, *J* = 11.0 Hz, 2H), 8.04 (s, 1H). LC-MS (5-95 MeCN in 20 mins) ^{t}R = 21.27 min, Purity = 94%, m/z = 878.40. Insufficient material for ^{13}C NMR.

7 Chapter 7: References

1 X. Sun, H. Gao, Y. Yang, M. He, Y. Wu, Y. Song, Y. Tong and Y. Rao, *Signal Transduct. Target. Ther.*, 2019, **4**, 64.

2 E. L. P. Chekler, J. A. Pellegrino, T. A. Lanz, R. A. Denny, A. C. Flick, J. Coe, J. Langille, A. Basak, S. Liu, I. A. Stock, P. Sahasrabudhe, P. D. Bonin, K. Lee, M. T. Pletcher and L. H. Jones, *Chem. Biol.*, 2015, **22**, 1588–1596.

3 S. H. Hassanpour and M. Dehghani, *J. Cancer Res. Pract.*, 2017, **4**, 127–129.

4 F. Bray, J. Ferlay, I. Soerjomataram, R. L. Siegel, L. A. Torre and A. Jemal, *CA. Cancer J. Clin.*, 2018, **68**, 394–424.

5 R. L. Siegel, K. D. Miller and A. Jemal, *CA. Cancer J. Clin.*, 2019, **69**, 7–34.

6 GOV.UK, Chapter 2: trends in mortality, https://www.gov.uk/government/publications/health-profile-for-england-2018/chapter-2-trends-in-mortality#leading-causes-of-death-in-2016, (accessed 21 June 2021).

7 CancerResearchUK, Cancer Statistics for the UK, https://www.cancerresearchuk.org/health-professional/cancer-statistics-for-the-uk#heading-Two, (accessed 21 June 2021).

8 M. M. Fidler, I. Soerjomataram and F. Bray, *Int. J. Cancer*, 2016, **139**, 2436–2446.

9 D. Hanahan and R. A. Weinberg, *Cell*, 2011, **144**, 646–674.

10 Y. Cao, *Cell Biosci.*, 2017, **7**, 1–14.

11 C. . Waddington, *Endeavour*, 1942, **1**, 18–20.

12 S. Sharma, T. K. Kelly and P. A. Jones, *Carcinogenesis*, 2009, **31**, 27–36.

13 S. Timmermann, H. Lehrmann, A. Polesskaya and A. Harel-Bellan, *Cell. Mol. Life Sci.*, 2001, **58**, 728–736.

14 B. M. Turner, *Nat. Cell Biol.*, 2007, **9**, 2–6.

15 S. Biswas and C. M. Rao, *Eur. J. Pharmacol.*, 2018, **837**, 8–24.

16 R. Beroukhim, C. H. Mermel, D. Porter, G. Wei, S. Raychaudhuri, J. Donovan, J. Barretina, J. S. Boehm, J. Dobson, M. Urashima, K. T. Mc Henry, R. M. Pinchback, A. H. Ligon, Y.-J. Cho, L. Haery, H. Greulich, M. Reich, W. Winckler, M. S. Lawrence, B. A. Weir, K. E. Tanaka, D. Y. Chiang, A. J. Bass, A. Loo, C. Hoffman, J. Prensner, T. Liefeld, Q. Gao, D. Yecies, S. Signoretti, E. Maher, F. J. Kaye, H. Sasaki, J. E. Tepper, J. A. Fletcher, J. Tabernero, J. Baselga, M.-S. Tsao, F. Demichelis, M. A. Rubin, P. A. Janne, M. J. Daly, C. Nucera, R. L. Levine, B. L. Ebert, S. Gabriel, A. K. Rustgi, C. R. Antonescu, M. Ladanyi, A. Letai, L. A. Garraway, M. Loda, D. G. Beer, L. D. True, A. Okamoto, S. L. Pomeroy, S. Singer, T. R. Golub, E. S. Lander, G. Getz, W. R. Sellers and M. Meyerson, *Nature*, 2010, **463**, 899–905.

17 S. Giuriato and D. W. Felsher, *Cell Cycle*, 2003, **2**, 328–331.

18 A. Sorolla, E. Wang, E. Golden, C. Duffy, S. T. Henriques, A. D. Redfern and P. Blancafort, *Oncogene*, 2020, **39**, 1167–1184.

19 P. Qin, H. Wang, F. Zhang, Y. Huang and S. Chen, *Cell Biochem. Funct.*, 2019, **37**, 266–272.

20 G. J. Yoshida, *J. Exp. Clin. Cancer Res.*, 2018, **37**, 1–20.

21 K. A. Bowen and D. H. Chung, *Curr. Opin. Pediatr.*, 2009, **21**, 350–356.

22 M. Henriksson and B. Luscher, *Adv. Cancer Res.*, 1996, **68**, 110–182.

23 C. V. Dang, *Mol. Cell. Biol.*, 1999, **19**, 1–11.

24 S. Jones, *Genome Biol.*, 2004, **5**, 1–6.

25 C. Murre, G. Bain, M. A. van Dijk, I. Engel, B. A. Furnari, M. E. Massari, J. R. Matthews, M. W. Quong, R. R. Rivera and M. H. Stuiver, *BBA - Gene Struct. Expr.*, 1994, **1218**, 129–135.

26 S. K. Nair and S. K. Burley, *Cell*, 2003, **112**, 193–205.

27 E. M. Flinn, C. M. C. Busch and A. P. H. Wright, *Mol. Cell. Biol.*, 1998, **18**, 5961–5969.

28 G. J. Kato, J. Barrett, M. Villa-Garcia and C. V Dang, *Mol. Cell. Biol.*, 1990, **10**, 5914–5920.

29 C. Murre, P. S. McCaw, H. Vaessin, M. Caudy, L. Y. Jan, Y. N. Jan, C. V. Cabrera, J. N. Buskin, S. D. Hauschka, A. B. Lassar, H. Weintraub and D. Baltimore, *Cell*, 1989, **58**, 537–544.

30 C. V Dang, M. McGuire, M. Buckmire and W. M. F. Lee, *Nature*, 1989, **337**, 664–666.

31 E. M. Blackwood and R. N. Eisenman, *Science.*, 1991, **251**, 1211–1217.

32 C. V. Dang, K. A. O'Donnell, K. I. Zeller, T. Nguyen, R. C. Osthus and F. Li, *Semin. Cancer Biol.*, 2006, **16**, 253–264.

33 H. Chen, H. Liu and G. Qing, *Signal Transduct. Target. Ther.*, 2018, **3**, 1–7.

34 L. R. Thomas, Q. Wang, B. C. Grieb, J. Phan, A. M. Foshage, Q. Sun, E. T. Olejniczak, T. Clark, S. Dey, S. Lorey, B. Alicie, G. C. Howard, B. Cawthon, K. C. Ess, C. M. Eischen, Z. Zhao, S. W. Fesik and W. P. Tansey, *Mol. Cell*, 2015, **58**, 440–452.

35 J. M. Gerlach, M. Furrer, M. Gallant, D. Birkel, A. Baluapuri, E. Wolf and P. Gallant, *Proc. Natl. Acad. Sci. U. S. A.*, 2017, **114**, E9224–E9232.

36 S. K. Madden, A. D. de Araujo, M. Gerhardt, D. P. Fairlie and J. M. Mason, *Mol. Cancer*, 2021, **20**, 1–18.

37 C. V. Dang, *Cell*, 2012, **149**, 22–35.

38 B. D. Strahl and C. D. Allis, *Nature*, 2000, **403**, 41–45.

39 L. Zeng and M.-M. Zhou, *FEBS Lett.*, 2002, **513**, 124–128.

40 P. Filippakopoulos, S. Picaud, M. Mangos, T. Keates, J.-P. Lambert, D. Barsyte-Lovejoy, I. Felletar, R. Volkmer, S. Müller, T. Pawson, A.-C. Gingras, C. H. Arrowsmith and S. Knapp, *Cell*, 2012, **149**, 214–231.

41 O. B. Cox, T. Krojer, P. Collins, O. Monteiro, R. Talon, A. Bradley, O. Fedorov, J. Amin, B. D. Marsden, J. Spencer, F. von Delft and P. E. Brennan, *Chem. Sci.*, 2016, **7**, 2322–2330.

42 S. Muller, P. Filippakopoulos and S. Knapp, *Expert Rev. Mol. Med.*, 2011, **13**, e29.

43 D. A. Hay, O. Fedorov, S. Martin, D. C. Singleton, C. Tallant, C. Wells, S. Picaud, M. Philpott, O. P. Monteiro, C. M. Rogers, S. J. Conway, T. P. C. Rooney, A. Tumber, C. Yapp, P. Filippakopoulos, M. E. Bunnage, S. Müller, S. Knapp, C. J. Schofield and P. E. Brennan, *J. Am. Chem. Soc.*, 2014, **136**, 9308–9319.

44 S. Picaud, O. Fedorov, A. Thanasopoulou, K. Leonards, K. Jones, J. Meier, H. Olzscha, O. Monteiro, S. Martin, M. Philpott, A. Tumber, P. Filippakopoulos, C. Yapp, C. Wells, K. H. Che, A. Bannister, S. Robson, U. Kumar, N. Parr, K. Lee, D. Lugo, P. Jeffrey, S. Taylor, M. L. Vecellio, C. Bountra, P. E. Brennan, A. O'Mahony, S. Velichko, S. Muller, D. Hay, D. L. Daniels, M. Urh, N. B. La Thangue, T. Kouzarides, R. Prinjha, J. Schwaller and S. Knapp, *Cancer Res.*, 2015, **75**, 5106–5119.

45 P. Filippakopoulos, J. Qi, S. Picaud, Y. Shen, W. B. Smith, O. Fedorov, E. M. Morse, T. Keates, T. T. Hickman, I. Felletar, M. Philpott, S. Munro, M. R. McKeown, Y. Wang, A. L. Christie, N. West, M. J. Cameron, B. Schwartz, T. D. Heightman, N. La Thangue, C. A. French, O. Wiest, A. L. Kung, S. Knapp and J. E. Bradner, *Nature*, 2010, **468**, 1067–1073.

46 P. V. Fish, P. Filippakopoulos, G. Bish, P. E. Brennan, M. E. Bunnage, A. S. Cook, O. Federov, B. S. Gerstenberger, H. Jones, S. Knapp, B. Marsden, K. Nocka, D. R. Owen, M. Philpott, S. Picaud, M. J. Primiano, M. J. Ralph, N. Sciammetta and J. D. Trzupek, *J. Med. Chem.*, 2012, **55**, 9831–9837.

47 J. Morinière, S. Rousseaux, U. Steuerwald, M. Soler-López, S. Curtet, A. L. Vitte, J. Govin, J. Gaucher, K. Sadoul, D. J. Hart, J. Krijgsveld, S. Khochbin, C. W. Müller and C. Petosa, *Nature*, 2009, **461**, 664–668.

48 J. Shi and C. R. Vakoc, *Mol. Cell*, 2014, 54, 728–736.

49 C. Dhalluin, J. E. Carlson, L. Zeng, C. He, A. K. Aggarwal and M. M. Zhou, *Nature*, 1999, **399**, 491–496.

50 J. Shi and C. R. Vakoc, *Mol. Cell*, 2014, **54**, 728–736.

51 M. A. Dawson, R. K. Prinjha, A. Dittmann, G. Giotopoulos, M. Bantscheff, W. I. Chan, S. C. Robson, C. W. Chung, C. Hopf, M. M. Savitski, C. Huthmacher, E. Gudgin, D. Lugo, S. Beinke, T. D. Chapman, E. J. Roberts, P. E. Soden, K. R. Auger, O. Mirguet, K. Doehner, R. Delwel, A. K. Burnett, P. Jeffrey, G. Drewes, K. Lee, B. J. P. Huntly and T. Kouzarides, *Nature*, 2011, **478**, 529–533.

52 Y. W. Jiang, P. Veschambre, H. Erdjument-Bromage, P. Tempst, J. W. Conaway, R. C. Conaway and R. D. Kornberg, *Proc. Natl. Acad. Sci. U. S. A.*, 1998, **95**, 8538–8543.

53 A. Dey, A. Nishiyama, T. Karpova, J. McNally and K. Ozato, *Mol. Biol. Cell*, 2009, **20**, 4899–4909.

54 J. Lovén, H. A. Hoke, C. Y. Lin, A. Lau, D. A. Orlando, C. R. Vakoc, J. E. Bradner, T. I. Lee and R. A. Young, *Cell*, 2013, **153**, 320–334.

55 F. Vollmuth, W. Blankenfeldt and M. Geyer, *J. Biol. Chem.*, 2009, **284**, 36547–36556.

56 Plexxicon., (2017), 'PLX51107 for CRUK Combinations Alliance', [PowerPoint presentation], Availiable at: https://www.ecmcnetwork.org.uk/sites/default/files/PLX51107%20CRUK%20Combinations%20Alliance%202017-10%20final.pdf, (Accessed: 10/05/2021).

57 E. Nicodeme, K. L. Jeffrey, U. Schaefer, S. Beinke, S. Dewell, C. W. Chung, R. Chandwani, I. Marazzi, P. Wilson, H. Coste, J. White, J. Kirilovsky, C. M. Rice, J. M. Lora, R. K. Prinjha,

K. Lee and A. Tarakhovsky, *Nature*, 2010, **468**, 1119–1123.

58 G. Zhang, A. N. Plotnikov, E. Rusinova, T. Shen, K. Morohashi, J. Joshua, L. Zeng, S. Mujtaba, M. Ohlmeyer and M. M. Zhou, *J. Med. Chem.*, 2013, **56**, 9251–9264.

59 S. Picaud, D. Da Costa, A. Thanasopoulou, P. Filippakopoulos, P. V. Fish, M. Philpott, O. Fedorov, P. Brennan, M. E. Bunnage, D. R. Owen, J. E. Bradner, P. Taniere, B. O'Sullivan, S. Müller, J. Schwaller, T. Stankovic and S. Knapp, *Cancer Res.*, 2013, **73**, 3336–3346.

60 G. Patrick, *An Introduction to Medicinal Chemistry*, Oxford University Press, London, England, 6th edn., 2017.

61 Y. Duan, Y. Guan, W. Qin, X. Zhai, B. Yu and H. Liu, *Medchemcomm*, 2018, 9, 1779–1802.

62 C. Berthon, E. Raffoux, X. Thomas, N. Vey, C. Gomez-Roca, K. Yee, D. C. Taussig, K. Rezai, C. Roumier, P. Herait, C. Kahatt, B. Quesnel, M. Michallet, C. Recher, F. Lokiec, C. Preudhomme and H. Dombret, *Lancet Haematol.*, 2016, **3**, e186–e195.

63 A. Stathis, E. Zucca, M. Bekradda, C. Gomez-Roca, J.-P. Delord, T. de La Motte Rouge, E. Uro-Coste, F. de Braud, G. Pelosi and C. A. French, *Cancer Discov.*, 2016, **6**, 492–500.

64 M. Boi, E. Gaudio, P. Bonetti, I. Kwee, E. Bernasconi, C. Tarantelli, A. Rinaldi, M. Testoni, L. Cascione, M. Ponzoni, A. A. Mensah, A. Stathis, G. Stussi, M. E. Riveiro, P. Herait, G. Inghirami, E. Cvitkovic, E. Zucca and F. Bertoni, *Clin. Cancer Res.*, 2015, **21**, 1628–1638.

65 S. Amorim, A. Stathis, M. Gleeson, S. Iyengar, V. Magarotto, X. Leleu, F. Morschhauser, L. Karlin, F. Broussais, K. Rezai, P. Herait, C. Kahatt, F. Lokiec, G. Salles, T. Facon, A. Palumbo, D. Cunningham, E. Zucca and C. Thieblemont, *Lancet Haematol.*, 2016, **3**, e196–e204.

66 Clinical-Trials.gov, A Two Part Study of RO6870810. Dose-Escalation Study in Participants With Advanced Solid Tumors and Expansion Study in Participants With Selected Malignancies, https://clinicaltrials.gov/ct2/show/NCT01987362, (accessed 30 April 2021).

67 Clinical-Trials.gov, A Study of RO6870810/TEN-010 in Participants With Acute Myeloid Leukemia and Myelodysplastic Syndrome, https://clinicaltrials.gov/ct2/show/NCT02308761, (accessed 30 April 2021).

68 I. A. Asangani, V. L. Dommeti, X. Wang, R. Malik, M. Cieslik, R. Yang, J. Escara-Wilke, K. Wilder-Romans, S. Dhanireddy, C. Engelke, M. K. Iyer, X. Jing, Y. M. Wu, X. Cao, Z. S. Qin, S. Wang, F. Y. Feng and A. M. Chinnaiyan, *Nature*, 2014, **510**, 278–282.

69 A. Chaidos, V. Caputo, K. Gouvedenou, B. Liu, I. Marigo, M. S. Chaudhry, A. Rotolo, D. F. Tough, N. N. Smithers, A. K. Bassil, T. D. Chapman, N. R. Harker, O. Barbash, P. Tummino, N. Al-Mahdi, A. C. Haynes, L. Cutler, B. C. Le, A. Rahemtulla, I. Roberts, M. Kleijnen, J. J. Witherington, N. J. Parr, R. K. Prinjha and A. Karadimitris, *Blood*, 2014, **123**, 697–705.

70 Y. Zhao, C. Y. Yang and S. Wang, *J. Med. Chem.*, 2013, **56**, 7498–7500.

71 B. K. Albrecht, V. S. Gehling, M. C. Hewitt, R. G. Vaswani, A. Côté, Y. Leblanc, C. G. Nasveschuk, S. Bellon, L. Bergeron, R. Campbell, N. Cantone, M. R. Cooper, R. T. Cummings, H. Jayaram, S. Joshi, J. A. Mertz, A. Neiss, E. Normant, M. O'Meara, E. Pardo, F. Poy, P. Sandy, J. Supko, R. J. Sims, J. C. Harmange, A. M. Taylor and J. E. Audia, *J. Med. Chem.*, 2016, **59**, 1330–1339.

72 P. C. Liu, X. M. Liu, M. C. Stubbs, T. Maduskuie, R. Sparks, N. Zolotarjova, J. Li, X. Wen,

M. Favata, P. Feldman, A. Volgina, D. DiMatteo, R. Collins, N. Falahatpisheh, P. Polam, Y. Li, M. Covington, S. Diamond-Fosbenner, R. Wynn, T. Burn, K. Vaddi, S. Yeleswaram, A. P. Combs, W. Yao, R. Huber, P. Scherle and G. Hollis, in *Experimental and Molecular Therapeutics*, American Association for Cancer Research, 2015, pp. 3523–3523.

73 O. Mirguet, Y. Lamotte, F. Donche, J. Toum, F. Gellibert, A. Bouillot, R. Gosmini, V. L. Nguyen, D. Delannée, J. Seal, F. Blandel, A. B. Boullay, E. Boursier, S. Martin, J. M. Brusq, G. Krysa, A. Riou, R. Tellier, A. Costaz, P. Huet, Y. Dudit, L. Trottet, J. Kirilovsky and E. Nicodeme, *Bioorganic Med. Chem. Lett.*, 2012, **22**, 2963–2967.

74 J. Seal, Y. Lamotte, F. Donche, A. Bouillot, O. Mirguet, F. Gellibert, E. Nicodeme, G. Krysa, J. Kirilovsky, S. Beinke, S. McCleary, I. Rioja, P. Bamborough, C. W. Chung, L. Gordon, T. Lewis, A. L. Walker, L. Cutler, D. Lugo, D. M. Wilson, J. Witherington, K. Lee and R. K. Prinjha, *Bioorganic Med. Chem. Lett.*, 2012, **22**, 2968–2972.

75 H. G. Ozer, D. El-Gamal, B. Powell, Z. A. Hing, J. S. Blachly, B. Harrington, S. Mitchell, N. R. Grieselhuber, K. Williams, T. H. Lai, L. Alinari, R. A. Baiocchi, L. Brinton, E. Baskin, M. Cannon, L. Beaver, V. M. Goettl, D. M. Lucas, J. A. Woyach, D. Sampath, A. M. Lehman, L. Yu, J. Zhang, Y. Ma, Y. Zhang, W. Spevak, S. Shi, P. Severson, R. Shellooe, H. Carias, G. Tsang, K. Dong, T. Ewing, A. Marimuthu, C. Tantoy, J. Walters, L. Sanftner, H. Rezaei, M. Nespi, B. Matusow, G. Habets, P. Ibrahim, C. Zhang, E. A. Mathe, G. Bollag, J. C. Byrd and R. Lapalombella, *Cancer Discov.*, 2018, **8**, 458–477.

76 D. S. Hewings, M. Wang, M. Philpott, O. Fedorov, S. Uttarkar, P. Filippakopoulos, S. Picaud, C. Vuppusetty, B. Marsden, S. Knapp, S. J. Conway and T. D. Heightman, *J. Med. Chem.*, 2011, **54**, 6761–6770.

77 D. Hay, O. Fedorov, P. Filippakopoulos, S. Martin, M. Philpott, S. Picaud, D. S. Hewings, S. Uttakar, T. D. Heightman, S. J. Conway, S. Knapp and P. E. Brennan, *Medchemcomm*, 2013, **4**, 140–144.

78 D. S. Hewings, O. Fedorov, P. Filippakopoulos, S. Martin, S. Picaud, A. Tumber, C. Wells, M. M. Olcina, K. Freeman, A. Gill, A. J. Ritchie, D. W. Sheppard, A. J. Russell, E. M. Hammond, S. Knapp, P. E. Brennan and S. J. Conway, *J. Med. Chem.*, 2013, **56**, 3217–3227.

79 A. R. Sekirnik (née Measures), D. S. Hewings, N. H. Theodoulou, L. Jursins, K. R. Lewendon, L. E. Jennings, T. P. C. Rooney, T. D. Heightman and S. J. Conway, *Angew. Chemie - Int. Ed.*, 2016, **55**, 8353–8357.

80 P. Filippakopoulos and S. Knapp, *Science.*, 2020, **368**, 367–368.

81 O. Gilan, I. Rioja, K. Knezevic, M. J. Bell, M. M. Yeung, N. R. Harker, E. Y. N. Lam, C. Chung, P. Bamborough, M. Petretich, M. Urh, S. J. Atkinson, A. K. Bassil, E. J. Roberts, D. Vassiliadis, M. L. Burr, A. G. S. Preston, C. Wellaway, T. Werner, J. R. Gray, A. M. Michon, T. Gobbetti, V. Kumar, P. E. Soden, A. Haynes, J. Vappiani, D. F. Tough, S. Taylor, S. J. Dawson, M. Bantscheff, M. Lindon, G. Drewes, E. H. Demont, D. L. Daniels, P. Grandi, R. K. Prinjha and M. A. Dawson, *Science.*, 2020, **368**, 387–394.

82 S. Picaud, C. Wells, I. Felletar, D. Brotherton, S. Martin, P. Savitsky, B. Diez-Dacal, M. Philpott, C. Bountra, H. Lingard, O. Fedorov, S. Müller, P. E. Brennan, S. Knapp and P. Filippakopoulos, *Proc. Natl. Acad. Sci. U. S. A.*, 2013, **110**, 19754–19759.

83 O. A. Kharenko, E. M. Gesner, R. G. Patel, K. Norek, A. White, E. Fontano, R. K. Suto, P. R. Young, K. G. McLure and H. C. Hansen, *Biochem. Biophys. Res. Commun.*, 2016, **477**, 62–67.

84 E. J. Faivre, K. F. McDaniel, D. H. Albert, S. R. Mantena, J. P. Plotnik, D. Wilcox, L. Zhang, M. H. Bui, G. S. Sheppard, L. Wang, V. Sehgal, X. Lin, X. Huang, X. Lu, T. Uziel, P. Hessler, L. T. Lam, R. J. Bellin, G. Mehta, S. Fidanze, J. K. Pratt, D. Liu, L. A. Hasvold, C. Sun, S. C. Panchal, J. J. Nicolette, S. L. Fossey, C. H. Park, K. Longenecker, L. Bigelow, M. Torrent, S. H. Rosenberg, W. M. Kati and Y. Shen, *Nature*, 2020, **578**, 306–310.

85 D. Chen, T. Lu, Z. Yan, W. Lu, F. Zhou, X. Lyu, B. Xu, H. Jiang, K. Chen, C. Luo and Y. Zhao, *Eur. J. Med. Chem.*, 2019, **182**, 111633.

86 A. Weilemann, M. Grau, T. Erdmann, O. Merkel, U. Sobhiafshar, I. Anagnostopoulos, M. Hummel, A. Siegert, C. Hayford, H. Madle, B. Wollert-Wulf, I. Fichtner, B. Dörken, S. Dirnhofer, S. Mathas, M. Janz, N. C. Tolga Emre, A. Rosenwald, G. Ott, P. Lenz, A. Tzankov and G. Lenz, *Blood*, 2015, **125**, 124–132.

87 P. Li, R. Spolski, W. Liao, L. Wang, T. L. Murphy, K. M. Murphy and W. J. Leonard, *Nature*, 2012, **490**, 543–546.

88 S. Sundararaj, S. Seneviratne, S. J. Williams, A. Enders and M. G. Casarotto, *Nucleic Acids Res.*, 2021, **49**, 2255–2265.

89 A. R. R. A. Levy, A. Rojas-villarraga and R. A. Levy, in *Cancer and Autoimmunity*, Elsevier, 2000, p. 77.

90 A. L. Shaffer, N. C. T. Emre, L. Lamy, V. N. Ngo, G. Wright, W. Xiao, J. Powell, S. Dave, X. Yu, H. Zhao, Y. Zeng, B. Chen, J. Epstein and L. M. Staudt, *Nat. Lett.*, 2008, **454**, 226–231.

91 J. Eguchi, X. Wang, S. Yu, E. E. Kershaw, P. C. Chiu, J. Dushay, J. L. Estall, U. Klein, E. Maratos-Flier and E. D. Rosen, *Cell Metab.*, 2011, **13**, 249–259.

92 S. Guo, Z. Z. Li, D. S. Jiang, Y. Y. Lu, Y. Liu, L. Gao, S. M. Zhang, H. Lei, L. H. Zhu, X. D. Zhang, D. P. Liu and H. Li, *Cell Death Differ.*, 2014, **21**, 888–903.

93 D. S. Jiang, Z. Y. Bian, Y. Zhang, S. M. Zhang, Y. Liu, R. Zhang, Y. Chen, Q. Yang, X. D. Zhang, G. C. Fan and H. Li, *Hypertension*, 2013, **61**, 1193–1202.

94 A. R. Conery, R. C. Centore, A. Neiss, P. J. Keller, S. Joshi, K. L. Spillane, P. Sandy, C. Hatton, E. Pardo, L. Zawadzke, A. Bommi-Reddy, K. E. Gascoigne, B. M. Bryant, J. A. Mertz and R. J. Sims, *Elife*, 2016, **5**, 1–17.

95 A. Agnarelli, T. Chevassut and E. J. Mancini, *Leuk. Res.*, 2018, **72**, 52–58.

96 N. G. Iyer, H. Özdag and C. Caldas, *Oncogene*, 2004, **23**, 4225–4231.

97 A. J. Bannister and T. Kouzarides, *Nature*, 1996, **384**, 641–643.

98 R. Eckner, M. E. Ewen, D. Newsome, M. Gerdes, J. A. DeCaprio, J. B. Lawrence and D. M. Livingston, *Genes Dev.*, 1994, **8**, 869–884.

99 M. V. Karamouzis, P. A. Konstantinopoulos and A. G. Papavassiliou, *Cell Res.*, 2007, **17**, 324–332.

100 T. P. Yao, S. P. Oh, M. Fuchs, N. D. Zhou, L. E. Ch'ng, D. Newsome, R. T. Bronson, E. Li, D. M. Livingston and R. Eckner, *Cell*, 1998, **93**, 361–372.

101 Y. Tanaka, I. Naruse, T. Hongo, M. J. Xu, T. Nakahata, T. Maekawa and S. Ishii, *Mech. Dev.*, 2000, **95**, 133–145.

102 V. Garcia-Carpizo, S. Ruiz-Llorente, J. Sarmentero, O. Graña-Castro, D. G. Pisano and M.

J. Barrero, *Epigenetics and Chromatin*, 2018, **11**, 1–15.

103 E. D. Pleasance, P. J. Stephens, S. O'Meara, D. J. McBride, A. Meynert, D. Jones, M. L. Lin, D. Beare, K. W. Lau, C. Greenman, I. Varela, S. Nik-Zainal, H. R. Davies, G. R. Ordõez, L. J. Mudie, C. Latimer, S. Edkins, L. Stebbings, L. Chen, M. Jia, C. Leroy, J. Marshall, A. Menzies, A. Butler, J. W. Teague, J. Mangion, Y. A. Sun, S. F. McLaughlin, H. E. Peckham, E. F. Tsung, G. L. Costa, C. C. Lee, J. D. Minna, A. Gazdar, E. Birney, M. D. Rhodes, K. J. McKernan, M. R. Stratton, P. A. Futreal and P. J. Campbell, *Nature*, 2010, **463**, 184–190.

104 M. Peifer, L. Fernández-Cuesta, M. L. Sos, J. George, D. Seidel, L. H. Kasper, D. Plenker, F. Leenders, R. Sun, T. Zander, R. Menon, M. Koker, I. Dahmen, C. Müller, V. Di Cerbo, H. U. Schildhaus, J. Altmüller, I. Baessmann, C. Becker, B. De Wilde, J. Vandesompele, D. Böhm, S. Ansén, F. Gabler, I. Wilkening, S. Heynck, J. M. Heuckmann, X. Lu, S. L. Carter, K. Cibulskis, S. Banerji, G. Getz, K. S. Park, D. Rauh, C. Grütter, M. Fischer, L. Pasqualucci, G. Wright, Z. Wainer, P. Russell, I. Petersen, Y. Chen, E. Stoelben, C. Ludwig, P. Schnabel, H. Hoffmann, T. Muley, M. Brockmann, W. Engel-Riedel, L. A. Muscarella, V. M. Fazio, H. Groen, W. Timens, H. Sietsma, E. Thunnissen, E. Smit, D. A. M. Heideman, P. J. F. Snijders, F. Cappuzzo, C. Ligorio, S. Damiani, J. Field, S. Solberg, O. T. Brustugun, M. Lund-Iversen, J. Sänger, J. H. Clement, A. Soltermann, H. Moch, W. Weder, B. Solomon, J. C. Soria, P. Validire, B. Besse, E. Brambilla, C. Brambilla, S. Lantuejoul, P. Lorimier, P. M. Schneider, M. Hallek, W. Pao, M. Meyerson, J. Sage, J. Shendure, R. Schneider, R. Büttner, J. Wolf, P. Nürnberg, S. Perner, L. C. Heukamp, P. K. Brindle, S. Haas and R. K. Thomas, *Nat. Genet.*, 2012, **44**, 1104–1110.

105 N. L. Lill, S. R. Grossman, D. Ginsberg, J. DeCaprio and D. M. Livingston, *Nature*, 1997, **387**, 823–827.

106 M. L. Avantaggiati, V. Ogryzko, K. Gardner, A. Giordano, A. S. Levine and K. Kelly, *Cell*, 1997, **89**, 1175–1184.

107 C. Pouponnot, L. Jayaraman and J. Massagué, *J. Biol. Chem.*, 1998, **273**, 22865–22868.

108 G. M. Pao, R. Janknecht, H. Ruffner, T. Hunter and I. M. Verma, *Proc. Natl. Acad. Sci. U. S. A.*, 2000, **97**, 1020–1025.

109 L. Fauquier, K. Azzag, M. A. M. Parra, A. Quillien, M. Boulet, S. Diouf, G. Carnac, L. Waltzer, H. Gronemeyer and L. Vandel, *Sci. Rep.*, 2018, **8**, 1–16.

110 D. C. Bedford, L. H. Kasper, T. Fukuyama and P. K. Brindle, *Epigenetics*, 2010, **5**, 9–15.

111 H. Ogiwara, M. Sasaki, T. Mitachi, T. Oike, S. Higuchi, Y. Tominaga and T. Kohno, *Cancer Discov.*, 2016, **6**, 430–445.

112 J. Maksimoska, D. Segura-Peña, P. A. Cole and R. Marmorstein, *Biochemistry*, 2014, **53**, 3415–3422.

113 X. Liu, L. Wang, K. Zhao, P. R. Thompson, Y. Hwang, R. Marmorstein and P. A. Cole, *Nature*, 2008, **451**, 846–850.

114 J. Bouchal, F. R. Santer, P. P. S. Höschele, E. Tomastikova, H. Neuwirt and Z. Culig, *Prostate*, 2011, **71**, 431–437.

115 J. M. Gajer, S. D. Furdas, A. Gründer, M. Gothwal, U. Heinicke, K. Keller, F. Colland, S. Fulda, H. L. Pahl, I. Fichtner, W. Sippl and M. Jung, *Oncogenesis*, 2015, **4**, e137–e137.

116 C. Demetriadou and A. Kirmizis, *Crit. Rev. Oncog.*, 2017, **22**, 195–218.

117 V. Di Cerbo and R. Schneider, *Brief. Funct. Genomics*, 2013, **12**, 231–243.

118 O. D. Lau, T. K. Kundu, R. E. Soccio, S. Ait-Si-Ali, E. M. Khalil, A. Vassilev, A. P. Wolffe, Y. Nakatani, R. G. Roeder and P. A. Cole, *Mol. Cell*, 2000, **5**, 589–595.

119 K. Balasubramanyam, V. Swaminathan, A. Ranganathan and T. K. Kundu, *J. Biol. Chem.*, 2003, **278**, 19134–19140.

120 K. Balasubramanyam, M. Altaf, R. A. Varier, V. Swaminathan, A. Ravindran, P. P. Sadhale and T. K. Kundu, *J. Biol. Chem.*, 2004, **279**, 33716–33726.

121 K. Balasubramanyam, R. A. Varier, M. Altaf, V. Swaminathan, N. B. Siddappa, U. Ranga and T. K. Kundu, *J. Biol. Chem.*, 2004, **279**, 51163–51171.

122 R. A. Fuchs and R. J. McLaughlin, *Neuropsychopharmacology*, 2017, **42**, 581–583.

123 S. Ting Chiu, *Drug Des. Open Access*, 2012, **02**, 1–2.

124 M. Heger, R. F. van Golen, M. Broekgaarden and M. C. Michel, *Pharmacol. Rev.*, 2014, **66**, 222–307.

125 K. M. Nelson, J. L. Dahlin, J. Bisson, J. Graham, G. F. Pauli and M. A. Walters, *J. Med. Chem.*, 2017, **60**, 1620–1637.

126 T. Esatbeyoglu, K. Ulbrich, C. Rehberg, S. Rohn and G. Rimbach, *Food Funct.*, 2015, **6**, 887–893.

127 J. Fang, J. Lu and A. Holmgren, *J. Biol. Chem.*, 2005, **280**, 25284–25290.

128 N. Jurrmann, R. Brigelius-Flohé and G. F. Böl, *J. Nutr.*, 2005, **135**, 1859–1864.

129 Y. Jung, W. Xu, H. Kim, N. Ha and L. Neckers, *Biochim. Biophys. Acta - Mol. Cell Res.*, 2007, **1773**, 383–390.

130 D. Chin, P. Huebbe, J. Frank, G. Rimbach and K. Pallauf, *Redox Biol.*, 2014, **2**, 563–569.

131 C. Schneider, O. N. Gordon, R. L. Edwards and P. B. Luis, *J. Agric. Food Chem.*, 2015, **63**, 7606–7614.

132 K. I. Priyadarsini, *J. Photochem. Photobiol. C Photochem. Rev.*, 2009, **10**, 81–95.

133 E. M. Bowers, G. Yan, C. Mukherjee, A. Orry, L. Wang, M. A. Holbert, N. T. Crump, C. A. Hazzalin, G. Liszczak, H. Yuan, C. Larocca, S. A. Saldanha, R. Abagyan, Y. Sun, D. J. Meyers, R. Marmorstein, L. C. Mahadevan, R. M. Alani and P. A. Cole, *Chem. Biol.*, 2010, **17**, 471–482.

134 W. Lu, H. Xiong, Y. Chen, C. Wang, H. Zhang, P. Xu, J. Han, S. Xiao, H. Ding, Z. Chen, T. Lu, J. Wang, Y. Zhang, L. Yue, Y. C. Liu, C. Zhang, Y. Yang, H. Jiang, K. Chen, B. Zhou and C. Luo, *Bioorganic Med. Chem.*, 2018, **26**, 5397–5407.

135 L. M. Lasko, C. G. Jakob, R. P. Edalji, W. Qiu, D. Montgomery, E. L. Digiammarino, T. M. Hansen, R. M. Risi, R. Frey, V. Manaves, B. Shaw, M. Algire, P. Hessler, L. T. Lam, T. Uziel, E. Faivre, D. Ferguson, F. G. Buchanan, R. L. Martin, M. Torrent, G. G. Chiang, K. Karukurichi, J. W. Langston, B. T. Weinert, C. Choudhary, P. De Vries, J. H. Van Drie, D. McElligott, E. Kesicki, R. Marmorstein, C. Sun, P. A. Cole, S. H. Rosenberg, M. R. Michaelides, A. Lai and K. D. Bromberg, *Nature*, 2017, **550**, 128–132.

136 Y. Yang, R. Zhang, Z. Li, L. Mei, S. Wan, H. Ding, Z. Chen, J. Xing, H. Feng, J. Han, H. Jiang, M. Zheng, C. Luo and B. Zhou, *J. Med. Chem.*, 2020, **63**, 1337–1360.

137 Z. Ji, R. F. Clark, V. Bhat, T. Matthew Hansen, L. M. Lasko, K. D. Bromberg, V. Manaves,

M. Algire, R. Martin, W. Qiu, M. Torrent, C. G. Jakob, H. Liu, P. A. Cole, R. Marmorstein, E. A. Kesicki, A. Lai and M. R. Michaelides, *Bioorganic Med. Chem. Lett.*, 2021, **39**, 127854.

138 J. H. Shrimp, A. W. Sorum, J. M. Garlick, L. Guasch, M. C. Nicklaus and J. L. Meier, *ACS Med. Chem. Lett.*, 2016, **7**, 151–155.

139 K. S. Smith, P. L. Smith, T. N. Heady, J. M. Trugman, W. D. Harman and T. L. Macdonald, *Chem. Res. Toxicol.*, 2003, **16**, 123–128.

140 J. L. Dahlin, K. M. Nelson, J. M. Strasser, D. Barsyte-Lovejoy, M. M. Szewczyk, S. Organ, M. Cuellar, G. Singh, J. H. Shrimp, N. Nguyen, J. L. Meier, C. H. Arrowsmith, P. J. Brown, J. B. Baell and M. A. Walters, *Nat. Commun.*, 2017, **8**, 1527.

141 B. E. Zucconi, J. L. Makofske, D. J. Meyers, Y. Hwang, M. Wu, M. I. Kuroda and P. A. Cole, *Biochemistry*, 2019, **58**, 2133–2143.

142 H. M. Chan and N. B. La Thangue, *J. Cell Sci.*, 2001, **114**, 2363–2373.

143 C. Dhalluin, J. E. Carlson, L. Zeng, C. He, A. K. Aggarwal and M. M. Zhou, *Nature*, 1999, **399**, 491–496.

144 R. Sanchez, J. Meslamani and M. M. Zhou, *Biochim. Biophys. Acta - Gene Regul. Mech.*, 2014, **1839**, 676–685.

145 S. Mujtaba, L. Zeng and M. M. Zhou, *Oncogene*, 2007, **26**, 5521–5527.

146 L. R. Vidler, N. Brown, S. Knapp and S. Hoelder, *J. Med. Chem.*, 2012, **55**, 7346–7359.

147 M. C. Hewitt, Y. Leblanc, V. S. Gehling, R. G. Vaswani, A. Côté, C. G. Nasveschuk, A. M. Taylor, J. C. Harmange, J. E. Audia, E. Pardo, R. Cummings, S. Joshi, P. Sandy, J. A. Mertz, R. J. Sims, L. Bergeron, B. M. Bryant, S. Bellon, F. Poy, H. Jayaran, Y. Tang and B. K. Albrecht, *Bioorganic Med. Chem. Lett.*, 2015, **25**, 1842–1848.

148 A. M. Taylor, R. G. Vaswani, V. S. Gehling, M. C. Hewitt, Y. Leblanc, J. E. Audia, S. Bellon, R. T. Cummings, A. Coîté, J. C. Harmange, H. Jayaram, S. Joshi, J. M. Lora, J. A. Mertz, A. Neiss, E. Pardo, C. G. Nasveschuk, F. Poy, P. Sandy, J. W. Setser, R. J. Sims, Y. Tang and B. K. Albrecht, *ACS Med. Chem. Lett.*, 2016, **7**, 145–150.

149 R. A. Denny, A. C. Flick, J. Coe, J. Langille, A. Basak, S. Liu, I. Stock, P. Sahasrabudhe, P. Bonin, D. A. Hay, P. E. Brennan, M. Pletcher, L. H. Jones and E. L. P. Chekler, *J. Med. Chem.*, 2017, **60**, 5349–5363.

150 A. Muthengi, V. K. Wimalasena, H. O. Yosief, M. J. Bikowitz, L. H. Sigua, T. Wang, D. Li, Z. Gaieb, G. Dhawan, S. Liu, J. Erickson, R. E. Amaro, E. Schönbrunn, J. Qi and W. Zhang, *J. Med. Chem.*, 2021, **64**, 5787–5801.

151 T. D. Crawford, F. A. Romero, K. W. Lai, V. Tsui, A. M. Taylor, G. De Leon Boenig, C. L. Noland, J. Murray, J. Ly, E. F. Choo, T. L. Hunsaker, E. W. Chan, M. Merchant, S. Kharbanda, K. E. Gascoigne, S. Kaufman, M. H. Beresini, J. Liao, W. Liu, K. X. Chen, Z. Chen, A. R. Conery, A. Côté, H. Jayaram, Y. Jiang, J. R. Kiefer, T. Kleinheinz, Y. Li, J. Maher, E. Pardo, F. Poy, K. L. Spillane, F. Wang, J. Wang, X. Wei, Z. Xu, Z. Xu, I. Yen, L. Zawadzke, X. Zhu, S. Bellon, R. Cummings, A. G. Cochran, B. K. Albrecht and S. Magnuson, *J. Med. Chem.*, 2016, **59**, 10549–10563.

152 F. A. Romero, J. Murray, K. W. Lai, V. Tsui, B. K. Albrecht, L. An, M. H. Beresini, G. De Leon Boenig, S. M. Bronner, E. W. Chan, K. X. Chen, Z. Chen, E. F. Choo, K. Clagg, K. Clark, T. D. Crawford, P. Cyr, D. De Almeida Nagata, K. E. Gascoigne, J. L. Grogan, G.

Hatzivassiliou, W. Huang, T. L. Hunsaker, S. Kaufman, S. G. Koenig, R. Li, Y. Li, X. Liang, J. Liao, W. Liu, J. Ly, J. Maher, C. Masui, M. Merchant, Y. Ran, A. M. Taylor, J. Wai, F. Wang, X. Wei, D. Yu, B. Y. Zhu, X. Zhu and S. Magnuson, *J. Med. Chem.*, 2017, **60**, 9162–9183.

153 N. Brooks, M. Raja, B. W. Young, G. J. Spencer, T. C. Somervaille and N. A. Pegg, *Blood*, 2019, **134**, 2560–2560.

154 M. Brand, J. Clayton, M. Moroglu, M. Schiedel, S. Picaud, J. P. Bluck, A. Skwarska, H. Bolland, A. K. N. Chan, C. M. C. Laurin, A. R. Scorah, L. See, T. P. C. Rooney, K. H. Andrews, O. Fedorov, G. Perell, P. Kalra, K. B. Vinh, W. A. Cortopassi, P. Heitel, K. E. Christensen, R. I. Cooper, R. S. Paton, W. C. K. Pomerantz, P. C. Biggin, E. M. Hammond, P. Filippakopoulos and S. J. Conway, *J. Med. Chem.*, 2021, **XXX**, XXX–XXX.

155 Study to Evaluate CCS1477 in Advanced Tumours, https://clinicaltrials.gov/ct2/show/NCT03568656, (accessed 2 July 2021).

156 R. Chopra, A. Sadok and I. Collins, *Drug Discov. Today Technol.*, 2019, **31**, 5–13.

157 M. H. Glickman and A. Ciechanover, *Physiol. Rev.*, 2002, **82**, 373–428.

158 R. Yau and M. Rape, *Nat. Cell Biol.*, 2016, **18**, 579–586.

159 M. S. Weiss and G. E. Schulz, *J. Mol. Biol.*, 1992, **227**, 493–509.

160 D. Komander and M. Rape, *Annu. Rev. Biochem.*, 2012, **81**, 203–229.

161 R. J. Deshaies and C. A. P. Joazeiro, *Annu. Rev. Biochem.*, 2009, **78**, 399–434.

162 Y. Ye and M. Rape, *Nat. Rev. Mol. Cell Biol.*, 2009, **10**, 755–764.

163 B. A. Schulman and J. Wade Harper, *Nat. Rev. Mol. Cell Biol.*, 2009, **10**, 319–331.

164 O. Kerscher, R. Felberbaum and M. Hochstrasser, *Annu. Rev. Cell Dev. Biol.*, 2006, **22**, 159–180.

165 D. Mukhopadhyay and H. Riezman, *Science.*, 2007, **315**, 201–205.

166 C. L. Brooks and W. Gu, *FEBS Lett.*, 2011, **585**, 2803–2809.

167 M. A. E. Lohrum, D. B. Woods, R. L. Ludwig, É. Bálint and K. H. Vousden, *Mol. Cell. Biol.*, 2001, **21**, 8521–8532.

168 M. Li, C. L. Brooks, F. Wu-baer, D. Chen, R. Baer, M. Li, C. L. Brooks, F. Wu-baer and D. Chen, *Science.*, 2003, **302**, 1972–1975.

169 J. H. Lee, S. M. Jung, K. M. Yang, E. Bae, S. G. Ahn, J. S. Park, D. Seo, M. Kim, J. Ha, J. Lee, J. H. Kim, J. H. Kim, A. Ooshima, J. Park, D. Shin, Y. S. Lee, S. Lee, G. Van Loo, J. Jeong, S. J. Kim and S. H. Park, *Nat. Cell Biol.*, 2017, **19**, 1260–1273.

170 H. J. Meyer and M. Rape, *Cell*, 2014, **157**, 910–921.

171 R. G. Yau, K. Doerner, E. R. Castellanos, D. L. Haakonsen, A. Werner, N. Wang, X. W. Yang, N. Martinez-Martin, M. L. Matsumoto, V. M. Dixit and M. Rape, *Cell*, 2017, **171**, 918-933.e20.

172 G. Bjørkøy, T. Lamark, S. Pankiv, A. Øvervatn, A. Brech and T. Johansen, *Methods Enzymol.*, 2009, **451**, 181–197.

173 E. Oh, K. G. Mark, A. Mocciaro, E. R. Watson, J. R. Prabu, D. D. Cha, M. Kampmann, N.

Gamarra, C. Y. Zhou and M. Rape, *Nature*, 2020, **579**, 136–140.

174 C. Liu, W. Liu, Y. Ye and W. Li, *Nat. Commun.*, 2017, **8**, 14274.

175 M. B. Metzger, V. A. Hristova and A. M. Weissman, *J. Cell Sci.*, 2012, **125**, 531–537.

176 C. E. Berndsen and C. Wolberger, *Nat. Struct. Mol. Biol.*, 2014, **21**, 301–307.

177 W. Li, M. H. Bengtson, A. Ulbrich, A. Matsuda, V. A. Reddy, A. Orth, S. K. Chanda, S. Batalov and C. A. P. Joazeiro, *PLoS One*, 2008, **3**, e1487.

178 E. S. Fischer, K. Böhm, J. R. Lydeard, H. Yang, M. B. Stadler, S. Cavadini, J. Nagel, F. Serluca, V. Acker, G. M. Lingaraju, R. B. Tichkule, M. Schebesta, W. C. Forrester, M. Schirle, U. Hassiepen, J. Ottl, M. Hild, R. E. J. Beckwith, J. W. Harper, J. L. Jenkins and N. H. Thomä, *Nature*, 2014, **512**, 49–53.

179 J. Weber, S. Polo and E. Maspero, *Front. Physiol.*, 2019, **10**, 1–8.

180 D. H. Lee, *Trends Cell Biol.*, 1998, **8**, 397–403.

181 R. Verma, L. Aravind, R. Oania, W. H. McDonald, J. R. Yates, E. V. Koonin and R. J. Deshaies, *Science.*, 2002, **298**, 611–615.

182 Y. Saeki, *J. Biochem.*, 2017, **161**, mvw091.

183 W. Baumeister, J. Walz, F. Zühl and E. Seemüller, *Cell*, 1998, **92**, 367–380.

184 J. Adams, *Nat. Rev. Cancer*, 2004, **4**, 349–360.

185 K. R. Landis-Piwowar, V. Milacic, D. Chen, H. Yang, Y. Zhao, T. H. Chan, B. Yan and Q. P. Dou, *Drug Resist. Updat.*, 2006, **9**, 263–273.

186 B. S. Moore, A. S. Eustáquio and R. P. McGlinchey, *Curr. Opin. Chem. Biol.*, 2008, **12**, 434–440.

187 G. Fenteany, R. F. Standaert, W. S. Lane, S. Choi, E. J. Corey and S. L. Schreiber, *Science.*, 1995, **268**, 726–731.

188 A. Paramore and S. Frantz, *Nat. Rev. Drug Discov.*, 2003, **2**, 611–612.

189 D. Chauhan, Z. Tian, B. Zhou, D. Kuhn, R. Orlowski, N. Raje, P. Richardson and K. C. Anderson, *Clin. Cancer Res.*, 2011, **17**, 5311–5321.

190 K. B. Kim and C. M. Crews, *Nat. Prod. Rep.*, 2013, **30**, 600–604.

191 J. B. Almond and G. M. Cohen, *Leukemia*, 2002, 16, 433–443.

192 P. J. Elliott, T. M. Zollner and W. H. Boehncke, *J. Mol. Med.*, 2003, **81**, 235–245.

193 J. Adams, M. Behnke, S. Chen, A. A. Cruickshank, L. R. Dick, L. Grenier, J. M. Klunder, Y.-T. Ma, L. Plamondon and R. L. Stein, *Bioorg. Med. Chem. Lett.*, 1998, **8**, 333–338.

194 P. Bonvini, E. Zorzi, G. Basso and A. Rosolen, *Leukemia*, 2007, **21**, 838–842.

195 R. A. Kyle and S. V. Rajkumar, *Clin. Lymphoma Myeloma*, 2009, **9**, 278–288.

196 B. C. Potts, M. X. Albitar, K. C. Anderson, S. Baritaki, C. Berkers, B. Bonavida, J. Chandra, D. Chauhan, J. C. Cusack, W. Fenical, I. M. Ghobrial, M. Groll, P. R. Jensen, K. S. Lam, G. K. Lloyd, W. McBride, D. J. McConkey, C. P. Miller, S. T.C. Neuteboom, Y. Oki, H. Ovaa, F. Pajonk, P. G. Richardson, A. M. Roccaro, C. M. Sloss, M. A. Spear, E. Valashi, A. Younes and M. A. Palladino, *Marizomib, a Proteasome Inhibitor for All Seasons: Preclinical*

Profile and a Framework for Clinical Trials, 2011, vol. 11.

197 A. J. Jakubowiak, D. Dytfeld, K. A. Griffith, D. Lebovic, D. H. Vesole, S. Jagannath, A. Al-Zoubi, T. Anderson, B. Nordgren, K. Detweiler-Short, K. Stockerl-Goldstein, A. Ahmed, T. Jobkar, D. E. Durecki, K. McDonnell, M. Mietzel, D. Couriel, M. Kaminski and R. Vij, *Blood*, 2012, **120**, 1801–1809.

198 R. Hájek, R. Bryce, S. Ro, B. Klencke and H. Ludwig, *BMC Cancer*, 2012, **12**, 415.

199 Q. Dou and J. Zonder, *Curr. Cancer Drug Targets*, 2014, **14**, 517–536.

200 W. Lenz, *Am. J. Dis. Child.*, 1966, **112**, 99–106.

201 T. Ito, H. Ando, T. Suzuki, T. Ogura, K. Hotta, Y. Imamura, Y. Yamaguchi and H. Handa, *Science.*, 2010, **327**, 1345–1350.

202 N. Vargesson, *Birth Defects Res. Part C - Embryo Today Rev.*, 2015, **105**, 140–156.

203 S. Gao, S. Wang and Y. Song, *Biomark. Res.*, 2020, **8**, 1–8.

204 A. K. Stewart, *Science.*, 2014, **343**, 256–257.

205 G. Lu, R. E. Middleton, H. Sun, M. V. Naniong, C. J. Ott, C. S. Mitsiades, K. K. Wong, J. E. Bradner and W. G. Kaelin, *Science.*, 2014, **343**, 305–309.

206 J. Krönke, N. D. Udeshi, A. Narla, P. Grauman, S. N. Hurst, M. McConkey, T. Svinkina, D. Heckl, E. Comer, X. Li, C. Ciarlo, E. Hartman, N. Munshi, M. Schenone, S. L. Schreiber, S. A. Carr and B. L. Ebert, *Science.*, 2014, **343**, 301–305.

207 T. Mori, T. Ito, S. Liu, H. Ando, S. Sakamoto, Y. Yamaguchi, E. Tokunaga, N. Shibata, H. Handa and T. Hakoshima, *Sci. Rep.*, 2018, **8**, 1–14.

208 C. Vitale, L. Falchi, E. Ten Hacken, H. Gao, H. Shaim, K. Van Roosbroeck, G. Calin, S. O'Brien, S. Faderl, X. Wang, W. G. Wierda, K. Rezvani, J. M. Reuben, J. A. Burger, M. J. Keating and A. Ferrajoli, *Clin. Cancer Res.*, 2016, **22**, 2359–2367.

209 A. List, G. Dewald, J. Bennett, A. Giagounidis, A. Raza, E. Feldman, B. Powell, P. Greenberg, D. Thomas, R. Stone, C. Reeder, K. Wride, J. Patin, M. Schmidt, J. Zeldis and R. Knight, *N. Engl. J. Med.*, 2006, **355**, 1456–1465.

210 A. Ladha, J. Zhao, E. M. Epner and J. J. Pu, *Exp. Hematol. Oncol.*, 2019, **8**, 1–9.

211 R. Gopalakrishnan, H. Matta, B. Tolani, T. Triche Jr and P. M. Chaudhary, *Oncogene*, 2016, **35**, 1797–1810.

212 P. R. Hagner, H.-W. Man, C. Fontanillo, M. Wang, S. Couto, M. Breider, C. Bjorklund, C. G. Havens, G. Lu, E. Rychak, H. Raymon, R. K. Narla, L. Barnes, G. Khambatta, H. Chiu, J. Kosek, J. Kang, M. D. Amantangelo, M. Waldman, A. Lopez-Girona, T. Cai, M. Pourdehnad, M. Trotter, T. O. Daniel, P. H. Schafer, A. Klippel, A. Thakurta, R. Chopra and A. K. Gandhi, *Blood*, 2015, **126**, 779–789.

213 Study of CC-122 to Evaluate the Safety, Tolerability, and Effectiveness for Patients With Advanced Solid Tumors, Non-Hodgkin's Lymphoma, or Multiple Myeloma, https://clinicaltrials.gov/ct2/show/NCT01421524, (accessed 5 July 2021).

214 M. E. Matyskiela, W. Zhang, H. W. Man, G. Muller, G. Khambatta, F. Baculi, M. Hickman, L. Lebrun, B. Pagarigan, G. Carmel, C. C. Lu, G. Lu, M. Riley, Y. Satoh, P. Schafer, T. O. Daniel, J. Carmichael, B. E. Cathers and P. P. Chamberlain, *J. Med. Chem.*, 2018, **61**, 535–542.

215 A Study to Determine Dose, Safety, Tolerability and Efficacy of CC-220 Monotherapy, and in Combination With Other Treatments in Subjects With Multiple Myeloma, https://clinicaltrials.gov/ct2/show/NCT02773030, (accessed 5 July 2021).

216 M. E. Matyskiela, G. Lu, T. Ito, B. Pagarigan, C. C. Lu, K. Miller, W. Fang, N. Y. Wang, D. Nguyen, J. Houston, G. Carmel, T. Tran, M. Riley, L. Nosaka, G. C. Lander, S. Gaidarova, S. Xu, A. L. Ruchelman, H. Handa, J. Carmichael, T. O. Daniel, B. E. Cathers, A. Lopez-Girona and P. P. Chamberlain, *Nature*, 2016, **535**, 252–257.

217 G. M. Burslem and C. M. Crews, *Chem. Rev.*, 2017, **117**, 11269–11301.

218 K. M. Sakamoto, K. B. Kim, A. Kumagai, F. Mercurio, C. M. Crews and R. J. Deshaies, *Proc. Natl. Acad. Sci.*, 2001, **98**, 8554–8559.

219 K. M. Sakamoto, K. B. Kim, R. Verma, A. Ransick, B. Stein, C. M. Crews and R. J. Deshaies, *Mol. Cell. Proteomics*, 2003, **2**, 1350–1358.

220 M. Ivan, K. Kondo, H. Yang, W. Kim, J. Valiando, M. Ohh, A. Salic, J. M. Asara, W. S. Lane and J. Kaelin, *Science.*, 2001, **292**, 464–468.

221 P. Jaakkola, D. R. Mole, Y. M. Tian, M. I. Wilson, J. Gielbert, S. J. Gaskell, A. Von Kriegsheim, H. F. Hebestreit, M. Mukherji, C. J. Schofield, P. H. Maxwell, C. W. Pugh and P. J. Ratcliffe, *Science.*, 2001, **292**, 468–472.

222 J. S. Schneekloth, F. N. Fonseca, M. Koldobskiy, A. Mandal, R. Deshaies, K. Sakamoto and C. M. Crews, *J. Am. Chem. Soc.*, 2004, **126**, 3748–3754.

223 P. Bargagna-Mohan, S. H. Baek, H. Lee, K. Kim and R. Mohan, *Bioorganic Med. Chem. Lett.*, 2005, **15**, 2724–2727.

224 H. Lee, D. Puppala, E. Y. Choi, H. Swanson and K. B. Kim, *ChemBioChem*, 2007, **8**, 2058–2062.

225 D. Zhang, S. H. Baek, A. Ho and K. Kim, *Bioorganic Med. Chem. Lett.*, 2004, **14**, 645–648.

226 X. Wang, S. Feng, J. Fan, X. Li, Q. Wen and N. Luo, *Biochem. Pharmacol.*, 2016, **116**, 200–209.

227 R. K. Henning, J. O. Varghese, S. Das, A. Nag, G. Tang, K. Tang, A. M. Sutherland and J. R. Heath, *J. Pept. Sci.*, 2016, **22**, 196–200.

228 J. Zheng, C. Tan, P. Xue, J. Cao, F. Liu, Y. Tan and Y. Jiang, *Biochem. Biophys. Res. Commun.*, 2016, **470**, 936–940.

229 T. T. Chu, N. Gao, Q. Q. Li, P. G. Chen, X. F. Yang, Y. X. Chen, Y. F. Zhao and Y. M. Li, *Cell Chem. Biol.*, 2016, **23**, 453–461.

230 A. R. Schneekloth, M. Pucheault, H. S. Tae and C. M. Crews, *Bioorganic Med. Chem. Lett.*, 2008, **18**, 5904–5908.

231 D. L. Buckley, I. Van Molle, P. C. Gareiss, H. S. Tae, J. Michel, D. J. Noblin, W. L. Jorgensen, A. Ciulli and C. M. Crews, *J. Am. Chem. Soc.*, 2012, **134**, 4465–4468.

232 D. L. Buckley, J. L. Gustafson, I. Van-Molle, A. G. Roth, H. S. Tae, P. C. Gareiss, W. L. Jorgensen, A. Ciulli and C. M. Crews, *Angew. Chemie - Int. Ed.*, 2012, **51**, 11463–11467.

233 C. Galdeano, M. S. Gadd, P. Soares, S. Scaffidi, I. Van Molle, I. Birced, S. Hewitt, D. M. Dias and A. Ciulli, *J. Med. Chem.*, 2014, **57**, 8657–8663.

234 D. P. Bondeson, A. Mares, I. E. D. Smith, E. Ko, S. Campos, A. H. Miah, K. E. Mulholland, N. Routly, D. L. Buckley, J. L. Gustafson, N. Zinn, P. Grandi, S. Shimamura, G. Bergamini, M. Faelth-Savitski, M. Bantscheff, C. Cox, D. A. Gordon, R. R. Willard, J. J. Flanagan, L. N. Casillas, B. J. Votta, W. Den Besten, K. Famm, L. Kruidenier, P. S. Carter, J. D. Harling, I. Churcher and C. M. Crews, *Nat. Chem. Biol.*, 2015, **11**, 611–617.

235 G. E. Winter, D. L. Buckley, J. Paulk, J. M. Roberts, A. Souza, S. Dhe-Paganon and J. E. Bradner, *Science.*, 2015, **348**, 1376–1381.

236 J. Lu, Y. Qian, M. Altieri, H. Dong, J. Wang, K. Raina, J. Hines, J. D. Winkler, A. P. Crew, K. Coleman and C. M. Crews, *Chem. Biol.*, 2015, **22**, 755–763.

237 K. Raina, J. Lu, Y. Qian, M. Altieri, D. Gordon, A. M. K. Rossi, J. Wang, X. Chen, H. Dong, K. Siu, J. D. Winkler, A. P. Crew, C. M. Crews and K. G. Coleman, *Proc. Natl. Acad. Sci.*, 2016, **113**, 7124–7129.

238 M. Zengerle, K. H. Chan and A. Ciulli, *ACS Chem. Biol.*, 2015, **10**, 1770–1777.

239 M. S. Gadd, A. Testa, X. Lucas, K. H. Chan, W. Chen, D. J. Lamont, M. Zengerle and A. Ciulli, *Nat. Chem. Biol.*, 2017, **13**, 514–521.

240 A. Testa, S. J. Hughes, X. Lucas, J. E. Wright and A. Ciulli, *Angew. Chemie - Int. Ed.*, 2020, **59**, 1727–1734.

241 A. H. Shain and J. R. Pollack, *PLoS One*, 2013, **8**, e55119.

242 R. C. Centore, G. J. Sandoval, L. M. M. Soares, C. Kadoch and H. M. Chan, *Trends Genet.*, 2020, **36**, 936–950.

243 C. Hodges, J. G. Kirkland and G. R. Crabtree, *Cold Spring Harb. Perspect. Med.*, 2016, **6**, a026930.

244 W. Farnaby, M. Koegl, M. J. Roy, C. Whitworth, E. Diers, N. Trainor, D. Zollman, S. Steurer, J. Karolyi-Oezguer, C. Riedmueller, T. Gmaschitz, J. Wachter, C. Dank, M. Galant, B. Sharps, K. Rumpel, E. Traxler, T. Gerstberger, R. Schnitzer, O. Petermann, P. Greb, H. Weinstabl, G. Bader, A. Zoephel, A. Weiss-Puxbaum, K. Ehrenhöfer-Wölfer, S. Wöhrle, G. Boehmelt, J. Rinnenthal, H. Arnhof, N. Wiechens, M. Y. Wu, T. Owen-Hughes, P. Ettmayer, M. Pearson, D. B. McConnell and A. Ciulli, *Nat. Chem. Biol.*, 2019, **15**, 672–680.

245 A. C. Lai, M. Toure, D. Hellerschmied, J. Salami, S. Jaime-Figueroa, E. Ko, J. Hines and C. M. Crews, *Angew. Chemie - Int. Ed.*, 2016, **55**, 807–810.

246 WO2020/092907, 2020.

247 R. Vannam, J. Sayilgan, S. Ojeda, B. Karakyriakou, E. Hu, J. Kreuzer, R. Morris, X. I. Herrera Lopez, S. Rai, W. Haas, M. Lawrence and C. J. Ott, *Cell Chem. Biol.*, 2021, **28**, 503-514.e12.

248 T. Neklesa, L. B. Snyder, R. R. Willard, N. Vitale, J. Pizzano, D. A. Gordon, M. Bookbinder, J. Macaluso, H. Dong, C. Ferraro, G. Wang, J. Wang, C. M. Crews, J. Houston, A. P. Crew and I. Taylor, *J. Clin. Oncol.*, 2019, **37**, 259.

249 J. J. Flanagan, Y. Qian, S. M. Gough, M. Andreoli, M. Bookbinder, G. Cadelina, J. Bradley, E. Rousseau, R. Willard, J. Pizzano, C. M. Crews, A. P. Crew, I. Taylor and J. Houston, *Cancer Res.*, 2019, **79**, P5-04-18 LP-P5-04–18.

250 X. Li and Y. Song, *J. Hematol. Oncol.*, 2020, **13**, 1–14.

251 M. Naito, N. Ohoka and N. Shibata, *Drug Discov. Today Technol.*, 2019, **31**, 35–42.

252 C. W. Wright and C. S. Duckett, *J. Clin. Invest.*, 2005, **115**, 2673–2678.

253 K. Okuhira, Y. Demizu, T. Hattori, N. Ohoka, N. Shibata, T. Nishimaki-Mogami, H. Okuda, M. Kurihara and M. Naito, *Cancer Sci.*, 2013, **104**, 1492–1498.

254 N. Ohoka, K. Okuhira, M. Ito, K. Nagai, N. Shibata, T. Hattori, O. Ujikawa, K. Shimokawa, O. Sano, R. Koyama, H. Fujita, M. Teratani, H. Matsumoto, Y. Imaeda, H. Nara, N. Cho and M. Naito, *J. Biol. Chem.*, 2017, **292**, 4556–4570.

255 K. Sekine, K. Takubo, R. Kikuchi, M. Nishimoto, M. Kitagawa, F. Abe, K. Nishikawa, T. Tsuruo and M. Naito, *J. Biol. Chem.*, 2008, **283**, 8961–8968.

256 G. V Los, L. P. Encell, M. G. McDougall, D. D. Hartzell, N. Karassina, C. Zimprich, M. G. Wood, R. Learish, R. F. Ohana, M. Urh, D. Simpson, J. Mendez, K. Zimmerman, P. Otto, G. Vidugiris, J. Zhu, A. Darzins, D. H. Klaubert, R. F. Bulleit and K. V. Wood, *ACS Chem. Biol.*, 2008, **3**, 373–382.

257 T. K. Neklesa, H. S. Tae, A. R. Schneekloth, M. J. Stulberg, T. W. Corson, T. B. Sundberg, K. Raina, S. A. Holley and C. M. Crews, *Nat. Chem. Biol.*, 2011, **7**, 538–543.

258 V. R. Agashe, M. C. R. Shastry and J. B. Udgaonkar, *Nature*, 1995, **377**, 754–757.

259 L. Lins and R. Brasseur, *FASEB J.*, 1995, **9**, 535–540.

260 H. Kubota, *J. Biochem.*, 2009, **146**, 609–616.

261 D. L. Buckley, K. Raina, N. Darricarrere, J. Hines, J. L. Gustafson, I. E. Smith, A. H. Miah, J. D. Harling and C. M. Crews, *ACS Chem. Biol.*, 2015, **10**, 1831–1837.

262 B. Nabet, J. M. Roberts, D. L. Buckley, J. Paulk, S. Dastjerdi, A. Yang, A. L. Leggett, M. A. Erb, M. A. Lawlor, A. Souza, T. G. Scott, S. Vittori, J. A. Perry, J. Qi, G. E. Winter, K. K. Wong, N. S. Gray and J. E. Bradner, *Nat. Chem. Biol.*, 2018, **14**, 431–441.

263 N. Mizushima and M. Komatsu, *Cell*, 2011, **147**, 728–741.

264 K. Lu, F. den Brave and S. Jentsch, *Autophagy*, 2017, **13**, 1799–1800.

265 A. M. K. Choi, S. W. Ryter and B. Levine, *N. Engl. J. Med.*, 2013, **368**, 651–662.

266 P. Jiang and N. Mizushima, *Cell Res.*, 2014, **24**, 69–79.

267 D. Takahashi, J. Moriyama, T. Nakamura, E. Miki, E. Takahashi, A. Sato, T. Akaike, K. Itto-Nakama and H. Arimoto, *Mol. Cell*, 2019, **76**, 797-810.e10.

268 M. Luo, X. Zhao, Y. Song, H. Cheng and R. Zhou, *Autophagy*, 2016, **12**, 1973–1983.

269 Z. Li, C. Wang, Z. Wang, C. Zhu, J. Li, T. Sha, L. Ma, C. Gao, Y. Yang, Y. Sun, J. Wang, X. Sun, C. Lu, M. Difiglia, Y. Mei, C. Ding, S. Luo, Y. Dang, Y. Ding, Y. Fei and B. Lu, *Nature*, 2019, **575**, 203–209.

270 G. P. Bates, R. Dorsey, J. F. Gusella, M. R. Hayden, C. Kay, B. R. Leavitt, M. Nance, C. A. Ross, R. I. Scahill, R. Wetzel, E. J. Wild and S. J. Tabrizi, *Nat. Rev. Dis. Prim.*, 2015, **1**, 15005.

271 Z. Li, C. Zhu, Y. Ding, Y. Fei and B. Lu, *Autophagy*, 2020, **16**, 185–187.

272 D. Takahashi and H. Arimoto, *Cell Chem. Biol.*, 2021, 1–11.

273 WO2019/183600A1, 2019.

274 M. Uhlen, L. Fagerberg, B. M. Hallstrom, C. Lindskog, P. Oksvold, A. Mardinoglu, A. Sivertsson, C. Kampf, E. Sjostedt, A. Asplund, I. Olsson, K. Edlund, E. Lundberg, S. Navani, C. A.-K. Szigyarto, J. Odeberg, D. Djureinovic, J. O. Takanen, S. Hober, T. Alm, P.-H. Edqvist, H. Berling, H. Tegel, J. Mulder, J. Rockberg, P. Nilsson, J. M. Schwenk, M. Hamsten, K. von Feilitzen, M. Forsberg, L. Persson, F. Johansson, M. Zwahlen, G. von Heijne, J. Nielsen and F. Ponten, *Science.*, 2015, **347**, 1260419–1260419.

275 K. J. Brown, H. Seol, D. K. Pillai, B. J. Sankoorikal, C. A. Formolo, J. Mac, N. J. Edwards, M. C. Rose and Y. Hathout, *Biochim. Biophys. Acta - Proteins Proteomics*, 2013, **1834**, 2454–2461.

276 S. M. Banik, K. Pedram, S. Wisnovsky, G. Ahn, N. M. Riley and C. R. Bertozzi, *Nature*, 2020, **584**, 291–297.

277 G. Ahn, S. M. Banik, C. L. Miller, N. M. Riley, J. R. Cochran and C. R. Bertozzi, *Nat. Chem. Biol.*, 2021, **28**, 1–13.

278 C. M. Walko and H. J. West, *JAMA Oncol.*, 2019, **5**, 1648.

279 P. M. LoRusso, D. Weiss, E. Guardino, S. Girish and M. X. Sliwkowski, *Clin. Cancer Res.*, 2011, **17**, 6437–6447.

280 M. Maneiro, N. Forte, M. M. Shchepinova, C. S. Kounde, V. Chudasama, J. R. Baker and E. W. Tate, *ACS Chem. Biol.*, 2020, **15**, 1306–1312.

281 P. K. Mahalingaiah, R. Ciurlionis, K. R. Durbin, R. L. Yeager, B. K. Philip, B. Bawa, S. R. Mantena, B. P. Enright, M. J. Liguori and T. R. Van Vleet, *Pharmacol. Ther.*, 2019, **200**, 110–125.

282 P. S. Dragovich, P. Adhikari, R. A. Blake, N. Blaquiere, J. Chen, Y. X. Cheng, W. den Besten, J. Han, S. J. Hartman, J. He, M. He, E. Rei Ingalla, A. V. Kamath, T. Kleinheinz, T. Lai, D. D. Leipold, C. S. Li, Q. Liu, J. Lu, Y. Lu, F. Meng, L. Meng, C. Ng, K. Peng, G. Lewis Phillips, T. H. Pillow, R. K. Rowntree, J. D. Sadowsky, D. Sampath, L. Staben, S. T. Staben, J. Wai, K. Wan, X. Wang, B. Q. Wei, I. E. Wertz, J. Xin, K. Xu, H. Yao, R. Zang, D. Zhang, H. Zhou and Y. Zhao, *Bioorganic Med. Chem. Lett.*, 2020, **30**, 126907.

283 A. C. Belkina, B. S. Nikolajczyk and G. V. Denis, *J. Immunol.*, 2013, **190**, 3670–3678.

284 F. Giles, M. Witcher and B. Brown, *Ann. Oncol.*, 2018, **29**, viii140–viii141.

285 Y. Yan, J. Ma, D. Wang, D. Lin, X. Pang, S. Wang, Y. Zhao, L. Shi, H. Xue, Y. Pan, J. Zhang, C. Wahlestedt, F. J. Giles, Y. Chen, M. E. Gleave, C. C. Collins, D. Ye, Y. Wang and H. Huang, *EMBO Mol. Med.*, 2019, **11**, 1–19.

286 F. Spriano, E. Gaudio, L. Cascione, C. Tarantelli, F. Melle, G. Motta, V. Priebe, A. Rinaldi, G. Golino, A. A. Mensah, L. Aresu, E. Zucca, S. Pileri, M. Witcher, B. Brown, C. Wahlestedt, F. Giles, A. Stathis and F. Bertoni, *Blood Adv.*, 2020, **4**, 4124–4135.

287 S. N. Meyer, C. Scuoppo, S. Vlasevska, E. Bal, A. B. Holmes, M. Holloman, L. Garcia-Ibanez, S. Nataraj, R. Duval, T. Vantrimpont, K. Basso, N. Brooks, R. Dalla-Favera and L. Pasqualucci, *Immunity*, 2019, **51**, 535-547.e9.

288 A. G. Cochran, A. R. Conery and R. J. Sims, *Nat. Rev. Drug Discov.*, 2019, **18**, 609–628.

289 V. Garcia-Carpizo, S. Ruiz-Llorente, J. Sarmentero, A. Gonzalez-Corpas and M. J. Barrero, *Mol. Cancer Res.*, 2019, **17**, 720–730.

290 C. O. Kappe and D. Dallinger, *Mol. Divers.*, 2009, **13**, 71–193.

291 M. Oghbaei and O. Mirzaee, *J. Alloys Compd.*, 2010, **494**, 175–189.

292 C. O. Kappe and D. Dallinger, *Nat. Rev. Drug Discov.*, 2006, **5**, 51–63.

293 C. Gabriel, S. Gabriel, E. H. Grant, B. S. J. Halstead and D. Michael P Mingos, *Chem. Soc. Rev.*, 1998, **27**, 213–223.

294 B. Wathey, J. Tierney, P. Lidström and J. Westman, *Drug Discov. Today*, 2002, **7**, 373–380.

295 Q. Yang, M. Sheng, X. Li, C. Tucker, S. Vásquez Céspedes, N. J. Webb, G. T. Whiteker and J. Yu, *Org. Process Res. Dev.*, 2020, **24**, 916–939.

296 N. Miyaura, K. Yamada and A. Suzuki, *Tetrahedron Lett.*, 1979, **20**, 3437–3440.

297 N. Miyaura and A. Suzuki, *Chem. Rev.*, 1995, **95**, 2457–2483.

298 L. Rocard, D. Hatych, T. Chartier, T. Cauchy and P. Hudhomme, *European J. Org. Chem.*, 2019, **2019**, 7635–7643.

299 M. R. Yadav, M. Nagaoka, M. Kashihara, R. L. Zhong, T. Miyazaki, S. Sakaki and Y. Nakao, *J. Am. Chem. Soc.*, 2017, **139**, 9423–9426.

300 T. N. Prize, The Nobel Prize in Chemsitry 2010, https://www.nobelprize.org/prizes/chemistry/2010/summary/, (accessed 12 May 2021).

301 D. Blakemore, in *RSC Drug Discovery Series*, 2016, vol. 2016-Janua, pp. 1–69.

302 Z. Ahmadi and J. S. McIndoe, *Chem. Commun.*, 2013, **49**, 11488–11490.

303 J. Sherwood, J. H. Clark, I. J. S. Fairlamb and J. M. Slattery, *Green Chem.*, 2019, **21**, 2164–2213.

304 N. A. Isley, M. S. Hageman and B. H. Lipshutz, *Green Chem.*, 2015, **17**, 893–897.

305 J. A. Mangravite, J. A. Verdone and H. G. Kuivila, *J. Organomet. Chem.*, 1976, **104**, 303–310.

306 A. J. J. Lennox and G. C. Lloyd-Jones, *Isr. J. Chem.*, 2010, **50**, 664–674.

307 P. A. Cox, A. G. Leach, A. D. Campbell and G. C. Lloyd-Jones, *J. Am. Chem. Soc.*, 2016, **138**, 9145–9157.

308 D. M. Knapp, E. P. Gillis and M. D. Burke, *J. Am. Chem. Soc.*, 2009, **131**, 6961–6963.

309 G. A. Molander, B. Canturk and L. E. Kennedy, *J. Org. Chem.*, 2009, **74**, 973–980.

310 J. T. Kuethe and K. G. Childers, *Adv. Synth. Catal.*, 2008, **350**, 1577–1586.

311 A. J. Close, P. Kemmitt, M. K. Emmerson and J. Spencer, *Tetrahedron*, 2014, **70**, 9125–9131.

312 A. J. J. Lennox and G. C. Lloyd-Jones, *Chem. Soc. Rev.*, 2014, **43**, 412–443.

313 S. S. Bhawal, R. A. Patil and D. W. Armstrong, *RSC Adv.*, 2015, **5**, 95854–95856.

314 T. Chandra and J. P. Zebrowski, *J. Chem. Heal. Saf.*, 2016, **23**, 16–25.

315 J. Spencer, N. Anjum, H. Patel, R. Rathnam and J. Verma, *Synlett*, 2007, **2007**, 2557–

2558.

316 C. Zhang, J. Lu, M. Li, Y. Wang, Z. Zhang, H. Chen and F. Wang, *Green Chem.*, 2016, **18**, 2435–2442.

317 N. R. Lee, A. A. Bikovtseva, M. Cortes-Clerget, F. Gallou and B. H. Lipshutz, *Org. Lett.*, 2017, **19**, 6518–6521.

318 A. A. Altaf, N. Khan, A. Badshah, B. Lal, Shafiqullah, S. Anwar and M. Subhan, *J. Chem. Soc. Pakistan*, 2011, **33**, 691–693.

319 T. A. Clohessy, A. Roberts, E. S. Manas, V. K. Patel, N. A. Anderson and A. J. B. Watson, *Org. Lett.*, 2017, **19**, 6368–6371.

320 D. Zhu, M. Lu, P. J. Chua, B. Tan, F. Wang, X. Yang and G. Zhong, *Org. Lett.*, 2008, **10**, 4585–4588.

321 A. Chinnappan and H. Kim, *RSC Adv.*, 2013, **3**, 3399.

322 G. Shen, L. Zhao, W. Liu, X. Huang, H. Song and T. Zhang, *Synth. Commun.*, 2017, **47**, 10–14.

323 G. La Sorella, G. Strukul and A. Scarso, *Green Chem.*, 2015, **17**, 644–683.

324 B. H. Lipshutz, S. Ghorai, A. R. Abela, R. Moser, T. Nishikata, C. Duplais, A. Krasovskiy, R. D. Gaston and R. C. Gadwood, *J. Org. Chem.*, 2011, **76**, 4379–4391.

325 M. Baron, E. Métay, M. Lemaire and F. Popowycz, *Green Chem.*, 2013, **15**, 1006–1015.

326 P. K. Mandal and J. S. McMurray, *J. Org. Chem.*, 2007, **72**, 6599–6601.

327 C. M. Gabriel, M. Parmentier, C. Riegert, M. Lanz, S. Handa, B. H. Lipshutz and F. Gallou, *Org. Process Res. Dev.*, 2017, **21**, 247–252.

328 R. J. Griffiths, W. C. Kong, S. A. Richards, G. A. Burley, M. C. Willis and E. P. A. Talbot, *Chem. Sci.*, 2018, **9**, 2295–2300.

329 A. Modvig, T. L. Andersen, R. H. Taaning, A. T. Lindhardt and T. Skrydstrup, *J. Org. Chem.*, 2014, **79**, 5861–5868.

330 P. Hermange, A. T. Lindhardt, R. H. Taaning, K. Bjerglund, D. Lupp and T. Skrydstrup, *J. Am. Chem. Soc.*, 2011, **133**, 6061–6071.

331 T. L. Andersen, M. W. Frederiksen, K. Domino and T. Skrydstrup, *Angew. Chemie - Int. Ed.*, 2016, **55**, 10396–10400.

332 S. D. Friis, A. T. Lindhardt and T. Skrydstrup, *Acc. Chem. Res.*, 2016, **49**, 594–605.

333 H. Yin, D. U. Nielsen, M. K. Johansen, A. T. Lindhardt and T. Skrydstrup, *ACS Catal.*, 2016, **6**, 2982–2987.

334 P. Vitale and A. Scilimati, *Recent Developments in the Chemistry of 3-Arylisoxazoles and 3-Aryl-2-isoxazolines*, Elsevier Ltd, 2017, vol. 122.

335 J. . Joule and K. Mills, *Heterocyclic Chemistry*, Wiley India Pvt., 2008.

336 N. C. Neyt and D. L. Riley, *Beilstein J. Org. Chem.*, 2018, **14**, 1529–1536.

337 N. C. Neyt and D. L. Riley, *React. Chem. Eng.*, 2018, **3**, 17–24.

338 M. B. Smith, *March's Advanced Organic Chemistry: Reactions, Mechanisms, and*

Structure, Wiley, 2019.

339 L. A. Carpino, H. Imazumi, B. M. Foxman, M. J. Vela, P. Henklein, A. El-Faham, J. Klose and M. Bienert, *Org. Lett.*, 2000, **2**, 2253–2256.

340 M. Wang, J. Lu, M. Wang, C. Y. Yang and S. Wang, *J. Med. Chem.*, 2020, **63**, 7510–7528.

341 M. Hanafi, X. Chen and N. Neamati, *J. Med. Chem.*, 2021, **64**, 1626–1648.

342 Y. Liu, Y. Zhen, G. Wang, G. Yang, L. Fu, B. Liu and L. Ouyang, *Eur. J. Med. Chem.*, 2020, **204**, 112505.

343 T. B. Nguyen, J. Sorres, M. Q. Tran, L. Ermolenko and A. Al-Mourabit, *Org. Lett.*, 2012, **14**, 3202–3205.

344 M. M. Heravi, M. Ghavidel and L. Mohammadkhani, *RSC Adv.*, 2018, **8**, 27832–27862.

345 US, 0075706 A1, 2013, 15.

346 US, 0002524 A1, 2004, 20.

347 V. Rauniyar and D. G. Hall, *J. Org. Chem.*, 2009, **74**, 4236–4241.

348 C. A. Lipinski, F. Lombardo, B. W. Dominy and P. J. Feeney, *Adv. Drug Deliv. Rev.*, 2001, **46**, 3–26.

349 C. A. Lipinski, *Drug Discov. Today Technol.*, 2004, **1**, 337–341.

350 H. J. Maple, N. Clayden, A. Baron, C. Stacey and R. Felix, *Medchemcomm*, 2019, **10**, 1755–1764.

351 A. Daina, O. Michielin and V. Zoete, *Sci. Rep.*, 2017, **7**, 1–13.

352 S. Krajcovicova, R. Jorda, D. Hendrychova, V. Krystof and M. Soural, *Chem. Commun.*, 2019, **55**, 929–932.

353 X. Han, C. Wang, C. Qin, W. Xiang, E. Fernandez-Salas, C. Y. Yang, M. Wang, L. Zhao, T. Xu, K. Chinnaswamy, J. Delproposto, J. Stuckey and S. Wang, *J. Med. Chem.*, 2019, **62**, 941–964.

354 J. R. Simard, L. Lee, E. Vieux, R. Improgo, T. Tieu, A. J. Phillips, S. L. Fisher, R. M. Pollock and E. Park, *SLAS Discov.*, 2021, **26**, 503–517.

355 A. Henssen, K. Althoff, A. Odersky, A. Beckers, R. Koche, F. Speleman, S. Schäfers, E. Bell, M. Nortmeyer, F. Westermann, K. De Preter, A. Florin, L. Heukamp, A. Spruessel, K. Astrahanseff, S. Lindner, N. Sadowski, A. Schramm, L. Astorgues-Xerri, M. E. Riveiro, A. Eggert, E. Cvitkovic and J. H. Schulte, *Clin. Cancer Res.*, 2016, **22**, 2470–2781.

356 P. Ottis, C. Palladino, P. Thienger, A. Britschgi, C. Heichinger, M. Berrera, A. Julien-Laferriere, F. Roudnicky, T. Kam-Thong, J. R. Bischoff, B. Martoglio and P. Pettazzoni, *ACS Chem. Biol.*, 2019, **14**, 2215–2223.

357 L. He, C. Chen, G. Gao, K. Xu and Z. Ma, *Aging (Albany. NY).*, 2020, **12**, 4547–4557.

358 C. M. Robb, J. I. Contreras, S. Kour, M. A. Taylor, M. Abid, Y. A. Sonawane, M. Zahid, D. J. Murry, A. Natarajan and S. Rana, *Chem. Commun.*, 2017, **53**, 7577–7580.

359 J. Hines, S. Lartigue, H. Dong, Y. Qian and C. M. Crews, *Cancer Res.*, 2019, **79**, 251–262.

360 X. Mu, L. Bai, Y. Xu, J. Wang and H. Lu, *Biochem. Biophys. Res. Commun.*, 2019, **521**,

833–839.

361 F. Zhang, Z. Wu, P. Chen, J. Zhang, T. Wang, J. Zhou and H. Zhang, *Bioorganic Med. Chem.*, 2020, **28**, 115228.

362 F. Jiang, Q. Wei, H. Li, H. Li, Y. Cui, Y. Ma, H. Chen, P. Cao, T. Lu and Y. Chen, *Bioorg. Med. Chem.*, 2020, **28**, 115181.

363 C. Shi, H. Zhang, P. Wang, K. Wang, D. Xu, H. Wang, L. Yin, S. Zhang and Y. Zhang, *Cell Death Dis.*, 2019, **10**, 815.

364 B. Zhou, J. Hu, F. Xu, Z. Chen, L. Bai, E. Fernandez-Salas, M. Lin, L. Liu, C. Y. Yang, Y. Zhao, D. McEachern, S. Przybranowski, B. Wen, D. Sun and S. Wang, *J. Med. Chem.*, 2018, **61**, 462–481.

365 G. E. Winter, A. Mayer, D. L. Buckley, M. A. Erb, J. E. Roderick, S. Vittori, J. M. Reyes, J. di Iulio, A. Souza, C. J. Ott, J. M. Roberts, R. Zeid, T. G. Scott, J. Paulk, K. Lachance, C. M. Olson, S. Dastjerdi, S. Bauer, C. Y. Lin, N. S. Gray, M. A. Kelliher, L. S. Churchman and J. E. Bradner, *Mol. Cell*, 2017, **67**, 5-18.e19.

366 G. M. Burslem, J. Song, X. Chen, J. Hines and C. M. Crews, *J. Am. Chem. Soc.*, 2018, **140**, 16428–16432.

367 J. W. Papatzimas, E. Gorobets, R. Maity, M. I. Muniyat, J. L. Maccallum, P. Neri, N. J. Bahlis and D. J. Derksen, *J. Med. Chem.*, 2019, **62**, 5522–5540.

368 M. R. Michaelides, A. Kluge, M. Patane, J. H. Van Drie, C. Wang, T. M. Hansen, R. M. Risi, R. Mantei, C. Hertel, K. Karukurichi, A. Nesterov, D. McElligott, P. De Vries, J. W. Langston, P. A. Cole, R. Marmorstein, H. Liu, L. Lasko, K. D. Bromberg, A. Lai and E. A. Kesicki, *ACS Med. Chem. Lett.*, 2018, **9**, 28–33.

369 D. Zaidman, J. Prilusky and N. London, *J. Chem. Inf. Model.*, 2020, **60**, 4894–4903.

370 M. L. Drummond, A. Henry, H. Li and C. I. Williams, *J. Chem. Inf. Model.*, 2020, **60**, 5234–5254.

371 M. J. Bond and C. M. Crews, *RSC Chem. Biol.*, 2021, **2**, 725–742.

372 S. J. Coles and P. A. Gale, *Chem. Sci.*, 2012, **3**, 683–689.

373 M. Philpott, J. Yang, T. Tumber, O. Fedorov, S. Uttarkar, P. Filippakopoulos, S. Picaud, T. Keates, I. Felletar, A. Ciulli, S. Knapp and T. D. Heightman, *Mol. Biosyst.*, 2011, **7**, 2899.

374 J. Spencer, C. B. Baltus, H. Patel, N. J. Press, S. K. Callear, L. Male and S. J. Coles, *ACS Comb. Sci.*, 2011, **13**, 24–31.

375 A. H. Lewin, J. Szewczyk, J. W. Wilson and F. I. Carroll, *Tetrahedron*, 2005, **61**, 7144–7152.

376 R. A. Tromp, S. S. G. E. Van Boom, C. M. Timmers, S. Van Zutphen, G. A. Van Der Marel, H. S. Overkleeft, J. H. Van Boom and J. Reedijk, *Bioorganic Med. Chem. Lett.*, 2004, **14**, 4273–4276.

377 J. B. Liu, X. H. Xu and F. L. Qing, *Org. Lett.*, 2015, **17**, 5048–5051.

378 L. S. Monteiro, F. Paiva-Martins, S. Oliveira, I. Machado and M. Costa, *Bioorg. Chem.*, 2019, **89**, 102983.

379 R. A. West, O. G. O'Doherty, T. Askwith, J. Atack, P. Beswick, J. Laverick, M. Paradowski,

L. E. Pennicott, S. P. S. Rao, G. Williams and S. E. Ward, *Eur. J. Med. Chem.*, 2017, **141**, 676–689.

380 P. Seetham Naidu and P. J. Bhuyan, *Tetrahedron Lett.*, 2012, **53**, 426–428.

381 M. Kollareddy, A. Sherrard, J. H. Park, M. Szemes, K. Gallacher, Z. Melegh, S. Oltean, M. Michaelis, J. Cinatl, A. Kaidi and K. Malik, *Cancer Lett.*, 2017, **403**, 74–85.